The Sedimentary and Geomorphic Signature of Subglacial Processes in the Tarfala Valley, northern Sweden, and the Links between Subglacial Soft-bed Deformation, Glacier Flow Dynamics, and Landform Generation

by

Joseph Anthony Pomeroy

A Doctoral Thesis

Submitted in partial fulfillment of the requirements
for the award of
Doctor of Philosophy of Loughborough University

July 2013

Abstract

The aim of this study is to understand the extent, depth, magnitude and significance of subglacial sediment deformation. It will examine the role of this deformation in controlling glacier dynamics and landform generation in glaciers in general, and polythermal glaciers in particular. A detailed multi-dimensional approach is used to study recently exposed glacigenic sediments on the forefields of three polyglaciers in the Tarfala Valley, northern Sweden. Overridden fluted moraines and diamicton plains occur in each forefield. These palimpsest landforms consist of multiple subglacial traction tills. Flutes have quasi-regular geometry and about half of those studied have no initiating boulder. It is suggested here that flute formation by forced-mechanisms was superimposed on flute formation related to a topographically-induced flow instability. In each forefield the depth of the deforming-bed averaged between 0.2m and 0.6m thickness, and in flutes, clast fabric results suggest that sediment advection was limited in extent. Detailed clast fabric data suggest the diamicton plain is composed of thin layers of traction tills that accreted over time as the zone of deformation moved upwards. Thin section analysis reveals that traction tills have been affected by cryogenesis, especially in the upper 0.35m, and that periglacial overprinting of subglacial signatures extends to at least 1m depth and affects tills subaerially exposed for as little as 30 years. Laboratory shear box tests show that subglacial deformation required elevated pore-water pressures, which suggests deforming-bed conditions were restricted to the temperate zones of polythermal glaciers and that flutes formed beneath warm-based ice. Although subglacial deformation appears to be widespread and produces similar uniform, homogeneous traction tills in each forefield, magnetic fabrics suggest strain magnitudes were moderate (≤ 10), rather than the very high strain magnitudes ($>10^2$) required by the deforming-bed model. Furthermore, the application of the micro-structural mapping technique demonstrates that subglacial deformation was multi-phase, heterogeneous, and partitioned into the softer and more easily deformed parts of the matrix. A conjugate set of cross-cutting micro-fabrics develops during a late-stage of deformation and is probably related to the stiffening of the diamicton as the sediment de-waters. Consequently, deformation is controlled by variations in sediment granulometry and pore-water pressure, and is likely to have been spatially and temporally variable, a finding that supports the ice-bed mosaic model. The strain magnitudes and deforming-bed thickness suggest that soft-bed deformation did not exert a major control on glacier dynamics during the Little Ice Age advance.

Table of Contents

List of Tables

List of Figures

The Sedimentary and Geomorphic Signature of Subglacial Processes in the Tarfala Valley, northern Sweden, and the Links between Subglacial Soft-bed Deformation, Glacier Flow Dynamics, and Landform Generation

---

Chapter 1 Context, Rationale, Aims and Objectives of the Study

1.1 Introduction

There is consensus in the glaciological community regarding the pivotal role subglacial processes play in controlling glacier dynamics, till genesis, and the generation of streamlined landforms (Murray, 1997; Alley, 2000; Boulton *et al*., 2001; Clarke, 2005; Evans *et al*., 2006), but considerable uncertainty regarding the relative contribution subglacial processes such as lodgement, meltout, and bed-deformation make to the generation of subglacial tills (Piotrowski *et al*., 2001; van der Meer *et al*., 2003; Piotrowski *et al*., 2004; Evans *et al*., 2006; Menzies *et al*., 2006; Larsen *et al*., 2007), and the subglacial mechanisms responsible for producing distinctive landforms such as drumlins, mega-scale glacial lineations and fluted moraines (Hoppe and Schytt, 1953; Boulton, 1983; Menzies, 1987; Rose, 1987; Gordon *et al*., 1992; Tulaczyk *et al*., 2001; Stokes and Clark, 2002; Clark *et al*., 2003; King *et al*., 2007; Smith and Murray, 2009; Evans *et al*., 2010). There is also uncertainty regarding the nature of subglacial soft-bed deformation, whether it can be a deep, widespread and pervasive process involving strains to very high magnitude in a deforming mobile bed, or whether deformation is a more depth-limited, discrete and incremental process (Hart and Boulton, 1991a; van der Wateren *et al*., 2000; Piotrowski *et al*., 2001; Boulton *et al*., 2001; van der Meer *et al*., 2003; Menzies *et al*., 2006; Larsen *et al*., 2007; Iverson *et al*., 2008; Thomason and Iverson, 2009). In addition, there are uncertainties regarding the relative contribution of glacier sliding and subglacial deformation to the total basal slip of glaciers underlain by weak, soft-beds (Alley *et al*., 1986; Boulton, 1986; Boulton and Hindmarsh, 1987; Iverson *et al*., 1995; Jansson, 1995; Piotrowski *et al*., 2001; Smith and Murray, 2009; Cuffey and Paterson, 2010).

Much of the uncertainty regarding subglacial processes stems from the difficulty of making direct observations in inaccessible subglacial environments (Clarke, 2005). Borehole studies and direct observations in subglacial tunnels only allow a restricted view of the glacier bed, often in ice-marginal areas which may not be typical of the glacier as a whole, and usually over short time periods (Murray, 1997; Clarke, 2005). Geophysical measurements using ground-penetrating radar or seismology can give insights into the nature of the glacier bed over wider areas (King *et al*., 2007; Smith and Murray, 2009), but such measurements are difficult or impossible to ground-truth which renders interpretations speculative (Blankenship *et al*., 1986; Englehardt and Kamb, 1997; Murray, 1997; Piotrowski *et al*., 2001). As such, the properties of glacigenic sediments and landforms left behind following glacier recession represent the primary source of evidence from which inferences about the nature of subglacial processes can be made (Piotrowski *et al*., 2001).

In the Tarfala Valley of northern Sweden, the recession of small polythermal glaciers from their Neoglacial maximum extent has exposed fresh glacigenic sediments and landforms. The aim of this study was to understand the nature and extent of subglacial deformation and its role in controlling glacier dynamics and landform generation in glaciers in general, and in polythermal glaciers in particular. This will be accomplished by undertaking detailed investigations into the glacigenic properties of forefield sediments and landforms in the Tarfala Valley so as to characterise the nature of the subglacial environment, with a specific focus on understanding the nature, extent, depth, and magnitude of soft-bed deformation and its role in the formation of fluted moraines and diamicton plains. Three forefields were studied: Storglaciären, Isfallsglaciären, and Kaskasatjåkkaglaciären. A multi-disciplinary approach was adopted, which, for the first time, attempted to constrain the polyphase history of sediment deformation in the Tarfala Valley using micro-structural mapping (van der Meer, 1993; Phillips *et al*., 2010b), employed ground-penetrating radar surveys and sediment analysis to investigate the architecture of fluted moraines, and used the anisotropy of magnetic susceptibility (AMS) to estimate strain magnitudes in subglacial sediments (Iverson *et al*., 2008). The multi-disciplinary approach allowed for a more detailed analysis of glacigenic sediments and landforms than had previously been achieved in the Tarfala Valley, adding to the sum of direct observations required for falsifying models of subglacial soft-bed deformation, whilst providing valuable field evidence with which to inform and refine our understanding of subglacial processes in general.

1.2 Rationale

The realisation that different subglacial processes operate beneath glaciers resting on soft, deformable beds compared to rigid beds (Alley *et al*., 1986; Boulton, 1986; Cuffey and Paterson, 2010), coupled with the observation that soft beds were widespread beneath contemporary and Quaternary glaciers and ice sheets (Alley, 1991; Boulton *et al*., 2001; Clarke, 2005), led to a paradigm shift in glaciology and the development of the soft-bed deformation model (Alley *et al*., 1986; Boulton, 1986; Alley, 1991). The essence of the soft-bed deformation model (hereafter referred to as the deforming-bed model), is that glaciers move by shearing their beds (Iverson *et al*., 2008); glaciers overriding soft-beds may impart sufficient stress to deform the bed, often to considerable depth, with up to 70-90% of the forward motion of a glacier accounted for by sub-sole deformation within the mobile soft-bed (Boulton and Hindmarsh, 1987). The paradigm shift and the focus on bed-deformation led to claims that all subglacial tills are deformation tills (van der Meer *et al*. 2003), that deformation-induced fast ice flow produces distinctive elongated landforms such as flutes, drumlins and Mega-Scale Glacial Lineations (Stokes and Clark, 2002), and that pervasive deformation produces a continental-scale sediment flux (Boulton *et al*., 2001). Furthermore, non-stable glacio-dynamic behaviours that result in rapid deglaciation, such as glacier surging or the onset of fast flow in ice streams, are thought to be initiated by soft-bed deformation (Clark *et al*., 1996; Fischer and Clarke, 2001; Boulton and Hagdorn, 2006; Passchier *et al*., 2010); conversely, ice stream shut-down may be caused by the development of a more rigid substrate and the cessation of soft-bed deformation (Christoffersen and Tulaczyk, 2003). The deforming-bed model has also been use to account for the lobate shape and volume of palaeo-ice sheets (Clark *et al*., 1996; Boulton and Hagdorn, 2006), the Mid-Pleistocene transition in the length of glacial cycles from 40kyr to 70kyr (Clark and Pollard, 1998), and binge-purge cycles in the Laurentide Ice Sheet that culminated in Heinrich events and abrupt climate change (MacAyeal, 1993).

Recent research has called into question many aspects of the deforming-bed model (Fuller and Murray, 2000; Piotrowski *et al*., 2001; Clark *et al.*, 2003; Piotrowski *et al.*, 2004; Clarke, 2005; Larsen *et al.*, 2006; Evans *et al*., 2006; Iverson *et al*., 2008; Thomason and Iverson, 2009), and alternative subglacial models have been developed. For example, the ice-bed mosaic model (Piotrowski *et al*., 2004) places less emphasis on bed-deformation as a primary control on glacier dynamics and suggests deforming soft-beds were much less widespread and deep than previously suggested (Piotrowski *et al*., 2001). The ice-bed mosaic model characterises subglacial deformation as a discrete, depth-limited, cumulative and time-transgressive process. Furthermore, the assumption of a non-linear viscous till rheology adopted in the deforming-bed model has been questioned by laboratory studies that suggest tills consistently behave as Coulomb plastic materials (Iverson and Iverson, 2001; Tulaczyk, 2006; Iverson *et al*., 2008). In addition, the mechanisms leading to bed-deformation remain poorly constrained, with uncertainty surrounding the role of clast-ploughing (Tulaczyk *et al*., 2001; Rousselot and Fischer, 2007; Thomason and Iverson, 2008), ice-keel ploughing (Tulackzyk *et al*., 2001; Clark *et al*., 2003), clast crushing (Hooke and Iverson, 1995), and sediment dilation, fluidisation and liquefaction (Evans *et al*., 2006; Thomason and Iverson, 2008).

It is important to resolve the uncertainties regarding subglacial processes because a better understanding of subglacial processes is required to parameterize ice sheet models, to predict glacio-dynamic response to climate change (including the influence of fast-flowing ice streams on sea level change), and to match modelled glacier dynamics to sediment-landform associations (Carr, 2004; Evans *et al*., 2006; Boulton and Hagdorn, 2006; Lemke *et al*., 2007; Passchier *et al*., 2010). For example, an understanding of the subglacial processes involved in the recession of former ice sheets is required to inform predictions about the impact of global warming on the stability of the West Antarctic Ice Sheet (Cuffey and Paterson, 2010). However, subglacial models and models of sediment-landform associations have often been based on limited observational data and untested assumptions about till formation (Evans *et al.*, 2006). As such, direct observations from new field sites are important because they have the potential to increase our understanding of the sedimentary and geomorphological signature of subglacial processes (Evans *et al*., 2010), and because they provide vital field evidence for falsifying models of bed-deformation and for testing assumptions about till genesis (Benn and Evans, 2010). Field measurements are also required to corroborate theories emerging from laboratory investigations, such as recent advances in the use of magnetic fabrics as proxies for strain magnitude (Iverson *et al*., 2008). In addition, although tills contain important information about palaeo-glaciology (Christoffersen and Tulaczyk, 2003), palaeo-glaciological reconstructions and the interpretation of Quaternary glacigenic sediments should be guided and informed by field observations from modern glacial environments (Benn, 1995; Evans *et al*., 2010).

Previous research in the Tarfala Valley has focused on the mass balance and glacier dynamics of Storglaciären, with relatively little research conducted on glacigenic sediments and landforms in forefield areas (Holmlund and Jansson, 2002). Borehole studies revealed a 0.3-0.7m thick subglacial till in the ablation zone of Storglaciären that was interpreted as a pervasively deforming till (Hooke *et al*., 1997), and subglacial deformation tills have been identified as the main component of the Storglaciären diamicton plain and the fluted moraine of Isfallsglaciären, with pervasive bed-deformation invoked to explain the formation of these landforms (Eklund and Hart, 1996; Etienne *et al*., 2003). As such, previous research suggests that the recently exposed forefields of the Tarfala Valley are an ideal natural laboratory in which to investigate subglacial processes and to test models of subglacial deformation.

More detailed and extensive field studies were required in the Tarfala Valley because previous forefield investigations have been limited by poor sediment exposure (Etienne *et al*., 2003) or by the small number of sites investigated (Eklund and Hart, 1996). In addition, the borehole experiments were spatially restricted and involved uncertainties regarding instrument insertion and location, and failed to identify a consistent relationship between basal water pressure, strain rates within the deforming bed, and glacier velocity in successive years of study (Fischer *et al*. 1996; Murray, 1997). The interpretation of tills as being pervasively deformed has been on the basis of their homogeneous appearance, planar fabric, and fractal grain-size distribution (Etienne *et al*. 2003), none of which can be considered diagnostic properties of deformation tills (Evans *et al*., 2006), or from the occurrence of non-linear deformation profiles in a very limited number of trenches excavated into just one flute (Eklund and Hart, 1996). Indeed, because no one criterion is diagnostic of deformation tills (Piotrowski *et al*., 2001), the interpretation of glacigenic sediments needs to be founded on a wide-range range of evidence, with the classification of a sediment as a subglacial deformation till requiring unequivocal evidence of sediment deformation having taken place (Evans *et al*., 2006). It had also been assumed that the properties of sediments in the proglacial areas, such as planar fabrics and clast fabrics, reflected subglacial processes and not periglacial or paraglacial processes. Planar fabrics can also be produced by dewatering and unloading (Muller, 1983), or by the growth of ice lenses and freeze-thaw activity in silt-rich tills (Lundqvist, 1983), whilst mass flows, slope wash, and frost heave processes can cause post-depositional disturbance to clast fabrics (Rose, 1991). The extent to which the signatures of subglacial activity in forefield sediments have been overprinted by periglacial activity or disrupted by paraglacial processes was unknown in the Tarfala Valley. As such, further field evidence was required to confirm the identification and distribution of pervasively deformed subglacial tills. Furthermore, the bed-deformation model predicts that subglacial tills will be strained to very high magnitudes (Larsen *et al*., 2006; Iverson *et al*., 2008). Therefore, falsifying the deforming-bed model requires evidence of strain magnitudes, the depth and extent of the deforming bed, and the nature of the deformation process, whether spatially partitioned, pervasive, times-transgressive and so on (Piotrowski *et al*., 2001; Iverson *et al*., 2008). As such, a multi-disciplinary approach is justified.

Finally, it should be noted that the vast scale and remoteness of ice sheets and the lack of accessible forelands makes investigations into subglacial processes expensive and difficult. By contrast, small, accessible polythermal glaciers in the Tarfala Valley, that are typical of polythermal glaciers in Arctic regions as a whole (Holmlund and Jansson, 2002), can be used as analogues to inform our knowledge of subglacial processes and glacier dynamics in glaciers and ice sheets in general. In addition, the small scale of glaciers in the Tarfala Valley makes characterising the nature of the subglacial environment a realistic proposition, while the ongoing mass balance programme conducted at the Tarfala Research Station provides a wealth of additional data with which to enrich this study, and affords an excellent base from which to conduct this research.

1.3 Outline of the Thesis

The remainder of Chapter 1 provides the context for this study, which includes a critical literature review leading to the formulation of the key questions to be addressed and a specific statement of aims and objectives. Chapter 2 provides an outline of the study area, providing relevant details about the glaciers, climate, and geology of the Tarfala Valley, and justifies the choice of the three forefields selected for research. The remainder of Chapter 2 focuses on methodological considerations and gives details and then justifies the laboratory and fieldwork techniques employed.

The results of the study are presented in Chapters 3, 4 and 5. These Chapters are structured around the key questions identified in the literature review. In Chapter 3, the description and interpretation of the lithofacies-landform associations of each forefield enables the character and extent of subglacial sediments and landforms to be identified and establishes the thickness of the deforming bed. In Chapter 4, the clast fabrics and magnetic fabrics of subglacial diamictons are analysed as strain signatures. Detailed clast fabrics taken from fluted moraine in Isfallsglaciären are combined with macro-scale observations and used to assess models of flute formation. Magnetic fabrics from subglacial diamictons are then used to estimate strain magnitudes and to test the bed-deformation model. In Chapter 4, one of the key uncertainties in subglacial processes is addressed, namely, whether strain magnitudes in subglacial diamictons are consistent with the very high strains required by the deforming-bed model (Iverson *et al*., 2008). In Chapter 5, micromorphology is used to assess the extent of periglacial overprinting in recently exposed subglacial sediments. The micro-structural mapping approach (Phillips *et al*., 2010b) is then applied to thin section samples in order to investigate the polyphase history of sediment deformation in subglacial diamictons from the Isfallsglaciären fluted moraine and the Storglaciären diamicton plain. Micro-scale data are integrated with macro-scale observations to provide detailed insights into the nature of soft-bed deformation.

In Chapters 3 to 5 the scale of investigation moves from the macro-scale to the micro-scale, with each scale of analysis providing additional insights and allowing for a more complete understanding of subglacial deformation processes. Chapter 6 provides a synthesis in which data from all scales are integrated and interpreted in terms of what they tell us about the nature of soft-bed deformation in the Tarfala Valley, the extent to which it controlled previous glacier dynamics, and its role in formation of fluted moraines and the diamicton plain. A model of flute formation is presented. The wider implications and relevance of the research are then addressed, specifically: the extent to which the research supports or falsifies the deforming-bed model and other subglacial models, and the extent to which the research findings are applicable to glaciers at larger scales. Chapter 7 provides a summary of the conclusions of the study, and is followed by the acknowledgements, references, and appendices. A glossary of technical terms used in the thesis is given in appendix 1.

1.4 Context

In the literature review that follows, the deforming-bed model is outlined in section 1.4.1 and its significance explained. In sections 1.4.2 to 1.4.5 the main uncertainties regarding subglacial processes and the deforming-bed model are considered. In sections 1.4.6 to 1.4.8 other subglacial models are introduced and the uncertainties relating to these models discussed. In section 1.4.9 the importance of the basal thermal regime in bed-deformation is addressed, and in section 1.4.10 uncertainties about the role of bed-deformation in the formation of flutes are considered.

1.4.1. The Dynamics of Glaciers with Soft-beds and the Deforming-bed Model

The first evidence of a link between fast glacier flow and bed-deformation came from the interpretation of seismic reflections from beneath the Whillans Ice Stream in Antarctica (formerly Ice Stream B). In a region of low driving stresses, well below those required to deform glacial ice, fast glacier flow was thought to be initiated and maintained by the pervasive deformation of a 6m deep, saturated and dilatant subglacial till that was hypothesized to be deforming as a viscous fluid and so accommodating the motion of the glacier (Blankenship *et al*. 1986; Alley *et al*. 1986). However, this hypothesis was challenged by observations from borehole studies that suggested the deforming bed was only a few centimetres thick, and that fast glacier flow was the result of basal sliding (Englehardt and Kamb, 1997). The processes of basal sliding and bed-deformation combine to produce the total basal slip of a glacier, and basal slip can account for up to 90% of a glacier’s velocity (Hooke *et al*., 1997). Fast-flowing Antarctic ice streams have been observed to have basal slip rates of 0.2 to 1km yr^{-1} despite low driving stresses of 2 to 20 KPa (Kamb, 1991), which suggests that well-lubricated soft-beds that reshape themselves in response to stress not only contribute to glacier flow through deformation, but offer little frictional resistance to glacier sliding and, as such, deformable beds play a key role in controlling the dynamics of active glaciers (Cuffey and Paterson, 2010).

The degree to which basal slip is partitioned between glacier sliding and bed-deformation is unknown for most glaciers, but observations from boreholes drilled into the ablation zone of Storglaciären in the Tarfala Valley of northern Sweden, suggest that sliding is the dominant process and accounts for up to 70% of basal slip (Hooke *et al*., 1997). However, Etienne *et al*. (2003) suggested that the presence of a (up to) 7m thick and volumetrically important pervasively deformed subglacial deformation till in the forefield diamicton plain indicates that bed-deformation may have been the dominant control on glacier dynamics over centennial timescales during the Neoglacial advance, with the current dominance of basal sliding merely reflecting the contemporary wetter climatic conditions. Similarly, Alley (1991) suggested that pervasive bed-deformation was the key control on glacier flow beneath the Laurentide Ice Sheet where the presence of a rough till bed would have rendered basal sliding a slow process.

Boulton and Hindmarsh (1987) made the first direct measurements of bed-deformation in a subglacial tunnel beneath Breiðamerkurjökull, Iceland. Strain markers inserted into the bed revealed a 0.6m deep non-linear pervasive deformation profile, with strain increasing towards the ice-bed interface. The deforming till had a two-tier structure, with a weak, saturated and dilatant upper A- type horizon, in which ductile deformation occurred and greater strain was encountered, and a stiffer, lower non-dilatant B-type horizon, in which brittle deformation occurred along discrete shear planes. The high rates of strain calculated (up to 55 yr^{-1}) suggested that bed-deformation was responsible for substantial till advection and geomorphological work. Boulton and Hindmarsh calculated that deformation of the bed accounted for up to 90% of the forward movement of the glacier in the terminus region, and if a Bingham non-linear viscous till rheology was assumed (see section 1.4.2 below) the flow relation fitted the form:

$$\dot{\varepsilon} = B_1 \tau^a N^{-b} \tag{1.1}$$

Where:

$\dot{\varepsilon}$ is the strain rate, τ is the basal shear stress, N is the effective pressure (that is, the overburden pressure – the pore-water pressure), and B_1, a and b are adjustable parameters. Boulton and Hindmarsh found values of a = 1.33, b = 1.80, and B_1 = 34.8 $(kPa)^{0.47}$ a^{-1} gave a good fit to the observed strain data. Basal shear stress τ was assumed to equate to the driving stress τ_b which was calculated from the simplified expression:

$$\tau_b = \rho ghsin\alpha \tag{1.2}$$

Where:

ρ is the density of ice; g is gravitational acceleration; h is the weight of overburden (usually taken as the ice thickness); and sin α is the surface slope of the glacier (Paterson, 1994). The effective pressure *N* depends on sediment conductivity and the ability of a bed to evacuate excess pore water, which in turn is controlled by the evolution of the basal hydrologic system (Boulton *et al*., 2001). In dry granular sediments effective pressure is high, which increases inter-granular friction and sediment strength. As sediments become saturated, the normal compressive stress is partitioned between the pore-water and the sediment framework, which reduces effective pressure and inter-granular friction and weakens the sediment to the point where deformation may occur (Paterson, 1994). A relatively dense sediment will dilate in response to shear as individual grains slide up and over each other (Craig, 1997), and, consequently, unconsolidated saturated sediments may deform grain by grain throughout a basal shear zone (that is, pervasively) in response to shear stress. According to the deforming-bed model, the strain rateincreases as shear stressincreases (in a slightly non-linear way), but decreases as effective pressure increases. The strain ratecan be predicted using equation 1.1, which anticipates widespread and pervasive deformation whenever glaciers override saturated soft-beds. Saturated soft-beds therefore exert a major control on glacier flow.

The Boulton and Hindmarsh deforming-bed model has become very influential in glaciology and widely incorporated into ice sheet models and reconstructions (MacAyeal, 1993; Clark *et al*., 1996; Clark and Pollard, 1998; Boulton and Hagdorn, 2006). Furthermore, bed-deformation has been invoked to explain drumlin formation by sediment deformation around a stiffer till core (Boulton *et al*., 2001), the homogenisation of till as a consequence of high strains(Eklund and Hart 1996; van der Wateren *et al*., 2000; van der Meer *et al*., 2003), and the non-linear deformation profile of palaeo-tills which are characterised by mixed zones, diffuse contacts, and homogenised beds (Hart and Rose, 2001; van der Meer *et al*., 2003; Evans *et al*., 2006). In addition, bed-deformation has been used to explain the formation of fluted moraine (Boulton, 1976; Eklund and Hart, 1996), the weakening of clast fabrics at high strain (Rose and Carr, 2001), the widespread distribution of massive, homogeneous tills beneath the Laurentide and European Ice Sheets (Alley, 1991; van der Meer *et al,*. 2003;

Alley 2000; Boulton *et al*., 2001), the distribution of past and present ice streams (Alley, 1991; Boulton and Hagdorn, 2006), and the continental scale flux of sediment responsible for building trough-mouth fans and terminal moraine lines (Alley, 1991).

1.4.2 Uncertainties Relating to Subglacial Processes and the Deforming-bed Model - Till Rheology, Constitutive Behaviour, and the Importance of Effective Pressure in Controlling Yield Strength

Because bed-deformation is a broad term that encompasses discrete failure along shear planes, ploughing by clasts, and pervasive deformation throughout an entire layer, and because tills display considerable spatial heterogeneity in their properties, devising simple failure criteria to model the subglacial deformation of soft-beds is problematic (Paterson, 1994). Laboratory ring-shear experiments using tills recovered from beneath glaciers consistently show that till rheology is best approximated as a Coulomb plastic material and not as a viscous linear (Newtonian) or non-linear fluid material as used in the deforming-bed model (Kamb, 1991; Iverson and Iverson, 2001; Tulaczyk *et al.,* 2001; Iverson *et al*., 2008). Till rheology is important because it determines the way a till deforms. A Coulomb plastic material fails by discrete slippage between grains along a shear plane or failure in a narrow shear band once shear stress τ, exceeds the yield strength τ_0, whereas a Newtonian viscous fluid deforms linearly in response to τ, with $\tau_0 = 0$, while a Bingham material deforms linearly in response to τ once τ_0 is exceeded (Benn and Evans, 2010; Cuffey and Paterson, 2010). Saturated granular soils behave as Coulomb plastic materials which dilate in shear until a critical state is reached, known as the residual shear strength, after which there is no further change in porosity or shear stress despite increasing strain (Head, 1982); it is believed granular tills behave in a similar way (Iverson and Iverson, 2001). In addition, the stresses generated in the sediment that oppose shearing do not increase with faster rates of shear, which means shear strength is independent of strain rate in a Coulomb plastic material (Head, 1982; Cuffey and Paterson, 2010). The Mohr-Coulomb failure criterion can be used to calculate the yield strength (or shear strength) of a Coulomb plastic material:

$$\tau_0 = c_0 + N tan\phi \tag{1.3}$$

Where: $c_0$is the sediment cohesive strength and ϕ is the internal angle of particle friction (Paterson, 1994).

Shear strength is not a fundamental property of sediment as it changes over time and depends on the prevailing drainage conditions and effective pressures (Head, 1982), the thickness of the glacier (overburden pressure), the applied stresses, and the pre-existing consolidation level of the sediment (Menzies *et al*., 2006). Furthermore, shear strength depends on the sediment mineralogy, texture, packing, and grain sorting, and is likely to vary spatially and as the granulometry of a subglacial till evolves through time in response to abrasion, particle crushing, and the washing-out of fines (Head, 1982; Craig, 1997; Benn and Evans, 2010). Clay rich tills have greater cohesive strength than sandy tills, and coarse-grained tills provide greater frictional resistance between grains and so support greater shear stresses than fine-grained tills. The range of cohesion and friction values in tills is generally considered to be small, which means that effective pressure is the most important control on sediment strength (Benn and Evans, 2010; Cuffey and Paterson, 2010).

Over hourly, diurnal and seasonal timescales, variations in effective pressure reflect variations in pore-water pressure, and these variations exert a fundamental control on sediment strength and the strain rate, as incorporated into equation 1.1 (Boulton and Hindmarsh, 1987). However, because yield strength is independent ofthe strain rate in a Coulomb plastic material (but the point at which failure occurs is linearly dependent on effective pressure), once $\tau > \tau_0$ the sediment no longer supports excess stress and glaciers slip over their beds (Tulaczyk *et al*., 2001; Benn and Evans, 2010). As such, deformation may be restricted to a shallow failure zone within the till which acts as a lubricating layer which facilitates basal sliding (Cuffey and Paterson, 2010). Such a situation is more likely to occur where there is a smooth bed consisting of fine-grained tills because they have sufficiently high surface tension to resist the infiltration of basal ice into the sediment by regelation, and because they lack coarser material capable of bridging through the substrate, which would resist sliding (Iverson *et al*., 2007). However, as shown in section 1.4.3 below, this does not appear to be the case in the Rutford Ice Stream where basal sliding seems to be associated with a rough bed (Smith and Murray, 2009). A stiff patch of till behaving as a Coulomb plastic material will deform elastically and store strain before the yield strengthis reached, potentially creating a sticky spot beneath a glacier which may support a significant proportion of the basal shear stress and whose eventual failure may result in stick-slip movement and the release of basal seismic energy (Fischer and Clarke, 2001). Sticky spots may prevent catastrophic ice acceleration over soft, deforming beds (Murray, 1997), and their distribution may account for the shutdown of some ice streams (Stokes and Clark, 2002).

Observations beneath contemporary glaciers show that basal shear stresses vary within a narrow range, typically 50 to 150 KPa (Cuffey and Paterson, 2010). As such, it is variations in sediment properties that control the timing, location, and extent of bed-deformation (Piotrowski *et al*., 2006). The importance of pore-water pressure in controlling yield strength is demonstrated by inserting values into equation 1.3; if basal shear stress is assumed to be 100 KPa, and the overburden pressure 2.2 MPa (exerted by a glacier 250m thick), then a granular till lacking cohesion, but with a typical friction angle of 30° would only deform if the effective pressure was less than 150 KPa, and this would require pore-water pressure to take up to 90% of the overburden load (Paterson, 1994). As such, subglacial tills should only deform when they are water saturated and pore-water pressure is high, and this implies deformation will vary spatially and temporally in response to variations in pore-water pressure, sediment porosity and hydraulic conductivity. It also implies bed-deformation is restricted to temperate ice and is favoured by regions of the bed having restricted drainage or distributed drainage systems (Piotrowski *et al*., 2001; Benn and Evans, 2010). However, as shown below (in section 1.4.7), deformation may occur beneath cold based-glaciers, especially where glacier-permafrost interactions take place (Waller, 2009). In addition, equation 1.3 assumes the pore-water is static, whereas in reality the seepage of water down a till profile can act to increase the local effective pressure and strengthen the till (Craig, 1997; Cuffey and Paterson, 2010). Conversely, grain-crushing at high effective pressures reduces inter-particle friction and reduces the yield strength (Craig, 1997). As such, it is not surprising that the relationship between effective pressure, till strength, and glacier flow is seldom straightforward.

Borehole experiments in the ablation area of Storglaciären indicate a complex relation exists between the strain rate of the subglacial till and effective pressure (Iverson *et al*., 1995). The till strain rate was estimated at $25yr^{-1}$ but the till was not deforming uniformly. Strain rates peaked during periods of rising basal water pressure, but reduced to zero at times of peak basal water pressure when the glacier was effectively decoupled from its bed and basal sliding dominated flow (Iverson *et al*., 1995; Fischer *et al*., 1996). Glacier flow accelerations were correlated with high basal water pressures and basal sliding initiated by intense rainstorms, and not with high strain rates in the till. Repetition of the experiments in subsequent years found the till strain rate, basal water pressure and glacier surface velocity remained out of phase, but that heavy rainstorms did not initiate fast flow later in the summer when the basal drainage system became better connected and efficient (Fischer *et al*., 1996; Hooke *et al*., 1997). However, the results of these borehole experiments are equivocal because instrument failure meant that simultaneous recordings of strain rates, glacier flow, and basal water pressures were seldom achieved (Fischer *et al*., 1996). In addition, the assumption that water-level variations in boreholes drilled to the glacier bed accurately reflected variations in basal water pressure has been questioned (Murray, 1997; Clarke, 2005). Topography may also exert an important control on Storglaciären's dynamics. Jansson (1996) argued that extensional flow across a prominent riegel generated crevasses which allowed surface water to access the bed in the lower ablation zone. Subsequent variations in basal water pressure caused hydraulic jacking in water-filled cavities, which resulted in flow acceleration as the whole glacier was pulled forward. The empirically derived velocity relation was:

$$u_s = 30N^{-0.40} \tag{1.4}$$

where$u_s$is the glacier surface velocity (Jansson, 1996). Figure 1.1 summarises what is known about Storglaciären's flow dynamics and highlights the role of effective pressure in controlling bed-deformation.

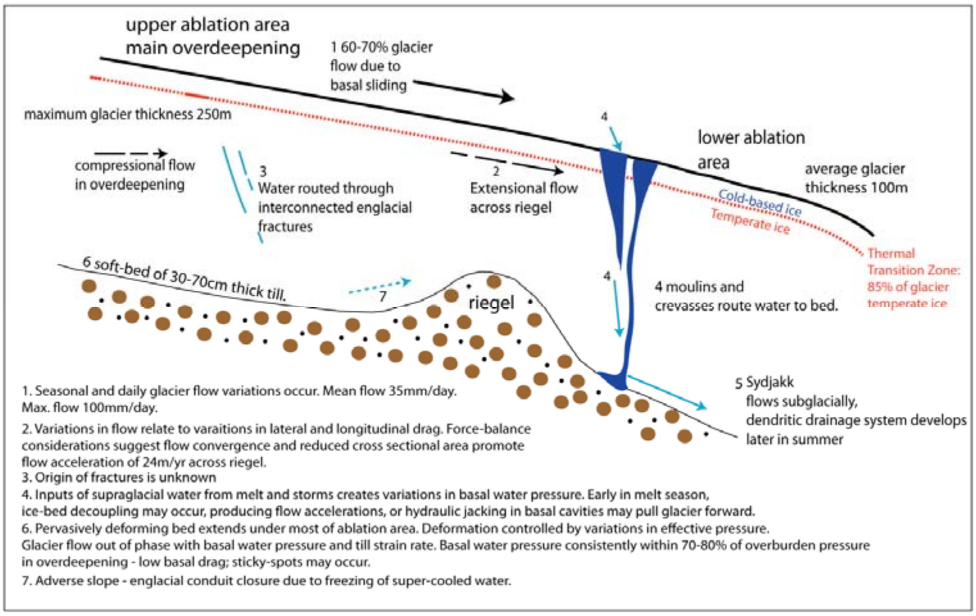

Figure 1.1 Factors Controlling the Glacial Dynamics of Storglaciären, This diagram summarises the research findings of Hooke and Pohjola (1994), Jansson (1995), Iverson *et al*., (1996), Holmlund *et al*., (1996), Holmlund and Jansson (2002), and Fountain *et al*., (2005).

Given the variable nature of shear strength in tills, the best rheology to use to parameterize ice sheet models remains contested (Clarke, 2005). Hindmarsh (1997) argued that deformation is scale-dependent; local plastic failures along discrete shear plans over length scales of 0.1 to 1m are distributed through a till in such a way as to resemble viscous failure when summed-up over length scales of 1km or more, scales which are more relevant to influencing glacier flow rates, and, as such, models should adopt a viscous till rheology. Fowler (2000) argued that till rheology is complex and that adopting a simple viscous rheology is justified when considering long-term strain under steady deformation because the effects of dilatancy, failure, irreversible elasticity and fabrics become irrelevant. However, Tulaczyk (2006), using observational data from the Whillans Ice Stream, rejected Hindmarsh's (1997) contention that till rheology is scale-dependent; till in laboratory tests behaves and deforms in the same way as till observed in the field when integrated over scales of 10 to 100km. However, laboratory experiments struggle to reproduce the load and temperature conditions typical of subglacial environments and, critically, it is often necessary to remove the coarsest fraction from remoulded tills before they can be used in ring-shear devices and shear box tests, which may significantly alter the response of the till to shear stress (Hart and Rose, 2001; Clarke, 2005; Benn and Evans, 2010). Boulders, for example, may act as immobile inclusions within till, distorting and intersecting shear planes, and stiffening the till and resisting sliding (Cuffey and Paterson, 2010). As such, even though laboratory experiments demonstrate that tills approximate the behaviour of Coulomb plastic materials, the extent to which small-scale laboratory experiments can be scaled-up to accurately capture the behaviour of tills beneath glaciers has to be questioned (Fowler, 2000).

1.4.3 Uncertainties relating to Subglacial Processes and the Deforming-bed Model - Depth of Deformation, Till Flux and Strain Magnitude

In tills behaving as Coulomb plastic materials, bed-deformation should be partitioned into narrow failure zones (Cuffey and Paterson, 2010). However, deeper and more distributed shear profiles can be produced in a Coulomb plastic material by clast-ploughing, or through transient variations in the loci of deformation brought about by vertical changes in pore-water pressure (Alley, 2000; Boulton *et al*., 2001). Diurnal variations in water pressure at the surface of a soft-bed take the form of a sine wave of frequency *f* whose rate of propagation through the sediment depends on hydraulic diffusivity *D*:

$$D\left(\frac{\partial^2 p}{\partial z^2}\right) = \frac{\partial p}{\partial t} \tag{1.5}$$

Where:

p iswater pressure, *z* is depth and *t* is time (Paterson, 1994).

As the pressure wave enters and travels down through the bed the amplitude of the sine wave is reduced, by approximately one third at a depth of 0.5m according to Paterson (1994). The significance of equation 1.5 is that a zone of plastic deformation is most likely to be located wherever the water pressure is greatest (and effective pressure lowest) at any given moment in time, and this zone moves up and down the sediment profile in response to the propagation of diurnal pressure waves. Over time, this may result in distributed shear throughout the deforming layer (Alley, 2000). Critically, the depth of deformation is limited by the exponential decay of the pressure wave, which may explain why the average depth of bed-deformation observed beneath contemporary glaciers is 0.3m to 0.5m; below this depth $\tau_0 > \tau$ because pore-water pressure increases at a slower rate with depth than overburden pressure (Alley, 1991, 2000; Cuffey and Paterson, 2010). Table 1.1 summarises the results of experiments in which the depth of subglacial sediment deformation has been cited, and shows that although conflicting and variable deformation depths have been recorded, often for the same glacier, most observations favour shallow deformation (< 0.5m) focused at or near the glacier bed, as would be expected with a sediment yielding as a Coulomb plastic material.

Table 1.1Deforming layer thickness measured from direct observations in subglacial tunnels, from borehole experiments, geophysical experiments, and foreland and laboratory analysis. Note that the application of different techniques to different types of glacier does not produce great differences in the depth of subglacial deformation measured.

Glacier	Experimental Outcomes	Deforming Layer Thickness (m)	References
Whillans Ice Stream W. Antarctica	Glacier velocity of $825ma^{-1}$. Highly dilatant and porous till (0.4). Strain rate 75 a^{-1}	Average 6 but up to 12	Alley *et al.*, (1986; 1989); Blankenship *et al.*, (1986)
Whillans Ice Stream W. Antarctica	High basal water pressure, 83% basal motion in shallow layer 0.33mm deep; basal sliding dominates	< 1mm to 2m max	Kamb (1991); Engelhardt and Kamb (1998)
Breiðamerkurjökull, Iceland (Maritime temperate glacier)	Net strain decreases with depth with 65-85% of forward motion accounted for by bed-deformation. Dilatant and porous A-horizon (0.4) pervasively deforms while less porous B-horizon (0.2) experiences brittle deformation	0.6	Boulton and Hindmarsh (1987)
Storglaciären, Sweden (polythermal sub-arctic glacier)	Borehole measurements suggest basal sliding under a large part of the ablation area is very high, 60-90% of measured surface velocity. Glacier decouples from its bed at high water pressures. Sliding occurs throughout winter. Sediment flux $0.67m^2\ a^{-1}$ per m section. Till supports basal shear stress of 55 KPa.	0.35	Iverson *et al.*, (1994); Jansson (1995)
Trapridge Glacier, Yukon (Sub Polar)	Time varying nature of strain in 10m deep bed; 40-65% of surface velocity due to sliding	0.3	Fischer and Clarke, (2001)
Trapridge Glacier	Deformation within 1m thick coarse till accounts for 25-45% of surface velocity	0.3	Blake (1992)
Black Rapids Glacier, Alaska	Décollement depth > 2m with deformation accounting for 50-70% of surface velocity	7.5 thick till	Truffer *et al.*, (2000)

Columbia Glacier, Alaska	Observations of bent drill rods	0.65	Humphreys *et al.*,(1993)
Urumqi Glacier no. 1. China	Frozen basal sediment layer in cold-based ice deforms and accounts for 60% forward motion of the glacier	0.36	Echelmeyer and Wang (1987)
Hagafellsjökull Vestari, Iceland	Continuous clay layer between tills in drumlins suggests shallow, non-pervasive sediment deformation. Main movement by sliding and main deformation by clast-ploughing	< 1cm	Fuller and Murray, (2000)
Bakaninbreen, Svalbard	Tilt cells inserted down borehole suggest till deforming as non-Coulomb plastic	0.2	Porter and Murray, (2001)
Batestown till, former Laurentide Ice Sheet lobe	AMS fabrics and ring shear experiments suggest strains to a few decimetres and to moderate strain magnitudes	< 0.3	Thomason and Iverson (2009)
Elisebreen, Svalbard	Detailed till analysis suggests limited and patchy deformation	0.3	Larsen *et al*., (2006)
Rutford Ice Stream, W.Antarctica	Patchy deforming bed, but widespread deformation of a dilatant, porous, and water-saturated bed in places. Streamlined bedforms developed rapidly and elongation ratios increase downstream	12	Smith and Murray (2009)

Paradoxically, thick layers of pervasively deformed sediments have been identified in the Quaternary till deposits of Europe and North America, although there are disagreements over the interpretation of some of these till sequences (Boulton *et al*., 1985; Alley, 1991; Hart and Boulton, 1991a and b; Clark, 1994; Clark *et al*., 1996; van der Wateren *et al*., 2000; Alley, 2000; Piotrowski *et al*., 2001; van der Meer *et al*., 2003; Menzies *et al*., 2006; Benn and Evans, 2010; Phillips *et al*., 2011a). Van der Wateren *et al*. (2000) suggested that the distribution of kinematic strain indicators in Pleistocene till sequences in NW Europe showed that there was an increase in finite strain towards the ice-bed interface where homogenised tills were generated through simple shear to high strains, and that the deforming layer was several metres thick. Alley (1991) favoured a deforming bed origin with pervasive shear to very high strains for the uniform and homogeneous till sheets of the Laurentide ice sheet, which extend over vast areas and are between 1 and 10m thick. Hart and Boulton (1991a) suggested that the depth of the deforming bed depended on the basal shear stress and could be thick (up to 10m) where excavational deformation occurred, that is, where the deforming layer was eroding into the underlying substrate, or thin (10cm) where constructional deformation occurred, that is, deformation was focused in a thin layer that moved up through the sediment profile over time.

Thick deforming beds up to 12m deep have also been identified in recent geophysical surveys beneath the Rutford Ice Stream in West Antarctica (Smith, 2006; King *et al*., 2007; Smith and Murray, 2009). Seismic and radar surveys in the onset zone suggest that the patchy but deep deformation of overridden marine sediments is capable of building (in just 7 years) drumlins that become increasingly elongated as they migrate downstream. In these studies, deforming beds are identified wherever regions of low seismic activity occur (Smith, 2006). The hypothesis is that deforming sediments produce a smooth, frictionless bed that generates few distinctive basal microseismic signals, whereas stable, non-deforming beds (where basal sliding or stick-slip movements dominate), are characterised by rougher beds which generate greater friction and high numbers of basal microseismic signals (Smith, 2006). Deforming beds are also identified by their lower levels of acoustic impedance which suggests that the sediment is in a highly porous and dilatant state, and is therefore assumed to be deforming (Smith and Murray, 2009). However, as was shown in the case of the Whillans Ice Stream (Blankenship *et al*., 1986; Englehardt and Kamb, 1997), care has to be taken in the interpretation of seismic surveys, especially where there are no direct observations to confirm the depth of the deforming bed. Moreover, high porosity alone is not a diagnostic criterion for identifying a deforming bed because subglacial melt out tills also have high porosity (Piotrowski *et al*., 2001).

The thickness of the deforming bed is important because it sets limits on the subglacial till flux (volume of till moved per unit time per unit width), which given the existence of thick grounding-line deposits, terminal moraines and trough-mouth fans cannot be negligible (Piotrowski *et al*., 2001; Clark *et al*, 2001; Cuffey and Paterson, 2010). As with glaciers, a subglacial till layer can be considered to adjust to changes in its 'mass balance' or 'continuity relation' (Alley 2000; Cuffey and Paterson, 2010); to persist, the flux of material transported from any part of the till layer must be replenished by an input of eroded material from up-glacier. Cuffey and Paterson (2010) use the continuity relation and estimated rates of erosion in modern glaciers to show that it is theoretically possible for a deforming layer to persist in a steady-state under a wide-range of subglacial conditions, as long as the deforming bed is thin (<1m). However, the deforming-bed model considers glaciers overriding pre-existing sediments, a situation not considered in Cuffey and Paterson's continuity relation, where erosion of the substratum through excavational-style deformation is thought to be an important process in the formation and regeneration of thick deforming beds, which can support high till fluxes with erosion rates of up to 1mm yr^{-1} (Hart and Boulton, 1991a; Piotrowski *et al*., 2002). Indeed, subglacial deformation tills are defined as admixtures of far-travelled material and local material (Dreimanis, 1998), and the presence of transported rafts of underlying sediment, intraclasts and soft-sediment inclusions in glacigenic sediments are useful criteria for identifying a deformation sequence, and shows the effectiveness with which underlying substrate can be incorporated (or cannibalised) into the base of a deforming layer (Menzies and Shilts, 2002; Benn and Evans, 2010).

The thickness of the deforming layer typically recorded in modern glacial environments and distributed shear profiles may also be explained by clast-ploughing in areas of debris-rich basal ice. A clast embedded in the glacier sole will plough through a weak bed and transmit stress to a depth of 1-5 times the diameter of the clast (Tulaczyk *et al*., 2001) and, given that many tills have average clast diameters of a few centimetres, this typically generates 0.3 to 0.5m of distributed shear (Boulton *et al*., 2001). The style and depth of deformation may be controlled by granulometry because clasts in coarse tills interlock and strongly couple to the glacier bed; stresses are then focused along grain alignments, such as imbricate stacks and grain lineations, which develop in response to shear, and which transmit stress to lower depths within the till (Boulton *et al*., 2001). The partitioned transmission of stress along discrete grain stacks does not occur in fine-grained deposits, where deformation is often limited to less than 0.1m (Tulaczyk *et al*., 2001), compared to a shear-zone depth in coarser tills that may be up to ten times the average clast diameter (Boulton *et al*., 2001). Pervasive deformation, rather than being the norm, may be restricted to viscous clay deposits in overridden marine and lake basins, while restricted depths of deformation impose severe limits on the continental-scale sediment flux proposed by the deforming-bed model (Boulton *et al.*, 2001; Piotrowski *et al.*, 2001).

1.4.4 Uncertainties relating to Subglacial Processes and the Deforming-bed Model - Deformation of Granular Tills by Clast Crushing

The extent to which shear stress is concentrated along grain alignments can be estimated by the degree of grain-crushing or fracturing in subglacial tills (Larsen *et al*., 2006). Laboratory tests suggest that effective stresses of between 15 and 75 MPa are required to fracture grains in unimodal sediments, which is far in excess of typical effective stresses recorded beneath contemporary glaciers (Hiemstra and van der Meer, 1997). However, in sheared granular tills, the highest inter-granular stresses are found where grains of a similar size are in direct contact along grain bridges, and stress concentrations at these contact points may be sufficient to cause grains to fracture (Hiemstra and van der Meer, 1997). Indeed, stress concentrations along clast alignments must be up to 400 times higher than the basal shear stress to allow fracturing to occur (Larsen *et al*., 2006b). Craig (1997) reported that some crushing can occur in dense sands in triaxial shear tests at normal pressures typically in excess of 500 KPa, which is well within the range of effective pressures that might be expected beneath glaciers at times of low pore-water pressure (Paterson, 1994). In addition, Craig (1997) noted that grain-crushing reduces particle interlocking and the internal angle of friction, which weakens the sediment and results in a curved Mohr-Coulomb failure envelope, which means that shear strength no longer increases linearly with effective pressure. At times of high effective pressures, grain-crushing and not sediment dilation, grain-sliding and grain-rolling may be the dominant mechanism of deformation in granular tills (Hooke and Iverson, 1995). The presence of fractured quartz grains, a by-product of grain-crushing, may be a useful criterion for identifying deformation tills in thin sections (van der Meer *et al*., 2003).

1.4.5 Uncertainties relating to Subglacial Processes and the Deforming-bed Model - The Extent of Subglacial Bed-deformation

Piotrowski *et al*. (2001) used detailed field observations to challenge the idea that bed-deformation was widespread beneath former-ice sheets, and raised a series of objections to the deforming-bed model based on detailed stratigraphical investigations into till sequences in Germany and Poland which they argued showed that:

1. supposed deformation tills often contained delicate shell material, inconsistent with the homogenisation of till at high strains, while weathering skins around highly rotten boulders showed no evidence of having been deformed. Striae were often restricted to upper surfaces of boulders, suggesting an origin through lodgement rather than deformation;
2. non-linear strain profiles, indicative of pervasive deformation and showing an increase in cumulative strain towards the ice-bed interface, with diffusive and mixed contacts between tills and underlying substrates, were seldom observed. Contacts between tills and underlying substrates were generally sharp and suggested erosion or deposition rather than deformation;
3. bedded and layered 'deformation tills', supposedly formed by the transposition of shear foliations (van der Wateren *et al*., 2000), were formed by meltout processes in subglacial cavities;
4. heterogeneous till sequences were formed by the melt out of englacial and subglacial debris, and were far more extensive than previously recognised;
5. till thickness did not usually increase towards the ice margins as might be expected with high till flux in a deforming bed; rather, tills wedged-out towards the margins;
6. englacial debris contributed more to ice-rafted debris than subglacial debris, suggesting the subglacial sediment flux was over-estimated;
7. bed-deformation, characterised by zones of diffusive mixing at the contact between homogeneous till and deformed substratum, occurred in close proximity to till resting with sharp contact on non-deformed substratum, suggesting deformation was a patchy and transient process;
8. the occurrence of numerous sand stringers, formed during phases of ice-bed decoupling, showed that basal sliding was the dominant control on glacier flow, whilst channelized subglacial drainage systems evacuated subglacial water efficiently and limited the areas of the bed where pore-water pressure were sufficiently high to induce deformation.

Furthermore, the Boulton and Hindmarsh (1987) deforming-bed model was based on only 5.5 days of field observations and 7 data points taken from beneath just 6m of ice, and was conducted at a site only 20m from the glacier margin where longitudinal stresses were likely to be significant; as such, the results may not be typical of glaciers in general (Paterson, 1994; Murray, 1997; Piotrowski *et al*., 2004). Piotrowski *et al*. (2001) concluded that, although bed-deformation did occur, it was not as widespread beneath former ice sheets as previously believed and bed-deformation processes merely recycled and smeared till across the bed wherever marine or lacustrine sediments were overridden; there was no significant addition of basal debris through subglacial erosion and transport.

Boulton *et al*. (2001) responded by arguing that delicate shell material could be protected in a dilatant till where effective pressure was low and that till thickness would attain a wave-like form during one glacial cycle and thin towards the margins. In addition, sharp sediment contacts were to be expected where failure had occurred along a distinct décollement surface, with non-deformed sediments occurring below the décollement plane. However, it is difficult to reconcile the preservation of delicate shell material with high levels of shear strain in a dilatant till layer which collapses once shearing ceases. Furthermore, décollement would limit the amount of substratum that could be cannibalised into the evolving deforming bed, and this would place limits on the potential till flux (Piotrowski *et al*., 2002). In addition, as shown in Table 1.1, basal sliding does seem to contribute more to glacier flow than bed-deformation, at least in contemporary glaciers.

1.4.6 The Ice-bed Mosaic Model

The criticisms of the deforming-bed model outlined in the previous section led to the development of the ice-bed mosaic model (Piotrowski *et al*., 2004). The key feature of the ice-bed mosaic model is that the subglacial bed is, at any one time, a mosaic of deforming and stable spots whose stability is essentially controlled by variations in effective pressure. A deforming spot may expand or contract over time. As such, strain is cumulative and time-transgressive, and the total strain a patch of sediment undergoes is the result of repeated phases of stability and deformation. The zone of deformation moves upwards through time as till accretion occurs and any given till sequence may represent multiple phases of deformation interspersed with phases of lodgement or meltout (Piotrowski *et al*., 2004). The implications of the ice-bed mosaic model are that deformation is depth-limited, generally discrete rather than pervasive, and nowhere near as widespread as previously believed. In addition, strain magnitudes are orders of magnitude lower than predicted by the deforming-bed model. Indeed, one way of validating the deforming-bed model is to measure the strain magnitude of subglacially deformed beds because the model predicts strain magnitudes in excess of 10^2 to 10^5 (Piotrowski *et al*., 2004). Unfortunately, measuring strain magnitude is extremely difficult and, although various proxy measures exist, accurately measuring strain magnitude remains a critical goal in glaciology (Piotrowski, *pers. comm*). One promising approach recently developed uses the anisotrophy of magnetic susceptibility (AMS) to map changes in shear direction and strain magnitude in subglacial tills, and initial results lend support to the ice-bed mosaic model as they suggest deformation is a patchy, transient process and strain magnitudes are well-below those required by the bed-deformation model (Iverson *et al*., 2008; Thomason and Iverson, 2009; Shumway and Iverson, 2009).

1.4.7 The Classification of Till and the Fluid-Flow Model of Massive Till Formation

One of the implications of the ice-bed mosaic model is that subglacial meltout and lodgement processes played important roles in the formation of thick Quaternary till sequences (Piotrowski *et al*., 2004; Larsen *et al*., 2007). Indeed, if the deforming-bed model is rejected, then alternative explanations for the development of extensive Quaternary till sheets consisting of homogeneous, matrix-dominated till have to be found. One possibility is what Alley (1991) termed the basal transport model, in which sediment is incorporated into the base of a glacier through shearing-in, net freeze-on, and regelation processes, and basal and englacial material is then deposited over wide areas by regelation, lodgement and meltout processes. Alley suggested that the bed-deformation model and basal transport model represent end members of the spectrum of subglacial processes that may have been in operation beneath palaeo-ice sheets.

Meltout tills may have a low preservation potential in ice-marginal locations due to the re-working of sediments by mass movement processes and water flow (Paul and Eyles, 1990). The lodgement process involves the plastering of subglacial debris across the bed as it is released from the base of a sliding glacier by mechanical means or by pressure melting (Dreimanis, 1998). Menzies and Shilts (2002) argued that the need for pressure melting places a limit on the rate at which till accretion by lodgement can occur, which maybe as little as a few $mmyr^{-1}$, and that it is difficult to envisage such a process being responsible for the development of 10-30m thick diamicton plains in which subglacial conditions must have remained uniform for considerable distances. Moreover, macroscopically massive subglacial tills show evidence of shear strain and deformation when viewed in thin section, leading van der Meer *et al*. (2003) to argue that all subglacial tills are deformation tills and should be classified as 'tectomicts', a term which reflects their structural rather than depositional origin. However, as Iverson *et al*. (2008) put it:

> *"the important question in Glaciology is not whether subglacial tills have been sheared, but by how much."*

In a major review paper concerned with the formation of till and the mechanisms of subglacial deformation, Evans *et al*. (2006) made the important point that lodgement and deformation are not mutually exclusive processes, but part of a subglacial continuum. Lodgement, deformation, flow-sliding, clast-ploughing, the freeze-on of sediment to the base of the glacier, meltout and erosion can all occur close together in space and time at the glacier bed. For example, a boulder can plough, then be lodged, then have matrix deform around it. The imprint of these processes are likely to be superimposed on evolving subglacial sediments, meaning that subglacial tills are likely to be 'hybrids' formed by multiple processes that overprint each other. It follows from this that the genetic classification of tills as 'deformation' tills or 'lodgement' tills is misleading (Evans *et al*., 2006). As such, the non-genetic term diamicton (Dm) is used in this study to describe poorly sorted glacigenic sediments, and the classification scheme devised by Evans *et al*. (2006), and extended by Benn and Evans (2010), is followed. Accordingly, subglacially sheared sediments that retain the characteristics of their parent material are termed glacitectonites, and subglacial traction tills are defined as:

> *"Sediment deposited at a glacier sole, the sediment having been released directly from the ice and/or liberated from the substrate and then disaggregated and completely or largely homogenized during transport."* (Benn and Evans, 2010).

It is important to stress that the term traction till encompasses tills that previously would have been classified as lodgement till, meltout till, or deformation till, and explicitly recognises that imprints of all these processes may be present in a hybrid traction till.

Evans *et al*. (2006) concurred with Piotrowski *et al*. (2001) in stating that the process of subglacial deformation is not in doubt, but that there are uncertainties over its timing, extent, and role. There also seems to be consensus over the pivotal role pore-water pressure plays in controlling sediment deformation. Indeed, Evans *et al*. (2006) expounded a fluid-flow model for subglacial till formation in which liquefaction, fluidisation, and hydro-fracturing are important processes. Subglacial tills are considered to consist of anatomising networks of dilatant zones enclosing domains of stiffer, non-dilatant till (these are akin to the A and B horizons identified by Boulton and Hindmarsh, 1987). Local variability in clast content and clay content, inherited from parent material, results in a variable strain response, with strain partitioned into clay-rich zones which deform more readily than stiffer, partially solidified sandy areas. The complex partitioning of deformation into discrete zones can occur at various levels within the active layer and produces a complex vertical strain profile. The active layer is the zone of maximum displacement and consists of the anatomising zones of dilatant, weak, water-saturated, 'fluid-like, A-horizons' in which clasts are free to rotate, and in which there is a partial liquefaction of fine material; consequently, a coherent matrix framework is absent. Indeed, it is the partial liquefaction of sediment that is thought to cause the homogenisation of till, and, critically, homogenisation may occur at low strains.

The mechanism of homogenisation by partial liquefaction at low strains is potentially important because, if it is true, it accords with the relatively low strain magnitudes reported for subglacial tills in recent magnetic fabric studies (Iverson *et al*., 2008; Thomason and Iverson, 2009), which are at odds with the subglacial bed-deformation model in which homogenisation is thought to occur when sediments are sheared to very high strains (Alley, 1991; Hart and Boulton, 1991a; van der Wateren *et al*., 2000; van der Meer *et al*., 2003). In the fluid-flow model, stiffer, non-dilatant 'B-horizons' are partially solidified due to lower pore-water pressure and these zones accrete over time as they de-water. Over-pressurized water can escape through complex transport pathways and results in hydro-fracturing and fluidisation of sediment. A number of recent studies have provided evidence of hydro-fracturing in subglacial sediments (Evans *et al*., 2006; Phillips and Auton, 2000; Phillips *et al*., 2007; Phillips *et al*., 2011a). According to the fluid-flow model, thick Quaternary till sequences, previously interpreted as deformation tills, are best interpreted as glacitectonites or glaciotectonites and traction tills, with the hybrid traction tills formed by multiple processes and polyphase-accretion over time (Evans *et al*., 2006; Phillips *et al*., 2011a).

Iverson *et al*. (2008) questioned the extent to which 'fluid-like' A-horizons exist, because laboratory experiments show that tills continue to behave as Coulomb plastic materials even when dilatant and under low effective pressures. Furthermore, there must be a limit to how ‘partial’ the ‘partial liquefaction’ suggested by Evans *et al*. (2006) can be, because complete liquefaction in an A-horizon would cause catastrophic glacier acceleration as effective pressure and till yield strength would effectively be at zero (Iverson *et al*., 2008). Evans *et al*. (2006) suggested that weak and variable clast fabrics recorded in many subglacial diamictons support the idea of weak dilatant zones where clasts are free to rotate under conditions of low effective pressure, and that these conditions are similar to conditions in debris flows, which produce similarly variable fabrics. But, as Iverson *et al*. (2008) pointed out, the two systems are not comparable because debris flows have greater momentum and more clast collisions than subglacial tills. As such, the most likely explanation for weak clast fabrics in subglacial diamictons is low strain magnitude, or a change in the shearing direction over time, or the partitioning of strain into discrete zones too small for the sampling procedure to detect (Iverson *et al*., 2008).

1.4.8 The Ice-keel Ploughing Hypothesis

Clark *et al*. (2003) argued that mega-scale glacier lineations (MSGL) and mega-flutes (Table 1.2) are formed subglacially in areas of fast ice stream flow by ice-keel ploughing. Ice-keel ploughing represents another potential mechanism capable of deforming soft-beds over extensive areas. The ice-keel acts as an asperity; as it ploughs, sediment flows around the keel, resulting in distributed shear in a Coulomb plastic material (Tulaczyk *et al*., 2001). A cavity forms behind the advancing keel which ploughs out a groove, and sediment is rucked-up into ridges in inter-keel areas, whose cores may preserve non-deformed sediments. The resulting topography consists of flow-parallel ridges and grooves whose spacing reflects the geometry of the glacier-base and whose grooves are erosional, not depositional, in origin (Clark *et al*., 2003).

For the groove-ploughing hypothesis to be verified, high-resolution geophysical observations over wide-areas are required to see the process in action (Clark *et al*., 2003). The groove-ploughing hypothesis provides a mechanism by which clast-poor basal ice is able to deform its bed and suggests that bridging by ice-keels may increase basal drag, helping to regulate ice stream flow and stability (Tulaczyk *et al*., 2003). Furthermore, a numerical groove-ploughing model suggests that ice stream sediment flux would be of sufficient magnitude to produce trough-mouth fans without the need to invoke a viscous till rheology, and that the sediment flux is an order of magnitude lower than that predicted by the viscous till conveyer of the deforming-bed model (Clark *et al*., 2003). The groove-ploughing hypothesis does not account for all subglacial landforms and it is uncertain to what extent the hypothesis is applicable to smaller landforms such as flutes (Benn and Evans, 2010). It is also uncertain whether ice keel asperities, which would be worn-down during groove-ploughing, would have sufficient longevity to produce MSGL (Clark *et al*., 2003).

1.4.9 Bed-deformation beneath Cold-based Glaciers and Subglacial-Permafrost Interactions

Numerical models assume that unfrozen sediments and warm-based glacier ice are essential boundary conditions for subglacial deformation and that cold-based glaciers are geomorphologically inactive (Waller *et al*., 2009). In cold-based glaciers, where ice is below the pressure melting point (PMP), basal sliding is assumed to be inhibited by a lack of lubricating meltwater and strong adhesion of ice to the bed, a situation which produces limited abrasion, although plucking may occur (Benn and Evans, 2010). However, subglacial sediment deformation has been observed beneath cold-based glaciers (Echelmeyer and Wang, 1987; Fitzsimmons *et al*., 2000; Christoffersen and Tulackzyk, 2003), and, in ice-marginal areas where glaciers override permafrost, subglacial deformation has been observed to produce thick layers of glacitectonic melange (Waller *et al*., 2009). Super-cooled water can exist in fine-grained sediments at temperatures below the PMP because high interfacial pressures locally reduce the freezing point (Waller *et al*., 2009), and because small pores inhibit ice crystal growth (Christoffersen and Tulackzyk, 2003). Waller *et al*. (2009) suggested glaciers overriding warm permafrost, that is, permafrost just below the PMP, transmit stress to considerable depths in the bed through grain bridges. In addition, the presence of super-cooled water facilitates pervasive deformation in the fine-grained matrix, while stiffer sandy sediments are more competent and resist deformation. Such a scenario was invoked to explain the presence of large intraclasts of undisturbed sand and gravel beds in Pleistocene glacitectonite sediments at West Runton, Norfolk, which seemed to ‘float’ in a pervasively deformed finer matrix. Waller *et al*. (2009) argued that the size and coherence of the intraclasts is inconsistent with formation by incremental deformation, and rejected a subglacial meltout origin for the sediment sequence on the grounds that a 30m thick debris-rich basal ice layer would be required to produce a 10m deep sediment sequence, which they suggested seems improbable.

The observation that glacier-permafrost interactions can render parts of cold-based glaciers geomorphologically active has important implications for interpreting Quaternary sediment sequences and for understanding ice-marginal processes in polythermal glaciers. The extent to which dynamic glacier-permafrost interactions are restricted to ice-marginal locations having specific thermal regimes and warm permafrost conditions is currently unknown. Christoffersen and Tulackzyck (2003) demonstrated that super-cooled water can be extracted from subglacial sediments beneath active ice streams by cryostatic suction if a steep temperature gradient exists across the ice-bed interface, leading to sediment de-watering and freeze-on and ice stream shutdown. Presumably, therefore, the model of deformation outlined by Waller *et al*. (2009) requires a temperature gradient across the ice-bed interface that impedes cryostatic suction towards the glacier and allows super-cooled water to remain in the sediment, and this requirement may place limits on the spatial extent of the process. Indeed, basal thermal conditions are thought to operate a first order control and topography a second order control on glacier flow dynamics in northern Sweden (Kleman *et al*., 2008). Relict non-glacial surfaces pre-dating the last glaciation were preserved beneath cold-based ice in the Tarfala area at higher elevations (1514 – 1296m a.s.l.) suggesting cold-based ice *was* geomorphologically inactive (Goodfellow *et al*., 2008). Meanwhile, throughout the Quaternary, zones of flow convergence in mountain ice sheets generated sufficiently deep ice to allow pressure melting to occur and for geomorphologically active warm-based ice to scour out zones of selective linear erosion, producing deep lakes, the Western Fjord zone, and glacial troughs such as the Tarfala Valley (Kleman *et al*., 2008).

1.4.10 The Role of Bed-deformation in the Formation of Fluted Moraines

The deforming-bed model has been used to explain the formation of elongate and streamlined subglacial landforms such as flutes, drumlins, and MSGL, and brief descriptions and a summary of the typical dimensions of these landforms, including the flutes of Isfallsglaciären in the Tarfala Valley, are given in Table 1.2 (Boulton, 1976; Åmark, 1980; Boulton, 1983; Menzies, 1987; Rose, 1987; Smalley and Piotrowski, 1987; Benn, 1994 and 1995; Eklund and Hart, 1996; Clark *et al*., 2003; Smith and Murray, 2009; Evans *et al*., 2010; Phillips *et al*., 2011b). Flutes are common landforms in deglaciated areas where they form groups of elongated sediment ridges which are aligned parallel to the glacier flow direction, which suggests a subglacial origin (Schoof and Clarke, 2008). Given that fluted moraines are known to occur in the Tarfala Valley, this section explores the links between subglacial bed-deformation and landform generation through a review of the literature associated with flute formation. Models of flute formation are considered under three headings:

i. forced mechanisms of flute formation which involve the deformation of sediment into basal cavities;
ii. depositional and erosional mechanisms of flute formation;
iii. instability mechanisms of flute formation.

The hypothesis that flutes are formed by subglacial meltwater erosion (Shaw and Freschauf, 1973) is not dealt with in detail here because it is rejected by most researchers (Benn and Evans, 2010) and because previous studies have shown that flute furrows in Isfallglaciären in the Tarfala Valley are straight and parallel, which rules out erosion by meltwater flow (Hoppe and Schytt, 1953; Åmark, 1980; Gordon *et al*., 1992).

Table 1.2 Definitions and Dimensions of Common Subglacial Landforms

Bedform	**Description**	**Length**	**Width**	**Elongation Ratio (length/width)**	**Other Observations**
Flutes[1]	Elongated ridges of sediment, usually diamicton but can be sand and gravel. Flute long axes parallel glacier-flow direction. Form in groups, often closely and quasi-regularly spaced. Can be long and parallel-sided, or short and tapering. Often, but not always associated with embedded boulders, projecting a minimum of 0.3 to 0.5m into basal ice	Variable typically *ca*. 100m But up to 500m to 1km	1-2m Up to 3m	2:1 up to 60:1	Height <1-2m. Generally uniform cross-section. Spacing, 0.4 to 1.5m. Clast fabrics can be herringbone pattern or flow-parallel
Isfalls-glaciären flutes[2]	Long, parallel-sided flutes and short tapering forms exist. Tapering flutes associated with angular boulders with few striae. All deeply embedded boulders have flutes. Some flutes merge	50m +	1-1.5m	50:1+	Closely spaced, 55% of flutes are spaced 1-1.5m apart, but some areas have uneven spacing. Smaller flutes superimposed on larger flutes. Flute heights typically 20-40cm
Drumlins	Streamlined hills, typically with a blunt stoss end and lee-side tail. Long axes parallel glacier flow direction. Can be hard rock cored, but more typically composed of a variety of sediments, which may or may not include deformation till. Occur in swarms, often with quasi-	Variable but typ. >100m Mean of UK forms 629m	Variable Mean of UK forms 209m	Typically 7:1 Mean of UK forms 2.9m	Variety of drumlinoid forms occur, including narrow spindles and parabolic forms

	regular morphology. May become more elongated and streamlined down-flow				
Mega-flutes	Large flutes, often with smaller flutes superimposed upon them. As they become more elongated, drumlins grade into mega-flutes or MSGLs	>100m to 1km +	Variable	Variable, but highly elongate	Rose (1989) reported a mega-flute 35m wide, and 3m high
Mega-Scale-Glacial-Lineations (MSGL)	Very large mega-flutes. Also known as giant glacial grooves, reflecting their possible erosional origin by ice-keel ploughing. Form in swarms; they may be related to fast flow in the trunk zones of palaeo-ice streams	>10km	>100m	Highly elongated 50:1 to 100:1	May be 15 - 25m high or more. Widths and depths of furrow and heights of flutes can decrease down-flow, consistent with ice-keel ploughing hypothesis (ice keel melts/is worn down in down-flow direction)

[1]Data in this table have been compiled from the dimensions stated in Rose (1989), Menzies and Shilts (2002), Stokes and Clark (2002), and Benn and Evans (2010). [2] Data concerning the Isfallsglaciären flutes are taken from Hoppe and Schytt (1953) and Åmark (1980). Note, length and elongation ratio are used to classify subglacial bedforms, although the divisions are arbitrary.

i) *Forced Mechanisms of Flute Formation*

Hoppe and Schytt (1953) and Schytt (1963) reported direct observations on the formation of two flutes in a 60m long subglacial tunnel drilled into the retreating terminus of Isfallsglaciären in 1949. Flute formation was thought to be initiated in the lee-side cavity of lodged boulders. Glacier pressure caused fine-grained water-saturated sediment to be squeezed-up from below a boulder into a cavity, where, due to a reduction in pressure, it froze to the base of the glacier. The flute formed as the frozen sediment was transported forward by glacier flow, which enabled more sediment slurry to be injected into the lee-side cavity. As such, flutes grew by the addition of sediment at their proximal ends and emerged frozen at the terminus of the glacier. Glacier ice in the tunnel was entirely cold-based, which suggested flutes were bedforms produced in the cold margins of polythermal glaciers.

Boulton (1976) also stressed the relationship between lodged boulders and flute formation, but argued that flutes were formed beneath warm-based glaciers by the ductile subglacial deformation of pre-existing water-saturated sediments. According to Boulton, the enhanced plastic deformation of glacier ice around obstacles at the glacier bed created furrows in the base of the glacier which were filled by subglacially deformed sediments, which, after deglaciation, formed flutes. Boulton argued that the furrows were flanked on either side by projecting ice-ribs, and that in the vicinity of the projecting ribs soft-sediment was subjected to vertical compression and horizontal extension, which caused the sediment to flow in - towards the furrow. Conversely, in the furrow, horizontal compression and vertical extension caused the sediment to flow upwards towards the base of the glacier. As such, subglacial deformation filled the cavity with saturated sediment which flowed more readily in response to stress than glacier ice, which prevented cavity closure, and folded the sediment into broad, open anticlines with axial planes parallel to the long axis of the emerging flute.

According to Schoof and Clarke (2008), implicit in Boulton's model is the suggestion that a lee-side furrow, or cavity, would be extended by the plug of till which somehow 'solidifies' after being injected into the cavity and forces basal ice upwards and over it. In this way, the sediment plug is able to generate its own lee-side cavity, and glacier flow and further till intrusions cause the cavity to move forward, enabling the flute to grow by the deformation of sediment into the cavity at its distal end. For Boulton, the width and height of the flute reflect the width and height of the obstruction, and oblique and transverse clast fabrics on the flanks of flutes reflect sediment flow into the cavity, whereas flow-parallel fabrics on the crest result from glacier-imposed shear stress and down-flow sediment advection. Schoof and Clarke (2008) rejected Boulton's 'forced mechanism' of flute formation on mechanical grounds; soft-sediment would simply fill the cavity and, because sediment is denser than ice, the sediment plug would not force the basal ice layers upwards. As such, no new cavity would form in the lee of the sediment plug and the initial cavity would attenuate down-flow.

Eklund and Hart (1996) provided evidence to suggest that the Isfallsglaciären flutes were formed by bed-deformation into lee-side cavities beneath warm-based ice. One trench (excavated in the proximal end of a flute near to a large embedded boulder) showed a non-linear deformation profile which Eklund and Hart argued was produced by constructional deformation and represented an upwards increase in shear strain towards the glacier bed. Figure 1.2 gives detail of the vertical profile described by Eklund and Hart and compares their model of flute formation at Isfallsglaciären with the model suggested by Hoppe and Schytt (1953). Figure 1.2 also identifies the testable predictions inherent in the Hoppe and Schytt (1953) and Eklund and Hart (1996) hypotheses, which can be used to validate these models. Eklund and Hart argued that excavational deformation occurred down-flute as a consequence of increased basal shear stress, which caused the base of the deforming layer to deepen by eroding into the sand substrate. They further suggested that clast fabric strengths increased as a function of strain magnitude and that clast fabric strength decreased with depth, was stronger on the flanks than the crest, and increased distally. Strong flute clast fabrics were associated with high strains in a pervasively deforming bed. Eklund and Hart only reported three clast fabrics themselves from Isfallsglaciären and relied on clast fabric data taken in Norwegian forefields by Benn (1994) and Rose (1989) to support these conclusions.

Benn and Evans (2010) suggested that there are two types of flutes: long parallel-sided flutes which have flow-parallel or slightly oblique clast fabrics, and shorter, tapering flutes which have herringbone fabrics. Benn (1995) argued that strong flow-parallel clast a-axis fabrics in parallel-sided flutes were formed by the cumulative extensional strain of till that was squeezed-up into ice-walled grooves, and that brittle deformation occurred along discrete failure planes. The shape of the groove constrained deformation and prevented lateral rotation of clasts, which facilitated homogeneous strain parallel to the flute axis. In this model, strong flow-parallel and elongate clast fabrics are produced because clast a-axes lie along the plane of slip, constrained by ice or stiff till, and strong preferred orientations develop parallel to the direction of shear due to drag effects (Benn, 1994). The flute grows as sediment is added to the distal end of an incipient sediment-filled subglacial cavity, and strong flow-parallel fabrics suggest sediment is sheared by overriding ice and advected down-flow (Benn, 1994;1995). By contrast, deformation is less laterally constrained in interflute areas where inhomogeneous strain produces weaker fabrics. Benn and Evans (2010) argued that pressure gradients within glacier ice are prevented from closing basal grooves filled with dilatant till because the till has a lower viscosity than the ice, and, as such, it deforms more readily and equilibrates the pressure differences within the ice, which keeps the groove open. Consequently, long parallel-sided flutes can form and their length is controlled by the flow rate of the glacier and the location of the glacier terminus. Shorter tapering flutes may be produced in stiffer, non-dilatant tills in which the viscosity contrast with glacier ice is less apparent, which allows ice flow to close the grooves. If this is true then till rheology is an important control on flute formation.

The ‘forced-mechanism’ of flute formation cannot account for the very regular spacing of flutes seen on forefields such as Aldegondabreen, Svalbard (Clark, C. *pers. comm.* 2011). In addition, care must be taken when making inferences about flute genesis based on the interpretation of clast fabrics because flutes exposed on forefields may not reflect the form of the original subglacial flute. Boulton (1976) observed that flutes in subglacial cavities often had a mushroom shape in cross-section, caused by ice ribs pinching in at the sides of the cavity, and that this shape collapsed upon deglaciation, inverting flute topography. Similarly, Hoppe and Schytt (1953) found that the subglacial flutes at Isfallsglaciären were twice the height of flutes on the forefield because they were full of frozen meltwater, and were very steep-sided. Flutes also have low survival potential and are rapidly modified by paraglacial processes such as frost heave, slope wash and solifluction (Rose, 1991), so it is incumbent upon researchers to demonstrate that clast fabrics reflect glacial and not paraglacial processes; clast fabrics taken from the top 10cm of a till or from the surface of a flute most likely reflect the latter (Rose, 1991). Unfortunately, some researchers did not specify the depth at which clast fabrics were taken, or stated that 'surface' fabrics were taken (Eklund and Hart, 1996; Benn, 1995).

ii) *Depositional and Erosional Mechanisms of Flute Formation*

Gordon *et al.* (1992), working on the fluted moraine of Lyngsdalen, Norway, argued that flutes were formed by deposition from debris-rich basal ice. Gordon *et al*. (1992) rejected Hoppe and Schytt's (1953) model because flutes were not restricted to polythermal glaciers, and because the freeze-on method advocated could not produce very long flutes as flute length would be limited by the width of the cold-ice margin. A groove-ploughing (erosional) origin for the flutes was rejected by Gordon *et al*. (2000) as they argued that the absence of till wedges and embedded boulders in furrows made flute formation by ploughing improbable. However, some Icelandic flutes have been observed to consist of outwash preserved in the lee of boulders, so an erosional origin for some flutes cannot be discounted (Fuller and Murray, 2000). According to Gordon *et al*. (1992) flutes are formed in basal ice by the streaming of basal-rich debris layers around embedded boulders, which explains why many flutes on forefields are observed to divert around large boulders. As such, flute fabrics are inherited from deformation in basal ice and flutes form when 'streams' of basal debris are deposited by meltout.

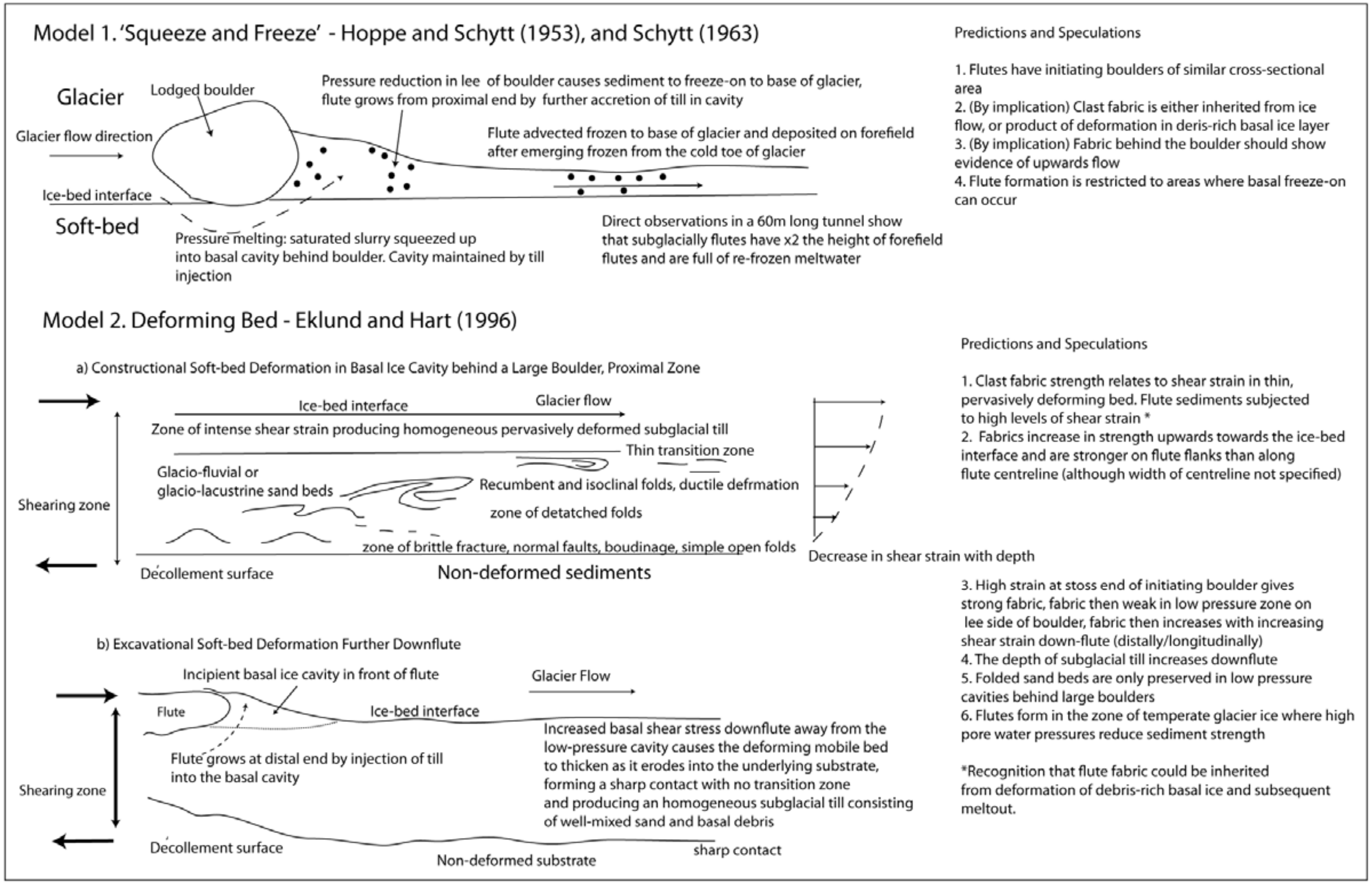

Figure 1.2 Models of Flute Formation at Isfallsglaciären

Gordon *et al*. (1992) found that short tapering flutes and long parallel-sided flutes could be formed in the same till, which suggests that mechanisms unrelated to till rheology must be sought to account for differences in flute form. In Lyngsdalen, short tapering flutes formed behind initiating boulders, whereas longer parallel-sided flutes had no obvious initiating boulder. Stokes and Clark (2002) argued that the occurrence of flow sets of MSGLs in palaeo-ice streams show that long glacial bedforms are indicative of fast-flow, so it maybe that long flutes are produced in regions of relatively fast glacier flow. Conversely, given the mechanical limits on the size of lee-side cavities suggested by Schoof and Clarke (2008), till injection into lee-side cavities may only be capable of producing short tapering flutes.

Hoppe and Schytt (1953) and Gordon *et al*. (1992) made observations on polythermal glaciers which were thinning and receding from positions reached during the recent Little Ice Age Maxima. As such, flutes may have formed by bed-deformation beneath active warm-based ice, which, in the case of Isfallsglaciären, may have covered most of the present-day forefield (Holmlund, *pers.comm*. 2011), and were subsequently frozen-on to the base of the glacier only as the glacier thinned and receded (Benn and Evans, 2010). In addition, flutes have been observed to form in Alpine glaciers which lack debris-rich basal ice (Phillips *et al*., 2011b), which indicates that not all flutes can form by the mechanism proposed by Gordon *et al*. (1992).

Detailed clast fabric studies by Benn in Slettmarkbreen, Norway (1994), and Breiðamerkurjökull, Iceland (1995), do not support a depositional origin for flutes because clast fabrics reflect strain in the sediment, rather than ice flow. Benn observed that striae on lodged boulders were generally parallel with flute long axes and indicated the glacier flow direction, but clast fabrics formed herringbone patterns with fabrics transverse and oblique to the glacier flow direction. If the depositional model was correct, then fabrics in the sediment should have corresponded to the glacier flow direction (Benn, 1994). Benn interpreted the herringbone fabrics as reflecting local stress gradients in the deforming bed, with pressure gradients directed towards low pressure lee-side cavities.

iii) *Instability Mechanisms of Flute Formation*

Some researchers have suggested that subglacial landforms form part of a subglacial bedform-continuum, which consists of a sequence of bedforms that becomes increasingly streamlined and elongated down-flow (Smalley and Piotrowski, 1987; Rose, 1987; Menzies, 1987; Lundqvist, 2004; Smith and Murray, 2009). 'Fields' of subglacial bedforms having similar dimensions may be generated by instabilities in the deforming bed (Hindmarsh, 1998; Fowler, 2000). The instability model assumes that an unstable uniform bed of deforming till, which is being sheared by a glacier, can produce a transition in bedforms from Rogen moraines, to drumlins, to flutes and mega-flutes in a way that is analogous to the way in which instabilities in fluid flow produce transitional bedforms such as anti-dunes and dunes in rivers (Fowler, 2000). Instability may be triggered by variations in topography which cause the bed to thicken at a given spot. The thickening of the bed causes an increase in normal and effective pressures which causes the deforming layer to stall and the bed to thicken further (Hindmarsh, 1998). The positive feedback mechanism thus amplifies the topographic effect and amplification favours the formation of bedforms of certain wavelengths, which accounts for the dominant wavelengths observed in subglacial bedforms and the 'quasi-regular' geometry typical of drumlin fields and fluted moraines (Fowler, 2000; Schoof and Clarke, 2008). Moreover, the instability model suggests that bed-deformation can generate flutes without the need for initiating boulders. Schoof and Clarke (2008) developed a numerical model that showed variations in normal pressure around bed obstructions triggered flow instabilities in basal ice, which in turn generated secondary corkscrew-like spiral flows capable of transporting sediment from flute troughs to crests. Such a system could explain herringbone fabrics, as was first proposed by Shaw and Freschauf (1973).

Recent geophysical evidence provides support for the subglacial bedform-continuum hypothesis. On the Antarctic continental shelf, bedforms generated beneath palaeo-ice streams become increasingly elongated down-glacier and MSGL and subglacial till are associated with the lower reaches of ice stream trunk zones (O'Cofaigh *et al*., 2002; Evans *et al*., 2004), while beneath the contemporary Rutford Ice Stream a transition from crystalline bedrock to drumlins occurs in the onset zone, and a transition from increasingly elongated drumlins to MSGL occurs in the ice stream trunk zone (King *et al*., 2007; Smith and Murray, 2009).

1.4.11 Synthesis of Flute Formation

According to Benn and Evans (2010), subglacial bed-deformation in the lee of an obstruction is the most widely accepted model of flute formation. However, the exact nature of this forced mechanism remains unclear as it is uncertain whether it occurs beneath warm-based ice or cold-based ice, involves pervasive deformation or discrete brittle shear, is the product of fast glacier flow or continuous steady flow, or whether flutes grow by sediment accretion at their distal or proximal ends. Moreover, the forced mechanism of flute formation beneath temperate ice does not account for the often-reported quasi-regular spacing of flutes, flutes without obvious initiating boulders, or the occurrence of flutes across bedrock areas (Gordon *et al*., 1992). Indeed, Gordon *et al*. (1992) suggested that flutes may be polygenetic and that formation may be a scale-dependent process as they are associated with, and often form on top of, larger subglacial bedforms such as mega-flutes and drumlins; the disparity in the size of these landforms (see Table 1.2) indicates that they may be formed by different processes (Schoof and Clarke, 2008). Observational evidence is required to validate the different models of flute formation in the Tarfala Valley and in Table 1.3 the observational evidence that could be used to support the different models of flute formation is identified.

Table 1.3 The Observational Evidence that can be used to Support Different Models of Flute Formation

	Forced Mechanism Models				**Deposition Model**	**Instability Model**
Authors	Hoppe and Schytt (1953) Cold-based ice	Boulton (1976) Warm-based ice	Benn (1994 and 1995) Warm-based ice	Eklund and Hart (1996) Warm-based ice	Gordon *et al*., (1992)	Hindmarsh (1998), Fowler (2000), Schoof and Clarke (2008)
Flute Geometry	Long, parallel-sided, quasi-regular spacing	Boulton - flute spacing depends on boulder density; higher density induces closer spacing, whilst flute width and height reflect the width and height of the initiating boulder. The axial plane of the flute is parallel to the glacier flow direction. Short tapering flutes form behind lightly embedded boulders, whereas deeper embedded boulders (≥ 0.3m) produce sediment prows and longer flutes Benn, and Eklund and Hart - long parallel-sided flutes with flute axis parallel to glacier flow direction			Long parallel-sided flutes, width increases with height, quasi-regular spacing. Short tapering flutes occur on same forefield. Flutes often superimposed, or merging, or diverging around boulders. Interflutes long and straight, so not formed by subglacial meltwater erosion	Regular spacing and consistent flute dimensions reflecting preferred wave-lengths of bed instabilities
Flute Distribution and Glacier Velocity	Form in cold margin, and can occur across bedrock areas as flutes frozen to glacier base	Form beneath warm based ice where pre-existing forefield sediments are deformed into basal cavity. Benn - long flutes represent if not fast flow, then at least a period of steady and continuous glacier flow.			Deposited from debris streams within debris-rich basal ice in polythermal glaciers and can be deposited across bedrock areas	Form wherever instability is induced in deforming bed e.g. where bed thickens due to topographic change. May be associated with larger elongated bedforms such as mega-flutes

Relationship to Boulders	Flutes are closely associated with embedded boulders, and may form near to areas of plucked bedrock which seed flute formation (Evans *et al*., (2010). Boulton - lightly embedded boulders could be removed by short-term re-advances, with removed boulders later deposited to form transverse push moraines. Large boulders can terminate flutes, with new flutes forming in cavities on their lee-sides. Sediment often piled-up against large boulders where they terminate flutes. Eklund and Hart - constructional deformation occurs in the protected lee of embedded boulders, whereas excavational deformation occurs away from the lee-side cavity due to increased basal shear stress.		Not all embedded boulders have flutes and not all flutes have embedded boulders. Short tapering flutes do have initiating boulders, whereas long flow parallel flutes do not. Sediment often piled- up against stoss end of boulders, with a gap on the lee-side, or flutes diverge around large boulders	Flute formation does not require initiating boulders. Secondary flow instabilities may be generated around boulders, with spiral-like flows transporting sediment from troughs to crest. Flutes may widen in the lee of large boulders
Flute Sediments	Re-frozen sub-glacial sediment slurry (Dm), maybe finer- grained than interflute material	Boulton - deformed pre-existing forefield sediments, so variable lithofacies. Underlying substrate typically up-domed into antiform mirroring the ground surface when seen in cross-section. Flutes sheared by overriding ice which encourages abrasion/comminution. Consequently, a silt-spike may occur in fluted sediment particle-grain size distributions. Benn - homogeneous subglacial diamicton (Dm) with planar fabric and stoss and lee/double stoss and lee boulders. Typically B-horizons. Up-doming of substrate also reported. Eklund and Hart - homogeneous Dm formed by bed deformation. Transitional or sharp contact with glacio-fluvial or glacio-lacustrine sands in lee of boulder, or sharp contact with coarser Dm elsewhere.	Homogeneous Dm with strong planar fabric. Sharp contact with older weathered Dm substrate. No up-doming of underlying substrate	Deforming bed material, typically subglacial till
Fabrics and Strain pattern *(MF = macro-fabric)*	Not specified, although may be flow-parallel a-axis MF if inherited from meltout of frozen-on sediment	Boulton – oblique and transverse MF in furrows/flanks. Strong flow parallel a-axis MF where shearing of flute crest by overriding ice. Steep clast dips on flanks and beneath crest. AMS ellipsoids reflect flow of fines inwards and upwards into cavity, caused by strong horizontal extension and vertical compression in trough and strong vertical extension and lateral compression in cavity. Complex strain patterns around boulders. Benn – strong flow parallel a-axis MF produced by steady, cumulative homogeneous strain in ice-walled furrow. High cumulative strain so MF strength should increase longitudinally. In interflute, strain is less-constrained and is inhomogeneous, producing weaker and more variable MF, with greater range of vectors and clast dips, more akin to A-horizons. MF reflect deformation in sediment with strain directed towards low pressure shadow in lee of boulders. Eklund and Hart – strong flow parallel a-axis MF in thin deforming layer. MF strength strongest on flanks, decreases with depth, and increases longitudinally away from initiating boulders.	Strong, flow-parallel a-axis MF in flute inherited from deformation in basal ice; interflute more variable with weaker MF more typical of debris flows	Not specified, although herringbone fabric might be produced by secondary spiral flows and strong flow-parallel a-axis fabrics by shearing by overriding ice
Nature of deformation	Not specified, but presumably ductile in slurry	Variable, but generally ductile | Brittle failure along discrete shear planes | Per-vasive, ductile to brittle	Not specified, but presumably brittle shear in debris-rich basal ice	Not specified, but presumably pervasive in deforming bed

1.5 Problem Formulation, Aims and Objectives

1.5.1 The Problem

The preceding discussion has demonstrated a general consensus that:

1. tills behave as Mohr-Coulomb plastic materials, at least in laboratory studies;
2. variations in effective pressure exert a major control on sediment yield strength;
3. tills deform when shear stress > shear strength;
4. bed-deformation does occur;
5. for glaciers with soft-beds, basal slip and pervasive bed-deformation exert a major control on glacier dynamics;
6. basal slip seems to be a more important process than pervasive deformation for many contemporary glaciers;
7. the thickness of the deforming bed is variable, but for many contemporary glaciers it is less than 0.5m.

However, uncertainties still surround many subglacial processes, especially those related to the nature and extent of bed-deformation and its role in tills genesis and landform generation, and there is an urgent need for further field observations with which to validate subglacial models such that realistic subglacial parameters can be incorporated into ice sheet models.

1.5.2 Statement of Aims and Objectives

The aim of this study is to understand the nature of subglacial deformation, its extent, depth, and magnitude and its role in controlling glacier dynamics and landform generation in glaciers in general, and polythermal glaciers in particular. This will be achieved by using observational evidence to characterise the nature of the subglacial environment in front of Storglaciären, Isfallsglaciären, and Kaskasatjåkkaglaciären, polythermal valley glaciers in the Swedish sub-arctic.

Specifically, the objectives are:

1. to establish the distribution and characteristics of subglacial landforms and sediments in each forefield to find out if similar subglacial processes operated in each area;
2. to determine which subglacial model, if any, best characterises the subglacial environment. To this end, it is necessary to determine the thickness of the deforming

bed and the lateral extent of recent deformation tills/subglacial traction tills, and to ascertain the nature of subglacial deformation (whether pervasive, partitioned, brittle or ductile and so on); in particular, whether subglacial tills have been deformed to the very high strain magnitudes (10^2 to 10^4) required by the deforming-bed model and the extent to which bed-deformation controls glacier dynamics;

3. to assess the polyphase nature of soft-bed deformation and to assess the extent to which periglacial and paraglacial processes have disrupted and/or overprinted the properties of subglacial sediments;
4. to establish the role of bed-deformation in flute formation and to test the different models of flute formation.

Observational evidence is required in the Tarfala Valley to validate the different subglacial models and in Table 1.4 the observational evidence that can be used to support the bed-deformation model, the ice-bed mosaic model, and the fluid-flow model is identified.

Table 1.4 The Observational Evidence that can be used to Support Three Different Subglacial Models (the Soft-bed Deformation Model, the Ice-bed Mosaic Model, and the Fluid Flow Model).

Observational Evidence	Soft-bed Deformation Model *(After Boulton and Hindmarsh, 1987; Alley, 1991; Eklund and Hart, 1996; van der Meer et al., 2003)*	Ice-bed Mosaic Model *(After Piotrowski et al., 2004)*	Fluid Flow Model *(After Evans et al., 2006)*
Depth of Deforming Bed	Potentially deep and pervasive Up to 10m +	Limited, thin, maybe as little as a few centimetres in places	Deforming bed part of hybrid traction till; depth variable, but may be limited
Extent of Deformation	Widespread. All subglacial tills are deformation tills. Deforming soft-beds can control glacier flow. Considerable till advection	Less widespread, lodged and melt-out sequences more common than previously realised. Deforming bed forms part of a patchy mosaic, with the deforming patches forming an anastomosing network (Shumway and Iverson, 2009)	Variable in time and space
Strain Magnitude	Very high 10^2-10^5	Patchy, but generally low $< 10^2$. In laboratory experiments, steady-state strain ellipsoids and fabrics are produced at moderate to high strains (7 to 30) by simple shear (Iverson *et al*., 2008).	Variable
Vertical Strain profile	Non-linear simple gradational profile typical of pervasive deformation, with strain increasing towards ice-bed interface. However, vertical variations in sediment strength, pore water pressure, and effective pressure can result in décollement plane moving upwards over time as bed accretes, which produces more complex profile	Non-linear simple gradational profile may be typical of pervasive deformation, with strain increasing towards ice-bed interface. However, bed mosaic can produce complex profile with rapid changes in fabric vectors and strength over small depth intervals. Lodgement and bed accretion can produce uniform profile	Variable but complex. Strain may be distributed uniformly within bed, with variations in strain response reflecting variations in sediment strength and dilatancy
Typical Fabrics	Macro-fabric strength decreases with depth in non-linear pervasive profile, but with uniform vector orientations. In a thin deforming bed, may get uniformly strong flow-parallel a-axis fabrics. Macro-fabrics may weaken at higher strain (Carr and Goddard, 2007) with clasts orientated transverse to flow, or may weaken in thicker deforming beds (Hart, 1994)	Fabric strength is a proxy for strain magnitude as fabric strength does not decrease at higher strain; meltout, lodgement and accretion of bed over time can produce a uniform profile with strong flow-parallel a-axis macro-fabrics. In ring shear experiments, strong flow-parallel a-axis fabrics and magnetic lineations are produced at moderate to high strains under pervasive shear, with up-glacier plunge. Fabrics do not weaken with increased strain once steady-state is achieved. Deviations from the steady state fabric/strain ellipsoid suggest low strains and variable strains over time (Iverson *et al*., 2008).	Variable, reflecting hybrid nature of traction till. Strong fabrics may be inherited from the melt-out of debris-rich basal ice. Dilatant 'fluidised' A-horizons produce variable macro-fabrics, with some weaker fabrics, akin to debris flows, and are characterised by ductile deformation. Fabrics will be stronger in B horizons where discrete brittle shear dominates.
Nature of Diamicton and Deformation at macro-scale	Homogenised subglacial till produced at high strain. In non-linear pervasive profile, this may gradate into tectonised layers and then non-	There are no diagnostic criteria for deformation tills. Lodgement tills can also be homogeneous and have strong planar fabrics. Non-linear	Subglacial tills originate through a variety of processes which operate in close

	deformed sediments beneath a décollement plane at depth. Till may contain intraclasts and rafts/wedges of substrate. At the macro-scale, evidence of brittle deformation occurs lower in the profile e.g. faulting, with evidence of increasingly ductile flow at higher strains towards the ice-bed contact e.g. sheath folds, overturned folds etc. Homogenised till consists of admixture of local and far-travelled material, with strong planar fabric common; the planar fabric represents shear planes which may be visible at the micro-scale. Clasts in deformation tills are typically sub-round to sub-angular, with blocky shapes indicative of subglacial transport. Calcite precipitate may also occur in the lee of fractures on boulder surfaces, and stoss and lee forms are common. Subglacial tills typically have pseudo-fractal patterns with slopes of approx -2.9 (Hooke and Iverson, 1995)	deformation profiles may be seen at the macro-scale, but these will be spatially variable and limited in extent. Deformation is typically partitioned into thin layers. Subglacial deformation profiles are characterised by a homogeneous appearance. Heterogeneous sequences are more typically of till accretion over time through meltout, lodgement, and deformation processes. Sand stringers within homogeneous till represent phases of ice-bed separation. Sand drapes over boulders, striae concentrated on upper boulder surfaces, the preservation of delicate material, and the presence of non-deformed weathering haloes within homogeneous till suggest a lodgement/meltout origin rather than deformation origin. Striae and wear marks all over clasts are more indicative of deforming beds. Stoss and lee boulders are indicative of lodgement; double stoss of lee boulders of ploughing followed by lodgement	space and time at the glacier bed, e.g. meltout, lodgement, ploughing, deformation, and erosion, and so subglacial tills are hybrids, whose character reflects over-printing by multiple processes. At the ice-bed contact, tills are likely to be in a dilatant state and deforming in a ductile 'fluidized' layer. Stiffer B horizons may deform in a more brittle manner. The escape of over-pressurized water will produce numerous water escape structures
Nature of Diamicton and Deformation at the Micro-scale	A range of S-matrix and Plasma fabrics and structures may be present such as rotational structures, till pebbles, water-escape structures, crushed grains, necking structures, kinking fabrics, unistrial and skelsepic plasma fabrics and crenulations foliations etc, depending on the exact nature of deformation e.g. brittle, ductile, compressional, extensional etc.	There are no diagnostic micro-structures and micro-fabrics for deformation tills. Discrete shear planes, represented by grain lineations and stacks become longer and lower in angle at higher strains, and the IL-index suggests strain magnitudes in deformation tills are low (Larsen *et al*., 2006a). Lodged clasts may have a sediment prow ahead of them with sand micro-fabrics draped over the top of the clast (Thomason and Iverson, 2006)	The polyphase history of sediment deformation may be discerned through the micro-structural mapping of micro-fabrics. Micro-fabrics may be seen to wrap around larger rigid clasts in a pervasively deforming bed where strain is preferentially partitioned into softer and more easily deformed matrix (Phillips *et al*., 2011b)
Nature of Contact between Homogeneous Diamicton and Substrate	Diffuse/mixed in thin transition zone, or sharp if the contact represents a plane of décollement produced by a change in lithofacies, or an increase in effective pressure beyond the critical point required for sediment failure	Deforming beds should be characterised by diffusive mixing at the contact between the till and underlying substrate. Sharp contacts are more indicative of erosion or deposition processes	Variable

Chapter 2 Study Area and Methods

2.1 Introduction to the Study Area

2.1.1 Location

The Tarfala valley is a NW-SE trending glacial trough with a drainage basin area of 20.6 km^2 located on the eastern side of the Kebnekaise Massif in northern Sweden (Holmlund and Jansson, 2002; Figs. 2.1 and 2.2). The trough floor has a minimum elevation of 800m above sea level (m a.s.l.) while peaks attain a maximum elevation of 2114m a.s.l. on Kebnekaise, Sweden's highest mountain. The Tarfalajåkk (Tarfala river) now occupies the trough floor and flows south-east from the Tarfalajaure Lake which is situated at the head of the valley. A number of small cirque glaciers occur at higher elevations above 1400m a.s.l. in the Tarfala area and 3 valley glaciers, of which Storglaciären is the largest, descend to minimum elevations of approximately 1200m a.s.l. on the western flank of the trough. Stockholm University's Tarfala Research Station (67° 55'N, 18° 35E) is the research base for this study as is located just to the south-east of Tarfalajaure at an elevation of 1135m a.s.l.

2.1.2 Climate

The Tarfala Valley has a sub-arctic climate with a mean annual temperature of -3.9°C, a summer average of 5.5°C (daily maxima between 10 and 15°C), and a winter average of -8.9°C (daily minima between -10°C and -20°C) (Grudd and Schneider, 1996). Typical annual precipitation totals are 950mm yr^{-1}, with about one third of this falling as summer rain (Hock *et al*., 1996). The Tarfala Valley comes under the influence of both Arctic and Polar Maritime air masses and cyclonic activity can bring intense storms into the region with precipitation intensities up to 80mmh^{-1} and wind speeds up to 81ms^{-1}, in extreme cases (Holmlund and Jansson, 2002). Net radiation dominates the energy budget of Tarfala's glaciers and provides 66% of the energy available for melt (Hock *et al*., 1996). Glaciers have receded rapidly (between 0.5 and 1km) from their Little Ice Age Maxima positions, which were attained in 1910 (Karlén, 1973). Holmlund *et al*. (1996a) showed that glacier net balance is strongly correlated to the average summer temperature, and that glacier retreat was the result of a 1°C rise in the mean summer temperature which occurred at the beginning of the 20th Century.

Figure 2.1 Location of the Tarfala Valley. The black circle on the inset map shows the location of the Tarfala Valley in northern Sweden above the Arctic Circle and close to the Norwegian border.

2.1.3 Glacier Dimensions, Mass Balance, and Site Selection

Mass balance observations have been made on Storglaciären since 1946 and represent the longest continuous mass balance record in the world (Holmlund and Jansson, 2002). Storglaciären has been the subject of intense research activity, which has focused on the relations between glacier flow dynamics, hydrology, and subglacial processes. By contrast, relatively little research in the Tarfala area has focused on other glaciers or their forefields. Indeed, despite much being known about Storglaciären's contemporary dynamics, relatively little research has been conducted on the forefield sediments and landforms, so it makes sense to select Storglaciären's forefield as one of the sites for this study. The dimensions and recent mass balance of the main glaciers in the Tarfala area are given in Table 2.1.

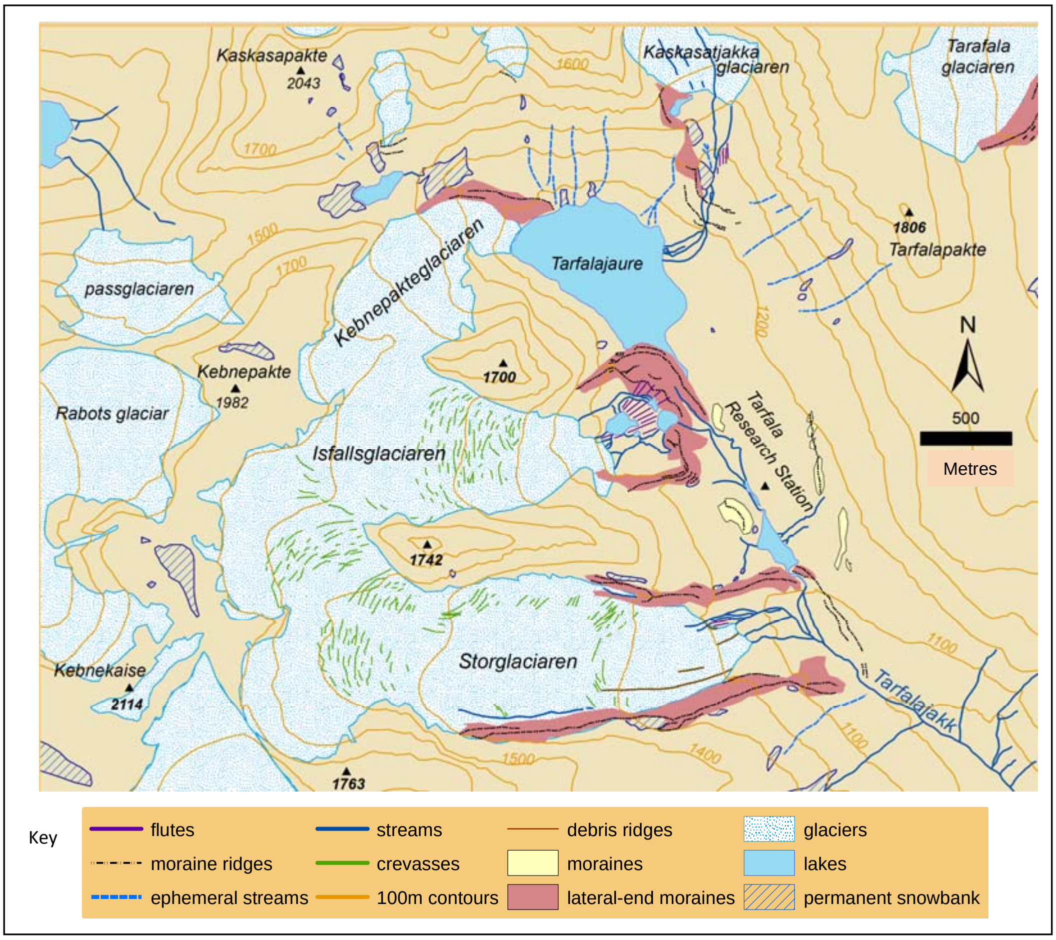

Figure 2.2 Outline geomorphological map of the Tarfala Valley. The black trainagles denote major peaks (figures in metres) and the moraine ridges are distinct ridges within the large lateral-end moraine complexes.

Tarfala's glaciers are generally small and polythermal in structure, with the ratio of temperate to cold-based ice varying as a function of glacier thickness and the speed with which cold layers are transferred through the glacier system (Holmlund and Eriksson, 1989). Tarfalaglaciären consists entirely of cold-based ice whereas Kaskasatjåkkaglaciären consists of mostly temperate ice (Holmlund and Jansson, 2002). Evidence for the thermal structure of Tarfala's glaciers comes from repeated ice-radar surveys, and for Storglaciären, these have shown a decrease in the proportion of cold-based ice over the last twenty years (Holmlund and Eriksson, 1989; Pettersson *et al*., 2003; Gusmeroli *et al*., 2010; 2012). About 85% of Storglaciären is temperate ice, with cold-based ice occurring at the glacier surface and margins in the ablation zone, where it extends to a depth of approximately 30m (Holmlund *et al*., 1996a). Climate is the dominant control cold-layer thickness (Gusmeroli *et al*., 2012). In the accumulation area, the re-freezing of spring meltwater releases latent-heat which advects warm ice into the glacier and keeps it temperate (Pettersson *et al*., 2003). In the ablation area, much of the meltwater rapidly runs-off the surface without penetrating the glacier and the glacier is frozen to its bed at the thin lateral margins (Pettersson *et al*., 2003). Gusmeroli et al. (2012) showed that the volume of the cold surface-layer was reduced by about one third between 1989 and 2009 (at an average rate of 0.8 +/- 0.24ma^{-1}), and they argued this thinning was caused by recent climatic warming in subarctic Scandinavia (for example, temperature records from the weather station at the Tarfala Research Station showed that the average winter temperature had increased by 1°C since the mid-1980's). Consequently, Storglaciären had become an almost entirely temperate glacier (Gusmeroli *et al*., 2012). Isfallsglaciären is thought to have a similar ratio and distribution of cold-based ice to temperate ice as Storglaciären (Holmlund, *pers.comm*. 2012).

Table 2.1The Dimensions and Mass Balance of Glaciers in the Tarfala Area

1996 Data[1]	***Area km^2***	***Volume $10^6 m^3$***	***Max. depth m***	***Mean depth m***	***Max. altitude m***	***Min. altitude m***
Storglaciären	3.12	306	250	99	1720	**1130**
Isfallsglaciären	1.32	93	220	72	1750	**1185**
Tarfalaglaciären	0.86	16	51	19	1790	**1390**
Bjorlings	1.47	139	225	94	2010	**1410**
Rabots	4.10	346	175	84	1940	**1060**
2001 data[1] Storglaciären	3.1	300	255	95	***Retreat since 1910***:550m	***Average annual velocity at equilibrium line***: **30m/yr**
2007/8 Data[2]	***Area km^2***	***Mass Balance mm water equivalent***	***Max. length m***	***Snowline elevation m a.s.l.***	***Max. altitude m***	***Min. altitude m***
Storglaciären	3.06	+580	3.7	1420	1828	**1125**
Isfallsglaciären	1.4	-----	2.1	1460	1750	**1175**
Tarfalaglaciären	0.9	-200	1.0	-----	1760	**1400**
Bjorlings	1.39	-----	2.1	1560	1790	**1420**
Rabots	4.22	+350	4.1	1360	1960	**1080**
So Kaskasatjåkka-glaciären	0.6	-----	1.4	1500	1720	**1340**
2009/10 Data[3]	***Mass Balance 2009 mm w.e.***	***Mass Balance 2010 mm w.e.***	***ELA m a.s.l. 2009***	***ELA_0***	***AAR 2009***	***AAR_0***
Storglaciären	-590	-690	1495	1463	37	**45**
Tarfalaglaciären	-1710	--------	1790	-------	0	**--------**

These data are taken from: [1] Holmlund *et al*., (1996a); [2]&[3] Mass Balance data, Equilibrium line data (ELA), and Ablation Area Ratios (AAR) from: *The World Glacier Monitoring Service* (2007/8 and 2009/10); all other data from: *The World Glacier Inventory* (2012). Storglaciären has continued to reduce in area in recent decades, whereas the location of the snout has remained fairly static in response to some positive mass balance years between 1996 and 2008. However, since then, Storglaciären's mass balance, like most glaciers in the Tarfala area, has been negative and the equilibrium line altitude (ELA) has increased in elevation beyond ELA_0, that is, the ELA elevation at which the glacier would attain a balanced state between annual accumulation and ablation.

Isfallsglaciären and Storglaciären (Fig. 2.3) face east, share similar bedrock geology and topography, and flow west to east. Storglaciären is 1.5km longer and covers just over twice the area of Isfallsglaciären, although their snowline altitudes are similar (see Table 2.1). The World Glacier Inventory (2012) classifies Storglaciären as a valley glacier with compound form (meaning it has more than one accumulation basin), with an even to slightly stepped longitudinal profile with a major overdeepening formed behind a bedrock riegel in the upper ablation area. Sporadic permafrost exists beneath the lower ablation area (Holmlund and Jansson, 2002).

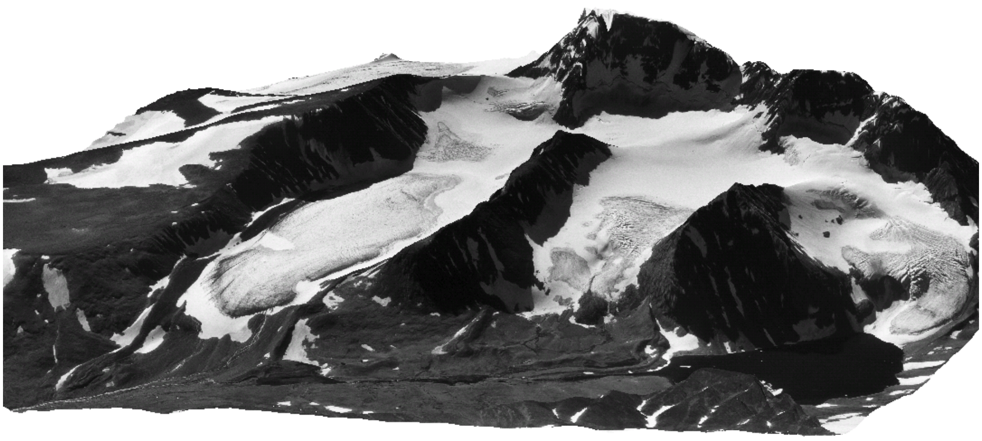

Figure 2.3 A View SW towards Kebnekaise showing the Storglaciären and Isfallsglaciären Forefields. Storglaciären is on the left and the northern stream (Nordjåkk) and the southern stream (Sydjäkk) are seen dissecting the central diamicton plain. Storglaciären and Isfallsglaciären are separated by the sharp ridge Södra Klippberget. The ice-cored lateral-frontal moraines in both forefields are clearly seen. This image was produced by combining a Lantmäteriet 2001 aerial image of Kebnekaise with a digital elevation model of the Tarfala Valley (produced by Stockholm University) in ArcGIS.

Isfallsglaciären is also classified as a valley glacier, but has a simple form (one accumulation basin) and a longitudinal profile dominated by an ice fall, which occurs across a 70m high rock bar which extends to an elevation of 1420m. In Storglaciären's forefield, Nordjåkk and Sydjåkk are eroding the central diamicton plain and the terminus position of the Little Ice Age advance is marked by a distinct line of boulder gravel (Etienne *et al*., 2003). By contrast, prominent fluted moraines and a number of lakes dominate the Isfallsglaciären forefield. The Isfallsglaciären forefield was selected for study because of the excellent exposure of fluted moraines.

Kaskasatjåkkaglaciären has a south-east facing aspect and Kaskasatjåkka (the forefield) a south facing aspect. Kaskasatjåkkaglaciären is classified as a mountain cirque glacier with an even longitudinal profile (World Glacier Inventory, 2012). The Lantmäteriet Kebnekaise 1:20 000 map shows that the terminus has receded over 800m from its 1910 Little Ice Age Maximum position to an elevation which is approximately 200m higher than the termini of Isfallsglaciären and Storglaciären. The forefield is relatively narrow and very steep in its upper section, where a diamicton sheet (so-named to distinguish it from the diamicton plain of Storglaciären) is deeply dissected by streams forming narrow, 2-3m deep, steep-sided gullies. Fluted moraine and lakes occur, and two large permanent snow banks exist on the western side of the forefield. The snow banks are cored by remnants of glacier ice (Holmlund, *pers.comm*.2011). Kaskasatjåkka was selected for study because it provides a valuable contrast to Isfallsglaciären and Storglaciären in terms of glacier thermal structure, glacier type, aspect, and forefield geomorphology.

It should be noted that, unlike many polythermal glaciers in Svalbard, none of the Tarfala glaciers have been observed to produce major surges, although flow accelerations or 'mini-surges' may be caused by the transit of kinematic waves on Storglaciären (Jansson, *pers.comm*. 2011).

2.1.4 Bedrock Geology and Superficial Deposits

The following summary is based on the analysis of the bedrock geology of the Tarfala Area given by Anderson and Gee (1989; Fig. 2.4). Geologically, the Tarfala Valley consists of hard, crystalline mafic rocks belonging to the Seve Nappe Complex of the Scandinavian Caledonides. The nappes dip 20-40° to the northwest and are composed of three main tectonic units, these being the Tarfala amphibolite, the Storglaciären gneiss, and the Kebne dyke complex. The Kebne dyke complex consists of sheeted dykes of mafic dolerite intruding sub-ordinate meta-sediments, mostly hornfelses. Resistant dolerite dykes form the high rugged relief of the Kebnekaise Mountains and the Kebne dyke complex underlies the accumulation areas and upper ablation areas of Storglaciären and Isfallsglaciären and the whole of the Kaskasatjåkka forefield. The Storglaciären gneiss crops out below the Kebne dyke complex and consists of a narrow band of garnet-rich mylonitic augen gneiss. The gneiss probably represents the deformed base of an overlying nappe. The hard mylonitic gneiss resisted glacial erosion and forms distinct morphological breaks in the Tarfala Valley, forming riegels in Isfallsglaciären and Storglaciären and sharp scarp slopes on Norra and Södra Kilppberget. The foliated Tarfala amphobolite crops out below the Storglaciären Gneiss and contains green epidote and sparse garnets.

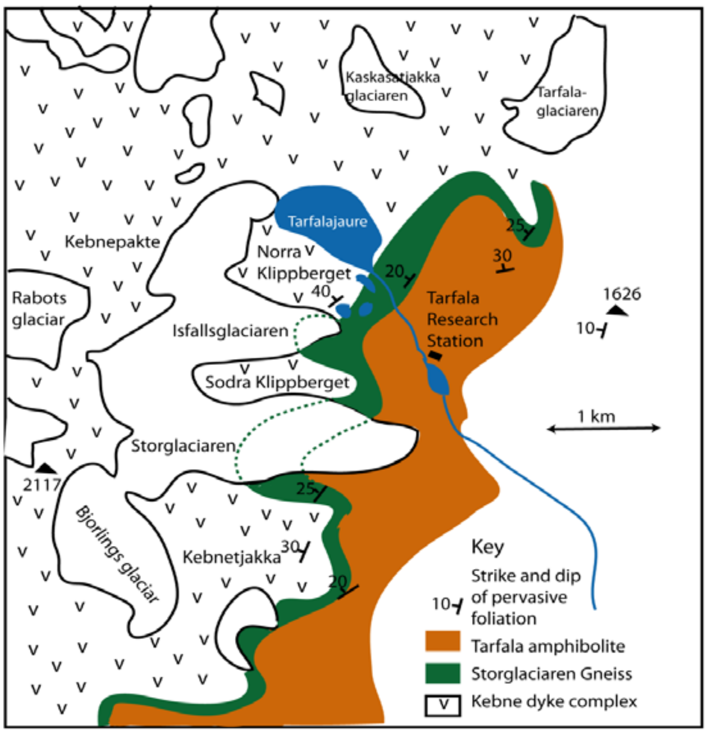

Figure 2.4 Simplified geology map of the Tarfala Valley based on Anderson and Gee (1989). The dashed lines project the boundaries of the Storglaciären mylonitic gneiss beneath Storglaciären and Isfallsglaciären and are speculative. The mylonite forms a resistant rock bar that is responsible for creating riegels in the longitudinal profiles of both glaciers. Projections of the bedrock across forefields presently covered by superficial deposits are also speculative.

Bronge (1996) estimated that it would have taken 300 000 years for a temperate glacier to excavate the Tarfala trough, and that 1.36km^3 of hard crystalline rock was removed. Plucked and polished and striated bedrock is exposed on eroded scarps at the margins of Isfallsglaciären and Kaskasatjåkkaglaciären and in roches moutonnées and eroded sections in the Storglaciären and Kaskasatjåkka forefields. However, most of the valley floor and forefields have superficial sediment cover. Tills, especially subglacial meltout and ablation tills, are known to dominate the superficial cover of Quaternary deposits in Sweden and tills cover 95% of the country (Lundqvist, 1983).

Etienne *et al*. (2003) produced the first description of the lithofacies–landform associations in the Storglaciären forefield and their work is summarised in Table 2.2. They estimated that a subglacial deformation till was the second most important deposit volumetrically, with a sandy gravel of glacio-fluvial origin the most important. According to Etienne *et al*. the central diamicton plain consists almost entirely of deformation till which formed during the Little Ice Age advance; Table 2.3 summarises their interpretation of the sequence of events that have shaped the Storglaciären forefield. However, Etienne *et al*. did not recognise the two-till sequence identified in the upper till plain by Baker and Hooyer (1996) and, as such, their volumetric estimates should be treated with caution. Baker and Hooyer's section is summarised in Figure 2.5 and shows a lower coarser till, highly weathered and containing angular clasts, in sharp contact with a thin layer of finer-grained, olive grey till which contains more sub-rounded to sub-angular clasts and which corresponds to subglacial deformation till identified by Etienne *et al*. (2003). The upper till was observed to extend beneath the contemporary glacier, which led Baker and Hooyer to conclude it was formed within the last 400 years during the Little Ice Age advance. They suggested that the Storglaciären sequence resembled a similar two-till sequence observed at nearby Passglaciären where organic material, found on a weathering surface that marked the boundary between the two tills, had been dated at ^{14}C 3260 +/- 80 yrs B.P. Baker and Hooyer speculated that the lower till in Storglaciären was possibly oxidised during an early Holocene warm period or was of Late Weichselian age. They suggested two possible reasons for the contrast in till properties:

(i) it was related to a change in basal thermal conditions, with the lower till deposited beneath cold-based ice where limited comminution occurred, whereas the finer-grained till related to abrasion beneath warm-based ice;

(ii) a lake formed in the main overdeepening during earlier glacier retreat and, subsequently, overridden glacio-lacustrine sediments sourced the formation of the finer-grained upper till during the LIA advance.

Table 2.2 Lithofacies – Landform associations at Storglaciären identified by Etienne *et al*. (2003)

Lithofacies Name and Code	*Matrix Particle grain Size Distribution (pgsd) % sand/silt/ clay*	*Key Characteristics: A = angular Clasts SA = Sub angular SR = Sub round R = Round Amp = amphibolite; Dol = dolerite, Gn = gneiss*	*Fractal Slope and R^2 Value*	*Interpretation*	*Lithofacies- Landform Associations*
Massive Diamicton Dm	61/32/7 Polymodal Peak 3.5φ	Mostly SA/SR, although one sample up to 25% A. Dark to light grey, loosely compact sand-silt matrix. Clasts of amp, dol, gn, gravel to boulder size. Chattermarks/striae on boulders, one nailhead striation. Calcite precipitate in lee of crescentric gouges. Well-developed pervasive planar fabric gives marked fissile weathering characteristic	-2.91 0.9931 Good fit	Subglacial deformation till: subglacial transport indicated by striae/chattermarks/ calcite precipitate (solute fallout from subglacial water films).Polymodal psd indicates active transport. Planar fabric produced by shears in actively deforming bed and fractal slope also indicates deformed basal till sheet	Zone 1 N Lateral Moraine: 20m high, 1km long, Ice-cored, 1-2m thick debris. Litho-facies: SG, minor ZGm/Dm
Sandy Gravel SG	70% gravel 28% sand, 1.8% silt, 0.2% clay	Boulder to granule size gravel, amp, dol, gn. SA/SR, more R/SR compared to dm.	-2.16 0.985 Poor fit	Similar deposits in banks and bed of contemporary glacio-fluvial rivers and palaeo-channels. Glacio-fluvial deposits	Zone 2 Moraine Mound Complex: <0.5->2m high elonogate mounds, N side of forefield. Sm, subordinate SG, ZGm, Dm
Silty Gravel ZGm	60% gravel 70% sand 27% silt 3% clay	Granules to cobbles, boulders rare; massive. Grades laterally to SG/DM. Slightly depleted in fines compared to dm.	-2.82 0.9941 Near linear	Deformed dm partially re-worked by glacio-fluvial activity. Winnowing of fines.	Zone 3 S Lateral Moraine: 25-30m high, 200m wide, 1km long. Boulder gravel in distal part, isolated Dm
Massive Sand Sm	94.4/5.5/0.1 Well sorted Medium to fine sand	Thinly inter-bedded (<4cm) with litho-facies Zs in glacio-lacustrine unit. Lacks internal structure.	-2.65 0.8617 Poor fit	Glacio-fluvial deposit in low discharge marginal streams and lining of channel bar tops. Re-worked in moraines	Zone 4 Active Glacio-fluvial Modified terrain, mostly braided rivers. SG dominant, minor Zs, Sm, Dm
Silty Sand Zs	67/31/2	Thin veneers on gravel bars and in backwaters and silting ponds or in lee of large boulders; typically overlies Sm in 1cm thick layers, or inter-laminated with Sm in backwaters	-2.95 0.9424 Curvi-linear	Vertical fining upwards sequence in modern day bar tops: SG – Sm – Zs so glacio-fluvial and glacio-lacustrine deposits. High fractal slope value indicative of abrasion and fracture, suggests Zs may be re-worked basal material	Zone 5 Diamicton Plain, 3 wide elongated ridges, asymmetric, trend WSW – ENE, up to 8m high, 400m long: Almost exclusively Dm incised by meltwater streams.
Boulder Gravel BG		SA-SR Boulders		Supra-glacial and subglacial origin to boulders	Form outer and inner terminal moraine lines

Columns 1-5 relate to lithofacies and should be read from left to right. Column 6 details the lithofacies-landform associations and should be read vertically. Two further landforms were described that are not listed in the table, these being zone 6: abandoned glacio-fluvial terrain dominated by SG with isolated Dm in palaeo-channels, and zone 7: a proglacial lake association in an ice stagnation hollow dominated by Sm, with thinly bedded (cm scale) fining upward sequences to Zs. The boundaries between lithofacies are not sharp but merge laterally. SG is the most important sediment volumetrically, followed by Dm and then BG, which is a similar distribution to that found in proglacial areas of other polythermal glaciers in the High Arctic (Etienne *et al*., 2003).

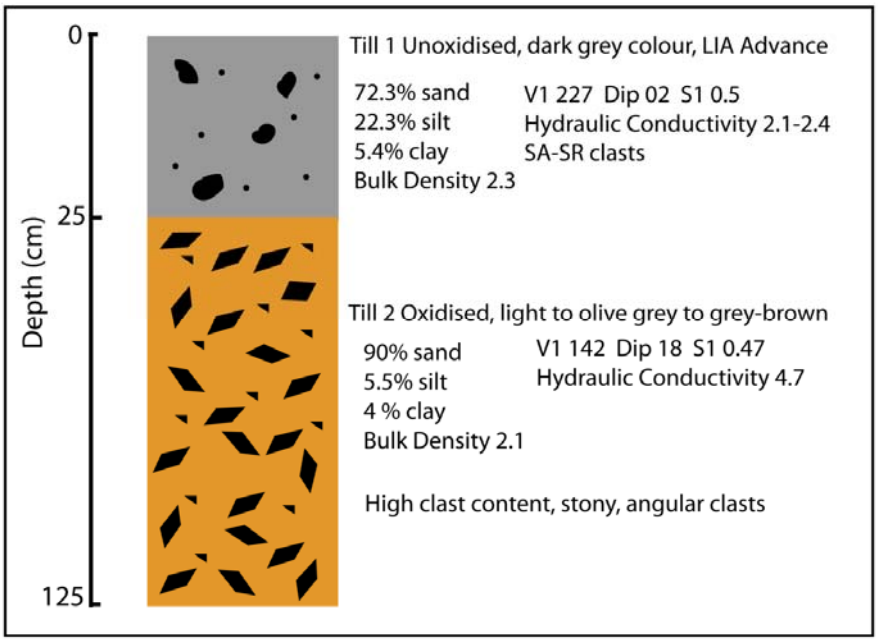

Figure 2.5 Section of Upper Till Plain, Storglaciären, based on Baker and Hooyer (1995). Baker and Hooyer excavated 3 pits of 1.8m depth and one 9m long trench to 4m depth in the central part of the upper till plain, near to the glacier terminus. The section shown represents a summary of their findings. The percentage sand, silt and clay refers to the till matrix. Bulk density is in gcm^{-3}. V_1 is the mean vector, and dip, in degrees, is the mean dip of 50 clasts; S_1 is the eigenvalue. Hydraulic conductivity was measured in a laboratory using a falling head permeameter and the units are x10^{-7}ms^{-1} for till 1 and x10^{-6}ms^{-1} for till 2. Till 2 therefore has an order of magnitude higher permeability than till 1, which reflects its sandy matrix and high clast content. Both tills have weakly clustered fabrics, with V_1 values 85° apart. Baker and Hooyer argued till composition and texture should remain fairly uniform between separate glacier advances in the same valley, and that the differences shown between the two tills represented either a switch in basal thermal conditions, or the cannibalisation of glacio-lacustrine sediments (see main text).

2.1.5 The Quaternary and Holocene Chronology of the Tarfala Valley

Little is known about the earlier glacial history of the Tarfala area as very few detailed multi-proxy stratigraphic studies or high-resolution dating studies have been performed (Rosqvist *et al*., 2004). It is probable that the mountains of northern Sweden acted as ice accumulation centres for mountain ice sheets and the Scandinavian Ice Sheet (SIS) throughout the Quaternary Period (Lundqvist, 2004). A summary table detailing what is known about the Quaternary history of northern Sweden is given in appendix 2. Basal thermal conditions and topography are thought to have exerted first and second order controls on glacier flow dynamics in northern Sweden, with cold-based glacial ice protecting relict non-glacial landscapes at higher elevations, while flow convergence produced thicker warm-based ice capable of scouring out glacial troughs (Kleman *et al*., 2008). Thick deposits of till and relict moraines on the eastern foothills of the northern Swedish mountains suggest that mountain ice sheets were dominant throughout the Early to Mid Quaternary, and that the last Fenno-Scandinavian Ice Sheet was probably cold-based over much of its area as it was incapable of eroding these features (Kleman *et al*., 2008).

Table 2.3 The Sequence of Events Responsible for the Lithofacies-Landform Associations at Storglaciären as Interpreted by Etienne *et al*., (2003).Note: the dates are based on the work of Karlén (1973) and Rosqvist *et al*., (2004).

	Late Holocene Sequence of Events at Storglaciären
7	Ice stagnation and formation of kettle hole on S side of forefield.
6	Recession, 1915 onwards. Drainage switches to W to East. Ice-marginal streams Sydjåkk and Nordjåkk erode till plain and become more central in location. Forefield terrain modified by glacio-fluvial activity. Sandy gravels incise Dm.
5	Deposition of inner block moraine at terminus marks LIA Maxima position.
4	LIA advance overtops N lateral moraine (historical photographic evidence from 1910).
3	LIA Advance (begins 1500 A.D.). Widespread actively deforming bed beneath temperate ice forms till plain consisting of thick deposits of homogeneous Dm; similar cold to warm-based ice ratio as today. Over centennial time scales, pervasive soft-bed deformation is important control on glacier dynamics.
2	Glacier recession, punctuated by ice-marginal fluctuations.
1	Holocene development of Ice-cored lateral moraines and deposition of outer block moraine at 2500 cal. yrs B.P. Ice-marginal meltwater drains N to S. Date, timing, and extent of earlier Holocene advances poorly constrained, but Neo-Glaciation possibly begins 6000 cal. yrs B.P.

With the exception of the Mid to Late-Holocene, the timing, extent and dynamic controls on previous glacier advances in the Tarfala Valley are poorly constrained (Karlén, 1973; Rosqvist *et al*., 2004; Lundqvist, 2004). Karlén (1973) conducted a multi-proxy study of 28 glacial forelands in the Kebnekaise Mountains from which he developed a Holocene glacial chronology. Karlén argued that moraine-mound complexes, composed of imbricate stacks of "*undifferentiated drift*", were the product of multiple glacier advances and represented a palimpsest landscape (Kleman, 1992). Later glacial advances were blocked by these large, ice-cored moraines, and so stacked 'drift' against their proximal slopes as the moraines grew by proximal enlargement. Karlén (1973) was able to recognise separate glacial advances from cross-cutting sedimentary relationships within the moraine mounds and he dated each advance using lichenometry. Four main Holocene advances were identified at: 8500, 5000, and 2700-2400 calendar years before present (cal. yrs B.P.), and at 1500 A.D., with frequent oscillations of glacier termini occurring throughout the Holocene. Karlén (1973) argued that the most extensive glacier advances were of roughly equal magnitude and occurred at 2700-2400 cal.yrs B.P., when the outer moraines of each forefield were formed, and during the most recent Little Ice Age Advance. Karlen (1973) dated the outer terminal moraine of Storglaciären at 2500 cal. yrs B.P.

Lichenometry data should be treated cautiously because lichen growth curves in northern Sweden are not well calibrated beyond 2700 cal. yrs B.P. because of the lack of datable organic material (Rosqvist *et al*., 2004). In addition, lichen-rich boulders can be incorporated into moraine-mound complexes by push-deformation processes (Shakesby *et al*., 2004), or transported to, and re-deposited on moraines in slush flows (Rapp, 1960). As such, lichen sizes may not indicate the date of moraine formation. In addition, late-lying snow can kill-off lichen and lichen will not grow beneath semi-permanent snow banks. Therefore, lichen sizes on moraine boulders may indicate the date at which the boulder surface became free of a semi-permanent snow cover, rather than the age of the moraine (Shakesby *et al*., 2004). Moreover, oxygen isotope analysis of diatom frustules from freshwater lake cores in the Abisko area of northern Sweden do not support Karlén's interpretation of Early-Holocene advances, and put the onset of Neo-glaciation at 6000 cal.yrs B.P., with an estimated mean annual temperature decline from the Early-Holocene warm phase of between 2 and 4° C (Rosqvist *et al*., 2004). As such, the age of moraines that pre-date the Neoglaciation remain poorly constrained. The analysis of isotopic signatures preserved in diatoms taken from the Abisko lake cores suggests that an increasing frequency of arctic air mass flows may have initiated the Neoglacial advance (Rosqvist *et al*., 2004).

2.2 Methods: the Need for a Multi-disciplinary Approach

A combination of data at the forefield scale, outcrop scale, and micro-scale are needed to meet the aims and objectives of this study, that is, a landsystems approach is required (Evans, 2003). At the outcrop scale, the systematic description of glacigenic sediments is required to identify lithofacies, to record structural evidence of sediment deformation, to ground-truth radar surveys, and to map lithofacies-landform associations. However, the identification and classification of glacigenic sediments is rendered problematic by issues of equifinality, till hybridization, and polygenesis and, as such, the interpretation of glacigenic sediments requires multiple lines of evidence and the use of a multi-disciplinary approach (Piotrowski *et al*., 2004; Evans *et al*., 2006; Larsen *et al*., 2006; Piotrowski *et al*., 2006, Evans *et al*., 2010; Phillips *et al*., 2011b). Furthermore, subglacial diamictons that appear massive and homogeneous at the outcrop scale may record evidence of deformation at the micro-scale (van der Meer, 1993; Carr, 2001; van der Meer *et al*., 2003), and the chronology of deformation may be revealed through micro-structural mapping and the analysis of two-dimensional clast micro-fabrics (Phillips *et al*., 2011b). As such, it is necessary to integrate observations at the outcrop scale with observations at the micro-scale in order to elucidate the polyphase nature of subglacial deformation (Hiemstra *et al*., 2005). Consequently, in this study, a range of field and laboratory techniques are used at the outcrop and micro-scale to describe and interpret sediments observed in excavated trenches and where good natural exposures occur. Data were collected at the outcrop scale during two summer field seasons at the Tarfala Research Station and some of the GPR surveys were conducted during a short spring campaign in 2011. Specific details of sampling methods, data collection and data interpretation techniques are given in the sections below and are organised as follows: section 2.3 describes data collection in the field and at the outcrop scale, and using ground-penetrating radar; section 2.4 deals with structural measurements made in the field (clast fabrics) and laboratory (micromorphology, micro-structural mapping, 2-D micro-fabrics, and magnetic fabrics); section 2.5 outlines the additional laboratory methods used to describe and analyse sediments.

2.3 Field Observations

2.3.1 Observations at the Forefield Scale

Field work surveys were used in conjunction with observations from aerial photographs of the Tarfala Valley taken in 1910, 1959, 1969, 2001, and 2008 to map the geomorphology of each forefield. The photographs were supplied by Per Holmlund at the Tarfala Research Station. A 2001 aerial image of the Kebnekaise Massif geo-referenced in the SWEREF 99 co-ordinate system was acquired from Lantmäteriet Images and used as the base map for digitizing landforms using ArcGIS software. The locations of landforms observed in the field were recorded using a handheld Garmin GPS unit, and these locations were added to the base map in ArcGIS. Flute geometry was measured in each forefield using ground transects. Flute widths, lengths and spacing (flute crest to flute crest) were measured using a 30m tape measure, and flute heights measured using a 1m ruler. Flute locations and sampling sites (trenches) were recorded using the Garmin GPS unit. The dimensions of landforms such as diamicton plains were measured from aerial images georeferenced in ArcGIS.

A map of Isfallsglaciären drawn by Enquist in 1910 when the glacier was near to its Little Ice Age Maxima was available at the Tarfala Research Station. This map shows surface contours across the glacier and allows estimates of the glacier surface slope to be made. Enquist's map was georeferenced in ArcGIS and superimposed on the Lantmäteriet map of the Tarfala Valley. Ground heights, obtained from dGPS measurements made during GPR surveys of fluted moraine, were added to the map. The difference in elevation between the GPR surveys and Enquist's contours allowed the thickness of the glacier in 1910 to be estimated at various points. Ice thickness and surface slope data were then used to estimate basal shear stresses beneath Isfallsglaciären in 1910 using equation 1.2.

2.3.2 Observations at the Outcrop Scale

Lithofacies is a non-genetic term which is used to describe distinct beds, layers or bodies of sediments that can be distinguished from each other by their sedimentary properties (Evans and Benn, 2004). One-dimensional graphic logs record vertical changes in lithofaces and are a convenient way of recording observations on sediment particle size, bed thickness and geometry, contacts, deformation and depositional structures, macro-fabrics, and inclusions (Kruger and Kjær, 1999). Two-dimensional graphic logs combined observations from several vertical sections into a sketch which shows the vertical and lateral changes in lithofacies and lithofacies architecture, and is a more useful sediment logging method where lateral and vertical changes in lithofacies are manifold (Evans and Benn, 2004). Graphic logs also record the stratigraphic sequence and allow lithofacies associations to be discerned; lithofacies associations show the relationships between different lithofacies and may give clues to their genetic origin (Evans and Benn, 2004).

In this study, variations in lithofacies and lithofacies associations were mapped using one and two-dimensional graphic logs. The graphic log coding system introduced by Kruger and Kjær (1999) was followed. In the Tarfala Valley, sediment exposure is poor and even where streams are incising into diamicton plains, sediment sequences are masked by slumps and mass flows. However, at Storglaciären in 2011, active erosion by Sydjåkk and a landslip exposed a fresh 100m+ long, 3-4m deep section of the diamicton plain, and although unstable and unsafe in places, 5 detailed logs were recorded along this section (specific locations are shown in Chapter 3). In addition, 5 detailed graphic logs were recorded at sites along the diamicton plain where incision by Nordjåkk created natural 'cliff' faces; fresh faces were exposed by digging away slumped/flowed material with a spade to depths of 2m+ and then using a trowel and sharp knife to carefully clean the face. The same method was used to clean faces at natural stream-cut sections into the diamicton sheets and moraines in Kaskasatjåkka, where 10 detailed graphic logs were taken. In Isfallsglaciären, twenty-three pits were excavated into fluted moraine and sketches and 2-D graphic logs used to record lithofacies and lithofacies associations. To limit further damage to a fragile environment, eight large pits, up to 2-3m wide and up to 1m deep, that had been dug (but not back-filled) by previous researchers, were carefully re-opened with a spade and faces cleaned with a trowel and sharp knife and 2-D graphic logs recorded (all pits were back-filled as far as possible after use). New pits, up to 1-2m wide and 1.9m deep, were excavated across flute and interflute areas in 3 different parts of the forefield (see Chapter 3) to sample lithofacies at the proximal, middle, and distal ends of flutes.

Where detailed graphic logs were taken, clast fabrics were recorded and samples were taken for laboratory investigations into particle-grain size distributions, clast morphology, and sediment porosity. In addition, a portable handheld shear vane was used to measure vertical variations in the *in situ* undrained shear strength of diamicton at 10cm intervals. Shear vane tests followed the methods used by Kjær *et al*. (2003), in which 5 readings were taken from within each 10cm layer, the highest and lowest values discarded, and an average attained from the remaining 3 values. In handheld shear vane tests a small disc of sediment is sheared by the rotation of the vane and the forces resisting rotation are automatically converted into a shear strength reading on a dial; torque is applied until a maximum shear strength reading is attained (up to a maximum value of 130 KPa in this study) and the sediment fails (Craig, 1997). Portable shear vane tests were developed by civil engineers to quickly assess shear strength in clays and may not be appropriate for use with other sediments because the vanes can stick during rotation against large clasts (Craig, 1997). However, Christoffersen and Tulaczyk (2003) and Kjær *et al*. (2003) successfully used portable shear vane tests to record variations in diamicton shear strength with depth in areas where natural sediment exposure was poor. In this study, shear vane readings where the vane obviously caught against larger clasts, or where it was not possible to fully insert the shear vane into the sediment, were discarded. It was not possible to insert the shear vane into some over-consolidated diamictons or clast-supported or very clast-rich diamictons. Vertical variations in the shear strength of subglacial diamictons were recorded in 8 shear vane experiments in Isfallsglaciären, and seven experiments each at Kaskasatjåkka and Storglaciären. Shear vane readings were also taken within the top 20cm of fluted moraine at various locations across the forefield of Isfallsglaciären.

In addition to the sites used for graphic logging and detailed sediment analysis, 84 smaller pits, typically excavated to 0.5m depth, were opened-up at Isfallsglaciären, and a combination of 38 pits and/or natural sediment exposures opened-up at Storglaciären and 41 at Kaskasatjåkka. In these additional pits and exposures, the lithofacies and the maximum and minimum depths of subglacial diamicton were recorded. The sites were selected to give good coverage of each forefield and to enable maps showing the distribution of lithofacies and the thickness of the subglacial diamicton to be constructed. In some pits, it was possible to use a soil auger (with extension rods) to recover sediment samples from depths of up to 2m. Site locations were recorded using a handheld Garmin GPS unit (which gave a ground accuracy reading of between 3 and 6m) and marked on a base map.

2.3.3 Ground-Penetrating Radar (GPR) Surveys

GPR surveys have been successfully used to investigate the sedimentary geometry, architecture, and stratigraphy of glacial forefield sediments and glacigenic landforms such as drumlins, outwash fans and moraines (Graham and Midgley, 2000b; Bennett, 2001; Bakker, 2002; Bennett *et al*., 2004; Kjær *et al*. 2004; Sadura *et al*. 2006), to study deformation in Quaternary tills (Busby and Merrit, 1999), to investigate the internal structure and formation of Pleistocene outwash deposits, sandy till formations, and Quaternary gravel sequences (Møller and Jakobsen, 2002; Kostic and Aigner, 2007; Gibbard *et al*., 2009), and to characterize geo-radar facies and to investigate deformation structures in ice-marginal zones (Overgaard and Jakobsen, 2001; Jakobsen and Overgaard, 2002; Schwanborn *et al*., 2008). Ground-penetrating radar (GPR) surveys are used in this study to investigate the sedimentary architecture and structure of fluted moraines and to help establish the depths and distributions of lithofacies across the forefields.

The strength and polarity of radar wave reflections between any two layers depends on the strength of the dielectric contrast:

$$R = \frac{\sqrt{\varepsilon_r 2} - \sqrt{\varepsilon_r 1}}{\sqrt{\varepsilon_r 2} + \sqrt{\varepsilon_r 1}} \tag{2.1}$$

Where:
R is the reflection coefficient, 1 and 2 are adjacent layers, and ε_r is the relative dielectric permittivity, a measure of a material's capacity to store electrical charge (Reynolds, 1997). Bedding planes and sedimentary structures separating media with different ε_r can generate strong reflections which represent stratigraphic bounding surfaces, whilst bodies of sediment with consistent reflectors represent radar-facies; bounding surfaces and radar-facies can be mapped using GPR (Neal, 2004). Different antennas are necessary to view structures at different scales (Jol and Bristow, 2003). High frequency antennas provide better vertical resolution, up to ¼ of the wavelength (λ), which gives a maximum vertical resolution of 0.21m and horizontal resolution of 0.43m for 200 MHz antenna, but poor penetration depth as wave attenuation is high; low frequency antennas give better penetration, but relatively poor resolution (Hubbard and Glasser, 2005).

GPR surveys and data-processing were carried out following the procedures recommended by Annan (1999), Jol and Bristow (2003), and Neal (2004) and involved co-polarised, broadside, common off-set surveys (meaning the transmitter and receiver were in the same direction and perpendicular to the line of section), which provide the most efficient and accurate method to detect geo-radar bounding surfaces and geo-radar facies geometry (Neal, 2004). Surveys were conducted using a pulseEKKO PRO GPR system with 50, 100 and 200MHz antennas and with a minimum trace stacking density of 64 (as recommended by Neal, 2004, for gravel and sand-rich sediments typical of glacial forefields). Table 2.4 summarises the antenna separation, step-size, and sampling intervals used with the 50, 100, and 200 MHz antennas. Multiple transverse and longitudinal surveys were conducted across the fluted moraine of Isfallsglaciären and the diamicton plain/sheet of Storglaciären and and Kaskasatjåkka during summer field seasons, and surveys lines were taken across the forefield of Isfallsglaciären and the ablation zone of Storglaciären during a spring campaign, which took place before the winter snow cover had begun to melt. The 200MHz surveys provided the best vertical resolution and were used specifically to investigate the near-surface sedimentary architecture of fluted moraines. During the spring surveys, the locations and topography of the GPR survey lines were recorded with centimetre accuracy using a Trimble differential Global Positioning System (dGPS) set to continuous recording mode. The dGPS system was unavailable during the summer GPR surveys, so locations and topography were determined using a handheld Garmin GPS unit (which typically measured ground locations to an accuracy of 3 to 6m), and verified by checking Garmin data against topographic heights taken from the Lantmäteriet 1: 20 000 Kebnekaise map or from Google Earth. Many of the pits excavated in each forefield were located at sites where sedimentary data could be used to ground-truth GPR surveys. Figure 2.6a-c shows the GPR transect lines in each forefield.

GPR data were processed using Ekko-View Deluxe Software following the recommended sequence outlined by Annan (1999), which included time zero adjustment, dewow filtering, topographic correction, gain application, deconvolution, and migration. Radar wave velocities, required for accurate depth determination, were calculated using the hyperbola matching method which is summarised in Table 2.5 (Neal, 2004). Initial analysis of the GPR data showed that the Trimble dGPS produced significant noise. Experimental processing showed that a very low background subtraction filter eliminated most of the noise without losing too much data or generating data distortions. A processing protocol for analysing the GPR data was established and is shown below in Table 2.5.

Table 2.4 Antenna Separation Distance, Sampling Intervals, and Step-Sizes used with 50, 100 and 200MHz Antennas

Antenna Centre Frequency	*Antenna Separation Distance (m)*	*Step-Size (m)*	*Temporal Sampling Interval (ns)*	*Time Window (how long/deep system probes subsurface)*	*Approximate Depth (m) of Penetration with Wave Velocity of 0.1mns^{-1} and specified Time Window*
50MHz	2	0.5	1.6	400ns	20
100MHz	1	0.25	0.8	200ns	10
200MHz	0.5	0.1	0.4	100ns	5

Note: these values are those recommended in the Sensors and Software Inc. PulseEkko Pro User's Guide (2006). If the sampling interval is too small data may be aliased. These sampling intervals are designed to properly sample signal waveforms with finer sampling for higher frequencies. PulseEkko Pro antennas are bistatic and unshielded. The depth of penetration (m) = V x T/2 where V is the radar wave velocity (mns^{-1}) and T is the two-way travel time (ns); 0.1mns^{-1} is a good average velocity for geological materials (Annan, 1999).

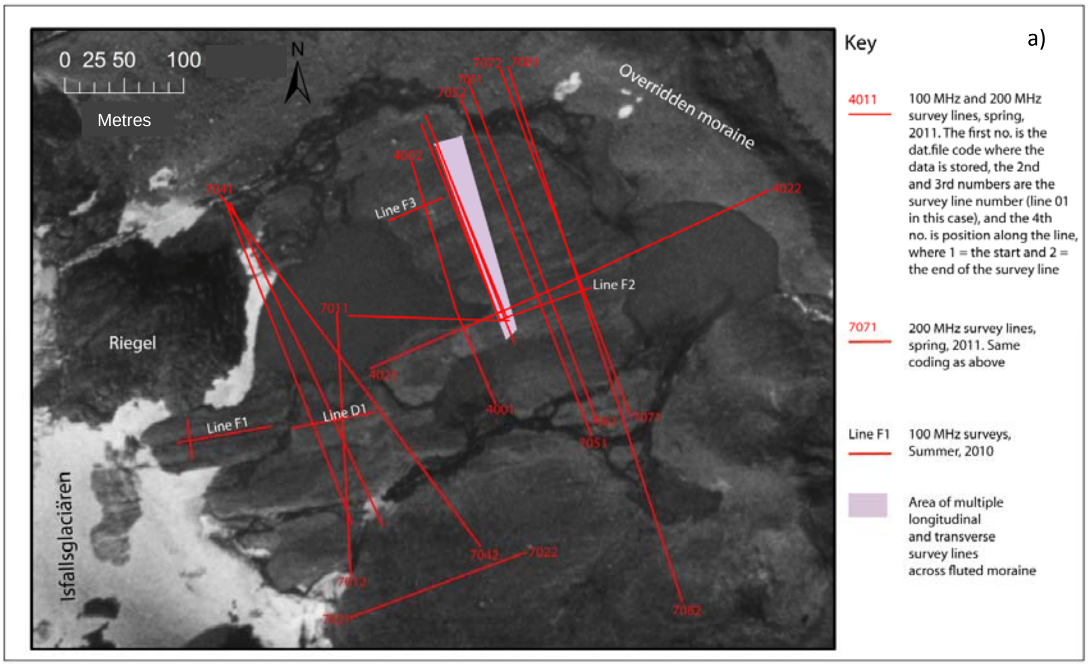

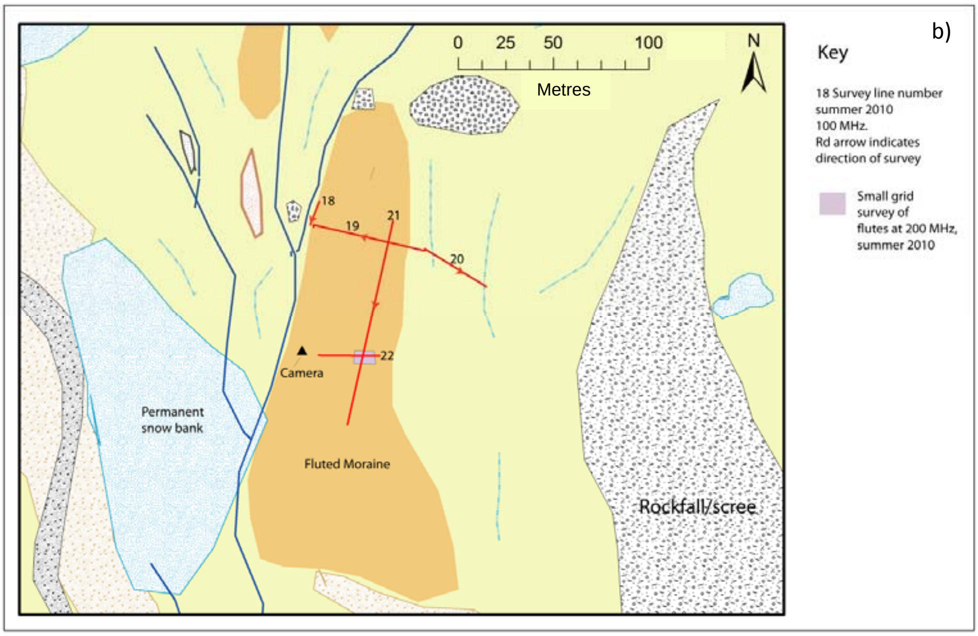

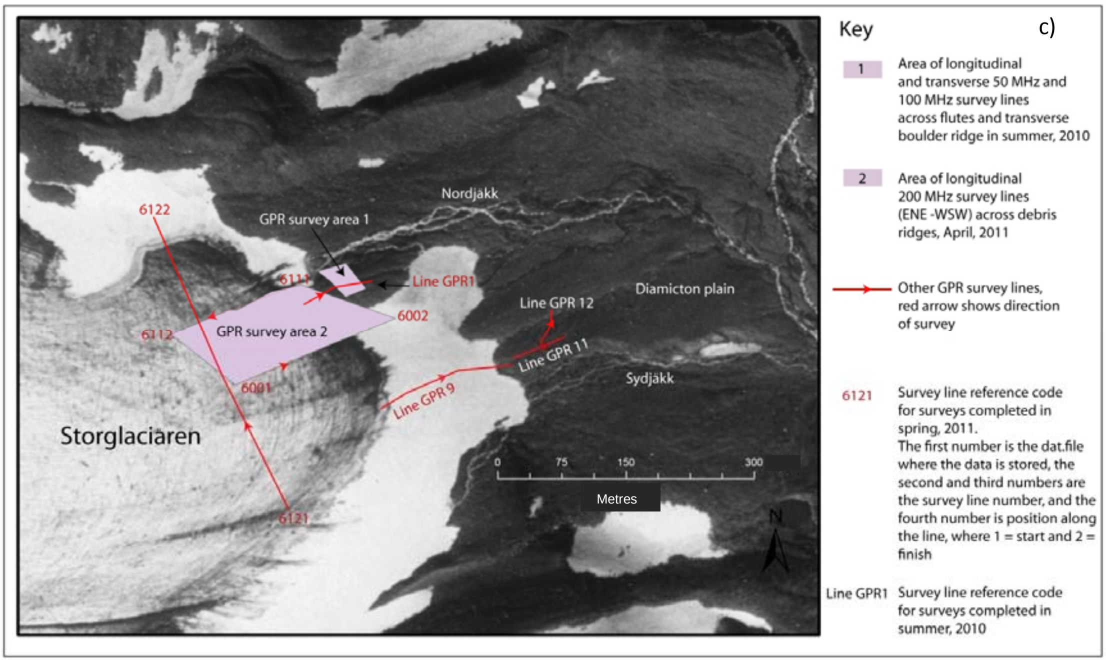

Figure 2.6 GPR transect lines at (a) Isfallsglaciären, (b) Kaskasatjåkka, and (c) Storglaciären

Table 2.5 A Processing Protocol for GPR Survey Data

Step	*Processing*	*Rationale*
1	Set system to automatic dewow	The radar system produces low frequency components that diffuse into the ground as eddy currents and return as slow-decaying transients; these can be removed by a high pass filter (dewow)
2	Re-set datum time zero on all traces	For each trace, time zero represents the first major break in the signal and is determined by the GPR system's computer. However, this is not always correct and time zero can drift between traces for multiple reasons. This process estimates the best position for time zero on each trace and moves traces up/down such that the value of the first break on each trace is aligned with the value of the first trace
3	Add dGPS file and convert to UTM. Re-calculate step-size for free runs	PulseEkko Pro creates a separate 'topographic file' when used in conjunction with a dGPS system and this has to be manually added to the GPR file. Where surveys were conducted over snow surfaces, the GPR system was attached to a pulk and easily moved. As such, traces were collected as a free run rather than using specified step-sizes. The topographic file includes elevation and location data for traces and once it is added the step-size can be re-calculated for free run data
4	Add elevation data	This merely combines the 'topographic file' with the GPR file - traces are not topographically adjusted until stage 8
5	Re-position traces (only necessary where two pulks were used, the lead pulk carrying the GPR transmitter/receiver and trailing pulk carrying the dGPS system	The distance between the two pulks is known and this distance is used to re-position traces accurately
6	Delete unwanted traces and establish radar wave velocity using hyperbola matching method	Unwanted traces include repeat traces or traces recorded accidentally or when the system was in free run mode but stationary. Each trace generated by the radar transmitter is a short pulse of electro-magnetic energy which travels down through the ground as a spreading 3-D cone; reflections from point objects in the ground can occur anywhere along the surface of the cone, but the GPR system places the reflector directly beneath the receiver. During the course of a survey this causes hyperbolic diffraction as the GPR system moves towards, over, and then away from a point reflector such as a large boulder. Theoretical hyperbola produced by known radar wave velocities are 'matched' against real hyperbola to establish the most appropriate radar wave velocity for the ground materials
7	Apply a background subtraction filter (set to c.10% of the trace number)	This removes much of the noise generated by the dGPS system. The background subtraction filter uses a running average; each original trace is replaced by the original trace minus the average trace of a specified window (in this case, the window represents 10% of the total number of traces in the section)
8	Add topography using a radar wave velocity of 0.06 to 0.17mns^{-1} depending on ground conditions	An estimate of radar wave velocity is required to add accurate topography to the section
9	Add a spreading and exponential compensation (SEC) gain	Gains are required because geometric spreading and the exponential dissipation of radar energy with depth cause radar signal strength to decrease with time; as such, gains are added to boost weaker signals at later times. SEC gains compensate for spherical spreading losses and the exponential dissipation of energy. As such, SEC gain produces profiles which are the closest to physical reality and allow the strength of reflectors to be compared
10	Migrate hyperbola back to single points if necessary	This transformation is necessary where there are many interfering hyperbola, but it requires accurate radar wave velocity and can produce artefacts in the data

Note: these processes can all be conducted using Ekko-View Deluxe editing software.

2.4 Structural Measurements

2.4.1 Clast fabrics

In this study, clast fabric refers specifically to the orientation of clast long-axes (a-axes) and to fabrics than can be measured without the need of a microscope (Bennett *et al*., 1999; Benn, 2004). Particle long-axes rotate in response to imposed stresses (Benn, 1994) and clast fabrics have been widely used in the analysis of sediments to infer relative strain magnitudes and strain histories in glacigenic sediments and fluted moraines, and to establish previous glacier flow directions (Boulton, 1976; Rose, 1991; Benn, 1994; 1995; Eklund and Hart, 1996; Kjær *et al*., 2003; Piotrowski *et al*., 2006; Evans *et al*., 2010). A-axis alignment is used in this study so that results are comparable with previous research where clast fabrics have been measured using a-axis alignment (for example, Boulton, 1976; Eklund and Hart, 1996). Clast fabric data are compared quantitatively using the eigenvector and eigenvalue method of Mark (1973; 1974). Three orthogonal eigenvectors are calculated from particle long-axis orientations: V_1 is the principal eigenvector which is parallel to the axis of maximum clustering in the data, V_2 is the intermediate eigenvector, and V_3 the minimum eigenvector (Mark, 1973; Benn, 2004). The strength of clustering around the eigenvectorsis given by the normalized eigenvalues $S_1 \geq S_2 \geq S_3$, where $S_1 + S_2 + S_3 = 1$, and where S_1 is the principal eigenvalue. Where $S_1 = S_2 = S_3 = 0.33$clasts show no preferred alignment and the fabric is isotropic;where $S_1 = 1$ there is a perfect alignment of clasts around V_1, the preferred plane of orientation (Iverson *et al*., 2008; Benn, 2004). Eigenvalue data are particularly useful as they indicate the 'shape' of a fabric, with the three eigenvalues visualized as the axes of an ellipsoid (Benn, 2004). Benn (1994) used an elongation index (E = 1- (S_2-S_1) and an isotropy index (I = S_3/S_1) to scale a fabric shape triangle which represents the continuum of all possible ellipsoid shapes. Sediments formed in different environments tend to produce a distinctive range of eigenvalues and fabric shapes and, as such, clast-fabrics have been used to aid the interpretation of glacigenic sediments (Dowdeswell and Sharp, 1986; Benn, 1995). However, Bennett *et al*. (1999) stressed that clast-fabric data alone cannot be used to discriminate the genetic origin of glacigenic sediments because the fabric shape envelopes of sediments formed in different environments overlap. Conversely, Benn (1994) demonstrated that fabric shape could be used to discriminate A-type horizons and B-type horizons in deforming beds, as B-type horizons had more elongate and flat fabric shapes.

Benn and Ringrose (2001) developed a bootstrapping technique for establishing confidence intervals around data points plotted on fabric shape ternary diagrams that are scaled using elongation and isotropy indices. They found that the 10th convex hull approximated the 90-95% confidence region around a sample point, and provided a quantitative way of establishing whether fabrics were drawn from different populations, that is, whether they had statistically different clast fabric shapes (although Benn, 2004 stressed that this is not a formal test for statistical difference). Benn and Ringrose's (2001) bootstrapping programme is used in this study to establish 10th convex hulls around data points for clast fabrics taken from different diamictons to see if there is a statistical difference between their fabric shapes. Specifically, the technique is used to examine differences in fabric shapes between flutes and interflutes, and between diamictons from different parts of the diamicton plain.

In this study, variations in the vertical, lateral, and longitudinal clast fabrics of the Isfallsglaciären fluted moraine are measured and the patterns of relative strain used to test the models of flute formation (Table 1.3). In addition, the isotropy and elongation indices are used to describe and compare the clast fabric shapes of flute and interflute sediments and the underlying substrate. In total, 49 macro-fabrics were measured from pits excavated into the fluted moraine in order to record the proximal to distal variations in fabric orientations and strengths (specific locations are given in Chapter 3). A Silva compass-clinometer was used to record clast a-axis dip and orientation (with a precision of +/- 1°). Clast fabrics are usually measured using prolate clasts of a specified size-range which are sampled from within a restricted sediment volume (Benn, 2004). The reasons for this are:

a) prolate clasts (in which the a-axis is longer than the b-axis) are considered more likely to develop preferred orientations as they rotate and align during transport more readily than clasts with similar a- and b-axes (Benn, 2004);
b) larger clasts are more prone to adopt parallel orientations than smaller clasts during transport (Kjær and Krüger, 1998; Carr and Goddard, 2007);
c) subtle changes in lithofacies and externally applied shear stresses can occur over small spatial scales and over time; sampling over wide areas and large vertical intervals fails to detect such variations (Piotrowski *et al*., 2004; Benn, 2004).

There is no 'standard' method for taking clast fabrics and different researchers have used different clast sizes, shapes, and samples sizes, and sampled over different areas, which means that clast fabrics collected in different studies may not be comparable (Benn, 2004). For example, Piotrowski *et al*. (2006) measured clast-fabrics using 30 prolate clasts with a-axes lengths 0.7 to 5.6cm long and, for each fabric reading, clasts were sampled from a restricted area (30 by 30cm) and vertical thickness (20cm). Similarly, Gordon *et al*. (1992) used 25 clasts to measure clast fabric when studying small-scale fabric variations in flutes. Benn (2004) recommended a sample size of at least 50 clasts as statistical variance is high for sample sizes of 25. However, Larsen and Piotrowski (2003) showed that statistical variance is within acceptable limits when a sample size of 30 clasts is used, as long as strong fabrics occur.

An important objective in this study is to see how strain signatures vary with depth over decimetre scales and this requires the measurement of clast fabrics over small vertical intervals. A pilot study using 50 clasts indicated that flute fabrics were generally strong (S_1>0.7) and, as such, a sample size of between 25 and 30 clasts was justified. The method employed here is based on the methods used by Kjær *et al*. (2003) and Piotrowski *et al*. (2006), who also measured clast fabric variations over small vertical intervals. The dip and orientation of clasts with a-axes lengths 0.6 to 6cm long and with a: b ratios >1.5:1 were measured (Kjær *et al*. also used a sample size of 25). Each clast fabric was taken from a restricted sediment volume, with the area measuring no more than 25 by 25cm, and the vertical thicknesses restricted to 10cm. Where insufficient clasts of the specified size and shape were found the sampling was extended to cover a 20cm thick vertical layer. The advantage of this approach is that it is sensitive to small vertical changes in clast alignments and fabric strength, which may reveal time-transgressive variations in bed-deformation. In addition, adjacent fabrics can be combined to produce a fabric reading having a sample size of 50+ clasts and lower statistical variance. Clast fabrics were not taken from flute areas that had obviously experienced sub-aerial disturbance or mass flows, and to minimise the effects of paraglacial disturbance clast fabrics were not taken from the top few centimetres of the flute or from flute surfaces (Rose, 1991).

The vertical resolution of clast fabric readings (0.1-0.2m intervals) was capable of picking up subtle changes in strain signature. For example, the 0.2m vertical sampling interval was capable of detecting a weak layer of clast fabrics in flute diamicton at 0.4-0.6m depths and differences in the tenth convex hulls between the clast-fabric readings of the weak layer and macro-fabric readings from other depths below the flute crest suggest that this difference is real and not just a function of the sampling interval or sampling method (see Chapter 4). Sampling clast fabrics over smaller depth intervals (0.1m) was frequently impossible due to a sparsity of clasts of the required shape and size, and so the majority of readings were measured over 0.2m vertical intervals.

The same method was employed at Storglaciären and Kaskasatjåkka to measure longitudinal and vertical changes in clast fabrics in fluted moraine and diamicton plain/sheet sections (at sites where graphic logs were recorded), and to compare the clast fabrics of different lithofacies. At Storglaciären, 40 clast fabrics were measured and at Kaskasatjåkka 23 clast fabrics were measured. Stereo32 software (Röller and Trepmann, 2012) has been used to calculate eigenvalues and eigenvectors and to generate rose diagrams, lower hemisphere, equal-area stereonet projections and contour plots of fabric data. Rose diagrams have been plotted using conventional linear scaling and density-distribution contour plots are shown on lower-hemisphere, equal-area projections. Density distribution has been calculated using a cosine sums function, which plots a continuous distribution on a 10-interval scale ranging from blue (minimum density) to red (maximum density).

2.4.2 Micromorphology, Micro-structural Mapping and Two-Dimensional (2-D) Fabrics

Macro-scale observations are often insufficient to reveal the genetic origin, environment of deposition, and strain history of glacial sediments. Micromorphology is the study of sedimentary textures and structures in thin section using a petrographic microscope at magnifications of x10 to x100 (van der Meer *et al*., 2010). It is a well-established approach which can be used in combination with macro-observations to guide facies interpretation (van der Meer, 1993; Carr, 2004), to discern pervasive and discrete deformation in subglacial sediments (van der Meer, 1993), and to detect polyphase strain histories in vertical till sequences from cross-cutting relations and over-printing structures (Phillips and Auton, 1998). A range of planar and rotational plasma fabrics and skeleton-matrix (S-matrix) deformation structures are commonly associated with subglacially deformed sediments (van der Meer, 1993; van der Meer *et al*., 2003). Plasma refers to the textural component < 20μm in size and plasma fabrics form when patches of platy clay minerals and fine silts develop similar orientations, often in response to movements along shear planes; the identification of plasma fabrics involves identifying areas of plasma having similar interference colours when viewed under cross-polarized light (Carr, 2004). A number of S-matrix deformation structures have been observed to form along discrete microshears in re-moulded subglacial tills used in ring-shear experiments (Thomason and Iverson, 2006; Larsen *et al*., 2007). S-matrix deformation structures included grain lineations, crushed and flaked grains, turbate structures, and grain stacks (Carr, 2004). Ring shear experiments suggest that most simple shear-strain is accommodated by microshears in subglacial sediments (Larsen *et al*., 2007). However, similar fabrics and structures have been recorded in other glacigenic sediments, such as debris flows and thus cannot be considered diagnostic of subglacial deformation tills (Piotrowski *et al*., 2006).

Micromorphology is increasingly used in multi-disciplinary studies to analyse glacigenic sequences and much systematic work has been done comparing the plasma fabrics and the number and type of S-matrix structures found in sediments derived from different depositional environments (van der Meer, 1993; Carr, 2001; Carr, 2004; Menzies *et al*., 2006; van der Meer *et al*., 2010b; Phillips *et al*, 2011b). However, Larsen *et al*. (2006a) found that a steady-state number of S-matrix deformation structures was achieved in subglacial tills at low strain (strain = 7), and, as such, the number of S-matrix deformation structures revealed little about strain magnitude. Furthermore, sediment composition influences the type of structures found in thin sections (plasma fabrics are not found in sediments devoid of clay, for example), and this has led to the misinterpretation of some depositional environments (Phillips *et al*., 2011b). In addition, simply identifying and counting the number of S-matrix structures in a thin section reveals nothing about the relations between the micro-structures or the sequence of events that produced them; this limitation has recently been overcome with the introduction of the micro-structural mapping methodology, which uses the methods and terminology of structural geologists to identify and analyse the polyphase history of deformation in glacigenic sediments (Phillips *et al*., 2011b). This approach involves the production of a detailed micro-structural map of a thin section and uses cross-cutting relationships to discern the relative chronology of micro-fabric development. Two-dimensional fabrics are used to identify domains, that is, areas of the 'map' where grains have the same preferred alignment, and detailed mapping of S-matrix structures reveals the relation between successive domains and micro-structure development. As such, the map reveals the complex (and for subglacial deformation tills, usually polyphase) history of deformation. The micro-structural mapping methodology is employed in this study to investigate the polyphase history of sediment deformation in fluted moraine sediments from

Isfallsglaciären and diamicton plain sediments from Storglaciären, and the method is fully summarised in Table 2.6.

Table 2.6 The Micro-structural Mapping Methodology of Phillips *et al*. (2011b)

Step	***Procedure***
1	Collect samples whose orientation with respect to the glacier flow direction is known. Subglacial diamictons have usually experienced multiple phases of deformation and kinematic indicators, such as asymmetric folds, can be used to provide information on the stress regime during different phases of deformation if the sample is correctly orientated to begin with. Produce thin sections from the collected samples
2	Take a high-resolution scan of a thin section and import it into a graphics package such as Adobe Illustrator
3	On separate layers, digitize the long-axes of skeleton grains and measure their length, and map any S-matrix structures present, such as grain lineations. Work systematically across the slide. Measure the 2-D orientation of skeleton grains using the angle-measure function.
4	Pick out trains of grains having the same alignment. Compare with rose diagrams of 2-D fabrics, which can be drawn for different areas of the 'map'. Use the grain alignments and rose diagrams to identify fabric domains, that is, areas of the map having the same preferred orientation of grains
5	Look for cross-cutting relationships that enable the sequence of events to be established; F1 is the earliest form fold, Fn the latest; S1 is the earliest formed fabric, Sn the latest
6	Use separate colours in separate layers to draw polygons around areas of the map having the same domains, that is, areas where skeleton grains have the same preferred alignment. Use different colour fills to identify the different micro-fabrics. Interpret the map by establishing the relative age of the micro-fabrics and structures

In the study of subglacial diamictons, thin section samples are usually taken from beneath the zone of active soil formation and below the zone where periglacial processes are/were active, which for Quaternary tills is usually taken to be below a depth of 2m (van der Meer *et al*., 2003). The current depth and extent of permafrost in forefields of the Tarfala Valley is unknown. However, sporadic permafrost is thought to exist beneath the ablation area of Storglaciären, moraine-mound complexes in Storglaciären and Isfallsglaciären are known to be ice-cored below a depth of about 2m, and the annual temperature range produces seasonal cycles of freeze-thaw activity (Holmlund and Jansson, 2002). As such, periglacial activity may have affected subaerially exposed forefield sediments. Periglacial processes related to the growth and thaw of ice lenses and interstitial ice produce a range of micromorphological structures (Van Vliet-Lanoe, 2010) which can overprint subglacial structures (Carr, 2004), whilst frost action can affect clast fabrics. For example, Rose (1991), working on flutes in the forefield of Austre Okstinbreen, Norway, found that macro-fabrics could be disrupted by frost heave processes and that frost penetrated deeper in exposed flute crests and ridges where there was a thinner cover of insulating snow. Similarly, Lundqvist (1983) suggested that a 'cleavage-like' planar fabric observed in some Swedish tills was formed by frost action.

The observations of Rose (1991) and Lundqvist (1983) are important because it has been assumed by previous researchers that the properties of glacigenic sediments exposed in diamicton plains and fluted moraines in the Tarfala valley are entirely subglacial in origin. The extent to which subglacial fabrics and structures have been over-printed by periglacial fabrics and structures is unknown in the Tarfala Valley, but it can also be investigated using the micro-structural mapping methodology. To that end, 7 thin section samples were collected from flutes in Isfallsglaciären from excavated pits where clast fabrics were recorded and sedimentary investigations carried out. Samples were collected from the proximal, middle, and distal ends of flutes to see if sediments exposed on the forefield for a longer period of time revealed more evidence of periglacial overprinting. In two pits where the deforming layer seemed to thicken, samples were collected from different depths beneath the flute crest to examine whether periglacial over-printing lessened with depth and whether subglacial fabrics and structures became more apparent with depth. In 3 pits, samples were taken across key lithofacies boundaries to examine the relation between the upper diamicton and underlying substrate. It should be noted that no flutes are currently emerging from beneath the ice margin of Isfallsglaciären and so it was not possible to recover samples from an environment where flutes were actively forming.

At Storglaciären and Kaskasatjåkka attempts were made to recover micromorphology samples from the base of deeper vertical sections where rivers had incised into the diamicton plain/sheet. However, this did not prove possible as some of the sections were unstable and unsafe to work near, or, despite repeated attempts, the diamicton was so fissile and fractured it crumbled apart when attempts were made to sample it. In Storglaciären, it proved possible to recover 5 samples from vertical sections where graphic logs were taken. The samples were taken from varying depths, with the deepest sample recovered from 2m depth, to sample across key lithofacies boundaries and to investigate vertical changes in subglacial micro-fabrics and structures. In Kaskasatjåkka, the diamicton from the diamicton sheet proved too fissile to recover a coherent sample from.

Micromorphology samples were taken following the procedures recommended by van der Meer *et al*. (2010a). Two types of sampling tin were used; a commercially produced Kubiena tin, dimensions 180 x 80 x 60mm, and a purpose built tin, dimensions 150 x 110 x 100mm. Where samples were collected from river-cut sections rather than freshly dug pits and trenches, a minimum of 30cm of sediment were cleared from the face to remove weathered or slumped material prior to sampling. Samples were carefully collected by cutting around sediment with a sharp knife and working the open-end of the tin into the face. The larger purpose built tin had the advantage of reducing the volume of the sample affected by any deformation produced whilst working the sides of the tin into the face, a process that could take an hour or more to complete. Sample orientation and dip data were measured using a Silva compass-clinometer and orientation data were checked against the Lantmäteriet 1:20 000 Kebnekaise map to ensure that local bedrock had not produced any magnetic deviations (Tarling and Hrouda, 1993). Where necessary, pebbles and clingfilm were used to pack the tin tightly so that the sample did not move around in transit, and clingfilm and parcel tape were used to seal lids to the samples to prevent drying out and to provide protection during shipment. Thin sections of dimensions 100 x 75mm were produced at the Centre for Micromorphology, Royal Holloway University of London, following the procedures recommended by Palmer *et al*. (2008), which involved samples being air dried, impregnated with epoxy resin, cut, ground, and mounted on slides. All thin sections were cut parallel to the assumed direction of previous glacier flow (that is, down-flute and down the diamicton plain) because flow-parallel orientations are likely to reveal the most complete record of sediment deformation (Phillips *et al*., 2011b).

2.4.3 The Anisotropy of Magnetic Susceptibility (AMS) and Strain Magnitude

AMS is a well-established, objective, precise, rapid and cost effective method used in geology to measure strain in rocks (Tarling and Hrouda, 1993), and it is increasingly used to assess strain in deformed glacigenic sediments (Iverson *et al*., 2008; Thomason and Iverson, 2009; Fleming *et al*., 2013). In this study, magnetic fabrics derived from AMS data were used to estimate strain magnitude in subglacial sediments and to investigate variations in strain in fluted moraines and diamicton plain sections. The following paragraph briefly describes the physics underpinning the method and is based on the detailed account given by Tarling and Hrouda (1993). The method involves collecting orientated samples of sediment and determining the strength of magnetism acquired by the sample when a magnetic field is applied at different directions. The strength of induced magnetism M depends on the magnetic susceptibility of the sample and the strength of the applied magnetic field:

$$M = KH = K\frac{B}{H_0}$$

(2.2)

Where:

M isthe magnetic dipole moment per unit volume (Am^{-1}), H is the magnetic field strength (Am^{-1}), B is the magnetic field strength measured in Tesla, H_0 is the permeability of free space ($4\pi \times 10^{-7}$ henrym^{-1}), and K is the magnetic susceptibility of the material. The application of an external magnetic field to a substance causes the spin of electrons to precess and generate a magnetization either in the direction of the applied field (which happens in materials having incomplete electron shells, which are described as paramagnetic), or opposite to the applied magnetic field (which happens in materials described as diamagnetic which have complete electron shells); the induced magnetism is usually weak and lost once the applied field is removed. Ferromagnetic materials behave paramagnetically but produce strong magnetization which is retained after the applied field is removed. The bulk susceptibility K_{bulk} of a sample is the sum of the susceptibilities of all the paramagnetic, diamagnetic and ferromagnetic materials present. However, if ferromagnetic minerals, such as the common iron oxide mineral magnetite, account for more than 0.1% of the volume of a sample they dominate the magnetic properties because they have high magnetic susceptibilities. If a known volume of sediment is subjected to a magnetic field of known strength H, and the strength of induced magnetism M is measured, then the bulk susceptibility is given by:

$$K_{bulk=}\frac{M}{H}$$

(2.3)

K_{bulk} is a dimensionless number (Tarling and Hrouda, 1993). If the same magnetic susceptibility is attained regardless of the orientation of the sample, then the material is described as isotropic. However, most materials are anisotropic and the extent of the anisotropy of magnetic susceptibility (AMS) depends on the alignment and distribution of particles (especially ferromagnetic particles) in the sample; strong preferred alignments give strong anisotropy in the direction of alignment (Tarling and Hrouda, 1993).

The variation in magnetic susceptibility with orientation can be visualized as an ellipsoid having three orthogonal susceptibility axes, K_1, K_2, and K_3, with the greatest intensity of magnetization induced along the long-axis, known as K_1, the principal axis of magnetic susceptibility, and the weakest intensity of magnetization induced along the short-axis, K_3.The mean susceptibility K_{mean} is given by:

$$K_{mean} = \frac{K_1 + K_2 + K_3}{3} \tag{2.4}$$

where $K_1 \geq K_2 \geq K_3$ in SI units (Tarling and Hrouda, 1993). Various statistical parameters exist to assess the strength of the AMS fabric and to describe the shape properties of the susceptibility ellipsoid. By convention, the strength of the magnetic fabric is measured using the corrected anisotropy degree P_j :

$$P_j = \ exp\sqrt{\{2\ [(\eta_1 - \eta_m)^2 + \ (\eta_2 - \eta_m)^2 + \ (\eta_3 - \eta_m)^2]\}} \tag{2.5}$$

Where:

η_1 = InK_1, η_2 = InK_2, η_3 = InK_3, and $\eta_m = (\eta_1 + \eta_2 + \eta_3)/3$ (Jelinek, 1981).

The shape of the susceptibility ellipsoid is described using lineation (L), foliation (F), and shape (T) parameters which are calculated using the ratios or differences between two or more of the principal susceptibility axes (Tarling and Hrouda, 1993). Lineation is defined by the K_1 axis with $L = K_1/K_2$, although the normalized lineation and foliation parameters of Khan (1962) are commonly used (for example, Fleming *et al*., 2013), whereby:

$$L = \frac{K_1 - K_2}{K_{mean}} \tag{2.6}$$

and:

$$F = \frac{K_2 + K_3}{K_{mean}}$$

(2.7)

The shape factor *T* is given by Jelinek (1981) as:

$$T = \left[\frac{2In\frac{K_2}{K_3}}{In\frac{K_1}{K_3}}\right] - 1$$

(2.8)

where:
$0 < T \leq 1$ defines oblate fabrics shapes (disc-shaped),
$-1 \leq T < 0$ defines prolate fabric shapes (rods),
and $T \approx 0$ defines neutral or triaxial shapes.

To sample the AMS fabric of an area of rock or sediment a number of sub-samples (typically 8-12cm^3) are taken. The AMS of each sub-sample can be thought of as an ellipsoid for which *Pj* and *T* parameters can be calculated. By convention, the orientations of the principal susceptibility axes of the sub-samples are displayed on a lower hemisphere equal-area stereonet which enables the fabric shape of the bulk sample to be seen (this is the bulk susceptibility ellipsoid). Strongly oblate fabrics are produced in subaqueous environments such as still water lakes where gravity settling causes platy magnetic minerals to align parallel to the depositional surface (Tarling and Hrouda, 1993). Where bottom currents occur, the long-axis of grains can be preferentially aligned and this produces flow-parallel lineations in magnetic fabrics (Rees and Woodall, 1975). Lineations may also be produced by post-depositional strain that causes grains to rotate and align with their long-axes parallel to the shear direction and their short-axes perpendicular to the shear plane (Schwer and Tauxe, 2003).

Recently, Iverson *et al*. (2008) and Thomason and Iverson (2009) have used magnetic fabrics to test the deforming-bed model by investigating the relation between fabric development and strain magnitude. In a series of ring-shear experiments using re-moulded subglacial tills, including one from the forefield of Storglaciären (although the location and depth of sample were not specified), subglacial tills were sheared to various strains and the resultant clast-fabrics and magnetic fabrics measured. Their experiments showed that strong, steady-state clast-fabrics (S_1 0.78-0.87) were attained at low to medium strains (7 – 30) by March-type clast rotation, in which clast long-axes rotate and become tightly clustered parallel to the shear direction and then act as passive markers as smaller grains slip over their surfaces. No weakening of the macro-fabric occurred at higher strains. Strong, steady-state magnetic fabrics, with K_1 tightly clustered in the direction of shear, were also attained at low to medium strains, suggesting that any subglacial till with a weak magnetic fabric has not been sheared to the very high strains required by the deforming-bed model (unless the magnetic fabric had been weakened by post-depositional disturbance, or there had been a strong element of pure shear involved in the deformation process). The relation between fabric development and strain was independent of till grain-size, and thermomagnetic and hysteresis experiments showed that magnetic fabrics in the Storglaciären till were controlled by silt-sized particles of magnetite.

Iverson *et al*. (2008) argued that sub-sample ellipsoids could be thought of as 'clasts', with their K_1 orientations analogous to clast long-axis orientations. As such, the sub-sample K_1 values were used to compute eigenvectors and eigenvalues for bulk samples. Eigenvalues were used to assess magnetic fabric strength, and Benn's (1994) isotropy and elongation indices were used in triangular diagrams to assess the change in magnetic fabric shape with increasing strain. Scattergraphs were also constructed to show the relation between the principal eigenvalue S_1 (attained from the K_1values) and strain. Although this is not a conventional way of analysing AMS data (Fleming, *pers.comm*.2012), it does enable eigenvectors and eigenvalues obtained from magnetic fabrics measured in this study to be compared to the values obtained in the ring-shear experiments of Iverson *et al*. (2008), and for estimates of strain magnitude in glacigenic sediments in the Tarfala Valley to be derived from their ternary diagrams and scattergraphs.

The conventional method for taking AMS sub-samples in soft-sediments is to press 2cm-sided cubes into sediment faces (Thomason and Iverson, 2009); some deformation of the sample is possible with this method (Fleming, *pers.comm*.2011). An alternative approach which avoids these sampling issues is to extract sub-samples from larger block samples which have been air dried and hardened by being impregnated with a non-magnetic epoxy resin, that is, from samples prepared for thin section analysis (Fleming *et al*., 2013). In this study, AMS sub-samples were extracted from the hardened resin blocks obtained from the orientated micromorphology samples taken from fluted moraine and diamicton plain sections. Between fifteen and twenty 2cm-sided cubes (the sub-samples) were cut from each resin block using a diamond-edge saw. The magnetic anisotropy and susceptibility of each sub-sample were measured at University of Birmingham, England, using KLY-3 Kappabridge operating at 300 Am^{-1} and 875 Hz. A total of 122 sub-samples were collected from 7 micromorphology samples taken from the Isfallsglaciären fluted moraine; 57 sub-samples were extracted from different depths in the same pit (pit MMT3, Figure 3.2) where detailed clast-fabrics were also taken to examine changes in fabric strength over small vertical intervals and to assess the effects of paraglacial activity on magnetic/clast-fabric development. Five thin section samples were extracted at sites where graphic logs were recorded from the diamicton plain (Figure 3.1c) and, after resin impregnation, it proved possible to take magnetic fabrics from three of these. The highly fissile nature of the diamicton made it difficult to recover thin section samples, and after resin impregnation, the samples were observed to contain numerous fractures which made it difficult to cut cube samples. As such, two of the five samples were abandoned and only between 11 and 15 sub-samples (cubes) were able to be recovered from each of the other three.

Iverson *et al*. (2008) argued that magnetic fabric is a better indicator of cumulative strain than clast-fabric. The reason for this is that magnetic fabrics measure a 'bulk' volume of sediment rather than individual grains. However, it should be borne in mind that in a pit where the flute is say 100cm wide and 50cm deep (cross-sectional area = 5000cm^2), a sample size of fifty-seven 4cm^2 AMS sub-samples only represents 4.6% of the cross-sectional area, whereas 4 clast-fabrics, taken at 10cm vertical intervals and each covering an area of 25 by10cm, represents a sample covering 20% of the cross-sectional area. Magnetic fabrics depend on what happens to the silt-sized (and smaller) magnetite grains and these may have a very different strain response to larger gravel-sized clasts (Evans *et al*., 2006). As such, both types of fabric have the potential to provide valuable insights into bed-deformation processes (Boulton, 1976).

Hooyer *et al*. (2008) argued that the resolution of clast-fabric sampling intervals can be too coarse to detect important changes in strain signature, especially in tills with low gravel contents, which is one reason why magnetic fabrics are preferred, as they sample fabrics from a bulk volume at higher resolutions. Sand micro-fabrics can be taken at even higher resolutions than magnetic fabrics, but sand micro-fabric evolution does not show such a progressive response to increasing strain magnitude as magnetic fabrics in ring shear experiments (Thomason and Iverson, 2006). Indeed, most of the re-orientation of sand particles towards a steady-state fabric occurs at strains as low as 5-10, and for this reason, magnetic fabrics are thought to give the best estimation of shear strain magnitude (Iverson *et al*., 2008). However, macro-fabrics may not be as susceptible as magnetic fabrics to post-depositional disturbance or disruption by initial soil forming processes, such as silt translocation. Ideally, magnetic fabrics would be taken from subglacial flutes, or from flutes emerging at the glacier margin, so as to minimize post-depositional disturbances to fabrics. Unfortunately, no such flutes currently occur at the ice margins of the three forefields. As such, a combination of clast fabrics, micro-fabrics, and magnetic fabrics were taken not only to provide fabric resolutions at different scales, but to see if the different types of fabrics told a consistent story with regards to strain magnitudes.

In their field studies of the Douglas till, Shumway and Iverson (2009) measured vertical changes in AMS fabrics over 0.2m depth intervals using between 25 and 50 sub-samples to represent each interval. In the ring shear experiments and the field study of the Douglas till, sub-samples were collected using 1.6-1.8cm sided cubes, giving total volumes of 102 – 145.8cm^3 per bulk sample when 25 sub-samples were collected (Iverson *et al*., 2008). In the present study, the tins used to collect samples were used in landscape or portrait orientation depending on the purpose of the sample and, depending on the orientation of the tin, sediment could be sampled over 0.15-0.18m or 0.08-0.1m depth intervals, similar to or about half the depth interval sampled by Shumway and Iverson (2009). In general, between 15 and 20 sub-samples, consisting of 2cm sided cubes (volume 8cm^3) were cut from the resin blocks, giving a total bulk volume per sample of 120-160cm^3, which compares favourably with the volumes used in ring shear experiments (Iverson *et al*., 2008). Figure 2.7 shows cut cubes with orientation data marked on them ready for AMS measurement.

A vertical sampling interval of 0.2m may not detect smaller scale changes in strain magnitude which may occur if strain is partitioned into the softer and more easily deformed diamicton matrix (Evans *et al*., 2006). As such, each AMS bulk sample in this study was further divided into an upper and lower vertical zone, each between 4 and 8cm thick, so as to examine changes in magnetic fabric at higher resolutions. Separating the sample into two vertical zones was also required in sample BYL where the sample was taken across the boundary of two lithofacies. Given the smaller number of sub-samples in each vertical zone (between 6 and 10, giving a total volume of 48 to 80cm^3), the results from these zones must be treated with caution as the statistical variance is likely to be very high. Hooyer *et al*. (2008) suggested AMS fabric readings require a minimum of 25 sub-samples of cubes having dimensions of 1.6-1.8cm along each side for statistical significance.

Figure 2.7 Cube of diamicton cut from resin block. Each side of the cube is 2cm long. The block has orientation data marked on the faces and is used in the kappa-bridge for Magnetic Fabric Measurements (Image courtesy of Mr E. Fleming).

AMS parameters are influenced by the mineralogical composition of diamicton, which may vary between sites (Hooyer *et al*., 2008). As such, if the experimental ring shear calibrations of Iverson *et al*. (2008) are to be used to estimate strain magnitude from AMS fabrics taken in the Tarfala Valley, it is important to demonstrate that the mineralogy of samples are similar to those used in the ring shear experiments. The dependence of bulk magnetic susceptibility on temperature allows thermo-magnetic experiments to be used to estimate the mineralogy controlling the AMS response (Fleming *et al*., 2013). When heated, paramagnetic minerals (e.g. chlorite) show a slight linear decrease in bulk magnetic susceptibility, following the Curie-Weiss law of paramagnetic minerals, whereas ferro-magnetic minerals (e.g. magnetite) give a steady susceptibility up to the Curie-point temperature (the point at which they lose magnetism), after which the bulk susceptibility falls (Tarling and Hrouda, 1993).

Dry samples of diamicton from the Isfallsglaciären flutes were used in temperature-dependent bulk susceptibility experiments to establish the mineralogy controlling bulk magnetic susceptibility. The thermo-magnetic experiments were conducted at the University of Birmingham. Samples were heated from room temperature (21°C) to 700°C and bulk susceptibility measured at 1-2°C intervals using an AGICO MFK-1A kappabridge with CS4 high temperature susceptibility attachment. The results (Chapter 4) indicate magnetite is the magnetic carrier and, as such, the Tarfala samples are comparable to the samples used in the ring shear experiments.

2.5 Laboratory Methods

2.5.1 Particle Grain-Size Distribution

A sediment's particle-grain size distribution (pgsd) reveals information about its origins, transport history, and mode of deposition (Hoey, 2004), and is a key property used to describe lithofacies and to aid lithofacies discrimination (Blott and Pye, 2001). In this study, particle grain-size distributions were measured for 50 samples taken from different lithofacies collected in Isfallsglaciären, 28 from Kaskasatjåkka, and 18 from Storglaciären. A trowel was used to remove each sample and approximately 1kg of freshly exposed sediment was sealed in a labelled sampling bag. Samples were oven dried at 105°C for 24 hours in the sediment laboratory at the Tarfala Research Station (as no samples contained any obvious organic matter, air drying was not required; Hoey, 2004). Each sample was then dry sieved for 15 minutes using a mechanical shaker and a sieve stack containing sieve meshes at half φ intervals in the 19mm to 2mm size-range. From the bottom retaining pan, 100g of sediment <2mm in size was removed and sealed in labelled bags and returned to the sediment laboratory at Loughborough University for further analysis. The sieving of the fraction >2mm was not done to estimate the pgsd of gravel (which would require a much larger sample size to be representative), but to collect 50 pebbles of comparable size from each sample for use in the assessment of particle morphology; clasts caught between the 8mm and 16mm sieves (-3 to -4φ) were used for this. The percentage gravel content of diamicton samples was estimated in the field over a 2m^2 area following the method of Etienne *et al*. (2003).

Dry-sieving is the standard method used to measure pgsd in the 4mm to 63μm size-range (Hoey, 2004). In the sediment laboratory at Loughborough University the 100g sediment samples were dry-sieved for 15 minutes using a mechanical shaker and a sieve stack containing sieve meshes at half φ intervals in the 2mm to 63µm size-range. The weight of sediment in each sieve was recorded in grams to two decimal places. Where the sample contained a lot of fines that could potentially clog the finer sieves, the quantity of sediment going through the stack was reduced by dividing the sample into two halves and sieving each half separately. The pgsd of the finest fraction (particles <63µm in size) was determined using a Coulter LS Series Laser Diffraction Particle Size Analyser. Initial experiments followed the procedures recommended by Swift (2002) in which particles were disaggregated and dispersed by mixing the fine fraction with a 5% aqueous Calgon solution and placing the solution in an ultra sonic bath for 3 minutes just before testing. However, this method produced an unacceptable number of air bubbles in the Coulter LS230 fluid module which could be detected as spikes on some pgsds. An alternative method was developed that gave reproducible results without bubble spikes and involved thoroughly mixing a dry sample of fines and adding 5 drops of 1% surfactant (Calgon) to aid dispersal. The sample was then mixed with 30ml of distilled water and a pipette used to place the solution in the fluid module. A minimum of 3 Laser Analyser runs were completed for each sample (with a run length of 60 seconds) to establish the percentage volume of sample in different channel diameter classes (the smallest channel diameter being 0.375µm) using a Fraunhofer optical model and an obscuration range between 5 and 8%. An average percentage volume of sediment in each channel diameter class was calculated for each sample.

In order to establish the full pgsd for each sample the (percentage volume) laser data and the (percentage weight) sieve data were merged together following the procedure recommended by Mason (2011). Laser analysers are known to over-estimate the percentage weight of sample in the size range > 1mm compared to dry sieving, so the Laser Analyser was used to establish the pgsd for everything smaller than 1mm in size, and the sieved data was used for everything $\geq$ 1mm in size (Mason, 2011). The data were merged by converting the percentage volume of sediment in each channel diameter class into a value representing the percentage weight of sample in specified φ size class as follows:

1. any laser data >1mm channel diameter size was ignored;
2. the percentage volume of sediment in each channel diameter class <1mm were re-calculated such that the sum of all classes <1mm = 100%;
3. channel diameter classes were converted into specified half φ classes (smallest 0.488µm = 11φ) using the interpolation function of the Coulter Laser Analyser;

4. percentage weight of sample in each half φ class <1mm = (weight in g of total sample fraction <1mm/100) x % volume in each half φ class.

Particle size-distribution data were analysed using Gradistat software version 12 (Blott and Pye, 2001), with statistical summaries based on the log-graphical methods introduced by Folk and Ward (1957). The log-graphical method is the most widely used method of calculating pgsd summary statistics and gives a better sorting value for poorly-sorted sediments (such as glacial tills) because it focuses on the central part of the data and ignores extreme values in the distribution tails, which could unduly affect summary statistics (Blott and Pye, 2001). In this study, particle grain-size classes follow the scheme introduced by Wentworth (1922).

2.5.2 Fractal Dimensions

Clast crushing may produce a fractal grain-size distribution which resembles that produced in fault gouge by tectonic shearing, in which:

$$N(d) = N_0 \left(\frac{d}{d_0}\right)^{-\mathrm{m}} \tag{2.9}$$

where:

N is the number of particles of diameter d,N_0 is the number of particles of reference size d_0,m is the fractal dimension, and $-m$ is the gradient of a straight line on a double logarithmic plot (Hooke and Iverson, 1995). Grain-crushing and abrasion increase the fraction of fines in a subglacial till as the till evolves; grain-crushing is most likely to occur where stress concentrations are at a maximum, which occurs where two grains of roughly equal size are in contact (Hiemstra and van der Meer, 1997). Crushing produces a cushion of finer particles around larger clasts and leads to a grain-size distribution which has a roughly equal-volume fraction of small and large clasts, that is, a fractal or self-similar distribution of grains (Cuffey and Paterson, 2010). In fault gouge, crushing was shown to produce a fractal grain-size distribution with a gradient of -2.65 (Sammis *et al*., 1987). Hooke and Iverson (1995) found that subglacial tills tended towards a fractal grain-size distribution, with average slopes of -2.92 (+/- 0.17). Hooke and Iverson argued that the greater slope value in subglacial tills compared to fault gouge was explained by subglacial abrasion, which produced an excess of fines relative to the particle grain-size distribution in gouge, which was produced by crushing alone. Furthermore, fractal dimensions might be used to discriminate between tills of different origins (Hooke and Iverson, 1995).

Fractal distributions with similar slopes to those reported by Hooke and Iverson occur in debris flow deposits and can be produced by the mixing of distinct populations of sorted sediments, and so fractal dimensions are not diagnostic of genetic modes (Benn and Gemmell, 2002). In addition, deformation till may be produced by cannibalising local sediments, and so fractal dimensions may be inherited from the underlying substrate, rather than produced by a combination of subglacial crushing and abrasion (Benn and Evans, 2010). Conversely, Etienne *et al*. (2003) argued that fractal dimensions can be used to discriminate between lithofacies at Storglaciären, with subglacial deformation till having a quasi-fractal particle grain-size distribution with a slope of -2.91, which they argued is very distinct and very different from other forefield lithofacies. As such, fractal dimensions were calculated in this study to see if they aid in the identification of lithofacies and to compare the relative contributions of crushing and abrasion to diamicton production.

2.5.3 Clast Morphology

The 50 clasts taken from the 16mm to 8mm sieves were used to assess the clast morphology of diamicton and gravel deposits. Lukas *et al*. (2010) argued that clast roundness should be assessed using 50 clasts of the same lithology, as lithology influences clast shape; conversely, Bennett *et al*. (1997) found lithology had no influence on clast shape. In this study, most clasts were of mafic rocks (dolerite and amphibolite) and relatively fewer clasts were of meta-sediments or gneiss. As such, clast roundness was assessed using the Powers' scale (Powers, 1953) using 50 mafic rock clasts. Clast shape was assessed using Sneed and Folk (1958) shape classes; the long, intermediate and short axes (a, b, and c) of 50 clasts were measured using digital callipers and the data were plotted on Sneed and Folk triangular diagrams using Triplot software (Graham and Midgley, 2000). Sneed and Folk triangular plots quantitatively define ten shape classes, with blocks, rods and discs forming the apexes of the triangular graph, and the plots are scaled using the c:a and b:a axial ratios and the disc-rod index (a-b)/(a-c) (Benn, 2004). Clast shape influences the ease with which clasts can be entrained during transport, with disc-shaped clasts the most easily entrained (Graham and Midgley, 2000).

By combining a roundness index (RA = percentage of angular or very angular clasts) with a shape index (C_{40} = the percentage of clasts with an c:a ratio ≤0.4) on a bivariate scattergraph, Benn and Ballantyne (1994) were able to distinguish between sediments that had been transported actively in a subglacial environment, and those that had been transported passively in englacial or supraglacial environments. Subglacially transported sediments are typically blocky in shape and sub-angular to sub-round because both clast fracture and clast abrasion occur during active transport (Benn, 1994; 1995; Kruger and Kjær, 1999). In addition, Lukas *et al*. (2010) found that a roundness index based on the percentage of rounded and well-rounded round clasts plotted against the C_{40} index allowed fluvial sediments to be discriminated from subglacial sediments. In this study, bivariate scattergraphs are plotted for roundness indices and the C_{40} index to aid identification of lithofacies.

Insights into the nature of subglacial processes can also be gleaned from clast wear patterns (Olsen, 1983; Benn, 1994; 1995). Wear patterns on embedded boulders in fluted moraine and diamicton plain deposits were recorded in the field (this included striae patterns and directions and the presence of chattermarks and crescentric gouges), and for the 50 clasts used in the assessment of roundness, the number of facets and the crushing index were recorded. The crushing index was first developed by Olsen (1983) and was defined as the percentage of round and well rounded clasts in a sample which had breakage zones with sharp edges, with at least one zone >5% of the clast area. As many processes can cause clasts to be crushed, the crushing index should be considered a guide to the relative intensity of strain experienced by sediments (Piotrowski *et al*., 2006). In this study, the clast size range examined did not yield many well-rounded clasts, and so a modified crushing index was used, defined as the percentage of sub-round to round clasts with breakage zones or sharp edges. This index cannot be compared to other studies, but it does provide a relative contrast in crushing intensity between different lithofacies in the Tarfala Valley.

2.5.4 Geotechnical Properties

The geotechnical properties of sediments include their porosity, void ratio, and shear strength. Variations in these physical properties impart an important control on sediment response to subglacial shear stress and the nature of subglacial deformation - for example, porosity and void ratio can influence subglacial drainage conditions and pore-water pressures (Paterson, 1994; Piotrowski *et al*., 2004). Porosity and void ratio were measured at various sites where graphic logs were taken so as to estimate the state of sediment dilatancy and to compare the porosities of different subglacial sediments. Laboratory shear strength tests were carried out using a shear box to ascertain the shear stress required to deform subglacial diamictons and to investigate the influence of sediment granulometry and pore-water pressure on sediment deformation. Shear box tests allowed for estimates of sediment cohesive strength and frictional strength to be established, which provided additional information to the hand-held shear vane tests.

To assess variations in the void ratio and porosity in vertical sequences in fluted moraines and the diamicton plain/sheet, 27 small aluminium tubes were used to take 'core' samples (13 from the Isfallsglaciären fluted moraine, 6 from Kaskasatjåkka and 8 from the Storglaciären diamicton plain sections). These cores ranged in volume from 50 to 60cm^3 and porosity and void ratio were established using expressions (2.10 to 2.14) shown below (Kezdi, 1974). The cores were weighed and then sealed with cling film and Duck Tape and returned to the sediment laboratory at Loughborough University. In the laboratory, one end of the tube was sealed with wax and water was slowly added to the core over a period of several days until the sediment became saturated. The core was re-weighed to give the saturated weight of the sediment (w_s) and the wet density (γb) calculated (γb (gcm^3) = w_s/volume). Samples were then completely dried in an oven at 105°C for 24 hours and re-weighed to give the dry weight of the sediment (w_d) and to establish the moisture loss m_l(m_l= $w_s - w_d$). The moisture content M (%) was given by:

$$M = \frac{m_l}{w_d} \times 100 \tag{2.10}$$

And the bulk density *γd:*

$$\gamma d = \frac{\gamma b}{1 + \frac{M}{100}} \tag{2.11}$$

Using these data the specific gravity G of the sample (similar to particle density) was established:

$$G = \frac{w_d}{(w + w_d) - w_s} \tag{2.12}$$

Where w is the weight the sampled volume would be if the volume were occupied entirely by water. The void ratio (e) is given by:

$$e = \left(\frac{G \times \gamma_w}{\gamma_d}\right) - 1 \tag{2.13}$$

Where γ_w is the density of water. From this, porosity (%) is given by:

$$N = \frac{e}{1 + e} \times 100 \tag{2.14}$$

Specific gravity ranged between 2.9 for samples from Storglaciären up to 3.2 for samples from Isfallsglaciären (dolerite typically has a density of 2.9-3.1 gcm^{-3}).

In addition to the small tube samples, a larger sample was taken from one flute in each forefield (from 0.25 to 0.3m depth below flute crests) and one sample from the Storglaciären diamicton plain (0.7m depth). Samples were collected by taking a 'core' of known volume using sections of 3mm thick plastic drain pipe which ranged in size from 76 by 26mm to 62 by 24mm. The plastic pipe cores had a bevelled leading edge to aid 'coring' into the sediment. Samples were sealed with cling film and Duck Tape to prevent moisture loss and returned to the Tarfala Sediment Laboratory where they were weighed, dried at 105°C for 24 hours, and the bulk density (BD) established (BD (gcm^3) = dry weight of sample/volume) and the moisture loss at 'field conditions' calculated (initial weight – dry weight). In these samples, porosity (%) was estimated using the following expression:

$$N = 1 - \frac{BD}{Pd} \times 100$$

(2.15)

Where Pd is the particle density (Craig, 1996). Particle density was estimated to be between 2.9 and 3.2 gcm^3.

The total undrained shear strength (KPa) was calculated for each plastic tube sample using shear box tests conducted at the department of Civil Engineering at Loughborough University. The tests followed the procedures for 100 by 100mm shear box tests stipulated in the British Standard (BS 1377-7) for Civil Engineering Tests. Shear box tests are suitable for free draining granular materials and measure the relative displacement and applied force along a pre-define failure plane (Head, 1982). The procedure involved removing clasts that exceeded 6mm diameter (the maximum clast size that can be used in a shear box of this size) and remoulding each sample by thoroughly mixing it. Known volumes of water were then added to each sample and the samples tamped into the shear box to the required density. Shear box tests were conducted at three normal loads (50, 80, and 130 KPa) using a cog speed of 1.2mm of horizontal displacement per minute. The force resisting displacement (the shear strength) was measured at every 0.5mm of horizontal displacement using a calibrated load ring, where shear strength τ was calculated from:

$$\tau = \frac{C_r \times R}{L^2}$$

(2.16)

Where C_r is the load ring calibration in N per division, R is the number of recorded divisions, and L is the length of the shear box in mm (Head, 1982). Shear box tests measure the angle of shear resistance and shear strength increases with force up to the point of failure, known as the peak shear strength (Head, 1982). The linear relationship between peak shear strength and normal load is plotted as a graph which defines the Coulomb failure envelope; apparent cohesion (the shear strength when normal load = 0) does not change with increasing normal load but the friction angle of shear resistance (the internal angle of friction) does. The friction angle is given by the inclination of the best fit line to the horizontal axis and the apparent cohesion is given by the intercept on the vertical axis (Head, 1982). Shear box tests were conducted using a range of moisture contents (from dry sediments to field conditions to 10% moisture content) and sediment densities (from field conditions to more consolidated samples). The coarse fraction (>6mm diameter) removed from the samples represented 11% of the total weight for the Storglaciären samples, 13% of the Isfallsglaciären sample, and 22.5% of the Kaskasatjåkka sample. Sladen and Wrigley (1983) suggested that gravel contents of less than about 40% have little effect on the shear strength of matrix dominated tills. Gravel comprised 17-23% of the Storglaciären samples by weight, 23% of the Isfallsglaciären sample, and 41% of the Kaskasatjåkka sample.

Finally, the hydraulic conductivity k (ms^{-1}) was estimated using the Hazen formula (Head, 1982):

$$k = C_1(D_{10})^2 \times 10^{-4} \tag{2.17}$$

Where: D_{10} is the effective grain size and represents the upper diameter of the finest 10% of the sample by weight (the assumption being that the hydraulic conductivity is controlled by the size and amount of fines in the sample), and C_1 is an empirical value ranging from 16 to 100, meaning k values range by factors of 6. Calculation of k using the Hazen formula with $C_1 = 100$ gave a value for the diamicton sampled from the upper section of the Storglaciären diamicton plain that was close to Baker and Hooyer's (1996) k value for the same sediment, which was calculated in laboratory tests using a falling head permeameter (Baker and Hooyer's values = 2.1 to 2.4×10^{-7}; using the Hazen formula in this study gave a value of 2.49×10^{-7}). As such, the Hazen formula with $C_1 = 100$ was used as a quick way to estimate k values in this study.

Chapter 3 Lithofacies-Landform Associations in the Tarfala Valley

3.1 Introduction

The aim of this Chapter is to compare the lithofacies-landform associations of each forefield so that the thickness, lateral extent, and nature of subglacial sediments can be established. Etienne *et al*. (2003) identified six lithofacies and seven lithofacies-landform associations at Storglaciären and this chapter builds on their study. What is new here is that the lithofacies of fluted moraines in each forefield and the diamicton plain (Storglaciären) and diamicton sheet (Kaskasatjåkka) are compared, and the lithofacies-landform associations of Isfallsglaciären and Kaskasatjåkka are described in detail for the first time. Figure 3.1 shows the sites investigated. In addition, multiple diamictons are observed in each forefield and three additional lithofacies-landform associations are identified (beyond those recognised by Etienne *et al*., 2003).The focus of this chapter is on using macro-scale observations and measurements of the glacigenic properties of sediments to characterise the nature of the subglacial environment and to establish the nature and extent of subglacial deformation. As such, particular emphasis is given to the analysis of sediments from fluted moraine and the diamicton plain/sheet, which are thought to represent the former subglacial bed (Eklund and Hart, 1996; Etienne *et al*., 2003).

The first section of this Chapter (3.2) summarises and justifies the codes used to denote each distinct diamicton. The main properties of each diamicton are then described, followed by a genetic interpretation and consideration of the role of bed-deformation in its formation (Sections 3.3-3.6). Section 3.3 includes a description of the contact between subglacial diamicton and a sequence of sand layers in the Frontsjön area of Isfallsglaciären (Figure 3.1). This was an important area of investigation as it was the only location where the sand sequence was observed and the nature of the contact gave important insights into the origin of the diamicton. Other forefield lithofacies are then described (Section 3.7). This is followed by a description of the main landforms and lithofacies-landform associations in section 3.8, which includes a description and interpretation of the radar facies identified in fluted moraine. The geomorphology and main features of each forefield are summarised in Figure 3.2.

Comment [DJG1]: I think this introduction was too detailed and will duplicate information from later iin the chapter. Feel free to undelete if you disagree.

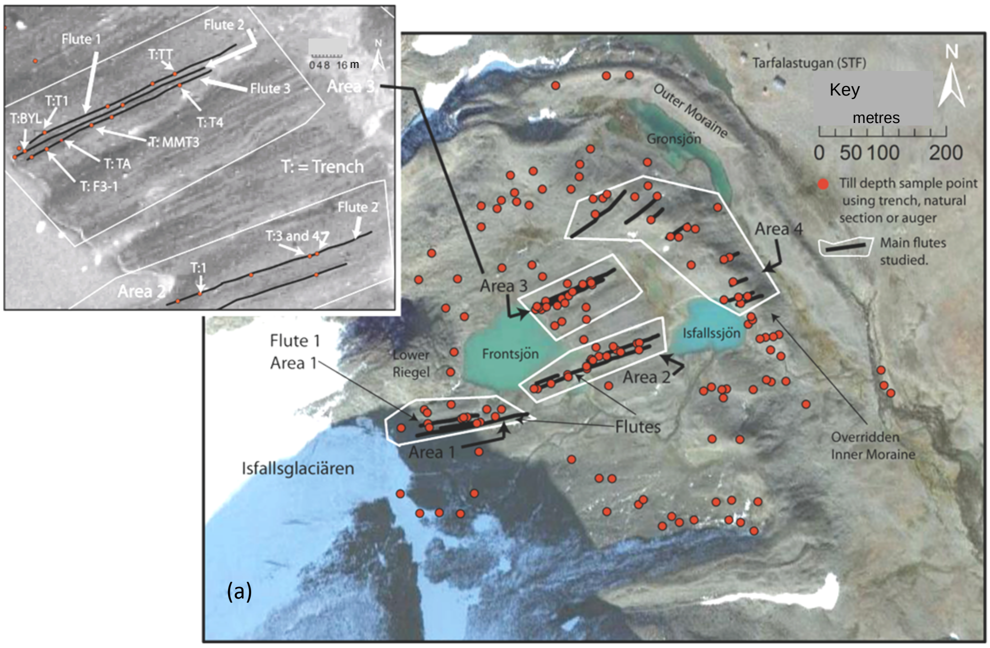

Flute 1
Flute 2
Flute 3
T:TT
T:T1
T:BYL
T:T4
T: MMT3
T: TA
T: F3-1
T: = Trench
Area 3
Area 2
T:3 and 4
T:1
Tarfalastugan (STF)
Key
metres
0 50 100 200
Till depth sample point using trench, natural section or auger
Main flutes studied.
Outer Moraine
Gronsjön
Area 4
Area 3
Area 2
Area 1
Flute 1
Area 1
Lower Riegel
Frontsjön
Isfallssjön
Flutes
Overridden Inner Moraine
Isfallsglaciären
(a)

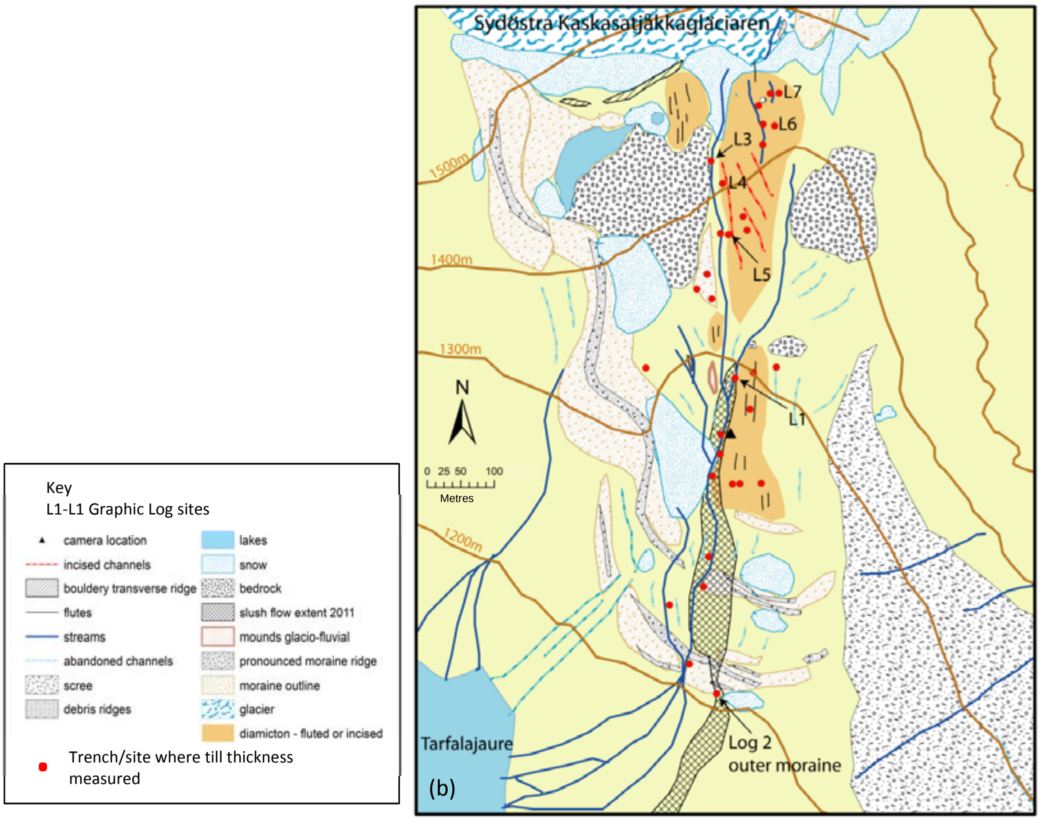

Key
L1-L1 Graphic Log sites
camera location
incised channels
bouldery transverse ridge
flutes
streams
abandoned channels
scree
debris ridges
lakes
snow
bedrock
slush flow extent 2011
mounds glacio-fluvial
pronounced moraine ridge
moraine outline
glacier
diamicton - fluted or incised
Trench/site where till thickness measured
Sydöstra Kaskasatjåkkaglaciären
L7
L6
L3
L4
L5
L1
1500m
1400m
1300m
1200m
N
0 25 50 100
Metres
Tarfalajaure
Log 2
outer moraine
(b)

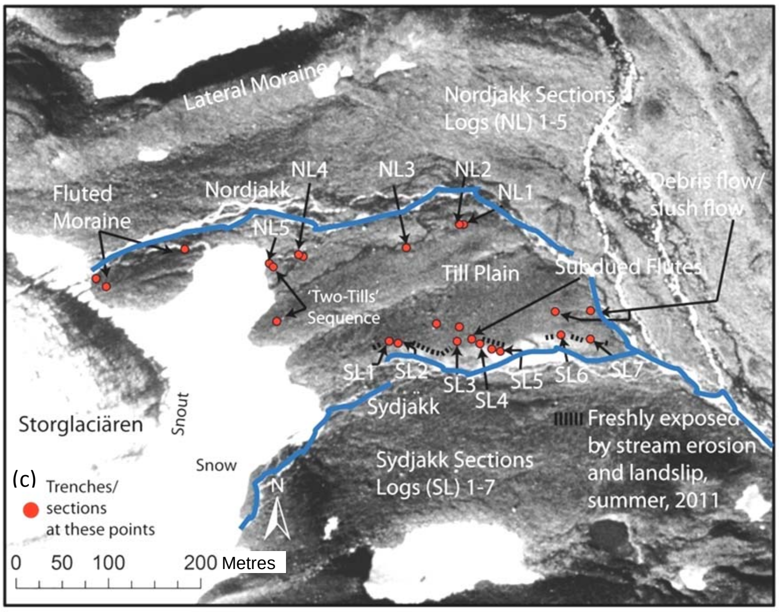

Figure 3.1 Study Sites (a) Isfallsglaciären (b) Kaskasatjåkka (c) Storglaciären. Note: the red dotes signify sites where pits, trenches or an auger where used to ascertain Dm thickness. 'L' denotes a site where a graphic log was taken, 'T' a trench.

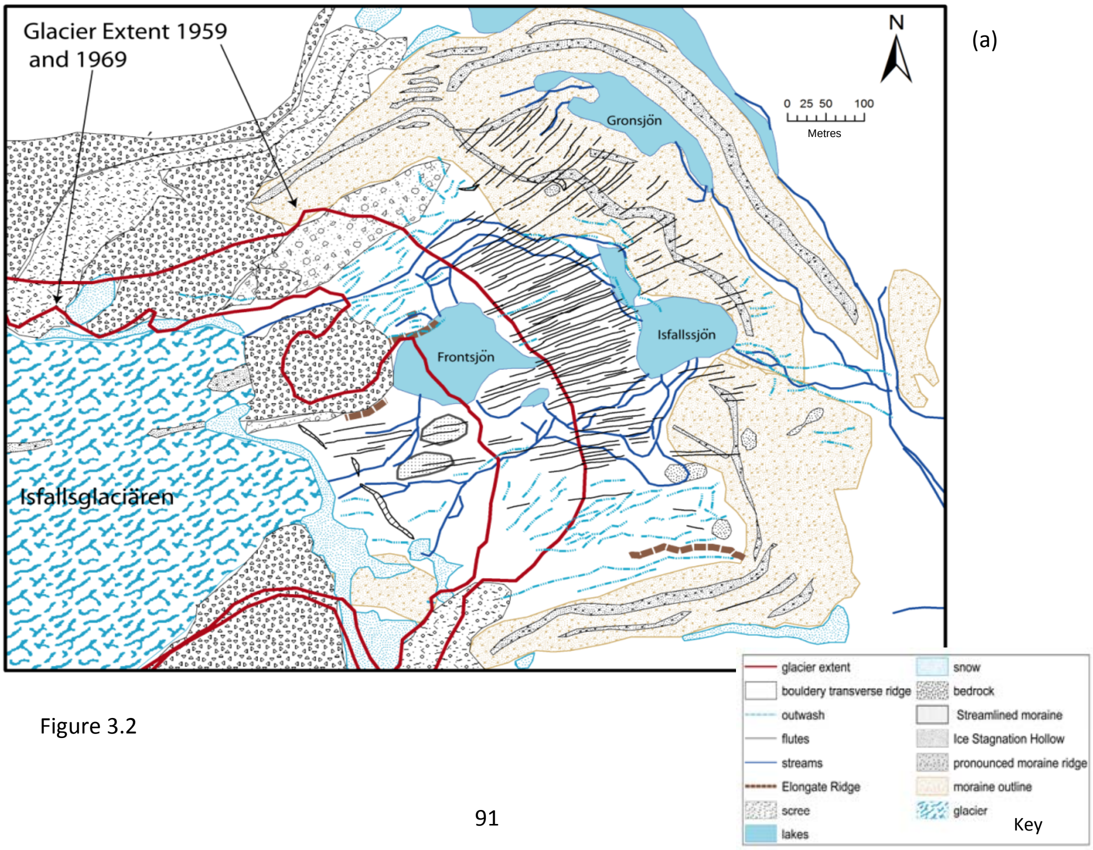

Figure 3.2

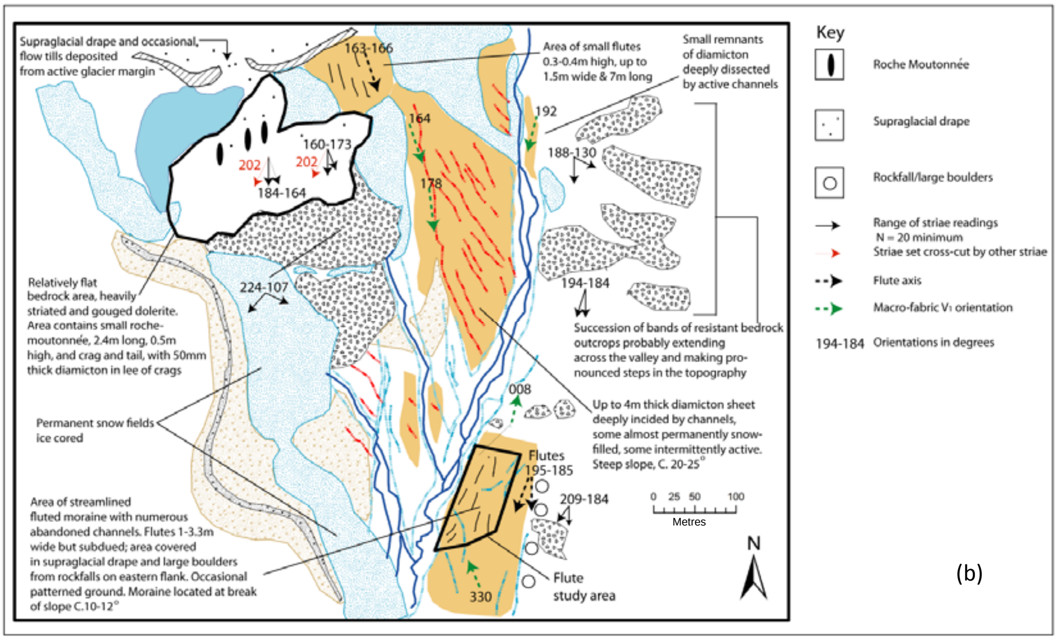

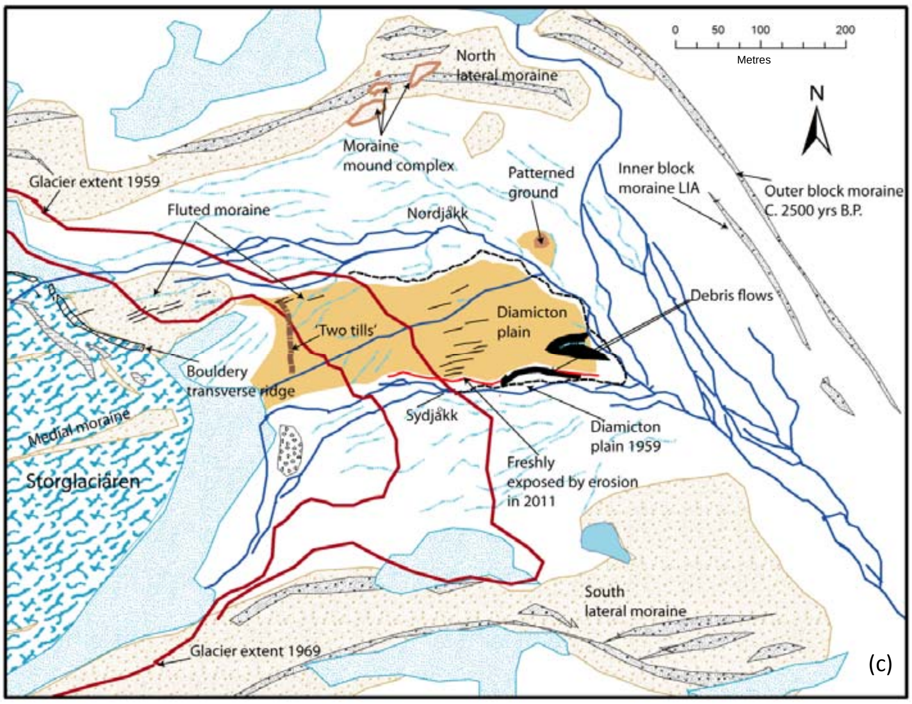

Figure 3.2 The Main Features and Geomorphology (a) Isfallsglaciären (b) Kaskasatjåkka (c) Storglaciären. The maps are based on aerial images such as the 2001 images shown in Figures 3.1 a & c and field observations.

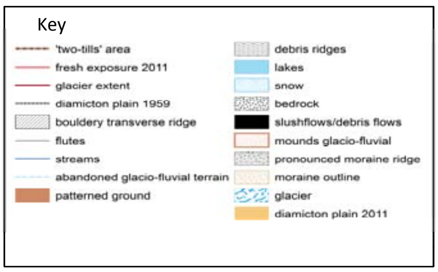

3.2 Diamicton and Diamicton Codes

Flint et al. (1960) first proposed the term diamicton to describe poorly sorted or non-sorted unlithified terrigenous sediments that displayed a wide-range of particle sizes, usually consisting of gravel in a sand or mud matrix. The term was non-genetic and applied to sediments of glacigenic and non-glacial origin (Hambrey, 1994). The term has since become widely-used in studies of glacigenic sediment sequences, (Eyles *et al*., 1983; Hambrey, 1994; Bennet and Glasser, 1996; Kruger and Kjaer, 1999; Benn and Evans, 2010), although different researchers have applied the term in different ways. Eyles *et al*. (1983) introduced a process-orientated approach to the description *and* interpretation of diamictons which used a coding system based on four symbols to describe and genetically interpret glacigenic sediment sequences. A distinction was made between matrix-supported and clast-supported diamictons. This genetic approach was criticised by Dreimanis (1984) because the coding system was too narrow to reflect the range of glacial diamictons, and because interpretation required additional information such as clast shape, size and orientation, which were not covered by the codes. Hambrey (1994) used the term descriptively and classified diamictons using a scheme adapted from Moncrieff (1989) for classifying poorly sorted sediments and sedimentary rocks. The classification involved quantifying the textural characteristics of diamictons, such that a distinction was made between clast-poor diamictons (<5% gravel) and clast-rich diamicton (>5% and up to 50% gravel), and between muddy and sandy diamictons based on matrix content. Clast-supported diamictons were considered a misnomer because the term implied high gravel content and consequently at least a moderate degree of sorting. Krüger and Kjaer (1999) and Benn and Evans (2010) have introduced lithofacies coding systems to describe diamictons and to genetically interpret glacigenic sediment sequences and these systems are based on the description of a much wider-range of elements than used by Eyles *et al*. (1983).

The objective description of lithofacies should preceed genetic classification (Hambrey, 1994), and so in the present study the term diamicton is used in its original sense to *describe* poorly sorted sediments. The genetic interpretation of lithofacies is arrived at only after detailed description has been presented. The coding system introduced by Krüger and Kjaer (1999) for glacigenic sediments was used in the field. The justification for using this system is that it aids the detailed and systematic observation of sediment sequences whilst the coding system aids the rapid recording of field data (Chapter 2.3.2). In this scheme, diamictons are described as clast-poor or clast-rich (based on a visual estimate of gravel content), matrix-supported (clasts dispered in a finer-grained matrix) or clast-spported (larger clasts in contact with each other forming a clast-supported framework with finer-grained material filling in the spaces between clasts), coarse-grained (sandy-gravelly), medium-grained (silty-sandy) or fine-grained (silty) depending on the dominant matrix content (Krüger and Kjaer, 1999). These descriptive terms are widely-used in a non-quantified way (cf. Hambrey, 1994) to describe diamictons (Eyles *et al*., 1983; Bennett and Glasser, 1996; Krüger and Kjaer, 1999; Evans and Benn, 2004; Benn and Evans, 2010). Clast-supported diamictons are rare in glacial sediments, although they can occur in mountainous environments (Dreimanis, 1984), which justifies using the term in the present study. Moreover, a clast-supported diamicton still contains some matrix and so it is likely to be relatively poorly sorted, and so the term diamicton is still apllicable. Lastly, as noted by Krüger and Kjaer (1999), diamicton layers can vary in gravel content over small scales, switching from being clast-supported to matrix supported, and any accurate description and coding system should reflect this.

The multiple diamictons observed in each forefield display similarities which enable them to be grouped into four main lithofacies (A-D). The four main diamictons identified are distinct and can be distinguished by their physical characteristics (Table 3.1). All diamictons have matrix particle-grain sizes that are very poorly sorted and polymodal or bimodal (Figure 3.3), and contain similar lithologies, with gravel content ranging in size from granules to boulders. Estimates of gravel conent (Chapter 2.5.1) are shown in Table 3.1. Diamicton codes are summarised in Table 3.2. Lithofacies A is a sandy diamicton that comprises the flutes of Isfallsglaciären. It also occurs in the main fluted areas of Kaskasatjåkka and Storglaciären (Figure 3.2b&c). Lithofacies B is a distinct silty, matrix-supported and highly fissile grey diamicton that forms the upper diamicton in the diamicton plain (Storglaciären) and diamicton sheet (Kaskasatjåkka). Lithofacies C is a clast-rich diamicton that is absent from Storglaciären. At Isfallsglaciären, it is restricted to the proximal parts of some flutes where it forms the substrate to Lithofacies A. At Kaskasatjåkka, Lithofacies C is occasionally observed to form the substrate to Lithofacies B in the diamicton sheet. In addition, a distinctive brown coloured version of Lithofacies C occurs widely across the lower forefield, where it forms the substrate to Lithofacies A. Lithofacies D is a very distinctive clast-rich and and coarse-grained diamicton that generally contains a high proportion of angular clasts and many very heavily weathered clasts. It has limited distribution, but where it occurs it forms the substrate to other diamicton facies in each forefield.

Table 3.1 The Distinguishing Characteristics of Diamictons in the Three Forefields. Note: I, S and K stand for Isfallsglaciären, Storglaciären, and Kaskasatjåkka. SD is the standard deviation. FSG is the fractal slope gradient. Facies = lithofacies. CI = Crushing Index. SR/SA = sub-round, sub-angular. PGSD = particle-grain size distribution. All diamictons have matrix pgsds that are polymodal or bimodal, and are very poorly sorted.

	colour	Pgsd (matrix)	Gravel content	a-axis clast fabric	Fissile texture	Roundness And C_{40}/RA Index (%)	Boulders	Weathering	Nature of contacts (u upper; l lower)	Other
Litho-facies A Flutes I, K, S	Grey to olive green (I) to brown- to charcoal grey (K/S)	Sandy with about 1/5th silt, <5% clay. Sandy Dm (snady-gravelly in some interflutes)	Clast-rich. (I) 20-35% gravel, but up to 40% in patches & in inter-flutes; (K/S) 35-50% gravel, quite stony in patches, with clast clusters and stone lines common. Granules to boulders	Flutes, strong and flow – parallel, elongate shapes, low isotropy (see Chapter 4). Interflutes, more variable	Strong, many planes of varying lengths	Low, SR-SA blocky clast shapes Mean (N = 12) C_{40} 15.8 SD 5.5 Mean RA 10.1 SD 6.9	Numerous, S&L and DS&L forms common, a-axis typically flow parallel or oblique	Relatively fresh look to clasts and matrix	Forms upper surface. L mostly sharp and wavy	Average mean FSG -2.9, but variable (see text). Typical thickness 0.3-0.5m
Litho-facies Bi S, K	Grey to light grey	Variable (S), but mean similar to Lithofacies A (S) Sandy Dm	Clast rich, (ca. 30% gravel) but less stony than Lithofacies A	Weaker than Lithofacies A and Bii, less elongate shapes, although V_1 similar orientations to Lithofacies B (Table 3.8&9)	Varies, Strong to weak	Higher C_{40}/RA than Lithofacies A and higher RA than Bii. Mean (S, N = 5) C_{40} 24.7, SD 7.3 RA 22.2, SD 3.6 Mean (K, N = 3) C_{40} 26.3, SD 1.6 RA 23, SD 3	Common, especially towards surface and on surface, where shapes variable	Relatively fresh	Forms upper surface. L Merges into Lithofacies Bii. Maybe the same Dm. Clast fabric/texture changes after 0.3-0.5m depth	Average FSG (S) lower than Lithofacies A/Bii (-2.81), but variable. Lower CI than Lithofacies A (Fig. 3.5)
Litho-facies Bii S, K	Grey	More silt and clay than Lithofacies A/Bi (S) 35% silt, 8% clay. Silty Dm to sandy Dm	Clast-rich (30-35% gravel), clast clusters common. Clasts often form lines which dip up-glacier at 6-20°. Granules to boulders	Stronger, more elongate than Lithofacies Bi (K and S, Nord. sections). V_1 orientations generally flow-parallel. More variable in Sydjåkk sections. (Fig. 3.9b & 3.29, Table 3.8)	Very Strong. Many Planes of varying lengths	Lower mean RA index than Lithofacies Bi. Similar to Lithofacies A (K). Higher RA than Lithofacies A (S). Mean (S, N = 7) C_{40} 23, SD 5.2 RA 16, SD 2.1 Mean (K, N = 5) C_{40} 20.8, SD 5.6 RA 14, SD 3.1	Numerous, wear marks similar to Lithofacies A. Some boulders have striae on multiple faces	Some badly weathered clasts with orange to rusty weathering halos. Some fractured clasts with broken pieces in situ	U merging (S) L sharp contact with sandy gravel(S) or Lithofacies D (K)	Average FSG higher than Lithofacies Bi and as for Lithofacies A (-2.9). Lower CI than Lithofacies A.
Litho-facies C_I	grey	Similar to Lithofacies A	Clast-rich (45-50% gravel). Coarse Dm,	Similar to Lithofacies A, generally strong,	Weaker than	Slightly more A and a few VA clasts, but	Numerous lodged with a-	Some clasts badly weathered	U & L contacts sharp, wavy.	Mean thickness 0.3-0.4m. Mean

		(Fig.3.13) Sandy-gravelly Dm	Cobbles 120mm long common, very stony patches up to 70% gravel)	flow parallel to oblique, elongate shapes	Litho-facies A, Lower Parts Non-fissile	C_{40}/RA similar to Lithofacies A Mean (N = 5) C_{40} 24, SD 4 RA 12, SD 2	axis flow parallel, as for Lithofacies A		Upper contact with Lithofacies A often forms a boulder pavement	FSG lower than Lithofacies A -2.68
Litho-facies D_I	Grey-Brown to Sandy yellow, Less homo-geneous	Contains more fines than Lithofacies A/C_I(46.5% mud)(Fig. 3.13)	Very clast-rich (50-60% gravel) and coarse Dm. Many large boulders and cobbles. Gravelly Dm	More isotropic fabric shapes and weaker fabrics than Lithofacies A/C_I (Fig. 3.9a – see Chapter 4).	Absent	Higher RA/C_{40} index than Lithofacies A/C_I, (Fig. 3.6a) Mean (N = 5) C_{40} 26, SD 8 RA 31, SD 13	High no. of SR-SA tabular boulders, many with steep dips	Many badly weathered clasts, oxidised appearance to matrix	L unseen. U consists of sand and gravel layer separating Lithofacies D from C or A. Sharp wavy contact (Fig. 3.13)	Mean FSG -2.85, similar to fLithoacies A but higher than Lithofacies C_I. Lenses of sands and silty sands occur within Lithofacies D
Litho-facies D_S	Light brown to greyish, Less homo-geneous than Lithoacies A/B_S	Distinctive mode of very coarse sand (Fig. 3.3g), 63.5% sand, 36.5% mud. Sandy-gravelly Dm	Very clast-rich Dm (45 – 55% gravel), medium-grained, with many cobbles and occasional large boulders	Weaker fabrics, more isotropic shapes than Lithofacies Bii (Log NL5) and different V_1 orientation (Table 3.8)	Weak to absent	On average, blades and compact blades comprise 56% of samples (N = 4), so similar shapes to Lithofacies A, but higher RA index Mean (N = 4) C_{40} 18, SD 3.6 RA 43, SD 4.3	Less evidence of lodgement and a-axis alignment with flow	Many badly weathered clasts, often has rusted orange hue	In Log NL5 Lithofacies D separated from Bii by 0.1-0.2m of sands and gravels which coarsen up to sharp contact. L unseen	Lower mean FSG -2.81 than Lithofacies A
Litho-facies C_{brown}	Brown, with orange to yellow hues where badly weathe-red	Very coarse sand mode (Fig. 3.3s). Sandy-gravelly Dm	Generally more clast-rich than Lithofacies A_K and B_K, (50-55% gravel) very stony in parts (70% gravel), although variable. Coarse Dm, clast clusters and stone-lines common	Weaker than Lithofacies A and Bii,, less elongated shapes (Table 3.9)	Varied, weak to very strong	Higher RA index than Lithofacies A and Bii but variable. Mean (N = 3) C_{40} 19.7 RA 24.7 SD 8.4	Varied, very bouldery sections, with stacked SA-SR boulders dipping up-glacier, to general absence of boulders	Many rotten, badly weathered clasts. Some amphibolite clasts show granular dis-integration to patches of coarse black sand	U & L sharp, wavy. Beds from 0.3 to 2m thick	Mean FSG lower than Lithofacies A_K and B_K at -2.76
Litho-facies D_K	Mottled Brown to rusty red and sandy yellow.	More fines than other Dm (K) with 48.8% mud, (see Fig. 3.3t)	Very clast-rich (50% gravel) and clast-supported in patches; coarse Dm with many cobbles and boulders, but muddy matrix	Slightly weaker than Lithofacies A and Bii, with different V_1 orientations plunging SSW or NNE	Weak to absent	Higher no. A and VA clasts than Lithofacies Bii_K , but similar to Bi and C_{brown} Mean (N = 3) C_{40} 15, SD 9.5 RA 22.7, SD 2.1	Tabular to rectangular shapes, some with faceted upper and lower faces	Many badly weathered clasts and oxidised appearance to matrix in places	L unseen. U sharp and wavy	Similar to Lithofacies A in high CI (75%), 89% Type 1 clasts, mean FSG -2.89

Table 3.2 Diamicton Codes

The subscripts I, K, and S refer to Lithofacies A at Isfallsglaciären, Kaskasatjåkka, and Storglaciären respectively

	Description
Dm	The use of Dm denotes a massive, homogeneous diamicton. Diamictons are poorly sorted, unlithified terrigenous sediments with a range of clast sizes and shapes (Benn and Evans, 2010)
Lithofacies A	The upper diamicton of the fluted moraine. Lithofacies A is a sandy, matrix-supported diamicton
Lithofacies B (i& ii)	The upper diamicton in the diamicton plain (S) and diamicton sheet (K). Bi refers to the *ca*. upper 0.3m of the diamicton which generally has weaker clast fabrics and a less silty particle grain size distribution (S), probably reflecting post-depositional modifications. Lithofacies B is grey, silty to sandy Dm, highly fissile, and matrix-supported. It is distinct from Lithofacies A. Flutes consisting of Lithofacies B are occasionally observed in the diamicton plain (S), but not in the diamicton sheet (K)
Lithofacies C	A scoarse-grained sandy-gravelly Dm which forms the substratum to Lithofacies A (I) in the proximal reaches of some flutes. It is absent from Storglaciären. A distinctive brown coloured version forms the substrate to Lithofacies A (K) and is exposed at the surface in the lower forefield area. Lithofacies C is occasionally observed separating Lithofacies B and D in the diamicton sheet (K)
Lithofacies D	A very clast-rich, coarse-grained gravelly Dm, often clast-supported in patches, which consists of very badly weathered clasts. It is occasionally observed to form the basal diamicton in the diamicton sheet (K). At Storglaciären and Isfallsglaciären, Lithofacies D contains a high proportion of very angular clasts, Lithofacies D forms the substrate to Lithofacies A in the fluted area of Storglaciären and to Lithofacies B in the upper part of the diamicton plain, where it forms the basal diamicton. In Isfallsglaciären, its distribution is restricted to the proximal zones of flutes where it is the substratum to Lithofacies A/C
StDm	A very clast-rich, coarse-grained diamicton that occurs in the lateral-frontal moraines of Kaskasatjåkka and Isfallsglaciären. It resembles Lithofacies D from Isfallsglaciären and Storglaciären in terms of pgsd, fractal slope gradient, and clast morphology. However, clasts are not as heavily weathered.

3.3 Lithofacies A and associated sediments

Comment [DJG2]: You also describe the underlying sand beds

Lithofacies A crops out widely across the forefield at Isfallsglaciären where it forms the upper diamicton in the flute field that extends from the southern side of the riegel and below Lake Frontsjön to the inner frontal moraine (Figure 3.2a). It also forms the upper diamicton in flute fields at Kaskasatjåkka and Storglaciären, but has a more limited distribution. At Kaskasatjåkka it occurs in flutes that form just below a distinct morphological break of slope (Figure 3.2b). At Storglaciärenit occurs in fluted moraine located on the northern side the present glacier marginand just west of Log NL5 (Figure 3.2c).

3.3.1 Description

In the main fluted areas of each forefield, flutes consisting of a matrix-supported, homogeneous grey to olive-green or grey-brown sandy diamicton. In the sediment matrix (<2mm), the polymodal and very poorly sorted particle grain-size distributions (pgsds) of Lithofacies A in each forefield display similarities (Figure 3.3a-c). The mean grain size is fine-sand, with approximately three quarters of the sample consisting of sand, about one fifth consisting of silt, with coarse silt being the dominant mode in the mud fraction, and less than 5% consisting of clay-sized material. Lithofacies A is clast-rich, and Lithofacies A from Kaskasatjåkka is generally coarser (primary mode very coarse sand) than Lithofacies A from Storglaciären and Isfallsglaciären (primary modes of fine sand). Clast clusters and smudges are common. When coarse pebbles and cobbles are carefully removed from Lithofacies A, leaving an impression, small, oval-shaped patches of coarse black sand often occur as inclusions preserved within the diamicton, sometimes, but not always, towards the lee-side of the impression. The porosity and void ratio vary between samples within each forefield, with porosity ranging between 20-37% and void ratio ranging between 0.25-0.56 (Table 3.3).

Comment [DJG3]: frequency implies in time

Lithofacies A has a friable, easily excavated matrix and is lacking in obvious macro-structure, except for a platy structure which weathers to give a fissile texture consisting of partings which dip and cross-cut in multiple directions, with common partings sub-parallel and near-vertical to the flute surface. The fissile partings exhibit variable spacing, with individual planes being a few centimetres to a few millimetres apart. In places, the fissility is difficult to see whilst in some trenches it appears more pervasive, with some planes continuous over decimetres while others, especially around embedded boulders, are very short and disrupted or intersected by the boulders.

Table 3.3 Bulk Density, Void Ratio, and Porosity Ranges for Lithofacies A, Flutes

	Bulk Density (g/cm^3)	Void Ratio	Porosity (%)	Average Porosity %	Standard Deviation (porosity)
Isfallsglaciären N=12	1.84 – 2.54	0.25 – 0.56	20 - 36	30	5.5
Kaskasatjåkka N=10	1.63 – 2.22	0.32 – 0.55	24 - 37	31	5.7
Storglaciären N=10	2.04 – 2.3	0.35 – 0.41	26 - 31	28	1.6

The surface of fluted moraines in each forefield consists of stony and bouldery armour, with some angular and non-striated boulders in evidence, although these tend either not to be embedded or are only lightly embedded in Lithofacies A. Large embedded boulders of amphibolite, dolerite, and occasionally gneiss form a prominent part of Lithofacies A in each fluted forefield. Large embedded boulders, typically between 1-3m in length, have their a-axes aligned parallel or slightly oblique to the flute axis. Boulders are sub-rounded to sub-angular and exhibit tabular blocky to slab-like shapes, with faceted upper (and occasionally lower) surfaces. Upper surfaces display numerous wear marks such as flow-aligned striae, crescentic fractures, and chattermarks. At Isfallsglaciären, calcite precipitate was observed to fill some gouges on the upper surface of boulders. Striae are particularly well-developed on the upper surfaces of amphibolite boulders at Isfallsglaciären, where they are straight, up to 0.2mm deep and 200mm long. They also occur on the sides of some embedded boulders in each forefield, where they are observed to dip up and down-glacier at between 10° and 40°, as well as forming sub-parallel to the flute surface. Striae are scarce on the lower surfaces of embedded boulders. On some large embedded boulders striae curve around the edges at the stoss-end before becoming straight and flow-parallel on the upper face. Stoss and lee forms are common in all three forefields and double stoss and lee forms are numerous at Isfallsglaciären.

The gravel component of Lithofacies A ranges in size from granules to boulders. In the 0.6mm to 60mm size-range clasts are dominated by sub-rounded to sub-angular modes, with Lithofacies A at Kaskasatjåkka exhibiting more sub-angular and angular clasts than at

Comment [DJG4]: gravel is a definition of size

Isfallsglaciären (Figure 3.4). All Lithofacies Asamples exhibit a high crushing index with typically 80% or more of rounded to sub-rounded clasts showing freshly fractured, chipped and worn surfaces and edges (Figure 3.5). Blades and compact blades are the most frequently occurring clast shapes, yielding low C_{40} indices (<25; Figure 3.6). Three main clast forms occur (Figure 3.7): Type 1 clasts are the most numerous (between 40-70% of clasts) and have one distinct flat faceted face and are generally sub-rounded to sub-angular; Type 2 clasts are common (20-30% of clasts), have two distinct flat faceted faces and are generally sub-rounded to sub-angular; Type 3 clasts are less common (10-20% of clasts), have no obvious flat faceted faces and are sub-angular to angular. The gravel component is dominated by relatively unweatheredclasts of mafic igneous rocks and metamorphic rocks (dolerite and amphibolite, with lesser amounts of gneiss, and meta-sediments). Bullet-shaped clasts are common. Shear vane tests indicate that the shear strength of Lithofacies A is very variable over small spatial scales, with the highest values attained in more clast-rich horizons at 0.5m depth(*ca*. 80KPa), and that shear strength generally increases with depth (average shear strength shows a 60% increase with depth in the upper half a metre of flutes; Table 3.4).

Comment [DJG5]: what do you meean by frexh?

Table 3.4 The Increase in Shear Strength with Depth in Lithofacies A, Isfallsglaciären Flutes

Depth Below Surface (m)	**Mean Shear Strength (KPa)**	**Standard Deviation**
0-0.1	48	15.03
0.1-0.2	52	16.4
0.2-0.3	52	20.1
0.4-0.6	77	14.8

Note: The mean shear strength is the average of 30 samples at each depth interval. For each sample, 5 readings were taken and the highest/lowest values discarded. The average of the remaining 3 was used as the sample value. The large standard deviations indicate that shear strength was variable, and even at the shallowest depths, values near to 100KPa could be obtained in clast rich horizons where the vane sometimes stuck against a large gravel-sized clast. These values were discarded. The increase in strength with depth is consistent with the increase in effective pressure resulting from the increased overburden pressure. The weakest values (3KPa) were obtained from shallow depths (0-0.1m) in a saturated sample taken in the proximity of the present ice-margin at Kaskasatjåkka, where lithofacies A was frequently observed to liquefy underfoot.

Both flutes and adjacent interflutes consist of Lithofacies A. However, macro-observations show Lithofacies A in interflutes to be, in most cases, coarser and more clast-rich than in adjacent flute crests. In the average particle grain-size distribution for the sediment-size fraction <5.6mm, the interflute sample is dominated by fine gravel (41%). Compared to the interflute samples, the flute samples are relatively depleted in fine to very fine gravel and coarse sand, and relatively enriched in fine sand and coarse silt (Figure 3.8). Most Lithofacies A clast a-axis fabrics taken from interflutes have S_1 eigenvalues <0.7 and exhibit weaker linear clusteringand greater isotropy than fabrics measured in adjacent flutes (Figure 3.9a). Most flute clast a-axis fabrics exhibit strong linear clustering with S_1 eigenvalues >0.7 and S_3 eigenvalues <0.15 (Figure 3.9a). Furthermore, flute and interflute samples can be distinguished by their mean fractal slope gradients (Figure 3.10a&b).The range of slope gradients is similar in Lithofacies A in flutes in each forefield (for example, at Isfallsglaciären they range from -2.63 to -2.98 whilst at Kaskasatjåkka they range from -2.67 to -3.02), and the mean of 28 flute samples is -2.91 (standard deviation = 0.09; R^2 = 0.998). By contrast, the mean fractal slope of six interflutes samples is -2.79 (Standard deviation = 0.075; R^2 = 0.995).

Comment [DJG6]: I'm uncertain why you're reporting an R^2 value here

Comment [DJG7]: ditto

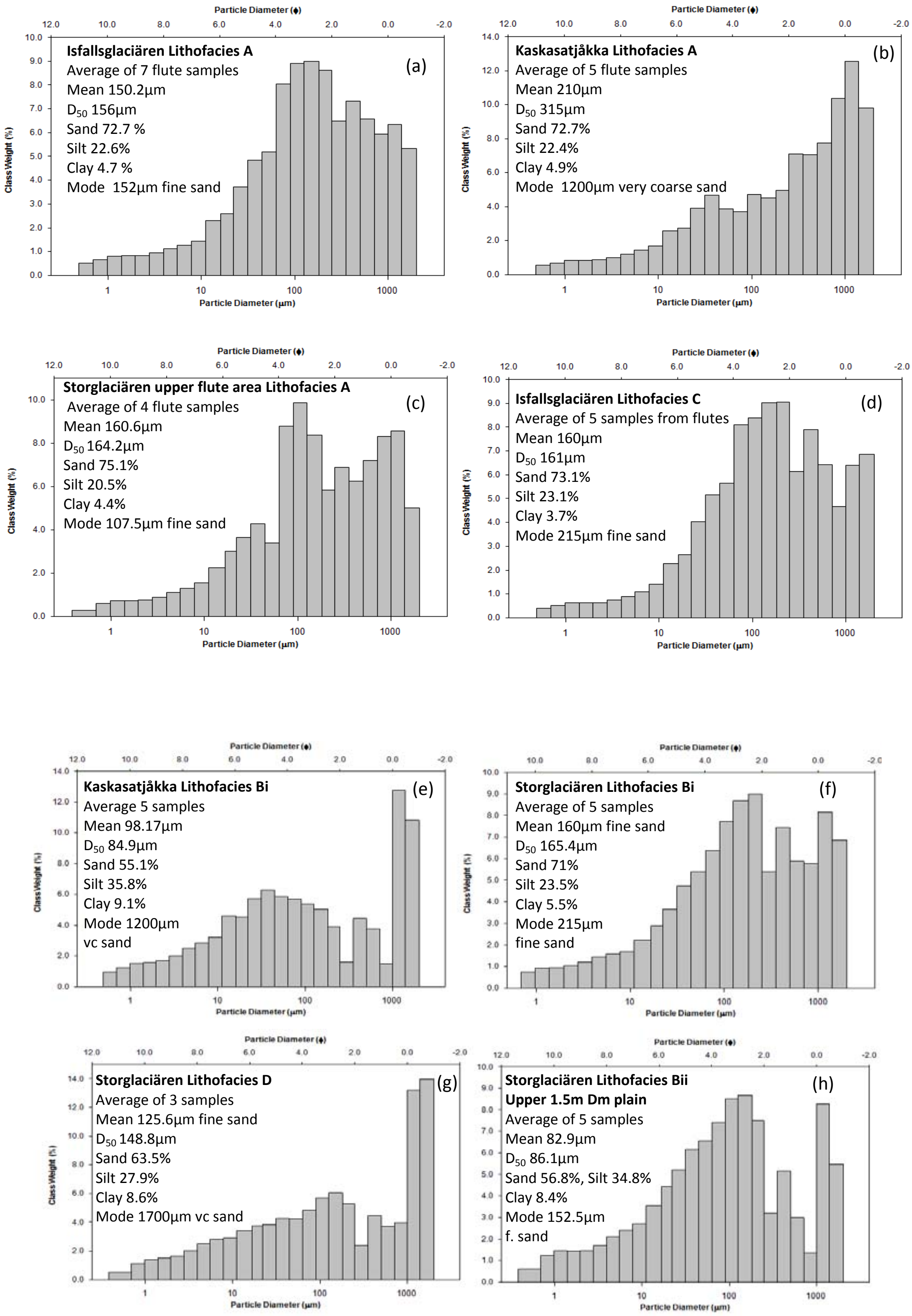
Isfallsglaciären Lithofacies A
Average of 7 flute samples
Mean 150.2µm
D50 156µm
Sand 72.7 %
Silt 22.6%
Clay 4.7 %
Mode 152µm fine sand
(a)
Kaskasatjåkka Lithofacies A
Average of 5 flute samples
Mean 210µm
D50 315µm
Sand 72.7%
Silt 22.4%
Clay 4.9%
Mode 1200µm very coarse sand
(b)
Storglaciären upper flute area Lithofacies A
Average of 4 flute samples
Mean 160.6µm
D50 164.2µm
Sand 75.1%
Silt 20.5%
Clay 4.4%
Mode 107.5µm fine sand
(c)
Isfallsglaciären Lithofacies C
Average of 5 samples from flutes
Mean 160µm
D50 161µm
Sand 73.1%
Silt 23.1%
Clay 3.7%
Mode 215µm fine sand
(d)
Kaskasatjåkka Lithofacies Bi
Average 5 samples
Mean 98.17µm
D50 84.9µm
Sand 55.1%
Silt 35.8%
Clay 9.1%
Mode 1200µm
vc sand
(e)
Storglaciären Lithofacies Bi
Average of 5 samples
Mean 160µm fine sand
D50 165.4µm
Sand 71%
Silt 23.5%
Clay 5.5%
Mode 215µm
fine sand
(f)
Storglaciären Lithofacies D
Average of 3 samples
Mean 125.6µm fine sand
D50 148.8µm
Sand 63.5%
Silt 27.9%
Clay 8.6%
Mode 1700µm vc sand
(g)
Storglaciären Lithofacies Bii
Upper 1.5m Dm plain
Average of 5 samples
Mean 82.9µm
D50 86.1µm
Sand 56.8%, Silt 34.8%
Clay 8.4%
Mode 152.5µm
f. sand
(h)
Particle Diameter (ϕ)
Particle Diameter (µm)
Class Weight (%)

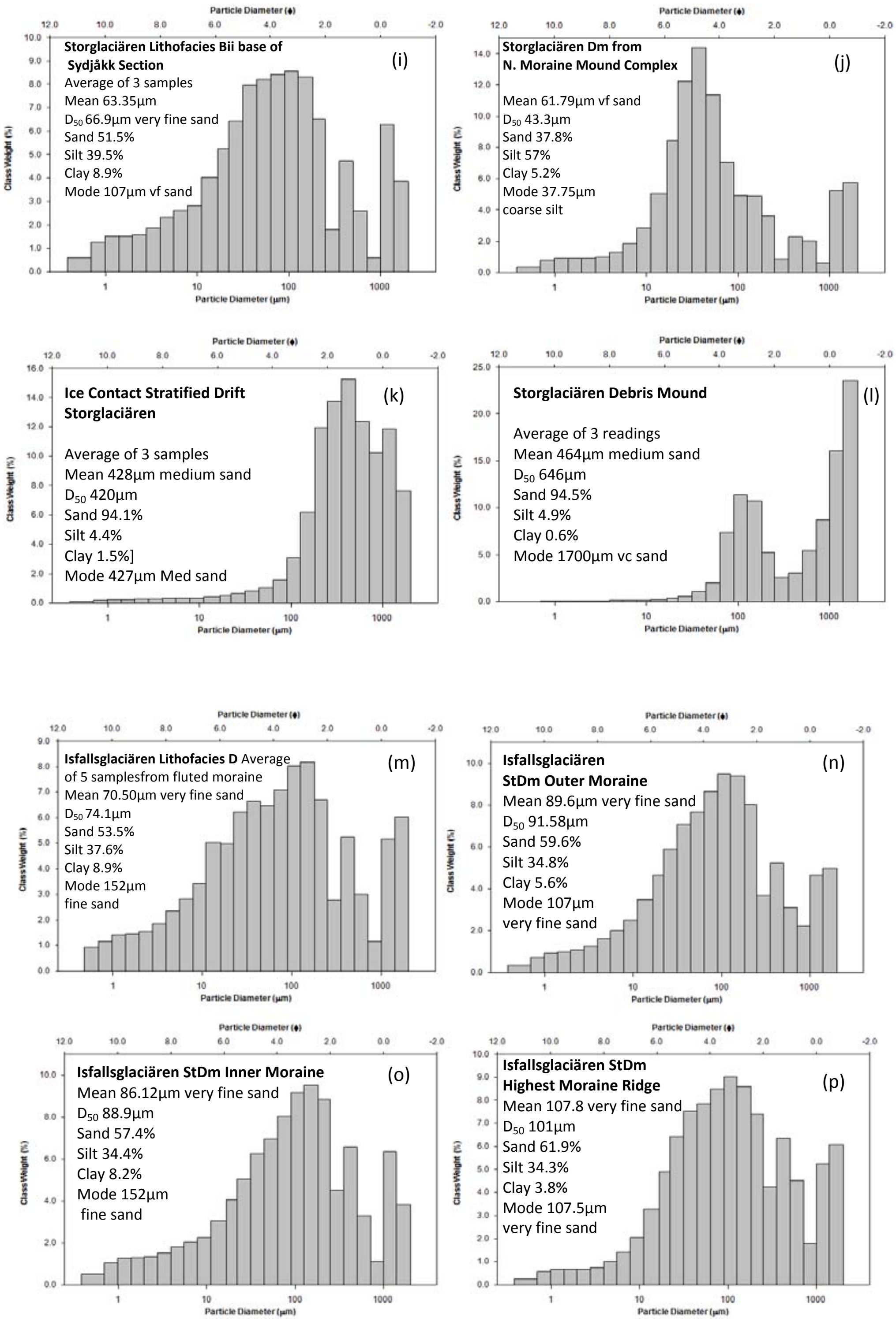
Storglaciären Lithofacies Bii base of Sydjåkk Section
(i)
Average of 3 samples
Mean 63.35µm
D50 66.9µm very fine sand
Sand 51.5%
Silt 39.5%
Clay 8.9%
Mode 107µm vf sand
Storglaciären Dm from N. Moraine Mound Complex
(j)
Mean 61.79µm vf sand
D50 43.3µm
Sand 37.8%
Silt 57%
Clay 5.2%
Mode 37.75µm coarse silt
Ice Contact Stratified Drift Storglaciären
(k)
Average of 3 samples
Mean 428µm medium sand
D50 420µm
Sand 94.1%
Silt 4.4%
Clay 1.5%]
Mode 427µm Med sand
Storglaciären Debris Mound
(l)
Average of 3 readings
Mean 464µm medium sand
D50 646µm
Sand 94.5%
Silt 4.9%
Clay 0.6%
Mode 1700µm vc sand
Isfallsglaciären Lithofacies D Average of 5 samplesfrom fluted moraine
(m)
Mean 70.50µm very fine sand
D50 74.1µm
Sand 53.5%
Silt 37.6%
Clay 8.9%
Mode 152µm fine sand
Isfallsglaciären StDm Outer Moraine
(n)
Mean 89.6µm very fine sand
D50 91.58µm
Sand 59.6%
Silt 34.8%
Clay 5.6%
Mode 107µm very fine sand
Isfallsglaciären StDm Inner Moraine
(o)
Mean 86.12µm very fine sand
D50 88.9µm
Sand 57.4%
Silt 34.4%
Clay 8.2%
Mode 152µm fine sand
Isfallsglaciären StDm Highest Moraine Ridge
(p)
Mean 107.8 very fine sand
D50 101µm
Sand 61.9%
Silt 34.3%
Clay 3.8%
Mode 107.5µm very fine sand
Particle Diameter (ϕ)
Particle Diameter (µm)
Class Weight (%)

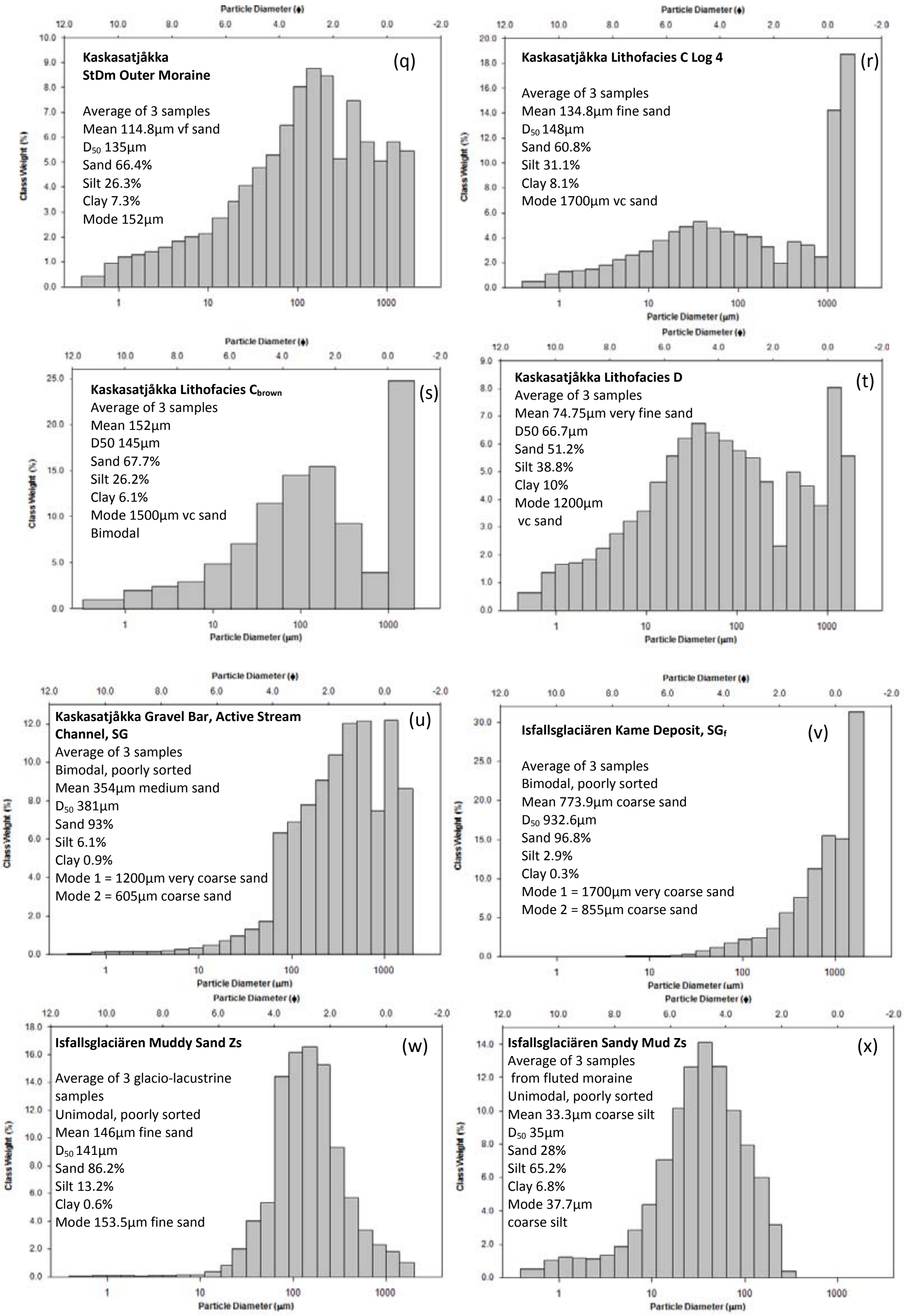
Particle Diameter (ϕ)
Class Weight (%)
Particle Diameter (µm)
Kaskasatjåkka
StDm Outer Moraine
(q)
Average of 3 samples
Mean 114.8µm vf sand
D_{50} 135µm
Sand 66.4%
Silt 26.3%
Clay 7.3%
Mode 152µm
Kaskasatjåkka Lithofacies C Log 4
(r)
Average of 3 samples
Mean 134.8µm fine sand
D_{50} 148µm
Sand 60.8%
Silt 31.1%
Clay 8.1%
Mode 1700µm vc sand
Kaskasatjåkka Lithofacies C_{brown}
(s)
Average of 3 samples
Mean 152µm
D50 145µm
Sand 67.7%
Silt 26.2%
Clay 6.1%
Mode 1500µm vc sand
Bimodal
Kaskasatjåkka Lithofacies D
(t)
Average of 3 samples
Mean 74.75µm very fine sand
D50 66.7µm
Sand 51.2%
Silt 38.8%
Clay 10%
Mode 1200µm
vc sand
Kaskasatjåkka Gravel Bar, Active Stream Channel, SG
(u)
Average of 3 samples
Bimodal, poorly sorted
Mean 354µm medium sand
D_{50} 381µm
Sand 93%
Silt 6.1%
Clay 0.9%
Mode 1 = 1200µm very coarse sand
Mode 2 = 605µm coarse sand
Isfallsglaciären Kame Deposit, SG_f
(v)
Average of 3 samples
Bimodal, poorly sorted
Mean 773.9µm coarse sand
D_{50} 932.6µm
Sand 96.8%
Silt 2.9%
Clay 0.3%
Mode 1 = 1700µm very coarse sand
Mode 2 = 855µm coarse sand
Isfallsglaciären Muddy Sand Zs
(w)
Average of 3 glacio-lacustrine samples
Unimodal, poorly sorted
Mean 146µm fine sand
D_{50} 141µm
Sand 86.2%
Silt 13.2%
Clay 0.6%
Mode 153.5µm fine sand
Isfallsglaciären Sandy Mud Zs
(x)
Average of 3 samples
from fluted moraine
Unimodal, poorly sorted
Mean 33.3µm coarse silt
D_{50} 35µm
Sand 28%
Silt 65.2%
Clay 6.8%
Mode 37.7µm
coarse silt

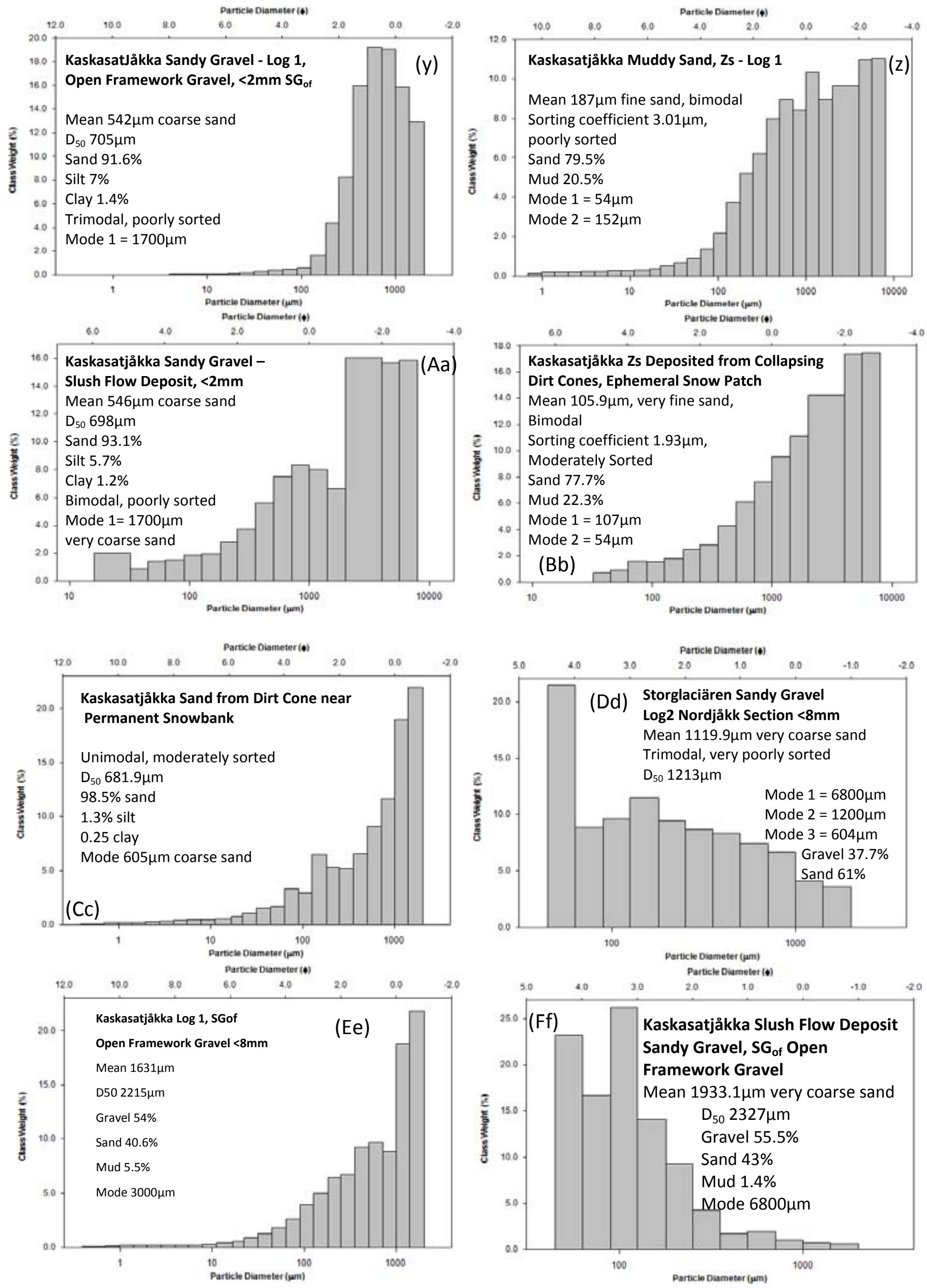

Figure 3.3 (a-Ff) Particle Grain-Size Distributions (pgsd) for Lithofacies from each Forefield. The pgsds have been constructed using GRADISTAT (version 8) software (Blott and Pye, 2001).

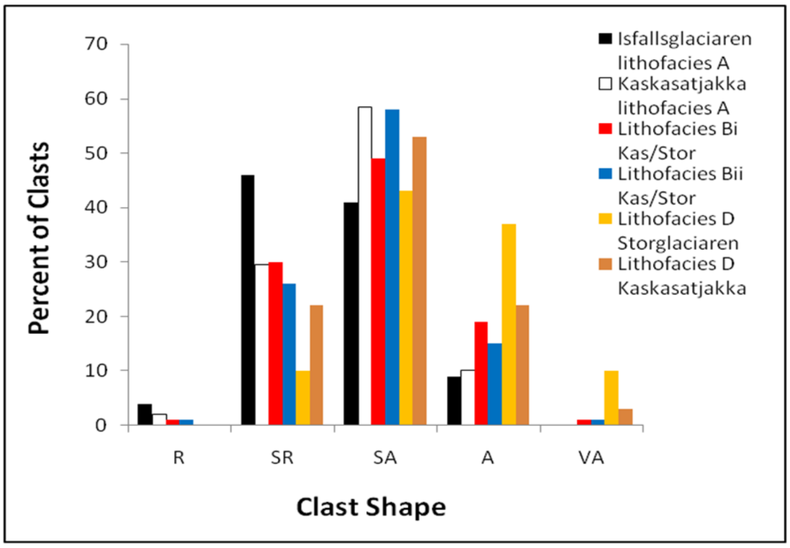

Figure 3.4 Clast Roundness. Lithofacies A values are the mean of 5 flute samples at Isfallsglaciären and Kaskasatjåkka (N = 50 in each sample, sum= 250 clasts in each area). Sub-rounded to sub-angular (SR-SA) clasts dominate. Lithofacies Bi & Bii sample values represent the average of 5 samples each from Storglaciären and Kaskasatjåkka (N = 50 in each sample). SR-SA forms still dominate, although there are a few more angular (A) clasts, and a few very angular (VA) clasts. Lithofacies D Stor (Storglaciären) and Kas (Kaskasatjåkka) are the average of two samples (N = 50 in each sample). Lithofacies D Stor is dominated by SA-A clasts, with a relatively high percentage of VA clasts.

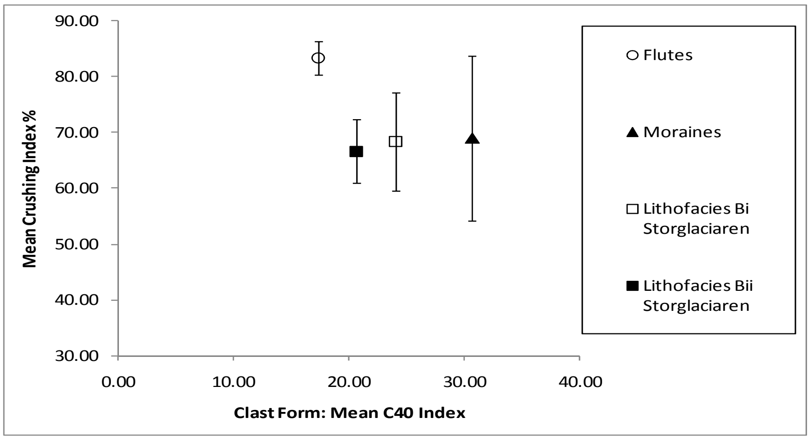

Figure 3.5 Crushing Index (CI) and Clast Form (C_{40} index). The mean CI of 10 Lithofacies A samples from flutes (N, the number of clasts observed = 50 in each sample) is 83.3% (standard deviation [SD] 4.55). The moraine samples (StDm) are taken from Isfallsglaciären. Note how Lithofacies Bi and Bii from Storglaciären have a similar CI with overlapping 95% confidence intervals, and slightly lower CI than Lithofacies A from flutes. The Moraines and Lithofacies B values are the average of 6 samples each.

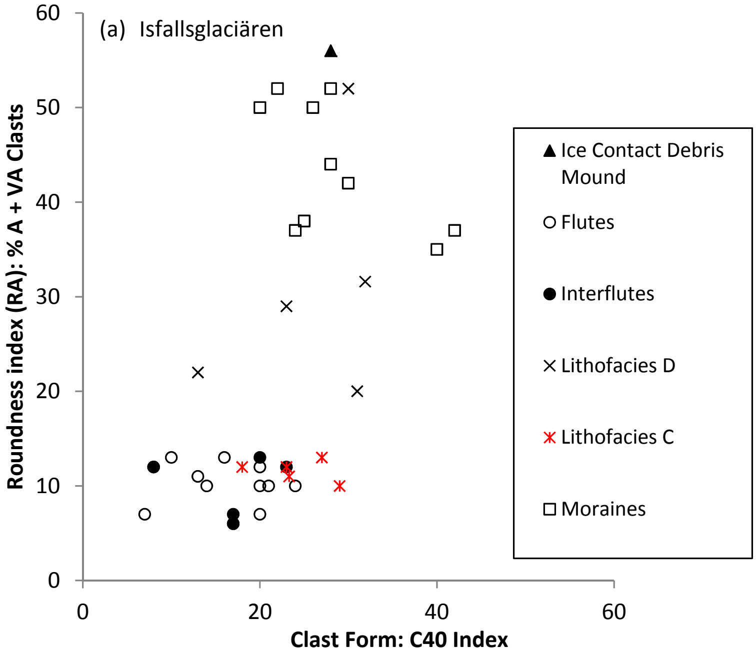
(a) Isfallsglaciären
Roundness index (RA): % A + VA Clasts
Clast Form: C40 Index
0
10
20
30
40
50
60
0
20
40
60
Ice Contact Debris Mound
Flutes
Interflutes
Lithofacies D
Lithofacies C
Moraines

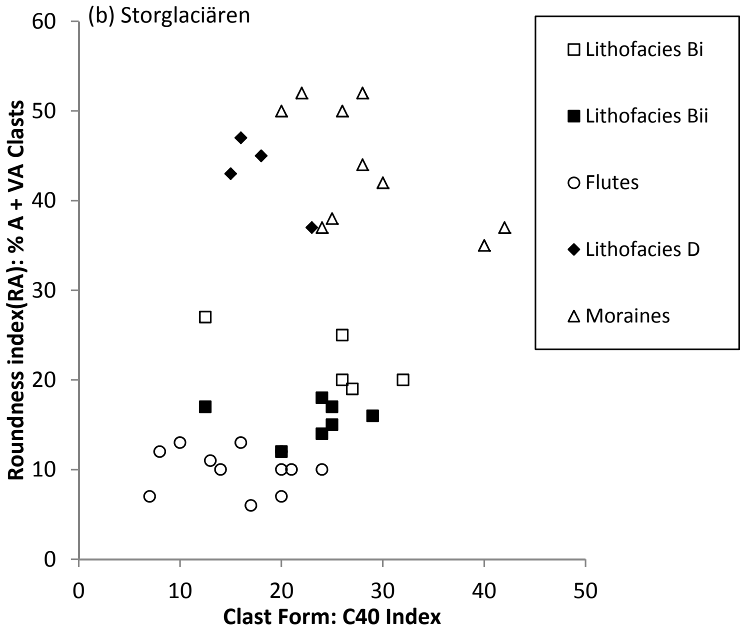
(b) Storglaciären
Roundness index(RA): % A + VA Clasts
Clast Form: C40 Index
0
10
20
30
40
50
60
0
10
20
30
40
50
Lithofacies Bi
Lithofacies Bii
Flutes
Lithofacies D
Moraines

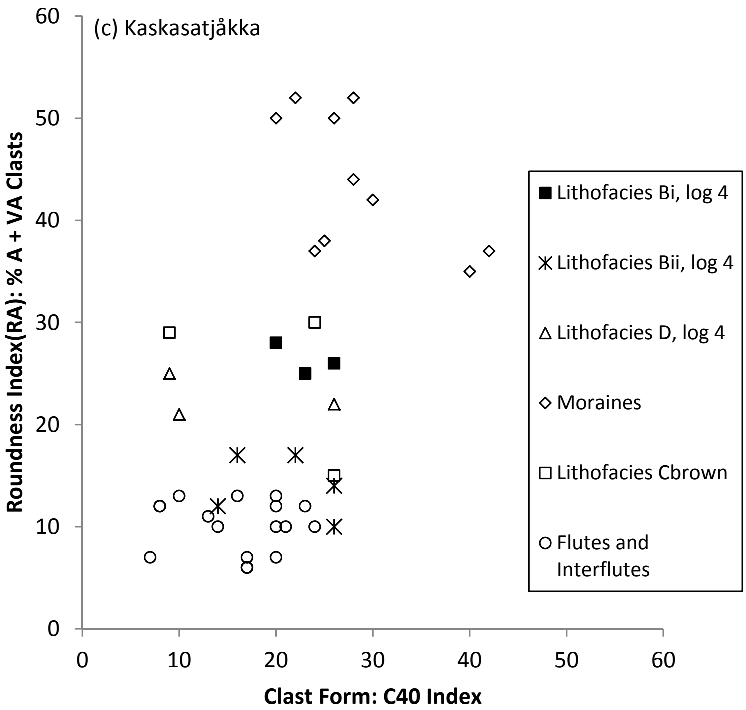

Figure 3.6a-c C_{40} Index and RA Index for Various lithofacies. On each graph, the flutes and interflutes represent samples taken from all 3 forefields from Lithofacies A. The moraine samples are stony diamictons (StDm) from the outer and inner moraines of Isfallsglaciären and Kaskasatjåkka. In Figure 3.6a these are contrasted with Lithofacies from Isfallsglaciären. Of the 12 lithofacies A samples (N = 50 in each sample) blades are the modal group in 50% of cases, with typically between 23-32% of clasts defined as blades and 20-25% compact-blades. The mean C_{40} index for Lithofacies A (flutes) is low (15.8%, standard deviation = 5.5), as is the mean RA index (10.1%, SD = 2.4), with C_{40} in the range 7-24% and RA 6-13%. Sediments produced in subglacial environments typically have low C_{40}/RA indices (Benn, 2004), because abrasion and crushing produce SR-SA equant shapes. Interflute samples plot in the same area of the graph. Lithofacies C is indistinguishable from the flute and interflute samples in most cases, suggesting a similar subglacial origin. Lithofacies D has more varied values, mostly halfway between the flutes and the moraines, but with some values identical to moraines. In Figure 3.6b a range of lithofacies from the Storglaciären diamicton plain are compared with Lithofacies A from flutes and diamictons from moraines, while in Figure 3.6c a range of lithofacies from Kaskasatjåkka are compared. Lithofacies Bi in Storglaciären and Kaskasatjåkka have higher mean RA indices than Lithofacies A and Bii (see Table 3.1), whilst some samples of Lithofacies Bi&ii contain slightly less blocky clast shapes than Lithofacies A. Lithofacies D from Storglaciären is clearly distinguished from Lithofacies A and Bby its high RA index, which is similar to the moraines.Lithofacies B in Kaskasatjåkka is similar to Lithofacies A, whereas Lithofacies C_{brown} is more variable.

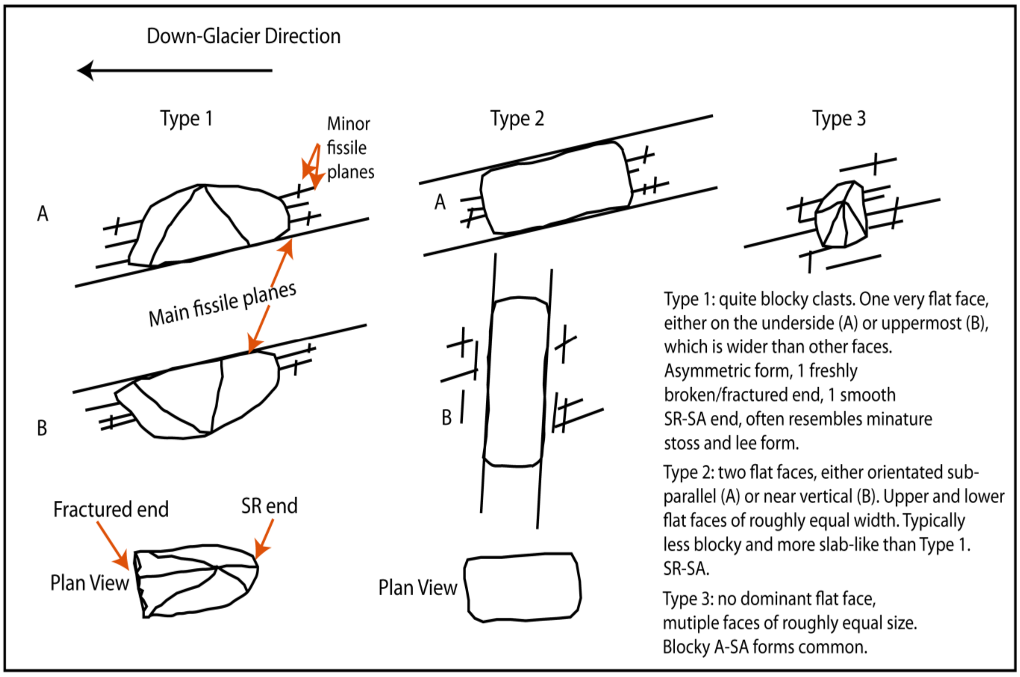

Figure 3.7 Common Clast Forms in Lithofacies A. A box sample from Trench MMT3, Flute 3, Area 3, Isfallsglaciären, which sampled Lithofacies A at 0.15-4m depth, was carefully dissected to investigate the relation between clast type and the orientation of the main fissile planes. 50 clasts of mostly dolerite and amphibolite in the 0.6-6cm size-range were studied. Of these, 88% were faceted and 84% had their a-axis orientated flow-parallel. Type 1 clasts comprised 50% of the sample, with 30% of the sample Type 1A clasts (lower flat face aligned in the orientation of the fissile planes or aligned along a main fissile plane), and 20% Type 1B (upper flat face aligned in the orientation of the fissile planes or aligned along a main fissile plane). Type 2 clasts comprised 38% of the sample, with 22% of the total Type 2A clasts (upper and lower flat faces aligned in the direction of sub-parallel fissile planes or lying along two main fissile planes), and 16% Type 2B clasts (as for Type 2A, but flat faces and fissile planes in near-vertical orientation). Type 1 and 2 clasts were very common in Lithofacies A and B. In six lithofacies A samples from Isfallsglaciären (N = 200) Type 1 clasts comprised 48% of the sample and Type 2 clasts 27%. Similarly, at Kaskasatjåkka, five lithofacies A samples (N = 150) yielded 68% Type 1 clasts and 23% Type 2 clasts.

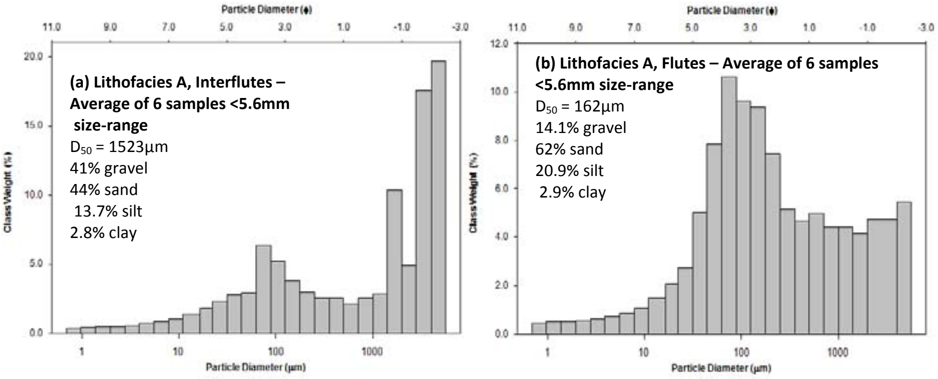

Figure 3.8 Lithofacies A Particle Grain-size Distributions for Interflute and Flute Samples in the Sediment-size Fraction <5.6mm. Both samples have similar clay components, and a spike in the fine to very fine sand (3 to 4ϕ), but the flute samples are relatively enriched in coarse silt (silt spike, 4.5 to 5ϕ) and fine sand compared to the interflute, whilst the interflute samples are skewed towards the fine-gravel mode.

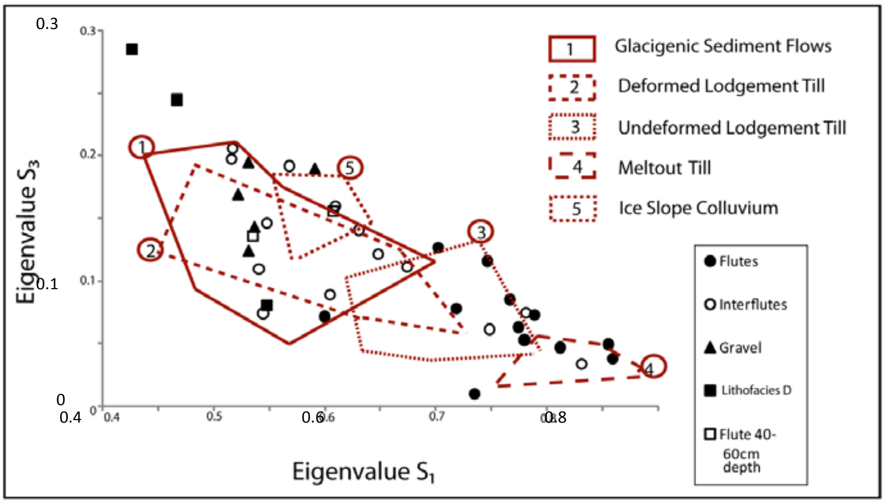

Figure 3.9a Various Lithofacies from Isfallglaciären plotted on a Bivariate Scattergraph showing Dowdeswell and Sharp's (1986) Process Fields. S_1 and S_3 are eigenvalues. The graph shows clast a-axis fabrics for Lithofacies A taken in flutes and interflutes. Nearly half the flutes samples plot as undeformed lodgement tills (equivalent to B-horizons). This contrasts with adjacent interflute samples where half plot as deformed lodgement tills/glacigenic sediment flows (equivalent to A-horizons). Sample points that plot towards the top left have increasingly isotropic fabric shapes with weak preferred alignment, whereas plots towards the bottom right are increasingly strong fabrics with preferred alignment and low isotropy.

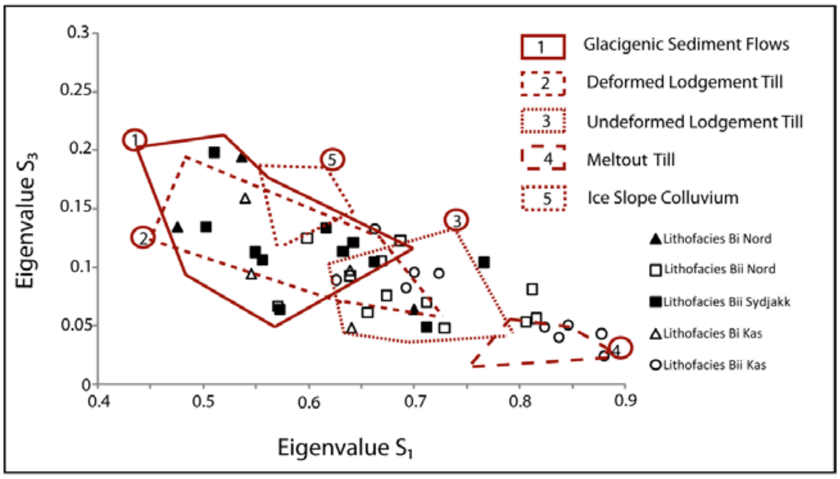

Figure 3.9b Lithofacies Bi and Bii from Storglaciären and Kaskasatjåkka plotted on a Bivariate Scattergraph showing Dowdeswell and Sharp's (1986) Process Fields. Nord is Nordjåkk and Kas is Kaskasatjåkka. Lithofacies Bii (N=7) samples plot mostly as deformed lodgement tills (5 from7) or glacigenic sediment flows (5 from 7). Lithofacies B from Nordjåkk (N=12) plot mostly as undeformed lodgement tills (7 from 12) with 2 from 12 plotting as melt out tills. This is similar to Lithofacies Bii from Kaskasatjåkka (N = 10) where 5 from 10 samples plot as melt out tills and 4from 10 as undeformed lodgement tills. Conversely, Lithofacies Bii from Sydjåkk (N = 11) has no points in the melt out process fields, but plots mostly as glacigenic sediment flows (9 from 11) and deformed lodgement tills (7 from 11).

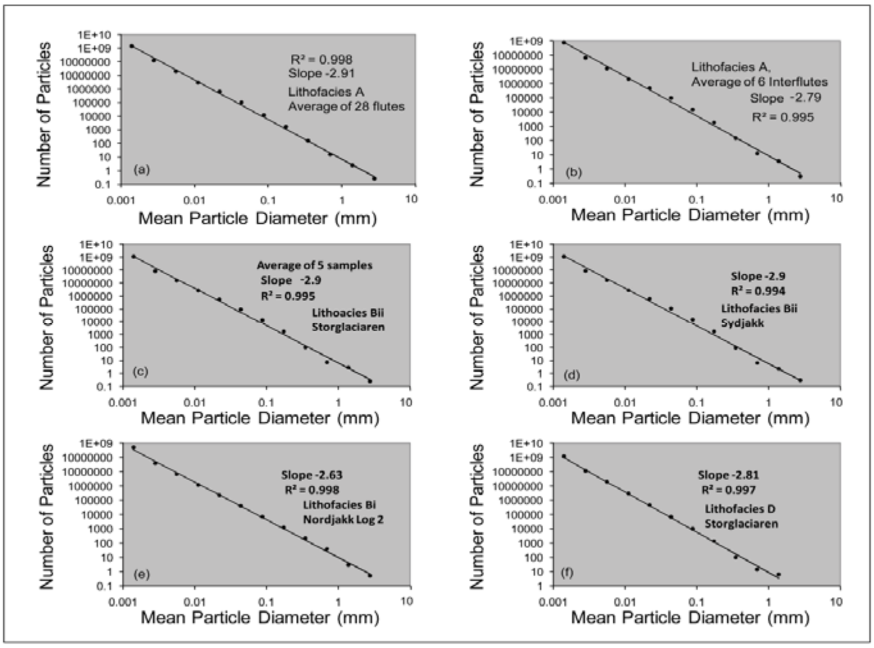

Figure 3.10 Fractal Slope Gradients

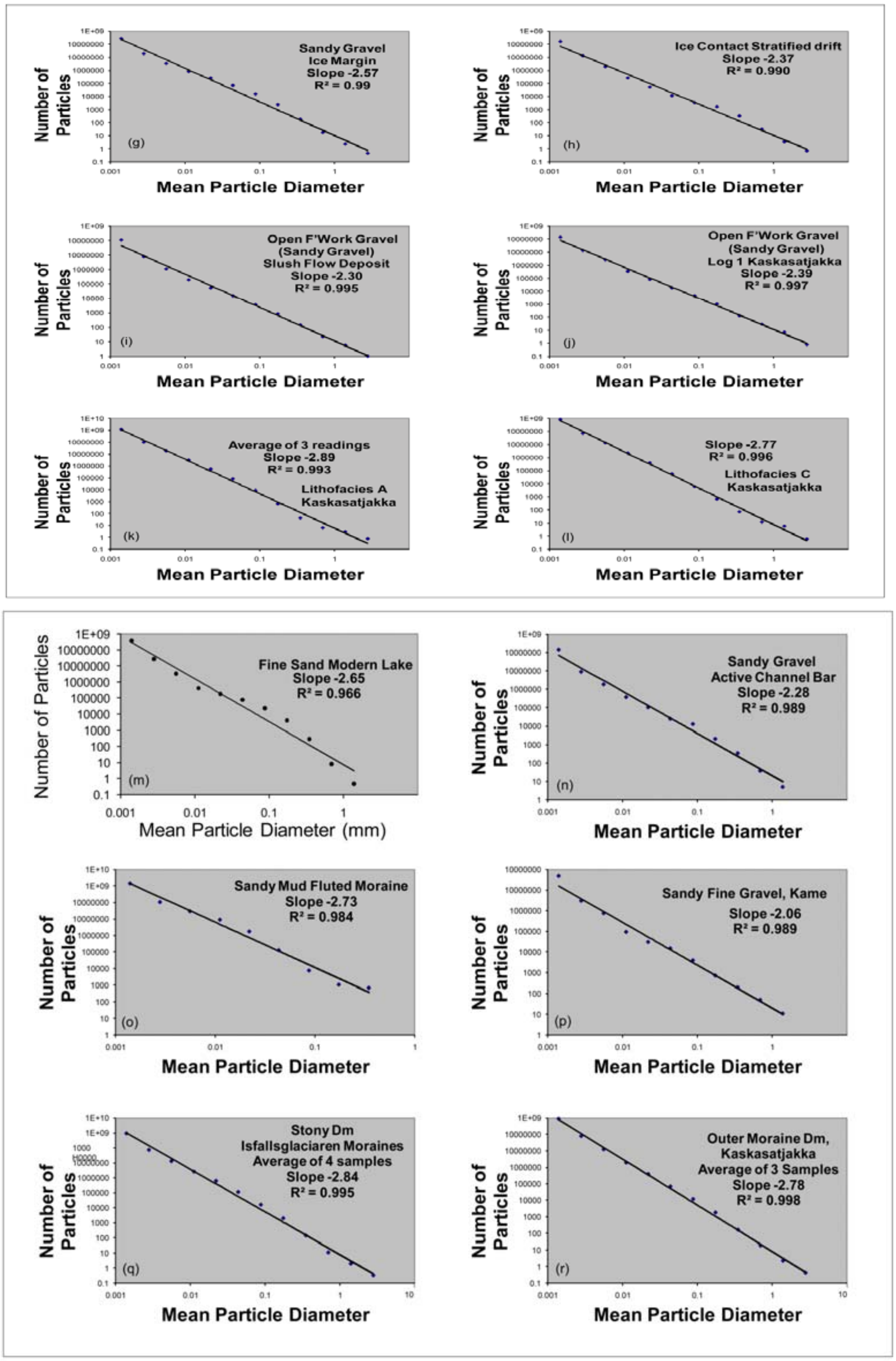

Figure 3.10 continued

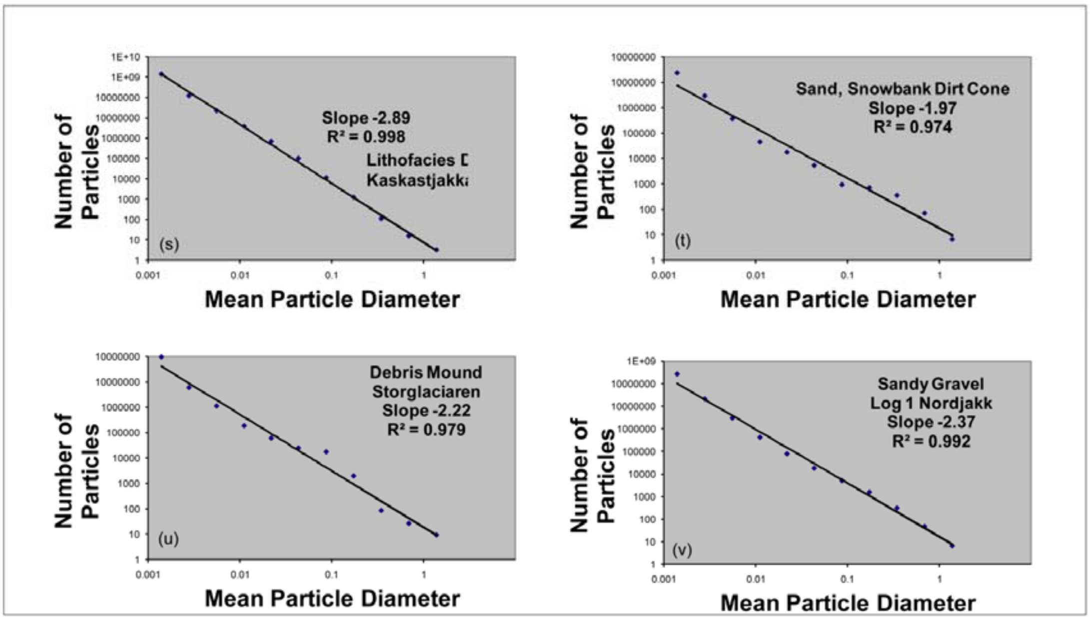

Figure 3.10a-v Fractal Slope Gradients, Various Lithofacies (facies on some diagrams). Mean particle diameter (mm) includes the very fine gravel fraction (<4mm) for most diamicton samples.

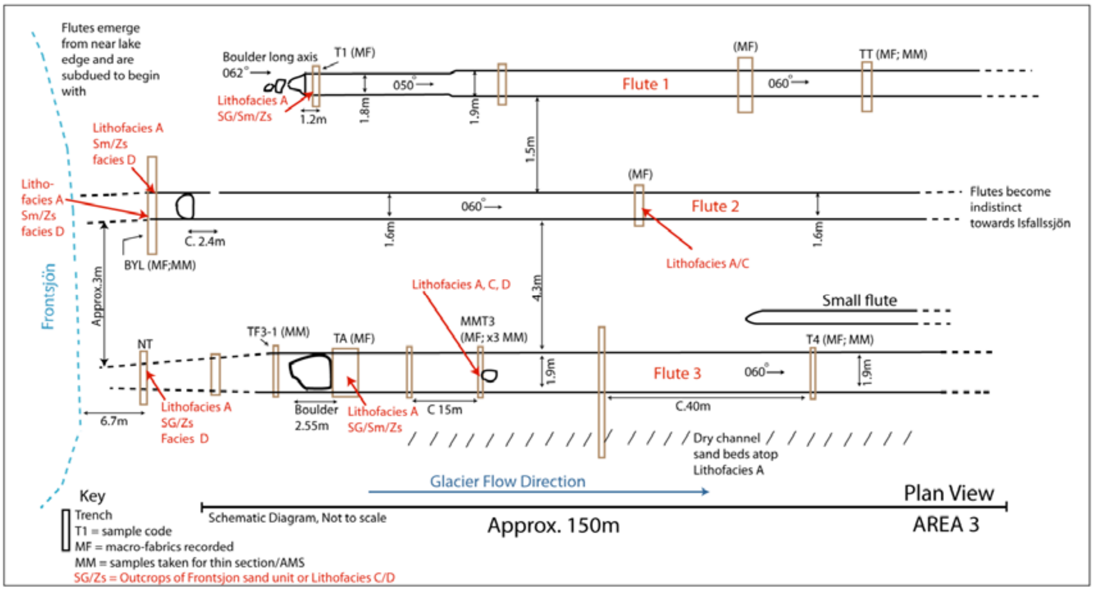

Figure 3.11 Location of Study Sites, Area 3, Isfallsglaciären and outcrops of Lithofacies including the Frontsjön sand unit. Note the irregular flute spacing and the restricted distribution of the Frontsjön sand unit to the proximal flute areas.

3.3.2 Relation to underlying sediments in the Frontsjön area, Isfallsglaciären

At Isfallsglaciären a relatively thick sequence (up to 2.5m) of sands formed the substratum to Lithofacies A in the proximal zones of flutes that occurred down-flow from Frontsjön (Areas 2 and 3 in Figure 3.1a). The Fronstjön sand unit consists of massive, coarse to medium sands interbedded with fine sands and fine to very fine silty sands. The sand beds varied in thickness – most were 1-2cm thick and exhibited variable dips. The contact between Lithofacies A and the sand substratum was extremely variable over short distances, with evidence of deformed, non-deformed, and erosional contacts occurring (Figure 3.12).

Comment [DJG8]: Note dip? Note thickness of beds?

Comment [DJG9]: This is interpretation

In some trenches, thin beds of silty sand and fine sand are folded into small, broad open antiforms with fold axes perpendicular to the glacier flow direction. These folds were observed at shallow depths (0.3-0.7m) below the contact with Lithofacies A and typically have fold amplitudes of 0.1m, although sometimes the folds appear detached (Figure 3.12a). Above the open folds thin sand beds become sub-parallel and display micro-laminations, or the sand becomes massive towards a sharp upper contact with Lithofacies A. Some trenches reveal more complex contacts, with what appear to be small recumbentfolds occurring at a few centimetres to decimetre depths below the contact with Lithofacies A, with axial planeshorizontal or inclined at shallow angles up-flow. These folds occurred where Lithofacies A was boulder-rich and where sediment prows formed in front of the leading edges of large embedded boulders and cobbles (Figure 3.12b). A few metres to the NW of the contact shown in Figure 3.12b, the contact becomes transitional, with a 2cm thick massive sand layer merging into Lithofacies A. In Trench T:T1, excavated 1.2m down-flute from an initiating boulder, 3-5cm thick beds of fine to medium sand dip up-glacier at between 20-40°and are separated from Lithofacies A by a sub-parallel sequence of 0.3-0.5m thick sands and gravels (Figure 3.12c). At the sharp contact, the sub-parallel sequence truncates the dipping sand layers and the boundary resembles an angular unconformity. A lens of gravel scours into the top of the dipping sand beds. The sub-parallel sand and gravel sequence exhibit grading and fining upwards sequences, with the fine and medium sand beds showing laminations. Individual fine-sand laminations can be traced longitudinally for over a metre with little visible sign of deformation, although the laminations bend-up over the lower gravel lens. A thicker layer of massive gravel scours into the upper part of the sub-parallel sand sequence and Lithofacies A makes sharp but wavy contact with this gravel.

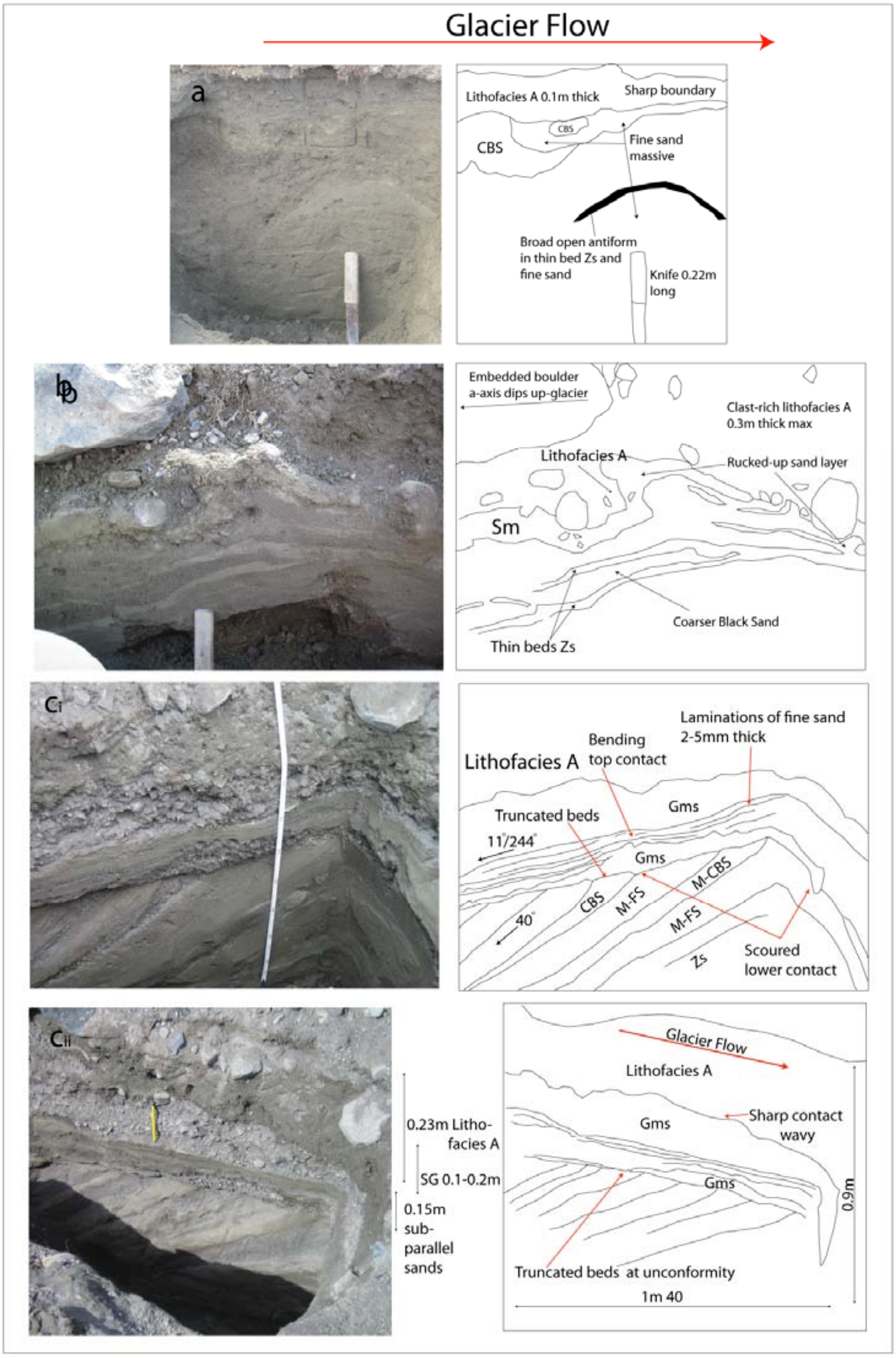

Figure 3.12 A variety of contacts between Lithofacies A and the Frontsjon sand unit

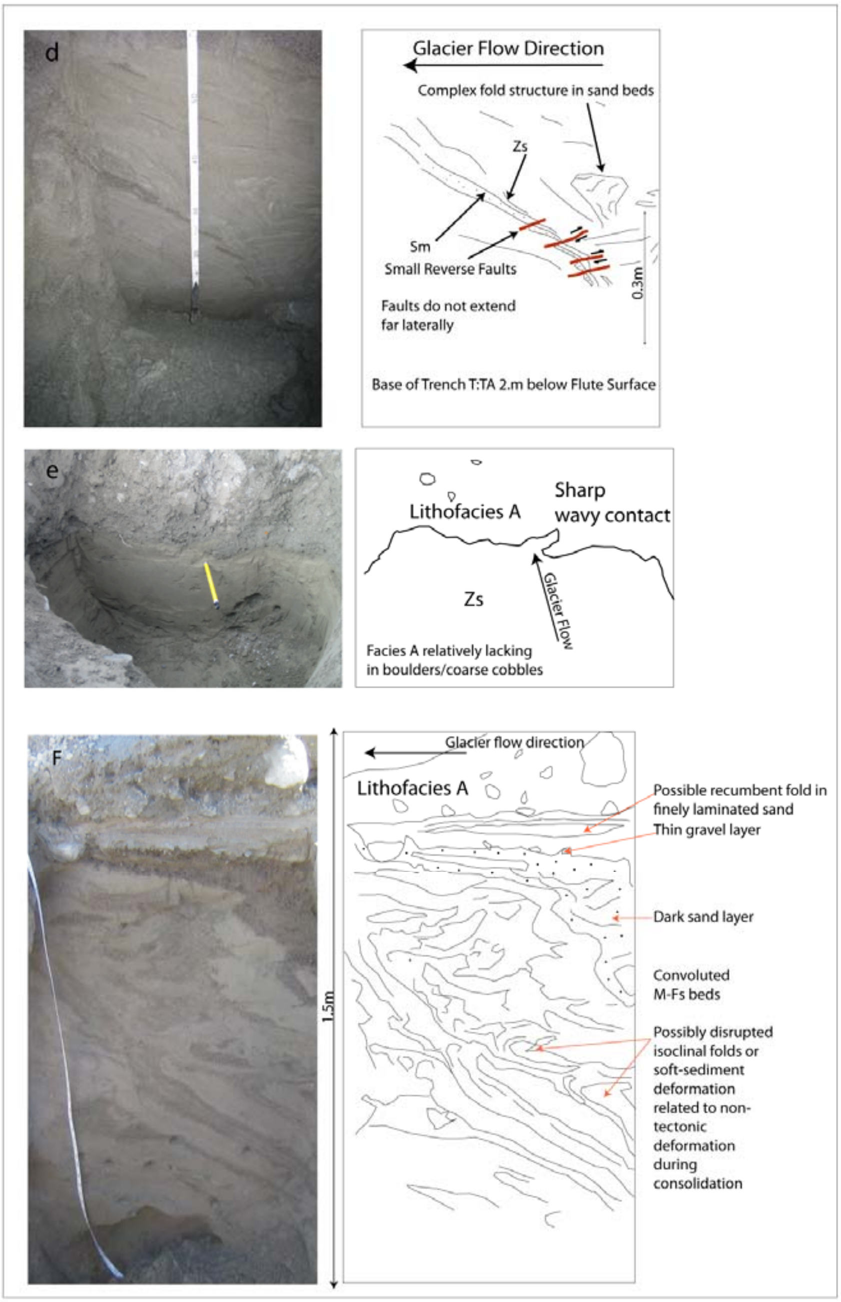

Figure 3.12 continued

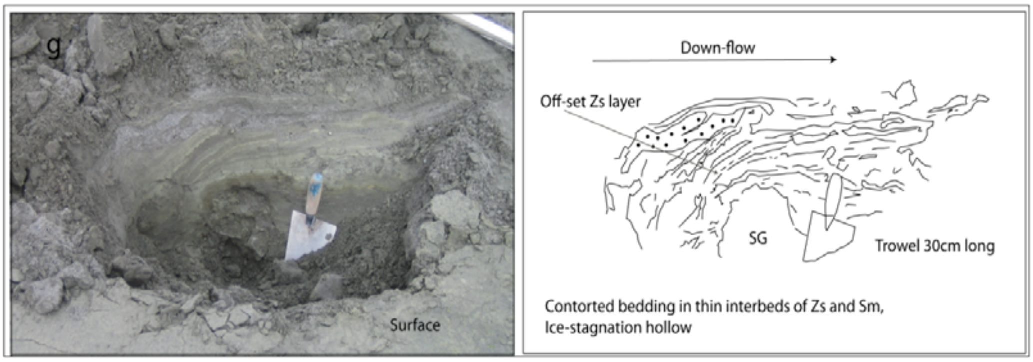

Figure 3.12 A Variety of Contact Types between Lithofacies A and the Frontsjön Sand Unit, Proximal Zone of Areas2 & 3, Isfallsglaciären. The Frontsjön sand unit consists of Zs, Sm, and CBS = coarse black sand, which is a poorly sorted variety of massive sand. SG occurs above the discontinuity in 3.12c, where it massive and matrix-supported (Gms). M-Fs = medium to fine sand layers, often with micro-laminations. Glacier flow direction is left to right unless otherwise indicated. (a) Left-hand side of trench TBYL looking NNW. Fine and silty sand layers form an open antiform at shallow depth. Sand layers become massive or display micro-laminations at the contact, which is sharp and wavy. Occasionally, similar contacts are demarcated by a 1-2cm thick fine massive yellow sand layer. (b) Same trench, right-hand side looking SSE, approximately 2m from previous image. A complex contact, with a coarser Lithofacies A which includes a large embedded boulder (a-axis flow-parallel and 0.7m long), which appears to have rucked-up a fine massive sand layer ahead of its leading edge at the contact. The boulder dips up-glacier at a shallow angle, which is consistent with embedded boulders which initially plough and form a prow, then lodged. (Ci&ii) Trench T:T1 left-hand side looking NNW, approximately 1.5-2m down-flute from initiating boulder. Two views of a complex sequence seen from different angles. Lithofacies A makes sharp wavy contact with a gravel layer which scours into a sub-parallel sequence of sands and gravels. These form a sharp and erosional contact with a sand unit that dips up-glacier. The contact resembles an angular unconformity. This trench is only *ca.*7m from the Trench where Eklund and Hart (1996) reported evidence of pervasive deformation (Trench T:TA). (d) Small reverse faults in black sand layertowards the base of Trench T:TA. (e) Sharp wavy contact with massive sand, Trench T1 area 2. (f) Trench T:TA which Eklund and Hart (1996) argued showed a pervasive deformation profile. Folding is supposed to become increasingly isoclinal and recumbent towards the contact in response to increased shear strain. This trench is 2m down-flute from an enormous embedded boulder which is 2.5m long and nearly 2m wide. Eklund and Hart(1996) argued the sequence was preserved in the pressure shadow behind this boulder, but it is also possible some of the deformation relates to the emplacement of this boulder. The sand layers appear contorted and disrupted, and it is unclear how much of the folding relates to, or pre-dates the emplacement of Lithofacies A, or is related to non-tectonic deformation related to the early stages of sediment consolidation. The contact between Lithofacies A and the sand is sharp; (g) Complex sequence of deformed Zs and Sm layers observed in ice-stagnation hollow. The contorted layers appear to resemble some of the deformation structures seen in the Frontsjön sand unit.

In Trench T:TA, small reverse faults with throw of a few centimetres are observed in a black sand bed towards the base of the trench. These faults give a sense of movement that is opposed to the former glacier-flow direction (Figure 3.12d).The faults are not laterally extensive and do not penetrate an adjacent fold structure. In some trenches, where Lithofacies A is relatively clast-poor, sharp or loaded contacts occur (Figure 3.12e).

3.3.3 Interpretation

The physical properties of Lithofacies A suggest active subglacial transport, ploughing, lodgement, and bed-deformation have been involved in its genesis. Subglacial abrasion produces striae and rock flour and so the numerous wear marks on embedded boulders and the polymodal particle grain-size distribution of Lithofacies A are characteristic of active subglacial transport rather than passive englacial or supraglacial transport (Boulton, 1978; Benn, 1994; Etienne *et al*., 2003). Calcite precipitate in gouges also suggests a subglacial origin as it is thought to be formed by solute fallout from subglacial meltwater in zones of localised ice-bed pressure reductions, such as on the lee-side of boulders (Weertman, 1957; Hallet, 1979; Hubbard and Sharp, 1993; Etienne *et al*., 2003). The sub-rounded to sub-angular blocky clast forms, which give low C_{40} and RA indices (Figure 3.6), are indicative of crushing and abrasion of clasts in a subglacial environment (Benn 1995; 2004). Stoss and lee forms are thought to be produced byglacier overriding and abrasion of lodged boulders, whilst double stoss and lee forms are thought to be formed by ploughing followed by lodgement (Krüger, 1984; Benn 1994). The concentration of wear marks on the upper surfaces of many embedded boulders and the general absence of striae and other wear marks on lower surfaces, also suggests many boulders were emplaced by lodgement and subsequently abraded by the movement of debris-rich basal ice across their upper surfaces (Piotrowski *et al.*, 2001). Boulders have greater buoyant weight and drag than matrix material and are more likely to bridge across layers and so preferentially lodge from basal ice (Benn, 1994). The presence of dipping striae on some boulder flanks and the general pattern of wear marks from the stoss to lee ends are indicative of sediment moving over and around lodged boulders, and are indicative of deforming bed conditions, at least for the finer fraction of Lithofacies A (Hubbard and Reid, 2006). Clast clusters are thought to form by the nucleation of clasts around lodged boulders (Evans and Benn, 2004). The presence of clasts clusters, stoss and lee boulders, bullet-shaped clasts, and embedded boulders with striae concentrated on upper surfaces suggest lodgement played an important role in the formation of Lithofacies A.

Deformation tills are admixtures of far-travelled subglacial sediment and locally derived sediments homogenised in a deforming bed (Piotrowski *et al*., 2001; Evans *et al*., 2006). In the Forntsjön area – where the substratum consists of relatively thick sand beds –Lithofacies A contains up to 80% sand in the matrix, whereas further down-flute where the substratum is other diamictons, the matrix contains more silt (Table 3.5).This suggests that cannibalisation of the sand beds in the Frontsjön area locally sourced part ofLithofacies A's matrix. As mafic-rich boulders and cobbles could not be derived from the cannibalisation of the sand beds, Lithofacies Ain the Fronstjön area was probably formed by the mixing of the sand withsubglacially derived sediment. At Isfallsglaciären, the occurrence of boulders of dolerite and unweathered clasts of dolerite and meta-sediments in Lithofacies A is consistent with material on the forefield being sourced by the glacial transport of clasts eroded from the Kebne Dyke Complex, which crops out further up-glacier.

Table 3.5 Longitudinal Variations in Fractal Slope Gradients and Particle Grain-size Distributions in Lithofacies A in Fluted moraine, Areas 2 and 3 Isfallglaciären

Trench code	**TBYL Right Flank**	**TBYL Left Flank**	**T1 Area2**	**TF3-1**	**T1**	**TA**	**MMT3**	**T4**	**TT**	**T4 Area 2**
Slope Gradient	-2.73	-2.75	-2.63	-2.87	-2.82	-2.72	-2.81	-2.88	-2.76	-2.91
R^2	0.994	0.993	0.995	0.995	0.996	0.985	0.994	0.987	0.995	0.997
Distance along fluted moraine (m)	6	6	19	25	30	32	50	75	80	90
% Sand	79	74.8	80.6	67	75	70	77	63	66	62
% Silt	19	20.4	19.4	28	19	25.4	20	31	29	35

Note: All samples were taken from the top 0.4m of flutes. Sample TA was taken from the lee of a large embedded boulder. Samples with 30%+ silt yield the highest slope gradients. The distances have been measured from the distal edge of Frontsjön

Eklund and Hart (1996) argued the contact between Lithofacies A and the Fronstjön sand unit showed unequivocal evidence of pervasive subglacial deformation. However, detailed excavations in this area (Figure 3.11) suggest a re-interpretation is required because the nature of the contact between Lithofacies A and the sand substratum is extremely variable over short distances (Figure 3.12).

The sand sequence underlying Lithofacies A in the Fronstjön area contains lithofacies associations that are typical of proglacial lakes and low discharge streams entering silting ponds (Etienne *et al*., 2003). The granulometry of Lithofacies Aseems to play a role in controlling the nature of the contact with the sand substratum. Cobbles and boulders in boulder-rich horizons seem to plough and then lodge into the underlying sand, as evidenced by rucked-up prows of sand (Figure 3.12b). Recumbent folds, illustrated in Figure 3.12b, may pre-date ploughing/lodgement, but may also be produced or affected by it because sand beds have weak shear strengths (at 1m depth in Trench T1, the average was 14 KPa) and, if saturated, a ploughing boulder in Lithofacies A could transmit sufficient shear stress to the sand to induce ductile deformation. In Figure 3.12b the large boulder has a diameter of 0.6m and the folds extend to 0.4-0.5m depth beneath the boulder. The depth of deformation is consistent with the estimate that ploughing boulders can transmit stress to depths of 1 to 5 times their diameter (Tulaczyk *et al*., 2001). Where Lithofacies A is relatively gravel-poor, the contact with the underlying sands tends to be sharp and lacks obvious folding (Figure 3.12e). Clast-poor horizons lacking grain bridges are unlikely to transmit shear stress to depth as effectively as clast-rich horizons (Tulaczyk *et al*., 2001), and are likely to be less stiff, meaning they will deform at lower shear stresses (Hubbard and Reid, 2006). Subglacial deformation in a thin but easily deformed layer may produce a décollement surface and sharp contacts, especially if a weak layer exists within the profile such as a layer of silty-sand (Alley, 1991; van der Wateren *et al*., 2000). Some of the sharp contacts observed in relatively clast-poor horizons in the Fronstjön area are consistent with being décollement surfaces because there is no evidence of deformation below the contact (Boulton *et al*., 2001). Where shallow décollement surfaces occurred, cannibalisation of the sand beds would have beenlocally restricted (Piotrowski *et al*., 2001).

Open antiforms are thought to be indicative of ductile deformation at relatively low strain (Park, 1989). In the Fronstjön area they generally occur at quite shallow depths suggesting that the underlying sand was deformed to a limited depth. In a pervasive deformation profile, the strain rate increases up-profile reaching a maximum just below the glacier sole (Boulton and Hindmarsh, 1987; Piotrowski *et al*., 2006), and so open antiforms should be followed up-profile by overturned and recumbent folds which characterise zones of greater strain (Eklund and Hart, 1996). This sequence was generally not observed, although it is possible that the massive sand and thin micro-laminated sand beds – observed above the antiforms – represent homogenised sands and tectonic laminations produced in a more intensely sheared zone (Eklund and Hart, 1996; Piotrowski *et al*., 2006). However, there was an absence of features such as ripped-up clasts and sand augens, and a low number of diffuse contacts with mixing zones, all of which are thought to be typical of pervasively deformed sequences (Piotrowski *et al*., 2001). Ductile deformation indicates that pore-water pressures were high, despite the relatively high hydraulic conductivity of the sand beds, and suggests deformation may have occurred at a relatively early stage of glacier advance when the sands were saturated (Piotrowski *et al*., 2006).

It is unclear as to how much of the deformation of the Frontsjön sand unit predates the emplacement of Lithofacies A or is related to shearing by overriding ice. The unconformity observed in Trench T:T1 suggests that the tilting and erosion of the main sand beds predates Lithofacies A emplacement (Figure 3.12c). In this trench, the sub-parallel sand and gravels that separate the lower sands from Lithofacies A are typical of the glacio-fluvial sediments associated with proglacial braided streams (Etienne *et al*., 2003). The discontinuity between the inclined sands and sub-parallel sands suggest a phase of proglacial erosion and deposition separated the tilting of the lower sands and the emplacement of Lithofacies A. The unconformity was excavated just down-flow from an initiating boulder, and only a few metres away from where Eklund and Hart (1996) reported pervasively deformed profiles, which suggests deforming-bed conditions were locally very variable. It is possible that much of the deformation of the sands related to the proglacial and ice-marginal transmission of glaci-tectonic stresses imposed by the advancing glacier, with erosion and further deformation related to a subsequent phase of glacier overriding, which produced Lithofacies A as part of a deforming bed.

Eklund and Hart (1996) reported evidence of a pervasive deformation profile preserved behind a large embedded boulder in Trench T:TA (Figure 3.12f). However, the direction of movement along the small reverse faults observed at the base of this Trench are opposed to the direction of shearing by overriding ice, which suggests the faults may be unrelated to the emplacement of Lithofacies A. Further up the profile and nearer to the contact with Lithofacies A, evidence of isoclinal and recumbent folding is equivocal;many of the 'folds' have a distinctly convoluted appearance (Figure 3.12f). An alternative explanation is that the sequence relates to soft-sediment deformation associated with sediment consolidation (Lowe, 1975).Such soft-sediment deformation is known to produce loading structures and convoluted laminations in water-saturated sands during the early stages of consolidation when pore-fluids are rapidly expelled from non-cohesive sands and coarse silts (Lowe, 1975; Allen, 1982). In such situations, slumps can produce overfolds and the lateral spreading of sand bodies under non-uniform confining loads can produce faults (Allen, 1982). Loading structures and non-tectonic soft-sediment deformation structures, which resemble some of the folding seen in the Fronstjön sands, were observed in lacustrine sand beds formed in recently drained ice-stagnation hollows at Isfallsglaciären (Figure 3.12g). This suggests that non-tectonic soft-sediment deformation may account for the small reverse faults and convoluted folds observed in Trench T:TA.

In summary, some trenches on the distal side of Fronstjön do reveal unequivocal evidence of deformed sands at the contact with Lithofacies A, confirming subglacial deformation has been an important process in the formation of Lithofacies A (Eklund and Hart, 1996). However, the depth of deformation is quite limited, whilst some trenches reveal little evidence of deformation, or substrate deformation that predates glacier overriding, or convoluted laminations that could related to sediment consolidation. The variable nature of the contact between Lithofacies A and the underlying sand beds, and the patchy nature of deformation, lends support to the ice-bed mosaic model (Piotrowski *et al*., 2004). Indeed, evidence of lodgement, ploughing and erosion within close spatial proximity suggests multiple processes are involved in the genesis of Lithofacies A and in flute formation, and that lithofacies A is best classified as a traction till (Benn, 1994; Evans *et al*., 2006).

3.3.4 The Nature of Subglacial Deformation in Lithofacies A

Observations at the macro-scale reveal Lithofacies A has relatively low void ratios and porosity values, strong a-axis clast fabrics, and fissile textures, all of which are consistent with B-type horizons (Benn, 1995; Evans *et al*., 2006). Few of the porosity readings approach the 40% figure thought typical of dilatant tills (Paterson, 1994), or have void ratios as high as those quoted by Benn (1995) for A-type horizons in diamictons with similar granulometry.

Comment [DJG10]: You haven't mentioned these yet. Need to incorporate into description.

Clast a-axis fabrics measured in Lithofacies A in flute crestsare generally strongly clustered and have low isotropy. Plots of the S_1 and S_3 eigenvalues on bivariate scattergraphs (Figure 3.9a) enable clast fabric data to be compared with the process fields identified by Dowdeswell and Sharp (1986) for glacigenic sediments. The process fields overlap and clast fabric alone does not provide a genetic classification of diamictons (Bennett *et al*., 1999). Nevertheless, the clustering of flute clast fabrics in the process field described as 'undeformed lodgement till' in Figure 3.9a, which is equivalent to B-Type horizons (Benn, 1994), lends weight to this interpretation. The most strongly clustered flute crest fabrics plot in the process fields of meltout tills and lodgement tills, whereas less clustered fabrics plot as deformation tills, which is consistent with the interpretation of Lithofacies A as a traction till formed by multiple processes.

Comment [DJG11]: This doesn;t really mean anything. Presumably you mean strongly clustered?

Comment [DJG12]: Doesn't this contradict itself?

Boulton (1976), Benn (1994; 1995) and Gordon *et al*. (1992) reported fissile textures inB-type horizons comparable to those observed in Lithofacies A. Benn (1994; 1995) suggested the fissile partings represented discrete, discontinuous shear planes formed by brittledeformation. The Lithofacies A fissile partings reveal similar sub-parallel and near-vertical orientations, and their uneven spacing and (often) disrupted or discontinuous nature, especially in the vicinity of embedded boulders, are consistent with them being discrete shear planes (Alley, 1991).Flat faceted faces of Type 1 and Type 2 clasts are generally aligned along major fissile partings (Figure 3.7), and this lends further support to the interpretation of fissile partings as discrete shear planes. Krüger (1984) and Benn (1995) observed clast forms in subglacial diamictons identical to the Type 1 clasts. Benn (1995) argued Type 1 clasts were formed by differential rates of shear above and below discrete shear planes which generated faceted faces as the surface of the clast was planed-off.Type 1A clasts were formed where the rate of deformation was fastest above the shear plane, such that the lower surface of the clast abraded as it was dragged along the shear plane. Type 1B clasts were formed where the diamicton was shearing fastest above the upper surface, which planed it flat. Type 3 clasts may resist abrasion more effectively, or may represent relatively freshly eroded fragments that have experience insufficient subglacial transport/subglacial deformation to abrade a prominent flat face. Their sub-angular to angular nature supports this interpretation. However, care must be taken in the interpretation of clast types because clast form is thought to be partly controlled by lithology (Lukas *et al*., 2010), and observations in Lithofacies A samples show that individual clasts can sometimes intercept multiple fissile partings, with the flat faceted face aligned to none of these.

Subglacial deformation in B-type horizons is thought to be characterised by discrete, brittle, or brittle-to-ductile shear in relatively stiff diamictons under higher effective pressures and lower pore-water pressures than are associated with ductile deformation in highly dilatant A-type horizons (Boulton and Hindmarsh, 1987; Benn, 1995; Evans *et al*., 2006). Such subglacial conditions might occur in the late-stages of flute formation, especially in better drained and relatively stiff coarse sandy diamictons, if the development of an efficient subglacial drainage system reduced pore-water pressures and produced a strong ice-bed couple (Evans *et al*., 2006).

Inclusions of patches of coarse black sand in Lithofacies A, revealed in the impressions of removed clasts, may represent intraclasts preserved in lee-side pressure shadows of larger clasts. The preservation of such patches may indicate that the homogenisation process was incomplete, but if this were the case, then other evidence of incomplete homogenisation, such as rafts of ripped-up sediment, would be expected. As this was not the case, Lithofacies A must be considered well-homogenised. Not all sand patches occurred in the lee of clasts and an alternative explanation is that the sand patches are lag deposits. Water flow lines within coarse diamictons converge on large clasts and washing and sorting in the immediate vicinity can produce lag deposits (Muller, 1983).

The average fractal slope gradient of Lithofacies A (-2.9) is very similar to the slope gradients reported by Hooke and Iverson (1995) and Etienne *et al*. (2003) for diamicton from Storglaciären (-2.91). The till beneath Storglaciären is known to deform in a shallow layer, albeit discontinuously (Iverson *et al*., 1994), and because Lithofacies A has similar fractal dimensions, this lends support to the interpretation of Lithofacies A as a deformation till (Etienne *et al*., 2003). However, of 28 flute samples analysed, fewer than half (43%) had slope gradients in the range -2.87 to -2.92, with 14% of samples greater than this (highest value recorded -3.02) and 43% below -2.87 (lowest -2.63). As such, the range of slope gradients for Lithofacies A overlap with other lithofacies and cannot be considered diagnostic of deformation processes (Benn and Gemmel, 2003).

Comment [DJG13]: Not convinced this should be here. You haven't presented these data yet. Does it add anything essential, or could it be removed?

In area 3 at Isfallsglaciären (Figure 3.1a) there is an overall increase in the matrix silt fraction of Lithofacies A in a down-flute direction (Table 3.5). Samples with silt fractions in excess of 30% yield the steepest fractal slope gradients. It is known that the particle grain-size affects fractal dimensions (Hooke and Iverson, 1995; Benn and Gemmel, 2003), but the question is whether the change in particle grain-size distribution reflects specific subglacial processes.

The overall increase in the silt-sized fraction is consistent with cumulative sediment advection down-flute through particle slippage along shear planes in a mobile bed, leading to an increase in fines through particle comminution and hence increases in the fractal slope gradient. Alternatively, the changes in the particle grain-size distribution may simply reflect changes in the particle grain-size distributions of the pre-existing sediments that were cannibalised to form Lithofacies A, with the sandy matrix of Lithofacies A in the proximal reaches of areas 2 and 3 derived from the erosion of the Fronstjön sand unit.

Fractal slopes nearer to the -2.58 value obtained by crushing alone (see section 2.5.2) point to the importance of grain fracture in areas where sediment advection and abrasion is likely to have been more limited, for example in Trench TBYL located in the proximal area of flute 2 (Table 3.5). Indeed, the numerous smudges and high crushing index observed in all Lithofacies A samples supports the idea that grain fracture is an important mechanism of deformation along the entire length of flutes. Haldorsen (1981) found that crushing of crystalline rocks produced spikes in the particle grain-size distribution in the fine sand to coarse silt modes, whereas abrasion produced spikes in the coarse silt to medium silt modes. In the matrix particle grain-size distributions of Lithofacies A spikes occur in the fine sand and coarse silt modes (Figure 3.3a) which is consistent with the idea that crushing has played a major role in particle comminution.

3.3.5 Contrasts in Lithofacies A Properties between Flutes and Adjacent Interflutes

The generally weaker and more isotropic clast fabric readings from interflutes plot in the process fields of Dowdeswell and Sharp (1986) as glacigenic sediment flows or 'deformed lodgement tills' (Figure 3.9a); 'deformed lodgement tills' are equivalent to dilatant A-type horizons characterised by pervasive and ductile deformation (Benn, 1994; Evans *et al*., 2006). Interflute porosities exhibit a smaller range than flutes (interflute range 32-38%, N = 10) but arebelow the 40% values thought typical of dilatant tills (Paterson, 1994). Fissile partings are often continuous between flutes and interflutes (Figure 3.13), and if these are shear planes, then this suggests that both have been subjected to brittle or brittle-to-ductile shear, at least in the latter stages of flute formation.

Roberson *et al*. (2011) noted that fluted diamictons were relatively depleted in gravel compared to non-fluted subglacial diamictons. Lithofacies A in flute samples is similarly depleted in gravel (and coarse sand) but relatively enriched in fine sand and coarse silt compared to interflute samples. The relative enrichment in fines in flutes could relate to the movement of finer sediment from interflutes into subglacial cavities during flute formation by subglacial deformation (Boulton, 1976). Different size sediment fractions exhibit varying responses to imposed shear stresses in a deforming bed (Benn, 1994; Evans *et al*., 2006), with boulders preferentially lodging (Benn, 1994), gravel-sized clasts acting as passive markers once a-axes become flow-aligned (Iverson *et al*., 2008), whilst matrix sediments, especially if saturated,may continue to deform in a ductile manner even at relatively low shear stresses(Phillips *et al*., 2001b). As such, subglacial deformation is a multi-phase process that preferentially acts on the finer sediment fraction, which may continue to deform after the coarser diamicton framework has become immobile (Benn, 1994; Phillips *et al*., 2011b). This is most likely to happen in granular sandy diamictons like Lithofacies A where there is a greater probability of inter-granular locking taking place (Alley, 1991). The contrasts in granulometry between flutes and interflutes suggest a ductile phase of deformation mayhave occurred in whichsaturated fine-grained sediments were preferentially removed from interflutes by high confining pressures and injected into lower pressure subglacial cavities(Boulton, 1976; Benn, 1994; Phillips *et al*., 2011b).

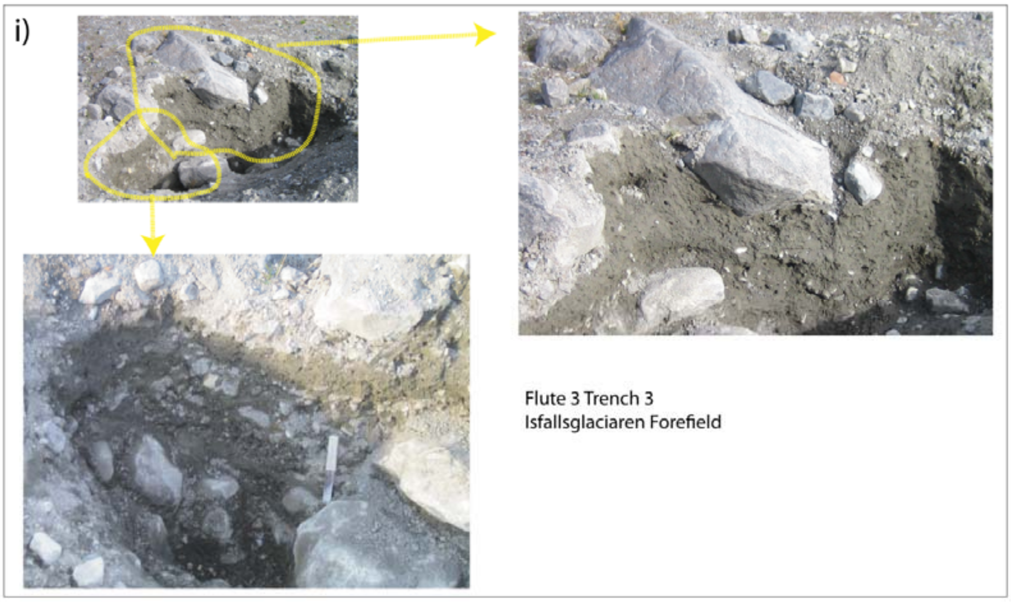

Figure 3.13 Details of Trench MMT3, Flute 3, Isfallsglaciären

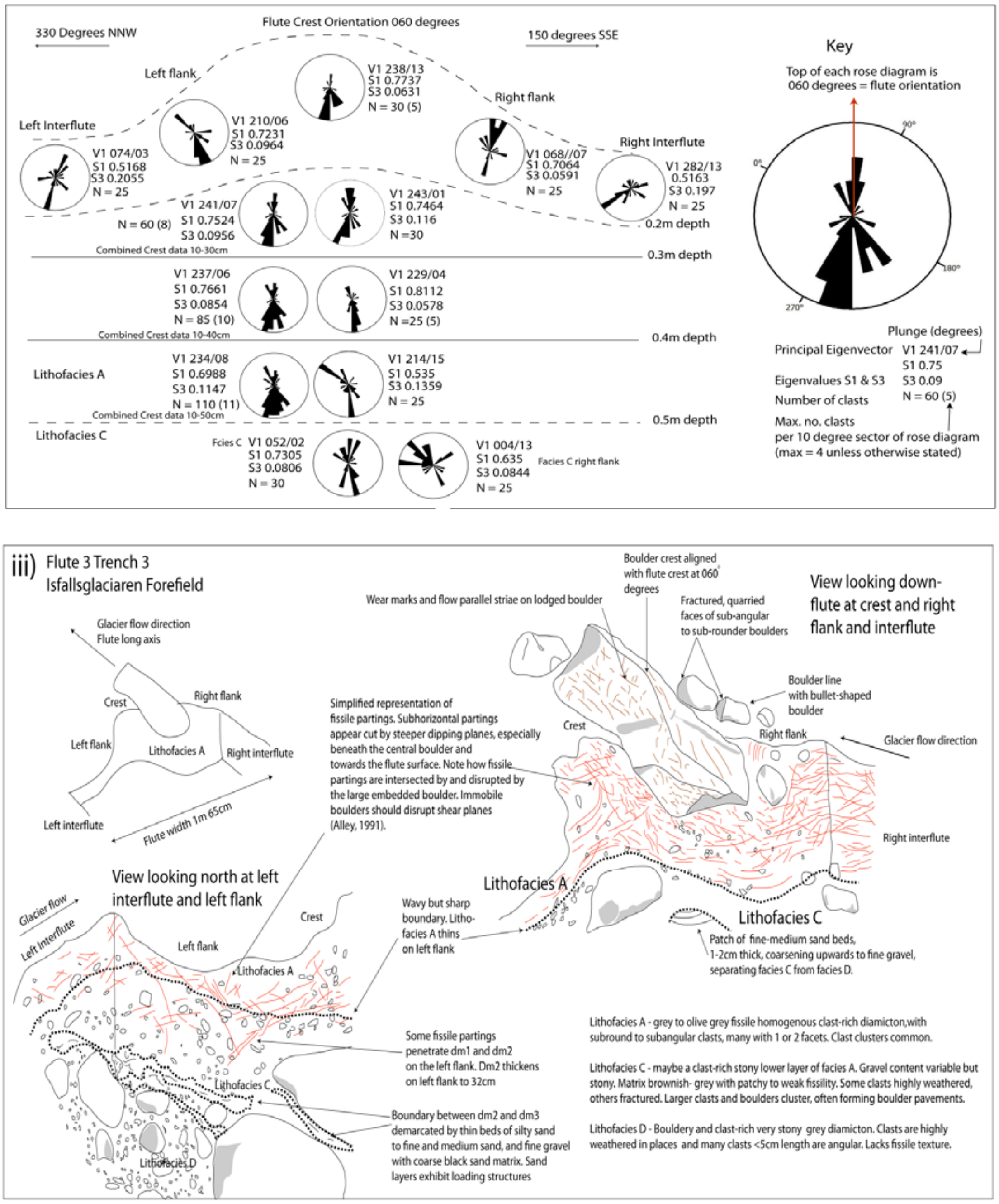

Figure 3.13 continued

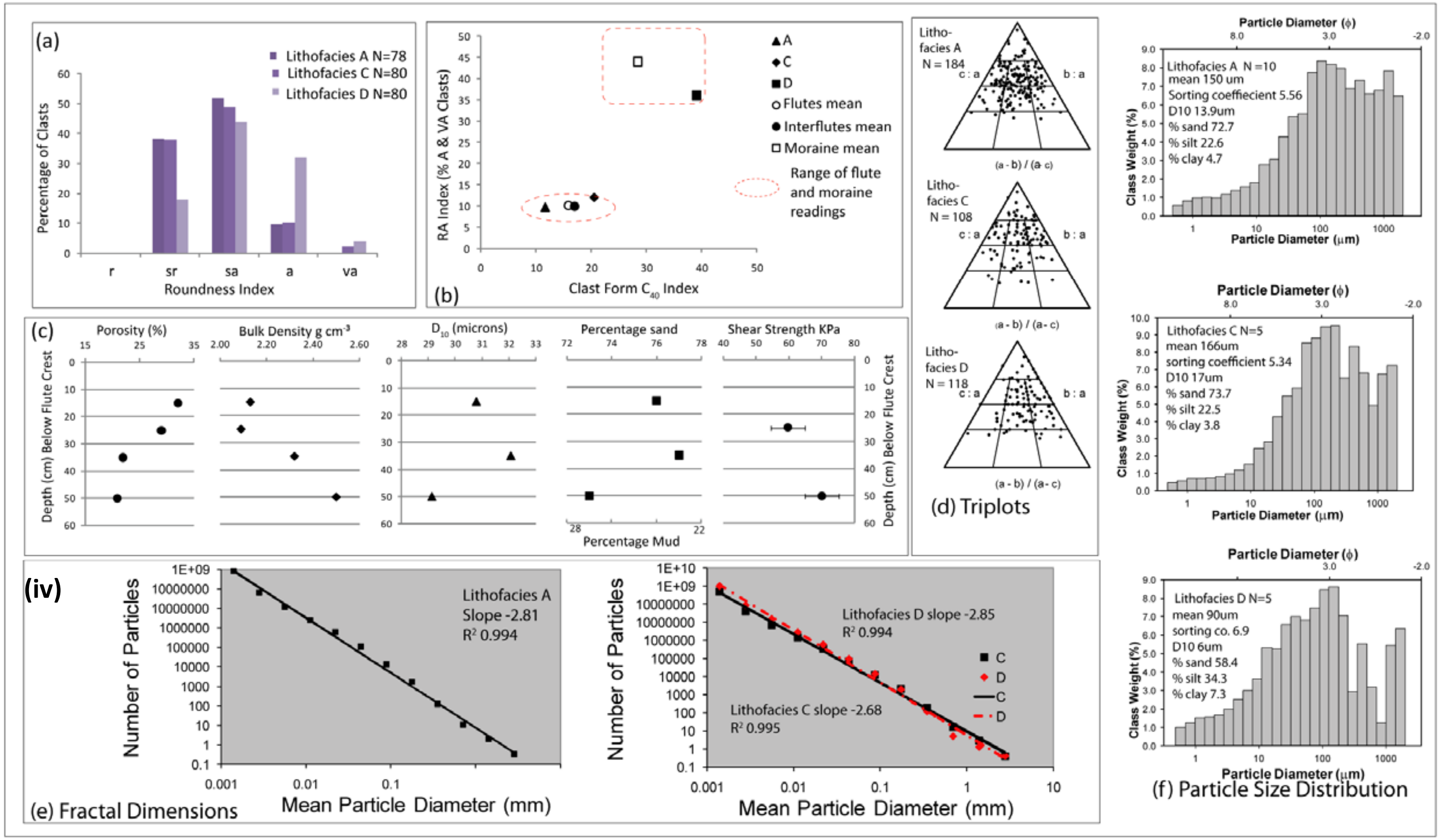

Figure 3.13 Details of Trench MMT3, Flute 3, Area 3, Isfallsglaciären. (i) View of trench looking ENE down-flute. (ii) Cross-section of flute showing clast fabrics at various depths and locations. (iii) Field sketch of lithofacies and contacts. (iv a-f) Physical properties of lithofacies. Note also the rapid decrease in porosity and increase in bulk density in Lithofacies A with depth, and the strong, flow parallel clast-fabrics beneath the flute crest. In iv f, the mean pgsd, sorting coefficient (sorting co.) and D_{10} are in μm.

In 30 samples taken from various subglacial lithofacies in the 3 forefields, steep fractal slopes (≥-2.9) are closely associated with strong and linearly clustered clast fabrics (Elongation index >0.65, see Figure 3.14a), and with particle grain-size distributions having high mud contents (>40%, see Figure 3.14b). One explanation for these relationships is that higher strain magnitudes – associated with greater sediment advection – resulted in significant particle comminution. This comminution produced silt spikes and steep fractal gradients, whilst the high strain magnitude induced strong flow-parallel clast alignments. However, this explanation does not account for the differences in particle grain-size distributions and clast fabrics between flutes and adjacent interflutes, which have been exposed to the same regional subglacial stress regime. An alternative explanation, and the one favoured here, is that the transfer of fines from interflutes to flutes during flute formation accounts, at least in part, for the differences in particle grain-size distributions and mean fractal slope gradients between flutes and interflutes. This transfer may also account for contrasts in clast fabrics between flutes and interflutes, although these can also be explained by the degree to which sediment was confined during deformation (Benn, 1994). It should be noted that the relations shown in Figure 3.14 also reflect a general increase in clast fabric strengths and mud content (and hence fractal slope gradients) with depth in the diamicton plain/sheet (see section 3.4 below).

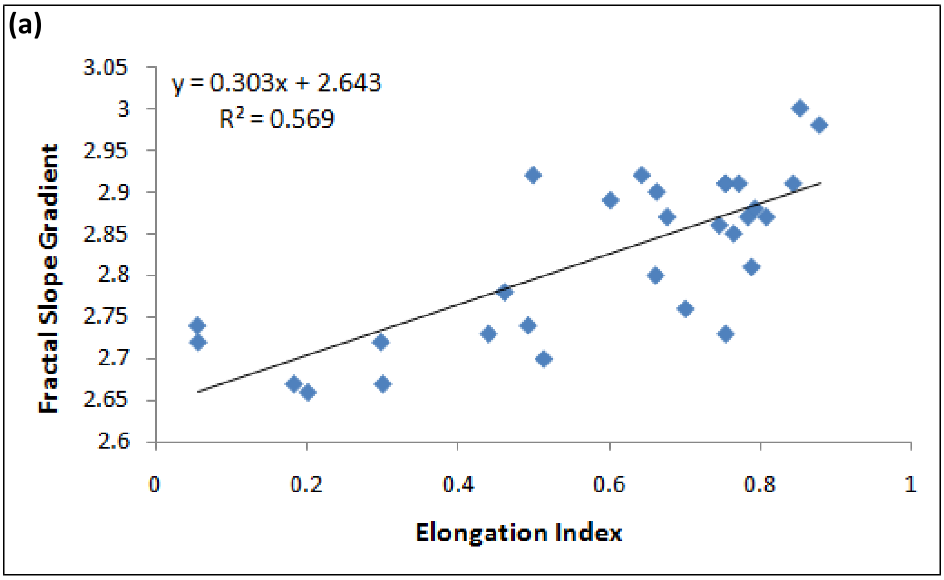

Figure 3.14 Fractal Slope Gradient, Elongation Index, and Mud Content for Lithofacies A, B, and C.

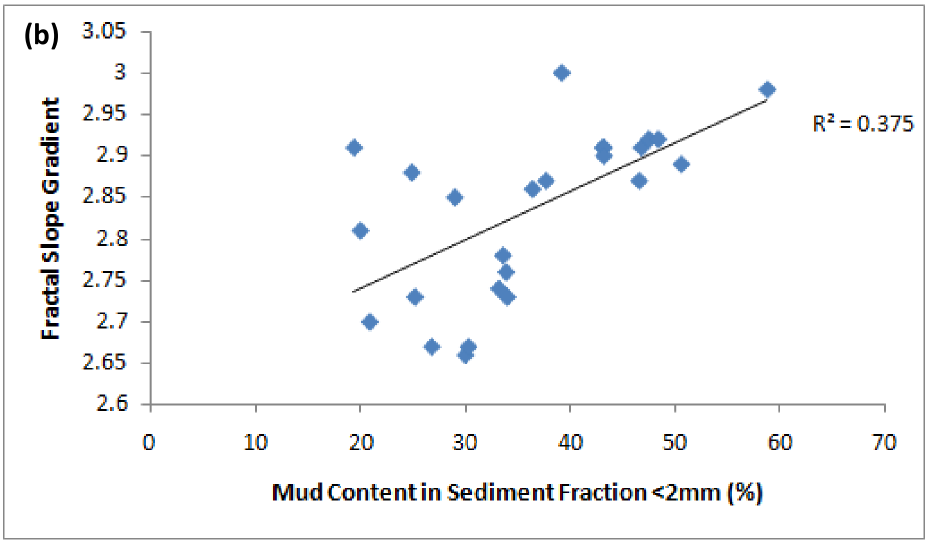

Figure 3.14 Fractal Slope Gradient, Elongation Index, and Mud Content for Lithofacies A, B, and C. Figure 14a shows the relation between fractal slope gradient and macro-fabric strength, as measured by the elongation index for 30 samples from flutes and interflutes are various depths, and from Lithofacies B and C from the diamictons sheet and plain. Negative fractal slope gradients have been converted into positive values for ease of plotting. There is a strong positive correlation (+0.75) and linear regression accounts for *ca*.57% of the variance. A 1-tail student t-test returns a t- value of 6.08 and a p-value of 7.44E-07, which is significant at the 0.01 level. Steep fractal slopes are associated with strongly elongate clast-fabrics. Figure 3.14b shows the relation between fractal slope gradient and percentage mud (silt and clay) content in the matrix for much of the same sample (N = 25). Linear regression accounts for about 38% of the variance, with a positive correlation (0.61). A 1-tail student t-test returns a t-value of 3.71 and p-value of 0.00056, which is significant at the 0.01 level. Steep fractal slopes are associated with high mud contents.

3. 3.6 The Shear Strength of Lithofacies A

Comment [DJG14]: Why isn't this incorporated into the description of the facies?

The peak shear strength, apparent cohesion, and internal angles of friction of Lithofacies A samples extracted from 0.2-0.4m depth in flutes from each forefield are shown in Table 3.6. These results were obtained from shear box tests. For comparison, results are also shown for a Lithofacies B sample taken from 0.7m depth in the diamicton plain (Storglaciären). Shear strengths and friction angles are similar in each Lithofacies A sample (Figure 3.15a), although sandy Lithofacies Afrom Isfallsglaciären is the weakest (shear strength 93KPa with 130KPa normal load), whilst the coarser diamicton from Kaskasatjåkka the strongest (shear strength 118KPa at the equivalent normal load). The samples were relatively dense and dilated in shear reaching peak shear strength slowly (Figure 3.15b). All samples have low hydraulic conductivities, although these can vary by an order of magnitude (range 2.82×10^{-6} to 3.89×10^{-8}, see Table 3.6).

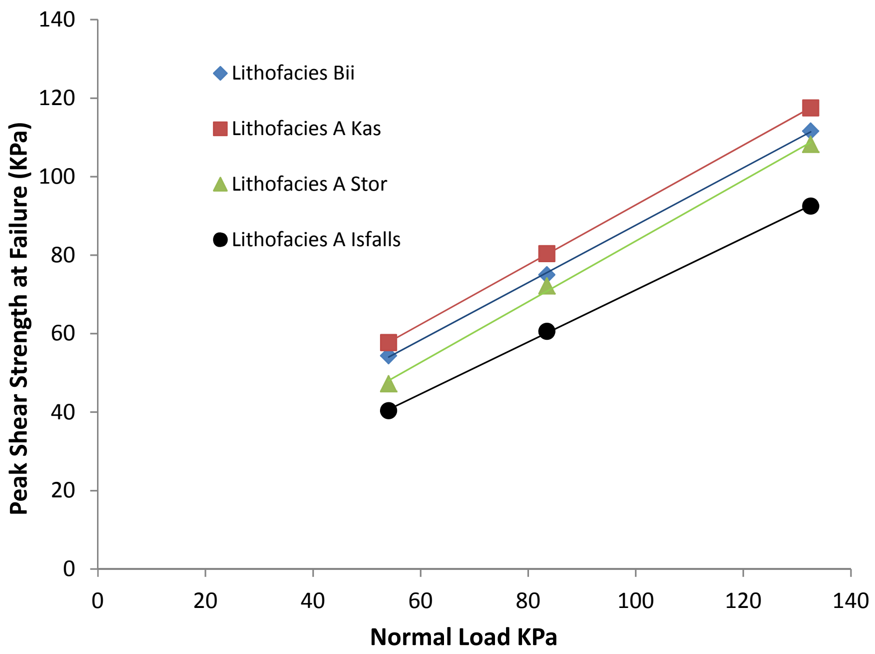

Figure 3.15a. Peak Shear Strengths under Increasing Normal Loads for Lithofacies A and B. Prior to shear box tests, the coarsest fraction (>6mm) was removed. This represented 13% by weight of the Isfallsglaciären (Isfalls) flute sample, and 11% of the Storglaciären samples (Syd = sample taken from log SL1 at Sydjåkk). The Kaskasatjåkka (Kas) flute sample was the coarsest and 22.5% of the sample by weight was removed. The samples were remoulded and tested at a range of moisture contents and densities. The above graphs represent the peak shear strengths at failure under three normal loads (54 KPa, 83 KPa, and 132 KPa) for sediments at field conditions, that is, the density and moisture contents sampled in the field. It can be seen that peak shear strength increases with normal load in a similar way for all samples, and that Lithofacies A from Isfallsglaciären consistently shows the weakest strength, whilst Lithofacies A from Kaskasatjåkka is the strongest under all loads. Facies A and B from Storglaciären have very similar strengths. For each line, the Y axis intersect gives the apparent cohesion value and the angle with the horizontal the internal fraction angle (Head, 1982).

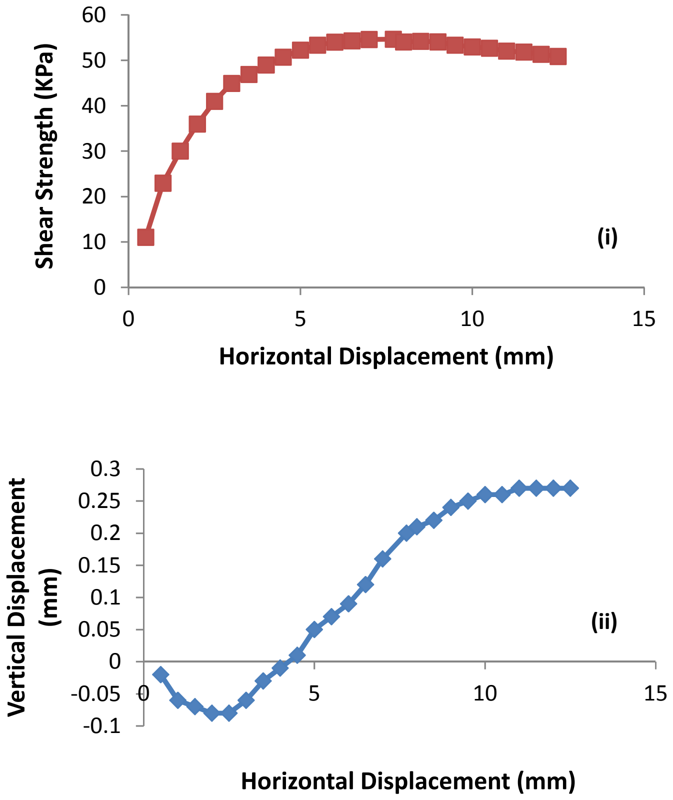

Figure 3.15b Changes in Shear Strength and Vertical Displacement during a Shear Box Test for a Dry and Remoulded Sample of Lithofacies Bii from Sydjåkk Log SL1 under 54 KPa Normal Load. Figure 3.15b(i) shows the changes in shear strength over time as the shear box moved with a horizontal displacement rate of 0.6mm s^{-1}. The shear strength initially increases to a peak value then tails off towards a residual value. Figure 3.15b(ii) shows the vertical displacement measured during horizontal shearing. Initially the sediment compacts in response to the applied normal load, before dilating slightly in response to shear. Dilation occurs in relatively dense sediments during shear and results from grains slipping over each other during shear, which requires additional force and hence a peak in strength occurs (Head, 1982). Dilation continues until the critical voids ratio is reached, after which no more dilation occurs with shear and the residual shear strengthis reached (Head, 1982). This seems to occur after about 11mm of horizontal displacement in the example above. The sediment is less dense and slightly more porous at the end of the test as a consequence of dilation (Craig, 1997), although the residual shear strength in this case appears to be only slightly lower than the peak value. Sediment density is a key control on peak shear strength (Head, 1982). All Lithofacies A samples under field conditions showed similar profiles to the one shown and were relatively dense, over-consolidated sediment.

Table 3.6 Sediment Characteristics and Shear Strength Values for Lithofacies A Samples (Flutes) and Lithofacies Bii (Sydjåkk Log SL1)

	D_{50} µm	D_{10} µm	Snd %	Silt %	Clay %	Hyd. Cond. m/s	Void Ratio	Por. %	BD g/cm^3	Sat. % F.C.	Coh KPa	Φ (°)	P.S. Ld 50 KPa	P.S. Ld 80 KPa	P.S. Ld 130 KPa
Is	102	8.6	83	13	4	2.82 x10^{-6}	0.56	36	1.84	32.2	8.2	33.5	40	61	93
Kas	98	1.9	56	27	17	3.89 x10^{-8}	0.32	24	2.22	48	20.5	37.3	58	80	118
Sfl	74	5.7	54	38	8	3.29 X10^{-7}	0.41	29	2.04	59	10	37.7	47	72	108
Syd	72	4.2	53	37	10	1.74 X10^{-7}	0.33	25	2.18	64	18	36	54	75	112

Note: Is = Isfallsglaciären Lithofacies A sample; Kas = Kaskasatjåkka Lithofacies A sample; Sfl = Storglaciären Lithofacies A flute sample; Syd = Sydjåkk Lithofacies B sample from the diamicton plain. The pgsd data relates to the matrix fraction. Por = porosity; BD = the bulk density of the sample; Hyd. Cond. = the hydraulic conductivity estimated using the Hazen formula (see section 2.5.4); Sat % F.C. is the degree of sediment saturation at field conditions (Head, 1982). Coh. is the apparent cohesion, that is, the shear strength when normal load = 0 (Craig, 1997); ϕ = the internal angle of friction; P.S. = peak shear strength under different Ld = loads for remoulded samples, such that particle densities and moisture contents matched the field conditions. Note that the Isfallsglaciären sample is the most porous and sandy, and has the lowest cohesion and internal friction angle, and lowest peak shear strengths. Note that the Kaskasatjåkka sample has the highest clay content and apparent cohesion, the lowest porosity and highest dry density, and the strongest peak shear strengths.

3.3.7 Discussion of factors affecting shear strengths

Comment [DJG15]: Specify what this is a discussion of.

The cohesion values and angles of internal friction are in the range of values quoted for typical subglacial tills(Paterson, 1994; Benn and Evans, 2010). The variations in hydraulic conductivity suggest pore-water pressures, and hence susceptibility to bed-deformation, are spatially variable. Indeed, Lithofacies A samples from the distal reaches of flutes in Isfallsglaciären in Area 3 have a higher silt content (Table 3.5) than the sample shown in Table 3.6 and would have lower hydraulic conductivities. At times of elevated pore-water pressure, Lithofacies Afrom Isfallsglaciären would be the weakest diamicton, as it is at field conditions, because it lacks cohesion and because the less dense sample has a lower friction angle, whilst the stonier nature of Lithofacies A from Storglaciären and Kaskasatjåkka would provide a stiffer framework to resist deformation. As such, the Isfallsglaciären Lithofacies A is likely to be the most easily deformed.

In the ablation area of contemporary Storglaciären, confining pressures are in the range 85 – 280 KPa (Iverson *et al*., 1999), whilst winter basal shear stresses are around 92KPa (Iverson *et al*., 1994). The Storglaciären Lithofacies A sample, with a cohesion value of 10KPa and friction angle of 37.7° yields shear strengths ranging from 75 – 226KPa (equation 1.3) under these confining pressures, and would require elevated pore-water pressures for deformation to occur (Cuffey and Paterson, 2010). This suggests that the production of deformation tills in the Tarfala Valley requires high pore-water pressures and this, in turn, requires warm-based ice (Piotrowski *et al*., 2006). As there is evidence that bed-deformation was involved in the formation of Lithofacies A, it follows that flutes must form under warm-based parts of glaciers (Eklund and Hart, 1996), which is contrary to the hypothesis of Hoppe and Schytt (1953) and Gordon *et al*. (1992). Furthermore, in Trench MMT3 at Isfallsglaciären (Figure 3.13), a less porous Lithofacies A occurred, with bulk density increasing from 2.19to 2.38 gcm^{-3}between 0.15 and 0.4m depths. Remoulded samples sheared at these densities under 130 KPa normal loads showed peak shear strength increased from 78 KPa to 117 KPa over these depths. This rapid increase in strength, linked to increased bulk density and friction angle (ϕ=38.4° at 0.4m depth), places a limit on the depth of deformation. As such, deformation is likely to be spatially and temporally variable and depth-limited, and these data support the ice-bed mosaic model of Piotrowski *et al*. (2004).

3.3.7 The Thickness of Lithofacies A

Lithofacies A in fluted moraine in each forefield generally averages between 0.3-0.5m thick and reaches a maximum thickness of 1m (Figure 3.16). At Isfallsglaciären, Lithofacies A displays variable thickness across the forefield, being thinner on the southern side of the proximal slope of the overridden outer moraine, on the immediate southern margin of the riegel, and where the substratum consists of sorted sediments in the proximal flute zones near Frontsjön. Lithofacies A is thickest in the proximal reaches of flutes in Area 2 and the distal flute reaches in Area 3 where the substratum consists of other diamicton facies. Non-fluted surfaces at Isfallsglaciären have similar average thicknesses. The influence of substratum type on the thickness of Lithofacies A is shown in Table 3.7. At Kaskasatjåkka and

Storglaciären the thickness of Lithofacies Ain fluted moraine seldom exceeds 0.3m (Figure 3.16b) whether the substratum consists of other diamictons or sands and gravels, and there is no obvious increase in Lithofacies A thickness in a down-flute direction.

Table 3.7 Lithofacies A Thickness and Underlying Substratum, Isfallsglaciären Areas 1-3

Lithofacies A Thickness (cm) – Substrate = Other Dm	**Lithofacies A Thickness (cm) – Substrate = Sorted Sediments (Sandy Gravels/Sand Beds)**	
65	20	
50	15	
35	14	
46	30	
90	8	
45	50	
50	10	
50	30	
20	10	
77	30	
85	9	
40	20	
10	28	
7		
23		
3		
20		
40		
100		
36		
60		
45.3	***21.1***	***Mean***
27.2	***12.2***	***St Dev***

Note: Average thickness is higher when the underlying substrate is other diamictons, although the high standard deviation (St Dev) shows thickness is very variable.

3.3.8 Discussion of factors affecting Lithofacies A thickness

Eklund and Hart (1996) suggested that, away from the pressure shadow of initiating boulders, Lithofacies A increased in thickness down-flute due to excavational deformation and increasing strain. In Area 3 of Isfallsglaciären, where they worked, Lithofacies A does increase in thickness distally along flutes, but this is not the case in the other forefields. Furthermore, in Area 2 (Isfallsglaciären), Lithofacies A is thickest in the proximal parts of flutes. An alternative explanation for the increase in thickness of lithofacies A in area 3 is that the greater matrix silt content (Table 3.5) facilitated higher pore-water pressures which enabled the bed to deform at lower shear stresses and promoted the formation of a thicker layer.

Variations in till thickness in a deforming bed have been related to the way in which the underlying substratum controls hydraulic conditions (Kjær *et al*., 2003). At Sléttjökull, Iceland, thicker tills formed where deformation occurred around stiff cores of impermeable substratum which encouraged high pore-water pressures and pervasive deformation (Kjær *et al*., 2003). The till was thinner where the substratum comprised sorted sediments. Similarly, at Isfallsglaciären, variations in the thickness of Lithofacies A seem to relate to the nature of the substratum, with thicker outcrops generally occurring where the substratum consists of other diamicton facies. The Fronstjön sand unit would have provided a relatively permeable substratum which would have encouraged better subglacial drainage conditions and lower pore-water pressures in Lithofacies A, resulting in less deformable conditions and a thinner deforming bed. This suggests that at the forefield scale, the subglacial system is highly sensitive to changes in drainage conditions (Kjær *et al*., 2003). However, at Isfallsglaciären, the thickness of Lithofacies A is locally very variable, and can be up to 0.5m thick on sorted sediments (presumably where restricted subglacial drainage conditions prevailed, allowing elevated pore-water pressures and a downward movement in the loci of deformation).

Comment [DJG16]: reference needed

At Kaskasatjåkka and Storglaciären Lithofacies A is generally thin regardless of the nature of of the substratum. As such, it is too simplistic to relate Lithofacies A thickness solely to the hydraulic conductivity of the substratum. A coarser subglacial bed, such as stony, bouldery diamicton, would provide a relatively stiff and rough surface which would exert considerable drag, and this is likely to encourage lodgement from debris-rich basal ice (Iverson *et al*., 2007; Cuffey and Paterson, 2010). As such, an increase in till thickness above coarser substratum might relate to increased lodgement as well as deformation. Sand beds are likely to provide a smoother surface with lower drag over which basal sliding can occur more easily and, at times of elevated pore-water pressures, a wet smooth bed acts as a lubricating layer which promotes basal sliding, with bed-deformation focused into a thin layer (Cuffey and Paterson, 2010). The base of the deforming layer may be demarcated by a décollement surface, especially if weak fine-grained sediments occur in the deforming pile (Alley, 1991).The sharp contacts between lithofacies A and the Fronstjön sand unit in Area 3 are consistent with décollement and the thickness of Lithofacies A is consistent with bed-deformation being focused into a relatively thin layer.

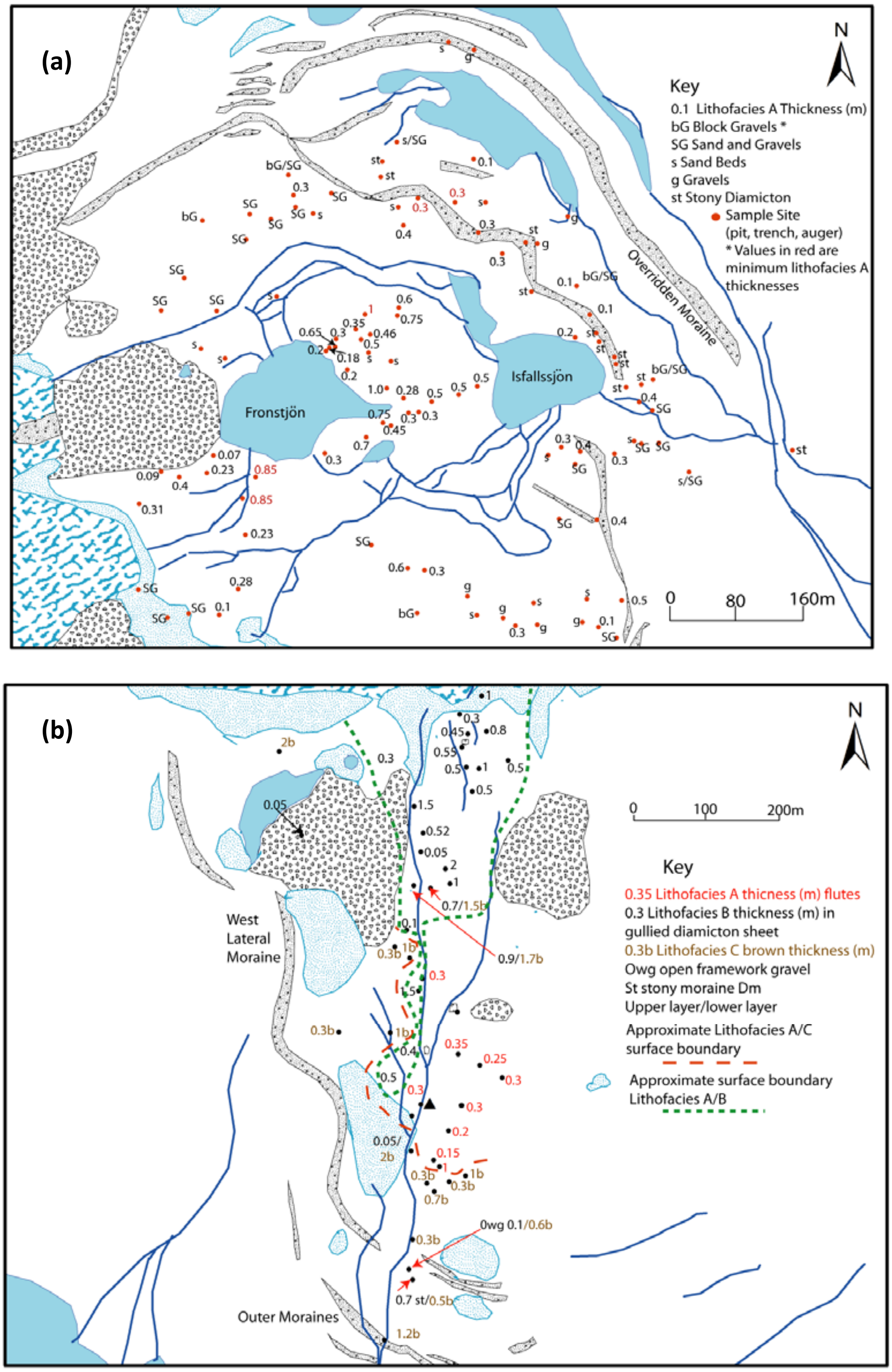

Figure 3.16 Lithofacies A Thickness in Isfallsglaciären (a) and Kaskasatjåkka (b).

The average thickness of Lithofacies A, whether from a fluted or non-fluted areas, is consistent with measured thicknesses of deforming beds from beneath contemporary glaciers, including Storglaciären (Iverson *et al.*, 1994; see Table 1.1), and suggests similar glacier dynamics prevailed during the Little Ice Age. The depth of deformation was limited. This is partly explained by the rapid increase in shear strength with depth in sandy, granular Lithofacies A. In most trenches, Lithofacies A was between 0.3-0.5m thick, and this consistency in thickness must also relate to the balance between sediment input (from erosion and lodgement) and output (by till advection) in the deforming bed (Cuffey and Paterson, 2010). The similarity in the average thickness of Lithofacies A in each forefield suggests that a similar balance between these forces existed in each glacier during the Little Ice Age Advance. Where Lithofacies A thickens, there was either an increase in sediment input, or increased cannibalisation of pre-existing sediments.

3.4 Lithofacies B, Diamicton Plain/Sheet

Lithofacies B forms the upper section of the diamicton sheet at Kaskasatjåkka (Figure 3.2b) and the diamicton plain at Storglaciären (Figure 3.2c). It also occurs as isolated patches between active meltwater channels in areas to the north and south of the diamicton plain at Storglaciären.

3.4.1 Description

Lithofacies B is the main diamicton of the diamicton plain/sheet. It appears homogeneous at the macroscale, and is a matrix-supported granular diamicton. Lithofacies B has a lighter grey colour than Lithofacies A, and has a higher proportion of angular clasts, with a small percentage of very angular clasts appearing (Figure 3.6b&c). As such, Lithofacies B can be discriminated from Lithofacies A using C_{40}/RA plots (Figures 3.6 a-c). Lithofacies B has a lower crushing index than Lithofacies A (Figure 3.5) and a finer matrix particle grain-size distribution. For example, at Kaskasatjåkka, Lithofacies B has 44.9% mud content and higher clay content (9.1% versus 4.9%) than Lithofacies A, but is less clast-rich (Figure 3.3b & e). Lithofacies B porosities are in the range 26-33% (N=10). The majority of embedded boulders in Lithofacies B are sub-angular to sub-rounded and exhibit similar forms and wear patterns to those observed in Lithofacies A. The surfaces of the diamicton plain and dissected diamicton sheet are strewn with numerous large boulders, some of which are not striated and

Comment [DJG17]: Add reference to appropriate figure/table angular to sub-angular; some embedded clasts near to the surface have very steep dips. Patterned ground was observed on the diamicton plain just north of logs NL1 and 2 (Figure 3.1c).

Lithofacies B can be divided into two sub-types based on its physical properties. Lithofacies Bi occurs in the upper *ca*. 0.3m of the diamicton plain/sheet. It forms a merging contact with Lithofacies Bii. Lithofacies Bi exhibits a variable fissile texture, with the upper 2-5cm often lacking fissility, whereas Lithofacies Bii is strongly fissile. Lithofacies Bi has a variable fractal slope gradient, ranging from -2.91 to -2.69, with a mean of -2.81 (Figure 3.10e), whereas most fractal slope gradients for Lithofacies Bii fall near to the average of -2.91 (Figure 3.10c). At Storglaciären, Lithofacies Bii has a consistently finer matrix particle grain-size distribution than Lithofacies Bi (Figures 3.3f & h), having less coarse sand and more clay-sized material (mean of 5 samples yields 56.8% sand, 34.8% silt and 8.4% clay). Furthermore, at both Kaskasatjåkka and Storglaciären, Lithofacies Bi can be discriminated from Lithofacies Bii by clast fabric shape (Tables 3.8 and 3.9; Figures 3.17 and 3.18). The elongation and isotropy indices for Lithofacies Bi and Bii clast fabrics have been plotted on a ternary graph in Figure 3.18a and Benn and Ringrose's (2001) bootstrapping programme used to establish 10th convex hulls. The Lithofacies Bii sample points have more linearly clustered shapes and the Lithofacies Bi sample point plots outside the 10th convex hulls of Lithofacies Bii, suggesting the clast fabric shapes are statistically different.

Lithofacies Bii displays a strongly fissile structure, with dip angle (and sometimes direction) and spacing of fissile partings varying over decimetre vertical and lateral scales. In the Storglaciären diamicton plain, the shear strength of Lithofacies Bi & Bii is variable with depth and correlates with the spacing of the fissile partings (Figure 3.17). Where the spacing is close (*ca*. 1mm or less) shear strength weakens, but where the spacing is wider (0.5– 3cm), shear strength increases. Weaker zones with very close (micro) fissility are typically between 0.1 and 0.3m thick.

Clast clusters and stone lines are common in Lithofacies Bii. Stone lines are similar to boulder pavements but consist of lines of granules and pebbles (Evans and Benn, 2004). Boulders commonly exhibit stoss and lee forms and removed boulders at log NL1 and NL2 show evidence of wear marks on all surfaces, or concentrated on upper surfaces. Type 1 and 2 clasts are common and show similar distributions and lithologies to those observed in Lithofacies A. Undisturbed bright orange weathering haloes are occasionally observed around fine-gravel clasts in Lithofacies Bii, as are fractured clasts which have fractures aligned with major fissile planes, but in which broken pieces remain in situ (Figure 3.19a).

Lithofacies Bii sampled from logged sequences on the Sydjåkk side of the diamicton plain (Storglaciären) are indistinguishable from Lithofacies Bii sampled from the Nordjåkk sections based on particle grain-size distribution (Figure 3.3h-i), fractal slope gradients (both yield average values of -2.9, Figure 3.10c-d), crushing index and clast types. However, the Sydjåkk clast fabrics are more variable (S_1 range 0.50 to 0.77; elongation index range 0.28 to 0.82, Table 3.8, and Figures 3.9b and 3.18b) and show considerable variation in V_1 orientation with depth (range 029° to 245°). In Figure 3.18b, Lithofacies Bii clast fabrics taken from logged sections on the Sydjåkk side of the diamicton plain are compared with clast fabrics from logged sections on the Nordjåkk side of the plain. The Sydjåkk sample points plot outside of the 10th convex hulls of Lithofacies Bii from the Nordjåkk sections, and have less linearly clustered fabric shapes, suggesting a statistical difference between the clast fabric shapes of the two areas.

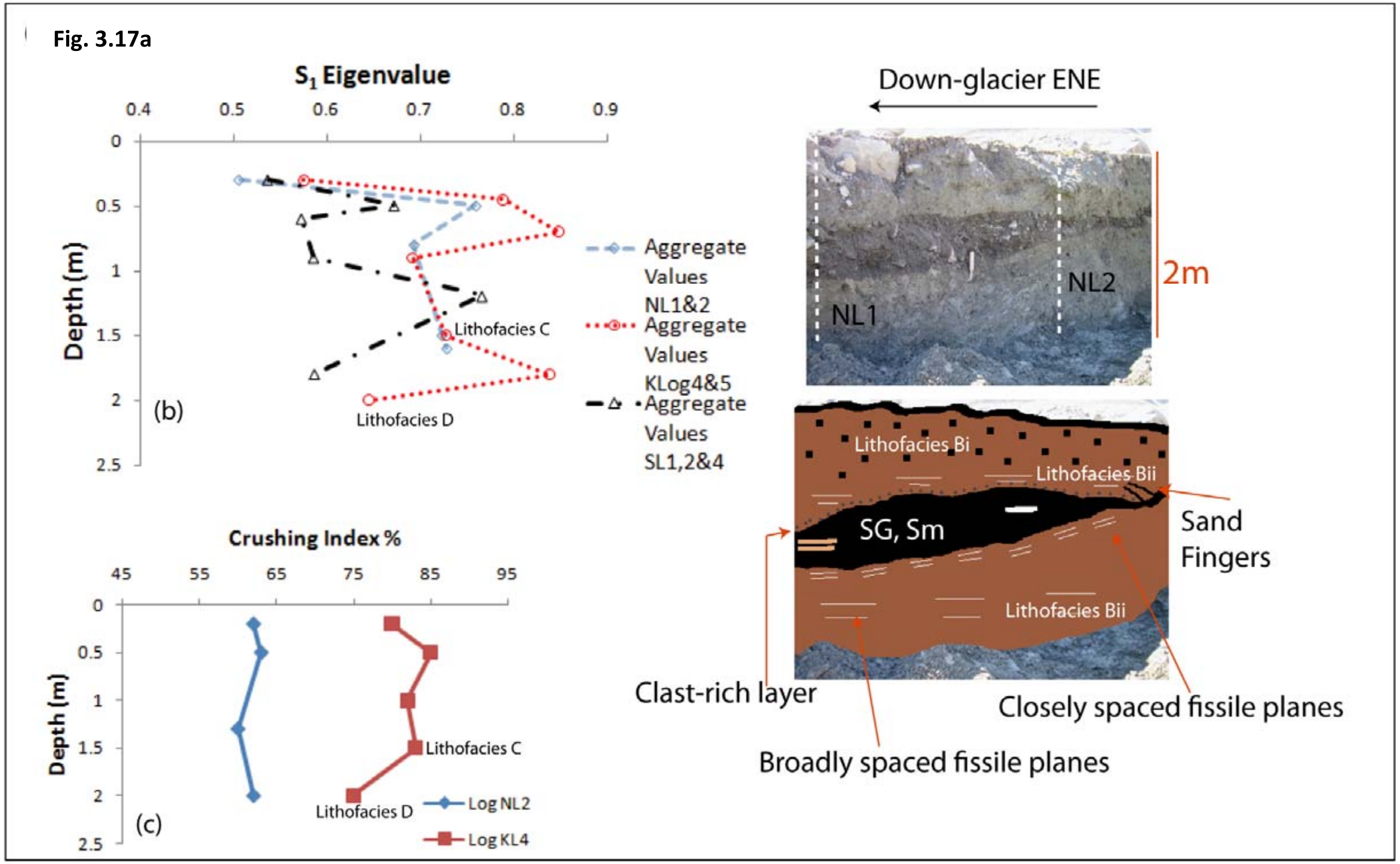

Figure 3.17 The Storglaciären Diamicton Plain at Nordjåkk Logs NL1 and NL2.

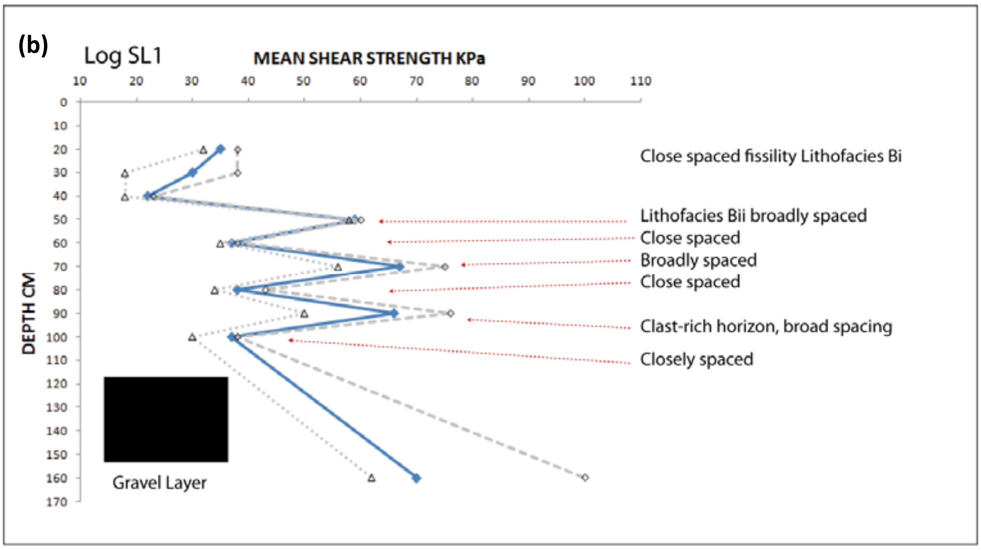

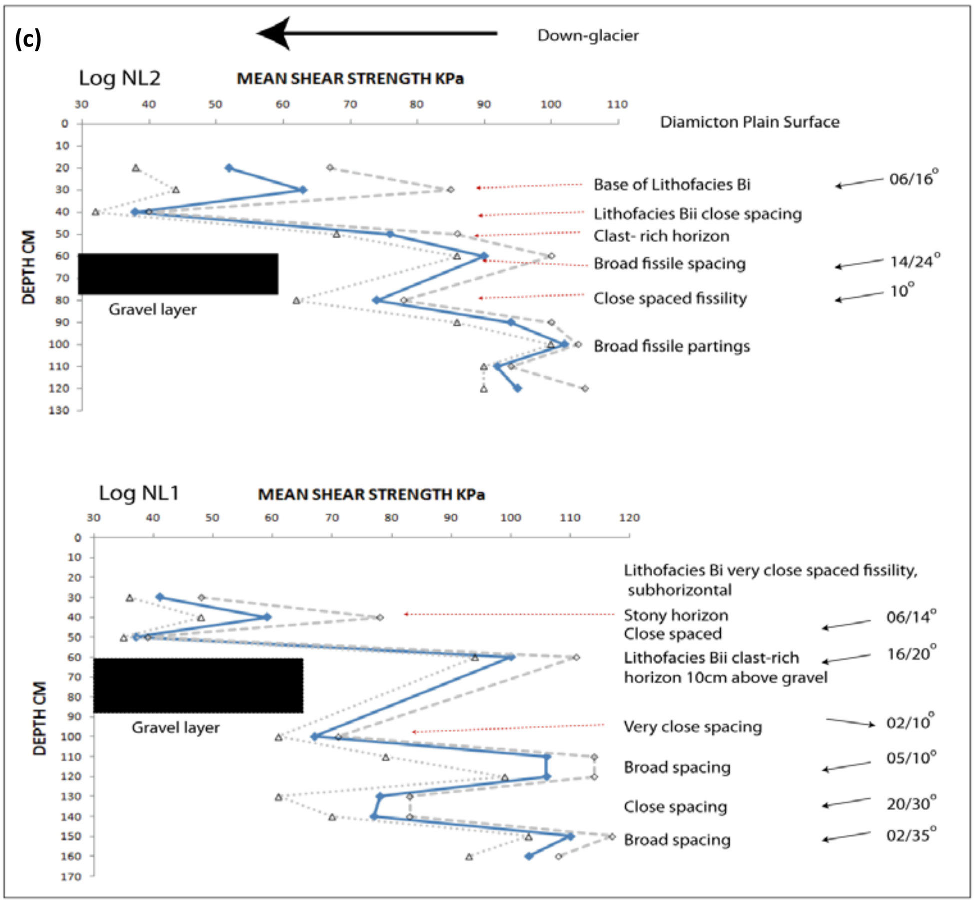

Figure 3.17 continued.

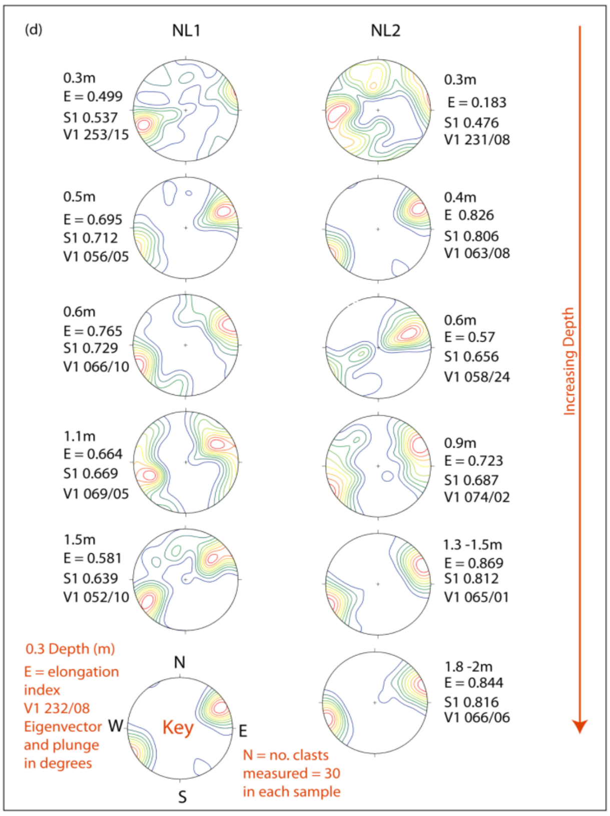

Figure 3.17 The Storglaciären Diamicton Plain at Nordjåkk Logs NL1 and NL2. (a) Field view and sketch of gravel sheet and variations in aggregate macro-fabrics in vertical sections in the Diamicton Plain and Sheet (the blue line NL1&2 shows aggregate clast fabrics from the Nordjåkk log sections 1 and 2 from the diamicton plain; the red line Klog 4&5 shows aggregate clast fabrics from logs 4 and 5 of the diamicton sheet; the black line SL1&2 shows aggregate data from logs 1 and 2 from the Sydjåkk side of the diamicton plain. (b & c) Variations in shear strength with depth and relation to spacing of fissile partings. (d) Variations in macro-fabric strength with depth in Lithofacies B, Logs NL1 and NL2. Note: in (b&c), the blue line is the average shear strength and the dashed lines represent the maximum and minimum shear strength readings at each depth, and hence give the shear strength range. The arrows indicate the dip direction of the main fissile partings and the numbers give the dip amounts (in degrees). Note the contrast in macro-fabric between Lithofacis Bi (top two macro-fabrics down to 0.3m depth, and Lithofacies Bii (all fabrics below 0.3m depth) in (d). In Logs NL1-5, the principal eigenvectors (V_1) for Lithofacies Bi are orientated between 231°-253° with an up-glacier plunge in the range 8°-15°. The principal eigenvalue (S_1) is weak, ranging from 0.476-0.555, with low elongation indices in the range 0.1828-0.4538. This contrasts with Lithofacies Bii for logs NL1-5 which have V_1 orientations between 043°-073° with down-glacier plunge ranging between 01°-24°, S_1 in the range 0.656-0.816, and elongation indices between 0.5701-0.869 (Table 3.8). Note the variable but generally strong S_1 values in Lithofacies Bii in (d) which range 0.639 to 0.816, with fabric strength increasing with depth in NL2, and the consistent V_1 orientations (range 052° to 074°).

Table 3.8 Clast a-axis Fabrics from Storglaciären Logs NL1-5 (Nordjåkk) and SL1-7 (Sydjåkk)

	Depth cm	N	V_1°	PL°	S_1	S_2	S_3	I	E
Nordjåkk									
Log NL2									
Lithofacies Bi	20-30	30	231	8	0.476	0.389	0.135	0.283	0.183
Lithofacies Bii	30-40	30	63	8	0.806	0.139	0.054	0.067	0.828
Lithofacies Bii	50-60	30	58	24	0.656	0.282	0.062	0.094	0.570
:ithofacies Bii	80-100	30	74	2	0.687	0.190	0.123	0.178	0.723
Lithofacies Bii	100-130	30	65	1	0.812	0.106	0.081	0.100	0.869
Lithofacies Bii	180-200	30	66	6	0.816	0.127	0.057	0.070	0.844
Log NL1									
Lithofacies Bi	20-30	30	253	15	0.5367	0.268	0.195	0.363	0.500
Lithofacies Bii	40-50	30	56	5	0.712	0.2178	0.070	0.099	0.695
Lithofacies Bii	50-60	30	66	10	0.729	0.171	0.1000	0.137	0.765
Lithofacies Bii	90-110	30	69	5	0.669	0.225	0.106	0.158	0.664
Lithofacies Bii	150	30	52	10	0.640	0.268	0.093	0.145	0.581
Log NL4									
Lithofacies A (flute)	15-25	30	253	5	0.776	0.1602	0.064	0.082	0.794
Log NL5									
LithofaciesBii	20-40	30	43	8	0.674	0.250	0.0761	0.113	0.630
Lithofacies D	40-60	50	90	1	0.516	0.314	0.1704	0.330	0.392
Lithofacies D	30-40	30	86	2	0.578	0.274	0.147	0.254	0.525
Lithodacies D	50-60	30	111	6	0.467	0.384	0.1486	0.318	0.177
Combined NL1-2									
Lithofacies Bi	20-30	80	238	13	0.555	0.303	0.141	0.255	0.454
Lithofacies Bii	>gravel	114	61	10	0.717	0.154	0.129	0.180	0.785
Lithofacies Bii	<gravel	143	66	4	0.720	0.175	0.105	0.145	0.756
Sydjåkk									
Log SL1&2									
Lithofacies Bii	40-50	30	114	18	0.633	0.253	0.114	0.180	0.600
Lithofacies Bii	60-80	30	174	18	0.504	0.362	0.135	0.268	0.282
Lithofacies Bii	230-250	30	62	1	0.766	0.129	0.105	0.136	0.831
Lithofacies Bii base of section	370-390	30	29	18	0.663	0.224	0.105	0.158	0.663
Log SL4									
Lithofacies Bi	20-30	25	147	18	0.525	0.386	0.089	0.169	0.265
Lithofacies Bii	30-45	25	134	13	0.712	0.238	0.050	0.070	0.665
Lithofacies Bii	70-90	25	57	4	0.573	0.362	0.064	0.112	0.368
Lithofacies Bii	90-100	25	189	9	0.617	0.249	0.134	0.217	0.596
Lithofacies Bii base of section	200	25	245	13	0.511	0.290	0.198	0.388	0.432
Log SL7									
Lithofacies Bi	20-40	25	12	5	0.550	0.337	0.113	0.206	0.388
Lithofacies Bii	60-80	25	124	12	0.643	0.236	0.122	0.189	0.633

Note: N is the number of clasts measured in each case. V_1 is the principal eigenvector and PL its plunge. I and E are the isotropy and elongation indices. S_1-S_3 are the eigenvalues. Lithofacies Bi has a weaker fabric than Lithofacies Bii, and facies Bii returns consistently strongly clustered fabrics in the Nordjåkk sections. The Sydjåkk sections exhibit more variable Lithofacies Bii fabrics in terms of strength and orientation and have, on the whole, less elongated fabric shapes.

Table 3.9 Clast a-axis Fabrics for Logs K4-K6, Kaskasatjåkka (column headings as for Table 3.8)

	Depth cm	N	V_1°	PL°	S_1	S_2	S_3	I	E
Kaskasatjåkka									
Log 4									
Lithofacies Bi	20-40	25	171	9	0.540	0.301	0.159	0.295	0.442
Lithofacies Bi	40-50	25	135	14	0.546	0.360	0.095	0.174	0.340
Combined	20-50	50	154	14	0.520	0.345	0.136	0.262	0.337
Lithofacies Bii	60-80	25	177	14	0.846	0.103	0.051	0.061	0.878
Lithofacies Bii	80-100	25	155	14	0.692	0.225	0.083	0.120	0.675
Combined	60-100	50	169	15	0.748	0.181	0.072	0.096	0.759
Lithofacies C	100-120	50	177	17	0.735	0.189	0.076	0.104	0.743
Lithofacies C	170-190	25	176	20	0.837	0.123	0.041	0.048	0.853
Lithofacies D	200	50	149	19	0.663	0.204	0.133	0.201	0.692
Log 5									
Lithofacies Bi	10-20	30	203	16	0.640	0.311	0.049	0.076	0.514
Lithofacies Bii	30-40	25	185	29	0.700	0.203	0.050	0.071	0.710
Lithofacies Bii	60-80	25	173	24	0.823	0.127	0.050	0.060	0.845
Lithofacies C	200	30	203	2	0.723	0.181	0.096	0.132	0.750
Log 6									
Lithofacies Bii	30-40	25	192	32	0.879	0.096	0.025	0.028	0.891
Lithofacies Bii	50-60	25	191	26	0.877	0.080	0.044	0.0500	0.909
Lithofacies D	150	30	339	27	0.626	0.284	0.0900	0.143	0.547
Log 1									
Lithofacies C_{brown}	150	30	008	41	0.616	0.290	0.114	0.186	0.564
Outer Moraine Lithofacies St Dm	100	50	048	20	0.509	0.274	0.217	0.426	0.462

Note: Lithofacies Bi can be discriminated from Bii by macro-fabric strength and fabric shape. As at Storglaciären, macro-fabrics show no simply decline in strength with depth, but vary in strength and fabric shape over small vertical intervals. However, V_1 orientation is similar for most lithofacies Bii readings in the same logged section.

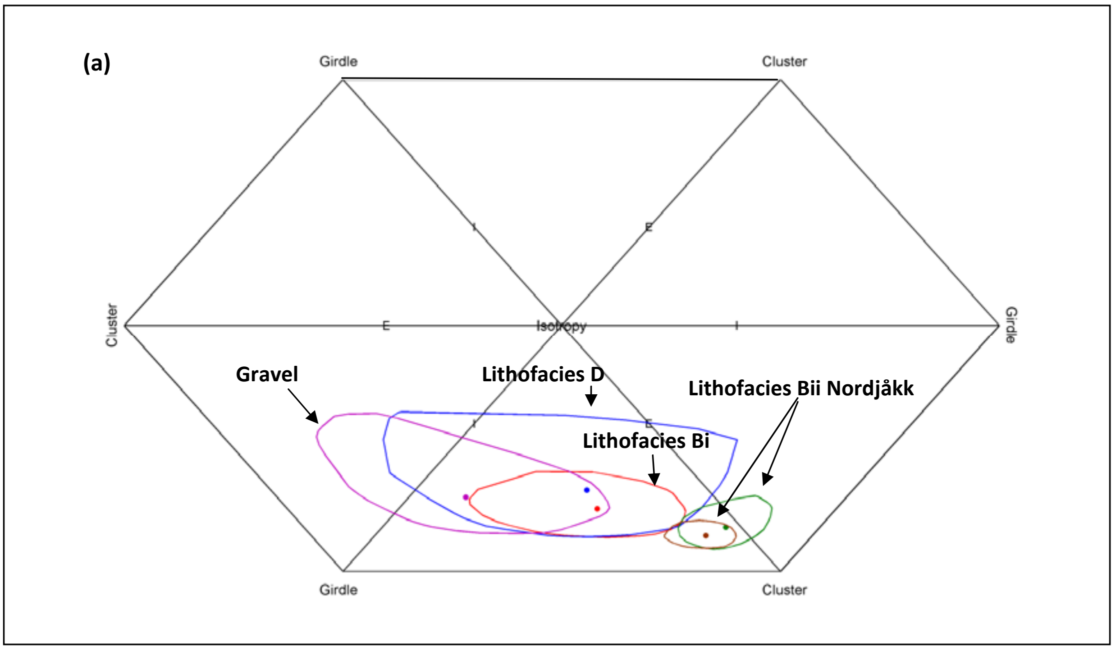

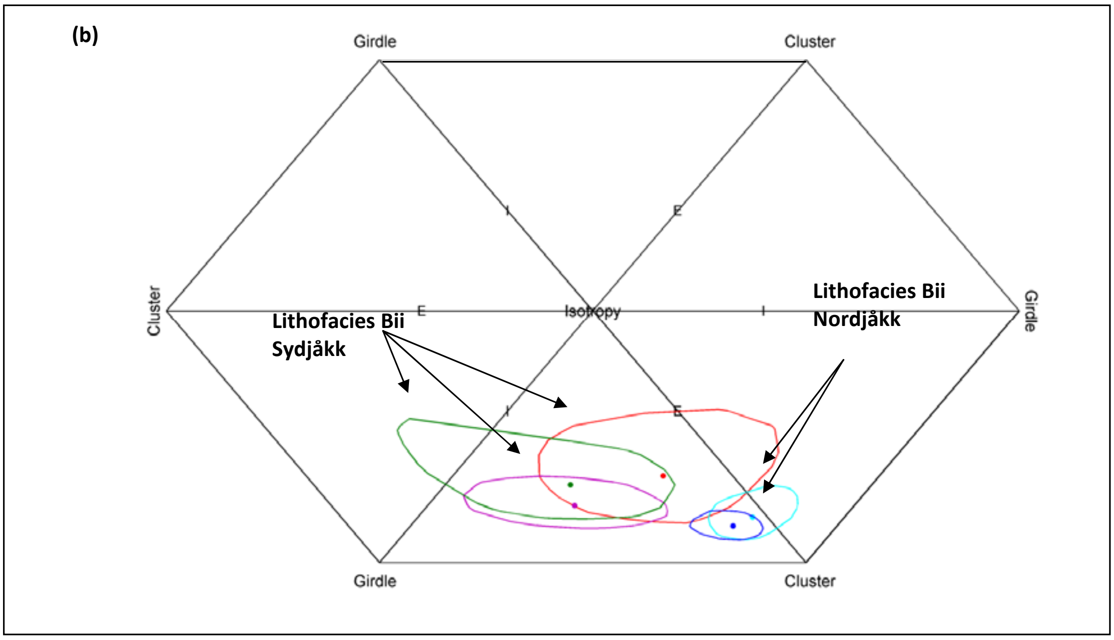

Figure 3.18 Ternary Diagrams and 10th Convex Hulls for Lithofacies from the Storglaciären Diamicton Plain plotted using Benn and Ringrose's (2001) Bootstrapping Programme. (a) Lithofacies from the Nordjåkk log sections NL1-5. Lithofacies Bii is from above and below the gravel sheet shown in Figure 3.15a. Note how these macro-fabrics plot towards the bottom right of the graph, indicating strong, linearly clustered macro-fabric shapes. The fabric points for Lithofacies Bi and D plot outside of the 10th convex hulls of Lithofacies Bii and have less clustered fabric shapes, suggesting there is a 90% probability that they are statistically different fabric shapes. (b) Various macro-fabrics from the Sydjåkk logs compared with Lithofacies Bii from the Nordjåkk logs. Note how the Sydjåkk samples have less linearly clustered fabric shapes compared to the Nordjåkk samples and are likely drawn from statistically different populations.

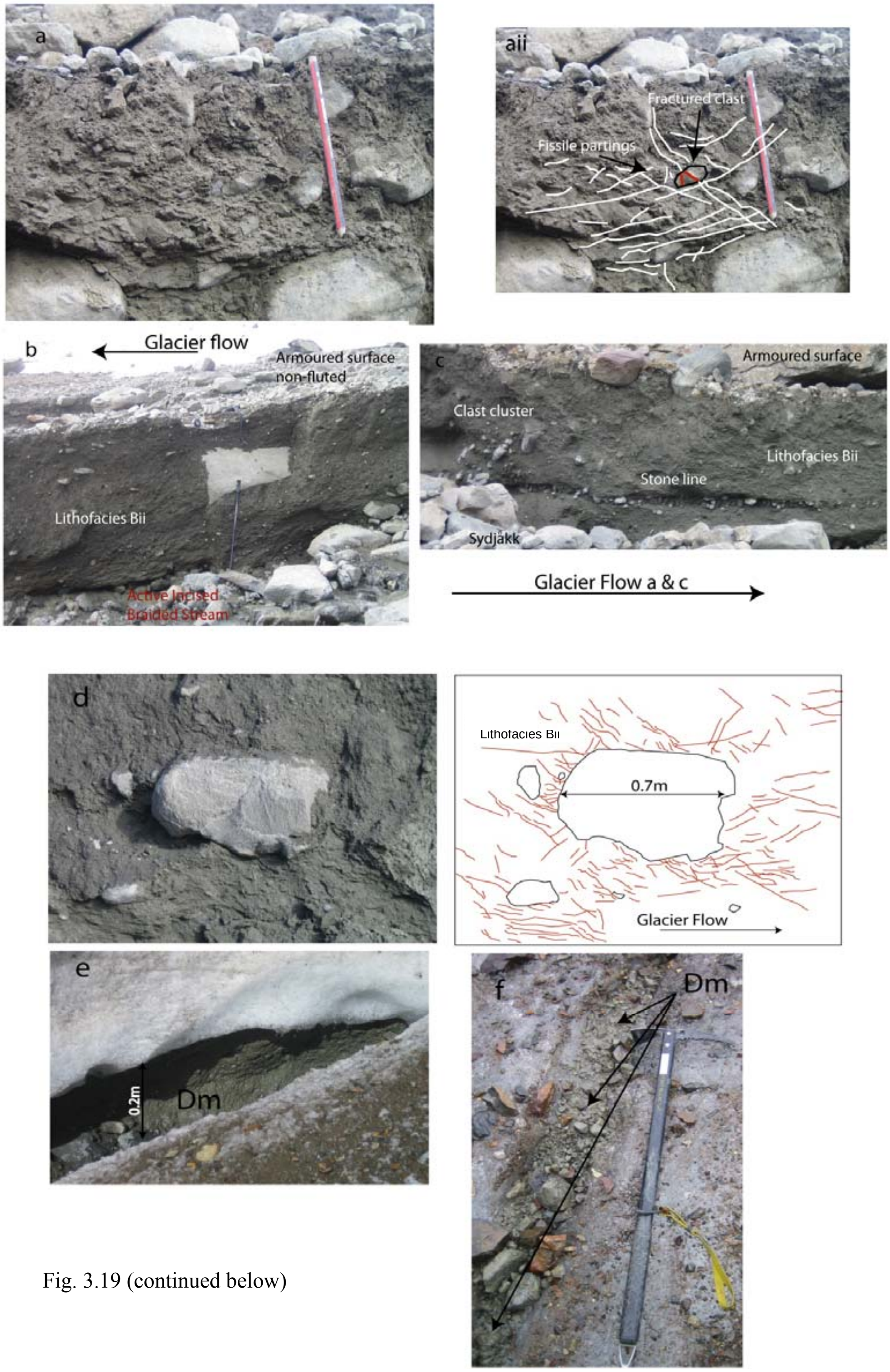

Fig. 3.19 (continued below)

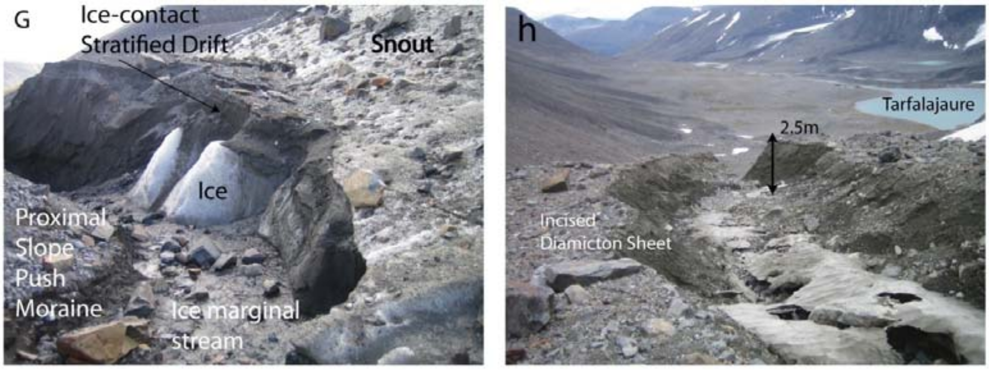

Figure 3.19 (continued) Features of the Storglaciären Diamicton Plain and Kaskasatjåkka Diamicton Sheet. (a) Fractured clast in fissile Dm, near to surface, Diamicton sheet. Note how the two fractures are aligned with fissile partings, and how the faceted faces of some clasts align with major partings (shown on the annotated version (ai) on the right). (b) Lithofacies B, Kaskasatjåkka, upper regions diamicton sheet, looking west. The walking pole is about 1m long. Note the highly fissile nature of the homogeneous diamicton, surface armour (with some SR boulders), large embedded boulder, and actively incising braided stream. The distinction between Lithofacies Bi and Bii is made on the basis of fabric. (c) Lithofacies B_S Diamicton Plain, Sydjåkk section near log SL6. The distinction between Lihtofacies Bi and Bii is made on the basis of fabrics and pgsd. The section is approximately 1.5m thick. Note the fissile nature of the diamicton, clast clusters, and stone line, thought to represent subglacially eroded and re-worked diamicton surfaces (Evans and Benn, 2004). (d) Embedded boulder in Lithofacies Bii_S near to log SL5, Diamicton Plain. The annotated version on the right shows the disruption of fissile partings around the boulder, with partings becoming very short, closely spaced, and terminating against the stoss-end. Not all partings are shown. Some partings form a platy structure, whereas others are more like micro-fractures. Common orientations are sub-parallel, with some dipping at a low angle up-glacier, and planes with steeper up or down-glacier dip. Some partings are relatively straight and continuous over decimetres, whereas others are shorter and curved. The partings do not cross-cut in any consistent manner, suggesting they formed contemporaneously. (e) Grey fissile diamicton resembling Lithofacies B observed at the bed beneath the present snout of Kaskasatjåkkaglaciären. (f) Photograph taken showing the surface of the glacier near to the previous image. A fluid Dm is squeezing-up through a fracture and forming a small flow till. The Dm is mixing with supraglacial drape. The survival potential is low, but similar flows were observed to form a thin drape across the current forefield at the glacier margin. (g) Terminus of Storglaciären, northern side. Ice contact stratified drift, dipping up-glacier, emerging at the glacier margin. The drift consists of interbedded SG and Sm and resembles layers observed in the Sydjåkk sections. However, its survival potential is low. Similar stratified sands and gravels were observed in englacial and subglacial streams at the ice-margin of Kaskasatjåkka. (h) View looking south from the summit of the diamicton sheet before it plunges down a steep slope. Note the armoured nature of the surface. This stream is intermittently active and good exposure is not seen due to active slope failure.

3.4.2 Interpretation

As with Lithofacies A, the polymodal particle grain-size distributions, sub-rounded to sub-angular blocky clast shapes, and wear-patterns on embedded boulders in Lithofacies B are characteristic of active subglacial transport (Etienne *et al*., 2003). Stone lines, such as those shown in Figure 3.19c, are thought to indicate periods of localised subglacial erosion and the re-working of diamicton surfaces (Evans and Benn, 2004). The co-existence of features indicative of lodgement (bullet-shaped clasts, clast clusters, stoss and lee boulders with striae concentrated on supper surfaces), deformation (embedded boulders with striae on all surfaces) and erosion in Lithofacies B suggest it is a hybrid lodgement/deformation till (Piotrowski *et al*., 2006) or traction till (Evans *et al*., 2006).The lower crushing index and greater degree of clast angularity in Lithofacies B compared to Lithofacies A suggests a lower intensity of deformation and with less effective particle comminution (Piotrowski *et al*., 2004).

Comment [DJG18]: layer?

Lithofacies Bii clast fabrics (Figure 3.17d) resemble clast fabrics considered typical of meltout or lodgement tills (Hicock *et al*., 1996), having high S_1 and low S_3 eigenvalues indicative of strong clustering around the V_1 eigenvector. These mechanisms of formation cannot be discounted because there is little unequivocal evidence of subglacial deformation at the macro-scale. For example, there are no macro-scale faults or folds, and an absence of strain markers to give a sense of shear or to confirm that fissile partings are shear planes. S_1 eigenvalues show no simple decrease in strength with depth (Figure 3.17a&d) but vary in strength with depth, indicating that the degree of clast alignment varies with depth in lithofacies B (Figure 3.17). Similar variations in clast fabric strength in vertical profiles have been reported in other subglacial diamictons (Piotrowski *et al*., 2004; Larsen *et al*., 2006) and related to variations in strain magnitude in thin deforming layers, with the upward movement of the zone of deformation over time allowing for the incremental accretion of the sequence.

Lithofacies Bii has a similar particle grain-size distribution to the lithofacies described by Etienne *et al*. (2003) for the diamicton plain and if, as they suggest, the fissile partings represent shear planes, then the variation in the spacing and attitude of fissile partings shows that the intensity of shear and/or the sediment response to shear varied markedly over small vertically and laterally scales. Such variation is difficult to reconcile with a homogeneous sequence deforming pervasively throughout its entire thickness, but is consistent with the incremental accretion of thin deforming layers in which time-varying changes in pore-water pressure exert a controlling influence on the extent and nature of deformation in each successive layer (Piotrowski *et al.*, 2004). The reduction in shear strength in layers with closely spaced fissile partings is consistent with the partings being shear planes, with the areas of closely spaced partings representing zones that have been more intensely sheared. A dense network of shear planes would weaken the diamicton and result in lower shear strength readings.

Comment [DJG19]: Potential confusion with 'yield strength' if used in this context

Fissile textures may be produced by the collapse of dilatant A-horizons or differential rates of shearing (Boulton, 1976). As with Lithofacies A, the flat faceted faces of Type 1&2 clasts were generally orientated with, and lying along major fissile partings in Lithofacies B, and fissile partings were much disrupted around embedded boulders (Figure 3.19d), consistent with them being shear planes (Alley, 1991). However, the presence of fissile partings in diamictons is insufficient to confirm a deformation origin because numerous processes can produce fissile textures in tills. In the upper few decimetres of Swedish tills, fissile partings have been interpreted as the product of segregated ice formation under periglacial conditions (Lundqvist, 1983). Strong fissile textures below about 1m depth in Swedish tills have been related to lodgement processes (Lundqvist, 1983). Lodgement is usually considered to be a slow process involving the particle-by particle meltout of clasts from basal ice where drag exceeds shear stress (Benn and Evans, 2010). However, matrix may also be lodged from thin sheets of overloaded basal ice and the dewatering of lodged layers during till accretion may produce fissile textures (Muller, 1983). Alternatively, fissile textures may be formed by the post-depositional unloading of tills (Evans *et al.*, 2006). Because the origin of the fissile partings cannot be confirmed at the macro-scale, inferences about the origin of homogeneous fissile diamictons (Boulton, 1976; Gordon *et al.*, 1992; Benn 1994; 1995; Etienne *et al.*, 2001) must be regarded as unsubstantiated unless micro-scale evidence is provided to support the interpretation.

Undisturbed weathering haloes and in situ broken clast fragments are difficult to reconcile with a strongly sheared bed as shearing would be expected to disrupt these features (Piotrowski *et al.*, 2001). However, these features may post-date diamicton emplacement; for example, fractured grains may be produced by frost action (Haldorsen, 1981). The occurrence of patterned ground and the steep dips of some near-surface clasts suggest periglacial frost heaving has been an active process in the area since the Little Ice Age recession, and vertical sorting of clasts by this process may explain the armoured nature of the fluted moraine and diamicton plain surfaces (Holmlund and Jansson, 2002; Etienne *et al*., 2003). However, Lithofacies Bi has a very similar average particle grain-size distribution to actively deforming till retrieved from boreholes beneath Storglaciären (Iverson *et al*., 1994), which suggests the particle grain-size differences between Lithofacies Bi and Bii relates to glacial and not periglacial processes, although silt translocation related to snowmelt and thaw consolidation would also account for the differences in particle-grain size. Lithofacies Bi clast fabrics plot in Dowdeswell and Sharp's (1986) process fields as deformed lodgement tills (A-Type horizons) and glacigenic sediment flows (Figure 3.9b), whereas Lithofacies Bii plots in the undeformed lodgement till (B-Type horizons) and meltout till fields. These results are consistent with the interpretation of Lithofacies B as a traction till. Lithofacies Bi does not have porosity values near to the 40% value thought typical of dilatant tills (Benn, 1994; Paterson, 1996), and is as consolidated as Lithofacies Bii, and generally fissile except for in the upper few centimetres. These observations suggest Lithofacies Bi is not a dilatant A-Type horizon.

The simplest explanations for less strongly clustered (more isotropic) clast fabrics are that parts of Lithofacies Bi were exposed to lower strain magnitudes (Iverson *et al*., 2008), or that fabrics have been disrupted by frost heave processes (Rose, 1991). Clast fabric disruption is not observed in flutes below about 0.1-0.2m depth (see extended discussion in Chapter 4), and so the extent of periglacial over-printing may be limited in depth. Patterned ground occurs near to logs NL1 & 2 in Storglaciären, where Lithofacies Bi fabrics show weak clast alignments at *ca*. 0.1-0.3m depth. These clast fabrics exhibit a greater number of steeply dipping clasts (Figure 3.17d), which is consistent with disruption by frost heave (Rose, 1991).

Comment [DJG20]: Isotropic?

Some of the non-striated angular boulders found on the forefield surface have steep dips and are probably of supraglacial origin, while striated sub-rounded to sub-angular boulders are indicative of a subglacial origin (Etienne *et al*., 2003). At the present glacier margins, angular supraglacial debris was observed to slide onto the forefield surface, and at Kaskasatjåkka, saturated subglacial sediment was observed to be squeezed-up through ice fractures onto the glacier surface, where it produced a thin grey homogeneous flow till which draped patches of the forefield surface (Figure 3.19e&f). As such, parts of Lithofacies Bi could have formed by similar processes and represent a drape of flow till or subglacial material re-worked at the glacier margin and mixed with supraglacial material deposited during glacier recession. This is consistent with the weaker clast fabrics and lack of fissile texture in the upper sections of Lithofacies Bi, and its higher RA index than Bii (Bii RA index generally<20%; Bi RA index ≈ 20-30%, Figure 3.6).

In summary, the similarities in particle grain-size distributions between Lithofacies Bi and subglacially retrieved deformation till, and evidence of lodgement and erosion occurring in close proximity to deformation, suggest Lithofacies B is a hybrid subglacial deformation/lodgement till (traction till). The contrasts between Lithofacies Bi & Bii probably relate to a combination of near-surface frost heave and slope wash processes, and the local re-working of subglacial sediments and mixing with supraglacial moraine during glacier recession.

3.5 Lithofacies C

Lithofacies C forms the substrate to Lithofacies A at Isfallglaciären where it crops out in patches in the proximal and middle zones of the flute field (Figure 3.11). It also occurs at Kaskasatjåkka where it forms the substrate to Lithofacies B in the diamicton sheet (Figure 3.1b). A distinctly brown-coloured version crops out widely to the south of the diamicton sheet at Kaskasatjåkka where it forms the substrate to Lithofacies A in the flute field (Figure 3.16b).

3.5.1 Description

Lithofacies C can be readily distinguished from Lithofacies A and B by its clast-rich nature Lithofacies C is found in areas 2 and 3 of Isfallsglaciären (Figure 3.1a) where it has a restricted distribution. Here, Lithofacies C has a similar colour, matrix particle grain-size distribution (Figure 3.3a & d) and clast morphology (Figure 3.13a, b, &d) to Lithofacies A, but a lower mean fractal slope (-2.68). Lithofacies C is also much less fissile than Lithofacies A, although some fissile partings are continuous across the Lithofacies A/C boundary. The boundary between Lithofacies A and C at Isfallsglaciären is often demarcated by a boulder pavement, where striae are concentrated on the upper surfaces of the boulders.

At Kaskasatjåkka, multiple diamictons interbedded with sands and gravels are exposed in some sections of the diamicton sheet and in sections cut through the frontal moraines (Figure

3.20b&c). Lithofacies C has a restricted distribution in the diamicton sheet, but is observed to form a sharp contact with Lithofacies B in logs 4 and 5 where it forms a tabular bed *ca*. 1m thick which extends laterally for over 20m (Figure 3.20b). Here, clast-rich Lithofacies C has a similar light grey colour and muddy matrix to Lithofacies B (Figure 3.3r), and exhibits similar strongly clustered clast fabrics (S_1 ranges from 0.72-0.84 with V_1 orientations plunging down-glacier towards the south; Figure 3.20b). At Kaskasatjåkka, a distinctive sub-set of Lithofacies C (Lithofacies C_{brown}) occurs widely across the lower forefield, where it forms the substrate to Lithofacies A and also occurs in river-cut sections of frontal moraines (Figure 3.16b and 3.20c). Lithofacies C_{brown}, like Lithofacies A, has a matrix particle grain-size distribution characterised by a primary mode of very coarse sand (Figure 3.3s). However, it is readily distinguished from Lithofacies A by its distinctive brown colour, clast-rich texture, and much weaker fissility. It also has a lower fractal slope dimension than Lithofacies A (-2.76, R^2 0.996) and some samples contain more angular and some very angular clasts, which give it a higher RA index (up to 30%, see Figure 3.6c). In samples taken from the outer frontal moraines, Lithofacies C_{brown} clast fabrics have relatively weak S_1 eigenvalues (≤ 0.62) compared to Lithofacies B and C from the diamicton sheet, with low elongation and more isotropic fabric shapes (Table 3.9).

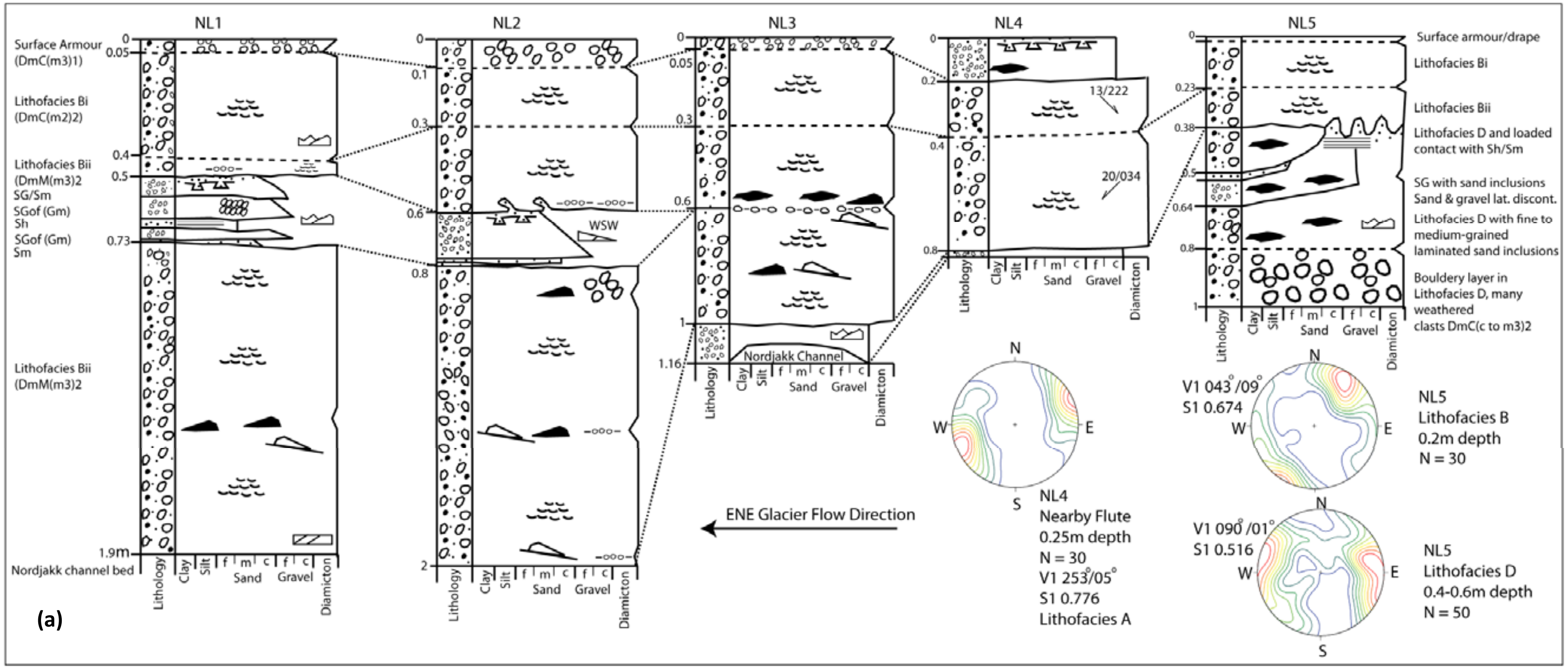

Figure 3.20(a) Graphic Logs from the Storglaciären Diamicton Plain, Nordjåkk section NL1-5

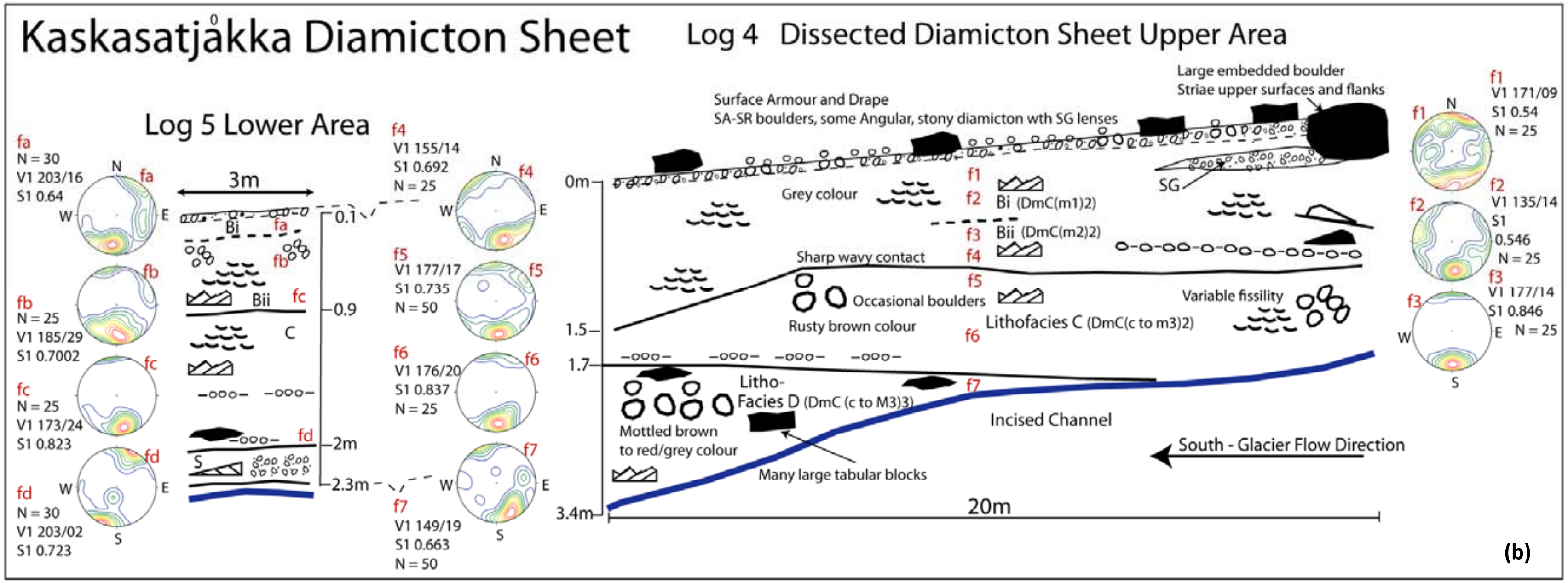

Figure 3.20(b) Graphic Logs from the Kaskasatjåkka diamicton sheet, Logs KL4&5

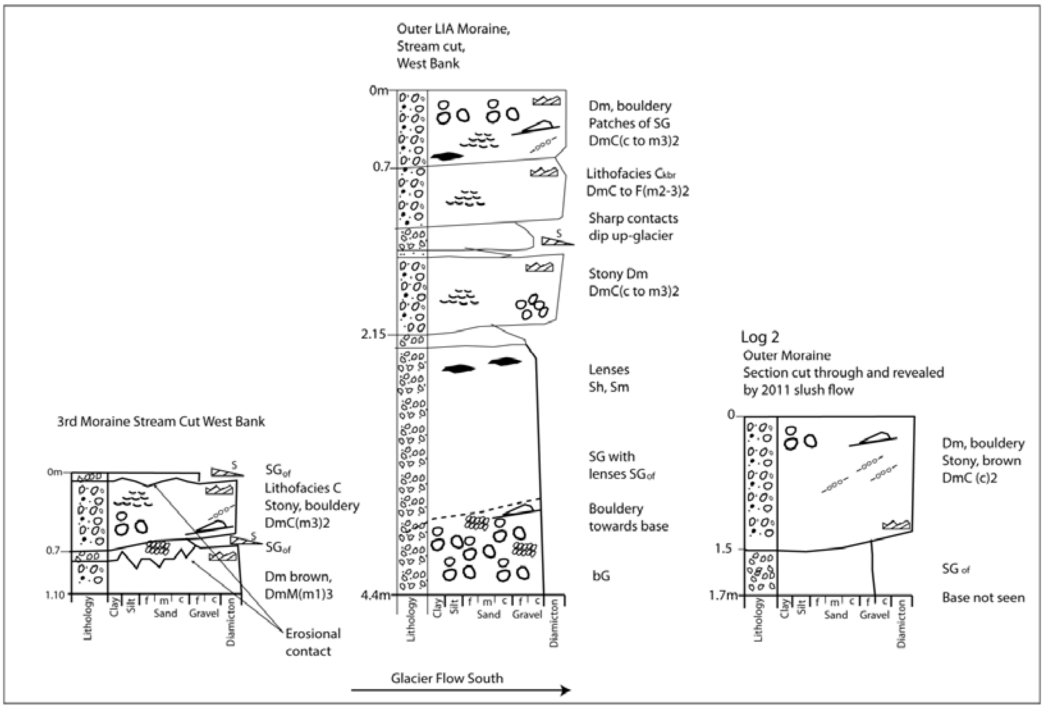

Key to graphic logs

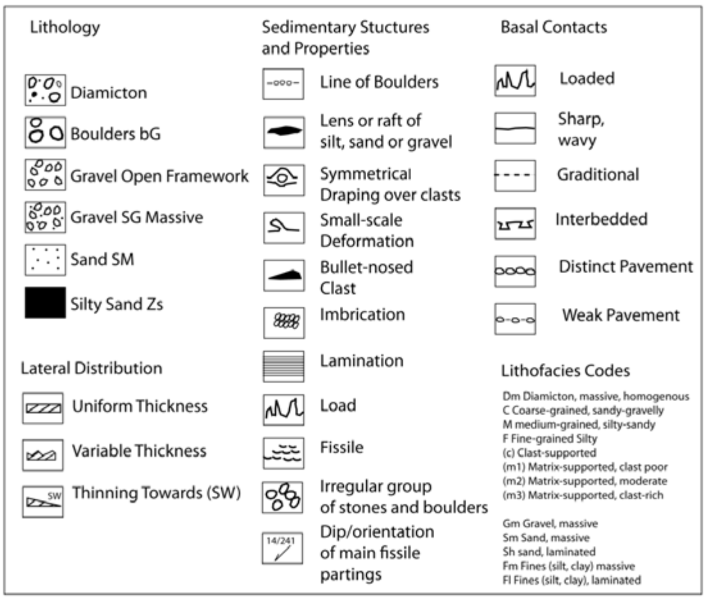

Figure 3.20 (c) Graphic Logs from Kaskasatjåkka moraine sections. Note how Lithofacies B thickness increases down-glacier in (a). Note the consistent V_1 orientations in macro-fabrics in (b), consistent with glacier flow towards the south, but variations in S_1 strength with depth. Note that most lithofacies contacts are sharp and wavy, and that tabular beds of Dm and SG commonly dip up-glacier in (b&c) at low angles (<10°).

3.5.2 Interpretation

The clast morphology and polymodal particle grain-size distributions of Lithofacies C (Table 3.1) are indicative of active subglacial transport (Etienne *et al*., 2003; Benn, 2004). The greater number of angular and very angular clasts in Lithofacies C_{brown}, especially in moraine samples, reflects an element of debris sourced from passive transport pathways. The presence of embedded boulders and clast clusters indicate that lodgement has been an important process in the formation of Lithofacies C (Evans and Benn, 2004). At Isfallsglaciären, Lithofacies C has very similar physical properties to Lithofacies A (Figure 3.13). As such, Lithofacies C may be a coarse-grained base layer of Lithofacies A. However, boulder pavements, such as those which often demarcate the boundary between Lithofacies A and C at Isfallsglaciären, are indicative of periods of erosion at the ice-bed interface which removes finer material, or the sinking of boulders through a ductile deforming layer (Benn and Evans, 2010). The concentration of striae on upper boulder surfaces in boulder pavements suggests lodgement occurred, and this is consistent with the boundary between Lithofacies A and C representing an erosional contact. As such, the emplacements of the lithofacies were separated in time.

The continuation of some fissile partings across the Lithofacies A/C boundary in Isfallsglaciären indicates that, if these are discrete shear planes (Benn, 1994), then a phase of discrete deformation affected both diamictons, at least during the latter stages of flute formation. The contact between Lithofacies A and C is often domed-up in flute crests. Boulton (1976) suggested such contacts were indicative of lateral compression and vertical extension in subglacial cavities, where flutes were thought to be formed by the squeezing of sediment into regions of low pressure. If this is true, then Lithofacies C may represent an earlier traction till that has been subsequently deformed during flute construction. The lower fractal slope dimension of Lithofacies C, and fine-sand spike in the particle grain-size distribution (Figure 3.3d), suggest that grain fracture was an important mechanism of particle comminution (Haldorsen, 1981). This relates to the effective transmission of stress along grain contacts in granular diamictons such as Lithofacies C (Hooke and Iverson, 1995).

Lithofacies C predates the emplacement of Lithofacies A and B, and so belongs to an earlier phase of glacier activity. However, clasts in Lithofacies C at both Isfallsglaciären and Kaskasatjåkka show little evidence of weathering and this suggests the diamicton has not been subjected to a prolonged phase of subaerial exposure and weathering. This suggests Lithofacies C was formed during the Little Ice Age Advance. The clast rich nature of the diamicton suggests an input of coarse material from subglacial transport, and/or the cannibalisation of proglacial sandy gravels. The strong S_1 eigenvalues (>0.72) and elongation indices (>0.74), and low isotropy indices (<0.13) of Lithofacies C are indicative of lodgement tills and meltout tills (Dowdeswell and Sharp, 1986). As such, Lithofacies C is interpreted as a subglacial traction till.

3.6 Lithofacies D

Lithofacies D occurs in all three forefields but its distribution is patchy and quite restricted. At Storglaciären it forms the substrate to Lithofacies A and B, but it is only observed in the upper sections of the diamicton plain (Figure 3.2c). At Isfallsglaciären it forms the substrate to Lithofacies B/C, but is only observed in the proximal parts of the flutes. At Kaskasatjåkka, Lithofacies D is occasionally observed to form at the base of the diamicton sheet where it forms the substrate to Lithofacies C.

3.6.1 Description

Lithofacies D is readily distinguished from other diamictons by its degree of weathering. Many clasts are rotten, fractured, and/or have weathering skins. Lithofacies D is a very clast rich, often clast-supported diamicton containing numerous boulders. It contains a relatively high proportion of angular and very angular clasts compared to other diamictons, which gives it a higher RA index than Lithofacies A and Bii. For example, at Storglaciaren, Lithofacies D has an RA index between 40% and 50%, whilst Lithofacies A and B have RA values below 20% (Figure 3.6b). S_1 eigenvalues are generally weaker and fabric shapes less clustered in Lithofacies D compared to other diamictons (Figure 3.9a). At Storglaciären, Lithofacies D is a sandy to light brown-grey diamicton. It was observed to form a sharp contact with Lithofacies Bii at log NL5 (Figure 3.20a). Here, Lithofacies D has less clustered and more isotropic clast fabric shapes than Lithofacies Bii and different V_1 orientations (V_1 Lithofacies D = 090°; V_1 Lithofacies Bii = 043° in log NL5, see Table 3.8). The matrix particle grain-size distribution is similar to Lithofacies Bii but contaims slightly less silt (Lithofacies D 63.6% sand, 27.9% silt and 8.6% clay; Lithofacies Bii 34.8% silt; Figure 3.3g&h).Thin layers of sand and gravel occur in patches within Lithofacies D and at the upper contact with Bii.

Lithofacies D also forms the substratum to Lithofacies A in fluted moraine in the upper part of the diamicton plain.

At Kaskasatjåkka, Lithofacies D has a restricted distribution but it is occasionally observed to form a tabular sheet at the base of the diamicton sheet (for example in log 4; Figure 3.20b). As at Storglaciären, Lithofacies D is very heavily weathered. The matrix has a mottled to oxidised appearance and displays brown to red to grey colours, whilst many clasts are fractured and some show evidence of granular disintegration. Lithofacies D at Kaskasatjåkka contains more fines in the matrix particle grain-size distribution than other diamictons at Kaskasatjåkka (48.8% mud; Figure 3.3t), and its clast fabrics are not as strongly clustered as Lithofacies B and C, whilst V_1 orientations plunge to the SSW or up-glacier to the NNE (Figure 3.20b).

At Isfallsglaciären a similar heavily weathered diamicton forms the substrate to Lithofacies A and C in the proximal to middle reaches of some flutes (Figure 3.11). This diamicton has also been denoted as Lithofacies D because it is also a clast-rich, heavily weathered diamicton with a high proportion of angular and very angular clasts (Figure 3.4), which enable it to be distinguished from Lithofacies A by its higher RA index (RA >20%; Figure 3.6a). It is also distinguished from other diamicton facies by its more isotropic clast fabrics (S_1 generally <0.5; S_3>0.25; Figure 3.9a). At Isfallsglaciären, Lithofacies D contains a large number of tabular sub-angular to sub-rounded boulders, many of which have steep dips. It lacks the fissile texture of Lithofacies A. The matrix particle grain-size distribution comprises 53.5% sand, 37.6% silt and 8.9% clay (Figure 3.3m). Thin, laterally discontinuous lenses of massive sand and fine gravel occur within Lithofacies D and at its upper contact (Figure 3.13).

Fractal slope gradients for Lithofacies D range from -2.81 at Storglaciåren to -2.89 at Kaskasatjåkka (Figure 3.10f&s).

3.6.2 Interpretation

Lithofacies D equates to the lower subglacial till identified by Baker and Hooyer (1996) at Storglaciären (Figure 2.5). The heavily weathered, oxidised nature of Lithofacies D in each forefield suggests it has experienced a period of proglacial exposure and weathering, possibly under relatively warm climatic conditions to induce oxidation, and that it belongs to a phase of glacier advance that pre-dates the Little Ice Age (Baker and Hooyer, 1996). The fine-sand/coarse silt spikes of Lithofacies D (Figure 3.3 g, m & t) are consistent with crushing being an important mechanism of particle comminution, whilst the greater ratio of coarse clasts to matrix is indicative of a lower intensity of comminution (Haldorsen, 1981). These observations lend support to Baker and Hooyer's (1996) suggestion that the differences in granulometry between Lithofacies B and D at Storglaciären indicate a switch in basal thermal regime from cold-based conditions during an earlier advance to warm-based conditions, where basal sliding and abrasion were important processes during the Little Ice Age Advance (Chapter 2.1.4).

Lithofacies D from the diamicton sheet has similar physical properties to Lithofacies C and B from Kaskasatjåkka and is interpreted here as a stony traction till (Table 3.11). An input of sediment from multiple transport pathways – including angular and very angular clasts from supraglacial pathways - and sediment re-working (for example by debris-flows and/or glaciofluvial meltwaters at the glacier margin) would explain the relatively high RA index of Lithofacies D at Isfallsglaciären and Storglaciären, the lack of fissile texture, the intercalation of sand and gravel beds, and the more isotropic clast fabrics. One clast fabric from Lithofacies D (Isfallsglaciären) plots as a glacigenic sediment flow in Figure 3.9a, whereas two other fabrics plot nearer to this process field than any other (Dowdeswell and Sharp, 1986). The similar fractal dimensions and matrix particle grain-size distributions between Lithofacies D and Bii at Storglaciären are consistent with Lithofacies D representing a re-worked subglacial traction till. As such, Lithofacies D from Isfallsglaciären and Storglaciären are interpreted as hybrid tills probably formed at the ice margin by the re-working of subglacial traction tills or the mixing of subglacial tills with passively transported material during glacigenic sediment flows. The greater angularity and stony nature of these deposits may simply reflect a different origin to Lithofacies A and B, rather than subglacial formation under a different thermal regime (Baker and Hooyer, 1996).

The evidence used to interpret Lithofacies A-D is summarized in Table 3.10.

Table 3.10 Interpretation of Diamictons (Note: the number of crosses in the table indicates the strength of the evidence – more crosses equates to stronger evidence)

	Lodgement till	**Deformation Till**	**Subglacial Melt Out Till**	**Flow Till**
Particle Shape	Basal transport rounds edges, spherical forms, striated and faceted. Bullet-shaped clasts. Lodged clasts striated on upper surface	Dominated by sedimentary characteristics of deforming sediment. Rotating clasts striated on all surfaces	Characteristics of basal transport being rounded, spherical, striated, faceted	Broad range but dominated by angular particles and non-spherical forms. Majority of clasts not striated or faceted
Lithofacies A and C_I	XXXXX	XXX	XXXXX	
Lithofacies Bi	XXXX	XXX	XXXXX	XX
Lithofacies Bii	XXXXX	XXX	XXXXX	
Lithofacies D_S	XX		XX	XX
Lithofacies D_I	XX		XX	X
Lithofacies C_{Kbrown}	XXXX	XXX	XX	X
Particle Size Distribution	Basal debris transport so either bimodal or multimodal	Diverse range. Rafts of original sediment may be present, causing marked spatial variability	Basal debris transport so either bimodal or multimodal. Sediment sorting associated with dewatering and sediment flow	Usually coarse and unimodal, though maybe locally well sorted
Lithofacies A and C_I	XXXXX	XX	XXXX	
Lithofacies Bi	XXXXX	XXX	XXXX	
Lithofacies Bii	XXXXX	X	XXXXX (Sydjåkk logs)	
Lithofacies D_S	XXXXX	XX	XXX	
Lithofacies D_I	XXXXX	X	XXXX	
Lithofacies C_{Kbrown}	XXXXX	X	XXXX	
Particle Fabric	Strong, elongated particles aligned closely with direction of local ice flow	Strong in the direction of shear. High angle clasts and chaotic patterns of clast orientation also common	Maybe strong in direction of ice flow, although may show greater range of orientations	Variable, maybe locally strong down flow
Lithofacies A and C_I	XXXXX (flutes)	XXXXX (flutes)	XXXX (interflutes)	XXX (interflutes)
Lithofacies Bi	XXX	XXXX	XX	XXX
Lithofacies Bii	XXXXX (Nordjåkk logs)	XXX	XXXXX (Sydjåkk logs)	XXXX (Sydjåkk logs)
Lithofacies D_S	XX	XX	XX	XX
Lithofacies D_I		X	X	XX
Lithofacies C_{Kbrown}	XX	XXX	XX	XX
Particle Packing	Typically dense, well-consolidated	Densely packed and consolidated	Maybe well packed and consolidated, but less so than lodgement till	Poorly consolidated with low density
All	XXX	XXX	XX (Bi)	
Particle Lithology	Dominated by local rock types	Diverse range of lithologies	Maybe inverse superposition	Variable, but far travelled erratics may be present
All	XXXX	XXXX		

Structure	Massive, well-developed shear planes and foliations. Brecciated clasts (smudges) or pavements may occur, along with evidence for ploughing	Fold, thrust and fault structures present if shear homogenisation low. Rafts of undeformed sediment may be present, and smudges.	Massive, but may contain flow structures. Sometimes crude stratification.	Flows may be visible with crude sorting and basal layers of tractional clasts. Sorted sand and silt layers associated with reworking by meltwater may be common. Flows may have erosional bases
Lithofacies A and C_I	XXXXX	XXX (folds in some sand substratum at Isfallsglaciären)	X	
Lithofacies Bi	XXXX	X	X	
Lithofacies Bii	XXXXX	X	XX (Sydjåkk logs)	XX (Sydjåkk logs)
Lithofacies D_S	XX	XX	X	X
Lithofacies D_I	XX	X	X	X
Lithofacies C_{Kbrown}	XXXX	X		

	Interpretation
Lithofacies A and C_I	Traction till formed by multiple processes at glacier bed during the Little Ice Age (LIA) advance. Processes involved ploughing, erosion, lodgement and deformation. Probably subjected to discrete brittle to brittle-to-ductile shear, at least in late-phase of formation. At Isfallsglaciären, C_I has restricted distribution – represents earlier phase of glacier activity as shown by boulder pavements at contact with Lithofacies A. The more stony appearance of C_I reflects either coarser input from lodgement, or more limited subglacial transport and comminution, possibly as traction layer frozen-on to cold ice margin during earlier Little Ice Age advance that was followed by a brief oscillation, or cannibalisation of coarser proglacial substrate, e.g. SG. Less stony Lithofacies A relates to either more effective and active comminution (suggested by its greater fractal slope), or finer debris input from cannibalisation of the Fronstjön sands (which pre-date A and C).
Lithofacies Bi	Hybrid Traction Till modified by surface processes and inputs of flow till in places
Lithofacies Bii	Hybrid Traction Till – evidence of lodgement, erosion, deformation in close proximity. Probably formed by incremental accretion from thin deforming layers. Sydjåkk sequence more indicative of meltout/ice-marginal deposition or glaci-tectonic origin
Lithofacies D	Dm related to pre-Little Ice Age advance in earlier part of the Holocene. Weathered appearance relates to period of prolonged subaerial exposure. Some clast angularity could relate to periglacial frost shattering during proglacial exposure. However, Lithofacies $D_{I\&S}$ are interpreted here as tills formed in ice-marginal moraines by multiple processes, including subglacial traction. They resemble stony diamicton samples from contemporary end moraines in terms of fractal slope dimension, pgsd, and similar C_{40}/RA index, with higher degree of clast angularity and high clast:matrix ratio. Includes input of debris from passive transport pathways in marginal moraine location, with possible re-working by glacio-fluvial activity/debris-flows. Major glacier advance in Tarfala area dated at 2400-2700 cal. yrs. B.P. by Karlén (1973), so Lithofacies D may relate to this phase of advance. Lithofacies D_K is similarly badly weathered and contains many angular clasts, but has other properties more reminiscent of traction till. Lithofacies D has restricted distribution in all 3 forefields, and in (I) and (S) form part of distinct moraine ridges, whereas (K) is lower part of dm sheet. As such,D_K is interpreted here as a traction till.
LithofaciesC_{brown}	Hybrid traction till. Lithofacies C forms after Lithofacies D but pre-dates Lithofacies A and B. The presence of Lithofacies C_{brown} in the inner end moraine is consistent with it forming during the Little Ice Age Maxima, which terminated against this moraine, or in the slightly more extensive advance which Karlén (1973) dated at 2400-2700 cal.yrs.B.P.

Note: The Table is based on the framework for the Interpretation of diamictons presented in Bennett and Glasser (1996). The weight of evidence suggests that all diamictons have experienced at least an element of subglacial transport. Lodgement processes, especially of clasts and boulders, seems to have been a common process. Some horizons may also have experienced deformation, although there is little evidence of folding, faulting, rip-up inclusions, or rafts of sediments. This suggests shear homogenisation, if it occurred, was high. A proglacial sequence of massive and silty sands and sandy gravels, overridden and mixed with basal debris, would produce something akin to a diamicton. However, homogenised tills can be produced by deformation in basal ice during transport, and lodgement also involves the lodgement of matrix material if basal debris becomes overloaded, especially in the lower ablation area. For flutes to form in ice-walled cavities, an element of flow into the cavity may be required. This may occur in more ductile matrix.

3.7 Other Forefield Lithofacies

Other lithofacies at Isfallsglaciären and Kaskasatjåkka are similar to the glaciofluvial, glacio-lacustrine, and ice-marginal lithofacies identified by Etienne *et al*. (2003) at Storglaciären (Chapter 2.1.4; Table 2.2), and their coding system is used in the descriptions of the lithofacies that follow. Each description is followed by an interpretation. Two variants of sandy gravel (SG) are identified, these being and open framework gravel (SG_{of}) and fine gravel (SG_{f}).

3.7.1 Sandy Gravels (SG)

Description

These are massive gravels with gravel ranging in size from granules to boulders. At Kaskasatjåkka and Isfallsglaciären, SG is also the most common forefield lithofacies. Samples collected from an active channel bar in a braided stream and from fluted moraine at Kaskasatjåkka reveal the matrix silt content is $\leq$ 7% (Figure 3.3u&y). Fractal slope dimensions range between -2.28 and -2.39 (Figure 3.10n), which is similar to the -2.16 quoted for SG at Storglaciären (Etienne *et al*., 2003). Blades form the modal particle shape giving C_{40} indices between 12-37%, whilst the percentage of rounded to sub-rounded clasts (R/SR index) is relatively high (56%) and enables SG to be distinguished from other forefield lithofacies (Figure 3.21). At Isfallsglaciären a sample of SG from fluted moraine comprised 78% gravel and 21% sand, which is similar to the 70% gravel content of SG identified by Etienne *et al*. (2003).

In logs NL1-4 (Storglaciären), SG forms a laterally discontinuous sheet some 13m long and 0.2-0.5m thick which exhibits 2-D pinch and swell geometry and sharp upper and lower contacts with Lithofacies B (Figure 3.3-Dd and Figure 3.17a). In some parts, crude a-axis imbrications are apparent and some patches of gravel have an open clast-supported framework, whilst the majority of the gravel sheet is matrix-supported. Some parts of the sheet show a crude fining upwards sequences with thin beds of massive fine to medium-grained sand occurring towards the upper contact with Lithofacies B. Two thin (*ca*. 2cm) sand 'fingers' are seen to project into the base of Lithofacies B, which has a 5cm thick layer enriched in gravel at its base.

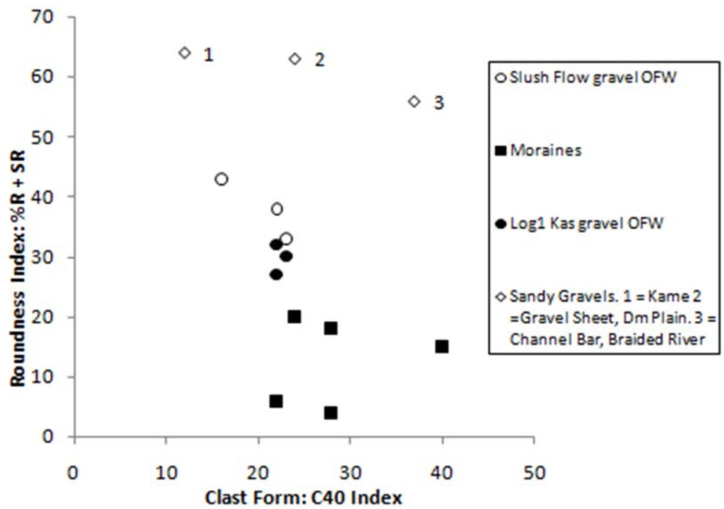

Figure 3.21 The Roundness Index and C_{40} Index for a Range of Lithofacies. Note: The channel bar deposit represents the average of 3 samples taken from an active bar in a braided stream in Kaskasatjåkka. This is a SG, as is the kame deposit (average of 3 samples) and gravel sheet deposit. Sandy gravels are discriminated by their relatively high R/SR index. Open framework gravels (OFW) are coded SG_{of} in the text. These samples come from moraines and fluted moraines, which plot in a similar area to open framework gravels recovered from the Kaskasatjåkka slush flow deposits in 2011.

Interpretation

SG occurs in fluted moraines and lateral and end moraines. It is the dominant lithofacies in palaeo-channels and the bed and banks of active braided channels in each forefield. SG is the most volumetrically important lithofacies at Storglaciären (and in the forefields of other polythermal Arctic glaciers). It occurs in a wide range of environments, especially in braided channel beds, and is thus interpreted as a glaciofluvial deposit (Etienne *et al*., 2003).

The gravel sheet in the Nordjåkk sections at Storglaciären (Figure 3.17) could be a proglacial or ice-marginal deposit formed during a Little Ice Age glacier oscillation (Karlén, 1973), or it could have formed subglacially. The gravel sheet resembles in scale and appearance the gravel sheets described by Boyce and Eyles (2000) which form inter-beds in till sheets in Canada. These are laterally discontinuous (length <10m) with pinch and swell 2-D geometry and thicknesses <1m. Boyce and Eyles (2000) interpreted such inter-beds as the product of ice-bed separation and localised incision by sub-glacial meltwater. Matrix-supported gravels with a-axis imbrications are known to be formed subglacially (Whiteman, 2002). The lower gravel contact is sharp and consistent with erosion of Lithofacies B. The enriched gravel horizon in Lithofacies B at the upper contact is consistent with a glaci-tectonic lamination produced by the local cannibalisation of the gravel sheet in a deforming horizon, as is the pinched nature of the sand inclusions (Ó Cofaigh *et al*., 2011). Lithofacies B has strong fissile texture and S_1 eigenvalues (which indicate strong clast alignment with consistent V_1 orientations to the ENE) above and below the gravel sheet, which indicates that the subglacial conditions that produced Lithofacies B were similar before and after gravel deposition. As such, it is possible that this sequence formed subglacially. However, whether it formed subglacially or represents glacio-fluvial deposition during a phase of recession followed by re-advance, the presence of the gravel sheet suggests that this sequence does not represent one continuous phase of pervasive deformation in which Lithofacies B was deforming through its entire thickness, but periods of till accretion separated by a phase of gravel deposition.

3.7.2 Silty Gravels (ZGm) and Fine Gravels (SG_f)

Description

Isolated patches of ZGm occur in moraines at Storglaciären (Etienne *et al*., 2003), but are absent at Isfallsglaciären and Kaskasatjåkka. ZGm contains 60% gravel (granules to cobbles, boulders rare), is massive, poorly sorted, contains 70% sand and 27% silt in the matrix, and has a fractal slope gradient (-2.82) very similar to Lithofacies Bii (Etienne *et al*., 2003). At Isfallglaciären and Kaskasatjåkka, fine-grained matrix-supported sandy gravel, SG_f comprises the main lithofacies in a series of steep-sided ridges and mounds which occur at the lateral margins of the forefield near to the proximal slopes of lateral moraines. SG_f contains variable gravel content, but it is usually greater than 60%, with granules and fine gravel dominant. Like ZGm, SG_f lacks coarser cobbles and boulders. It is distinguished from ZGm and SG by its matrix particle grain-size distribution - which is dominated by very coarse and coarse sand modes, with a black coloured sand comprising 96.8% of the matrix sample (Figure 3.3V) – and by its fractal slope gradient (SG_f = -2.06, R^2 0.989; SG = -2.28, R^2 0.989; Figures 3.10n&p). SG_f is massive and has a relatively high R/SR index (>60%; Figure 3.21).

Comment [DJG21]: You need to add a brief description of its physical properties

Interpretation

The relatively high R/SR index of SG_f is consistent with glaciofluvial transport and the lack of fines and coarser gravels and boulders is consistent with a moderate degree of sorting in a glaciofluvial environment (Benn, 2004). As such, SG_f is interpreted here as a glaciofluvial deposit and is considered a sub-set of lithofacies SG. Etienne *et al*. (2003) interpreted ZGm as a subglacial diamicton (Lithofacies Bii) re-worked and winnowed by glaciofluvial activity because of the similarities in fractal dimensions and particle grain-size distributions.

3.7.3 Open Framework Gravels (SG_{of})

Description

In fluted moraines in each forefield, end moraines and the diamicton sheet and plain, thin (<0.3m), laterally discontinuous layers of open framework gravels (SG_{of}) form sharp wavy contacts with diamictons and sand units. Like SG_f, there is an absence of boulders, and clasts are typically sub-rounded to sub-angular granules and cobbles. Fractal slopes range from -2.37 (R^2 0.99) to -2.39 (R^2 0.99; Figure 3.10i&j). SG_{of} has a lower R/SR index than SG/SG_f (≈ 30%, Figure 3.21). The matrix particle grain-size distribution is poorly sorted and consists of 91.6% sand, with a mode of very coarse sand and a low silt content of 7% (Figures 3.3y & Ee).

Interpretation

SG_{of} was observed in active channel bars in braided streams in each forefield. It is a glaciofluvial deposit that forms where fluvial currents are able to winnow fines from SG layers. However, gravels with open frameworks can also be produced in ice-marginal environments where subglacial sediment freezes-on to the base of the glacier during a winter advance, and then melts out during summer recession, when meltwater winnows away the fines (Menzies and Shilts, 2002). Thin beds of SG_{of} were also formed in levees and lobes during a major slushflow event at Kaskasatjåkka in 2011 (Figure 3.3Ff, and see section 3.6.c below). As such, SG_{of} is polygenetic.

3.7.4 Block Gravels (bG)

Description

Block gravels lack a coherent matrix and clasts range in size from cobbles to boulders. They occur on the distal slopes of the outer overridden moraine at Isfallsglaciären and on lateral moraines of all three forefields. They also occur in linear to arcuate discontinuous ridges which form transverse to glacier flow near to the present glacier terminus in all three forefields. At Isfallsglaciären, the boulders in the transverse ridges are typically 2-3m in length and form loose imbricate stacks. About half consist of sub-rounded to sub-angular forms with striae present on multiple faces. Striae dip at high angles and in multiple directions, and striae on adjacent boulders have very different orientations. Other boulders are angular and non-striated.

Interpretation

Block gravels are a common lithofacies of Arctic forefields where they are formed at glacier margins by the deposition of cobbles and boulders which derive from multiple glacial transport pathways (Etienne *et al*., 2003). Striated sub-rounded to sub-angular boulders are typical of subglacially transported material, whereas more angular boulders are typical of englacial or supraglacial transport pathways.

3.7.5 Massive Sand (Sm)

Description

At Storglaciären, Sm is a medium to fine-grained sand (94% sand) that is well-sorted and comprises mounds up to 3m high (Etienne *et al*., 2003). It is found in active and abandoned meltwater channels in all three forefields. A similar moderately-sorted but coarse-grained sand (98.5% sand) having a unimodal particle grain-size distribution (Figure 3.3Cc) was observed to form ephemeral dirt cones on the surface of permanent snowbanks at Kaskasatjåkka. At Isfallsglaciären Sm forms thin, laterally discontinuous layers that lack sedimentary structure. It occurs inter-bedded with muddy sand in the Fronstjön sand unit. It occasionally occurs in flutes as single thin (<2cm) layers within Lithofacies A, where it extends down-flow for about 20cm and dips at low angles (≈ 8°) up-flow. It also forms isolated patches on the proximal slope of the outer moraine, and forms graded sequences with

SG in fluted moraine. Sm samples from Isfallsglaciären and from mounds at Storglaciären were poorly sorted, medium to fine-sands with unimodal particle grain-size distributions (94-95% sand). Typical fractal slope gradients were in the order of -2.33 (with a relatively low R^2 value of 0.905).

Interpretation

Sm was interpreted by Etienne *et al*. (2003) as a glaciofluvial deposit associated with low discharge marginal streams and channel bank tops, and the occurrence of Sm in active channels in each forefield supports this interpretation. The thin, laterally discontinuous Sm layers within Lithofacies A have dimensions that resemble stringers (Piotrowski *et al*., 2004). Stringers are thought to form during a phase of ice-bed decoupling and deposition from subglacial meltwater. However, it is also possible the sand layers represent rafts of deformed substrate cannibalised into Lithofacies A (Evans *et al*., 2006). Dirt cones form by differential ablation of debris-covered snow; the debris can be windblown, originate from slides above the snowbank, or be deposited by meltwater flowing across the snowbank in early spring when the main channels are blocked with snow (Rhodes *et al*., 1987; Betterton, 2001). The dirt cones consist of SGf and Sm, and the coarse-grained nature and moderate sorting of Sm are consistent with the debris being sourced by meltwater flow across the snowbank.

3.7.6 Muddy (Silty) Sand (Zs)

Description

Zs typically contains 80% sand and 20% mud (mud contents vary between 13-22%). It has a fine-sand mean, unimodal to bimodal particle grain-size distribution, and moderate to poor sorting (Figure 3.3w, z & Bb). Porosities ranged between 45 and 50%. Zs forms thin beds (typically <2cm) which can be micro-laminated or massive. Fractal slope gradients range between -2.63 (R^2 0.996) and -2.61 (R^2 0.998). Zs is the dominant lithofacies in the Frontsjön sand unit and it occurs in ice-stagnation hollows, proglacial lakes, and in fluted moraine. At Isfallsglaciären, fining-up sequences of SG, Sm and Zs sometimes form the substrate to Lithofacies A in fluted moraine. In these areas, some Zs samples contain up to 65% silt and are sandy muds (Figure 3.3x).

Interpretation

Zs has been interpreted as a suspension deposit associated with glacio-lacustrine and active and palaeo-glaciofluvial terrain, where it forms in backwaters and silting ponds fed by low discharge rivers and forms thin veneers on gravel bars (Etienne *et al*., 2003). The mean fine-sand to very-fine sand grain-sizes and relatively high mud contents suggest deposition in low-energy environments, whilst fining-up sequences (SG, Sm, Zs) suggest deposition from waning currents, as might be expected in areas where meltwater channels enter small silting ponds and lakes (Ashley, 2002; Etienne *et al*., 2003). At Kaskasatjåkka, thin patches of Zs are also associated with the re-working of sands and gravels by meltwater following the collapse of snow bank dirt cones (Figure 3.3Bb).

3.7.7 Stony Diamicton (StDm) from End Moraines

Description

St(Dm) occurs widely in end moraines and lateral moraines at Isfallsglaciären and Kaskasatjåkka, where it forms the upper diamicton or, at Isfallsglaciären, forms the substrate to Lithofacies A. StDm is clast-rich to clast-supported (granules to boulders) and has a high RA index (>30% and up to 55%; Figure 3.6 and Figure 3.13b) with numerous angular and very angular clasts. Clasts appear unweathered. At Isfallsglaciären, StDm has a mean fractal slope gradient of -2.8 (R^2 0.995) and approximately a third of the matrix consists of silt, with modes of very fine to fine sand (Figure 3.3n, o&p).

Interpretation

StDm has similar physical properties to Lithofacies D (Table 3.1), for example, high RA indices that are indicative of transport along active and passive transport pathways (Benn, 2004). StDm occurs in end moraines and end moraines are characterised by inputs of material from multiple transport pathways and re-working of sediments by glaciofluvial meltwaters and debris flows (Menzies and Shilts, 2002). StDm at Isfallsglaciären has similar fractal dimensions and particle grain-size distribution to Lithofacies D at Isfallsglaciären (Figure 3.3m,n,o &p). This supports the interpretation of Lithofacies D as a till formed at an ice-marginal moraine. StDm does not contain large numbers of heavily weathered clasts, which indicates it is a till of more recent Little Ice Age origin.

Comment [DJG22]: This is a strange place to introduce new data of a different facies.

3.8 Lithofacies-Landform Associations

The lithofacies-landform associations of each forefield are shown in Figures 3.22a-c and described below.

3.8.1 Transverse Ridges

Description

Transverse ridges have asymmetric shapes and are steeper on their proximal sides. They form discontinuous features of between 100-200m length, and 1-3m height in each forefield, where they are located close to the present glacier margins. They are dominated by bG, with lesser amounts of SG and Lithofacies A. Flutes form immediately down-flow from the distal edges of transverse ridges.

Interpretation

The chaotic orientations of striae on adjacent sub-rounded to sub-angular boulders in bG suggest that these boulders have been remobilised from their initial embedded subglacial positions and rotated into their present positions during a subsequent glacier advance, and this is consistent with the transverse ridges being small push moraines formed by push-deformation processes (Boulton, 1976; Shakesby *et al*., 2004). Glaciers in the Tarfala Valley are known to have experienced small advances during the 1990s (Holmlund, *pers.comm.*), which were probably responsible for forming the asymmetric ridges. The angular boulders were either deposited from supraglacial transport pathways, or were entrained during advance over the proglacial area (Etienne *et al*., 2003).

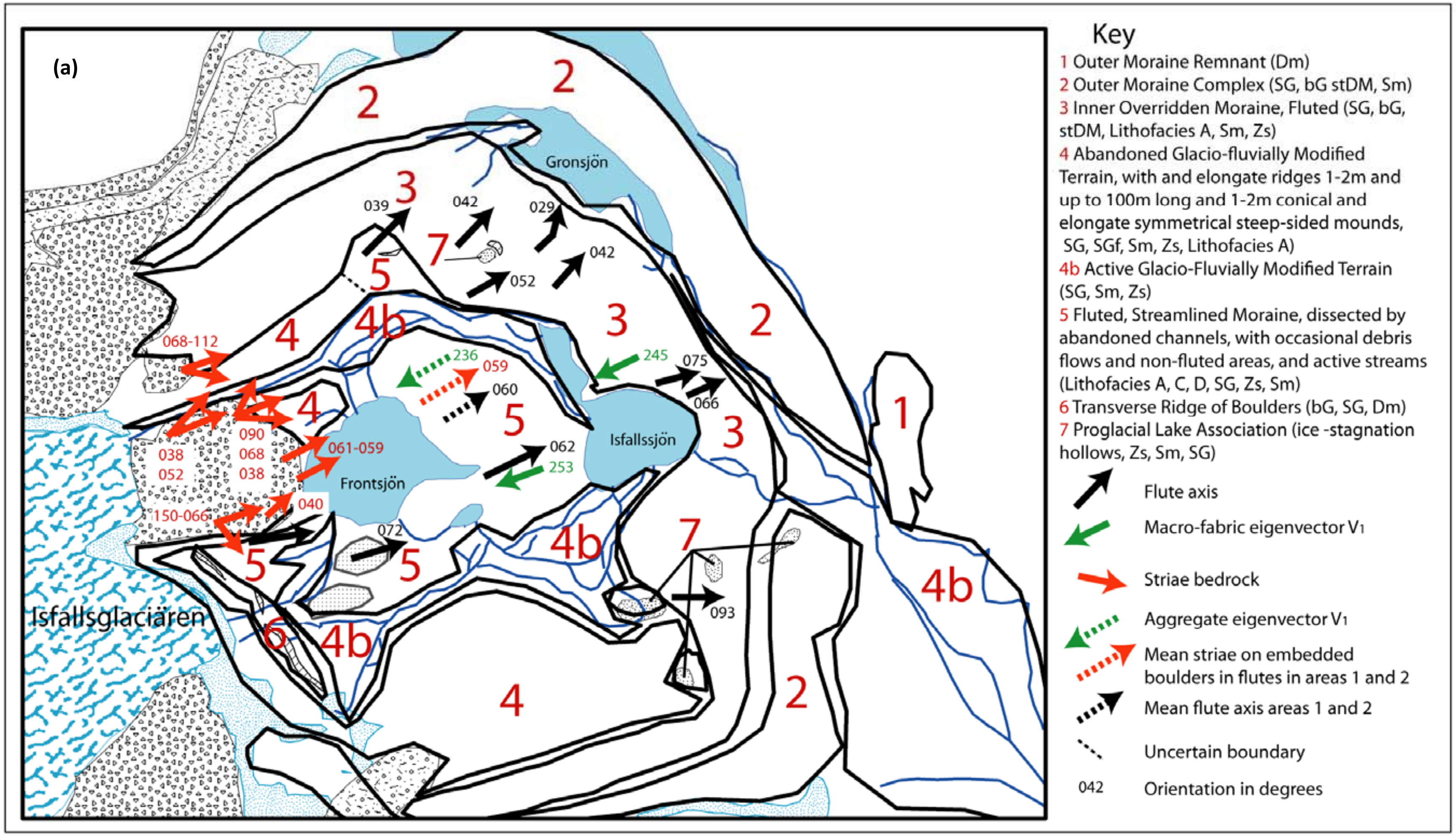

Figure 3.22a Lithofacies-Landform Associations at Isfallsglaciären

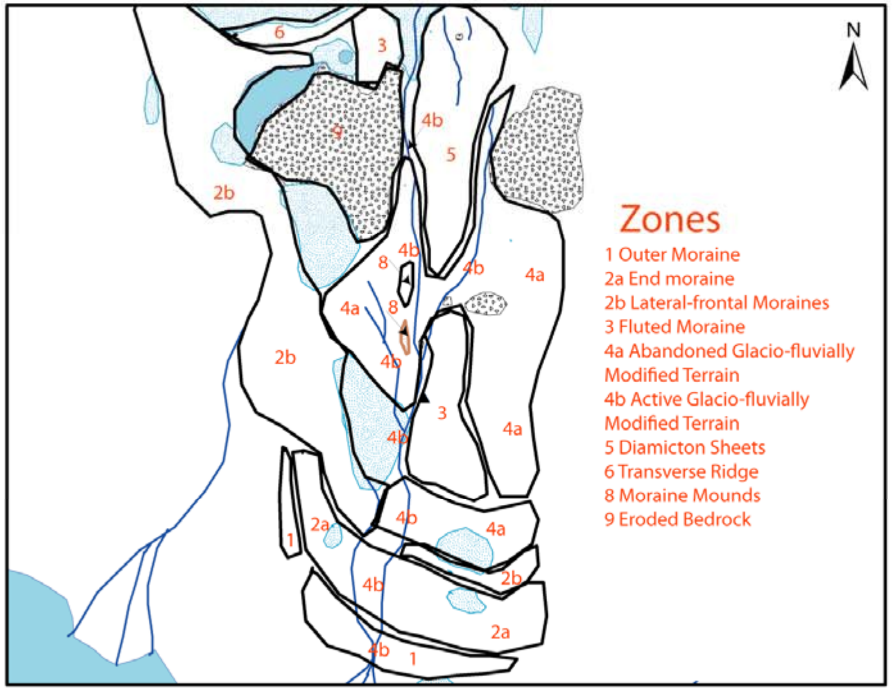

1 Outer Moraine dissected by active and abandoned channels and 2011 slushflow. Dm, stDm, SG, SGof,

2a End Moraine, subdued on eastern flank, approx extent of glacier 1916. Dm, stDM, bG, SG

2b Lateral-frontal Moraines, large lateral western moraine probably ice-cored. more subdued on eastern flank. SG, bG, occasional Dm & Sm/Zs

3 Streamlined Fluted Moraine dissected by active and abandoned channels, evidence of previous slushflows, occasional bedrock outcrops, and patterned ground in southern area 3. Lithofacies A, Cbr, SG

4a Abandoned Glacio-fluvially Modified Terrain, with evidence of active paraglacial re-working of sediments, glacier scoured bedrock outcrops, bouldery rockfalls and scree at foot of the steep eastern slopes of the valley. SG dominates channels with Sm/Zs, some bG, occasional Lithofacies Cbr south and west of area 3

4b Active glacio-fluvially Modified Terrain, SG, sub-ordinate Sm/Zs

5 Diamicton Sheets, up to 4m thick, resting on bedrock on steep slope, heavily dissected by channels, some intermittently active. Lithofacies B, C, D, SG

6 Transverse Ridge, bouldery, within 5m of glacier snout. bG, SG, Lithofacies B

8 Moraine Mounds, elongate ridges 1-2m high, SGf &SG, Glacio-fluvial deposits, Possibly Kames

9 Eroded Bedrock area with roches-moutonnee and crag and tail features, some supraglacial drape from active margin

Figure 3.22b Lithofacies-Landform Associations at Kaskasatjåkka

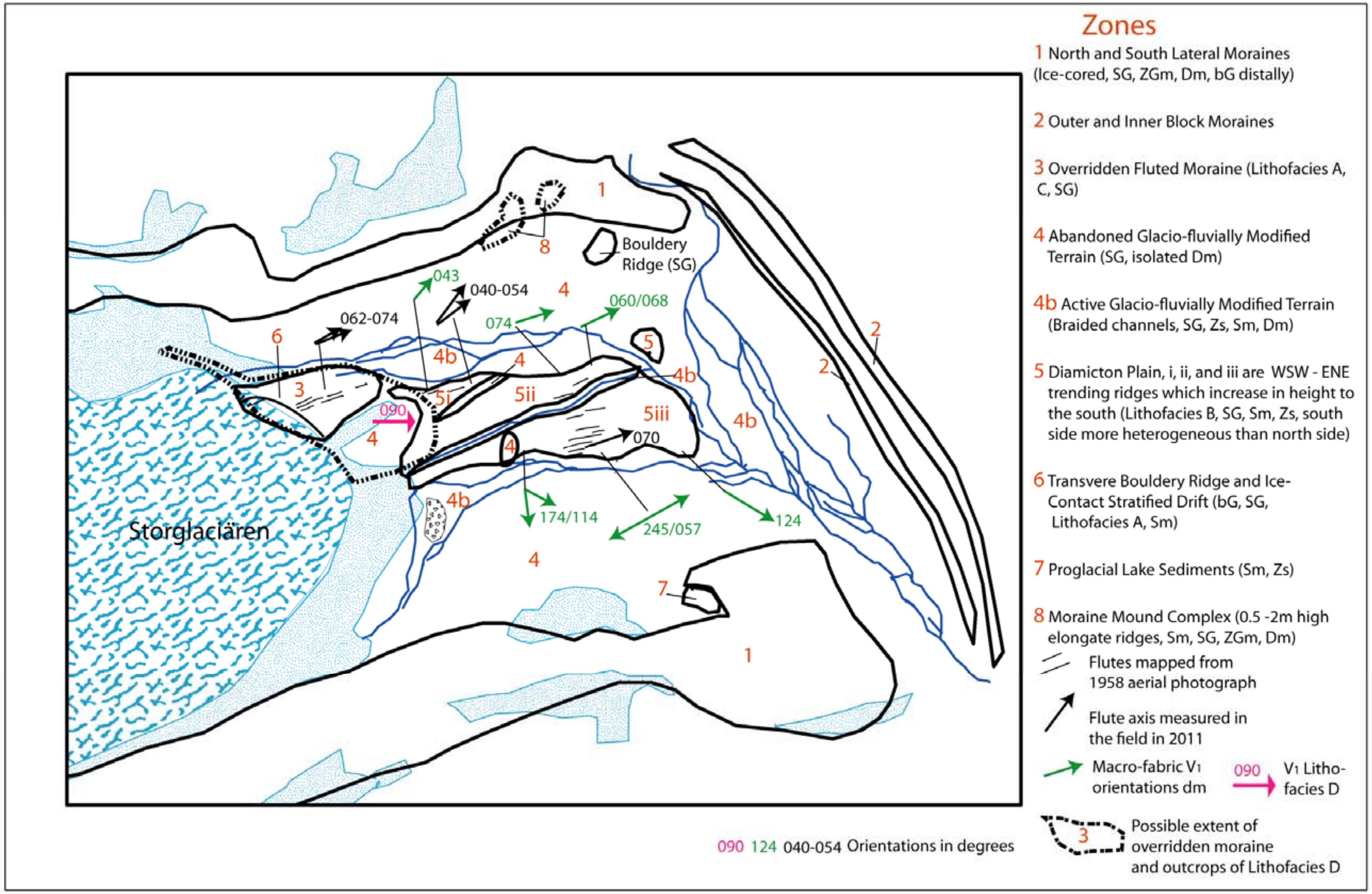

Figure 3.22c Lithofacies-Landform Associations at Storglaciären. The key and scale are the same as shown in Figures 3.2a-c.

3.8.2 Flute Fields

Description

Flutes are best exposed at Isfallsglaciären where they are over 100m long, straight, parallel-sided, and below the lower riegel they extend in a radial pattern across the lower forefield (Figure 3.22.a). The flute field extends across an extensive area (approximately 400m wide) area between Fronstjön and Isfallsjön where flutes are between 0.2-0.4m high. In Figure 3.23a the widths of all flutes measured at Isfallsglaciären are grouped into 0.5m class intervals and the frequency shown; flutes have a distinct modal width of 1.5-2m and interflutes a modal width of 0.5-1m. The flute field merges into active and abandoned glacio-fluvially modified terrain on either side of the forefield. The flutes extend over the inner frontal moraine – known to have been overridden during the Little Ice Age advance (Holmlund and Jansson, 2002) – but become increasingly indistinct on its distal face. Flutes emerge near the distal edge of Frontsjön on the adverse slope of what Eklund and Hart (1996) termed four drumlinized ridges, although the 'ridges' are better described as a distinct arcuate mound oriented transverse to glacier flow and extending across the entire fluted area (Figure 3.24). The top of the transverse mound has a similar elevation (1180m) to the overridden frontal moraine. Only about half of the flutes have distinct initiating boulders. Of the 25 flutes studied in detail across the three forefields, 17 had no initiating boulder. Flute widths and heights are generally consistent longitudinally (Hoppe and Schytt, 1953), and some flutes terminate against large embedded boulders or thicken on their stoss sides.

Although a distinct modal group emerges when all flute widths are considered (Figure 3.23a), individual transects across different parts of the forefield show that flute spacing (distance from flute crest to flute crest) can be uneven. For example, a transect conducted across the crest of the transverse moraine from Area 2 to Area 3 at Isfallsglaciären (Figure 3.1a) shows uneven flute spacing, with multiple modes occurring (Figure 3.23e). However, flute widths in excess of 4m along this transect mostly represent zones of lower-topography (*ca.*2m depressions) which are several metres wide and extend down-flow towards Isfallsjön. In these lower areas, a thin cover (<0.3m) of SG, Sm, and Zs makes sharp contact with underlying Lithofacies A (Figure 3.24).

Comment [DJG23]: Doesn't this contradict the start of the previous para?

Flutes at Kaskasatjåkka and Storglaciären have a more limited distribution (Figures 3.22b&c). At Storglaciären, a prominent zone of flutes occurs on a distinct transverse mound on the northern side of the forefield (zone 3, Figure 3.22c) where subdued flutes occupy an area approximately 50m wide and which extends for 100m down-flow in an ENE direction. Flutes are 0.1-0.3m high, 1-3m wide, and of variable lengths (~10-30m). The fluted surface is actively eroded by the Nordjåkk channel. Flutes are occasionally observed on parts of the diamicton plain (Figure 3.2c) where they are subdued in height (<0.15m) and difficult to trace longitudinally, although one flute near Log SL3&4 was traced for 20m. These flutes consist of Lithofacies B.

Comment [DJG24]: Give a range

The main fluted area at Kaskasatjåkka (zone 3, Figure 3.22b) extends across two distinct longitudinal mounds which occur to the east of the main braided channel. The mounds are up to 4m higher in elevation than the channel floor, and the upper mound occurs just below a distinct morphological break of slope. The two longitudinal mounds are separated by an east-west trending palaeo-channel. They cover an area approximately 100m wide which extends 150-200m to the south. To the south and east the mounds merge into zones of active and abandoned glacio-fluvially modified terrain. The longitudinal mounds are heavily dissected by palaeo-channels, and flutes in this area are often difficult to follow. Flutes are up to 60m long, between 1 and 4m wide, and 0.2-0.4m high. Flute widths at Kaskasatjåkka and Storglaciären are more variable than at Isfallsglaciären, although interflute widths are more consistent and generally <1m (Figure 3.23).

Diamicton is the dominant lithofacies within the flute fields in each forefield. The subglacial Lithofacies A forms the flutes, with Lithofacies C and D (base not seen) forming the substratum. SG also forms substratum to Lithofacies A, and in the Fronstjön sand unit, glaciofluvial sequences consisting of fining upwards cycles of SG, Sm and Zs occur, as well as glaciolacustrine sequences of interbedded Zs and Sm. At Kaskasatjåkka, stream incision revealed a 3-4m high section through part of the upper longitudinal mound at log 1 (Figure 3.1b). The longitudinal mound consists of a sequence of stony diamictons and SG (including 0.2-0.3m thick, discontinuous and contorted layers of SG_{of} and patches of micro-laminated Zs) which generally dip up-glacier and are capped by Lithofacies A which forms a sub-parallel layer that pinches-out down-flow (Figure 3.25).

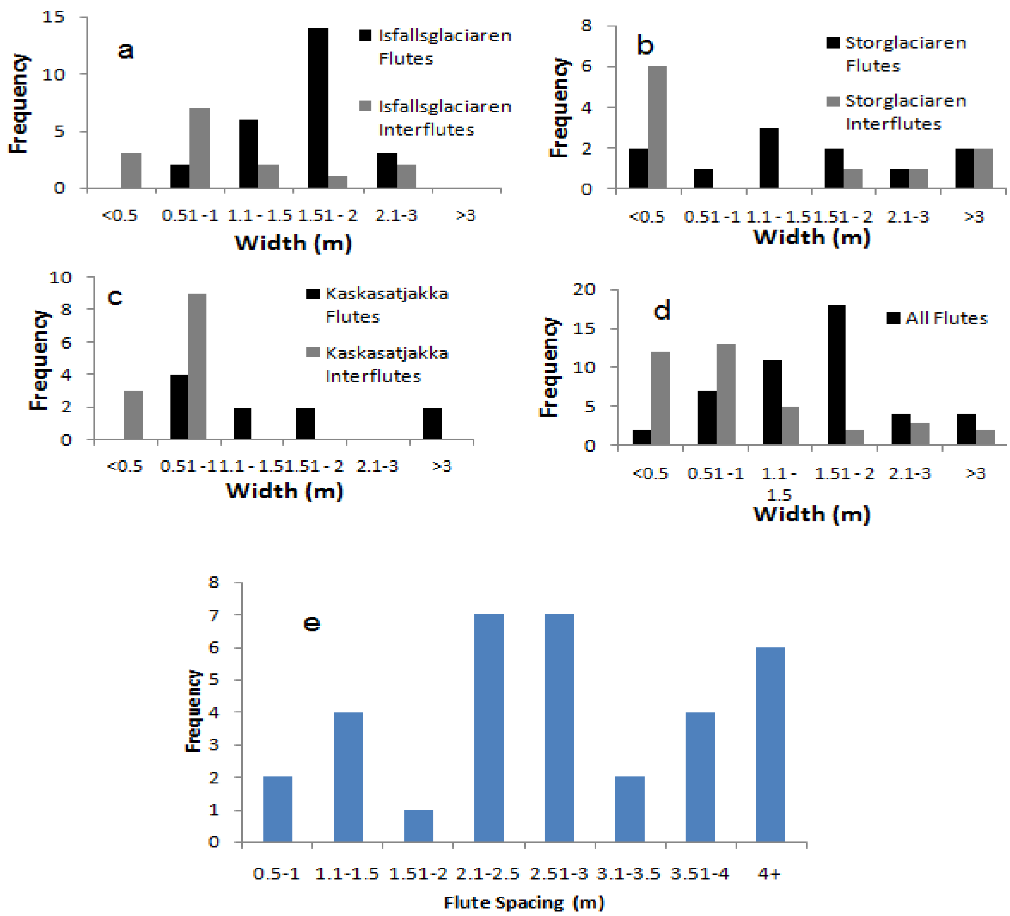

F

	Modal Width (m)	Width Range (m)	Height (m)	Typical Length (m)	Elongation Index
Isfallsglaciären	1.5-2	0.5 - 3	0.2-0.4	100	50 -67
Kaskasatjåkka	0.5 -1	0.5-4	0.2-0.4	40-60	60 - 80
Storglaciären	1-1.5	<0.5 - >3	<0.15	Variable, up to 20 - 30	20 - 30

Figure 3.23 Flute and interflute widths and spacing. Figure 3.23a shows the width of flutes in Areas 2 and 3 Isfallsglaciären, Figure 3.23b the widths at Storglaciären, and Figure 3.23c the widths at Kaskasatjåkka. Widths were measured at various points along flutes and at Isfallsglaciären flutes widths have a distinct modal width as do interflutes in each forefield. Flute widths are largely consistent along flutes, as are flute heights. Figure 3.23d shows the aggregate data (N = 46 flutes, 40 interflutes) for all three forefields. Figure 3.23e shows the spacing of flutes along a transect across Areas 2 and 3 at Isfallsglaciären (see Fig.4.1). Spacing was measured from flute crest to flute crest using a 50m tape measure. Flute spacing shows multiple modes.Figure 3.23f compares flute geometry in each forefield. The elongation index is the typical flute length divided by modal flute width.

Interpretation

Lithofacies A has an extensive coverage across the central part of the Isfallsglaciären forefield and the long flutes that extend across the forefield are consistent with an uninterrupted period of continuous glacier flow and deforming-bed conditions during the Little Ice Age advance (Benn and Evans, 2010). Flute fields are an important component of each forefield. Fluted moraine probably had a more extensive distribution at Kaskasatjåkka and Storglaciären originally. For example, the 1959 aerial photograph of Storglaciären shows a number of flutes which are no longer visible on the ground and a slightly more extensive diamicton plain (Figure 3.2c). Ice-marginal lateral streams have increasingly incised into the centrally located fluted field at Isfallsglaciären and Kaskasatjåkka, and the diamicton plain/sheet as glaciers have thinned and receded (Etienne *et al*., 2003), and paraglacial re-working of sediments is rendering flutes difficult to see at Kaskasatjåkka.

The Little Ice Age advance was characterised by a phase of flute formation related to deforming-bed conditions that occupied the central parts of each forefield. The deformation of Lithofacies A required elevated pore-water pressures and this required warm-based ice (Section 3.3.6&7), which is known to occur beneath the thicker central parts of polythermal glaciers in the Tarfala Valley to within *ca*.30m of their termini (Holmlund and Jansson, 2002). Lithofacies A is characterised by embedded boulders with heavily striated upper surfaces, consistent with overriding and abrasion by active ice, and this, combined with the necessity for elevated pore-water pressures, suggests basal sliding was an active process and probably a significant control on glacier dynamics, as it is known to be beneath contemporary Storglaciären (Iverson *et al*., 1995). The thickness of the deforming bed was limited during the flute formation phase and macro-observations suggest deformation was characterised by discrete, brittle or brittle-to-ductile shear, at least in the latter stages. Erosion of the Frontsjön sand unit sourced sediment to Lithofacies A in Isfallsglaciären and the sandy diamicton was more readily deformable than the coarser, stonier Lithofacies A at Storglaciären and Kaskasatjåkka, and this may help to explain why flutes are more extensive at Isfallsglaciären.

Comment [DJG25]: Evidence? Or refer back to where this is discussed

Lithofacies D has similar physical properties to the stony diamictons in end moraines, with sediment sourced from multiple transport pathways. The outcrop of Lithofacies D on the proximal slopes of the transverse mounds suggests that these features represent older frontal moraines that were formed by glacier advances that pre-date the Little Ice Age advance and have subsequently been overridden. As such, the flute fields in front of each glacier represent palimpsest landforms (Kleman, 1992). The overriding of moraines is known to occur in the Tarfala Area and is thought to cause little modification to the original moraine, except for a limited amount of rounding and streamlining of moraine summits (Karlén, 1973), a morphology that is consistent with that observed in each forefield.

The Fronstjön sand unit has a limited outcrop on the proximal slopes of the overridden fluted moraine. The lithofacies assemblage suggests it represents a proglacial lake association. The superposition of the sand unit (below Lithofacies A and C but above Lithofacies D), suggest the proglacial lake formed prior to the most recent Little Ice Age advance that formed the flutes. The proglacial lake was probably dammed by the adverse proximal slope of the transverse moraine. Similar lakes occur at contemporary Isfallsglaciären behind the large and extensive end moraines, and the presence of these transverse moraines explains the greater number of lakes at Isfallsglaciären. The moraine would have acted as a pinning point for the glacier (Ó Cofaigh *et al*., 2011) and saturated sediments probably occurred in zones of restricted drainage behind cold-based ice associated with thin termini (Eklund and Hart, 1996). Saturated sands at Isfallsglaciären would have been readily deformed, so contemporary Fronstjön may also occupy a moat where relatively weak sediments were easily eroded. The cannibalisation of the sand provided the constituent material of Lithofacies A.

Outcrops of SG substratum in the flute fields are consistent with proglacial glacio-fluvial deposition prior to the Little Ice Age advance across the moraine surface. The topographic low areas on the distal slopes of the transverse moraine surface consist of a glaciofluvial lithofacies association typical of outwash streams (Etienne *et al*., 2003), and it is probable that these areas represent former meltwater channels that drained from the receding glacier margin. Lithofacies A forms the substratum to the outwash deposits in these areas and flutes have probably been eroded by meltwater or buried beneath glaciofluvial deposits.

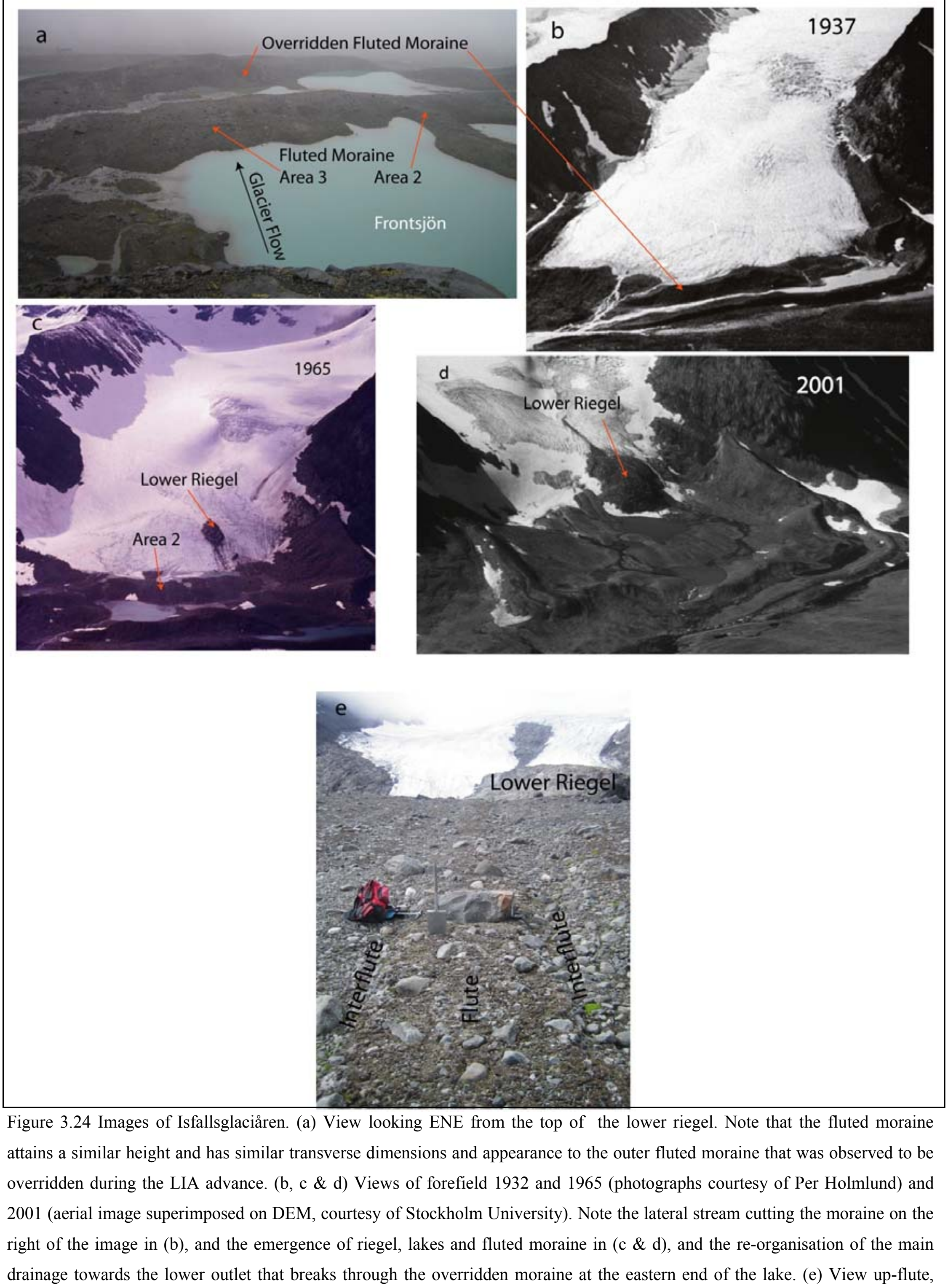

Figure 3.24 Images of Isfallsglaciåren. (a) View looking ENE from the top of the lower riegel. Note that the fluted moraine attains a similar height and has similar transverse dimensions and appearance to the outer fluted moraine that was observed to be overridden during the LIA advance. (b, c & d) Views of forefield 1932 and 1965 (photographs courtesy of Per Holmlund) and 2001 (aerial image superimposed on DEM, courtesy of Stockholm University). Note the lateral stream cutting the moraine on the right of the image in (b), and the emergence of riegel, lakes and fluted moraine in (c & d), and the re-organisation of the main drainage towards the lower outlet that breaks through the overridden moraine at the eastern end of the lake. (e) View up-flute, flute 1, area 2. The flute is parallel-sided and has a consistent height and width over 100m length. The spade is about 1m long.

Ground-Penetrating Radar (GPR) Surveys of Flute Fields and Overridden Moraines

GPR surveys were used to investigate the internal architecture of the flute fields and overridden moraines in order to provide further insights into the origin of these landforms (Chapter 2.3.3). GPR surveys were conducted across the northern flank of Storglaciären and down-flow onto the overridden fluted moraine, the flute field of Isfalsglaciären, and across the overridden fluted moraine at Kaskasatjåkka (Figure 2.6a-c).

Description

The 3m section at log 1, Kaskasatjåkka, allowed ground-truthing of the radargrams. In Figure 3.25 the radargram of log 1 shows the upper diamicton bounding surfaces form bright sub-parallel reflectors that pinch-out down-glacier, whilst the stony and bouldery Dm/SG sequence below forms a series of interfering hyperbola diffractions and reflectors that dip up-glacier; ground-truthing shows that the reflectors corresponded to lithofacies contacts or boulder pavements.

At Storglaciären, GPR transects in survey area 2 on the northern side of the glacier and across the fluted moraine mound show the glacier bed consists of a series of bright reflectors and strongly interfering hyperbola diffractions. Radargrams of longitudinal transects (200MHz) show a complex series of strong, laterally continuous sub-parallel and shorter up-glacier dipping reflectors at shallow depths in the terminus zone (Figure 3.26a). Similarly, at Isfallsglaciären, the unmigrated radargarm of transect line F3 (Figure 3.26b) across the transverse fluted mound shows that it is dominated by interfering hyperbolic diffractions, and ground-truthing reveals these areas are associated with bouldery diamictons or SG layers. Ground-truthing along line F3 also reveals that the series of bright, concave-up but asymmetric reflectors extending to 2-3m depth at 0 to 28m along the transect correspond to the Fronstjön sand unit.

Migrated radargrams across the Isfallsglaciären transverse mound allow two distinct radar facies (R1 and R2) to be identified. Both form bright, laterally continuous, wavy, sub-parallel or dipping reflectors, with R1 commonly occurring at 1-2m depth and R2 at 3-4m depth. Both reflectors often pinch-out to the east (that is, down-glacier). In some longitudinal transects, R1 and R2 dip up-glacier on the proximal side and crest of the transverse mound, and down-glacier on the distal side. In transverse section (Figure 3.25e) reflector R1 is concave-up and defines a lenticular body of bright and tightly packed hyperbola diffractions.

Radargrams processed using SEG gain, which allows comparison of reflector brightness (Neal, 2004), reveal patchy regions within the moraine beneath 2-3m depth where hyperbola diffractions are much less bright or where very few reflectors occur (Figures 3.26b-e).

Interpretation

Isotope studies have shown that subglacial sediment freezes-on to the base of Storglaciären and that compressive flow near the terminus brings subglacial and englacial debris to the surface, forming a series of ice-marginal debris bands and ice-contact stratified drift deposits on the northern side of the glacier (Moore *et al*., 2012). The elevation of frozen-on subglacial and englacial sediments by compressive flow is thought to be an important process in the ice-marginal terrestrial landsystems of active temperate glaciers in Iceland, where winter advances produce imbricate stacks of till and flutes on overridden moraines, with the stacks dipping up-glacier (Evans, 2003). Thick basal sequences of till are also elevated in subpolar glaciers by compressive flow, and form composite ridges of thrust sediments, dipping back up glacier (Ó Cofaigh *et al*., 2003). It is possible that some of the strong continuous reflectors dipping up-glacier in radargrams from Storglaciären (Figures 3.26a-d) represent ramps and that low-angle thrusting was involved in the formation of the transverse fluted moraine mounds (Bennett *et al*., 2004). However, Moore *et al*. (2012) found no evidence of thrusting near the terminus of Storglaciären. They did find inverted stratigraphy in debris bands which they argued was the product of over-folding associated with compressive flow. The transverse moraine mound would supply a suitable adverse slope which would enhance longitudinal compression and induce folding in the northern terminus zone. Sediment within ice is likely to reflect strongly because of the strong dielectric contrast (Neal, 2004). The strong dipping reflectors in line 09 (Figure 3.26a) are consistent with a sequence of frozen-on sediments that have been stacked against an older moraine mound, whilst some of the strong sub-parallel reflectors may represent debris-rich basal ice layers. This interpretation is consistent with Karlén's (1973) suggestion that older moraines form barriers to flow in the Tarfala Valley and grow by proximal enlargement as imbricate stacks of till are deposited on their proximal sides.

Areas of less bright reflectors are likely to occur where radar wave energy has been highly attenuated or where the dielectric contrast is small, whilst areas with very few/no reflectors are characteristic of ice (Neal, 2004). In the Isfallsglaciären radargrams, some areas characterised by few reflectors and less bright reflectors are underpinned by brighter

Comment [DJG26]: Do you mean areas with no reflectors? This would be characteristic of ice. Sediment within the ice is likely to reflect strongly because of the strong dielectric contrast. IF the reflectors themselves are weak, this suggests there's little energy left or that the dielectric contrast is small reflectors (for example, Figure 2.6ci), which demonstrates that wave attenuation is not causing the less bright areas/areas with fewer reflectors in these cases. The large lateral-frontal moraines at Storglaciären and Isfallsglaciären are known to be ice-cored below about 2 m depth (Holmlund and Jasson, 2002), and the areas of less bright/fewer reflectors begin below R1 at 2m depth in the radargrams. As such, these patches probably indicate ice-cored parts of the overridden moraines which are more transparent to radar waves (Neal, 2004). R1 occurs at a depth that generally exceeds the thickness of Lithofacies A and C combined. At 1m depth, outcrops of Lithofacies D or SG commonly occurred in the Isfallsglaciären trenches. It is unclear whether R1 and R2 represent structural or lithofacies boundaries. However, the ground-truthing of Log 1 at Kaskasatjåkka shows that dipping bounding surfaces and sub-parallel reflectors in the moraine represent contacts between different lithofacies. As such, although it was not possible to successfully ground-truth R1 and R2 at Isfallsglaciären, it is suggested here that they represent contacts between older diamictons and/or SG layers within the overridden moraine, which is consistent with it being a palimpsest landform.

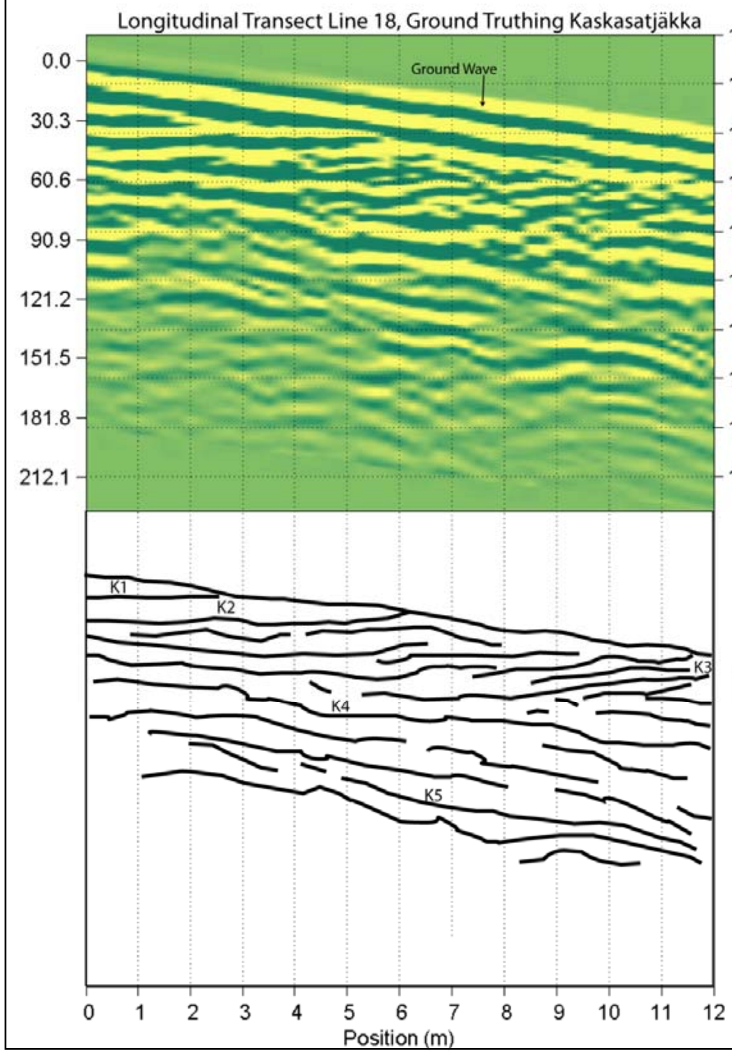

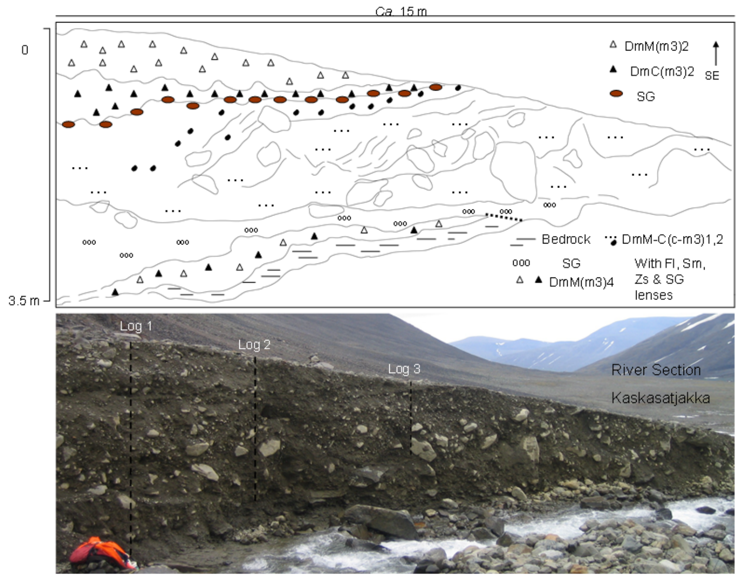

100 MHz survey, summer 2010 Log 1, heading south down stream-cut section. Background subtraction filter applied, topography added using wave velocity of 0.8,/ns attained from hyperbola matching. SEC gain x100, image interpolated so as to emphasise low angle reflectors

K1 and K2 - Strong bright continuous reflectors pinching out to the south - bounding surfaces between two upper fine-grained diamictons
K3 Bright reflectors dipping up-glacier, some short, discontinuous - clast rich layers in coarser Dm and dipping contacts between tabular Dm layers
K4 Strong continuous reflector dipping down-glacier and sub-parallel to surface slope - base of main bouldery Dm
K5 Strong reflector, subparallel, continuous, dipping down glacier, 4-5m below the surface - boulder pavement at base of sequence resting on bedrock

Figure 3.25 Kaskasatjåkka Log 1 river section, image, 2-D graphic log, and radargram with interpretation from ground-truthing. The radargram starts at Log1 on the image and heads south towards Log 3

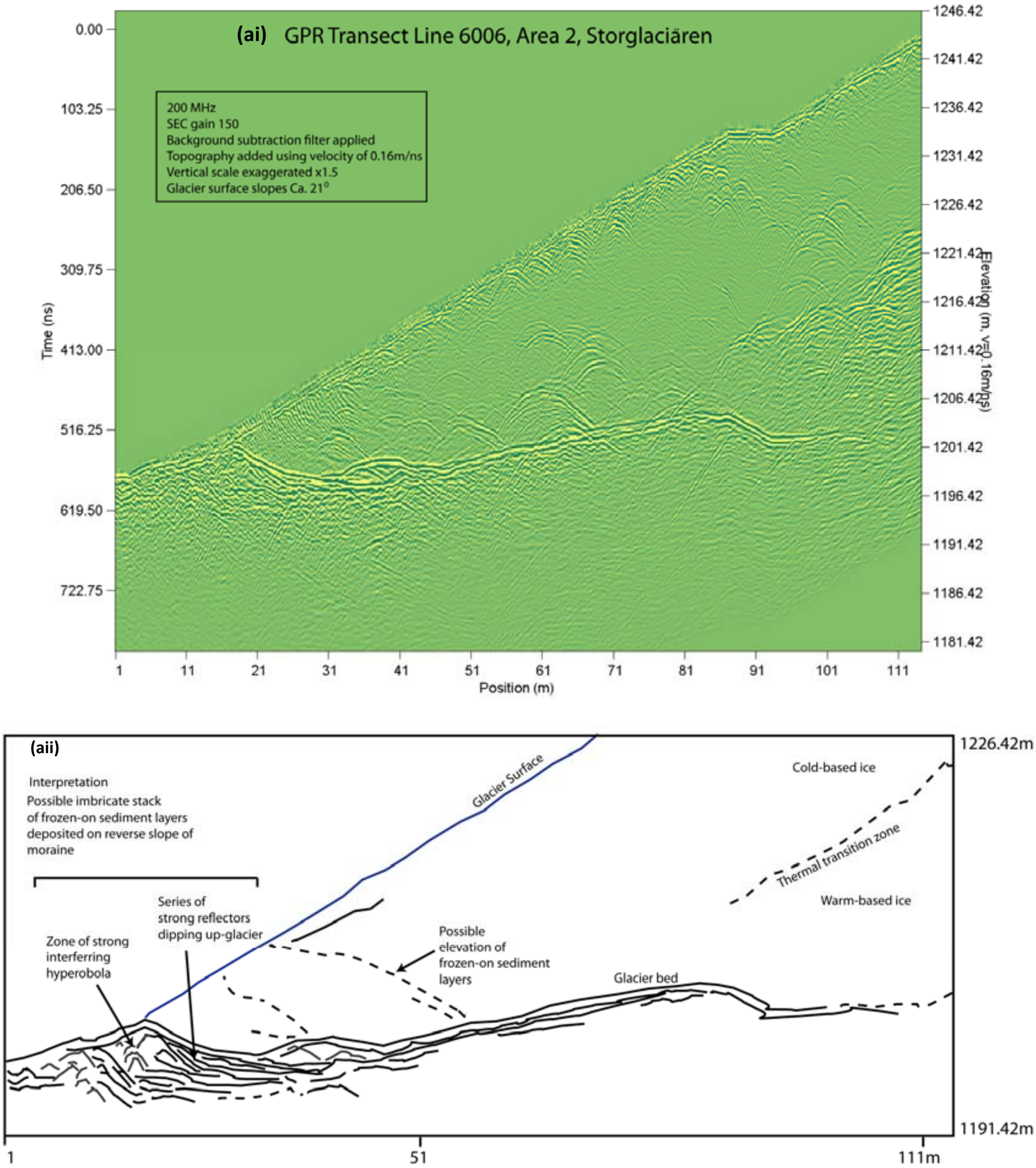

Figure 3.26 Radargrams (i) and interpretations (ii); (a) longitudinal profile across terminus region of Storglaciären and moraine.

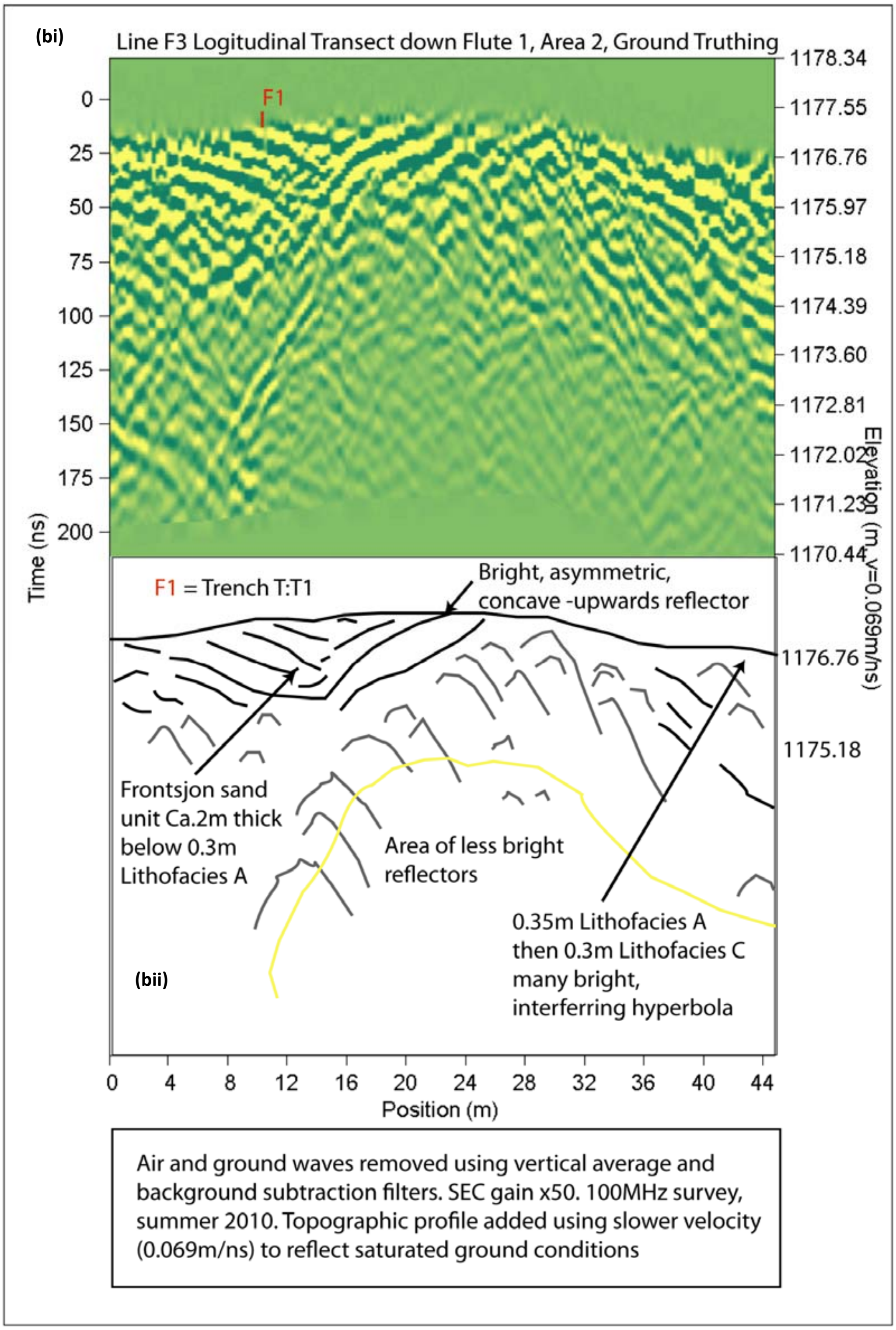

Figure 3.26 Radargrams and interpretations (b) longitudinal transect down Flute 1, Area 3, Isfallsglaciären.

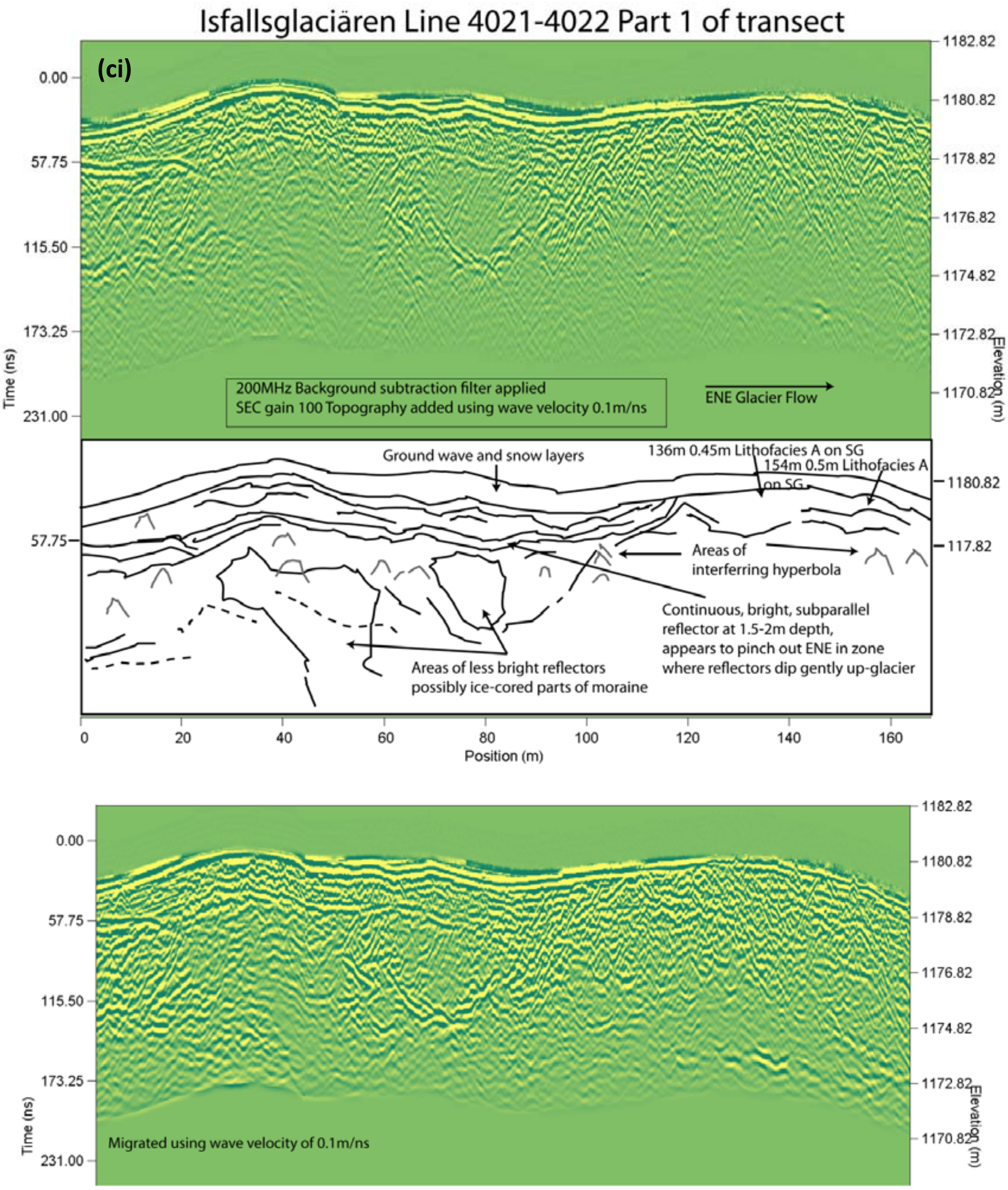

Figure 3.26 Radargrams and (c) longitudinal transect down fluted moraine, Isfallsglaciären (part 1 ci, part 2 cii below). Migrated profile shown below the interpretation in (ci) for comparison with the unmigrated profile.

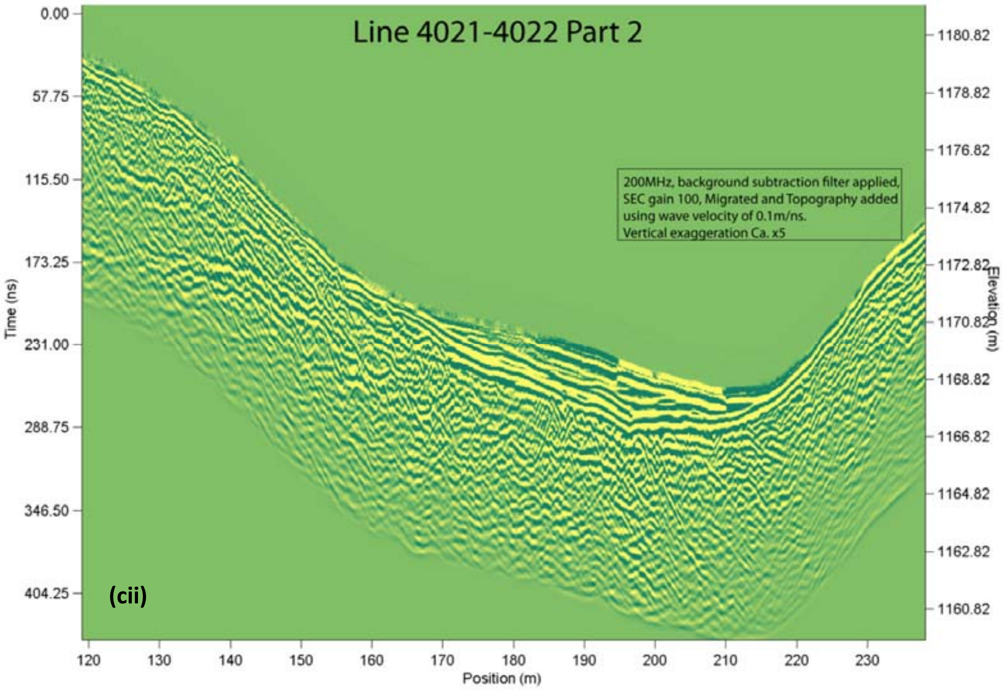
Line 4021-4022 Part 2
200MHz, background subtraction filter applied, SEC gain 100, Migrated and Topography added using wave velocity of 0.1m/ns. Vertical exaggeration Ca. x5
(cii)
Time (ns)
Elevation (m)
Position (m)
0.00
57.75
115.50
173.25
231.00
288.75
346.50
404.25
1180.82
1178.82
1176.82
1174.82
1172.82
1170.82
1168.82
1166.82
1164.82
1162.82
1160.82
120
130
140
150
160
170
180
190
200
210
220
230

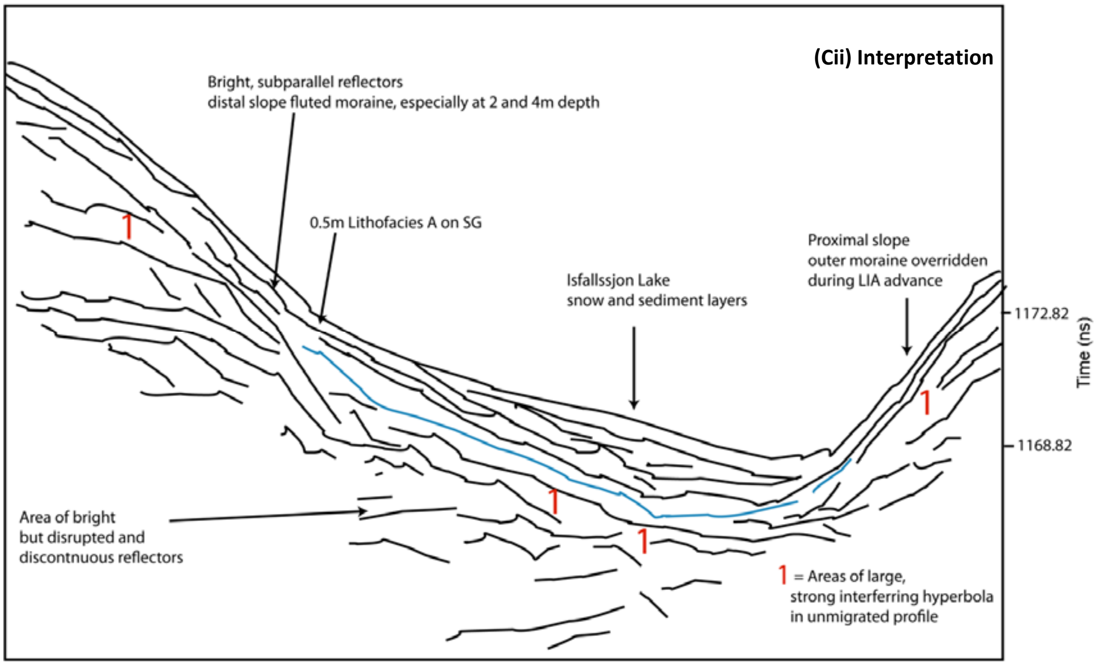
(Cii) Interpretation
Bright, subparallel reflectors
distal slope fluted moraine, especially at 2 and 4m depth
0.5m Lithofacies A on SG
Isfallssjon Lake
snow and sediment layers
Proximal slope
outer moraine overridden
during LIA advance
Area of bright
but disrupted and
discontnuous reflectors
1 = Areas of large,
strong interferring hyperbola
in unmigrated profile
1172.82
1168.82
Time (ns)

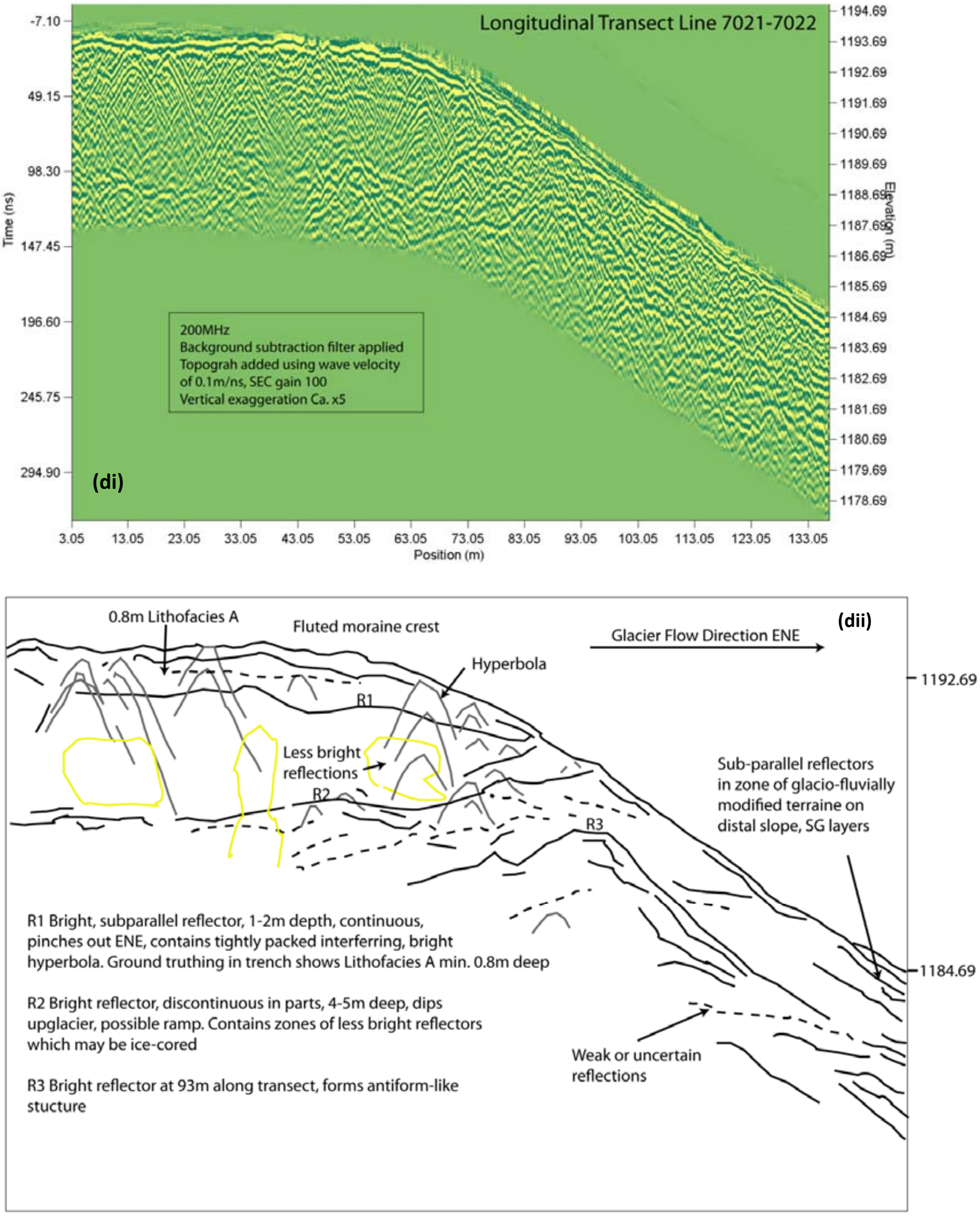

Figure 3.26 Radargrams and interpretations (d) detail of longitudinal profile across fluted moraine, Isfallsglaciären.

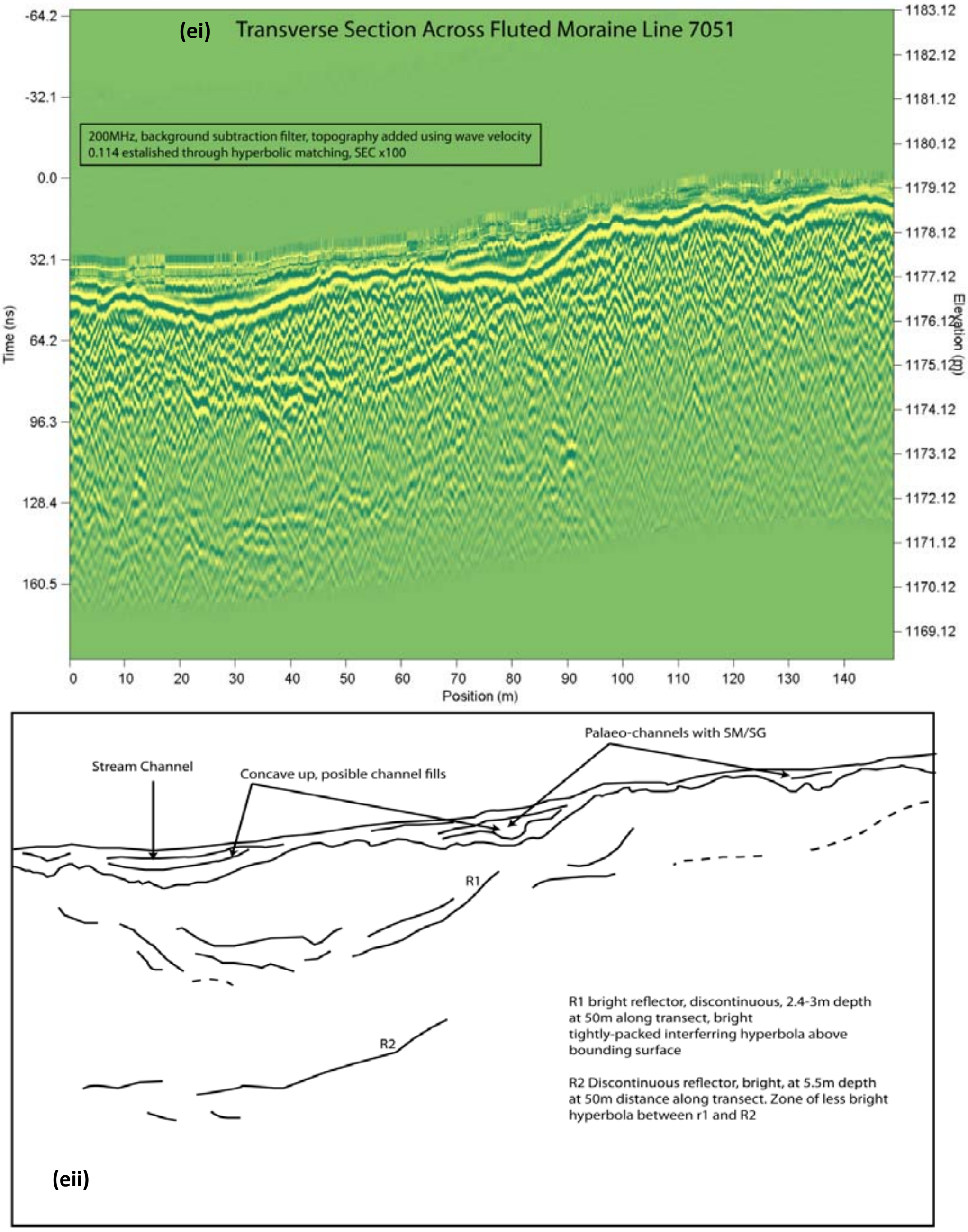

Figure 3.26 Radargrams and (e) transverse profile across fluted moraine, Isfallsglaciären. Note: the transect lines are shown on Fig.2.6.

3.8.3 Terrain Modified by Slushflows

Description

A time-lapse camera installed at Kaskasatjåkka revealed the impacts of a major slushflow that was witnessed by observers at the Tarfala Research Station and associated with a sudden warming event on the 7th June in 2011 (Figure 3.27a&b), when daily temperatures went from below freezing to 8-9°C over a 24 hour period (Matthews, *Pers. Comm*. 2012). Slushflows are initiated where the collection of meltwater in a snowpack causes it to lose cohesion and become mobilised (Scherer *et al*., 1998). They are high magnitude-low frequency events characterised as dense, turbid flood-wave torrents that resemble debris flows (Blikra and Nemec, 1998). Slushflows mobilise sediments that have been blown or washed or have fallen onto the snowpack, as well as eroding and re-working sediments in their paths, creating a range of distinctive erosional and depositional landforms (Figure 3.27 c-I; Table 3.11).

The Kaskasatjåkka slushflow was at least 1km long and up to 50m wide in places, and it followed a path along the main stream channel and fluted moraine (zone 3, Figure 3.22b) before breaking through the outer moraine and flowing down to Tarafalajaure, where it formed a fan as it entered the lake (Figure 3.28). The slush flow deposited considerable debris across the lower forefield area in the form of scattered clasts, snow-cored debris mounds, and more organised sedimentary deposits such as small debris ridges and lobes. Lithofacies included SG, SG_f, SG_{of}, Sm, and Zs, as well as stacks of large, precariously balanced boulders, sometimes showing imbrication, which had inverse to normal graded sand and SG_f drapes up to 14cm thick on upper surfaces. Some boulders and clasts were observed to have very steep dips. The gravels occurred in debris horns and debris shadows, small levées, and small patchy and digitated lobes (Figure 3.27 & Table 3.11). In vertical section, some gravel patches revealed lenses of fine massive sand interlaminated with Zs. Stratified waterlain matrix infill is thought to relate to the ablation of blocks of snow incorporated in the flow (Blikra and Nemec, 1998). The slushflow also deposited coarse to medium black sand, fine gravel, and finer debris on non-mobilised snow patches at the margins of the flow and within a few days differential ablation had produced dirt cones on the snow surface (Figure 3.27h). The dirt cones had low survival potential and ablation produced thin layers (<1cm) of Zs deposited across the forefield in meltwater flows and chaotically organised dumps of fine gravel (Figure 3.27i).

Table 3.11 Landforms, Features and Lithofacies Associated with Slush Flows

Feature/Landform	Description	Inferred Processes	Observed at Kaskasatjåkka	Lithofacies
Levees	Often 1 clast or a few clasts thick ridges of gravel	Surficial debris shouldered aside in flow	Yes, SA-SR pebbles - cobbles	SG, SG_{of}, SG_f
Debris horns	Mounds of coarse gravel and cobbles deposited chaotically on the stoss side of large boulders. Thins to up-valley apex. Chaotic, meltout fabric	Local freezing of plastic flow	Yes	SG, SG_{of} Sm
Debris shadows	Mounds of coarse debris deposited in the lee of large boulders, becoming tapered down-flow	Deposition from turbulent flow in lee of obstruction where flow divides, or erosional in origin	Occasionally, less frequent that debris horns	SG, SG_{of}
Tool mark grooves	Eroded scours, maybe removed boulders, and ripped-up earth	Boulders dragged over ground in flow	Yes, in lower forefield area and on outer moraine crest where flow broke through	NA
Debris ridges, patchy lobes, small digitated lobes, and scattered clasts	Low relief features, clasts scattered across forefield, often with steep dips; small lobes of gravel, often fingering out from a central channel. Small lobes often associated with frontal outwash of sands.	Sediment source in snowpack is windblown or weathered debris falling/sliding onto pack. Material is also eroded at the base of the flow and swept from apex. Debris is deposited in lobes and patches in distal parts of flow as flow wanes or obstacles encountered. Snow matrix in deposits melts post-flow, and sediments settle. Planar stratification and matrix infill relates to action of melt-waters, which can create low relief scours and sandy infills in fine gravel, or winnow gravel to produce open framework	Yes, widespread across lower part of forefield, masking substratum and armouring surface. Flow narrows to small channel towards distal end, before fanning out into lake where dominant lithofacies is laminated sands. Flow sediments sourced from glacial diamicton, slope colluvium and braided channel deposits	SG, SG_f, SG_{of}, Sm, Zs
Melt out clasts in precarious positions	Large boulders and cobbles, often stacked, at various angles. May be inverse grading, resting on small layer of sand and gravel. As snow melts, may collect sand and fine gravel on upper surface (may show inverse to normal grading)	Rigid plugs of snow can support huge boulders in dense flows. Kinematic sieving or dispersive pressures in debris-like flows may induce inverse grading	Yes, sometimes showing crude a-axis imbrications. Large gneiss and dolerite boulders up to 3m long and 2m wide. Often stacked on-top of snow cores	bG, SG_f, Sm, SG_{of}
Dirt cones on snow Patches	Conical symmetric to asymmetrical mounds and ridges of sand and fine gravels forming on snow patches. Low	Flow sweeps debris across snow patch. Subsequent differential ablation produces dirt cones. Rapid ablation	Yes, formed at foot of permanent snowbank in 2010 where debris may	SG_f, Sm (coarse), Zs

	survival potential	causes dirt cones to collapse and scatters sand and gravel and silty flows across forefield	have been sourced from re-working of lateral moraine above the snow bank, and on snow in upper forefield in 2011 after debris input from slush flow

Note: the description and inferred processes in this table are based on the work of Blikra and Nemec (1998). The slush flow re-worked sediments across the forefield and generated landforms comprising lithofacies that are also associated with glacio-fluvial meltwater deposition (SG, SG_f, SG_{of}, Sm, Zs), or glacial deposition (bG). Slush flows are initiated under rapid spring warming conditions and break out on slopes of between 2-40° in situations where the collection of melt water in a snow pack >0.5m deep (and in which drainage is retarded by impermeable frozen ground and/or substrate) causes the snow pack to lose cohesion and become mobilised (Scherer *et al*., 1998). Beylich and Gintz (2004) recorded eight slush flow events in one year in a valley in Swedish Lapland which moved 6-14 tonnes of sediment between 40- 170m. Slush flows may have been more common at the end of the LIA as permafrost degraded, and during the Holocene warm period (5500 Cal.yrs. B.P.;Blikra and Nemec,1998).

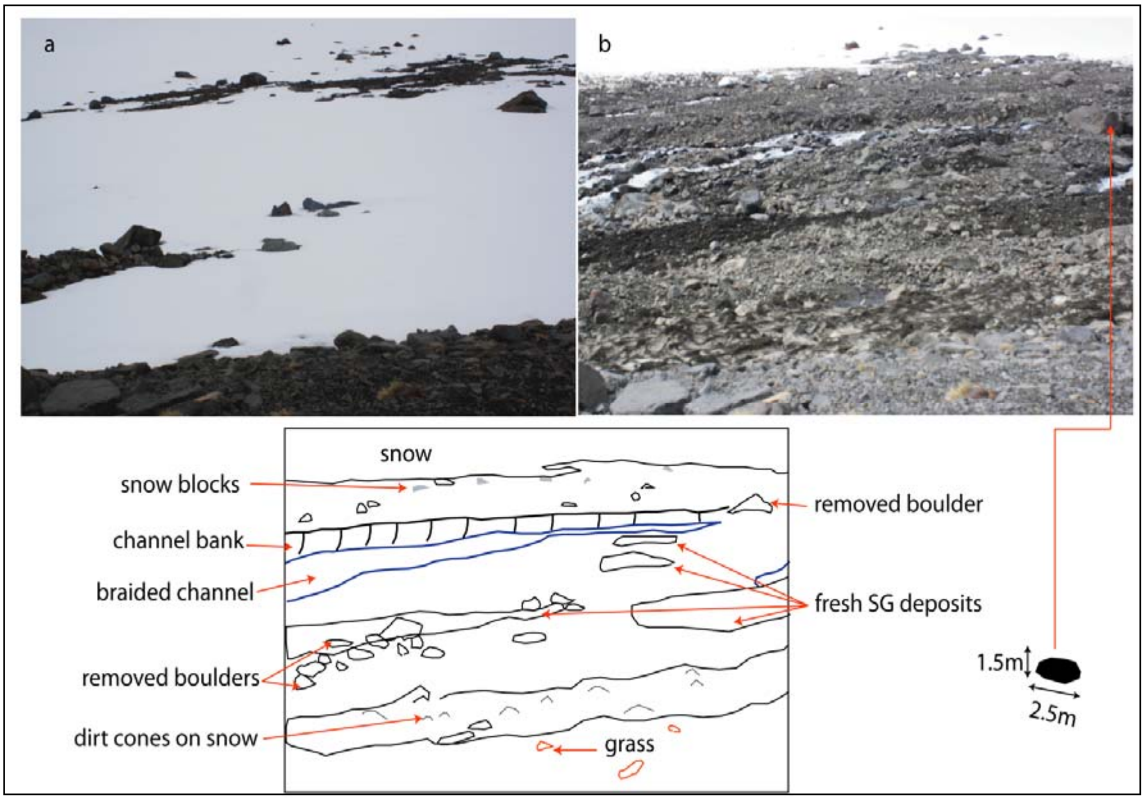

Figure 3.27 Features of the 2011 Slushflow at Kaskasatjåkka. Figure 3.27a time lapse camera image looking south west from fluted moraine towards permanent snow bank on June 7th at 1500 hours (camera location in area 2 on Figure 3.28). The image shows the scene prior to slushflow and rapid warming event. Figure 3.27b same view on June 9th at 15:00 hours after the slushflow event. The diagram shows the main changes between the two images and the size of the large boulder for scale. The flow seems to have followed the path of the main channel. Note the rapid formation of dirt cones in the foreground, the fresh deposits of SG, and the removed boulders.

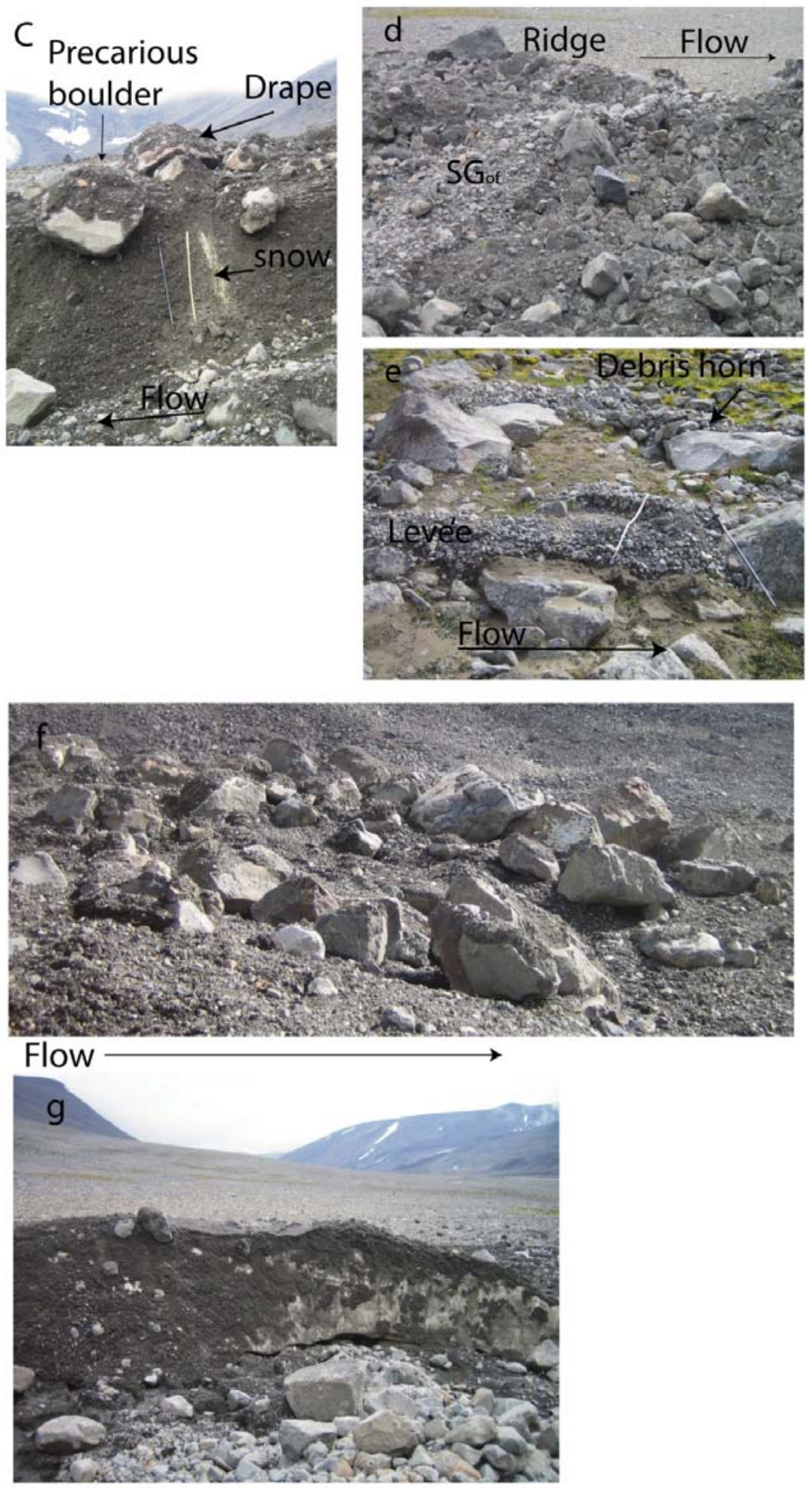

Fig. 3.27 continued

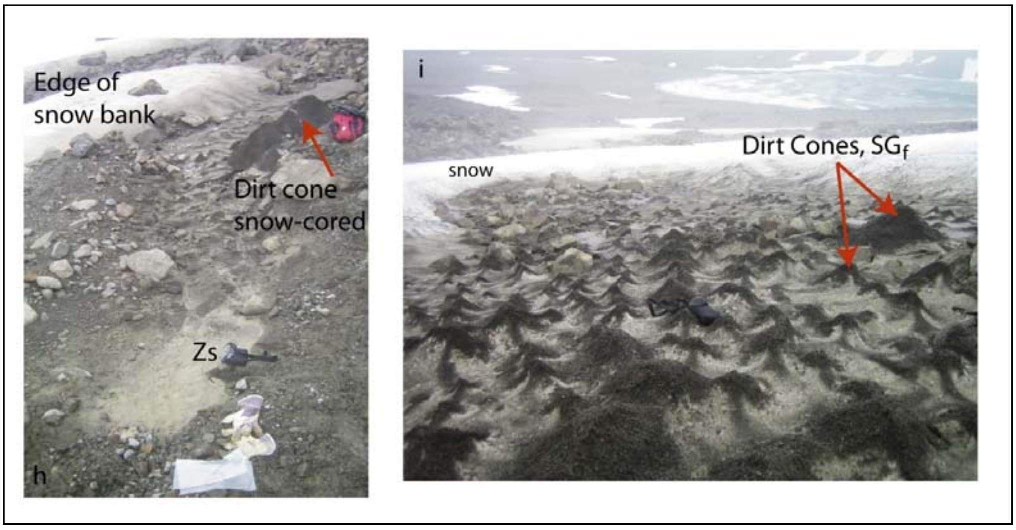

Figure 3.27 continued: (c) Precarious boulders with drape perched on dirt covered snow block. For scale, the walking stick is approximately 1m long. This image was taken at P5 (Figure 3.28). The drape is formed by deposition of debris from post-flow snow ablation and is up to 0.14m thick, and shows normal to inverse grading. (d) Small, discontinuous ridge of SG, approximately 1m high, and tongue of SG_{of} and churned-up ground with chaotic gravel deposits in lower part of flow (location P2, Figure 3.28). (e) Debris horn and levee, upper part of flow (location P6, Figure 3.28). (f) Large stacked boulders with relatively thick drape, location P5 (Figure 3.28). Note the steep dips of some boulders and crude imbrication. These boulders were deposited on top of fresh deposits of SG and snow. (g) Lower part of flow (location P3, Figure 3.28) showing drape and boulders on an approximately 2m high core of ice. Note the fresh deposit of bouldery SG_{of} in the foreground. (h&i) Images taken near the foot of the permanent snowbank in July 2010 (area 5, Figure 3.28). (h) Note the dirt cone consists of 20mm thick SGf atop a snow-core. The cone is 2m long and 0.3m wide. Note also the small flow of Zs produced by ablation of the dirty snowbank. Debris accumulates on the snowbank from the weathering of the large southern lateral moraine that crops out above the permanent snowbanks, from windblown sources, and from material washed onto the snow surface. (i) Dirt cones 80-100mm high consisting of SG_f. These cones were ephemeral and deposited SG across the forefield when they rapidly ablated during a storm.

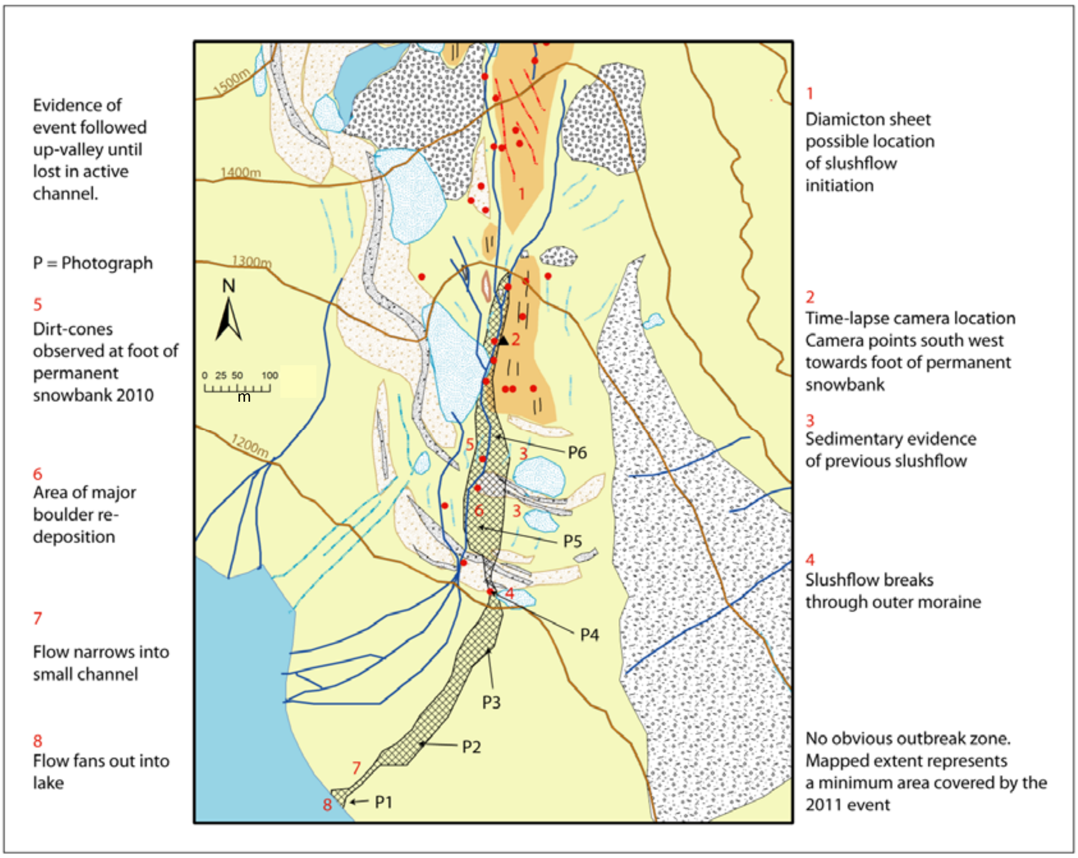

Figure 3.28 Extent of the 2011 Slushflow (key as for Figure 3.2b)

Discussion

In Swedish Lapland, slushflows may be the chief mechanism by which glaciated landscapes are modified (Rapp, 1961). Evidence of previous slushflows (precariously stacked boulders with sand and gravel drapes showing inverse grading) were observed to the east of the 2011 flow in the area of fluted moraine (zone 3, Figure 3.22b), and it is probable that slushflows occur relatively frequently at Kaskasatjåkka, where a combination of steep slopes, impermeable diamicton substrate, and south-facing aspect - (which allows for greater annual solar radiation input) - render the snow pack vulnerable to spring warming events and mobilisation. Convincing evidence of previous slushflows were not observed at Storglaciären or Isfallsglaciären, but evidence of recent small debris flows were seen in the proximal and distal sections of the diamicton plain, and in the distal sections of fluted moraine. This suggests paraglacial processes are actively re-working subglacial sediments in each forefield.

SG_{of} sampled from slushflow ridges and lobes had a very similar RR/C_{40} index and matrix particle grain-size distribution to SG_{of} sampled from sedimentary sections (Figure 3.3y&Aa and 3.21) and it is possible that some of the thin, discontinuous sand and gravel layers in the overridden moraine sections (for example, Log 1 Figure 3.26) represent former slushflow deposits.

Slushflows represent the interaction of glacial and paraglacial systems, as it is the impermeable diamicton substrate which helps to impede meltwater drainage and also sources much of the debris carried in the flow. The 2011 slushflow showed that these events are responsible for re-working diamicton deposits and help to armour the forefield surface and are responsible for some of the steep dips and chaotic assemblages of clasts. Not all SG, Sm and ZS deposits relate to glaciofluvial activity. Many of the large boulders that litter the forefield were not deposited directly by glaciers, and near-surface clasts with steep dips do not necessarily indicate periglacial frost heave processes. Paraglacial re-working of glacial sediments by slushflows, debris flows, active channel erosion, and ablation and sediment re-working related to snowbank processes seem to be a much more active process in south facing Kaskasatjåkka, where fluted moraine is very subdued and masked by surface armour, the diamicton sheet is deeply incised, and where no subglacial landforms are observed in the lower forefield. This active modification helps to explain some of the differences in appearance between the three forefields.

3.8.4 Diamicton Plain/Sheet

Description

The diamicton plain (Storglaciären) occupies a central position and is composed of the subglacial Lithofacies B, interbedded with glaciofluvial SG (including SG_{of} and SG_{f}), and Lithofacies D. The diamicton plain is asymmetric in height, being as much as 7m above Sydjåkk (log SL6) but only 2m above Nordjåkk (log NL1). It is up to 150m wide, and 400m long, and consists of three WSW-ENE trending ridges (Etienne *et al.*, 2003). Lithofacies B is the most volumetrically important lithofacies, and it thins towards the present glacier margin on the Nordjåkk side, but can be several metres thick in the lower parts of the plain (Figure 3.20a). Graphic logs from the Sydjåkk side of the diamicton plain (Figure 3.29) reveal a much more heterogeneous sequence than the Nordjåkk logs, with thin, laterally discontinuous beds of laminated sands inter-bedded or intra-bedded with Lithofacies B (Figure 3.30). The sand beds occasionally show loading structures and fining upwards cycles. In log SL1 sand beds form symmetrical drapes over the upper surfaces of embedded boulders and cobbles. Gravel beds are numerous, varied in thickness, laterally discontinuous, often show internal grading and evidence of imbrications, and consist of rounded to sub-angular clasts. Towards the base and top of log sections, gravel beds occasionally exceed 1m thickness and appear to cut trough-shaped channels into Lithofacies B.

The diamicton sheet (Kaskasatjåkka) occupies a steep slope in the upper forefield and extends down-slope to the south for up to 350m. It is up to 90m wide and 3-4m above the surface of the numerous palaeo and intermittently active channels that deeply dissect it. It is composed of subglacial Lithofacies B, C and D which form tabular beds which are up to 2m thick and interbedded with SG. Lithofacies B is the most volumetrically important lithofacies and shows a general increase in thickness towards the distal part of the sheet (Figure 3.20b).

Interpretation

Iverson *et al*. (2008) have recently demonstrated in laboratory experiments that pervasive shearing produces strong flow-parallel a-axis clast fabrics at relatively low strain magnitudes in glacial diamictons. As such, if the diamicton plain/sheet represents sequences that have pervasively deformed through their entire thicknesses, then clast fabric strength (as measured by the S_1 eigenvalue which shows the degree of clast alignment) and sediment properties should show a systematic change with depth, with fabric strength increasing upwards towards the glacier sole where shear strain was at a maximum (Boulton and Hindmarsh, 1987; Piotrowski *et al*., 2006). Clast fabrics from the Nordjåkk logs and the Kaskasatjåkka diamicton sheet are generally moderate to strong in Lithofacies Bii and C (S_1>0.6; Table 3.8&9) and have consistent V_1 orientations (indicative of glacier flow to the ENE in the Nordjåkk sections and to the south in the Kaskasatjåkka sections (Figure 3.2b&c). Clast fabrics with unidirectional V_1 orientations are consistent with pervasive deformation profiles (Shumway and Iverson, 2009). However, similar profiles with consistent V_1 orientations have also been interpreted as the product of the lodgement and the incremental accretion of thin deforming layers in a deforming bed (Larsen *et al*., 2006).

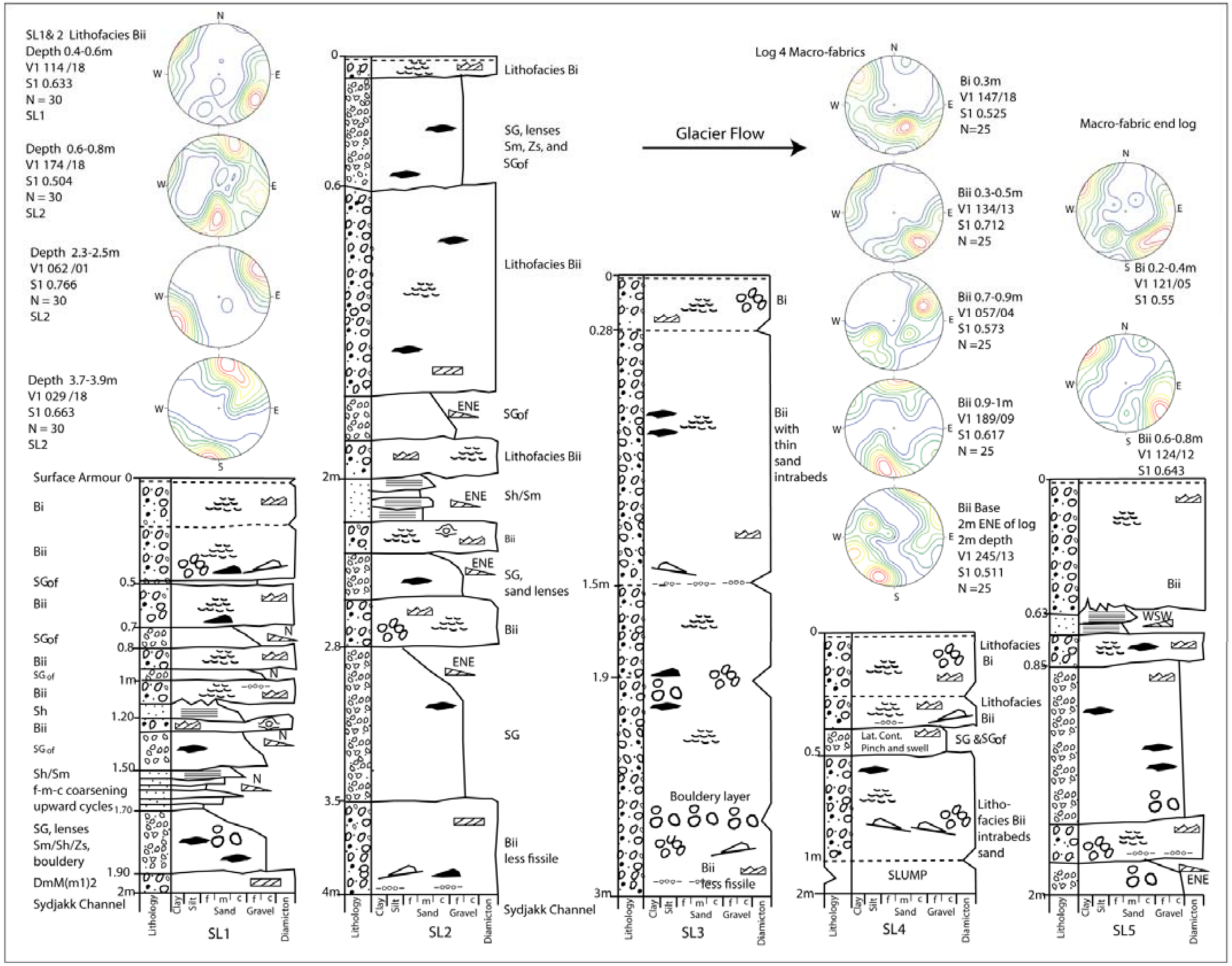

Figure 3.29 Graphic Logs from Storglaciären Diamicton Plain, Sydjåkk Sections SL1-5. Note the more heterogeneous nature of the logs compared to the Nordjåkk sections, and the more variable Macro-fabric V_1 orientations and strengths.

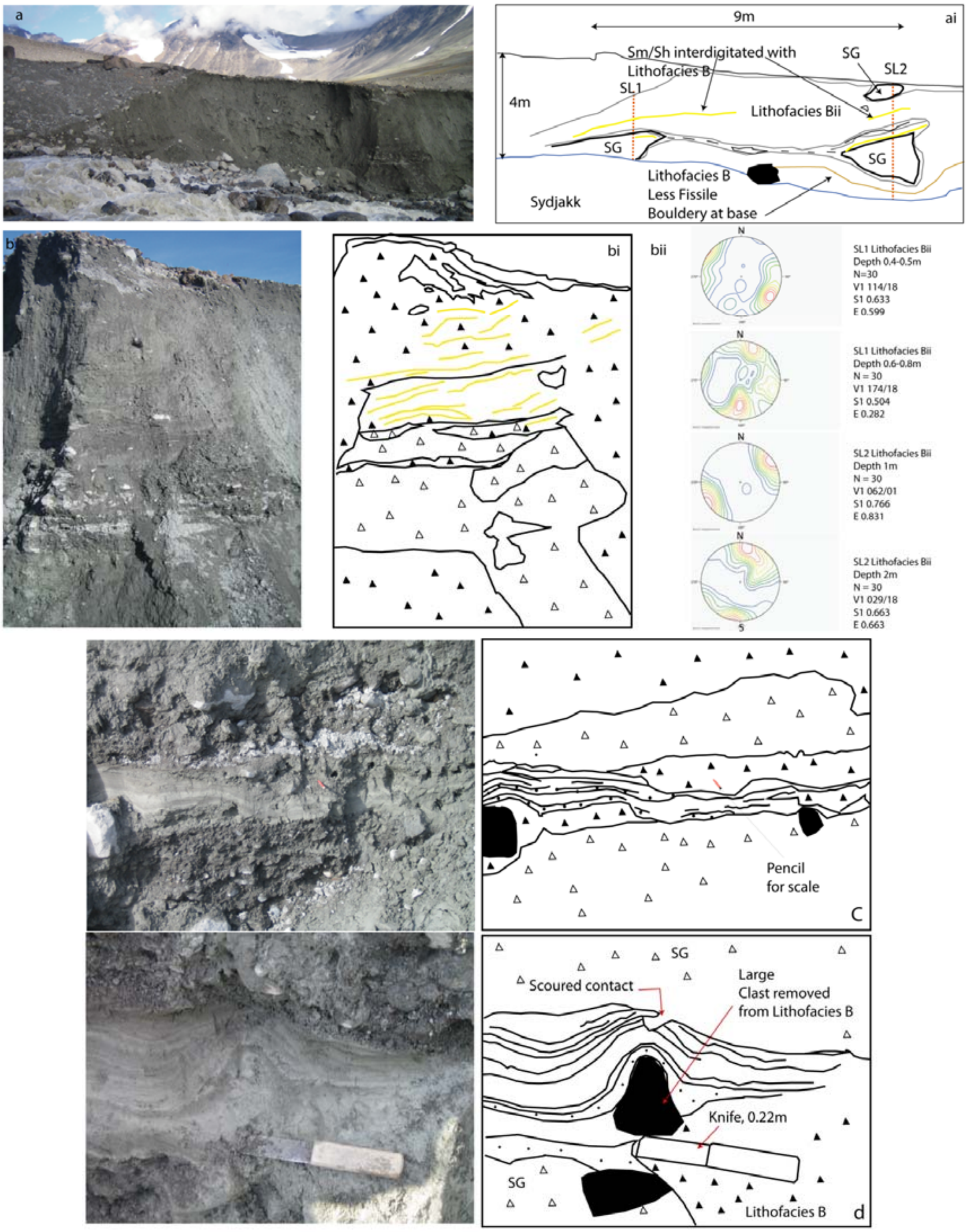

Figure 3.30 Details of Lithofacies Contacts from Sydjåkk Logs SL1 and SL2 (a &ai). The yellow lines represent sand layers, the black triangle Dm, and the open triangles SG; (bi&ii) Detail from Log SL2 and clast fabrics (biii); (c&d) Detail from Log SL1 showing interdigitating Dm/Sh beds and drapes over boulder in Lithofacies Bii. Note that in c&d glacier flow is towards the viewer, and so the upward bends in the sand layers are not antiforms.

d

d

Critically, the Nordjåkk and Kaskasatjåkka clast fabrics do not show any systematic increase in S_1 eigenvalues up-profile; they vary in strength with depth (Figures 3.17a&d, 3.20b; Tables 3.8&9). S_1 eigenvalues increase in strength to *ca*. 0.5-0.6m depth, indicating fabrics have stronger linear clast alignments, then decline, and then increase again between 1m and 1.5-2m depth. In log NL2 (Figure 3.17d) the strongest fabric is found towards the base of the section. The variations in fabric strength with depth are inconsistent with profiles that have pervasively deformed through their entire thickness (Piotrowski *et al*., 2006). In Lithofacies Bii, the crushing index and particle grain-size distribution, which can be considered proxies for particle comminution, show no systematic change with depth (Figures 3.17a, 3.3h&i). This is again inconsistent with a sequence that has pervasively deformed through its entire thickness as these proxies would be expected to show systematic changes down-profile as shear strain decreased (Piotrowski *et al*., 2006).

The variations in fabric strength in vertical profiles in the Nordjåkk and Kaskasatjåkka profiles can be interpreted in two ways. They either represent strain-partitioning (Evans *et al*., 2006), or variations in strain magnitude that occurred in thin deforming/lodged layers that accreted incrementally (Piotrowski *et al*., 2004). If granulometry controlled the response to strain (strain-partitioning) and the strength of fabric development, then stony diamictons such as Lithofacies C in logs 4 and 5 from the diamicton sheet of Kaskasatjåkka, which resist strain best, should yield weaker fabrics than matrix-supported Lithofacies B. But, as can be seen in Table 3.9, this is not the case as S_1 eigenvalues in Lithofacies C are as strong as or stronger than in Lithofacies B in the same vertical profiles. As such, the variations in clast fabric strength with depth, and the variations in the spacing of fissile partings in the diamicton plain/sheet (Section 3.4.1&2), are interpreted here as reflecting variations in strain magnitude in thin, deforming layers, with the vertical sequence building-up slowly through incremental accretion. The upward movement of the zone of deformation as the bed accretes prevents the mixing of layers and protects previously lodged and striated clasts from re-orientation (Piotrowski *et al*., 2006). According to Piotrowski *et al*. (2006), the thickness of each deforming layer is constrained between two points in the vertical profile between which an increase in fabric strength is observed. Applying this to Figure 3.17a, the thickness of each deforming unit in the diamicton plain/sheet is seen to vary between 0.2-0.3m up to 0.6m. These values are consistent with the reported thickness of the deforming bed beneath contemporary Storglaciären where basal sliding is known to dominate glacier dynamics

(Iverson *et al*., 1995). The correspondence in deforming-bed thicknesses suggests bed-deformation may also have had a limited control on glacier dynamics during the Little Ice Age Advance.

The thickening of Lithofacies B distally is consistent with the incremental accretion of mobile traction layers, which have been shown to thicken to within a few hundred metres of glacier margins (Evans and Hiemstra, 2005; Ó Cofaigh *et al*., 2011). The presence of Lithofacies D suggests that the upper parts of the diamicton plain/sheet are palimpsest landforms. Most of the Sydjåkk graphic logs reveal heterogeneous sequences which have similarities with the Sveg till from Central Sweden in that they exhibit variable clast fabrics, sediment drapes over embedded boulders (which are thought are to be formed by subglacial deposition associated with the static volume reduction of glaciers; Piotrowski *et al*., 2001), and intra-beds of sorted sediments. Shaw (1983) interpreted the Sveg till as a subglacial meltout deposit. The sharp contacts and the heterogeneous nature of the Sydjåkk sequences resemble meltout tills described by Piotrowski *et al*. (2001) which were thought to consist of accumulations of subglacial and englacial sediments. However, sediment drapes are not diagnostic of subglacial environments and it is possible they form by differential compaction of ice-marginal sediments (Phillips *et al*., 2011a). The association of SG, Sm and Zs in the Sydjåkk logs are consistent with ice-marginal/proglacial sediments and shows that the diamicton plain is more complex than previously thought, and in parts is not composed almost entirely of a single diamicton (cf. Etienne *et al*., 2003). The Sydjåkk sequence may represent:

Hypothesis 1: a proglacial/ice-marginal assemblage of sands and gravels that have been overridden and glaci-tectonised to various degrees by the Little Ice Age advance; or

Hypothesis 2: an accumulation of subglacial/englacial meltout deposits and ice-marginal deposits formed during Little Ice Age glacier oscillations.

Sequences of laminated and fissile tills similar to those observed in the Sydjåkk logs are thought to be formed by deformation partitioning (hypothesis 1) during glacier overriding, with rafts of sorted sediments (which form the laminations) retaining their original sedimentary stratigraphy lower down the sequence where shear strain was reduced, whilst beds becoming increasingly homogenised nearer to the glacier sole (Ó Cofaigh *et al*., 2011). This is only partly consistent with the Sydjåkk sequence as there is little evidence of increasing homogenisation vertically, little evidence of internal folding or faulting within sand layers, an absence of water escape structures (which might be expected with high pore-water pressures in deforming sand beds), and no evidence of diffuse sediment contacts. Moreover, the interdigitation of lithofacies observed in the sequence is known to occur in ice-marginal sequences (Menzies and Shilts, 2002). Further consideration of these hypotheses is given in Chapter 5 after micro-scale evidence has been introduced.

3.8.5 Small Moraine Mounds

Description

At Isfallsglaciären, a 100m long discontinuous ridge with a distinct kink along its course occurs near to the south lateral moraine and is composed almost entirely of SG_f. This ridge is orientated down-glacier and terminates near to an ice-stagnation hollow. The ridge is approximately 1.5-2m high and at its proximal end decays into an area of conical and symmetrical mounds, which are *ca*. 1m high and commonly composed of SG_f, although some mounds are composed of SG, Sm, or Lithofacies A, or varying amounts of all of these. Some parts of the ridge reveal a thin covering of SG or Lithofacies A. Straight ridges 30-50m long and 2m high, and 1-2m high mounds composed of SG_f occur to the north of the riegel and fluted moraine. At Kaskasatjåkka, elongated mounds composed of SG and SG_f occur on the proximal side of the large western lateral moraine.

Interpretation

The elongated ridges and mounds resemble in size and shape the moraine-mound complex that occurs on the proximal side of the north lateral moraine at Storglaciären, which Etienne *et al*. (2003) suggested were ice-marginal moraines formed by glaciofluvial activity. In terms of morphology and sediment content, the mounds and ridges at Isfallglaciären resemble kames, and the long kinked ridge an esker (Whiteman, 2002). Kames, eskers and ice-stagnation hollows tend to form in close association at glacier margins and kames can be formed by ice-contact or supraglacial glaciofluvial deposition (Menzies and Shilts, 2002). Kames can be formed of multiple or single lithofacies (Benn and Evans, 2010). In the moraine-mound complex of Storglaciären, a trench excavated into one mound composed of sands and gravels showed normal faults and slump folds, which are structures typically associated with the melt-out of stagnant ice in kames (Benn and Evans, 2010). As such, the conical and elongate mounds are interpreted here as kames.

Comment [DJG27]: In what way? Sediments? Morphology?

3.8.6 Large Lateral-Frontal Moraines

Description

The dimensions and geometry of lateral-frontal moraines at Isfallsglaciären and Kaskasatjåkka have previously been described by Karlén (1973), and the lithofacies of the Storglaciären moraines by Etienne *et al* (2003). At Storglaciären, the dominant lithofacies in lateral moraines were SG and bG, with minor amounts of ZGm and subglacial till (Etienne *et al*., 2003; Table 2.2). At Isfallsglaciären and Kaskasatjåkka, the dominant lithofacies are bG, SG, and StDm. Minor amounts of Sm occur. Flutes consisting of Lithofacies A occur on the inner frontal moraine at Isfallsglaciären which was overridden by the Little Ice Age advance (Hoppe and Schytt, 1953). At Kaskasatjåkka, Lithofacies C_{brown} forms tabular beds which dip up-glacier (~8-20°) in the inner frontal moraine (Figure 3.20c). These beds are observed on the proximal slope of the moraine.

Comment [DJG28]: Are you implying this is on distal slopes, or elsewhere?

Comment [DJG29]: Ref needed

Interpretation

The large lateral-frontal moraines are likely polygenetic palimpsest landforms which have developed as successive glacier advances have stacked subglacial tills against their proximal slopes (Kárlen, 1973). Lithofacies C_{brown} is interpreted here as a traction till. The up-glacier dip of this Lithofacies observed in moraine sections is consistent with sediments being stacked against the proximal slope of the moraine. The basal freeze-on of sediment is known to occur at Storglaciären (Moore *et al*., 2012) so it is probable that traction tills are carried forward onto proximal slopes of moraines frozen to cold-based ice at the glacier margin. Subsequent melt-out would result in the re-working of the traction tills (for example, by winnowing fines), and evidence for this is provided by the presence of ZGm, which has been interpreted as re-worked subglacial till (Etienne *et al*., 2003). Glaciofluvial activity at the ice margin would also account for the presence of SG and Sm. StDm contains a high proportion of angular and very angular clasts which indicates inputs of material from passive transport pathways, that is, inputs of supraglacial and/or englacially transported material. The presence of bG also indicates sediment input from multiple transport pathways, as these contain many sub-rounded boulders and some angular boulders. Subglacially transported boulders could be transported frozen-on to the base of the glacier, or transported and then deposited on moraines by push-deformation processes (Shakesby *et al*., 2004).

3.8.7 Other Lithofacies-Landform Associations

Proglacial lakes and abandoned and active glacio-fluvially modified terrain at Storglaciären have been analysed by Etienne *et al*. (2003). Similar lithofacies-landform associations occur at Isfallsglaciären and Kaskasatjåkka:

i) **Proglacial Lake Association**: ice stagnation hollows and lakes consist of a glacio-lacustrine sequence consisting of thin interbeds (4 to <2cm thick) of Sm and Zs;

j) **Active and Abandoned Glacio-fluvially Modified Terrain**: glaciofluvial modified terrain is particularly concentrated at the lateral margins of each forefield, consistent with the location of former ice-marginal streams, which are known to be important features of the landsystems of polythermal glaciers where cold-based ice at glacier margins inhibits meltwater drainage through glaciers (Ó Cofaigh and Evans, 2003). Numerous braided meltwater streams and abandoned palaeo-channels occur in each forefield where they dissect fluted moraine and the diamicton plain/sheet. The dominant lithofacies is SG in channel beds, with lesser amounts of SG_{of}, SG_f, Sm, and Zs.

3.9 Conclusions

Each forefield contains similar lithofacies-landform associations, suggesting similar processes operated in each area (Table 3.12). Some of the contrasts in forefield appearance relate to the active paraglacial re-working of glacial diamictons at south facing Kaskasatjåkka and the presence of large overridden transverse moraines at Isfallsglaciären which effectively dam lakes on their proximal slopes. The chief subglacial landforms are overridden fluted moraines and the diamicton plain/sheet, which are palimpsest landforms occupying central locations in each forefield and consist of multiple diamictons, with the upper diamictons identified as subglacial traction tills. The diamicton plain reveals interbeds of SG and some heterogeneous sequences on the Sydjåkk side that show this landform is more complex than previously realised, and suggests that subglacial conditions were far from uniform across the forefield. Clast fabric strengths show no systematic change with depth in diamicton plain/sheet sequences, indicating that the dominant diamicton (Lithofacies B) was not pervasively deformed through its entire thickness. The vertical variations in clast fabric S_1 eigenvalues and the variable spacing and attitude of fissile partings suggest the diamicton plain/sheet developed by incremental accretion from deforming layers of traction till≈ 0.2-0.3m to 0.6m thick. The estimated thicknesses of the deforming layers are consistent with the depth of deforming till reported from beneath contemporary Storglaciären, where basal sliding is known to dominate glacier dynamics, and this correspondence in thickness suggests bed-deformation may have had a limited control on glacier dynamics during the Little Ice Age advance.

Table 3.12a The attributes of each forefield – lithofacies description and interpretation (I: Isfallsglaciären; K: Kaskasatjåkka; S: Storglaciären).

Code	Lithofacies Description	Lithofacies Interpretation
A	Homogeneous, clast-rich sandy Dm, fissile	Subglacial traction till
B	Homogeneous, clast-rich grey sandy to silty Dm, highly fissile	Subglacial traction till
C	Coarse-grained, clast-rich sandy-gravelly Dm	Subglacial traction till
D	Coarse-grained, clast-rich sandy to muddy-gravelly Dm with badly weathered clasts	Subglacial traction till (K). Re-worked subglacial traction till (I, S)
SG **Sub-types:** **(SG_f)** **(SG_{of})**	Sandy gravel, 70% gravel, massive. SG_f – fine sandy gravel, fine gravel dominant (60%). SG_{of} Open framework gravel – lacks matrix	Mostly proglacial glaciofluvial deposits (braided channel bars and beds), although some ice-marginal or subglacial. Some SG, SG_f and SG_{of} are slushflow deposits
ZGm	Silty gravel, massive, 60% gravel, 27% silt in matrix	Subglacial traction till re-worked by glacio-fluvial activity
bG	Block gravels, lack coherent matrix, clasts are cobbles to boulders	Ice-marginal glacial deposits, or slushflow deposits
StDm	Resembles Lithofacies D but clasts unweathered	Ice-marginal deposit with re-worked traction till
Sm	Massive sand (coarse to fine-grained; well to poorly sorted)	Glaciofluvial deposits associated with low discharge streams and channel bank tops, or slushflows
Zs	Silty sand (20-65% mud), moderate to poorly sorted	Suspension deposit formed in active and abandoned glacio-lacustrine and glaciofluvial terrain (I, K, S) in silting ponds and gravel bars from waning currents. Re-worked SG from collapsed dirt cones (K).

Table 3.12b The attributes of each forefield – lithofacies-landform associations

Lithofacies-Landform Associations	**Key Attributes**		
	Isfallsglaciären	***Kaskasatjåkka***	***Storglaciären***
Transverse Ridges (bG, Lithofacies A, SG)	Asymmetric arcuate ridge near to glacier terminus, up to 200m long, 3m high. Push moraine.	Asymmetric ridge 100m long, 2m high, west side of present terminus - push moraine.	Small ridge 2m high on north side of present glacier – push moraine.
Flute Fields (Lithofacies A,C,D,SG Sm, Zs). Flute dimensions given in Figure 3.23	Radiates across 400m wide area of central forefield. Flutes override moraines; about half have no initiating boulder. Coarser Lithofacies A in interflutes. Flute field forms down-flow of bedrock riegel.	Flute field 200m long, 100m wide, occurs across two distinct longitudinal moraine-mounds towards centre of the forefield; occurs down-flow from bedrock riegel. Flutes subdued.	Prominent flute field on transverse moraine-mound on northern side of forefield (50m wide, 100m long). Flutes subdued.
Terrain Modified by Slushflows (SG, Sm, Zs)	Not observed (I, S). At Kaskasatjåkka, evidence of older and recent slushflows across lower forefield. Recent flow 1km long, 50m wide. Considerable debris re-worked and deposited across lower forefield (Figure 3.28) as levees, debris-horns, and chaotic boulders.		
Diamicton Plain(S) and Sheet (K) (Lithofacies B, C, D, SG)	Not observed (I). At Kaskasatjåkka extends for 350m, 90m wide, 3-4m high. Clast fabrics vary in strength in vertical profiles. Contacts between Lithofacies sharp. Palimpsest landform. Formed by incremental accretion of subglacial traction till interspersed with phases of glaciofluvial incision and deposition.		(S) Central position, 150m wide, 400m long, up to 7m high (but asymmetric). Dominated by Lithofacies B on northern side. Southern side has more heterogeneous sediment sequence. Palimpsest landform. Formed by incremental accretion of traction till or subglacial/ice-marginal meltout processes.
Small Moraine-Mounds	(I, K) Elongate and conical mounds 1-2m high comprising SG_f, SG, Sm. Form near lateral margins and ice-stagnation hollows. Ice-marginal moraines (kames) formed by glaciofluvial activity.		(S) Moraine-mound complex proximal side north lateral moraine. Kames and ice-marginal moraines.
Large Lateral-frontal Moraines	Largest moraines ice-cored, e.g. west lateral (K), north lateral (S). Dominant Lithofacies (I, K) bG, SG, StDm, with minor Sm and Lithofacies A; (S) SG, bG, ZGm, and Lithofacies B. Palimpsest landforms formed by incremental stacking of subglacial traction till on proximal slopes. Older moraines act as barriers to subsequent advances. Evidence of ice-marginal glaciofluvial re-working of till e.g. ZGm		
Proglacial Lake Association	Numerous lakes and ice-stagnation hollows form behind transverse moraines (I). Lake forms behind large lateral moraine and riegel (K). Ice-stagnation hollow formed on the south-side of forefield (S). These areas comprise glacio-lacustrine sequences with thin interbeds of Sm, Zs, and SG. Modern sequences reveal non-tectonic soft-sediment deformation structures akin to sequences observed in the Fronstjön sand unit (I).		
Active & Abandoned Glacio-fluvially Modified Terrain	Particularly concentrated at lateral margins consistent with location of former ice-marginal streams. Active and palaeo-channels dissect flute field. Dominant Lithofacies SG, Sm, Zs.	Numerous palaeo-channels and active braided streams dissect diamicton sheet and fluted moraine. SG is most volumetrically important Lithofacies in forefield.	Active channels concentrated at lateral margins. Diamicton plain heavily dissected by active braided channels and palaeo-channels. SG is the most volumetrically important Lithofacies in forefield.

The physical properties of Lithofacies A indicate it is a B-type horizon characterised by brittle or brittle-to-ductile deformation. However, deformation was likely to have been multiphased, as contrasts in particle grain-size distributions and fractal dimensions suggest fines were preferentially transferred from interflutes to flutes by ductile deformation. Unequivocal macro-scale evidence that Lithofacies A is a deformation till is only seen in the deformation of the Fronstjön sand units, although it is uncertain how much of the deformation pre-dates the emplacement of Lithofacies A. The shear strength of Lithofacies A indicates elevated pore-water pressures were required for deformation to occur, and this indicates warm-based ice occurred across the central parts of each forefield during the Little Ice Age advance. The thickness of Lithofacies A at Isfallsglaciären is variable and shows some sensitivity to the hydraulic conditions of the substratum, although Lithofacies A thickness in general shows little variation within and between forefields and averages 0.3-0.5m thick. The genesis of Lithofacies A, and therefore flutes, involved lodgement and deformation processes.

Chapter 4 Clast Fabrics and Magnetic Fabrics as Strain Signatures in Subglacial Diamictons

4.1 Introduction

The careful analysis of clast a-axis fabrics can reveal important information about the history of strain and the nature of deformation in fluted moraines (for example, Rose, 1989; Benn, 1994 and 1995), while strain magnitudes can be estimated using magnetic fabrics and used to test the deforming-bed hypothesis (Iverson *et al*., 2008). In Chapter 3 it was shown that fluted moraines and the Storglaciären diamicton plain were composed of subglacial traction tills. The aim of this chapter is to analyse the fabric signatures of these diamictons in order to investigate the nature of subglacial deformation and flute formation, and to assess the extent to which these fabrics are consistent with the very high strain magnitudes required by the deforming-bed model.

This chapter is divided into two parts; the first part analyses clast fabric variations in Lithofacies A from the fluted moraine of Isfallsglaciären. This forefield was chosen for detailed clast fabric analysis because it is where the most continuous and prominent flutes are exposed. The second part analyses the magnetic fabrics of Lithofacies A from flutes and Lithofacies B from the Storglaciären diamicton plain. This is the first detailed examination of clast fabrics in the Isfallsglaciären flutes and the first time magnetic fabrics have been used to estimate strain magnitude in Lithofacies A. If flutes are the product of soft-bed deformation and considerable sediment advection (Boulton, 1976; Benn, 1994; 1995; Eklund and Hart, 1996), then the clast fabrics and magnetic fabrics should be consistent with high cumulative strains. Moreover, in a pervasively deformed profile in which considerable sediment advection has taken place, strain magnitude should decrease systematically with depth (Eklund and Hart, 1996; Piotrowski *et al*., 2006) and increase distally along flutes (Eklund and Hart, 1996). Furthermore, if Lithofacies B, which is the dominant lithofacies of the diamicton plain, has been formed through pervasive deformation that was of sufficient magnitude to exert a controlling influence on Storglaciären's dynamics during the Little Ice

Age advance (Etienne *et al*., 2003), then magnetic fabrics should be consistent with very high strain magnitudes (Iverson *et al*., 2008).

The chapter begins by describing changes in clast a-axis fabric strength distally along-flutes at Isfallsglaciären. The extent to which clast a-axis fabric measurements (hereafter referred to as clast fabric) are consistent with high cumulative strain is then discussed. Changes in flute clast fabric strength and orientation with depth are then described, and these clast fabrics are then discussed in relation to pervasive deformation and deforming-bed thickness. Changes in clast fabric strength and orientation across flutes are then described, and these data, combined with macro-scale observations from each forefield, are used to assess models of flute formation. In part two, magnetic fabrics are described for Lithofacies A and B. The nature of strain is considered through an analysis of the variations in strain ellipsoids and the orientation of the principal magnetic susceptibility axes. Estimates of strain magnitude are given and reasons for the variations in the strength of magnetic fabrics discussed. The chapter ends by considering the extent to which the magnetic fabrics lend support to the deforming-bed hypothesis.

Section 1 Clast Fabrics of the Isfallsglaciären Flutes

4.1.i Flute Terminology and Clast Fabric Diagrams

In cross-section, the flute apex is generally found in the centre of the flute and is referred to here as the flute crest. Right and left flanks refer to the right-hand and left-hand sides of the flute when viewed in a down-flute direction. Right and left interflutes refer to the furrows that separate adjacent flutes on the right-hand and left-hand sides of the flutes when viewed in a down-flute (down-flow) direction. The flute axis is the flute bearing measured from the crest in a down-flow direction (mean striae vectors are obtained in the same way). For ease of comparison, rose diagrams and density-distribution contour plots have been orientated so that the mean flute vector (or in some cases, the local flute orientation) is at the top (‘north’) of the diagram.

4.1.ii Flute Orientations and Study Areas

The orientation of 47 flutes measured in the zones where fabrics were taken (Figures 4.1 & 4.2) are shown in Figure 4.3 and show strong clustering around a mean vector of 060°, with the axis of most flutes falling between 235-to-055° and 255-to-075°. Figure 4.3 also shows the orientation of 84 striae measured on initiating boulders or boulders deeply embedded in flutes near to where clast fabric measurements were taken. Most striae are orientated between 225-to-045° and 255-to-075° with a mean down-flute vector of 059°. The close agreement between flute and striae orientations concurs with previous published studies and suggests that flute orientations are both controlled by, and reflect the previous glacier flow direction (Boulton, 1976; Benn, 1994).

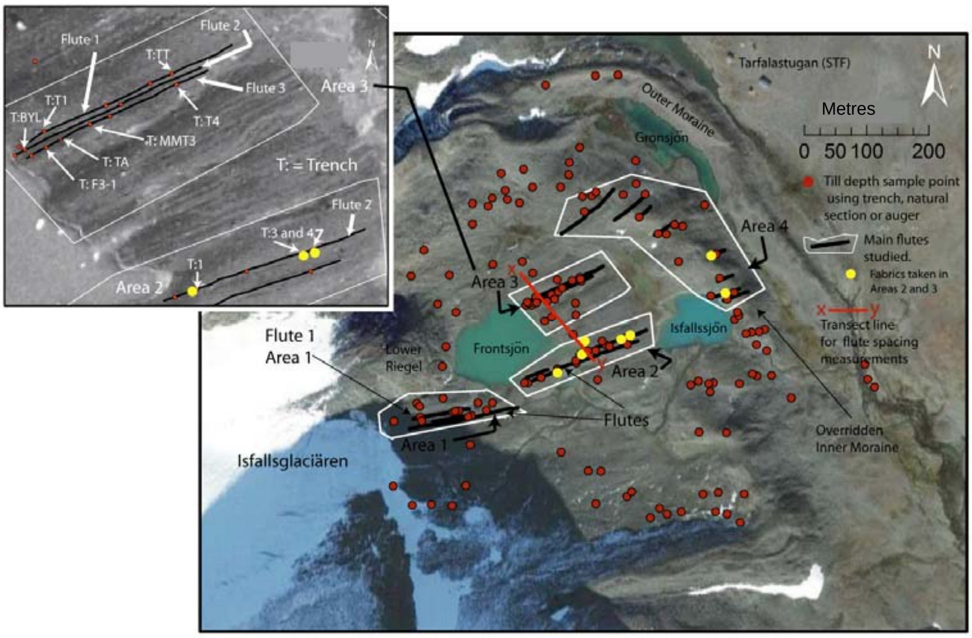

Figure 4.1 Location of study areas, Isfallsglaciären

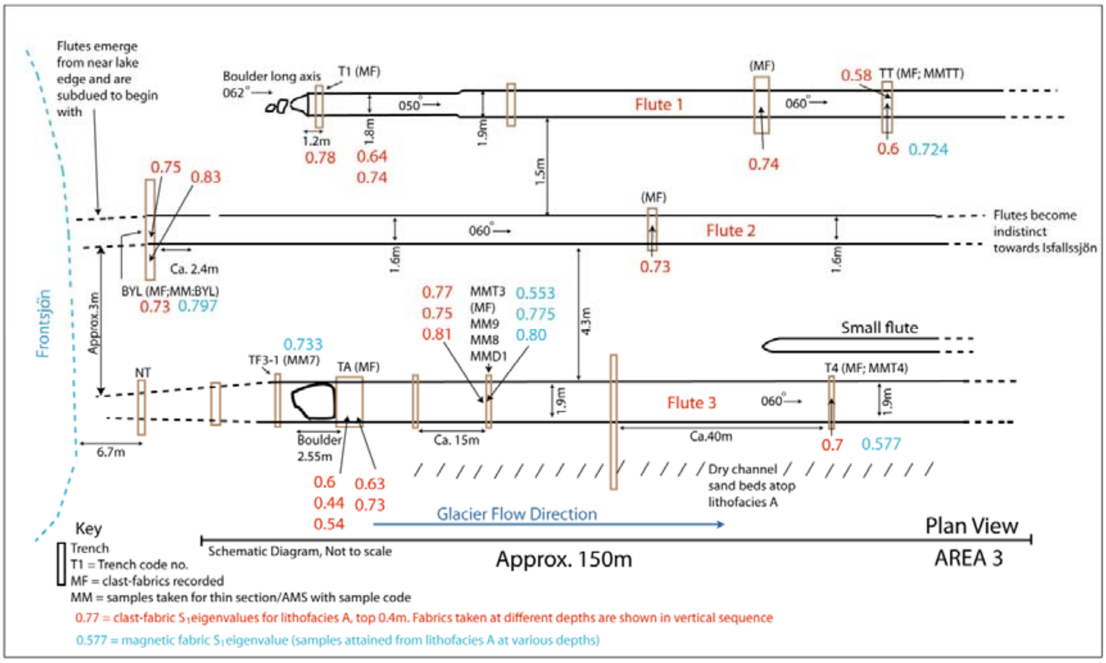

Fig.4.2 Location of AMS (magnetic fabric) and clast-fabric samples Area 3, Isfallsglaciären
(Note how S_1 eigenvalues show no simple decline with depth within the top *ca*. 0.5m of Lithofacies A and how S_1 eigenvaules from both clast fabric measurements and magnetic fabric measurements can be as strong in the proximal parts of flutes as distally).

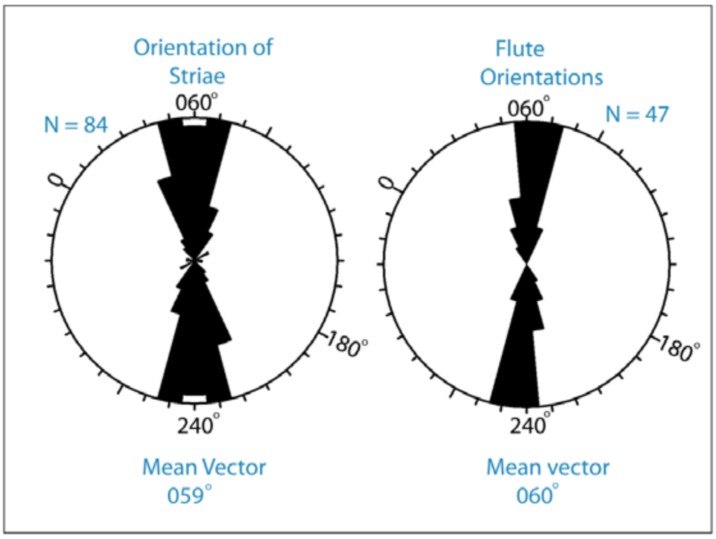

Figure 4.3 Flute and striae orientations

4.1.2 Longitudinal Variations in Clast Fabrics – the Influence of Large Embedded Boulders

In flute 2 in Area 2 (Figure 4.1), longitudinal variations in clast fabrics were measured in the top 0.2m of Lithofacies A. This flute is described in detail because it illustrates typical flute clast fabrics at Isfallsglaciären and the influence of large embedded boulders on clast fabrics and flute geometry (Figures 4.4 and 4.5). In Trench T1, taken in the proximal zone, the flute crest shows a typically strongly clustered clast fabric (S_1 0.7013) with a flat and linearly clustered shape (low isotropy and high elongation indices), with V_1 orientated within 8° of the flute axis with a low up-glacier plunge (3°) (Figure 4.3). As in most flutes at Isfallsglaciären, clast fabric strength shows asymmetry. In this case, the right-hand side reveals stronger S_1 eigenvalues and elongation indices, and lower isotropy indices. Typically, clast fabric strengths and vector orientations are very variable laterally over decimetre scales (S_1 decreases from 0.748 on the right flank to 0.508 on the far left interflute over ≈1.5m distance). Herringbone fabric patterns (Benn, 1994), apparent in Trench T1, flute 2, are also observed in Trenches T:A (flute 3) and T1 (flute 1) in Area 3 (Figure 4.2). In flute 2, the flute crest fabric increases in strength approximately 50m down-flute (Trench T3, Figure 4.5), where it has a stronger S_1 eigenvalue and elongation index. Typically, clast fabric strength varies longitudinally over metre scales and approximately 3.5m further down-flute from T3 (and approximately 0.5m down-flute from the end of a large embedded boulder) the crest fabric weakens (S_1 decreasing from 0.854 to 0.636) and the elongation index decreases, which indicates a less clustered fabric shape. V_1 has an oblique orientation at 13° to the east of the flute axis and now has horizontal plunge in a down-glacier direction.

The large embedded boulder near to Trench 3 in flute 1 (Figure 4.5) has a stoss-and-lee form with numerous striae on its upper surface and upper exposed flanks. The flute narrows and thickens on the stoss-side of the large embedded boulder, where Lithofacies A is piled-up against the stoss face, making the flute crest about 0.3m higher than the average crest height. The pile-up of sediment on the stoss-side of large embedded boulders is observed in the majority of flutes in all three forefields, and Lithofacies A is usually more clast-rich on the stoss-side of boulders. On the lee-side of the boulder, the flute crest is lower in height and the flute rapidly widens-out in a down-flute direction to become more than twice the width of the boulder. On the left-hand side of the stoss-face the crest fabric weakens (fabric 2, Figure 4.5). The density distribution plot reveals a polymodal distribution, with clast orientations transverse and oblique to the glacier flow direction. Some clasts dip at high angles, and the mean vector plunge is 36° to the north (354°). The stoss-face of the boulder in the immediate vicinity of the fabric measurement is orientated at 161-to-341°; most clasts are aligned with this face and dip away from the crestline towards the north (between 340° and 350°). Conversely, on the right-hand side of the boulder at the stoss-end, a very strong fabric is recorded (fabric 3, Figure 4.5; $S_1 = 0.813$) with a strongly clustered and flat fabric shape (E = 0.8585). Here, the V_1 eigenvector (247°, plunge 15°) is aligned with the side-edge of the boulder which is orientated at 070° to 250°.

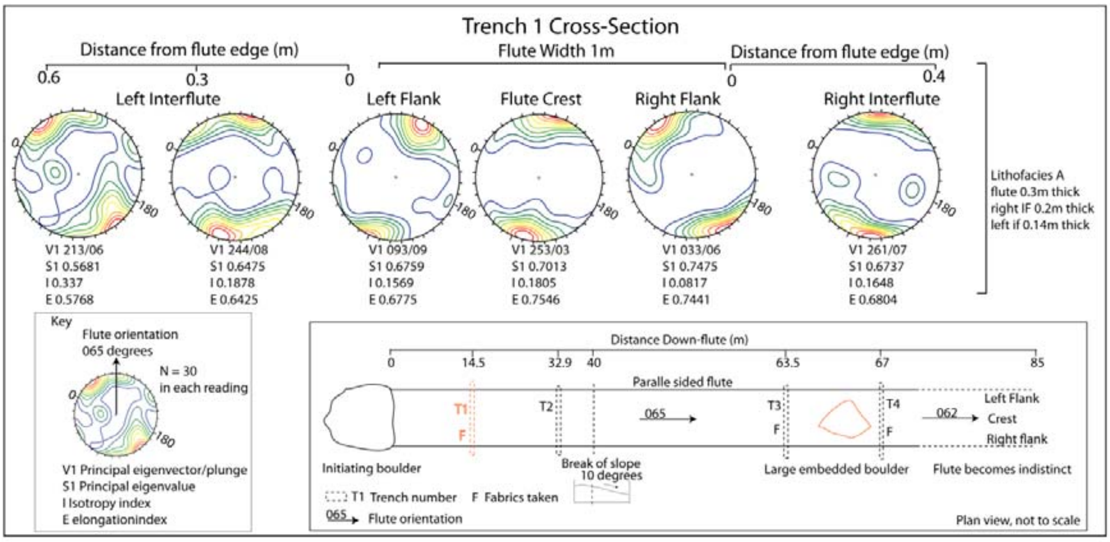

Figure 4.4 Clast fabrics in Flute 2, proximal end in Area 2, seen in cross-section

4.1.3 Longitudinal Variations in Clast Fabrics, Area 3

Clast fabric strength varies with distance along flutes in area 3 (Figure 4.2). At the proximal ends and within the first 5-6m of the flute, crest fabrics measured in the top 0.2m of Lithofacies A are generally strongly clustered, with S_1 eigenvalues ranging from 0.779 to 0.734 and elongation indices 0.784 to 0.660 (with isotropy < 0.065, which indicates fabric shapes are flat and linearly clustered). V_1 is generally aligned parallel to the flute axis. Clast fabrics show no systematic increase in strength towards the distal parts of the flutes 1 and 3, with flute fabrics within the top 0.2m of Lithofacies A having S_1 values ranging from 0.700 to 0.582.

In the flute studied by Eklund and Hart (1996) in Area 3, a large embedded boulder – 1.9m wide and 2.55m long – occurs in the proximal zone of the flute (although the boulder does not initiate flute formation as the flute is observed on the stoss-side of the boulder (Figure 4.2). Fabrics taken on the right flank in the lee of the boulder (0.8m down-flow), have relatively weak S_1 eigenvalues and less clustered to more girdle-like fabric shape (Table 4.1). However, at 1.2m from the lee-end of the boulder, the right flank fabrics show an increase in strength (S_1 = 0.63 in the top 0.1m, and S_1 = 0.76 at 0.5m depth) and fabrics form linear clusters rather than girdles. Similarly, clast fabric strength in flute 1 is strong with V_1 parallel to the flute axis at a distance of only 1.4m from the end of a large, initiating boulder.

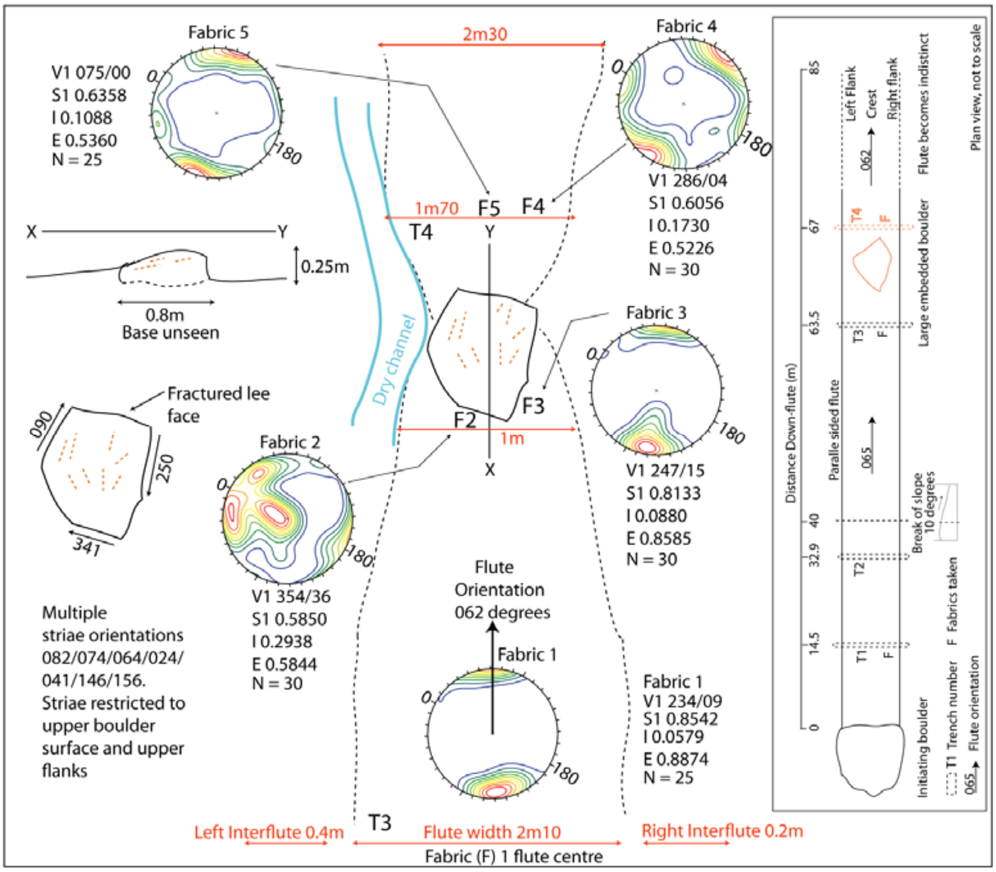

Figure 4.5 Clast fabrics around an embedded boulder, Flute 2, Area 3, distal end

Table 4.1 Right Flank clast fabric measurements from Trench TA, Flute 3, Area 3

Depth below Surface 0.8m from Boulder	N	V_1	V_1 Plunge (°)	S_1	I	E
0-20cm Lithofacies A	30	190	1	0.440	0.328	0.056
20-30cm Lithofacies A	30	27	6	0.544	0.136	0.299
40-50cm Clast-supported Lithofacies C	30	12	3	0.445	0.450	0.202
Depth below Surface 1.2m from Boulder						
0-20cm Lithofacies A	25	262	3	0.644	0.233	0.379
50-60cm Clast-supported Lithofacies C	25	48	9	0.757	0.087	0.766

Note how S_1 eigenvalues show no simple decline with depth and how the fabric becomes more organised and aligned with flow within a short distance from the end of a huge embedded boulder.

4.1.4 Clast Fabric Strength and Distance Down-flute – Statistical Analysis

The overall relation between clast fabric strength and distance along flutes for all data collected in the top 0.4m of the flutes is shown Figures 4.6a-c. The fabric data in the immediate vicinity of the large embedded boulders has been omitted because complex patterns of strain occur around boulders (Boulton, 1976; Benn, 1995) and, as shown above, weakened fabrics can occur in the lee of large embedded boulders. As such, clast fabrics taken near large boulders have been omitted from all subsequent clast fabric calculations, tabulations and graphs. Flute lengths in areas 2 and 3 are measured along the crest-line from the onset zone to their termini near to Isfallssjön, where flutes become indistinct and lose surface expression. Clast fabrics were not taken from the last 10-15m or so of the flutes in this area because the saturated ground showed clear evidence of sediment flows.

In assessing the relation between clast fabric strength (S_1 eigenvalue) and distance along flutes, the influence of depth and lateral position on clast fabric strength have been controlled for by restricting clast fabric measurements to the top 0.2m of the flute crest (Figure 4.6a). The relation between S_1 eigenvalues and distance along flute for all crest and flank readings in the top 0.4m of Lithofacies A (N = 26) is shown in Figure 4.6b, and the relation between the elongation index and distance along the flute for the same fabric readings is shown in Figure 4.6c.

None of the scattergraphs (Figure 4.6a-c) suggest a significant relation between clast fabric strength and distance along the flute. For Lithofacies A from the top 0.2m of the flute crest (Figure 4.6a), linear regression only gives a R^2 value of 0.054 with a weak correlation coefficient of 0.233, which suggests that, with the influences of depth and lateral position controlled, longitudinal position along a flute accounts for only about 5% of the variance in S_1 eigenvalues. Moreover, although the two highest individual eigenvalues are located in the distal parts of two flutes in area 2 (highest S_1 0.858; highest E 0.887), and two of the lowest values are attained in proximal flute locations on the left flank in area 3, crest and flank clast fabrics can be just as strong in the proximal zones of flutes as the middle and distal zones. Flute crest and flank clast fabrics generally return moderate to strong S_1 values (77% of readings $\geq$ 0.7), with moderate to strong linear clustering (69% of elongation indices $\geq$ 0.7 and with Isotropy indices < 0.1), with clast long-axes in the crest aligned approximately parallel to the glacier flow direction and with low (<10°) up-glacier V_1 plunge (Figure 4.7).

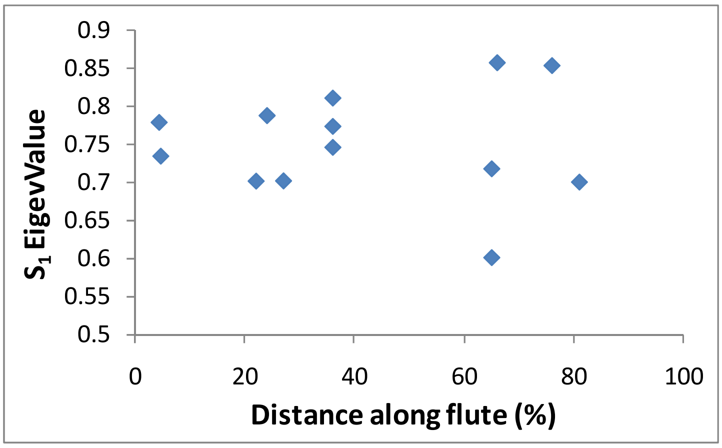

Fig. 4.6a Longitudinal Variations in S_1 Eigenvalues with distance down-flute in flute crests, 0-0.2m depth. Fabrics were taken from top 0.2m of Lithofacies A below the crest. As such, the influence of lateral position and depth has been controlled. In addition, no data from within the vicinity of large embedded boulders has been included. With all 13 fabric measurements plotted R^2 = 6E^{-07} and the correlation coefficient = 0.0008.

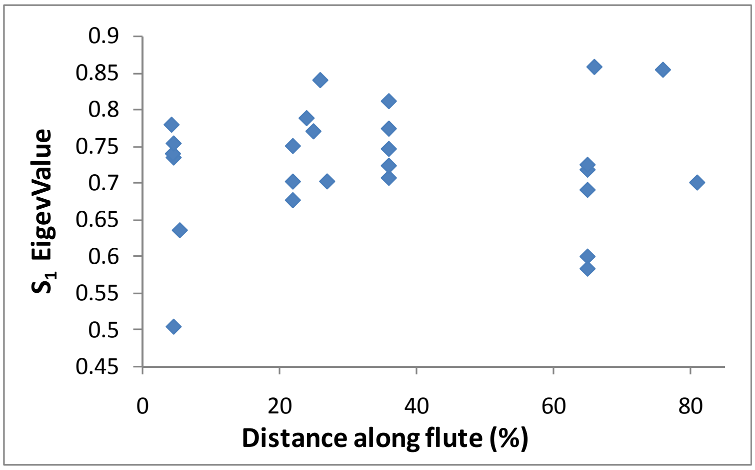

Figure 4.6b Longitudinal variations in S_1 Eigenvalues with distance down-flute, Lithofacies A, crest and flanks, 0-0.4m depth. Clast fabrics have been taken from the top 0.4m of Lithofacies A in flute crests and flanks. N = 26. R^2 = 0.006 and the correlation coefficient = 0.079 which is not significant at the 95% level.

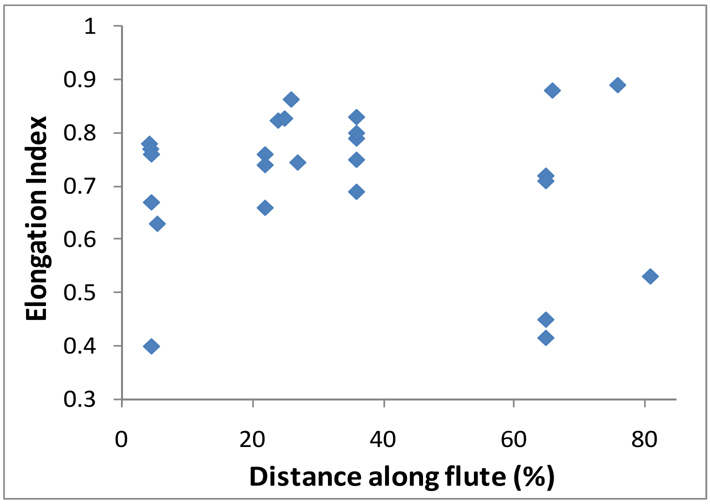

Figure 4.6c Longitudinal variations in Elongation Index and distance down-flute, Lithofacies A, crest and flanks, 0-0.4m depth. As in Fig. 4.6b, fabric readings are taken from the top 0.4m of Lithofacies A from flute flanks and crest. N = 26. R^2 = 0.0 and the non-significant correlation coefficient = 0.007.

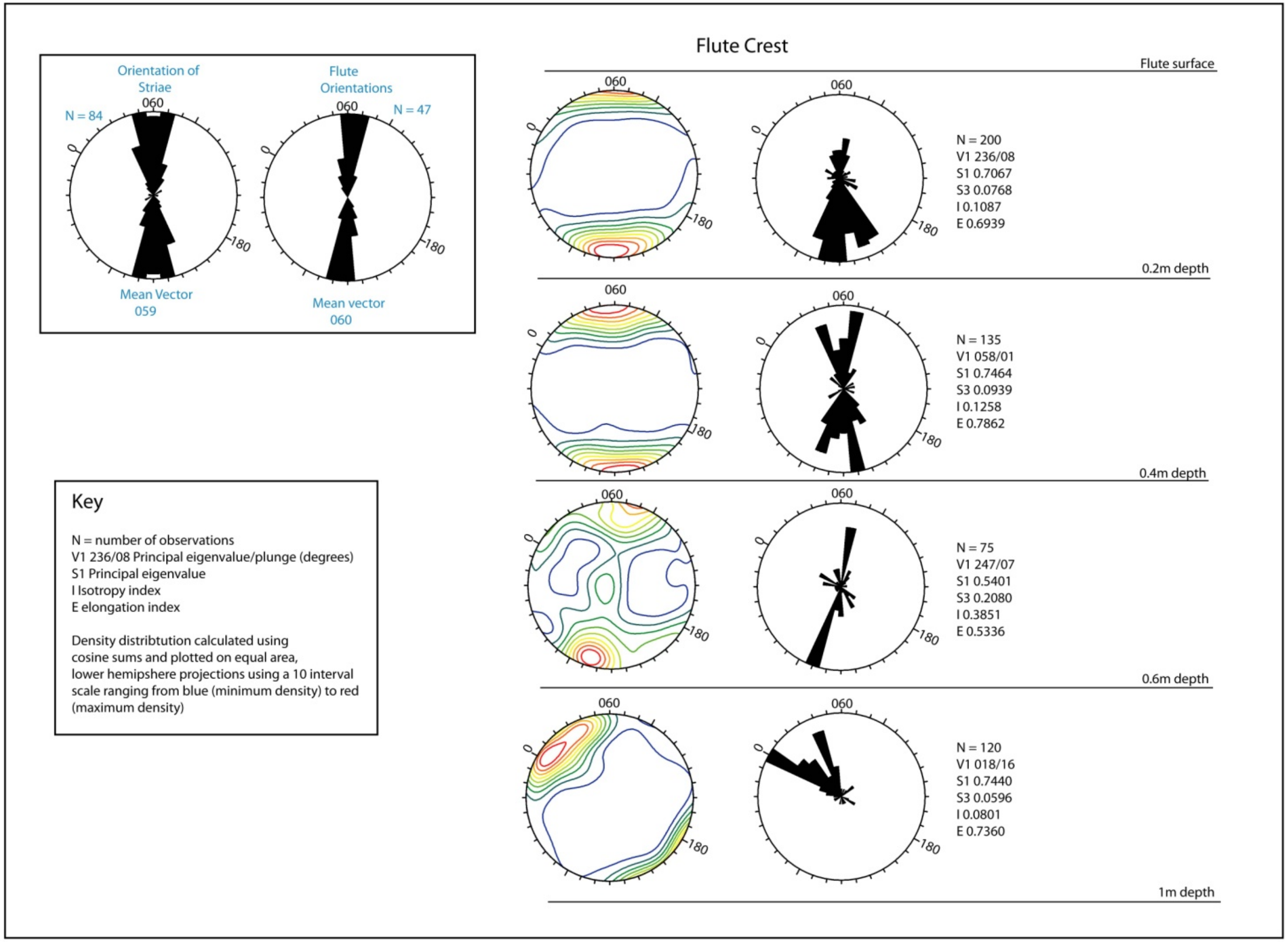

Figure 4.7 Rose diagrams and contour plots showing clast a-axis macro-fabric variations with depth beneath the flute crest, Lithofacies A.

4.1.5 Discussion - Clast Fabrics and Strain Magnitude

In ring shear experiments, clast a-axis fabric strength increases with increasing shear strain until steady-state fabrics are produced (Iverson *et al*., 2008). If cumulative shear strain increases distally along flutes in a pervasively deforming bed (Eklund and Hart, 1996), then S_1 eigenvalues should be positively correlated with longitudinal distance down-flute. Likewise, if flutes are the product of constrained subglacial deformation involving homogeneous and cumulative extensional strain in ice-walled furrows, and considerable till advection (Benn, 1995), then clast fabric strength might also be expected to increase in a down-flute direction. This does not appear to be the case at Isfallsglaciären as clast fabrics can be as strong in the proximal as distal parts of flutes.

Within the top 0.4m of the flute crest, whether in the proximal, middle, or distal zones of flutes, clast a-axis fabrics are generally strong and linearly clustered, and have flow-parallel V_1 orientations that plunge up-glacier at low angles. This fabric signature is consistent with the steady-state clast fabrics produced in ring-shear experiments by pervasive simple shear to moderate and high strains (Iverson *et al*., 2008), with steady-state fabrics characterised by strong S_1 values (S_1 = 0.78 to 0.89) and flow-parallel V_1 orientations which plunge 'up-glacier' at 4° - 8° (Iverson *et al*., 2008). As such, the Isfallsglaciären flute crest fabrics are consistent with shearing by overriding ice (Boulton, 1976), and the clast fabric signature suggests that shear strain was of sufficient magnitude to induce fabric organisation which approached steady-state conditions.

S_1 eigenvalues attained in ring shear experiments can be used as a guide to the relative changes in clast fabric strength across the forefield as fabric strength increases with increasing strain until the steady-state fabric is achieved, which can occur at moderate strains after only limited horizontal displacement (Iverson *et al*., 2008). Only 18% (9 from 49) of flute clast fabrics yield S_1 eigenvalues equivalent to the steady-state eigenvalues achieved in ring shear experiments. Fabric strength does not go on increasing once steady-state conditions have been achieved (Iverson *et al*., 2008) and so the flute fabric signatures equivalent to 'steady-state' values may represent very high strain magnitudes. Whilst ring shear experiments are not designed to reproduce subglacial environmental conditions and results are not directly comparable to field conditions (Hooyer *et al*., 2008), the strongest S_1 values do indicate the areas of highest cumulative strain. Of the nine S_1 values equivalent to steady-state eigenvalues, two came from the proximal zone of flutes, three from the middle zone (approximately a third of the way along the flute), and four from the distal reaches. That is, equivalent steady-state clast fabrics were as likely to occur in the first third of the flutes as distally, an observation that supports the idea that strong clast fabric may be produced at moderate strains, and this may account for the lack of correlation between clast fabric strength and distance down-flute. Larsen and Piotrowski (2003) argued that strong flow-parallel clast a-axis fabrics are inconsistent with a viscous till rheology, which they argue produces weaker girdle fabrics. The similarity between clast fabrics produced in ring-shear experiments, where diamictons are observed to behave as Coulomb plastic materials (Iverson *et al*., 2008) and flute crests suggests that Lithofacies A also behaved as a Coulomb plastic material during deformation.

For Iverson *et al*. (2008), the sensitivity of fabric evolution to strain magnitude means that the simplest explanation for weak subglacial fabrics, such as those recorded in some flank and interflute areas (Figure 4.4), is that sediment has not been strained to high magnitude. In gravel-sized clasts, much of the March-type rotation towards the steady-state position is achieved at low to moderate strains, with steady-state S_1 eigenvalues achieved at strains as low as 7. Iverson *et al*. (2008) argued that attributing variations in fabric strength to factors such as dilatancy (Evans *et al*., 2006) or till thickness (Hart, 1994) are speculative unless variations in strain magnitude are known. In the present study, 82% of flute clast fabric readings were not equivalent to steady-state S_1 values. Moreover, some relatively weak clast fabrics were recorded in flute flanks and crests and fabric strength changed over decimetre to metre scales. These fabric data suggest that the sediment response to strain was spatially variable across the forefield and that strain was not homogeneous (Benn 1994; 1995; Evans *et al*., 2006).

One of the implications of ring shear experiments is that relatively strong flow-parallel clast a-axis fabrics may be produced by relatively limited horizontal displacement of diamicton. At Isfallsglaciären, evidence for this comes from Trench T:A (flute 3, Area 3). V_1 orientations on the right flank, 0.8m from the end of the large embedded bolder, exhibit weak girdle fabrics with clast a-axis modes transverse and oblique to the flute crest, consistent with sediment being squeezed-in towards a lee-side cavity (Boulton, 1976). However, the influence of the low-pressure shadow zone only seems to extend for a longitudinal distance that is approximately equal to half the boulder length, because clast fabrics are more linearly clustered and stronger 0.4m further down-flute (Table 4.1). At 4m from the end of the boulder, clast fabrics are very strong and flow-parallel (a clast fabric taken at this distance on the right flank by Eklund and Hart (1996) gave S_1 = 0.84 and V_1 flow-parallel). That is, the clast fabric changed from weak and girdled to strong, flow-parallel and steady-state equivalent over a distance of 4m. Similarly, a flute crest measurement taken approximately 2m from the end of an initiating boulder in flute 1, Area 3, also recorded a strong and linearly clustered fabric (S_1 = 0.78) that was equivalent to a steady-state S_1 value. These data suggest that, if diamicton is being squeezed-in to subglacial furrows and advected down-flute as part of a deforming bed in the manner envisaged by Boulton (1976) and Benn (1995), then strong flow-parallel fabrics can be achieved by limited horizontal displacement. The diamicton in Trench T:A is up to 0.5m thick and makes sharp contact with Lithofacies C, so if it is assumed that this represents the deforming-bed thickness, then a horizontal displacement of 4m divided by a bed thickness of 0.5m gives a shear strain magnitude of 8, which is within the lower range of shear strain magnitudes required to produce steady-state S_1 eigenvalues in ring shear experiments (Hooyer *et al*., 2008).

If the strong S_1 eigenvalue 4m from the embedded boulder does represent a steady-state fabric, then further down-flute till advection would not be expected to increase the S_1 value any further, despite the increase in cumulative strain. In trench MMT3, approximately 20m further down-flute, the right flank clast fabric at 0.2m depth is flow-parallel but has a slightly weaker fabric (S_1 = 0.77). Similarly, in flute 1, the flute crest clast fabric decreases in strength towards the distal end of the flute (S_1 = 0.599 Trench TT) and is not equivalent to a steady-state fabric, and this is not consistent with high cumulative strain. The Isfallsglaciären data suggest that, in some cases at least, the down-flute advection of diamicton in flutes may be limited to relatively short distances and that strong flow-parallel clast fabrics can be produced by moderate shear strains. If this is true, then flutes may be formed by the local deformation of pre-existing material injected into basal furrows and then not advected very far in a longitudinal direction by overriding ice (Boulton, 1976). Limited till advection and moderate shear strains suggest bed-deformation exerted a limited control on glacier dynamics (Iverson *et al*., 2008).

However, caution must be exercised when using laboratory experiments to inform the interpretation of clast fabrics as strain signatures. Ring shear experiments require the coarsest fraction (> 0.6 to 0.8mm) of sediment to be removed from the sample as the chamber has finite capacity (Thomason and Iverson, 2006). This led Iverson *et al*. (2008) to remove between 3 and 16% of the sample weight of subglacial tills before use in shearing experiments. Larger particles and boulders bridge across shear planes and stiffen diamictons, transmit stress to lower depths, and take-up a disproportionate amount of basal shear stress (Cuffey and Paterson, 2010). As such, the inclusion of the coarser sediment fraction in ring shear experiments would be likely to increase the shear strain required to produce steady-state fabric strengths (Hooyer *et al*, 2008), and so S_1 eigenvalues at Isfallsglaciären might reflect higher strain magnitudes than equivalent S_1 eigenvalues achieved in laboratory experiments. Moreover, the pre-existing alignment of particles at Isfallsglaciären (and in other field settings) is unknown, and so the exact strain magnitude required to re-orientate particles to produce steady-state fabric strengths is also unknown (Shumway and Iverson, 2009). As such, clast fabric strengths attained in ring shear experiments cannot be directly compared with field conditions. However, because steady-state fabrics can be achieved at moderate strains, strong S_1 eigenvalues and flow-parallel clast a-axis fabrics in flutes are not necessarily the product of high cumulative strains, as previous researchers have suggested they are (Boulton, 1976; Rose, 1989; Benn 1994; 1995; Eklund and Hart, 1996).

Comment [DJG30]: have previous researchers suggested they cannot conclusively be related to high cumulative strain, or that they can? It's unclear

4.1.6 Variations in Clast Fabric Strength with Depth – Mean and Aggregate Data

In order to assess lateral and vertical variations in clast fabrics, mean S_1 eigenvalues and isotropy and elongation indices were calculated at various depths in the crest, flanks and interflutes and these are shown in Table 4.2. For comparison, all the dips and orientations of clasts from individual clast fabric readings have been combined using Stereo32 software and new *aggregate* eigenvalues, eigenvectors, and isotropy and elongation indices calculated. Aggregate data can provide valuable insights into the relationship between clast orientations and the general glacier flow direction; the relationship may be less clear in individual cases (Shumway and Iverson, 2009). The aggregate values, shown in Table 4.3, are calculated by combining all clast readings measured at specific depth intervals within the crest, flanks and interflutes. As is shown in the remainder of section 4.1 below, the mean and aggregate values generally give a consistent picture of the lateral and vertical changes in flute clast fabric.

Table 4.2 Mean S_1 Eigenvalues, Isotropy Indices, and Elongation Indices for the Isfallsglaciären Flute Clast Fabrics

Depth (cm)	***Left Interflute***	***Left Flank***	***Flute Centre (Crest)***	***Right Flank***	***Right Interflute***
0-10 only	N = 50 (2) *S_1 0.532* I 0.332 **E 0.452**	N = 50 (2) *S_1 0.613* I 0.239 **E 0.554**	N = 50 (2) *S_1 0.7962* I 0.0302 **E 0.778**	N = 25 (1) *S_1 0.754* I 0.082 **E 0.755**	N = 81 (3) *S_1 0.688* I 0.137 **E 0.655**
10-20 only	N = 115 (4) *S_1 0.651* I 0.220 **E 0.664**	N = 50 (2) *S_1 0.700* I 0.150 **E 0.720**	N = 55 (2) *S_1 0.776* I 0.075 **E 0.787**	N = 75 (2) *S_1 0.696* I 0.119 **E 0.677**	N = 75 (2) *S_1 0.646* I 0.209 **E 0.623**
0-20 combined* ***Standard Deviation(SD)*** ***Range [R]*** ***Confidence Interval 95% (Ci)***	N = 165 (6) *S_1* *0.612SD(0.09)* *R [0.517-0.781]* *Ci 0.075* I 0.258 SD (0.11) R [0.095-0.398] **E 0.593** **SD (0.14)** **R [0.441-0.814]** **Ci 0.108**	N = 150 (5) *S_1 0.679* *SD (0.10)* *R [0.503-0.724]* *Ci 0.091* I 0.179 SD (0.09) R [0.133-0.345] **E 0.675** **SD (0.19)** **R [0.358-0.827]** **Ci 0.162**	N = 250 (8) *S_1 0.761* *SD (0.08)* *R [0.599-0.858]* *Ci 0.058* I 0.080 SD (0.06) R [0.01 –0.185] **E 0.767** **SD (0.15)** **R [0.453-0.887]** **Ci 0.103**	N = 150 (5) *S_1 0.737* *SD (0.07)* *R [0.635-0.84]* *Ci 0.064* I 0.099 SD (0.05) R [0.054-0.193] **E 0.730** **SD (0.09)** **R [0.618-0.863]** **Ci 0.08**	N = 156 (5) *S_1 0.667* *SD (0.11)* *R [0.516-0.83]* *Ci 0.088* I 0.173 SD (0.12) R [0.082-0.382] **E 0.639** **SD (0.15)** **R [0.444-0.836]** **Ci 0.118**
20-40	N = 29 (1) *S_1 0.669* I 0.159 **E 0.665**	N = 35 (1) *S_1 0.609* I 0.262 **E 0.621**	N = 135 (4) *S_1 0.760* *SD (0.04)* *R [0.718-0.811]* *Ci 0.038* I 0.109 SD (0.04) R [0.109-0.155] **E 0.790** **SD (0.05)** **R [0.715-0.825]** **Ci 0.048**	N = 25 (1) *S_1 0.739* I 0.118 **E 0.765**	N = 85 (3) *S_1 0.543* *SD (0.002)* I 0.169 SD (0.05) **E 0.326** **SD (0.04)**
40-60			N = 75 (3) *S_1 0.571* *SD (0.05)* *R [0.535-0.607]* *Ci 0.069* I 0.255 SD (0.002) R [0.254-0.256] **E 0.497** **SD (0.16)** **R [0.385-0.609]** **Ci 0.207**		
55-65 Facies C		N = 30 (1) *S_1 0.731* I 0.110 **E 0.742**		N = 25 (1) *S_1 0.635* I 0.133 **E 0.558**	N = 25 (1) *S_1 0.757* I 0.087 **E 0.766**

>60 Facies A	N = 25 (1) *S_1 0.680* I 0.092 **E 0.622**	N = 25 (1) *S_1 0.704* I 0.113 **E 0.693**	N = 120 (4) *S_1 0.772* *SD (0.026)* *R [0.744-0.796]* *Ci 0.029* I 0.073 SD (0.008) R [0.063-0.08] **E 0.777** **SD (0.04)** **R [0.736-0.824]** **Ci 0.05**

(Key: 'N = 50' is the number of clasts measured and '(8)' is the number of fabric measurements; *0.532 S_1* Eigenvalue; 0.332 S_I Isotropy index; **0.452S_E Elongation Index**) *Note: Combined values at 0-20cm depth contain additional observations not included in the 0-10 or 10-20cm depth ranges. The additional observations are fabrics taken where insufficient clasts were found at 0.1m depth intervals and so data collection was extended over 0.2m depth intervals instead.

Table 4.3 Aggregate data for the Isfallsglaciären Flutes and Interflute clast fabrics

Location (depth in cm)	**N**	***V_1***	**Plunge°**	***S_1***	***S_2***	***S_3***	**I Index**	**E Index**
crest 0-10	50	235	9	0.767	0.204	0.029	0.038	0.734
crest 10-20	55	232	14	0.767	0.174	0.059	0.077	0.773
combined crest 0-20	200	236	8	0.707	0.217	0.077	0.109	0.694
crest 20-40	135	58	1	0.746	0.160	0.094	0.126	0.786
crest 40-60	75	245	7	0.540	0.252	0.208	0.385	0.534
crest >60	120	18	16	0.744	0.196	0.060	0.080	0.736
Crest Mean	***sum = 535***		***9***	***0.712***	***0.201***	***0.088***	***0.136***	***0.709***
Crest Standard Deviation			***5***	***0.087***	***0.033***	***0.063***	***0.126***	***0.092***
right flank 0-10	25	58	2	0.754	0.185	0.062	0.082	0.755
right flank 10-20	75	58	2	0.629	0.274	0.097	0.154	0.564
right flank 0-20 combined	100	58	1	0.660	0.251	0.089	0.134	0.619
right flank 20-40	25	7	36	0.739	0.174	0.087	0.118	0.765
Dm2 right flank 60	25	4	13	0.635	0.281	0.084	0.133	0.558
Right flank mean	***sum = 250***		***11***	***0.683***	***0.233***	***0.084***	***0.124***	***0.652***
Right Flank St Dev			***15***	***0.059***	***0.050***	***0.013***	***0.027***	***0.101***
right if 0-10	50	240	7	0.685	0.222	0.043	0.063	0.676
right if 10-20	75	243	4	0.548	0.324	0.127	0.232	0.408
right if combined	131	259	4	0.570	0.303	0.127	0.223	0.469
right if 20-40	65	231	2	0.559	0.317	0.123	0.220	0.433
Dm2 right if 60	25	48	9	0.757	0.177	0.066	0.087	0.766
Right IF mean	***sum = 346***		***5***	***0.624***	***0.269***	***0.097***	***0.165***	***0.550***
Right IF St Dev			***3***	***0.083***	***0.058***	***0.036***	***0.074***	***0.144***

left flank 0-10	50	205	7	0.606	0.254	0.135	0.223	0.560
left flank 10-20	50	73	9	0.655	0.238	0.107	0.164	0.637
left flank combined 0-20	100	52	2	0.560	0.316	0.124	0.220	0.436
left flank 20-40	35	240	3	0.609	0.231	0.160	0.262	0.621
left flank >80	25	265	14	0.704	0.216	0.080	0.113	0.693
Dm2 left flank 60	30	52	2	0.731	0.189	0.081	0.110	0.742
Left Flank mean	***sum = 290***		***6***	***0.644***	***0.241***	***0.114***	***0.182***	***0.618***
Left Flank St Dev			***5***	***0.065***	***0.043***	***0.032***	***0.063***	***0.106***
left interflute 0-10	50	235	14	0.491	0.316	0.194	0.395	0.356
left if 10-20	115	229	5	0.634	0.226	0.141	0.222	0.644
left if combined 0-20	165	230	7	0.588	0.252	0.160	0.272	0.572
left if 20-40	29	62	0	0.669	0.224	0.107	0.159	0.665
left if >80	25	235	1	0.680	0.257	0.063	0.092	0.622
Left IF mean	***sum = 384***		***5***	***0.612***	***0.255***	***0.133***	***0.228***	***0.572***
Left IF St Dev			***6***	***0.077***	***0.037***	***0.050***	***0.115***	***0.125***

Note: I and E refer to the isotropy and elongation indices. Figures in bold are mean values and standard deviations (ST Dev = 1 standard deviation). N = the number of clasts used in calculating the aggregate values.

4.1.7 Variations in Clast Fabric with Depth

Average ($_{av}$) and aggregate ($_{ag}$) data show that the flute crest fabric is strong in the first 0.4m of Lithofacies A (0-20cm depth: S_{1av} 0.761 and S_{1ag} 0.707; 20-40cm depth: S_{1av} 0.760 and S_{1ag} 0.746), with low isotropy (all readings < 0.126) and high elongation indices (0-20cm depth: E_{av} 0.761 and E_{ag} 0.694; 0-40cm depth E_{av} 0.790 and E_{ag} 0.786), showing fabric shapes are flat with strong linear clustering. In Figure 4.7, aggregate data are plotted on rose diagrams and density distribution contour plots to show the variations in Lithofacies A fabric with depth below the crest. The V_1 eigenvector (V_1 058°) is orientated parallel to the mean flute vector (060°) at 0.2-0.4m depth, and in the top 0.2m V_1 plunges gently up-glacier at 8° and is orientated within 004° of the mean flute axis (240°–to-060°). In flutes 1-3 in the middle-to-distal regions of area 3 (Figure 4.2), Lithofacies A is thicker than 0.4m and extends to a depth of more than 1m in places. In these flutes, clast fabric readings gave much weaker fabrics at a depth interval of 0.4-0.6m below the crest (S_{1av} 0.571; S_{1ag} 0.540), and gave less clustered and more girdle-like shapes (I_{av} 0.255, E_{av} 0.497; I_{ag} 0.385, E_{ag} 0.534), with greater variations in dip and clast orientations. However, below the weaker 0.4-0.6m horizon S_1 eigenvalues are once again strong (S_{1av} 0.772; S_{1ag} 0.744), and the fabric shape has a strong linear cluster

Comment [DJG31]: explain how these differ

(I_{av}0.073, E_{av} 0.777; I_{ag} 0.080, E_{ag}0.736), but with V_1 oblique to the mean flute axis and having a down-glacier plunge to the north.

Aggregate data show that fabrics below 0.6m depth have bimodal clast distributions, as shown in Figure 4.7, which is the product of combining fabric measurements that are orientated to the north east at 0.6-0.8m depth with fabric measurements orientated to the north at 0.8-1.0 m depth. Trench TT (Figure 4.2) gives a detailed picture of how clast fabric changes over 0.2m depth intervals in trenches where Lithofacies A is relatively thick, and this sequence is shown in Figure 4.8. Here, Lithofacies A is at least 0.8m deep and is separated from a similar looking diamicton below (which extends to at least 1.9m depth) by a 20mm thick and massive sand layer. Clast fabric strength in the flute crest varies with depth and is actually stronger at depth than it is in the top 0.2m in this section. There is no simple gradational decline in fabric strength with depth below the flute crest where Lithofacies A is relatively thick. Moreover, V_1 switches from having a down-glacier-plunge to up-glacier and then back again over a 1m-depth interval, with the down-glacier plunge varying in orientation by 63°.

4.1.8 Variations in Clast fabric with Depth where Lithofacies A is thinner than 0.5m

The mean S_1 eigenvalues and elongation indices (Table 4.3) confirm that clast fabric can be as strong, if not stronger below 0.6m depth as in the top 0.2m of Lithofacies A in the crests, flanks and interflutes. Where Lithofacies A is relatively thin (<0.3m), clast fabric measurements tend to be strong and linearly clustered, with V_1 parallel to the flute axis. In these areas, the clast fabric strength and fabric shape of the underlying substrate varies by lithofacies (Figure 4.9); unlike Lithofacies A and C, sandy gravel (SG) and Lithofacies D invariably have weak to moderate S_1 eigenvalues, with more isotropic to girdle-like fabric shapes.

The influence of lithofacies on clast fabric can be seen in Trench 1, flute 1 in Area 3 where an angular unconformity occurs (Figure 4.2 and Figure 3.12c). Clast fabric is strong in the 0.24m thick Lithofacies A layer (S_1 0.779, V_1 224° with 15° plunge), whereas the gravel substrate has girdle fabric shapes and weaker S_1 values (upper gravel = 0.531; lower gravel = 0.522), with different V_1 orientations and much steeper plunges (upper gravel oblique to the flute axis at 207° with 29° plunge; lower gravel transverse to the flute axis at 134° with 42° plunge). Lithofacies A is slightly thicker on the right flank of this trench (0.35m) and clast fabric here shows an increase in strength with depth even within this relatively thin layer (S_1 0.635 at 0.1-0.2m depth, increasing to 0.739 at 0.2-0.3m depth). Finally, where a thin layer of Lithofacies A is underlain by the clast-rich Lithofacies C, clast fabrics in Lithofacies C are as strong (if not stronger) than Lithofacies A (Figure 4.9).

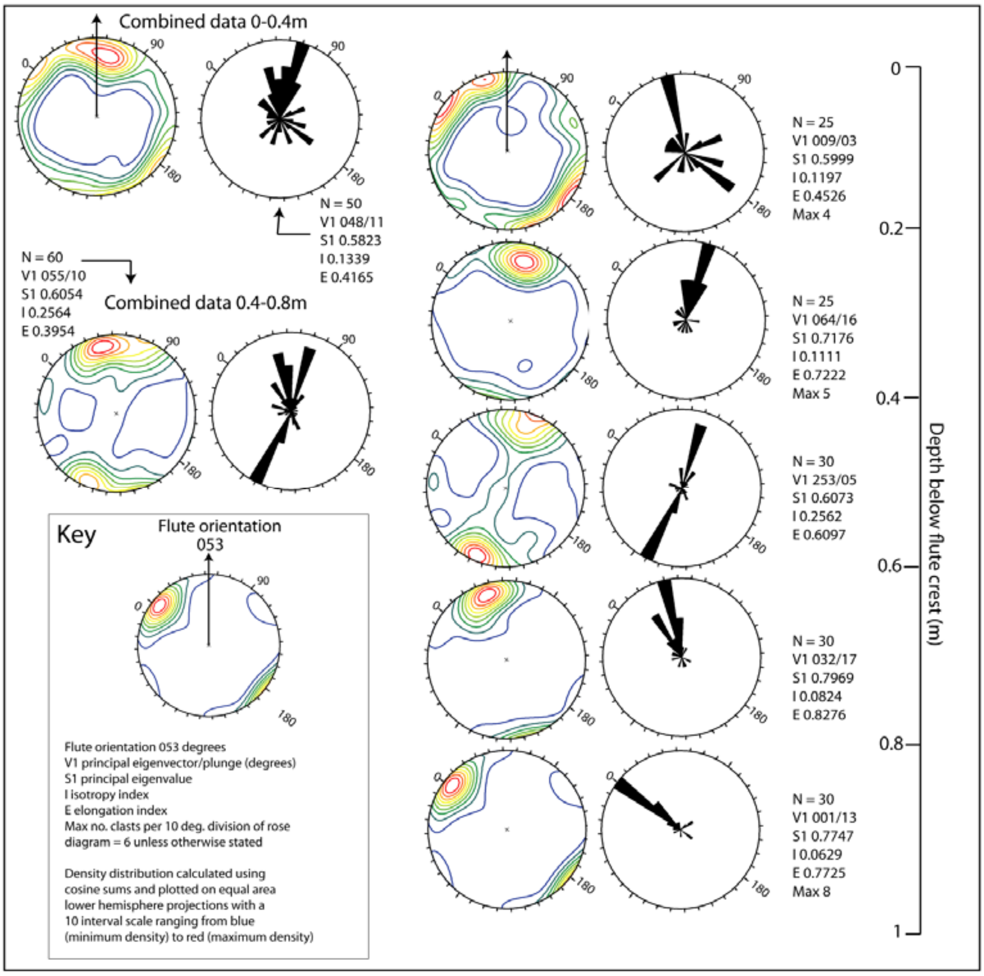

Figure 4.8 Changes in clast fabrics with depth beneath Flute Crest, Trench TT.

(Note how S_1 values do not decrease systematically with depth and the change in V_1 orientation down the profile. Clast fabric readings taken at 0.2m depth intervals have been combined over 0.4m depth intervals to increase N, the number of observed clasts to at least 50. At 0-0.4m depth, N = 50 and the combined clast fabric is weak (S_1 = 0.5823). Although N is greater, the fabric measurement over this depth interval lacks the sensitivity to detect the strong and linearly clustered a-axis fabric at 0.2-0.4m depth (S_1 = 0.718).

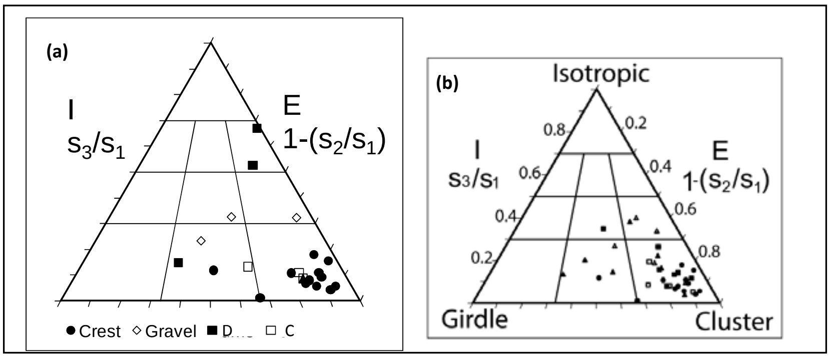

Figure. 4.9a Ternary Diagram showing variations in clast fabric shapes for different flute lithofacies (D and C refer to Lithofacies D and C; Crest to Lithofacies A from the flute crest); 4.9b shows the key for Figure 4.9a.

4.1.9 Clast Fabric Strength and Depth – Statistical Analysis

The relation between clast fabric strength and depth below the surface of the fluted moraine is shown in Figures 4.10a-c. All crest and flank clast fabric data taken in Lithofacies A and C between 0.1 and 1.0 m depths are shown in Figure 4.10a, whilst in Figure 4.10b, the influence of lateral position on clast fabric strength is minimized as only fabrics taken below the crest are shown. Only clast fabrics measured to 0.5m depth in flute crests are included in Figure 4.10c.

No correlation between S_1 eigenvalue and depth is apparent in the scattergraphs shown in Figures 4.10a and 4.10b, and linear regression analysis returns an R^2 value of 0.007 for all flank and crest readings (Figure 4.10a, number of fabric readings N = 44), and $R^2 = 0.044$ for crest readings to 1.0 m depth (Figure 4.10b, N = 30); clast fabric strength is variable with depth. However, the data in Figure 4.10c give a weak inverse correlation between the S_1 eigenvalue and depth below the crest for readings to 0.5m depth (N = 17, correlation coefficient -0.535), and from linear regression ($R^2 = 0.286$) a t-test value of 2.45 is obtained with P = 0.0135 for a one-tailed test (H_1: fabric strength decreases with depth), which is significant at the 95% level of confidence. It can be seen in Figure 4.10c that clast fabric measurements are generally strong in the top 0.4m of Lithofacies A ($S_1 > 0.7$), and that the correlation is influenced by the two strongest values ($S_1 > 0.84$) being obtained in the top 0.2m, whereas the two weakest values ($S_1 < 0.7$) occur below 0.4m depth and come from the relatively weak layer identified in section 4.1.7 above (and shown in Figure 4.11).

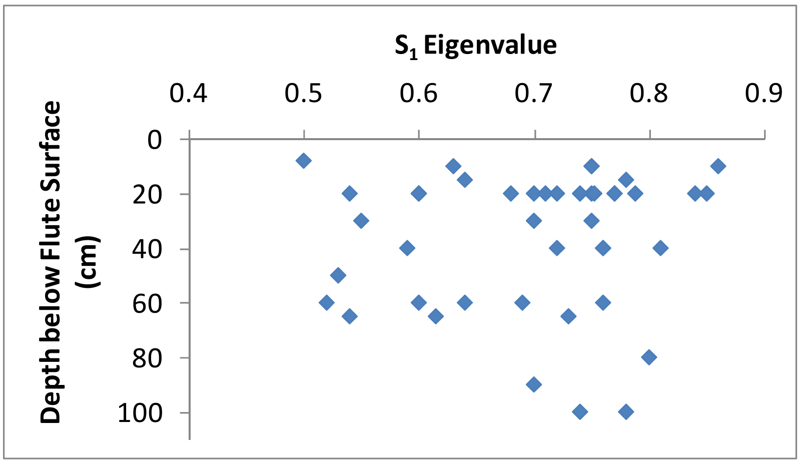

Figure 4.10a Variations in crest and flank S_1 Eigenvalues with depth.

Fabrics were taken from the flanks and crests of flutes from Lithofacies A/C at 0-1m depth (N = 44). $R^2 = 0.007$.

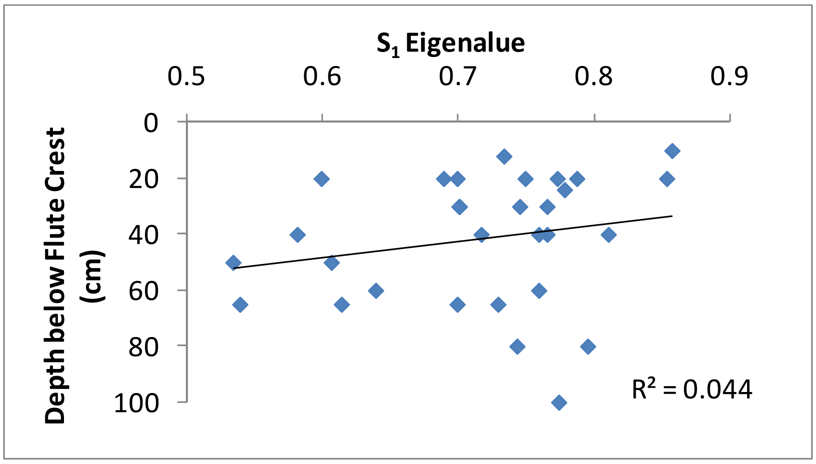

Figure 4.10b Variations in S_1 Eigenvalues with depth for flute crest readings only.

The correlation is not significant (correlation coefficient = -0.19), $R^2 = 0.044$, N = 30. A P- value of 0.144 and a t-value of 1.082 were obtained at the 95% confidence level using a one-tailed t-test.

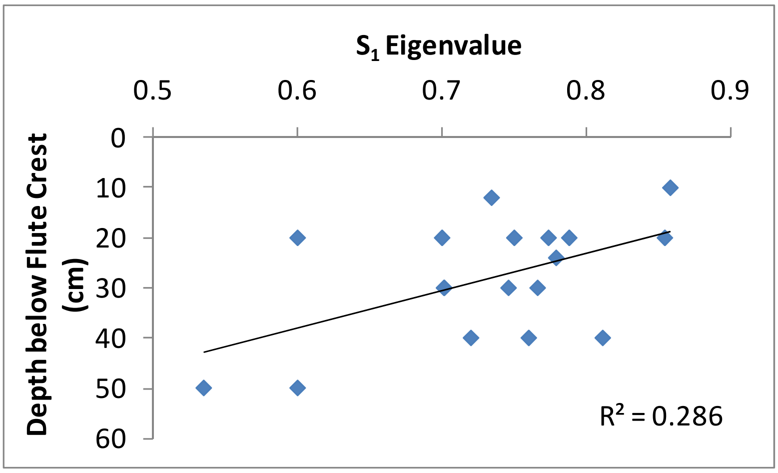

Figure 4.10c Variations in S_1 Eigenvalues in the top 0.5m of Lithofacies A.

Correlation coefficient = -0.535, N =17, R^2 = 0.286. Depth (the independent variable) is plotted on the vertical axis to show more readily the vertical changes in S_1 values with depth. The correlation is weak, but a t-test shows a significant relationship at 0.95% level of confidence, but not at the 99% (P-value = 0.0135, t = 2.45, one-tailed test). The R^2 value suggests that, in this case, depth accounts for about 28% of the variance in S_1 values. Fabrics are generally strong (>0.7) in the top 0.4m of the flute and consistent with shearing by overriding ice, whereas the weaker readings <0.4m come trenches where Lithofacies A is relatively thick, and a layer of weak fabrics are found between 0.4-0.6m depth. The weak fabrics suggest limited strain, and may be below the depth at which overriding ice is able to re-orientate clasts into flow-parallel alignment.

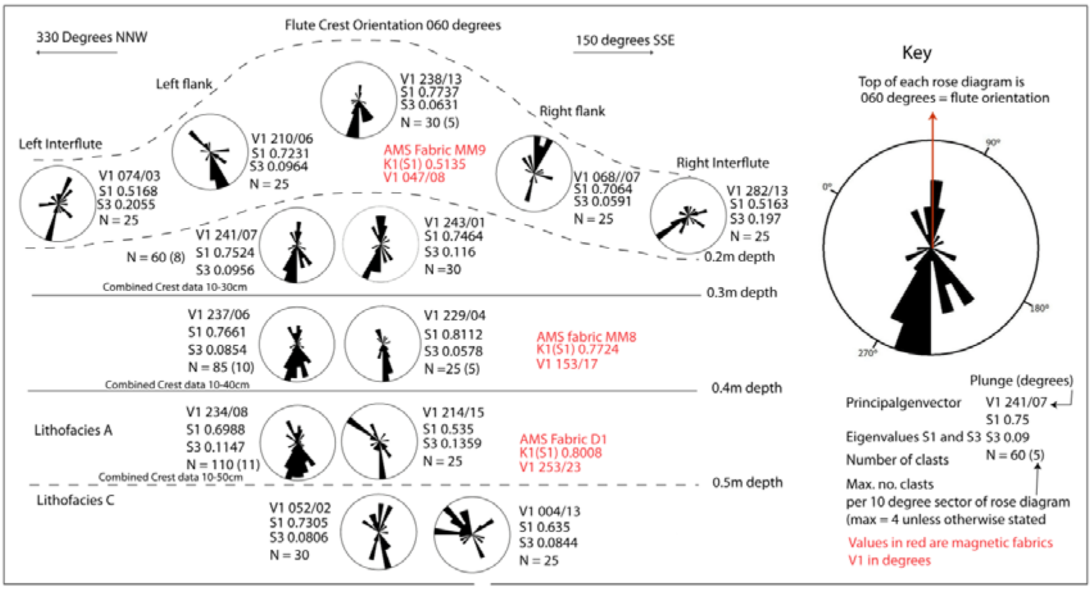

Figure 4.11 Clast a-axis macro-fabrics in Trench MMT3.

4.1.10 Statistical Analysis of Variations in Clast Fabric Shapes

Benn and Ringrose's (2001) bootstrapping programme has been used to establish 10th convex hulls around data points for the flute crest and the left and right interflutes using aggregate data at 0-0.2m depth intervals (Figure 4.12a). The aggregate sample point for the weak horizon lies outside the 10th convex hulls of the other crest data, which means that there is a high statistical probability (90-95%) that it belongs to a different population and has a statistically different clast fabric shape.

The statistical difference between the weak horizon and crest fabrics from other depths is also seen when 10th convex hulls are established for the fabric data from Trench MMT3 (Figure 4.12b) and for Trench TT (Figure 4.12c). In Figure 4.12d, crest fabric readings from Trenches MMT3 and TT have been combined and 10th convex hulls established. It is evident that the two sample points from the weak horizon plot outside of all the confidence intervals established around the other crest sample points, confirming that there is a high probability that the weak layer has a statistically different clast fabric shape. By contrast, in Trench MMT3, the sample point for Lithofacies C plots within the 10th convex hull of the fabric reading from 0.2m depth, suggesting that Lithofacies A and C are drawn from the same population.

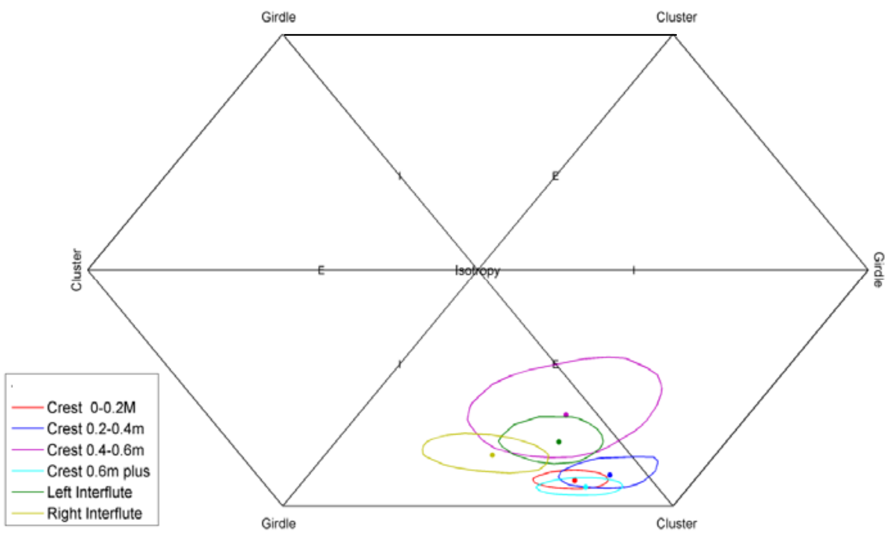

Figure 4.12a 10th Convex Hulls for aggregate data at 0.2m depth intervals. Most crest clast fabric shapes, defined by I and E indices, plot as linearly clustered shapes, except for the weak layer between 0.4-0.6m depths.

The fabric shape point for the weak layer plots outside the 10th convex hulls of other crest fabrics. As such, there is a significant statistical difference in fabric shapes (90% confidence interval) between the weak layer and other crest fabrics. Aggregate interflute fabric shapes are also less linearly clustered than most crest fabrics.

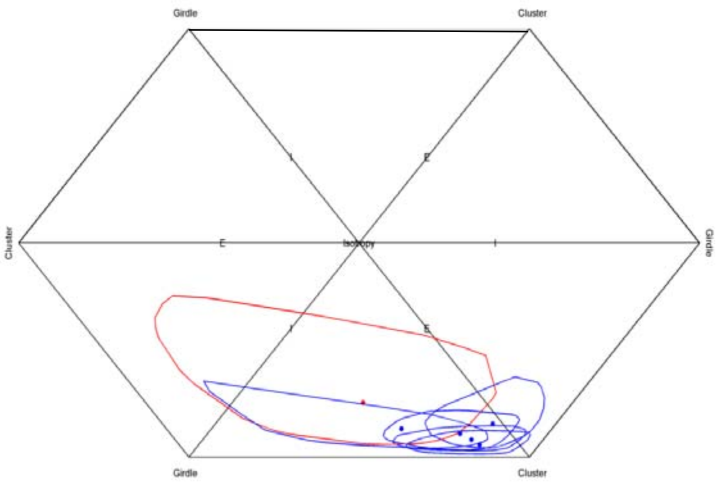

Figure 4.12b 10th Convex Hulls for fabric data from Trench MMT3. The red convex hull and data point represent the fabric shape for the weak layer 0.4-0.5m depth beneath the crest. The other points and 10th convex hulls are for all other crest fabric readings at various depths in Trench MMT3, including Lithofacies C, which plots within the 10th convex hulls of most Lithofacies A fabrics, showing there is not a statistical difference in these fabric shapes and they are probably drawn from the same population.

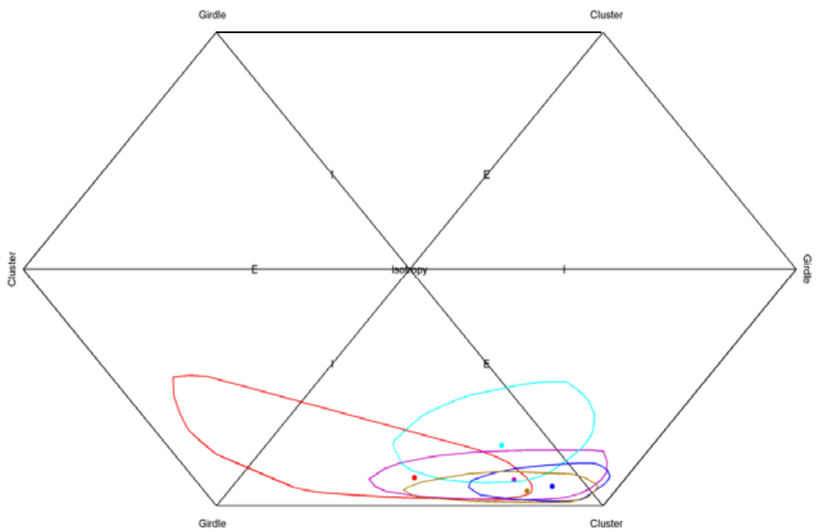

Figure 4.12c 10th Convex Hulls for fabric data from Trench TT. The weak layer is shown in red, other colours relate to flute crest measurements from various depths beneath the flute crest. The fabric shape for the weak layer is less linearly clustered and has a more girdle-like fabric shape).

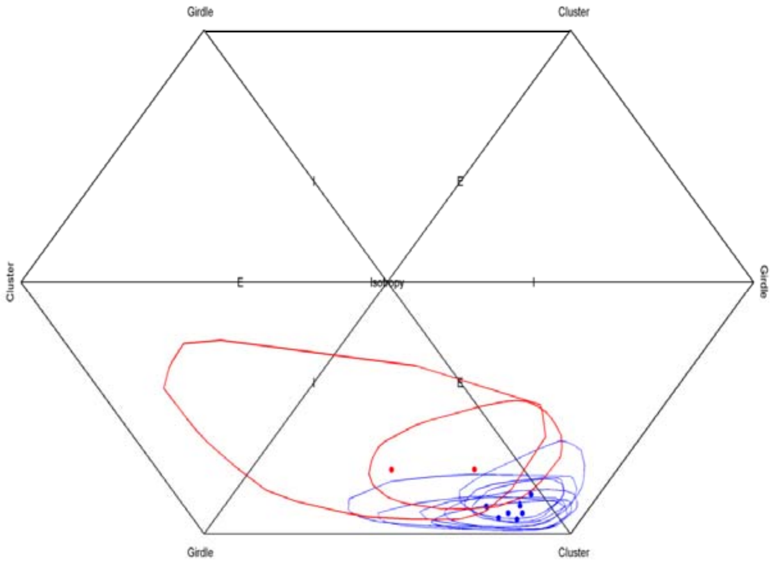

Figure 4.12d 10th Convex Hulls for combined fabric data at 0.2m depth intervals from Trenches MMT3 and TT. The two 10th convex hulls and data points in red represent fabric readings from weak layers beneath the crest (0.4-0.6m depth). 10th convex hulls and data points in blue represent all other crest fabrics combined over 0.2m depth intervals from these two trenches. Most crest fabric shapes form strong linear clusters except for the fabrics from the weak fabric layer, which are more isotropic and less linearly clustered, and plot outside the 10th convex hulls of the other fabric points.

4.1.11 Discussion - Clast Fabrics and Deforming-bed Thickness

In Chapter 3.3.8 it was shown that Lithofacies A averaged *ca*. 0.3-0.5m thickness and it was argued that the thickness of the deforming bed was limited. Variations in clast fabric strength and orientation with depth lend further weight to this interpretation. The variations in clast fabric strength with depth where Lithofacies A >0.5m thick (Figures 4.7, 4.8, & 4.11) indicate a more complex relation than the gradational decrease in strength suggested by Eklund and Hart (1996). Eklund and Hart (1996) did not measure changes in clast fabric strength with depth and only reported three clast fabric readings in total from Isfallsglaciären. Their interpretation was based on the analysis of a few trenches dug into one flute (flute 3, Area 3), which they argued showed evidence of pervasively deformed sediment sequences. As such, their assertions must be considered largely unsubstantiated because they are not supported by detailed clast fabric observations. A pervasively deforming bed should yield unidirectional V_1orientations (Shumway and Iverson, 2009), but where Lithofacies A is relatively thick this is not the case, and the variations in V_1 orientation and plunge and S_1 eigenvalues with depth (Figure 4.7& 4.8) are not consistent with a sequence deforming through its entire thickness (Piotrowski *et al*., 2006). Even where Lithofacies A is relatively thin (< 0.3m) and the substrate has a weaker S_1 value, V_1 orientations are not unidirectional. For example, in Trench T1, flute 1, Area 3 (Figure 3.12c) Lithofacies A and gravels do not share similar V_1 orientations. In addition, crude sedimentary grading within the upper gravel suggests structures in this layer are of primary depositional origin rather than produced by subglacial shear and, as such, the gravel clast fabrics probably reflect primary depositional processes. If this is true, then subglacial deformation was restricted in depth and contained within the thin Lithofacies A layer.

The clast fabric measurements in Trench TT, flute 1, Area 3 (Figure 4.8) suggest that this section represent more than one phase of bed-deformation or deposition. The vertical changes in fabric strength and vector orientation and plunge, especially above and below the sand layer at 0.8m depth where the V_1 orientation changes by 31° over a 0.2m depth interval, suggest a change in the basal stress regime or flow direction. The clast fabrics suggest that the similar looking diamictons above and below the sand layer belong to different phases of deformation or deposition and, as such, the depth of the deforming bed was limited to a maximum of 0.8m in Trench TT.

Rose (1989) argued that unidirectional pervasive shear in a thin deforming bed could produce uniform and strong flow-parallel clast fabrics rather than a profile exhibiting a gradational decline in strength. The clast fabrics from the top 0.4m of the flute crests at Isfallsglaciären are consistent with this interpretation, and the weak layer at 0.4-0.6m depth may represent the base of a thin, pervasively forming layer in which clast fabrics in the upper 0.4m show no systematic decline in strength with depth. However, the clast fabric data are also consistent with the model of Benn (1995) in which similar fabrics are produced by confined, discrete and brittle or brittle-to-ductile shear in ice-walled furrows. In Chapter 3.3.4 evidence was given to support the idea that Lithofacies A had experienced discrete and brittle or brittle-to-ductile shear, at least in the latter stages of flute formation.

In Trench MMT3 (Figure 4.11 and Figure 3.13) the top 0.4m of Lithofacies A below the crest has very strong, flow-parallel clast fabrics (with the strongest S_1 value at 0.3-0.4m depth).

These fabrics are indicative of simple shear to at least moderate or high strains. The relatively weak fabric at 0.4-0.6m depth (also apparent in Trench TT) are indicative of weak shear strain and may represent the base of a deforming bed where a combination of reduced basal shear stress by overriding ice, stiffer sediment and reduced pore-water pressures resulted in reduced strain (Evans *et al*., 2006). The statistical difference between fabrics in the weak layer and layers above (Figure 4.12) suggests that the weak layer may mark the depth at which shearing by overriding ice was no longer able to re-orientate clasts into strong flow-parallel alignment (Boulton, 1976). If these vertical changes in clast strength were due to strain partitioning (Evans *et al*., 2006), then fabrics should be weaker in stony Lithofacies C. However, this is not the case as clast fabrics are stronger in Lithofacies C which occurs below the weak fabric layer in Lithofacies A in Trench MMT3. The contrast in clast fabric strength and V_1 orientations between Lithofacies A and C in this Trench, and the sharp contact between Lithofacies A and C, which is often demarcated by a boulder pavement, suggest that the boundary probably represents erosion and removal of fines at a former ice-bed interface (Benn and Evans, 2010), or a décollement surface (Boulton, 1976).

Alley (1991) argued that in a pervasively deforming bed the plane of décollement could move upwards over time as the deforming-bed thickened through accretion. The vertical changes in fabric in Trench TT and MTT3 could be explained by such a process, with the changing V_1 orientations and S_1 values reflecting an upwards movement of a décollement plane over time. However, lodgement and meltout processes are known to produce strong unimodal and bimodal clast fabrics similar to the clast fabrics observed in Trench TT and MMT3 (Bennett *et al*., 1999; Larsen and Piotrowski, 2003). As such, where Lithofacies A is relatively thick, changes in clast fabric with depth probably reflect the accretion of a subglacial diamicton over time through a combination of processes (Piotrowski *et al*., 2004; Shumway and Iverson, 2009), with only the upper 0.4-0.6m relating to simple shear by overriding ice during flute formation.

4.1.12 Lateral Variations in Clast Fabrics - Variations between Area 2 and Area 3

Average S_1 eigenvalues and elongation indices calculated for flutes in Area 2 and Area 3, which are approximately 120m apart, show little difference and have similar value ranges (Table 4.4); crest clast fabric measurements are generally strongly clustered, and flank and interflute fabrics are more variable over scales of a few tens of metres in Area 2 and in Area 3.

Table 4.4 Clast fabric measurements from Area 2 and Area 3 compared

	Area 3	Area 2
Mean S_1 Eigenvalue	0.716	0.706
S_1 Standard Deviation	0.089	0.100
S_1 Confidence Interval	0.043	0.065
Mean Elongation Index	0.7	0.687
E Standard Deviation	0.150	0.160
E Confidence Interval	0.080	0.105
IF/Flute Range		
Upper S_1 value	0.830	0.81
Lower S_1 value	0.504	0.541

S_1 is the principal eigenvalue and E the elongation index and the means have been calculated using crest and flank data from the top 0.2m of Lithofacies A in each area. N, the number of fabric measurements = 13 in Area 3 and 9 in Area 2. Confidence intervals are at the 95% level. IF = interflute, and the IF/Flute range refers to the strongest (upper) and weakest (lower) S_1 values recorded in each area.

4.1.13 Lateral Variations in Flute Cross-Sections – Mean and Aggregate Data

The mean and aggregate data (Tables 4.2 and 4.3) show that clast fabrics in the top 0.2m of flute crests have stronger S_1 eigenvalues and elongation indices than the flanks, with the flanks and interflutes displaying asymmetry in terms of fabric strength and shape. The asymmetry in clast fabric between the right and left-hand sides of flutes is also shown in Figures 4.13a-c; in Figure 4.13a and Figure 4.13b contour plots and rose diagrams show lateral variations in aggregate clast fabric at 0-0.4m depth, with data summarised at 0.1m intervals for the top 0.2m of the flute. Interflute and flank fabrics have greater numbers of clasts orientated oblique to the flute axis compared to the flute crest, but all fabrics, with the exception of the left flank at 0-0.2m, show a primary or secondary mode of clasts with orientations close to the mean flute axis.

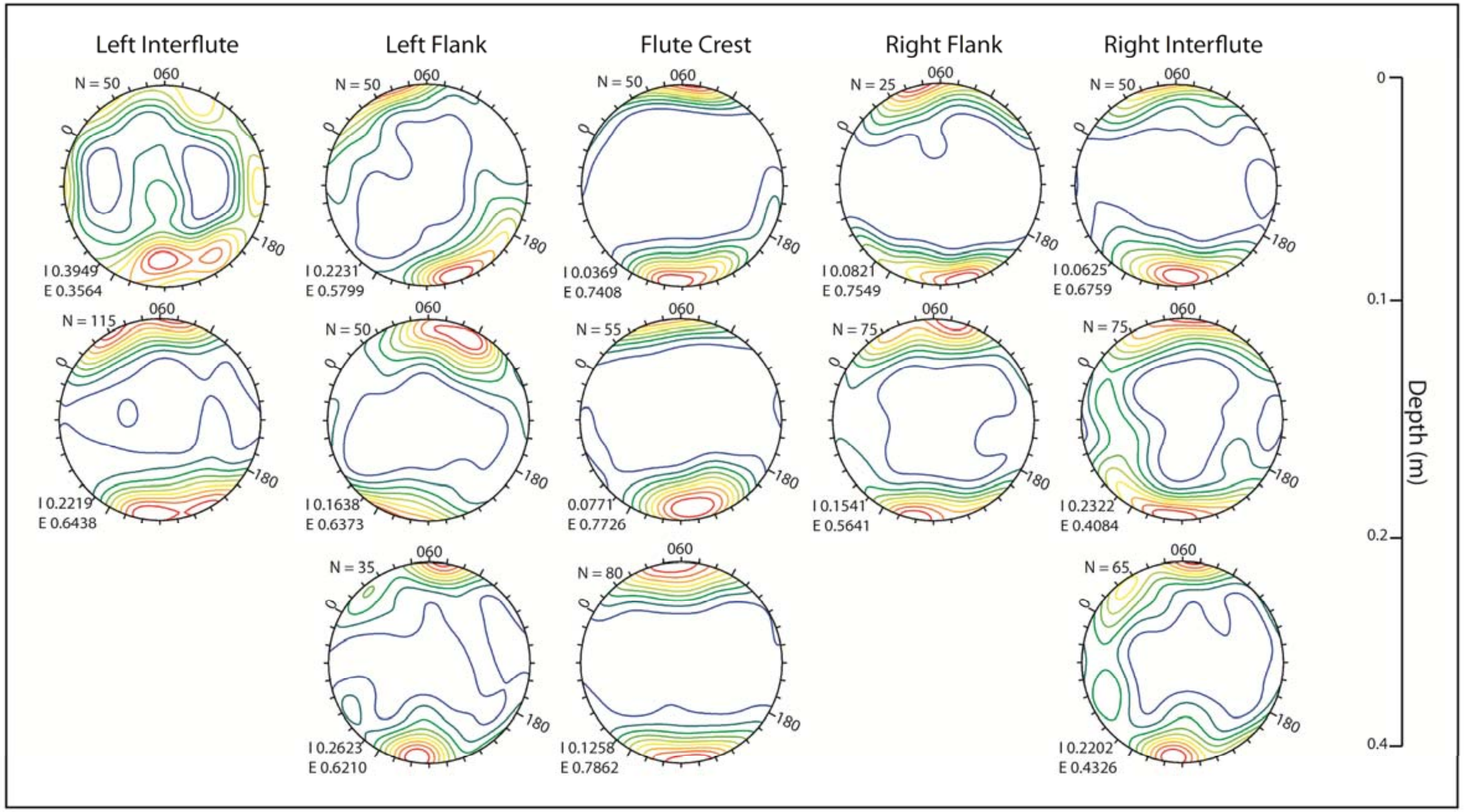

Figure 4.13a Contour plots showing lateral variations in clast fabric, aggregate data, 0-0.4m depth. N = the number of clasts used in calculating the aggregate values.

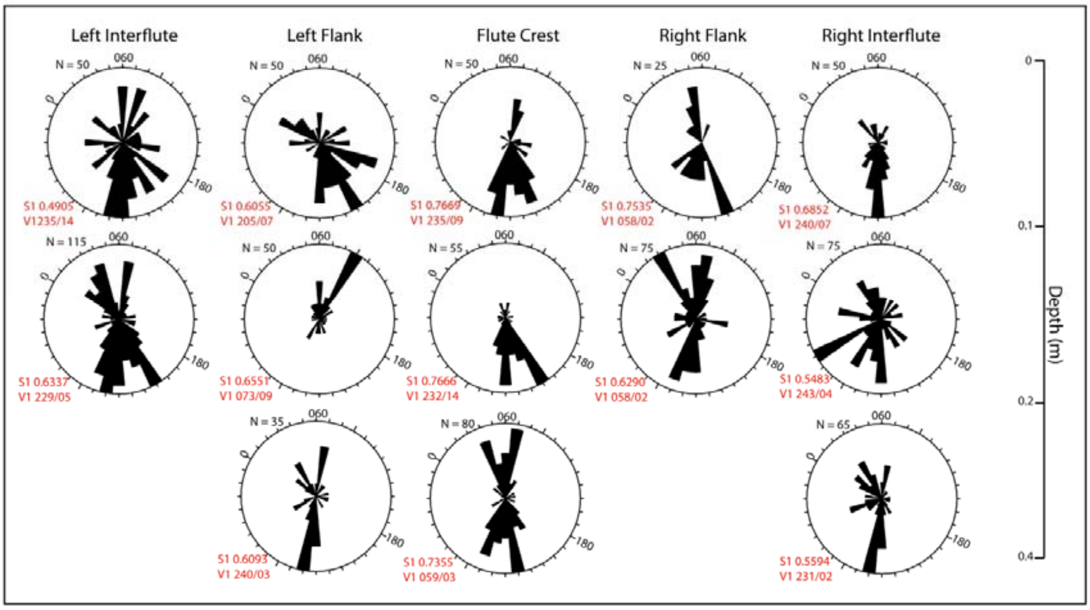

Figure 4.13b Rose diagrams showing lateral variations in clast fabric, aggregate data, 0-0.4m depth.

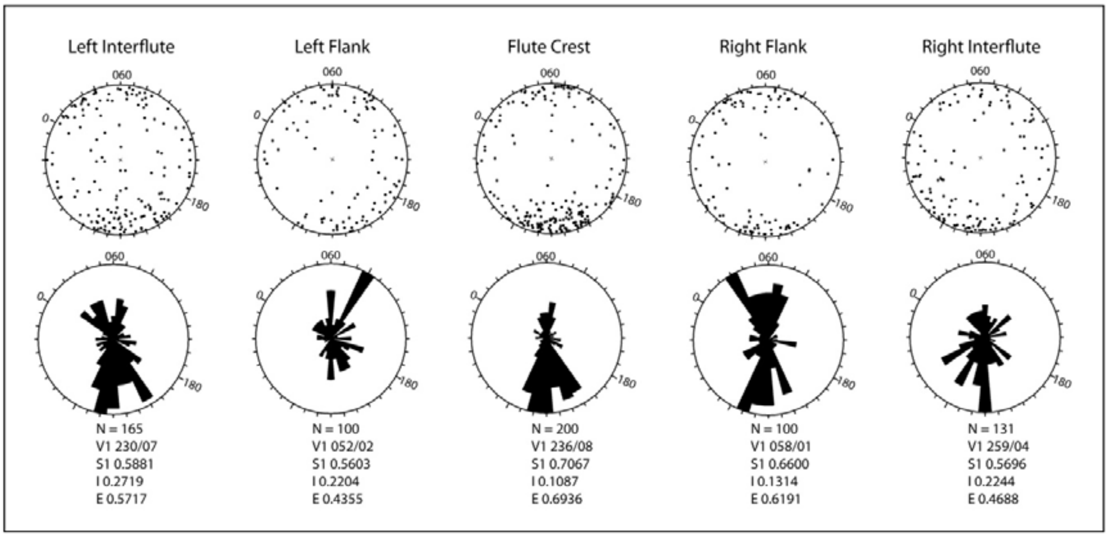

Figure 4.13c Lateral variations in clast fabrics, aggregate data, crest, flanks and interflutes, 0-0.2m depth (N = the number of clasts measured).

All crest, flank and interflute clast fabric measurements taken within the top 0.2m of flutes are aggregated and shown on stereoplots and rose diagrams in Figure 4.13c such that N (the number of clasts measured in each case) ≥ 100. As with the mean data, Figure 4.13c shows that the crest has the strongest linearly clustered a-axis fabric with V_1 flow-parallel. Clast fabrics become increasingly polymodal with distance away from the crest, with clast orientations on the flanks and interflutes exhibiting primary or secondary modes oblique to the mean flute axis, with clasts on the left flank and both interflutes exhibiting a wider range of dips and orientations, giving generally less clustered fabric shapes.

Clast fabric shapes for measurements taken from Lithofacies A within the top 0.2m of flute crests and interflute areas are compared using a ternary diagram (Figure 4.14) which is scaled using elongation and isotropy indices (Benn, 1994). With one exception, the flute crest readings cluster towards the lower right corner of the graph (high elongation, low isotropy), whereas the interflutes display a greater range of values.

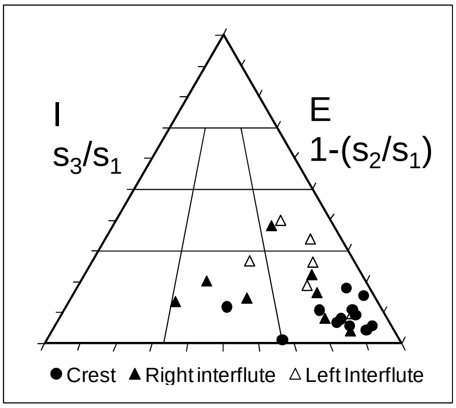

Figure 4.14 Ternary Diagram comparing clast fabric shapes from Interflutes and Flute Crests, Isfallsglaciären. The interflutes are generally less elongate and more girdle or isotropic in shape and cover a greater range of fabric shapes than flutes. Key as for Figure 4.9.

4.1.14 Lateral Variations within Area 3

Mean and aggregate data mask some interesting lateral variations in clast fabric within Area 3. For example, Figure 4.15 shows a cross-section from the proximal zone of flute 2 which is exceptional in that the right interflute has the strongest S_1 eigenvalue and elongation index, and values decrease in a northerly direction across the flute. However, clast fabric measurements taken only a few metres away in the proximal zones of flute 1 and flute 3

(Figure 4.3), show the crest to have the strongest fabric and the flanks to have stronger fabrics than the interflutes, although the fabric readings taken by Eklund and Hart (1996) near this area (flute 3) shows the right flank to be stronger than the crest. About one third of the way along flute 3 the crest fabric is stronger than the flanks and the flanks stronger than the interflutes, but this time the left flank has a stronger fabric than the right flank (Figure 4.11). In the distal zone of flute 1, clast fabrics measured in Trench TT show that the left interflute has a stronger fabric than the left flank or crest. Lateral variations in clast fabric strength are characterised by asymmetry, but neither the left nor right-hand sides of flutes show a consistently stronger or weaker clast fabric; the strongest S_1 values can switch between the crest and left-to-right flanks/interflutes over scales of tens of metres within the same flute. These individual cases show how variable clast fabrics are in one small area of fluted moraine.

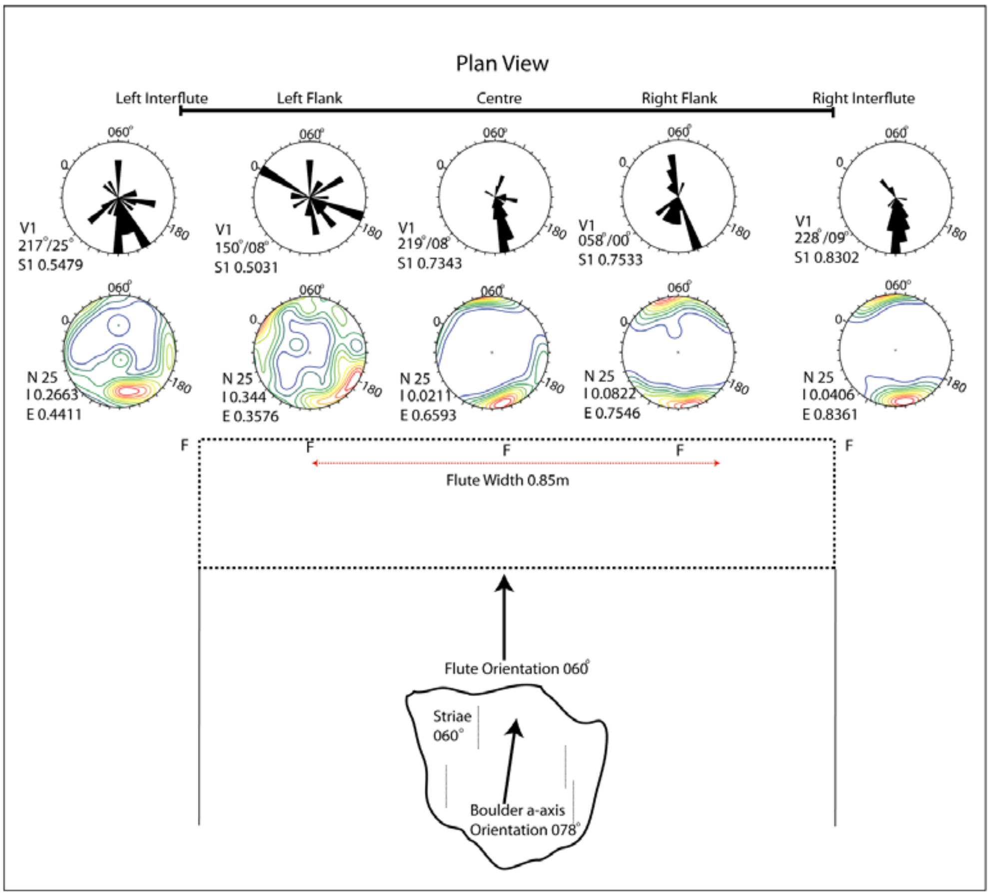

Figure 4.15 Cross-section of Flute 2, Area 3 showing clast fabric readings in the proximal zone.

4.1.15 Discussion - Clast Fabrics, Macro-observations and Models of Flute Formation

a) The Eklund and Hart Model

The detailed study of flute clast fabrics at Isfallsglaciären reveals a more complex picture than presented in the deforming-bed model of Eklund and Hart (1996). Contrary to their interpretation, clast fabrics, even behind embedded boulders, show no simple gradational decline in strength with depth (Table 4.1), the mean crest fabric is stronger than the flanks (Table 4.2 and Figure 4.7), and fabric strength is not correlated with distance down-flute (Figures 4.6a-c). The Eklund and Hart (1996) model must be considered an over-interpretation of events based on a small and limited data set, and the origin of the Isfallsglaciären fluted moraine needs re-interpreting in the light of the more detailed observations presented here. Flutes are more complex in structure and origin than envisaged by Eklund and Hart (1996). The observations reported here reveal a similar picture to those made by Gordon *et al*. (1992) and Benn (1994; 1995) in similar forefields of polythermal arctic and sub-arctic glaciers, lending support to the conclusion that flutes exhibit similar characteristics in these environments. However, these authors reached very different conclusions regarding the origin of flutes (see section 1.4.10). Indeed, macro-observations and clast fabric measurements taken from adjacent flutes at Isfallsglaciären provide supporting evidence for different models of flute formation (Table 4.5), which suggests that multiple processes may be involved in flute genesis (Benn, 1994).

b) Forced Mechanisms of Flute Formation beneath Warm-based Ice

The observations from Isfallsglaciären partly support the forced mechanism model of flute formation by bed-deformation beneath warm-based ice (Boulton, 1976; Benn 1994 and 1995). Some trenches in long, parallel-sided flutes reveal herringbone fabrics, or V_1 orientations oblique to the flute axis, which are consistent with the movement of sediment into subglacial cavities. Flow-parallel crest (and some flank) fabrics are consistent with shearing by overriding ice and sediment advection in a sediment-filled incipient subglacial cavity (Benn, 1995), at least to a depth of 0.4m. That neither the left- or right-hand sides of flutes showed consistently stronger fabrics suggests that, according to Boulton's (1976) model, the asymmetry in clast fabric strength was not caused by asymmetry in the regional glacier stress field, but reflects local variations in sediment strength, with weaker sediment on one flank preferentially deformed and advected. The up-doming of underlying substrate, observed in numerous trenches, is consistent with ice keels/ribs or ploughing boulders in troughs causing strong lateral compression which moves sediment upwards into subglacial cavities, where reduced pressure and vertical extension results in sediment up-doming (Boulton, 1976). The observed increase in gravel-sized material in the stoss of embedded boulders could be produced by pressure melting in a zone of increased compressive stress, which might encourage the removal of fines, or the preferential lodgement of coarser clasts (Benn, 1994). Weak lee-side clast fabrics are also consistent with models of flute formation by forced mechanisms (Table 4.5).

The strong flow-parallel flute crest and flank clast fabric readings are consistent with the model of constrained bed deformation in ice-walled furrows (Benn, 1995). However, the thin nature of the deforming bed, the lack of increase in Lithofacies A thickness towards the distal ends of flutes, and the lack of correlation between clast fabric strength and distance down-flute, suggest that till advection may have been more limited than envisaged by Benn (1995).

At Isfallsglaciären, interflute clast fabrics are weaker and display a greater range of vector orientations and clast dips than flutes. Benn (1995) argued that weaker interflute fabrics reflect ductile deformation in dilatant A-horizons, or are the product of high cumulative strain, but under inhomogeneous and less-constrained conditions, which allows particles to pitch up and down and rotate laterally in response to stress. The majority of interflute clast fabrics at Isfallsglaciären are much stronger than those reported by Benn (1994; 1995) and Gordon *et al*. (1992), and some have more flow-parallel a-axis alignments. Although significant differences in clast fabric shape occur between most flute crest and interflute observations (Figure 4.13), some interflute fabrics are indistinguishable from strong flute crest fabrics and must reflect similar strain magnitudes.

The idea that flute and adjacent interflutes have been subjected to similar shear strains and yet produce different clast fabric strengths is contested by Iverson *et al*. (2008), who argued that weak clast a-axis fabrics are incompatible with high strains in deformation tills. An alternative explanation for some of the weaker interflute and flank clast fabric measurements is that they reflect an element of post-depositional disturbance. Post-depositional disturbance could relate to slumping or sediment flows that occurred during deglaciation as supporting ice walls in basal cavities were removed (Boulton, 1976), liquefaction or flow of saturated material (Benn, 2004), subaerial modifications due to surface wash and frost heave (Rose, 1991), or a combination of these processes. This is especially true on the left flank, that is, the more shaded north-facing flank, where some of the weakest fabrics were recorded. For example, in Figure 4.15 the left flank and interflute fabrics of flute 2 in Area 3 are relatively weak and show polymodal clast orientations, with oblique and transverse orientations and some clasts with high angles of dip, which may have been produced by an undetected post-depositional slump on the left-hand side of the flute.

Rose (1991), investigated the ways in which paraglacial processes modified flutes at Austre Okstindbreen, Norway. He found that surface wash generally affected silt and sand-sized particles which were re-worked into flute troughs, whereas frost heave preferentially affected boulders and larger clasts due to their higher coefficients of heat loss. Over time, Rose (1991) found that subaerial modifications of fluted moraine resulted in particles becoming orientated down-slope and down the flanks of flutes, and some large clasts developed steeper dips, although mass movement was restricted to a depth of 10cm on slopes of 10 to 14° (at Isfallsglaciären, most flutes occur on slopes of between 5 and 10°). The one crest fabric taken by Eklund and Hart (1996) had a S_1 eigenvalue of 0.789. Equally strong clast fabrics were recorded nearby during this study, for example in the adjacent flute ≈7m to the north (S_1 = 0.78). The similarity in fabric readings between Eklund and Hart's study in 1996 and these readings taken in 2011 in nearby locations suggests that paraglacial processes have not greatly affected the fabric strength or orientation of gravel-sized clasts in the top 0.2m of Lithofacies A over the last 15 years. The two strongest flute crest fabric readings (S_1 0.85) occurred at the distal end of a flute in Area 2 and on the overridden moraine mound (Area 4). Paraglacial disturbances do not seem to have significantly weakened these fabrics despite their greater exposure time. Moreover, few clast fabric measurements record large numbers of clasts with steep down-flank dips. Indeed, in Table 4.3 it can be seen that aggregate data for flutes and interflutes at 0.2m depth yield V_1 orientations that are generally within a few degrees of the mean flute axis and with up-glacier plunges of between 1 and 8°. As such, the aggregate data indicates that flute and interflute clast fabrics have, overall, not experienced significant post-depositional disturbances, although where individual interflute clast fabric measurements are relatively weak, a number of clasts with higher dips and down-flank orientations are usually present. This can be seen, for example, in the far-left interflute fabric in Figure 4.4, which is consistent with a degree of subaerial modification. Indeed, it is possible that some of the very weak interflute fabrics recorded by Benn (1994; 1995) reflect similar disturbances, especially as these fabrics were recorded from the ground surface and within the zone particularly affected by surface wash and mass movement (Rose, 1991).

On two occasions the interflute clast fabric was stronger than fabrics in the adjacent flanks and crest, a finding not previously reported in the literature. The strong interflute clast fabrics are consistent with the idea that cumulative strains in interflute areas are equivalent to cumulative strains in flutes, although weaker fabrics are usually recorded (Benn, 1995). The influence of the large embedded boulder on clast fabrics at the distal end of flute 2, shown in Figure 4.5, suggests a possible mechanism capable of producing strong and weak interflute clast fabrics. Where the stoss-face of a lodged boulder is slightly oblique to the flute axis, sediment being advected down-flow in a deforming bed is only slightly deflected along the edge of the boulder, and the boulder edge acts as a constraining plane, like the ice wall of a furrow (Benn, 1995). Clasts in the deforming layer align parallel to the orientation of the boulder face, producing a strong clast a-axis fabric. Where the stoss-face is transverse to flow, the diamicton or debris-rich basal ice piles-up behind the boulder. The pile-up of sediment behind the boulder suggests this is a zone of relatively high compressive stress (Boulton, 1976), where numerous clast collisions promote steeper dips and clasts with orientations transverse and oblique to flow, which forms a weaker fabric. As such, this example suggests weaker fabrics can be produced in deformation tills at potentially high cumulative strains where there is a significant element of compressive stress, and similar transient stresses might occur in interflute areas ahead of ploughing clasts or in the vicinity of lodged clasts (Benn, 1995). Where deformation is constrained along a face that is approximately flow-parallel, stronger fabrics can be formed. The pile-up of sediment against the boulder in Figure 4.5 is consistent with sediment advection in a deforming bed (Benn, 1995). In interflute troughs or adjacent flute flanks, ploughing or lodged boulders might, on occasion, provide suitably aligned edges that could locally constrain deformation within the interflute and produce strong, flow-parallel fabrics (V_1 is near-flow-parallel in the two very strong interflute fabrics recorded at Isfallsglaciären). The operation of such a mechanism suggests the genesis of Lithofacies A and flute formation reflects interplay between lodgement and deformation processes.

The biggest problem with the forced mechanism models of flute formation is that about half of all flutes observed in the three forefields have no obvious initiating boulder behind which a subglacial cavity could form, and of 25 flutes studied in detail for fabric and sediment analysis, 17 had no initiating boulder. Boulton (1976) suggested flutes without initiating boulders could be explained by local glacier re-advances which preferentially removed lightly embedded boulders and stacked them into small transverse push moraines. Small push moraines are observed near-to the present glacier margins (Chapter 3.8.1). However, if this mechanism were responsible for the absence of initiating boulders in many flutes at Isfallsglaciären, then evidence of more push moraines should have been found across the forefield, but this was not the case. Sub-glacial cavities may also form behind bed obstructions (Boulton, 1976), but no obvious bed obstructions were observed at Fronstjön where flutes without boulders occurred. However, a relation does exist between boulders and about half the flutes observed, and some long, parallel-sided flutes are initiated by boulders, for example, flute 1, Area 3 (Figure 4.2). In this case, the width of the flute corresponds to the width of the boulder. Boulton (1976) suggested that flute dimensions reflected the size of lee-side cavities which were controlled by the dimensions of initiating boulders, so modal flute widths reflected the modal size of boulders. However, this explanation does not account for the distinct modal sizes of interflutes (Figure 3.23). The main fluted areas occur in close proximity to eroded bedrock riegels which probably sourced many of the large boulders which seeded flute formation (Evans *et al*., 2010). The forced mechanism of flute formation accounts for at least some of the flutes in the Tarfala Valley and flute formation involves interplay of boulder lodgement and bed-deformation processes.

c) Forced Mechanisms of Flute Formation beneath Cold-based Ice and Depositional Models of Flute Formation

In Chapter 3.3.7 it was argued that deformation of Lithofacies A required elevated pore-water pressures and so flute formation was associated with warm-based ice. For this reason, forced-mechanism models of flute formation beneath cold-based ice are rejected here as an explanation for the Tarfala flutes. Roberson *et al*. (2011) argued that isotope evidence from flutes at Midre Lovénbreen supported the idea that flute sediments had frozen-on to the base of the glacier. They extended the Hoppe and Schytt (1953) model of flute formation by suggesting that flutes form by the freeze-on of fluid sediment in a lee-side cavity in temperate ice where the Robin heat-pump produces a cold patch of ice. As with other forced-mechanism models, this model works best where there are large embedded boulders to initiate lee-side cavities, and so it is unlikely to account for all flutes observed in this study. Moreover, evidence of freeze-on does not necessarily relate to flute formation as flutes formed beneath temperate ice in polythermal glaciers can freeze-on as they enter regions of cold-based ice near the termini (Benn and Evans, 2010). Schytt (1963) observed cold-based ice with frozen-on flutes extending up-glacier for 60m from the glacier terminus in a subglacial tunnel at Isfallsglaciären. It is uncertain how the freeze-on model beneath temperate ice (Roberson *et al*., 2011) relates to clast-fabric observations. To point source a flute that is 100m long would require a considerable source of sediment to be continually moved into the subglacial cavity and considerable sediment advection. This suggests high cumulative strains and an increase in fabric strength down-flow, similar to Benn's (1995) model. As such, it is uncertain as to how applicable this model is to the Tarfala Valley.

Strong flow-parallel clast fabrics can also be produced by the melt-out of debris-rich basal ice (Lawson, 1979; Bennett *et al*., 1999) and are consistent with the Gordon *et al*. (1992) deposition model of flute formation. Indeed, many of the observations made at Isfallsglaciären concur with those made by Gordon *et al*. (1992) at Lynsdalen (Table 4.5). However, at Isfallsglaciären, although some flutes were observed to merge, no flutes were observed to diverge around or in between embedded boulders, which was a key piece of evidence used by Gordon *et al*. (1992) to support the theory of flute formation by deposition from debris-rich basal ice streams. Furthermore, it is difficult to reconcile herringbone fabrics with deposition from basal ice when local striae patterns on embedded boulders indicate glacier flow parallel to the flute axis (Benn, 1994), as seen, for example, in Trench 1, flute 2, Area 2 (Figure 4.4). Gordon *et al*. (1992) observed flutes forming across bare bedrock areas where there were no pre-existing sediments to source flute formation by bed-deformation processes, and used this observation in support of the theory that flutes were formed by the melt-out of streams of debris-rich basal ice. However, no flutes were observed crossing or forming on bedrock surfaces in Area 1 at Isfallsglaciären, or at Kaskasatjåkka. Although subglacial lodgement contributed material to Lithofacies A, the deposition model is rejected as an explanation for the Tarfala flutes because herringbone clast fabrics and flow-parallel striae are inconsistent with deposition from debris-rich basal ice, and because flutes are not observed to diverge around boulders or to form across areas of bedrock.

Table 4.5 Macro-scale Observations of Flutes in the Tarfala Valley and Models of Flute Formation

	Forced Mechanism Models				**Deposition Model**	**Instability Model**
Authors	Hoppe and Schytt (1953) Cold-based ice	Boulton (1976) Warm-based ice	Benn (1994 and 1995) Warm-based ice	Eklund and Hart (1996) Warm-based ice	Gordon *et al*. (1992)	Hindmarsh (1998), Fowler (2000), Schoof and Clarke (2008)
Flute Geometry	Long, parallel - sided, quasi-regular spacing	Boulton - flute spacing depends on boulder density; higher density induces closer spacing, whilst flute width and height reflect the width and height of the initiating boulder. The axial plane of the flute is parallel to the glacier flow direction. Short tapering flutes form behind lightly embedded boulders, whereas deeper embedded boulders (≥ 0.3m) produce sediment prows and longer flutes Benn, and Eklund &Hart - long parallel-sided flutes with flute axis parallel to glacier flow direction			Long parallel-sided flutes, width increases with height, quasi-regular spacing. Short tapering flutes occur. Flutes often superimposed, or merging, or diverging around boulders . IF long and straight, so not formed by subglacial meltwater erosion	Regular spacing and consistent flute dimensions reflecting preferred wave-lengths of bed instabilities
Field Evidence	**XXXXX**	**XXXXX** ***Short tapering flutes behind lightly embedded boulders observed*** ***Flutes in Is/Kas long, parallel-sided – some relate to initiating boulders where flute widths reflect boulder widths (Fig.4.2)***			**XXXX** ***No diverging flutes observed*** ***Long and straight IF furrows common***	**XXXX** ***Consistent flute dimensions in Is, but spacing less regular. Consistent flute heights in Stor, but widths/heights less regular in Kas (Fig.3.23)***
Flute Distribution and Glacier Velocity	Form in cold margin, and can occur across bedrock areas as flutes frozen to glacier base	Form beneath warm based ice where pre-existing forefield sediments are deformed into basal cavity Benn - long flutes represent if not fast flow, then at least a period of steady and continuous glacier flow			Deposited from debris streams within debris-rich basal ice in polythermal glaciers and can be deposited across bedrock areas	Form wherever instability is induced in deforming bed e.g. where bed thickens due to topographic change. May be associated with larger elongated bedforms such as mega-flutes
Field Evidence	***No flutes observed on bedrock***	**XXXXX** ***Deformation of Lithofacies A_1 requires elevated PWP, suggesting warm-based glacier conditions. Flutes in Is, continuous across forefield. Embedded boulders in Lithofacies A with striae concentrated on upper surfaces suggest lodgement and basal sliding***			***No flutes observed on bedrock***	**XXXXX** ***Flutes occur down-flow from riegels in Is/Kas, where distinct topographic change occurs. In Is., flutes radiate across forefield as glacier escapes confines of valley***
Relationship to Boulders	Flutes are closely associated with embedded boulders, and may form near to areas of plucked bedrock which seed flute formation (Evans *et al*., 2010). Boulton - lightly embedded boulders could be removed by short-term re-advances, with removed boulders later deposited to form transverse push moraines. Large boulders can terminate flutes, with new flutes forming in cavities on their lee-sides. Sediment often piled-up against large boulders where they terminate flutes. Eklund and Hart - constructional deformation occurs in the protected lee of embedded boulders, whereas excavational deformation occurs away from the lee-side cavity due to increased basal shear stress.				Not all embedded boulders have flutes and not all flutes have embedded boulders. Short tapering flutes do have initiating boulders, whereas long flow parallel flutes do not. Sediment often piled- up against stoss end of boulders, with a gap on the lee-side, or flutes diverge around large boulders	Flute formation does not require initiating boulders. Secondary flow instabilities may be generated around boulders, with spiral-like flows transporting sediment from troughs to crest. Flutes may widen in the lee of large boulders
Field Evidence	**XXX** ***Form in areas down-glacier from eroded bedrock outcrops which sourced many embedded boulders in Lithofacies A which may have seeded flute formation. Many flutes have no initiating boulder in Is.. Some large boulders do terminate flutes, but new flutes not observed on their lee-sides. Sediment is piled-up against large embedded boulders which do not terminate flutes. Constructional deformation profile not observed behind initiating boulder in Trench 1, flute 1, Area 3, Is. Macro-fabric can be strong behind boulders. Depth of Lithofacies A1 does not increase distally in most areas***				**XXXXX** ***All observations accord with observations in Is/Kas, Except divergence around large boulders***	**XXXXX** ***About half of flutes have no initiating boulder and of 25 flutes studied in detail, 17 had no initiating boulder. Flutes often widen behind large embedded boulders***

Flute Sediments	Re-frozen sub-glacial sediment slurry (Dm), maybe finer- grained than interflute material	Boulton - deformed pre-existing forefield sediments, so variable lithofacies. Underlying substrate typically up-domed into antiform mirroring the ground surface when seen in cross-section. Flutes sheared by overriding ice which encourages abrasion/comminution. Consequently, a silt-spike may occur in fluted sediment particle-grain size distributions Benn -homogeneous subglacial diamicton (Dm) with planar fabric and stoss and lee/double stoss and lee boulders. Typically B-horizons. Up-doming of substrate also reported Eklund and Hart - homogeneous Dm formed by bed deformation. Transitional or sharp contact with glacio-fluvial or glacio-lacustrine sands in lee of boulder, or sharp contact with coarser Dm elsewhere	Homogeneous Dm with strong planar fabric. Sharp contact with older weathered Dm substrate. No up-doming of underlying substrate	Deforming bed material, typically subglacial till
Field evidence	**XXXXX** ***Flute Dm less coarse than inter-flute Dm***	**XXXXX** ***Flutes consist of homogeneous Lithofacies), interpreted as traction till with a strong planar fabric. Long and tapering flutes contain same Dm, so differences in flute form NOT related to till rheology (Benn and Evans, 2010). S&L and DS&L boulders common. Up-doming of Lithofacies C_1 and SG substrate observed in some flutes. Lithofacies A pgsd suggests fine sand/coarse silt spike related to crushing/particle comminution. Porosities and void ratio indicate B-type horizons. Contacts with substrate mostly sharp and wavy***	**XXX** ***Up-doming observed***	**XXXXX**
Fabrics and Strain pattern ***(MF = macro-fabric)***	Not specified, although may be flow-parallel a-axis MF if inherited from meltout of frozen-on sediment	Boulton – oblique and transverse MF in furrows/flanks. Strong FP a-axis MF where shearing of flute crest by overriding ice. Steep clast dips on flanks and beneath crest. AMS ellipsoids reflect flow of fines inwards and upwards into cavity, caused by strong horizontal extension and vertical compression in trough and strong vertical extension and lateral compression in cavity. Complex strain patterns around boulders Benn – strong FP a-axis MF produced by steady, cumulative homogeneous strain in ice-walled furrow. High cumulative strain so MF strength should increase longitudinally. In IF, strain is less-constrained and is inhomogeneous, producing weaker and more variable MF, with greater range of vectors and clast dips, more akin to A-horizons. MF reflect deformation in sediment with strain directed towards low pressure shadow in lee of boulders Eklund and Hart – strong FP a-axis MF in thin deforming layer. MF strength strongest on flanks, decreases with depth, and increases longitudinally away from initiating boulders	Strong, FP a-axis MF in flute inherited from deformation in basal ice; IF more variable with weaker MF more typical of debris flows	Not specified, although herringbone fabric might be produced by secondary spiral flows and strong FP a-axis fabrics by shearing by overriding ice
Field Evidence	**XXX** ***Flute crest readings in top 0.4m are strong and FP***	**XXXXX** ***(Benn), although MF not correlated with distance down-flute. MF in crest/flanks mostly FP and strong in top 0.4m. IF MF more variable. Some herringbone MF indicate strain in bed directed towards furrow, whilst striae on boulders indicate glacier flow down-flute. Herringbone fabric in long flutes*** **XXX** (***Boulton) Strong, FP MF in crest, but not all flank/IF MF oblique/orientated towards crest. Clasts mostly have low dips, and AMS ellipsoids have much lower dips than suggested by Boulton and are consistent with FP simple shear rather than lateral compression/vertical extension in a cavity*** **XX** ***Eklund and Hart, MF stronger in crest than***	**XXXXX**	**XXX** ***Some herringbone fabric observed, but in close proximity to FP crest fabrics. Some flank/IF fabrics also suggest flow away from the crest***

	flanks, varies with depth but not gradationally, and does not increase distally, except over short (4m) distances. Crest MF strong, FP with weak layer below 0.4m suggests pervasive shear in bed 0.4m thick	

This table is a reproduction of Table 1.3 and includes observational evidence from Tarfala to assess which model(s) best account for observed flute characteristics. The number of crosses indicates the strength of match between model and field evidence. Is = Isfallsglaciären, Kas = Kasakastjåkka, Stor = Storglaciären, MF = Clast a-axis Macro-fabric, IF = interflute, FP = flow-parallel.

d) The Instability Model of Flute Formation

The absence of initiating boulders in many flutes provides support for the flow instabilities model (Fowler, 2000; Schoof and Clarke, 2008), which does not require boulders to generate flutes (Table 4.5). Flute and interflute widths at Isfallsglaciären (and interflute widths at Kaskasatjåkka and Storglaciären) display distinct modes, and flute heights in all three forefields are consistently between 0.2-0.4m, except where heights increase on the stoss-side of embedded boulders (Figure 3.23; Table 4.5). The quasi-regular pattern of flute dimensions is consistent with the instability model, which relates regular flute dimensions to the preferred wavelengths of bed instabilities (Fowler, 2000; Schoof and Clarke, 2008).

At Isfallsglaciären, flutes form down-flow from an area of eroded bedrock that forms a prominent riegel, and hence in a zone where there was a transition from a hard-bed to a soft-bed and a significant reduction in slope angle. At Kaskasatjåkka, the most prominent flutes also begin to form just down-flow from a major break of slope (Figure 3.2a&b). It is suggested here that flow instabilities may have been initiated by these distinct changes in topography. Up-flow of the fluted moraine, glacier flow would have been fast and extending over prominent bedrock riegels (Hedfors *et al.*, 2003). Glacier flow would have become slower and more compressive as the glacier diverged across the shallower slopes of the lower forefield, and especially upon the adverse slopes of overridden moraine mounds. At Isfallsglaciären, the radial orientation of flutes suggests glacier flow widened-out across the lower forefield as the glacier escaped the relatively narrow confines of the upper valley (Figure 3.2a&b). The changes in topography and associated glacier flow dynamics may have been responsible for generating flow instabilities at the ice-bed interface that acted to re-mould the bed into flutes with quasi-regular dimensions.

There are three problems with the application of the flow instabilities model in the Tarfala Valley. First, it is difficult to see how flow instabilities – in which secondary spiral flows move sediment from troughs to crests – can account for some stronger flow-parallel clast fabrics recorded in interflutes rather than adjacent flutes. Second, many flutes are associated with initiating boulders. Third, a transect across the flutes at Isfallsglaciären showed flute spacing had multiple modes (Figure 3.23) and spacing was not as regular as required by the flow instability model. Even though some of the variance in spacing along this transect can be explained by the burial and/or erosion of flutes by glacio-fluvial activity, spacing is irregular between flutes in some parts of Isfallsglaciären (see for example Figure 4.2). It is suggested here that a possible reason for this is that forced mechanisms of flute formation were superimposed on a region where flutes were also forming through flow instabilities. This would account for the quasi-regular dimensions of flutes, the relation between some flutes and boulders, the large number of flutes without initiating boulders, and the irregular spacing of flutes.

4.1.16 Conclusions

Clast fabric data and macro-observations from the Isfallsglaciären and Tarfala flutes provide evidence which can be used to support aspects of the forced-mechanism model and flow instabilities model of flute formation (Table 4.5). The presence of lodged boulders and ploughing clasts in Lithofacies A supports the idea flute formation involves interplay between lodgement, ploughing, and deformation processes. Strong flow-parallel crest fabrics are consistent with simple shear to moderate or high strains by overriding ice. Where Lithofacies A is relatively thick, the statistical difference between a weak layer of fabric readings and other flute crest fabric readings suggests that flute formation related to a phase of deformation by overriding ice that was limited in depth to 0.4-0.6m. The long length of parallel-sided flutes, the contrast in interflute and flute fabrics, the strong, flow-parallel fabrics, the location of flutes down-flow of areas of eroded bedrock that likely provided boulders to seed flute formation, and the occurrence of herringbone fabrics are all consistent with the forced mechanism model of flute formation beneath warm-based ice. However, clast fabric strengths do not increase distally and indicate strain magnitudes and till advection may be relatively limited in extent. Moreover, this model only provides a possible explanation for about half of the flutes observed in the Tarfala valley as many flutes have no initiating boulder. Flutes without boulders have either had their initiating boulders removed by some unknown process, or relate to flow instabilities at the ice-bed interface.

The quasi-regular dimensions of flutes in the Tarfala Valley and the lack of initiating boulders in many flutes lends support to the flow instability model of flute formation. The instability model also requires bed-deformation beneath warm-based ice, and the interpretation of Lithofacies A as a traction till produced beneath temperate ice during the Little Ice Age advance is consistent with this model. The main fluted areas at Isfallsglaciären occur where there is a longitudinal transition from a hard bed to a soft-bed, and at Isfallsglaciären and Kaskasatjåkka – where there is a distinct change in topography – and these changes may have generated flow instabilities that produced flutes through bed-deformation. The observations suggest that flutes at Tarfala are polygenetic, with both flow instabilities and the forced mechanism of flute formation in operation at the same time.

Section 2 - Magnetic Fabrics, Simple Shear and Strain Magnitude

In ring-shear experiments, pervasive simple shear produces a distinctive steady-state AMS strain ellipsoid and magnetic fabric strength increases with strain until steady-state conditions are achieved (Thomason and Iverson, 2006; Iverson *et al*., 2008). Subglacial soft-bed deformation is thought to be characterised by simple shear (McCarroll and Rijsdijk, 2003; Evans *et al*., 2006), and the deforming-bed model requires very high strain magnitudes (Piotrowski *et al*., 2006; Hooyer *et al*., 2008). In this section, magnetic fabrics from fluted moraine (Isfallsglaciären) and the diamicton plain (Storglaciären) are described and then analysed in terms of how closely they match the steady-state strain ellipsoid produced by pervasive simple-shear, and what they tell us about strain magnitudes.

4.2.1 Using Calibrations from Ring Shear Experiments to Estimate Strain Magnitude

In a series of laboratory-based ring shear experiments Thomason and Iverson (2006), Hooyer *et al*. (2008) and Iverson *et al*. (2008) demonstrated that the evolution of AMS fabric shape and strength were very sensitive to shear strain magnitude in a number of subglacial tills (see section 2.4.3). The rate at which clast fabric S_1 eigenvalues evolved and the strain magnitude required to attain steady-state magnetic fabrics were dependent on the particle grain-size distribution of the till (Thomason and Iverson, 2006). Sandy tills lacking gravels generally developed steady-state fabrics at lower strains and had weaker steady-state S_1 eigenvalues than coarser tills, which Thomason and Iverson (2006) suggested was because the chances of grain collisions between similar sized-particles was increased in tills with smaller particles. In addition, AMS parameters can be influenced by the mineralogical composition of the till, which may vary between sites (Hooyer *et al*., 2008). As such, if the experimental ring shear calibrations of Iverson *et al*. (2008) are to be used to estimate strain magnitude from magnetic fabrics taken in the Tarfala Valley, it is important to demonstrate that both the mineralogy and particle-grain size distribution of samples are similar to those used in the ring shear experiments. These issues are addressed in the next two sections.

4.2.2 AMS Parameters and Magnetic Mineralogy

Isfallsglaciären flows over the same basic igneous rocks and metamorphic rock units as Storglaciären, and so the mineral composition of the proglacial sediments is likely to be similar in each forefield. Hooyer *et al*. (2008) used thermo-magnetic experiments to demonstrate that AMS fabrics in the tills used in ring shear experiments, which included a subglacial diamicton from Storglaciären, were controlled by the long-axis alignment of silt-sized and smaller grains of magnetite. By comparison, the results of the thermo-magnetic experiments using Lithofacies A from Isfallsglaciären in this study are shown in Figure 4.16. The results show that bulk susceptibility is dependent on temperature, with the susceptibility remaining fairly steady with increasing temperatures up to 550-560°C, after which there is an abrupt reduction in susceptibility up to ≈600°C, beyond which the sample behaves paramagnetically (Chapter 2.4.3). Magnetite has a Curie-point temperature within the range at which the abrupt reduction in susceptibility occurs (Tarling and Hrouda, 1993, quoted a Curie-point value of 575°C for magnetite) which suggests magnetite is the magnetic carrier in the Isfallsglaciären diamicton. Hooyer *et al*. (2008) reported an abrupt reduction in susceptibility at ≈590-600°C for the Batestown and Douglas tills used in ring shear experiments. This suggests that the diamicton from the Isfallsglaciären flutes has a comparable magnetic mineralogy to the diamictons used in the ring shear experiments (Iverson *et al*., 2008). Furthermore, like the Douglas till, but unlike the Batestown till, the Isfallsglaciären diamicton does not show a marked increase in susceptibility at ≈500°C (known as the Hopkinson Peak), which is caused by very fine-grained single domain magnetite (<0.1μm) having greater susceptibility at higher temperatures (Hooyer *et al.*, 2008). This suggests the Isfallsglaciären diamicton does not contain very fine-grained magnetite.

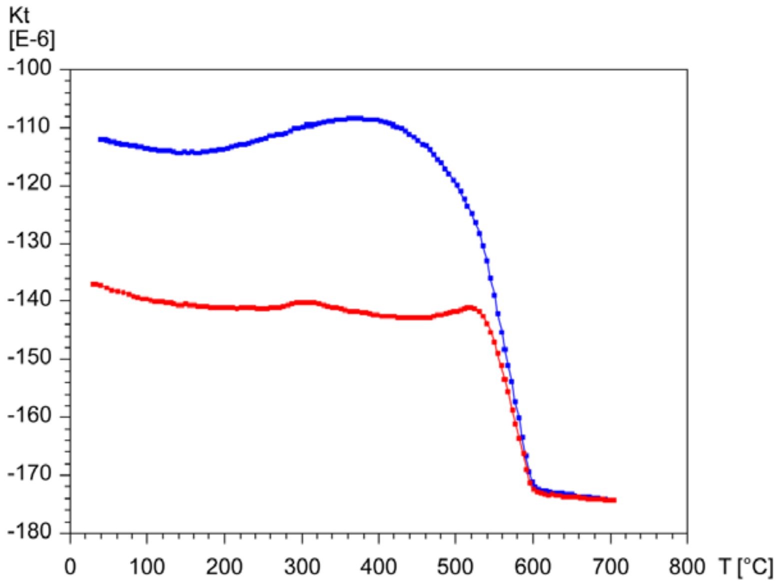

Figure 4.16 Graph showing relation between bulk magnetic susceptibility (K) and temperature. The Y axis is the bulk susceptibility (Kt) in SI units. A small sample of sediment (2g) is ground down and placed in a furnace within the kappabridge and heated. At 1-2° C intervals the susceptibility of the sample is measured during the heating leg of the experiment (shown by the red line), and during the cooling leg of the experiment (shown by the blue line). The dependence of bulk susceptibility on temperature allows an estimate of the mineralogy controlling the magnetic fabric to be made; paramagnetic minerals have a slightly inverse relationship with temperature, whereas ferro-magnetic minerals lose magnetism at the Curie temperature (the temperature at which their electrons switch from being ordered to fully disordered) (Tarling and Hrouda, 1993). As shown in the graph, the susceptibility shows little change with temperature until 550-560°C when it suddenly falls. Magnetite has a Curie temperature in this range and so is the likely magnetic carrier of the bulk susceptibility in this sample. At higher temperatures, the material behaves paramagnetically.

All the Isfallsglaciären samples give a strong mean susceptibility (K_{mean}) relative to values quoted by Tarling and Hrouda (1993) for sedimentary rocks. The mean susceptibility for all sub-samples (N = 118) is equal to 1767 +/- 90 (SI units, 95% confidence interval), which is consistent with material derived from mafic igneous and metamorphic rocks rich in ferro-magnetic minerals such as magnetite, which has very high susceptibility (Tarling and Hrouda, 1993). In six of the seven bulk samples from Isfallsglaciären, foliation (F) exceeds lineation (L) suggesting AMS ellipsoid shapes are mainly oblate. However, Figure 4.17 shows the shape parameter (*T*) plotted against the corrected anisotropy degree (P_j), which is a measure of the magnitude of the anisotropy, and this suggests that five of the AMS ellipsoid shapes are more triaxial than oblate, as they plot near to $T = 0$ (Tarling and Hrouda, 1993). Figure 4.17 also shows that ellipsoid shape is not dependent on the magnitude of the anisotropy of susceptibility, as might be the case if susceptibility at different sites was controlled by different mineral phases (Fleming *et al.*, 2013). In subglacial tills from Wisconsin, AMS ellipsoids also tended to be triaxial and remained so with increasing strain; it was the *orientation* of the ellipsoids that became progressively aligned with increasing strain (Hooyer *et al.*, 2008). In Figure 4.18, the range in the magnitude of the anisotropy and mean susceptibility are shown as P_j is plotted against K_{mean} for all 118 sub-samples from Isfallsglaciären, and it can be seen that the majority of sub-samples fall within a relatively narrow range of values, consistent with the AMS response being controlled by the same ferro-magnetic minerals in each sample area. The AMS parameters for the Isfallsglaciären flute samples are summarised in Table 4.6.

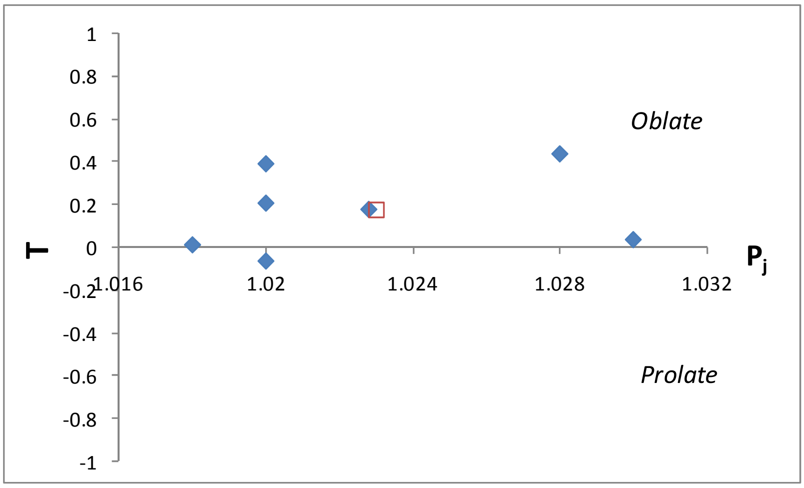

Figure 4.17 AMS Fabric shape parameter (T) plotted against the corrected anisotropy degree (P_j). For oblate fabric shapes T > 0 < +1; for prolate fabric shapes T is negative but < -1, and spheres plot at or near-to zero. The red square is the average magnetic fabric shape and strength (P_j) for the 7 fluted moraine samples and, as shown, most of the 7 samples have spherical to oblate shapes. The graph also shows that fabric shape is independent of the magnitude of the anisotropy, as T shows no correlation with P_j.

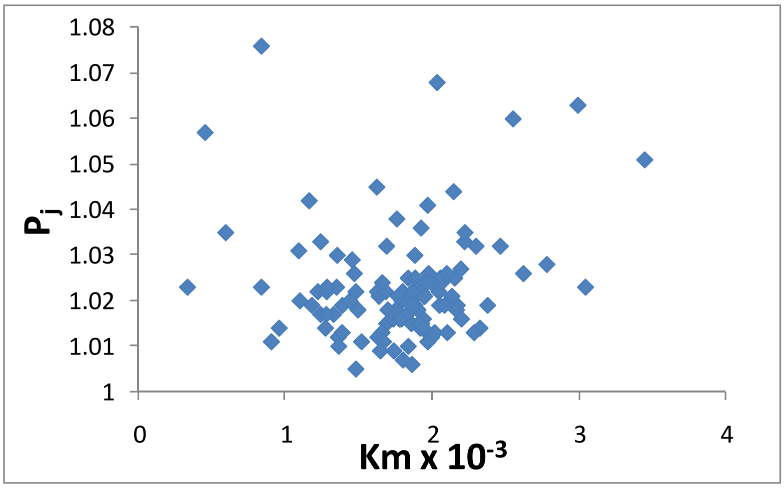

Figure 4.18 The Corrected anisotropy degree (P_j) plotted against mean susceptibility (K_m) for all sub-samples from the 7 Isfallsglaciären fluted moraine samples. P_j is a measure of magnitude of the anisotropy and, as shown, shows no appreciable change with increasing mean susceptibility.

Table 4.6 AMS Parameters, Isfallsglaciären Fluted Moraine

Mean AMS Parameters for each Sample								
Sample Code	**$K_m 10^{-3}$**	**L**	**F**	**P_j**	**T**	***K_1* inc**	***K_2* inc**	***K_3* inc**
BYL	1.162	1.006	1.015	1.023	0.390	17.6	15.1	63.5
MM7	1.692	1.008	1.009	1.018	0.015	34.7	33.7	31.7
MM9	2.088	1.007	1.020	1.029	0.436	19.0	17.3	59.7
MM8	1.689	1.009	1.008	1.016	-0.059	17.7	41.5	38.3
D1	2.028	1.009	1.013	1.023	0.179	21.3	19.5	58.1
MMt4	1.676	1.008	1.012	1.020	0.208	38.0	26.9	34.6
TT	1.846	1.014	1.017	1.033	0.040	24.4	25.5	48.6
All sub-samples	*1.767*	*1.009*	*1.014*	*1.023*	*0.177*	*24.1*	*25.4*	*48.5*
Standard Deviation	*0.486*	*0.006*	*0.010*	*0.012*	*0.411*	*15.7*	*19.1*	*20.0*
Confidence Interval	*0.088*	*0.001*	*0.002*	*0.002*	*0.074*	*2.9*	*3.5*	*3.6*

K_m is the mean susceptibility (SI units), *L* the lineation, *F* the foliation, P_j the Corrected Anisotropy Degree, *T* the shape factor, and K_1, K_2 and K_3 inc the inclination (plunge) of the three principal susceptibility axes in degrees. The final three rows (in italics) show the mean values with 1 standard deviation and 95% confidence intervals for all 117 sub-samples.

4.2.3 Comparison of Particle-grain Size Distributions

The particle grain-size distribution of tills used in ring shear experiments (Iverson *et al.*, 2008) are shown in Table 4.7 alongside the particle grain-size distribution of diamictons collected in this study from fluted moraine in each forefield, and from the Storglaciären diamicton plain. The particle grain-size distributions of sediments in this study closely resemble the particle grain-size distributions used in the ring shear experiments. As such, the similarities in magnetic mineralogy and particle grain-size distribution mean that the diamictons from Isfallsglaciären and Storglaciären are likely to show a similar magnetic fabric evolution in response to increasing shear strain as the tills used in ring shear experiments (Iverson *et al*., 2008), and the calibrations derived from ring shear experiments can be used to estimate shear strain magnitude from magnetic fabrics measured in this study.

Table 4.7 Comparison of Particle Grain-size Distributions (pgsd) of Subglacial tills used in Ring Shear Experiments (shown thus #) by Iverson *et al*. (2008) and Bulk Samples of Diamictons from Fluted Moraine and the Diamicton Plain.

	Gravel (% wt)*	**Sand (%)**	**Silt and Clay (%)**	**Silt (%)**	**Clay (%)**
Storglaciären #	10 (2)	65	25	-------	-------
Douglas #	5 (2)	72	23	-------	-------
Batestown #	17 (14)	49	34	-------	-------
Horicon #	19 (15)	70	11	-------	-------
Isfalls, Flute 3, MMT4, Distal	15	65	20	17	3
Stor, Log 1, Nordjakk Till Plain	13.5	65	21.5	18	3.5
Stor, flute, upper Till Plain, Proximal	11	48	40	34	6
Kas, flute, Distal	24	42	34	21	13

The Isfallsglaciären diamicton most closely resembles the Horicon till in pgsd, and has a similar sand, silt and clay content to the Douglas till. The Douglas, Batestown and Horicon tills were formed by the Superior Lobe of the Laurentide Ice Sheet, Wisconsin. Note the greater silt content in the Storglaciären fluted moraine compared to the diamicton plain, and the much coarser diamicton from Kaskasatjåkka. Key: Isfalls = Isfallsglaciären, Stor = Storglaciären, and Kas = Kaskasatjåkka. Distal and proximal relate to the location of the sample within the flute. The percentage weight of sample (%) is shown in each column, except *, where the number in brackets shows the % by weight of gravel after the coarsest fraction (> 0.6-0.8mm) was removed from the sample prior to use in ring shear experiments. The bulk samples in this study were extracted using plastic cylinders of varying volume (range, 575 – 772 cm^3). Each cylinder recovered a sample weight, when dried, >1kg (range 1.157 – 1.716kg).

4.2.4 AMS Parameters from the Storglaciären Diamicton Plain Samples

Magnetic fabrics were taken at 0.45-0.6m depth (code NL2upper) and 1.5-1.7m depth (code NL2lower) at log NL2, and from 0.7-0.88m depth at log SL1 (Figure 3.1c). The samples were of Lithofacies B. Only sample SL1 provided sufficient sub-samples to enable the bulk sample to be divided into two separate depth intervals (0.7-0.8m and 0.8-0.88m depth), which allowed strain magnitude to be estimated at a higher spatial resolution. The AMS parameters for the diamicton plain samples (Table 4.8) are very similar to those for Lithofacies A from Isfallsglaciären, with the aggregate K_m, P_j, and T values for each area being very similar. As in Isfallsglaciären, slightly stronger F than L values suggest AMS ellipsoids are more oblate than prolate, although the low T values indicate most ellipsoids are triaxial. Hooyer *et al.* (2008) demonstrated that magnetite was the magnetic carrier in diamicton samples from Storglaciären.

Table 4.8 AMS Parameters from the Diamicton Plain, Storglaciären

Column1	N	K_m10^{-3}	T	L	F	Pj	S_1	V_1	Plunge	I	E
Nord. Log 2 Upper 0.45-0.6m depth	15	1431	0.194	1.01	1.010	1.029	0.803	48	12	0.02	0.777
Nord. Log 2 Lower 1.5-1.7m depth	11	1730	0.149	1.02	1.024	1.04	0.690	241	7	0.10	0.655
Syd. SL1 0.7-0.88m depth	15	1095	0.220	1.01	1.072	1.03	0.648	202	3	0.23	0.690
Syd SL1 bottom 0.8-0.88m of sample	7	1042	0.220	1.02	1.016	1.03	0.694	189	4	0.14	0.696
Syd. SL1 top 0.7-0.8m of sample	8	1142	0.220	1.01	1.018	1.031	0.743	31	2	0.01	0.669
Aggregate	41	1419	0.190	1.01	1.035	1.033	0.679	43	4	0.17	0.701

Nord = Nordjåkk, Syd = Sydjåkk. Aggregate = the sum of all AMS sub-samples. Column headings as for Table 4.6, with the addition of N = the number of AMS sub-samples, S_1 is the principal eigenvalue and V_1 (in degrees) the principal eigenvector calculated using the orientation of K_1 susceptibility axes (V_1 plunge in degrees). I and E are the isotropy and elongation indices.

4.2.5 The Aggregate AMS Strain Ellipsoid for Flute Samples

Seven samples were taken from fluted moraine in Area 3 of Isfallsglaciären (Figure 4.2 shows the location of the sample sites). The orientation and plunge of the K_1, K_2 and K_3 susceptibility axes of all the sub-samples cut from these seven samples are shown separately as contour plots on lower hemisphere, equal area stereographical projections in Figure 4.19 a-c. In Figure 4.19a the principal susceptibility axes (K_1) have a bimodal distribution, with the maximum density of K_1 readings orientated at 248° with 20° plunge up-glacier, with a secondary mode at 174° with 25° plunge. Magnetic lineation is defined by the K_1 axis, and the main cluster of K_1 readings define a lineation that is parallel and aligned to within 8° of the mean flute axis (240°-060°). By comparison, in ring shear experiments steady-state S_1 eigenvalues (S_1 = 0.87 – 0.95) were achieved at moderate to high shear strains (7 to 30), with K_1 axes tightly clustered with an up-glacier plunge of between 18° and 26° (Hooyer *et al*., 2008). In Figure 4.19b it can be seen that that the K_3 axes form a tight cluster and unimodal distribution with V_1 having a steep down-glacier plunge (V_1 = 046°, plunge 64°). Similarly, in ring shear experiments the steady-state strain ellipsoid was characterized by a tight clustering of K_3 axes which had a steep, down-glacier plunge. Together, the alignment of the K_1 and K_3 susceptibility axes define the orientation of the longitudinal flow plane, while the orientation of the K_2 axis develops transverse to flow, but with the plunge of the K_2 axis defining the plunge of the shear plane (Shumway and Iverson, 2009). In Figure 4.19c the K_2 axes have a polymodal distribution with considerable variation in orientation and plunge, with V_1 plunging 8.5° to the north (355°) and a secondary mode plunging 6° to the south east (156°). However, the main clusters of K_2 axes are transverse to the mean flute axis and have low angles of plunge.

In Figure 4.19d the K_1, K_2 and K_3 susceptibility axes for all 118 sub-samples are combined and displayed as a contour plot which defines the aggregate strain ellipsoid. The aggregate strain ellipsoid for the Isfallsglaciären flutes closely resembles the steady-state strain ellipsoid produced in subglacial tills sheared to moderate and high strains in ring shear experiments (Figure 4.20) (Iverson *et al*., 2008; Shumway and Iverson, 2009). In Figure 4.19.d it can be seen that the longitudinal flow plane defined by the K_1-K_3 susceptibility axes is very closely aligned to the mean flute axis. As such, the aggregate strain ellipsoid for the Isfallsglaciären flutes is consistent with simple shear by overriding ice to moderate or high strains.

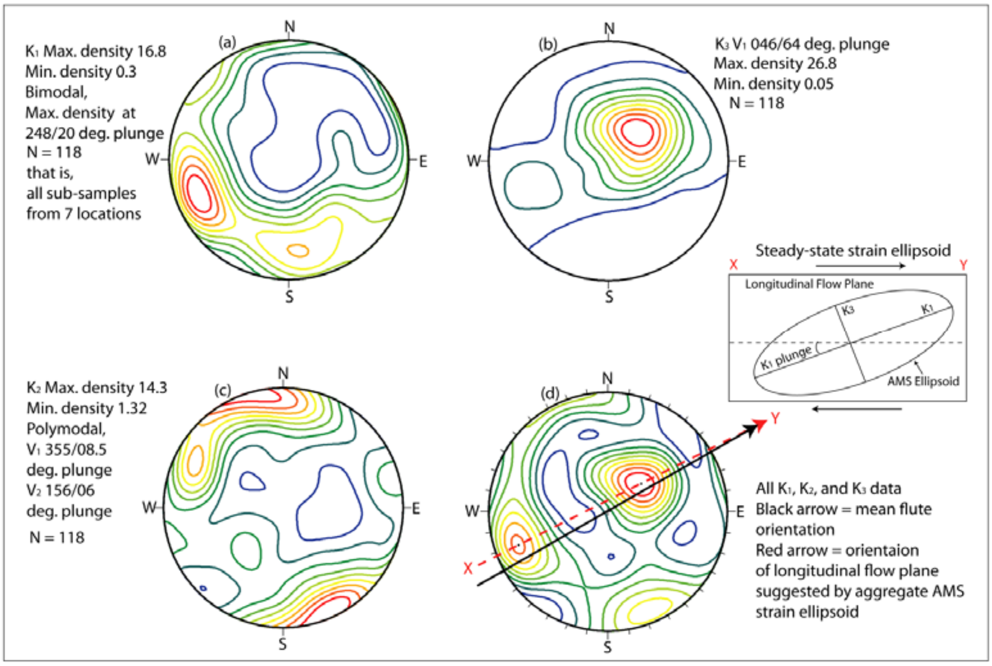

Figure 4.19 Stereonets showing orientation and plunge of principal susceptibility axes (K_1, K_2, K_3) for aggregate data (a-c) and the aggregate strain ellipsoid (d).

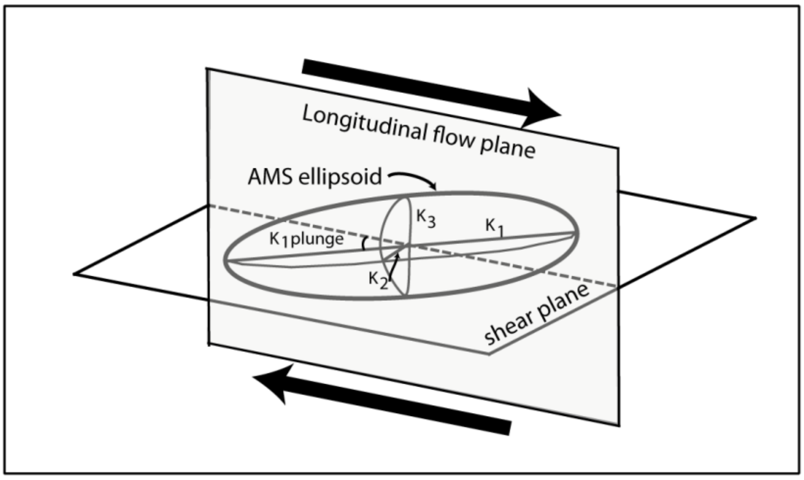

Figure 4.20 The idealised AMS strain ellipsoid produced by simple shear to high strains in ring shear experiments (From Shumway and Iverson, 2009).

4.2.6 The Aggregate AMS Strain Ellipsoid for the Diamicton Plain Samples

All the AMS sub-samples from Storglaciären have been aggregated together and the orientation of the K_1, K_2, and K_3 susceptibility axes displayed on an equal area, lower hemisphere stereograph projection which defines the aggregate AMS strain ellipsoid (Figure 4.21). Although it has similarities with the aggregate strain ellipsoid for flute samples and the steady-state strain ellipsoid produced in ring shear experiments, the K_1, K_2 and K_3 susceptibility axes show less clustering and a greater range of orientations than seen in the aggregate flute strain ellipsoid. Clast fabric measurements in Logs NL1-5 suggest glacier flow direction was to the ENE. The K_1 susceptibility axes form a distribution with clusters plunging at low angles to the ENE and WSW, with V_1 orientated 043° with 04° plunge down-glacier. Unlike the flute strain ellipsoid and steady-state strain ellipsoid, the majority of K_1 susceptibility axes do not plunge up-glacier and the V_1 plunges at a much lower angle. Likewise, the K_3 susceptibility axes are less tightly clustered than in the aggregate flute strain ellipsoid and steady-state strain ellipsoid, and the greatest concentration plunge up-glacier rather than down-glacier, with V_1 orientated at 277° with a 67° plunge. The K_2 susceptibility axes display a range of orientations and plunges, with V_1 at 126° with 27° plunge, which is consistent with a WSW-ENE longitudinal flow plane and shear plane plunging to the ESE (Shumway and Iverson, 2009).

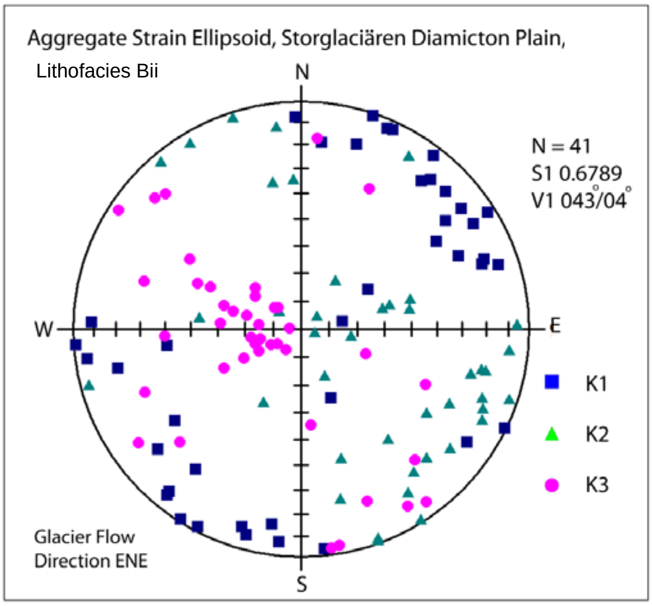

Figure 4.21 The orientation and plunge of the principal susceptibility axes, aggregate data, Storglaciären diamicton plain

4.2.7 Variation in AMS Strain Ellipsoids between Sites at Isfallsglaciären

Stereographic projections of the 7 samples taken from flutes are shown in Figure 4.22. Sample D1 shows the best approximation to the steady-state strain ellipsoid. The K_1 and K_3 axes are tightly clustered, with K_1 plunging up-glacier and K_3 plunging down-glacier, with the K_1 orientations defining a lineation in a flow-parallel direction. K_2 is transverse to the longitudinal flow plane and indicates the shear plane plunges at a shallow angle towards the north. The stereographic projections for samples MMTT and BYL show that they have similar AMS strain ellipsoids to D1, although the orientation of the K_1 lineation deviates significantly from the mean flute axis. In sample MMTT, the stereographic projection indicates a strain ellipsoid with a K_1 lineation to the south and a longitudinal flow direction to the northeast, which is consistent with the clast fabric recorded at this depth (Figure 4.8). Sample BYL was taken from a flute flank and across the boundary of Lithofacies A and underlying beds of very coarse silty sand (which had a silt content of 13-37% hence a magnetic fabric was recoverable). When analysed separately, both lithofacies yield similar strain ellipsoids, as shown in Figure 4.23. V_1 orientations, calculated from the orientation and plunge of the K_1 axes, are oblique to the flute axis for Lithofacies A (288° with 10° plunge) and for the silty sand (256° with 22° plunge).

Four of the seven samples have more complex AMS strain ellipsoids which deviate significantly from the simple shear steady-state strain ellipsoid, with the three samples taken from the shallowest depth showing considerable deviance. In Figure 4.22, MM8 is plotted using 20 sub-samples. However, analysis of AMS parameters suggests that three sub-samples differ significantly from all other sub-samples in terms of susceptibility, which suggests that these outliers are being produced by a different magnetic mineral or size of mineral (Tarling and Hrouda, 1993). As such, the stereographical projection of MM8 has been re-plotted with the outliers removed, and this is shown in Figure 4.24 alongside plots of the AMS parameters which show the outliers. The re-plotted sample for MM8 shows that the V_1 orientation, calculated from the orientation of the K_1 axes, is 153° with 17° plunge. There is a reasonably strong clustering of K_1 values transverse to the flute axis although K_2 and K_3 form less clustered distributions, with the majority of K_3 reading plunging down-glacier. By contrast, MM9 (Figure 4.22) has the most oblate shape ellipsoid of all the samples (T = 0.436), with the K_3 axes clustered and plunging at a high angle towards the north, and K_1 and K_2 forming a girdle fabric.

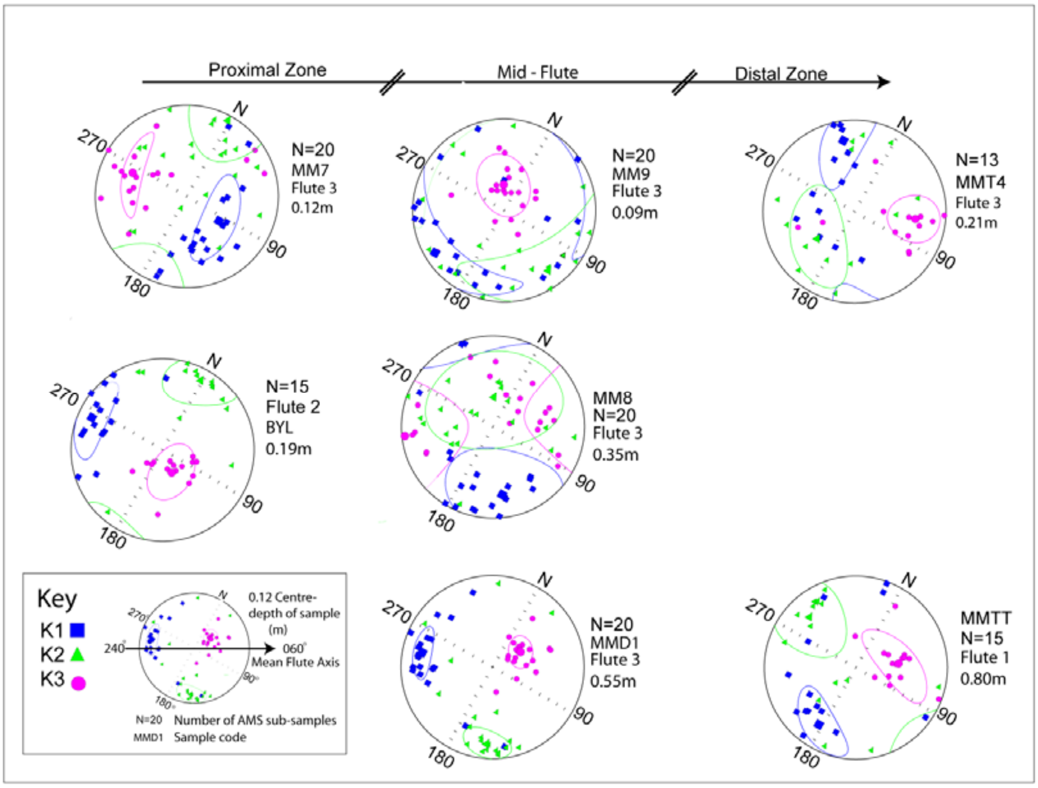

Figure 4.22 Stereonets showing the orientation and plunge of the principal susceptibility axes (K_1, K_2, K_3) for 7 bulk samples from the Isfallsglaciären flutes. Note: the large blue square, green triangle and pink circle are mean values for K_1, K_2, and K_3, respectively, and the lines encircling the K_1, K_2 and K_3 values represent the 95% confidence ellipsoids, that is, the area in which 95% of the K_1, K_2 and K_3 data lies.

Sample MM9 resembles the asymmetric girdle fabrics produced at moderate- to low-shear strains in ring shear experiments (Thomason and Iverson, 2006). The vertical profile in Trench MMT3 (samples D1, MM8 and MM9) shows considerable variation in magnetic fabric strength and vectors over 0.6m depth and some of the variation accords with the vertical clast fabric profile from this trench (Figure 3.13). D1 corresponds to the strong flow-parallel clast fabric recorded below 0.5m depth just to the left of the crest, and MM8 corresponds to the weak, less linearly clustered clast fabric measured between 0.4 and 0.5m depth. A clast fabric was not recorded in the top 0.1m of this trench, but the clast fabric taken over a 0.2m depth interval, in contrast to MM9, is strong with a-axis alignment parallel to the flute axis.

Sample MM7 was taken at an equally shallow depth to MM9, but approximately 30m up-flute in the proximal zone and a few metres from the stoss-side of a large embedded boulder. By comparison, MM7 yields a relatively strong S_1 eigenvalue, and a very different strain ellipsoid to MM9. In MM7, the K_1 axes form a tighter cluster than in MM9 but have relatively steep plunge and are oblique and transverse to the flute axis. The K_3 values plunge at a lower angle up-glacier rather than down, and the K_1-K_3 plane suggests a longitudinal flow direction towards the west (and deviating 30° from the flute axis). Sample MM4 yields the second strongest oblate ellipsoid shape (T = 0.203) with K_1 and K_2 less tightly clustered but with K_3 tightly clustered and plunging down-flute. The K_1 axes form an asymmetric girdle and have relatively high plunges; similar fabrics were produced by weak to moderate shear strain in ring shear experiments (Iverson *et al*., 2008).

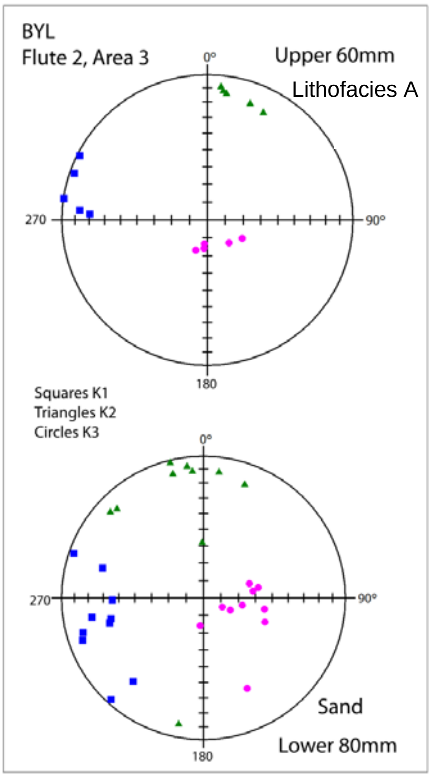

Figure 4.23a & b Sample BYL, re-plot showing K_1, K_2, K_3 orientations for upper Lithofacies A (a) and Lower Sand (b). The distributions of the principal susceptibility axes in Lithofacies A are similar to the steady-state strain ellipsoid produced by simple shear to moderate-high strains. K_1 and K_3 are clustered parallel to the longitudinal flow direction (which in this case suggests flow oblique to the flute axis and in towards the flute crest, consistent with sediment squeezing into a subglacial cavity). K_1 has up-glacier plunge of about 20°. K_3 is clustered and plunging at a high angle down-glacier, and K_2 plunges with an angle < 10° transverse to the flow

direction. K_2 defines the plunge of the shear plane. Note that the underlying sand has a similar fabric shape, although K_1 is less clustered. The sand ellipsoid is also consistent with simple shear, with a longitudinal flow plane less oblique to the flute axis than Lithofacies A. The sand ellipsoid could also have been produced by strong current flow during deposition. In such depositional fabrics, K_3 plunges up-flow and K_1 is orientated transverse to flow (Tarling and Hrouda, 1993), which would mean that, in this case, flow was towards the NW. However, the presence of a small, open asymmetric anticline in the sands a few decimetres below the contact with Lithofacies A, and the down-flute inclination of the fold axis, suggests that the sands have been sheared by overriding ice and that the AMS fabric represents simple shear rather than primary deposition.

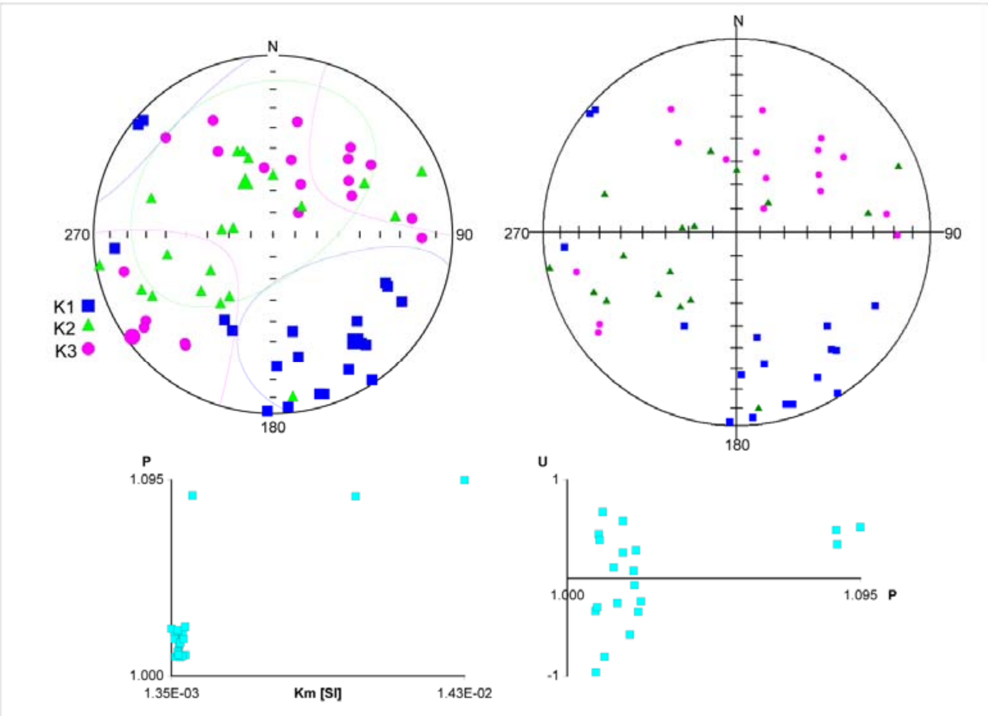

Figure 4.24 Sample MM8, re-plot of stereonet showing orientation of principal AMS Axes. The stereonet on the left shows the bulk sample with 20 sub-samples plotted and the stereonet on the right shows the same data minus the three outliers (see text).

4.2.8 Variations in AMS Strain Ellipsoids between Sites at Storglaciären

Stereographic projections of the K_1, K_2 and K_3 susceptibility axes for the Storglaciären samples define strain ellipsoids that show a considerable degree of variability (Figure 4.25). Samples NL2upper and SL1 have many of the features of a steady-state strain ellipsoid produced by simple shear, with a tight clustering of K_1 and K_3 axes and the majority of K_1, K_2, and K_3 axes forming perpendicular clusters. However, NL2upper deviates from the steady-state simple shear strain ellipsoid in that the K_1 susceptibility axes plunges down-glacier rather than up, and K_3 plunge up-glacier rather than down. By contrast, in sample NL2lower, which was taken approximately 1m further down the section from NL1upper, the K_1 axes plunge up-glacier (V_1 202° with 03° plunge) whilst the majority of K_3 axes plunge at a low angle to the SSE. In sample SL1 the K_1-K_3 axes suggest a longitudinal flow plane orientated towards the SW. This is not consistent with the direction of glacier flow suggested by the clast fabrics in logs NL1-5 (ENE). At Storglaciären, vectors obtained from the orientation of the K_1 axes have relatively low plunges compared to flute samples and the steady-state strain ellipsoid produced by simple shear.

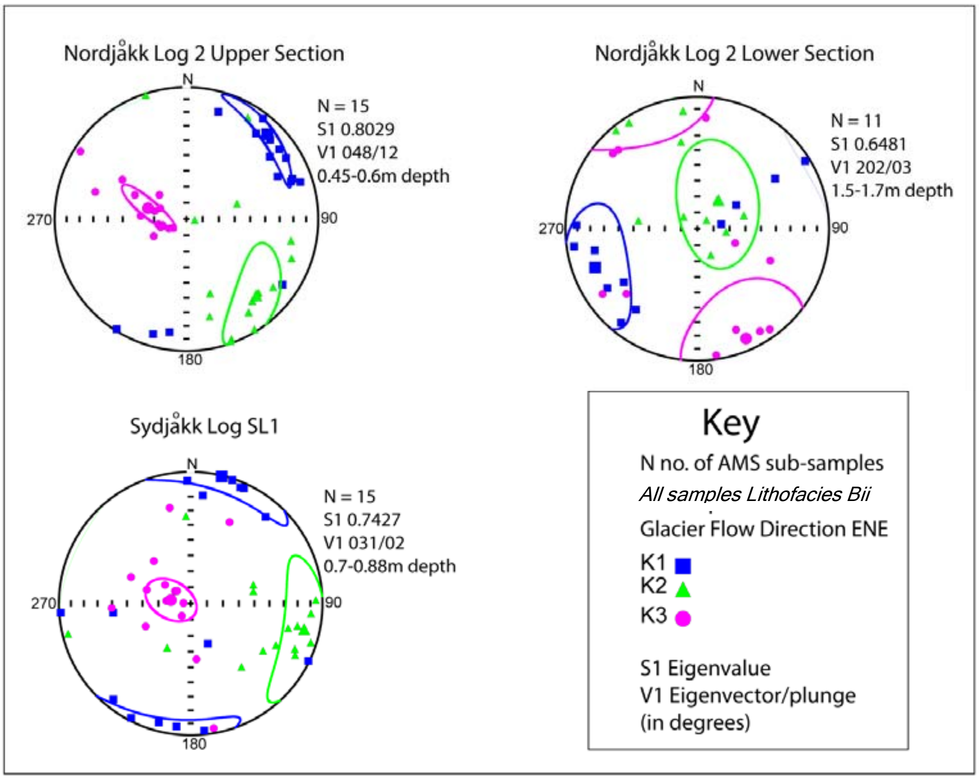

Figure 4.25 Stereonets showing the orientation and plunge of the principal susceptibility axes of the diamicton plain samples. The glacier flow direction is estimated from the clast fabric measurements from the Nordjåkk Logs NL1-5.

4.2.9 Estimating Strain Magnitude

The extent to which laboratory ring shear experiments are applicable to field conditions requires further investigation, and ring shear calibrations of strain magnitude should be treated with caution (Hooyer *et al*., 2008). An important uncertainty in field conditions is that the pre-existing fabric is unknown, and so the strain required to produce a steady-state fabric cannot be definitely known (Shumway and Iverson, 2009). However, comparison of magnetic fabrics derived from field data with magnetic fabrics attained in ring shear experiments under controlled conditions probably gives the best estimate of strain magnitude currently available for macroscopically homogeneous subglacial diamictons (Shumway and Iverson, 2009).

The relation between shear strain and magnetic fabric strength (S_1 eigenvalue determined from the orientation and plunge of K_1 axes) determined in ring shear experiments is shown in Figure 4.26, which is reproduced from Iverson *et al*. (2008). S_1 eigenvalues, calculated for the Isfallsglaciären samples, are shown in Table 4.9, alongside estimates of the strain magnitude required to produce these S_1 eigenvalues according to the regressed lines shown in Figure 4.26. As can be seen, none of the Isfallsglaciären samples has an S_1 eigenvalue ≥ the minimum value (S_1 = 0.83) attained at steady-state during ring shear experiments. Sample D1 has the strongest S_1 eigenvalue (0.801) which indicates moderate to high shear strain, and the weakest value is obtained for MM9 (0.533), which was taken approximately 0.4m higher up the vertical sequence in trench MMT3. Shumway and Iverson (2009) reported some similarly weak S_1 eigenvalues from field studies, but a greater range of S_1 values, with much higher values at the top end (0.59-0.99) than seen in the flutes of Isfallsglaciären. Most of the flute samples suggest low to moderate strain magnitudes (≤10).

Iverson *et al*. (2008) also mapped the influence of shear strain on magnetic fabric evolution by plotting ternary graphs scaled using the isotropy and elongation indices of Benn (1994) and these results are reproduced in Figure 4.27a. For comparison, Figure 4.27b shows the results from the Isfallsglaciären flutes plotted on an identical ternary graph. The black circles represent the fabric shapes for the 7 bulk samples, while the blue diamonds represent the results for the upper and lower vertical zones (S_1 eigenvalues for upper and lower vertical zones are shown in Table 4.9). None of the 7 bulk samples from Isfallsglaciären have elongation indices E >0.8 which suggests these samples have been moderately strained (<10). Samples MM9 and MMT4 have girdle shapes indicative of low strain (<2). However,

S_1values obtained at higher spatial resolutions by dividing the bulk samples into upper and lower vertical intervals yield 5 values where S_1 >0.83 and E >0.8, although, as previously stated (Chapter 2.4.3), these values should be treated with caution because of the small sample size. Nevertheless, the values from the upper and lower vertical intervals do suggest significant changes in magnetic fabric strength and K_1 orientation over cm scales. For example, in sample BYL the upper 60mm of the sample consists of Lithofacies A, and the lower 80mm silty sands. Both lithofacies yield strong S_1 values >0.83 with tightly clustered K_1 axes but, as shown in the stereoplot in Figure 4.23, they have different V_1 orientations and plunge.

In Trench MMT3, the orientation of the K_1 axes in the vertical sequence beneath the flute crest reveals significant variations in V_1 orientation and plunge; magnetic fabric strength also varies over 0.6m depth (Figure 4.28). Samples D1 and MM8 both have reasonably strong fabrics, and when divided into upper and lower vertical intervals the lower 50mm of D1 has an S_1 value of 0.880 (the strongest fabric recorded), while the upper section of MM8 has an S_1 value of 0.827. However, sample MM9 from nearer the flute surface reveals consistently weaker fabrics (although the lower 40mm of this sample has a moderate fabric strength S_1 = 0.664), giving an S_1 range of 0.533 – 0.880 over a depth of 0.6m.

As with the clast fabric, there is no evidence that magnetic fabric strength increases down-flute. Sample MM7 was taken from the proximal zone of flute 3 and MMT4 from the distal zone; MMT4 has a consistently weak magnetic fabric, even when divided into small upper and lower vertical intervals, while MM7 has a strong fabric, with the upper 80mm showing a tight clustering of K_1 axes with an S_1 value of 0.858, which is equivalent to steady-state S_1 values from ring shear experiments and suggests relatively high strain magnitude (≈20-25). Again, as with clast fabrics, it can be seen in Figure 4.29 that magnetic fabric strength shows no simple correlation with depth. Within 1m of the flute surface moderate to strong fabrics can be obtained at any depth, although the 3 weakest values (S_1 <0.6) are obtained at shallow depths (<0.3m), which causes the mean S_1 value to be slightly stronger below 0.3m depth (mean S_1 value 0-0.3m depth = 0.699, +/- 0.121 at 1 standard deviation; mean S_1 value >0.3m depth = 0.782, +/-0.075 at 1 standard deviation).

None of the S_1 values obtained from the K_1 axes orientations in the Storglaciären samples are equivalent to the steady-state S_1 values obtained in ring shear experiments (Table 4.9), and the strongest S_1 value (0.8 for NL2 upper) suggests a strain magnitude of ≈ 10. Most of the S_1 values indicate only moderate strain magnitudes. Sample SL1 was divided into two vertical intervals and the upper interval (0.7-0.8m depth) reveals a stronger S_1 value than the lower interval (0.8-0.88m depth) and a significant change in the V_1 orientation (from 031° to 189° over a 0.1m depth interval).

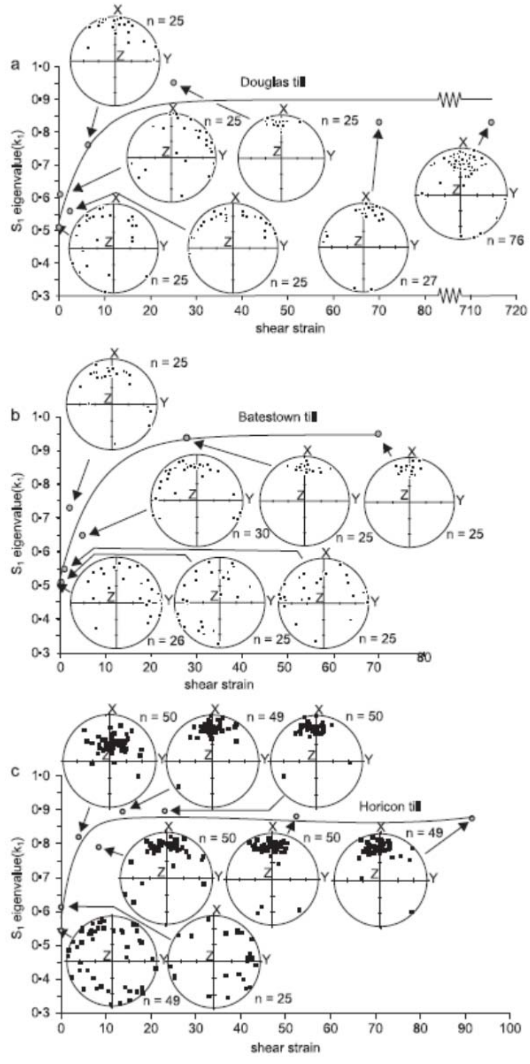

AMS k_1 fabric development as a function of shear-strain magnitude in the (a) Douglas till, (b) Batestown till and (c) Horicon till. Exponential fits to S_1 values had standard errors of 0·063, 0·067 and 0·041 for the Douglas, Batestown and Horicon tills, respectively. Orientations of k_1 are shown in lower-hemisphere stereonets, with n the number of samples. The direction of shearing is along the x axis, and the sense of shearing is bottom north and top south, such that k_1 orientations plunge 'up-glacier' at high strains. The uncertainty of shear-strain values is ±5%.

Figure 4.26 The development of steady-state AMS fabrics with increasing shear strain in ring shear experiments with three subglacial tills (from Iverson *et al*., 2008).

Table 4.9 Strength of magnetic fabric measurements from fluted moraine

Location in Area 3 & Sample Code	SO	SL mm	Sampling Int/Depth	N	S_1	S_2	S_3	V_1	Plunge	I	E	Sst Other	Sst Horicon
Flute 2 Proximal Left Flank BYL	***P***	***180***	***0.10 - 0.28m***	***15***	***0.797***	***0.163***	***0.040***	***267***	***19***	***0.050***	***0.796***	***8 to 9***	5 to 6
Flute 2 proximal left flank, Litho-Facies A, BYL	P	180	upper 60mm	6	0.874	0.104	0.022	288	10	0.025	0.881	20 to 25	>13+
Flute 2 proximal left flank, sand, BYL	P	180	lower 80mm	10	0.850	0.168	0.031	256	22	0.037	0.803	12 to 20	8 to 9
Flute 3 Proximal Crest mm7	***P***	***180***	***0.03 - 0.21m***	***17***	***0.733***	***0.243***	***0.024***	***141***	***39***	***0.033***	***0.669***	***4 to 5***	2 to 4
Flute 3 Proximal Crest mm7	P	180	upper 60mm	7	0.688	0.290	0.022	166	17	0.032	0.578	1 to 3	2 to 3
Flute 3 Proximal Crest mm7	P	180	lower 80mm	10	0.858	0.120	0.023	130	45	0.026	0.861	15 to 20	8 to 9
Flute 3 Middle Crest mm9	***L***	***85***	***0.05 - 0.14m***	***20***	***0.533***	***0.356***	***0.114***	***210***	***15***	***0.214***	***0.332***	***< 1***	< 1
Flute 3 Middle Crest mm9	L	85	upper 40mm	10	0.603	0.364	0.033	152	13	0.055	0.397	1 to 2	< 1
Flute 3 Middle Crest mm9	L	85	lower 40mm	10	0.664	0.227	0.108	227	11	0.163	0.658	1 to3	2 to 3
Flute 3 Middle Crest mm8	***L***	***85***	***0.31-0.39m***	***17***	***0.775***	***0.170***	***0.055***	***153***	***17***	***0.071***	***0.781***	***7 to 8***	4 to 5
Flute 3 Middle Crest mm8	L	85	upper 40mm	7	0.827	0.147	0.026	171	22	0.031	0.822	14 to15	6 to 7
Flute 3 Middle Crest mm8	L	85	lower 40mm	10	0.716	0.221	0.064	147	18	0.089	0.692	4 to 5	2 to 4
Flute 3 Middle Crest D1	***L***	***100***	***0.5-0.6m***	***20***	***0.801***	***0.174***	***0.025***	***253***	***23***	***0.032***	***0.783***	***9 to 10***	> 5 to 7
Flute 3 Middle Crest D1	L	100	upper 50mm	11	0.791	0.183	0.026	267	20	0.032	0.769	9 to 10	5 to 6
Flute 3 Middle Crest D1	L	100	lower 50mm	9	0.880	0.110	0.010	241	25	0.011	0.875	20 to 25	> 13+
Flute 3 Distal Crest MMT4	***L***	***85***	***0.165 - 0.25m***	***15***	***0.577***	***0.371***	***0.053***	***296***	***47***	***0.092***	***0.357***	***<1 to 2***	< 1
Flute 3 Distal Crest MMT4	L	85	upper 40mm	7	0.575	0.354	0.072	265	59	0.125	0.385	< 1 to 2	< 1
Flute 3 Distal Crest MMT4	L	85	lower 40mm	6	0.641	0.331	0.026	310	34	0.041	0.484	1 to 2	1 to 2
Flute 1 Distal Crest MMTT	***P***	***150***	***0.72 - 0.87m***	***15***	***0.724***	***0.249***	***0.028***	***202***	***31***	***0.039***	***0.656***	***4 to 5***	2 to 4
Flute 1 Distal MMTT	P	150	upper 60mm	6	0.874	0.115	0.011	184	17	0.012	0.868	20 to 25	> 13+
Flute 1 Distal MMTT	P	150	lower 60mm	9	0.653	0.296	0.051	247	32	0.078	0.546	1 to 2	1 to 2

Comment [DJG32]: Give values to 3sf

Eigenvalues and V_1 eigenvector and Isotropy (I) and Elongation (E) indices calculated from K_1 data. N is the number of sub-samples. Rows in italic and bold are the 7 bulk samples and sampling depths are depths below the flute crest or flanks. Each of the 7 samples is divided into an upper and lower depth interval (Int). SO is the sample orientation, P = portrait, and L = landscape orientation. SL is the slide length in the vertical plane. Sst = shear strain magnitude – these values are crude estimates based on applying the S_1 values to the S_1 shear strain calibrations presented by Iverson *et al*. (2008) for the Horicon till (Sst Horicon) and Batestown and Douglas tills (Sst other). In the ring shear experiments, steady state fabrics were achieved at $S_1 = 0.83+$.

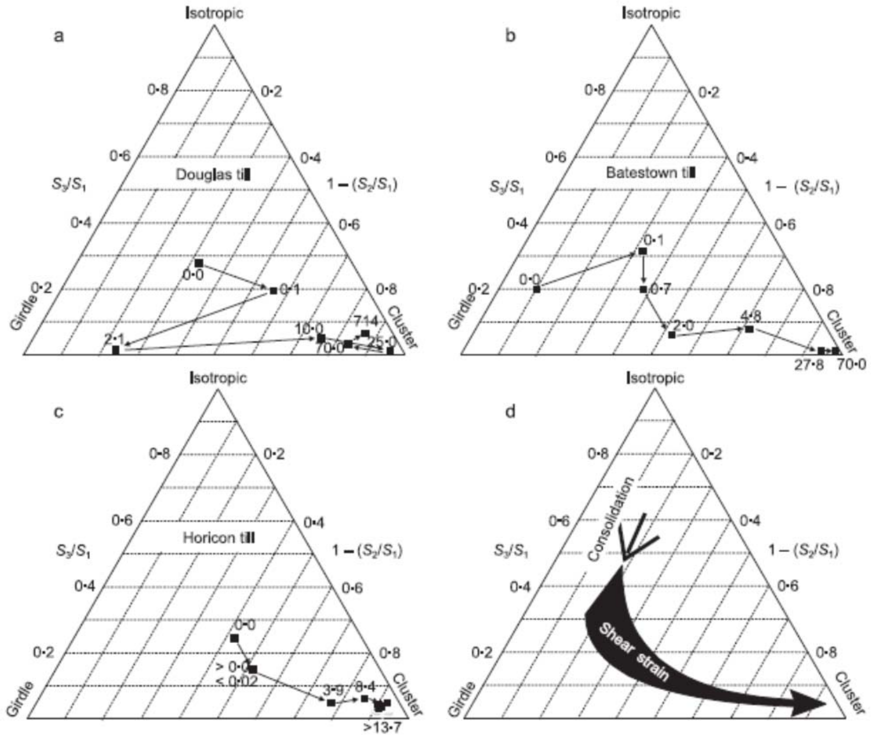

. Evolution of AMS k_1 fabric shape as a function of shear-strain magnitude (numbers next to points) for the (a) Douglas till, (b) Batestown till and (c) Horicon till, with (d) a generalization of the data. The change in fabric shape due to consolidation in (d) was not measured but is inferred from studies of consolidation fabrics (e.g. Deamer and Kodama, 1990; Schwehr *et al.*, 2006).

Figure 4.27a Ternary Diagrams showing the evolution of AMS fabric shape with increasing shear strain in ring shear experiments (from Iverson *et al*., 2008).

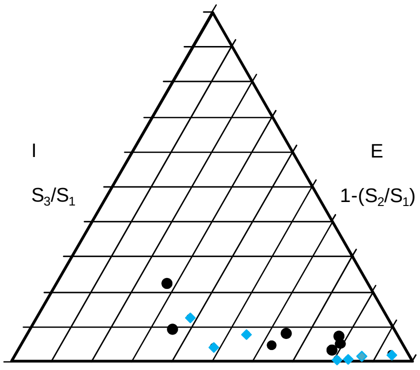

Figure 4.27.b Ternary Diagram showing AMS fabric shapes for the Isfallsglaciären flutes. Black circles are the fabric shapes for the 7 bulk samples, blue diamonds are the fabric shapes for the upper and lower vertical intervals (see text). The diagram is scaled using the same values as shown in Fig.4.27.a. Eigenvalues have been calculated from the orientation and plunge of the principal susceptibility axes (K_1).

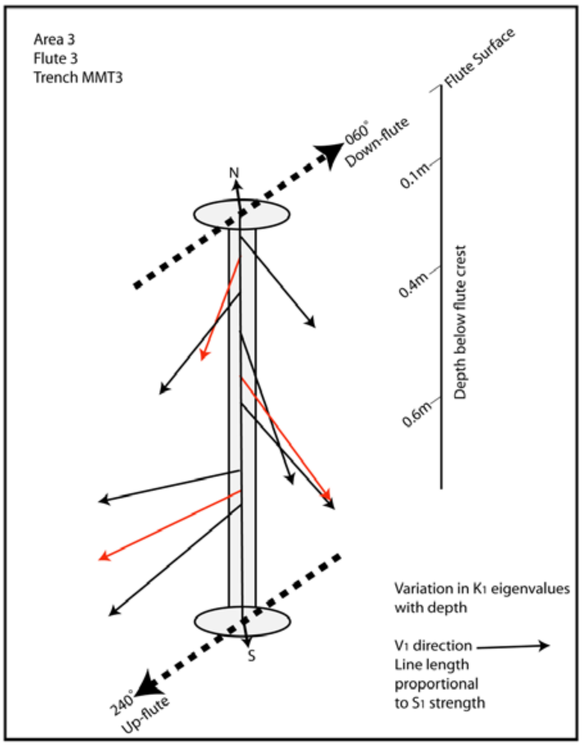

Figure 4.28 Changes in K_1 orientation and S_1 (K_1) strength over small vertical depth intervals, Trench MMT3. Note: MM9, MM8, and D1 were sampled from Lithofacies A.

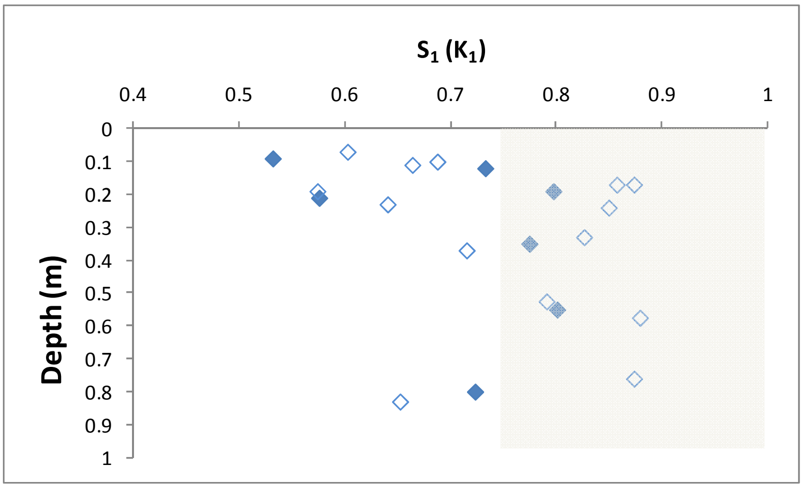

Figure 4.29 The Change in AMS fabric strength (S_1 Eigenvalue calculated from K_1 Data) with depth below the flute crest and flanks. Solid diamonds represent the 7 bulk samples and unfilled diamonds the upper and lower depth intervals within each sample. The shaded area represents the range of steady state S_1 eigenvalues quoted by Shumway and Iverson (2009) for the Douglas Till, in which sample points falling outside of the shaded area

had a less than a 5% chance of having been formed by unidirectional simple shear to strain magnitudes capable of inducing steady-state fabric strength. It can be seen that about half of the samples and 4 of the bulk samples fall outside of the shaded area and suggest only moderate strain magnitudes. Linear regression analysis returns an R^2 value of 0.083 for the data shown on the graph, with a t-test value of 1.31 and a p-value for a 1-tail test (H_1: AMS fabric strength decreases with depth) of 0.103, which is not significant at the 0.05% level of significance. Indeed, the weakest values are obtained nearer to the surface.

4.2.10 Discussion

a) Shear Strain and the Deforming-bed Model

The deforming-bed model is associated with very high shear strains in a pervasively deforming bed, typically estimated to be in the order of 10^2–10^4 (Hooyer *et al*., 2008). None of the bulk samples from the fluted moraine or diamicton plain suggest shear strain magnitudes >10, which in a pervasively deforming bed 0.5 to 1m thick would give a maximum horizontal displacement of between 5 and 10m. If this is true, then the deforming bed may have exerted a relatively minor influence on glacier dynamics during the Little Ice Age advance. One of the implications of limited till advection in a deforming bed is that macroscopically homogeneous subglacial diamicton and strong flow-parallel clast a-axis fabrics must be capable of being produced at moderate strains. The magnetic fabrics suggest that, although bed-deformation may have occurred, the magnitude of strain was orders of magnitude lower than required by the deforming-bed model.

b) Magnetic Fabrics and Shear Strain Magnitude

The aggregate strain ellipsoid for the flute samples is consistent with flow-parallel simple shear to moderate or high strains (rather than very high strains). Shumway and Iverson (2009) reported rapid changes in the plunge and orientation of K_1 and K_2 vectors over decimetre vertical scales in subglacial deformation tills, and similar changes are seen in the flutes and diamicton plain samples (for example, in Trench MMT3, Figure 4.28). The K_2 vector defines the plunge of the shear plane. In Trench MMT3, eigenvectors calculated using the orientation of the K_2 axes change with depth over 0.2m intervals. Near to the surface, V_1 plunges 14° at 119° (sample MM9), which changes to a plunge of 50° at 252° approximately 0.2m lower in the section (sample MM8), and then changes over the next 0.2m to 16°

plunge at 155° (that is, approximately transverse to flow in sample D1). Even if the estimates of shear strain magnitude based on comparisons with ring shear calibrations are uncertain, the variation in S_1 strength and K_1, K_2 and K_3 vectors over decimetre scales in Trench MMT3 are inconsistent with the notion of pervasive deformation to very high strain, which should produce unidirectional vector orientations (Shumway and Iverson, 2009). Likewise, at Storglaciären, the K_1 vector and S_1 strengths vary markedly over a 0.1m depth interval in sample SL1 (Table 4.8). In the Nordjåkk section, the plunge of the K_2 vector changes from NE to SE between the upper and lower samples. That is, the direction of plunge of the shear plane changed over a vertical interval of 0.9m.

Small-scale variations in magnetic fabrics in vertical till sequences have been interpreted as evidence of time-varying changes in strain and shearing direction in thin deforming layers, which accumulate to form thick diamicton sequences through slow incremental accretion (Shumway and Iverson, 2009). The vertical changes in the Storglaciären magnetic fabrics are consistent with this interpretation and the subglacial model of Piotrowski *et al*. (2004), which anticipates spatial and temporal variations in deforming-bed conditions. They are also consistent with the clast fabric data which suggested that Lithofacies B accumulated by the incremental accretion of deforming layers 0.3 to 0.6m thick.

Clast fabric data suggests the deforming-bed that produced the flutes was approximately 0.5m thick. Variations in magnetic fabric strength and vector orientation within this layer (for example, in MMT3) reflect either incremental accretion as the loci of deformation moved upwards over time, or strain partitioning. Although evidence has been provided to show that strain partitioning does not account for changes in macro-fabric strengths throughout the vertical profiles measured in the diamicton plain and fluted moraine sequences (Chapter 3.8.4), it may account for variations in magnetic fabric strengths measured at a smaller scale in relatively thin deforming beds. Strain is heterogeneous in a thin deforming bed because of micro-scale variations in granulometry and, critically, because low-strain zones develop in pressure shadows adjacent to larger clasts and embedded boulders (Evans *et al*., 2006; Phillips *et al*., 2001b). It is argued here that in a deforming bed 0.5m thick that contains a large number of lodged boulders and clasts, variations in magnetic fabrics likely reflect strain partitioning associated with the pressure shadows that develop adjacent to these boulders and clasts (see section e below).

The aggregate strain ellipsoid for the Storglaciären samples shows significant deviation from the steady-state simple shear strain ellipsoid. Indeed, the low plunge of the K_1 vectors is consistent with an element of pure shear superimposed on the strain ellipsoid (Evans *et al*., 2006). Pure shear is more dominant in proglacial and ice-marginal areas (McCarroll and Rijsdijk, 2003), where sediment compaction may result in the flattening of strain ellipsoids and a reduction in V_1 vector plunge (Evans *et al*., 2006). As such, the estimates of strain magnitude in the Storglaciären samples relate to a combination of simple shear and pure shear, whilst the less-clustered nature of the K_1 and K_3 axes relates to a greater degree of sediment compaction. However, none of the ellipsoids reveal particularly oblate ellipsoid shapes, as might be expected if there had been a significant element of pure shear (Tarling and Hrouda, 1993; Hus, 2003), and so the extent to which the ellipsoids have been flattened by compaction appears to be modest.

c) AMS Fabrics of Upper and Lower Vertical Intervals

The bulk AMS samples were taken over depth intervals of 0.09-0.18m. An important question to address is the extent to which this sampling interval is able to detect important variations in strain signature. By dividing the samples into upper and lower vertical intervals, some stronger S_1 values were obtained (Tables 4.8 & 4.9), some of which were equivalent to steady-state fabrics measured in ring-shear experiments. In addition, changes in vector plunge and orientation were observed over cm scales. For example, Figure 4.30 shows a closer clustering of K_1 and K_3 axes for 10 sub-samples taken from the lower 80mm of sample MM7 compared to the bulk sample. However, the reduced number of sub-samples in these smaller intervals would be expected to have an influence on S_1 values simply because the sample size is smaller, which means that less variation is likely to be measured and outliers will have a disproportionate effect; the stronger S_1 values may simply reflect the smaller sample size. As such, the estimated strain magnitudes for the smaller vertical intervals need to be treated with caution.

In Figure 4.28, the vertical changes in V_1 and S_1 (calculated for K_1 data) for three bulk samples (MM9, MM8 and D_1) are shown in red, with V_1 and S_1 values for the upper and lower vertical intervals for each bulk sample shown in black. The bulk samples (red) are sufficiently sensitive to detect changes in V_1 orientation and S_1 strength (each bulk sample covered approximately a 0.1m depth interval). However, the smaller sampling interval suggests that subtle variations may be missed. For example, the weak MM9 fabric seems to comprise two fabrics with near-perpendicular vectors, while both D1 and MM8 have one vertical interval that yields a much stronger S_1 value than the bulk sample. As such, the variations in magnetic fabrics from upper and lower vertical intervals may be recording evidence of strain partitioning (Evans *et al*., 2006), or time-transgressive variations in deformation in very thin accreting layers (Piotrowski *et al*., 2004; Shumway and Iverson, 2009). Alternatively, differential compaction may explain some of the small-scale variations in magnetic fabrics. Thin layers that have compacted more will have flattened strain ellipsoids with K_1 plunging at a lower angle compared to layers that experience less compaction (Evans *et al*., 2006). Differential compaction may explain the variations in sample MM7 (Table 4.9), where the upper layer records a weaker magnetic fabric and K_1 plunges at a relatively low angle (17°) compared to the lower layer which has a strong fabric and much steeper K_1 plunge (45°). In field situations, there are potentially several factors that can cause small-scale variations in magnetic fabrics, and it cannot be assumed that these variations reflect incremental accretion from thin deforming layers.

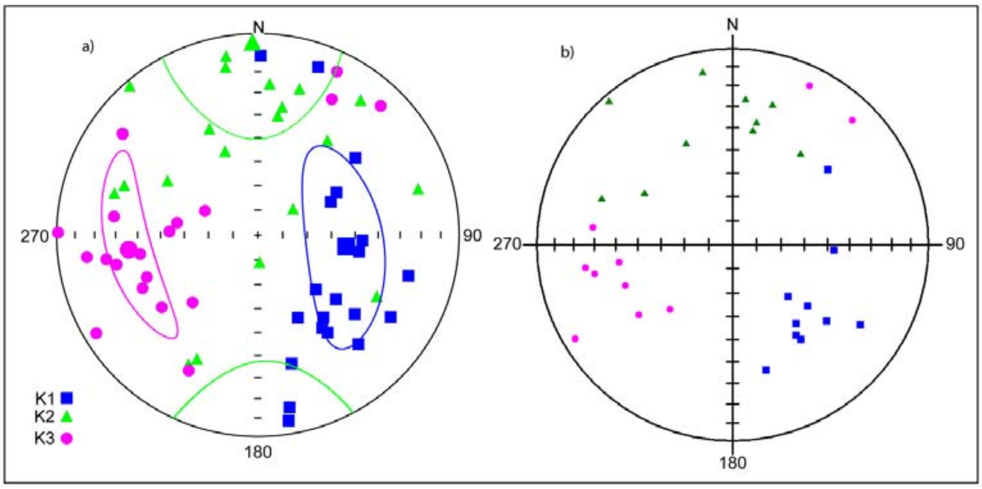

Figure 4.30 Stereoplots comparing the orientation of the principal susceptibility axes for the bulk sample (a) and lower interval sample (b) of Sample MM7.

d) Weak Magnetic Fabrics and Post-Depositional Disturbance

Weak magnetic fabrics can be indicative of post-depositional disturbances such as weathering, freeze-thaw and bioturbation (Hus, 2003; Iverson *et al*., 2008). An important question to address is the extent to which post-depositional processes may have modified magnetic fabrics at Isfallsglaciären and Storglaciären. Of the two weakest magnetic fabrics recorded in the flutes, MM9 was taken at a shallow depth near to the surface, and MMT4 was taken in the distal zone of flute 3. Aerial photographs show that the glacier had retreated from area 3 by 1959, and Karlén (1976) suggested the distal end of Area 3 may have been subaerially exposed by 1940 (Figure 4.1). As such, samples from the distal part of Area 3 may have been exposed to paraglacial processes for 20 years longer than samples from the proximal flute zone where near-surface magnetic fabrics are stronger (BYL/MM7), and this may explain the weaker magnetic fabric in MMT4. The magnetic fabric from Trench TT, taken at 0.8m depth in the distal zone shows a relatively strong S_1 value, which suggests that it is the near-surface samples (top 0.2m) that may have been most affected by post-depositional disturbances.

Hus (2003) showed that large deviations in the principal and minimum susceptibility axes in magnetic fabrics could be caused by bioturbation; cryoturbation, which involves a similar mixing of sediment layers, is likely to have a similar impact on magnetic fabrics. In addition, Hus (2003) demonstrated that weathering and soil forming processes produced a less open microfabric due to the redistribution of fines and clay translocation, which produced a decrease in anisotropy and foliation, whilst increased compaction upon burial caused an increase in oblateness and foliation with depth. However, most of the seven flute samples and diamicton plain samples have only weakly oblate or triaxial strain ellipsoids, and most of the flute magnetic fabrics show relatively strong K_1 lineations that are consistent with simple shear. There is little evidence of overprinting by weathering or soil-forming processes. For example, oblateness and foliation do not increase with depth (Table 4.6), and the near-surface samples BYL and MM7 both have relatively strong magnetic fabrics. In sample BYL the strong magnetic fabric for Lithofacies A and strain ellipsoid is consistent with steady-state simple shear. However, there is a slight decrease in the magnitude of the anisotropy nearer to the surface, which may indicate a degree of disturbance to some near-surface magnetic fabrics. The relatively wide-range of K_1 and K_3 orientations and plunges in samples MM9 and

MM8 may reflect disturbance by cryoturbation, and this will be investigated further in the next chapter where thin sections are analysed.

AMS sub-samples are 2cm^3 cubes and AMS readings are for bulk volumes. Such a volume samples many particles and intervening matrix – some of which might be disturbed, some not– and given that magnetite is the magnetic carrier of the AMS signature, it is the ratio of disturbed to undisturbed magnetite grains that likely controls the extent to which a subglacial fabric is overprinted by post-depositional disturbances. Given that cryogenic influences decrease with depth (Harris, 1998), it is likely to be the shallow magnetic fabrics that are most disturbed. Another possible source of disturbance is the flow of water along the fissile partings, which might cause silt-sized grains of magnetite to re-align. However, in sample D1 the fissile partings mainly dip down-flute and so deposition from flowing water should produce a fabric with K_1 transverse to the flute axis and K_3 plunging up-glacier (Tarling and Hrouda, 1993). As this is not the case (Figure 4.22), this hypothesis can be rejected for D1. However, some secondary clusters of K_1 axes that are transverse to flow (for example, in MM7) may relate to this process. Overall though, the aggregate flute strain ellipsoid is consistent with simple shear to moderate or high strains, which suggests that the influence of post-depositional disturbances on magnetic fabrics maybe localized to very shallow depths and limited in effect.

e) Transverse AMS Fabrics, Ploughing and Lodgement

Complex strain gradients may occur in the vicinity of ploughing and lodged boulders in a deforming bed (Boulton, 1976; Benn, 1994). Some of the flute magnetic fabrics which develop K_1 lineations transverse to the glacier flow direction may relate to the influence of complex strain patterns adjacent to boulders. For example, an element of horizontal compression ahead of a ploughing boulder, applied to sample D1, would produce a strain ellipsoid like that shown for sample MM8. In Trench MMT3 a large boulder is embedded on the right flank (see Figure 3.13). The long-axis of the boulder parallels the flute axis and flow-parallel striae occur on the boulder surface, suggesting the boulder was transported subglacially then lodged. The base of the boulder is at 0.4-0.47m depth, adjacent to where the magnetic fabric (MM8) with a K_1 lineation transverse to the flute axis occurs. If this boulder did plough prior to lodgement then it could explain the transverse fabric. Alternatively, the silty-fine sand matrix may have continued to flow or deform around the lodged boulder.

Strain would have been directed towards the lee-side pressure shadow (Benn, 1994) and this could have locally disrupted the magnetic fabric, especially to the lower left-hand side of the boulder at approximately 0.3-0.45m depth where the boulder face is oblique to the flute axis. Similarly, sample MM7, which has a longitudinal flow plane pointing more up-glacier than down, was taken a few metres up-flow from a huge embedded boulder, and the magnetic fabric may reflect local deviations from simple shear in the vicinity of the boulder where horizontal compression was high. That similar magnetic fabrics are not produced in ring shear experiments probably reflects the inability of laboratory experiments to handle larger clasts and the uniform nature of shear in ring-shear apparatus. Finally, it should also be borne in mind that subglacial diamictons can be highly variable in magnetic mineralogy, with different suites of minerals producing different strain ellipsoids and AMS values, and that it may be an over-simplification to equate K_1 lineations to strain (Fleming *et al*., 2013).

4.2.11 Conclusions

Estimates of strain magnitude derived from magnetic fabrics measured in field studies and calibrated against magnetic fabrics derived from ring shear experiments need to be treated with caution. Nevertheless, the flow-parallel aggregate AMS strain ellipsoid for flutes is consistent with simple shear to moderate or high strains by overriding ice, an observation which accords with the clast fabric findings from Isfallsglaciären. Strain ellipsoids for individual samples are variable and S_1 values obtained from the orientation of K_1 susceptibility axes suggest strain magnitude varied over small vertical and spatial scales. S_1 values from the bulk samples (measured over 90 to 180mm depth intervals) from flutes and the diamicton plain indicate moderate strain magnitudes (≤10) rather than the very high strain magnitudes required by the bed-deformation model ($>10^2$). Sampling at higher spatial resolutions (40 to 80mm depth intervals) did reveal some S_1 values indicative of higher strains in Lithofacies A from flutes. At the higher spatial resolution of sampling K_1 vectors and strengths varied markedly over ≈0.1m depth intervals.

The magnetic fabrics and aggregate strain ellipsoid are generally consistent with the clast fabric measurements for Isfallglaciären, except that weaker magnetic fabrics are recorded near to flute surfaces. The moderate to high strain magnitudes indicated by the bulk magnetic fabric measurements are consistent with clast fabric observations in Isfallsglaciären which suggest that the advection of Lithofacies A was limited. At Storglaciären, variations in K_1

vector orientation and strength over small vertical scales are consistent with clast fabric observations that suggest Lithofacies B formed by accretion from thin deforming layers rather than by pervasive deformation throughout its entire thickness. The very high strain magnitudes required by the deforming-bed model are not observed in the Storglaciären samples, even at higher spatial resolution. The estimated strain magnitudes for the diamicton plain samples are only moderate (≤10), which suggests bed deformation may have had a limited control on glacier dynamics during the Little Ice Age advance. However, the aggregate strain ellipsoid deviates from the simple-shear strain ellipsoid in that K_1 vectors have relatively low plunges, consistent with an element of sediment compaction and pure shear. Other deviations from the strain ellipsoid indicative of flow-parallel simple shear most likely relate to post-depositional disturbance by cryoturbation for near-surface samples (top 0.1 to 0.3m depth), deviations from simple shear in the vicinity of ploughing or lodged boulders, or localised variations in strain magnitude over time in an accreting layer. Indeed, some of the small-scale variations in K_1, K_2 and K_3 vectors and S_1 values lend support to the ice-bed mosaic model in that they suggest deforming-bed conditions were variable in time and space. However, these variations may also reflect a degree of strain partitioning or differential sediment compaction.

Chapter 5 The Micromorphology and Micro-structural Mapping of Subglacial Sediments

Introduction

In this chapter, thin sections are used to establish information on glacial sediment processes such as till genesis and transport. Specifically, micromorphology and micro-structural mapping are used for the first time to investigate the nature and history of sediment deformation and the extent of periglacial overprinting in thin section samples taken from the Isfallsglaciären flutes and the Storglaciären diamicton plain. The thin sections were taken from sites where graphic logs, clast fabrics and magnetic fabrics were recorded. As such, the micro-scale analysis provides additional insights into the nature of deformation at these locations and compliments and informs the larger-scale observations. The chapter begins with a description of thin sections and a presentation of micro-structural maps for flute samples. The flute thin sections are then analysed and the extent of periglacial overprinting established. The nature and polyphase history of deformation is then discussed in relation to the soft-bed deformation model and models of flute formation. Thin sections from the diamicton plain are then described and micro-structural maps presented. The diamicton plain samples are then analysed and the nature and polyphase history of sediment deformation discussed. The terminology used to describe the relationship between different elements revealed by the micro-structural map is summarised in Figure 5.1 (Phillips *et al*., 2011b). In combination, micromorphology and micro-structural mapping reveal information about the nature and history of subglacial deformation and the extent of periglacial overprinting that is not apparent at the macro-scale in homogeneous diamictons (van der Meer, 1993; Harris, 1998; Phillips *et al*., 2011b).

5.1 Thin Sections from the Isfallsglaciären Flutes

Six thin sections were selected for detailed micro-scale analysis from Area 3 of Isfallsglaciären (the location of the sample sites are shown in Figure 3.11 and the Trench and thin section codes explained in Table 5.1). Area 3 was selected for investigation because it is where flutes are best exposed and because the thin section analysis complemented the detailed magnetic fabrics and clast fabrics taken in this area. Three of the thin sections (MM9, MM8 and D1) were taken in vertical sequence below the flute crest in Trench MM3, which occurs about a third of the way along flute 3 (Figures 3.2 and 5.2.a) in a part of the forefield that was subaerially exposed between 1945 and 1965 (Karlén, 1973). The reason for sampling at different depth intervals was to see whether the nature of deformation and the extent of periglacial overprinting changed with depth. This site was chosen because flute 3 is a prominent flute and Trench MM3 was a major trench excavated for detailed lithofacies, clast fabric and magnetic studies. Furthermore, Lithofacies A was relatively thick and well-exposed and sufficiently friable to allow micromorphological samples to be extracted. The high cost of thin section production meant that a limited number of samples could be prepared, so vertical sequences were not established for other trenches. Thin section BYL was taken from the left flank in the proximal zone of flute 2. This site was chosen because it allowed sampling across the boundary between Lithofacies A and the Frontsjön sand unit, enabling the nature of the contact to be examined (Figure 5.2.b). Samples HF1 and MMTT were taken from the proximal and distal zones of flutes in order to contrast Lithofacies A samples that were subaerially exposed to paraglacial processes for different lengths of time. Sample MMTT was taken from the distal reaches of flute 1, which was exposed shortly after 1945 (Figure 5.2.c). This site was chosen because it was where Lithofacies A was thickest and it allowed a sample to be collected from a depth of 0.75 to 0.85m. Sample HF1 was taken from a flute crest in Area 1 (Figure 5.2d). The historical photographic archive at the Tarfala Research Station shows Area 1 was still occupied by the glacier in 1969 (Figure 3.2a) but was exposed some time before 1987.

Table 5.1 Trench and Thin Section Codes

Trench and Thin Section Codes	Explanation
Trench MMT3	The MM signifies that micromorphology samples (MM) were taken from this trench. T3 was the 3rd trench excavated into flute 3 in area 3
Thin sections MM9 MM8	MM9 and MM8 were the 8th and 9th MM samples taken during the study and were extracted in vertical sequence below the flute crest. The base of the sample tin was at 15cm in sample MM9 and at 40cm in sample MM8. Both sample Lithofacies A.
D1	The base of D1 was at 60cm depth. This sample was taken below the flute crest and samples across the lithofacies A and C boundary. D1 signifies that this was the first sample collected with the purpose made sample tin (D for 'Daves's tin') as opposed to a standard kubiena tin (see Chapter 2.4.2). The code D1 enabled this sample tin to be easily identified from other samples
Thin section BYL	The base of the tin was at 30cm depth. BYL signifies that this sample comes from a trench taken 'by the lake', that is, near to Fronstjön. The sample was taken from the left flank of a flute across the boundary of Lithofacies A and the Fronstjön sand unit
Trench and thin section MMTT	MM signifies a micromorphology sample was taken from this trench. The TT signifies that this trench was the 'terminal trench' excavated in flute 1, that is, the one excavated at the distal end of the flute. The same code was used for the thin section as it was the only sample collected in this trench. The base of the sample tin was at 90cm and sampled across Lithofacies A and a similar looking diamicton substrate
Thin section HF1	The base of the sample tin was at 30cm depth and sampled Lithofacies A from the crest of flute 1 (F1) in area 1. The H signifies this sample was excavated from the 'high' point of the forefield nearest to the present glacier terminus
Thin section MMS2	MMS2 refers to the second micromorphology (MM) sample taken in Storglaciären (S2). The base of the tin was at 80cm depth and sampled Lithofacies B at log NL2 (that is, Nordjåkk log 2)
Thin section SL1	The first micromorphology sample taken at Storglaciären and extracted at Sydjåkk log 1 (SL1). The base of the tin was at 80cm depth and sampled across Lithofacies B and SG

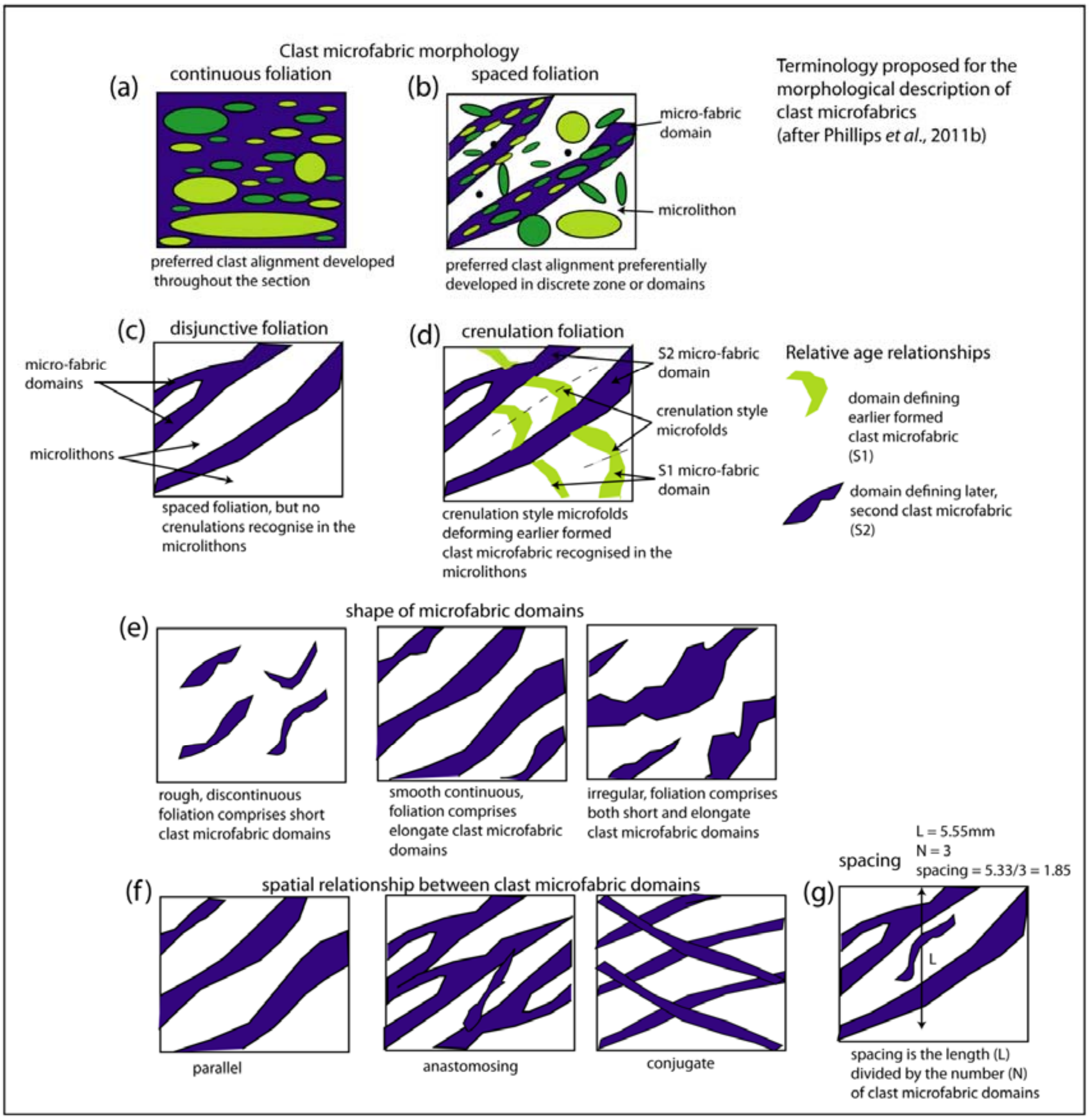

Figure 5.1 Terminology used to describe micro-structural maps (after Phillips *et al*., 2011b).

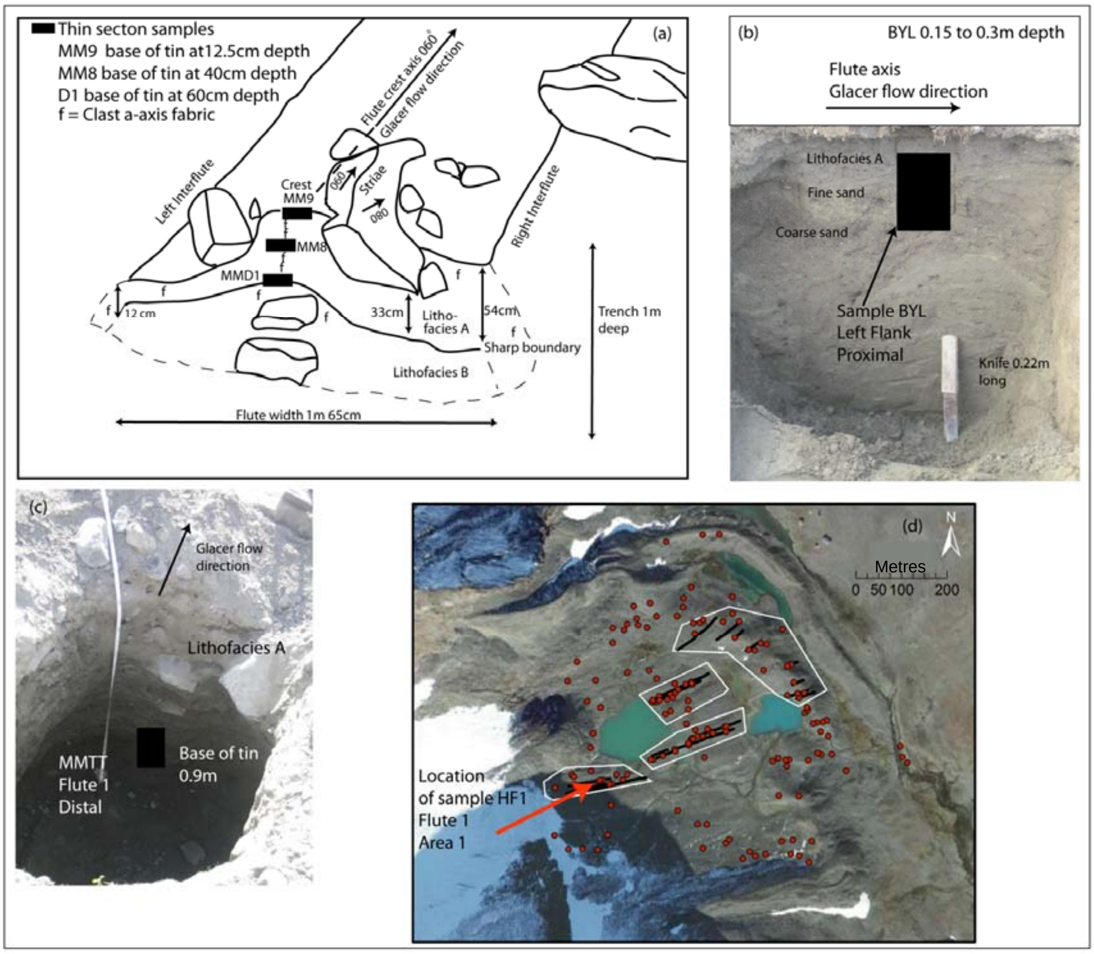

Figure 5.2a-d Locations of thin section samples, Isfallsglaciären flutes. (a) Trench MMT3 Area 3, flute 3, mid-way along the flute, samples MM9, MM8 and D1 from Lithofacies A. (b) Sample BYL, taken from the left flank of Flute 2 across the Fronstjön sand unit and Lithofacies A contact. (c) Sample MMT3 from flute 1, Area 3, distal zone, taken across two similar looking diamictons separated by a 2cm thick sand layer. (d) Location of sample HF1 from flute crest, flute 1, Area 1, more recently subaerially exposed, probably within the last *ca*. 30 years.

5.2 Description of Flute Thin Sections

5.2.1 Thin Section Samples from Trench MMT3

Thin section MM9 taken from the shallowest depth shows a relatively coarse, homogeneous Lithofacies A with an open and highly porous texture consisting of numerous void spaces (Figure 5.3). Like all Lithofacies A samples, the diamicton is poorly sorted and contains sub-angular to sub-rounded lithic clasts from many different sources, of which dolerite and amphibolite are the most abundant. Most dolerites in Lithofacies A consist of unweathered interlocking crystals of plagioclase feldspar and pyroxenes, some of which exhibit good 90° cleavage (that is, two cleavage planes intersecting at 90°, which is a diagnostic feature of pyroxenes). Olivine-rich dolerites also occur and occasional dolerite clasts exhibit a more rotten and weathered appearance. The amphibolite in Lithofacies A is dominated by fresh crystals of twinned plagioclase feldspars and by amphiboles. The amphiboles show strong pleochroism (typically brown to blue) and 120° cleavage. Lesser amounts of garnet-mica schist and banded gneiss occur. A few large lithic fragments are composed of weakly metamorphosed sandstones (meta-sediments) which exhibit relict primary sedimentary structures. In thin section MM9, the largest clasts have diameters of 12 to 18mm. These are concentrated in the top right of the thin section, where the clasts show a crude preference for being relatively steeply inclined (25° to 30°) in an up-flow direction. The diamicton matrix has a 'washed' appearance with slightly darker matrix patches reflecting areas of the thin section relatively rich in silt.

There are three main types of voids present in sample MM9:

1) vughs, which are irregular-shaped voids occurring in isolation within the matrix (Kilfeather and van der Meer 2008). Some vughs are observed to be star-shaped (Figure 5.4);

2) linear voids consisting of strings of bubble-shaped or irregular shaped voids (vughs) that are between 0.1and 0.25mm thick. Linear voids are relatively short in MM9 being 1 to 3mm long, and form sub-parallel to steeply inclined structures (Figure 5.3b);

3) the lower part of the thin section is dominated by larger voids (up to 1mm thick) which have smooth-shaped walls. Many of these larger voids form around or along the edges of larger lithic clasts (Figure 5.4).

All three types of voids display a clean appearance with little evidence of fine sediment deposition within them.

On the upper surface of each large lithic clast and coarse sand grain in sample MM9, thick caps of silt and grains of very fine sand form graded and crudely laminated structures known as silt caps (Harris, 1998; Van Vliet-Lanoe, 2010). Different types of silt caps have been observed in polar sediments; Type 1 silt caps are restricted to the upper surfaces of clasts, whereas Type 2 silt caps occur on upper surfaces and the sides of clasts, whilst Type 3 silt caps encircle clasts and occur on their undersides as well as upper surfaces (Bockheim and Tarnocai, 1998; Van Vliet-Lanoe, 2010). In thin section MM9, silt caps are 0.1 to 1.5mm thick and Types 1, 2 and 3 occur in the upper 40mm of the sample. Type 2 and 3 silt caps form rounded asymmetric coatings which occur on the sides and undersides of clasts. In some cases Type 1 silt caps have become detached from the upper surfaces of larger clasts (Figure 5.4). The thickest silt caps contain crude laminations of very fine sand and fine silt which parallel the surface of the clast. Irregular-shaped vughs and lenticular voids occasionally occur within the thicker silt caps.

In thin section MM9, 46 clasts with silt caps were counted in the upper 1.5mm of the sample, of which 80% were Type 1 silt caps. In the central 1.5mm of the sample, 51 clasts with silt caps were counted, with 88% being Type 1 silt caps. In the bottom 1.5mm of the sample a smaller number of silt caps occurred, with 34 clasts having silt caps with no Type 2 or 3 silt caps in evidence. In general, below the top 40mm of sample MM9, Type 2 and Type 3 silt caps are very rare and they are not observed at 0.5 to 0.6m depth in thin section D1. Type 3 silt caps are generally restricted to the upper *ca*. 0.1m of Trench MMT3. Indeed, silt caps become thinner and less frequent with depth in the flute samples (Figures 5.5 and 5.6). In thin section MM8, silt caps are only between 0.1 and 0.2mm thick, whilst in thin section D1 silt caps are 0.08 to 0.1mm thick. In samples MM8 and D1 silt caps occur on the upper surfaces of many steeply inclined clasts (Figures 5.5 and 5.6). In sample MM8 a prominent clast has a triangular shaped silt cap on its upper surface (Figure 5.5a) which grades upwards from coarse to fine and is followed up-sequence by faint laminations which resemble micro-ripples (Figure 5.7). The faint laminations and graded laminations are truncated on the right hand side by silty laminations.

The upper part of thin section MM8 is dominated by a large dolerite clast with an apparent long-axis diameter of 55mm inclined up-flow at an angle of 20°. Many large lithic clasts have apparent long axes steeply inclined (40° to 70°) up-flow. Below the large dolerite clast the diamicton has a platy structure and is highly fissured (Figure 5.5b). The fissures in the lower part of the thin section are inclined down-flow at 10° to 15°, whereas the fissures immediately below the large clast are steeply inclined up-glacier. The fissures in sample MM8 consist of linear strings of bead-like voids which are bubble-shaped or irregularly shaped and up to 0.4mm thick. The fissures appear generally clean and devoid of sediment, although under higher magnifications (x40) very thin films of silt can occasionally be seen lining the walls of some linear voids. Some of the fissures can be traced for several centimetres. Similar laterally extensive fissures consisting of linear voids are observed in all flute thin sections, although they are shorter and less well-developed in samples MM9 and HF1, and these linear voids, along with contraction voids, demarcate the fissile partings of Lithofacies A (Figure 5.8).

In thin section D1 there are fewer fissures than in sample MM8 and the diamicton has a more compact and less porous appearance (Figure 5.6). Small vughs occur in sample D1 and some of these have silty coatings around the edges of the voids which are known as silt cutans (Carr, 2004). Larger smooth shaped contraction voids occur along the edges on larger lithic clasts (Figure 5.8). The sample tin was cut across the boundary of Lithofacies A and C but this boundary, which appears sharp and wavy at the outcrop scale and is readily demarcated by a contrast in gravel content, is not obvious in the thin section. Lithofacies boundaries that appear obvious at the outcrop scale are often not seen in thin sections (van der Meer *et al*., 2010a).However, the thin section can be divided into two areas, which probably correspond to the two lithofacies present; area A occurs in the upper section of the sample and has a greater concentration of linear voids (fissures) which are mostly inclined down-flow at *ca*. 25° (Figure 5.6b). Area A consists of numerous pebble-sized clasts with diameters of 4 to 7mm and a greater concentration of Type 1 silt caps occurs in this zone. The lower part of the thin section, Area B, has fewer linear voids, fewer and thinner silt caps, and a number of lithic clasts mainly inclined up-flow.

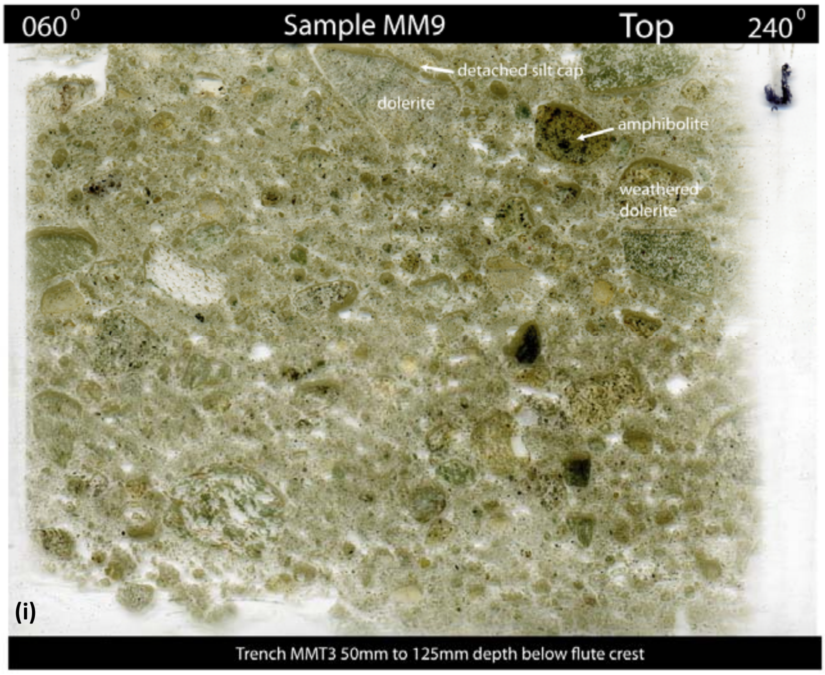

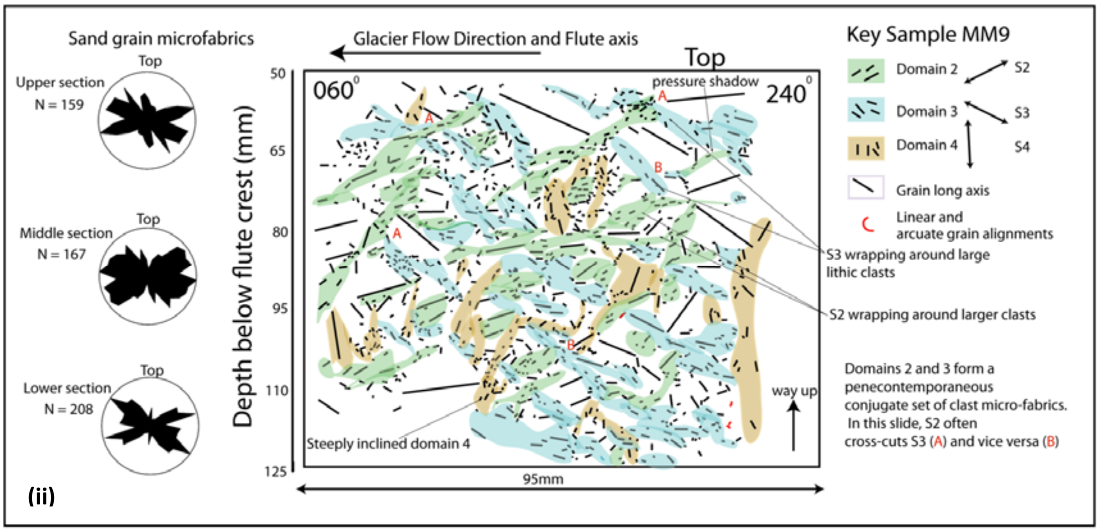

Figure 5.3a(i) Thin section MM9 from near the flute surface, Trench MMT3 and (ii) Micro-structural Map. Note the relatively open, porous nature of Lithofacies A in this sample and the abundance of silt caps.

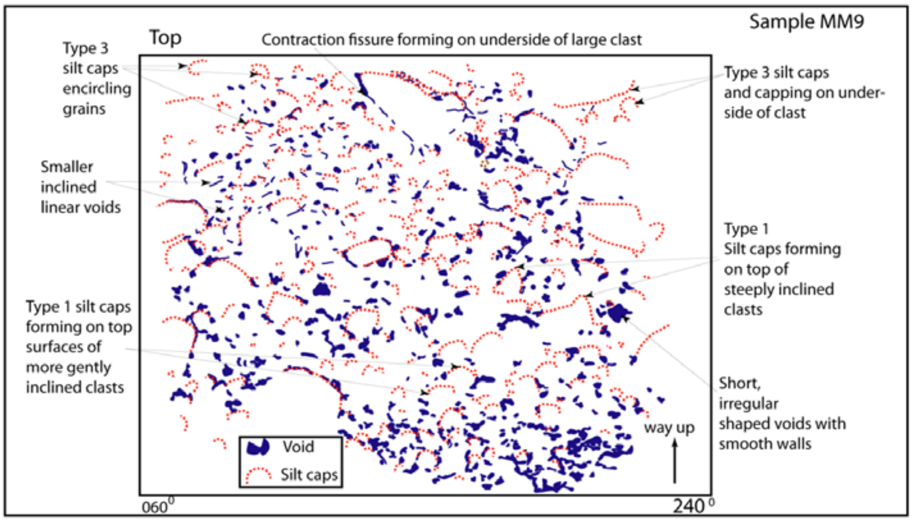

Figure 5.3b Silt Caps and voids in Sample MM9

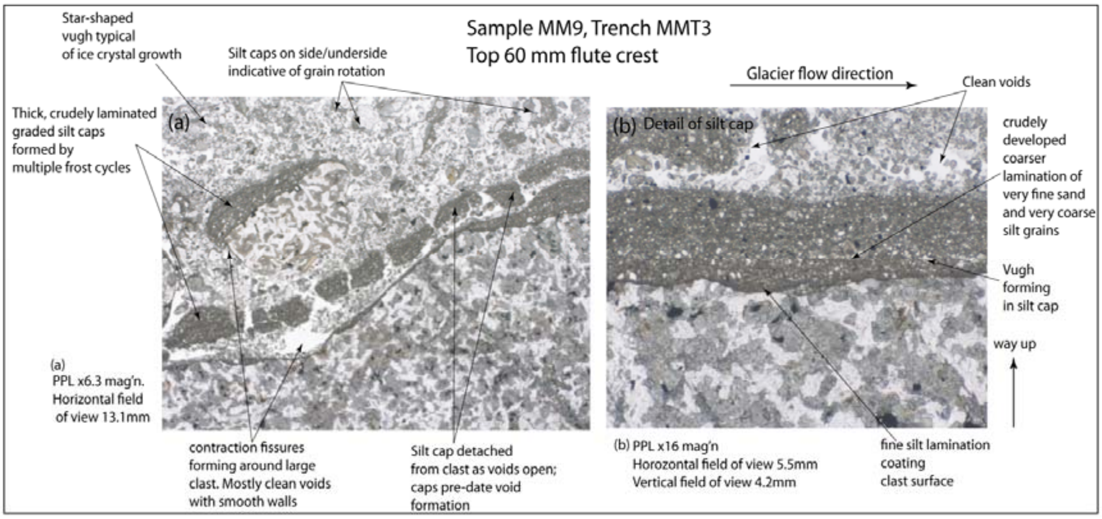

Figure 5.4 Magnified view of silt caps and voids, Sample MM9. (a) Detached Type 1 silt cap forming on top of a lithic clast of dolerite. (b) Close up of Type 1 silt cap on dolerite clast.

Figure 5.5a(i) Thin Section MM8, Trench MMT3, Flute 3, Area 3, Isfallsglaciären. The scale bar is shown in Figure 5.5a (ii) below. Note the highly fissured area, especially to the bottom left of the large dolerite clast, and the slightly lighter coloured matrix area, which has a 'washed appearance' in the centre of the section just below the large dolerite clast. The 2-D micro-fabrics shown on rose diagrams in Figure 5.5a (iii) below are constructed by measuring the orientation of the long axis of clasts with the top of the thin section acting as 'north'. N = the number of clasts measured in each case. Note how the fabric becomes multi-modal in the centre area below the large dolerite clast, consistent with a relative lack of strain and hence grain alignment in a pressure shadow. The red box in Figure 5.5a (i) demarcates the area where a triangular shaped silt cap occurs. This silt cap is shown in detail in Figure 5.7 below.

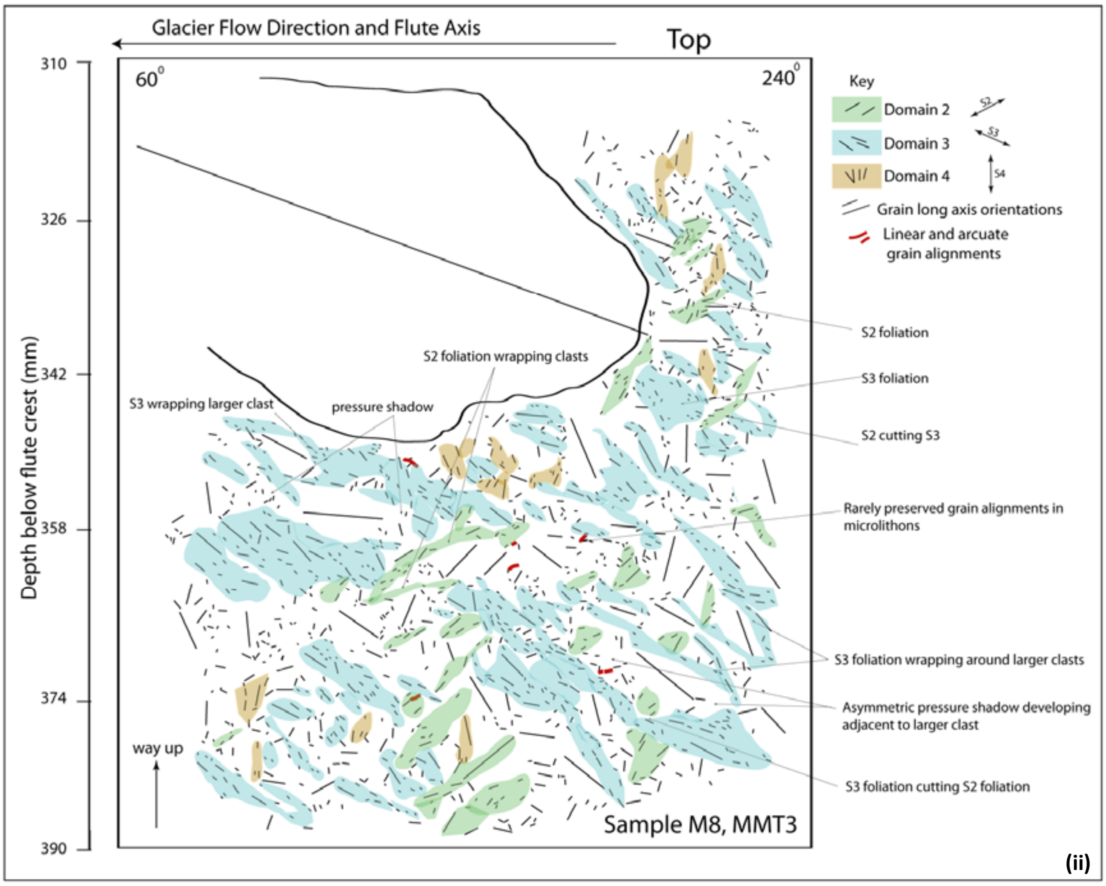

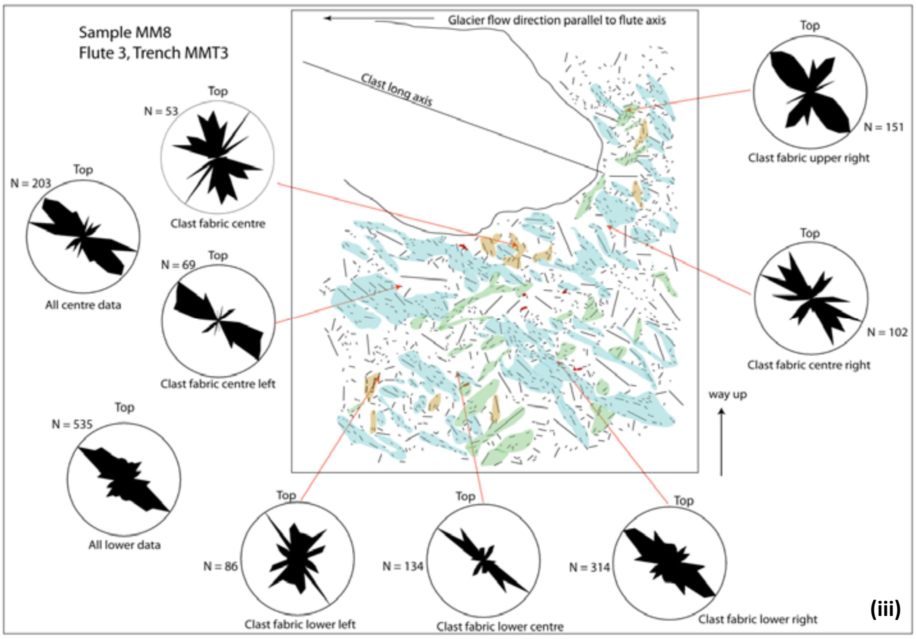

Figure 5.5a(ii) Micro-structural map sample MM8 with scale bar. (iii) 2-D Micro-fabrics Sample MM8.

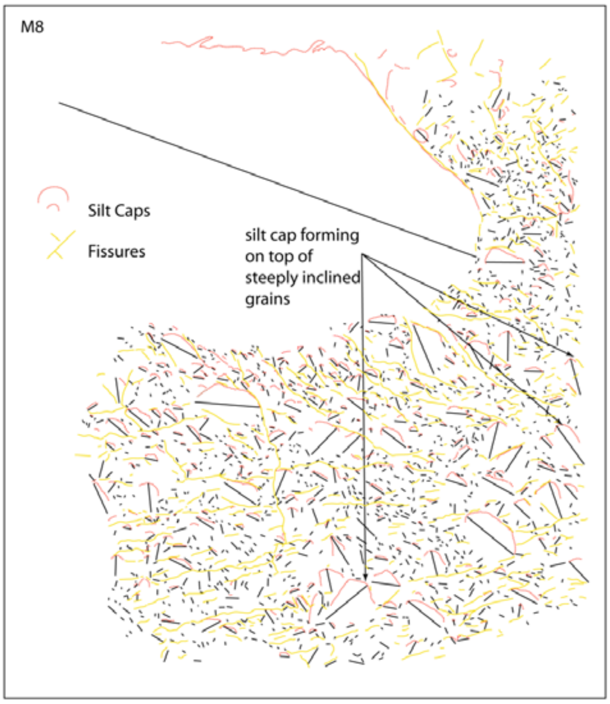

Figure 5.5b Fissures and silt caps, Sample, MM8 (apparent clast long-axes are shown as black lines)

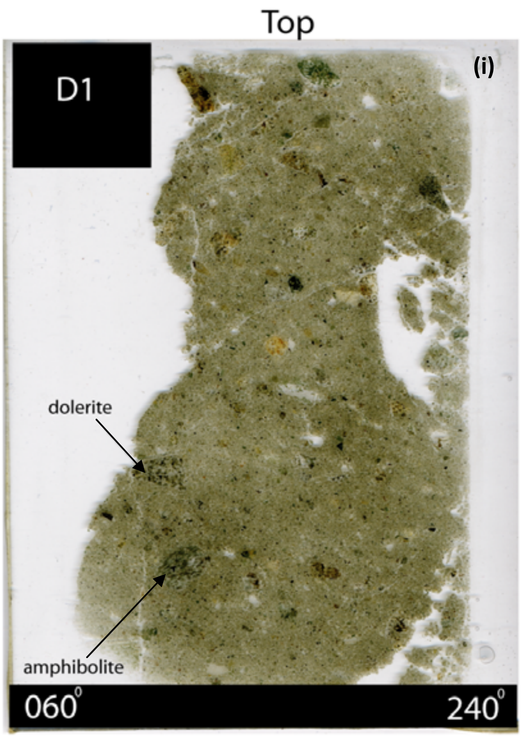

Figure 5.6a(i) Thin section D1, 0.5-0.6m depth, Trench MM3 (scale bar shown below of Figure 5.6a(ii).

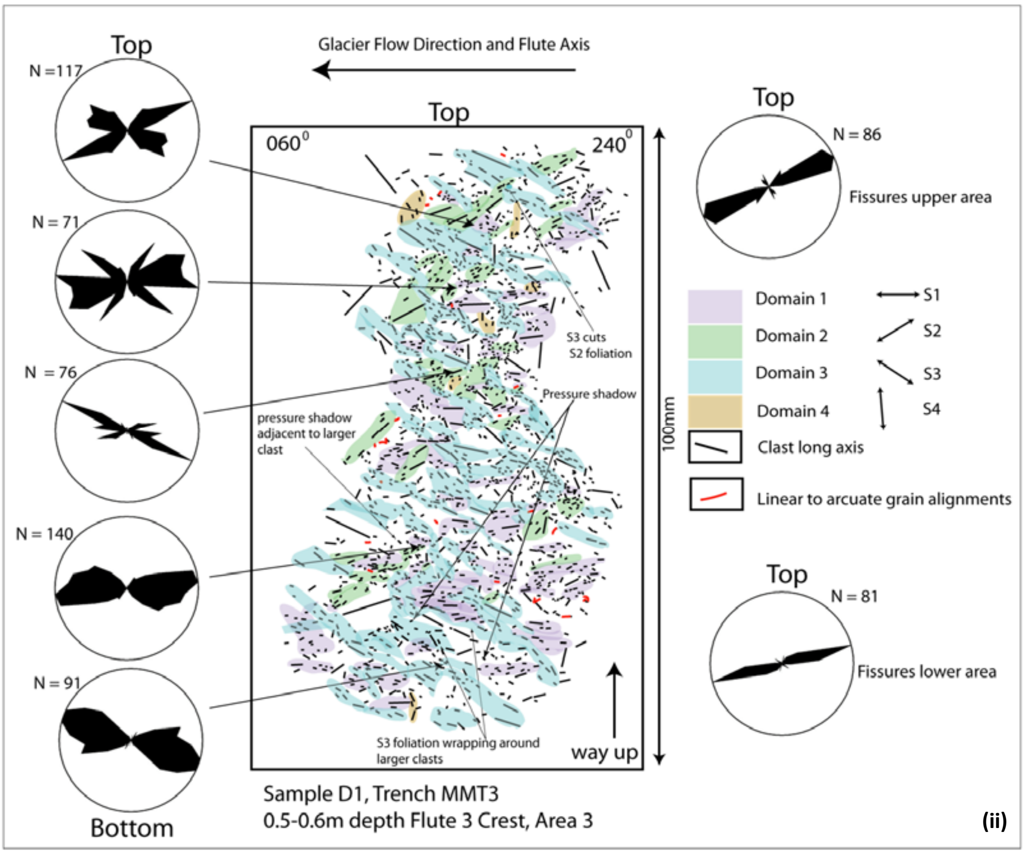

Figure 5.6a (ii) Micro-structural map for Thin Section D1. Note the appearance of the S1 micro-fabric which forms short lens-shaped domains (domain 1), especially in the lower half of the thin section.

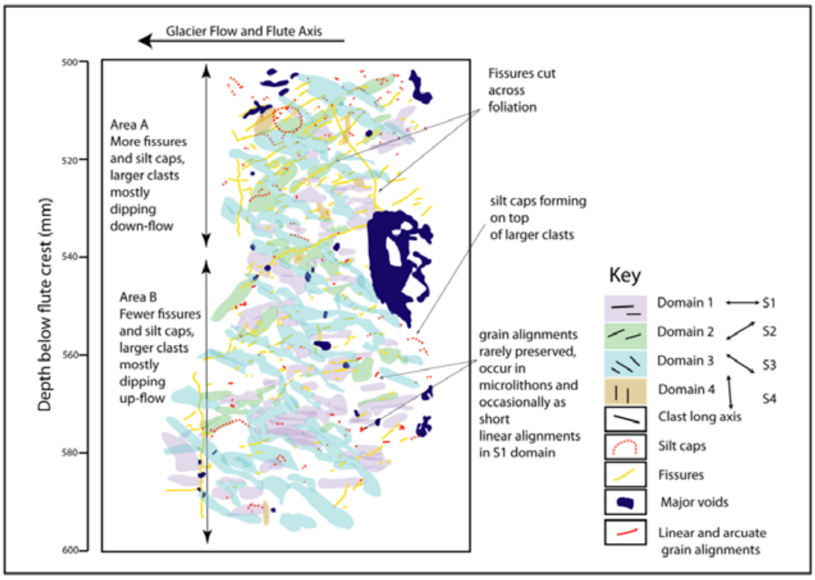

Figure 5.6b Fissures, voids and silt caps in Sample D1.

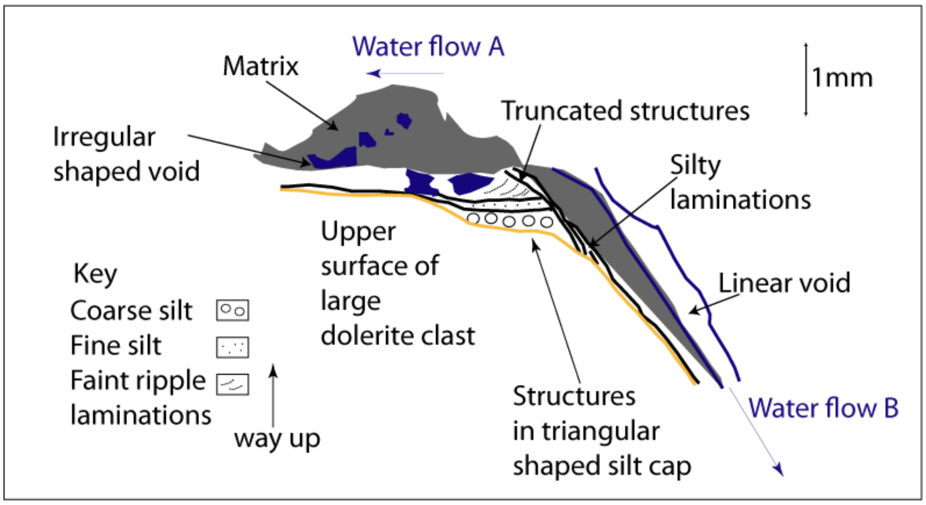

Figure 5.7 Detail of erosion and deposition in silt cap structure from thin section MM8. The coarse silt layer and faint ripple laminations were deposited first by water moving along the upper surface of the large dolerite clast (area shown in Figure 5.5a (i) above). The inclination of the ripple laminations suggest water moved right to left. These structures are truncated by the silty laminations on the right-hand side of the large clast, which suggest water flow along the linear void (water flow B). This silt cap structure relates to water flow, probably following thaw consolidation or snowmelt. These silt caps represent multiple phases of erosion and deposition.

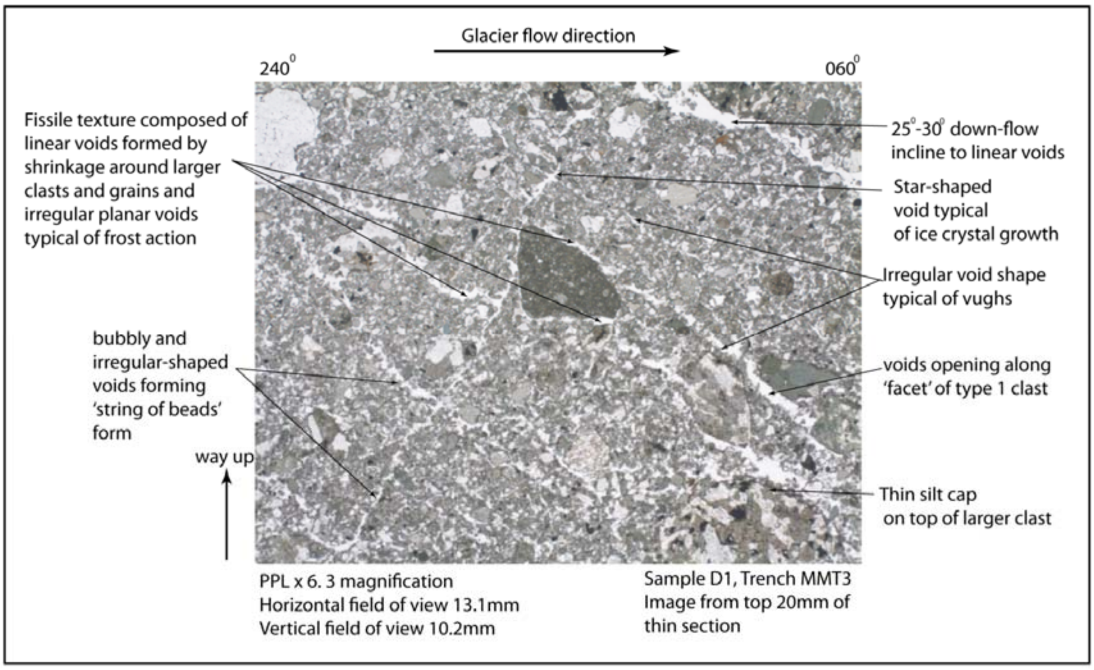

Figure 5.8 Detail of voids in Thin Section D1.

5.2.2 Thin Section Samples from the Distal and Proximal Flute Zones

Thin section MMTT represents the deepest flute sample and was taken from the distal end of flute 1 in Area 3. The thin section reveals a relatively compact diamicton with a silty matrix. A number of large smooth-edged voids up to 3mm wide and 21mm long occur in the middle and lower part of the section. Some of these voids have irregular shapes and are steeply inclined (Figure 5.9). The upper part of the thin section has a slightly darker colour compared to the more 'washed' lighter appearance of the lower and middle sections. The upper section has more sub-parallel linear fissures than the lower section. Compared to other flute samples, the linear voids in MMTT are thin and Type 1 silt caps are very thin and only observed at higher magnifications (thickest cap observed 0.1mm thick). The fissures are not as laterally extensive as seen in other flute samples and are generally clean, although thin silt coatings are observed on some steeply inclined linear voids at higher magnifications (x40). Isolated vughs occur throughout the matrix. A number of larger clasts with apparent long-axes up to 15mm occur in the bottom right of the sample. Clast long-axes vary in orientation throughout the sample; many have steep inclinations up or down-flow or are sub-parallel. The central part of the slide is relatively devoid of larger clasts. A few clasts are observed to have coatings of fine matrix encircling and adhering to their outer surfaces (van der Meer *et al*., 2010a). Linear grain alignments occasionally occur along the edges of fissures in sample MMTT. A linear grain alignment is defined as four or more similar-sized grains that are in contact and have their long-axes aligned in the same orientation (Larsen *et al*., 2006). In the flute thin sections, linear grain alignments are rare. Where they occur, they are sub-parallel or inclined at angles of 20° to 40°, and they are very short (typically comprising four or five grains).

Thin section BYL from the left flank of flute 2 in the proximal zone shows the contact between Lithofacies A and sands from the Frontsjön sand unit (Figure 5.10). The thin section can be divided into three areas: (1) the upper third consisting of Lithofacies A which is relatively clast-rich, with the largest clast having an apparent long-axis of 17mm; (2) the middle section which shows the contact between Lithofacies A and a fine-grained, massive sand; (3) the lower third of the thin section which shows convoluted folding in coarser sands. The diamicton resembles the sample in MM9 in having a relatively open and porous texture, with relatively few long linear fissures. Graded and laminated Type 1 silt caps, 0.4 to 1.5mm thick, occur on most clasts but are uncommon in the underlying sands (Figure 5.10b). Type 2 silt caps occasionally occur in the diamicton. A few vertically inclined clasts have silt caps forming on one side; however, most steeply inclined clasts have silt caps forming on their upper surfaces. On the left hand side of the sample, in the area just above the contact with the underlying sands, the diamicton matrix is relatively rich in silt. The silt forms thin (*ca*. 0.4 to 0.8mm thick) laterally discontinuous sub-horizontal bands up to 5mm long which are known as silt droplets (Carr, 2004;van der Meer *et al*., 2010a). The sharp wavy contact between Lithofacies A and the sand unit observed in the field is also seen across most of the thin section, although the contact becomes less certain on the left-hand side of the sample (Figure 5.10). The wavy contact is inclined approximately 10° up-glacier and a poorly sorted fine sand layer occurs below Lithofacies A. The fine-sand layer is compositionally and texturally immature and up to 3.8mm thick. It consists of fractured angular to sub-angular crystals of amphibolite and feldspars, with subordinate amounts of quartz. Grains range in diameter from 0.15 to 0.78mm. The poorly sorted coarse sand below the fine sand layer contains grains up to 1.8mm in diameter and contains occasional lithic fragments. The upward transition from coarser to finer sand shows an element of sedimentary grading occurs. The sand from the base of the section is silty and it contains many voids. The voids are 0.5 to 1mm thick and dominated by vughs and lens-shaped voids, although a few more spherically-shaped voids occur.

Comment [DJG33]: what does this mean?

Thin section HFL1 from the most recently exposed flute in Area 1 consists of a relatively fine-grained sandy Lithofacies A which is clast-poor. It contains relatively few linear fissures and silt caps compared to other flute samples from comparable depths, such as BYL and MM8 (Figure 5.11). The silt caps are generally thin and only seen under higher magnifications (x40). Most silt caps are Type 1 although a few Type 3 silt caps are observed in the upper part of the sample. Many clasts have no silt caps. Silt droplets occur towards the top of the thin section.

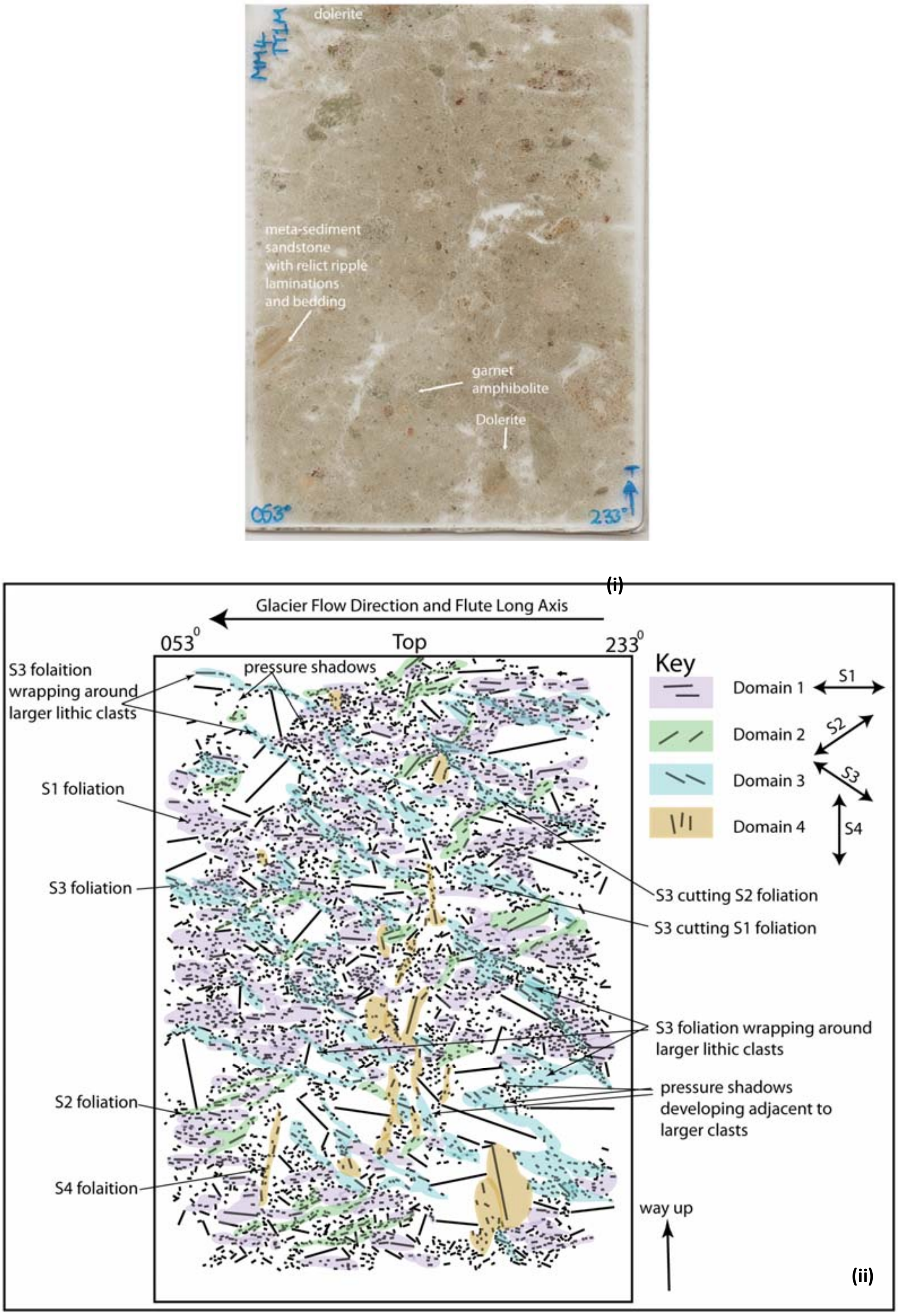

Figure 5.9a(i) Thin section MMT3, distal end flute 3, 0.75-0.85m depth. (ii) Micro-structural map (scale bar on Figure 5.9b below).

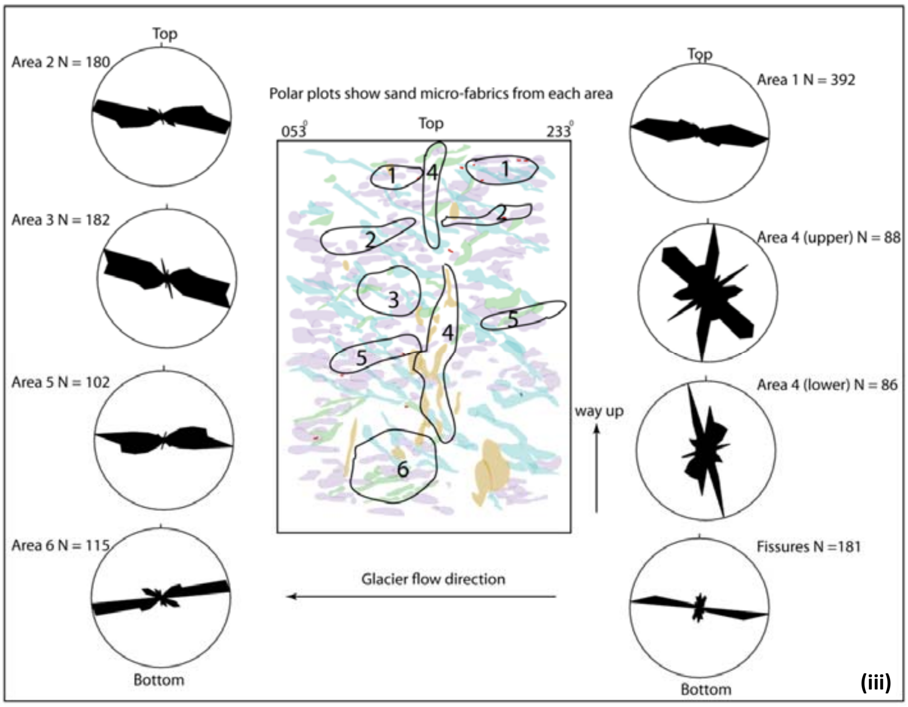

Figure 5.9a(iii) 2-D Micro-fabrics for Areas 1-6, Sample MMT3. Note the more vertical clast orientations in Area 4, and the dominance of the S1 micro-fabric (S1 domains in purple) throughout the other areas.

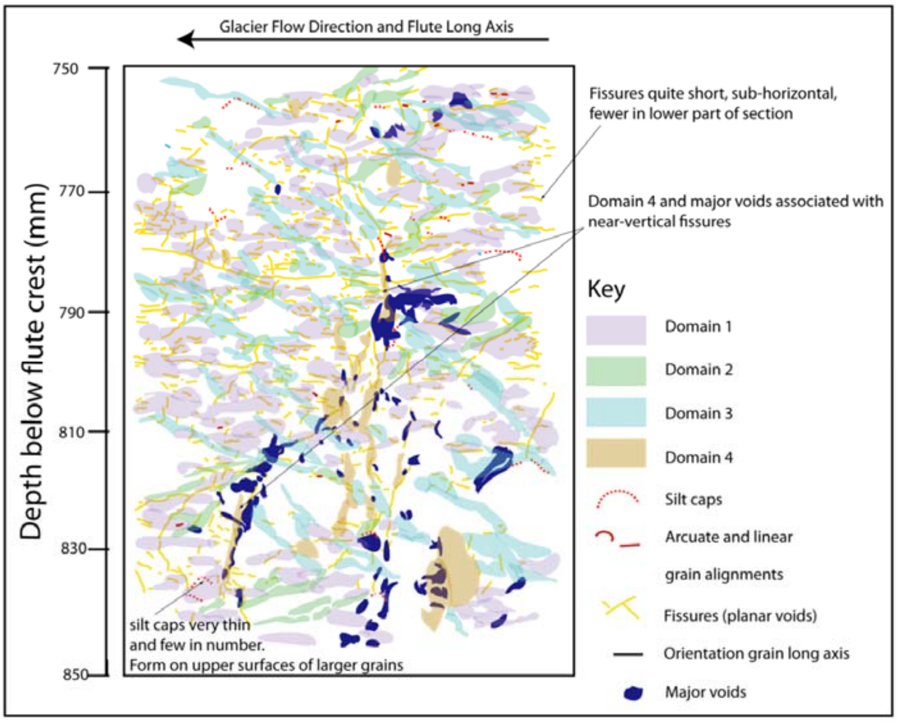

Figure 5.9b Fissures, voids, and silt caps, Thin Section MMTT.

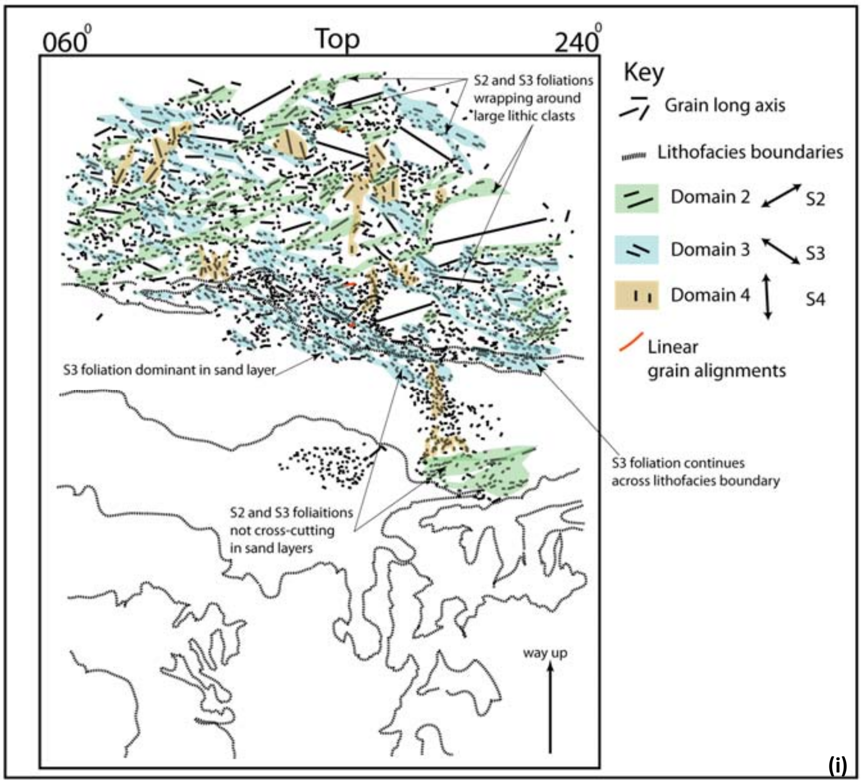

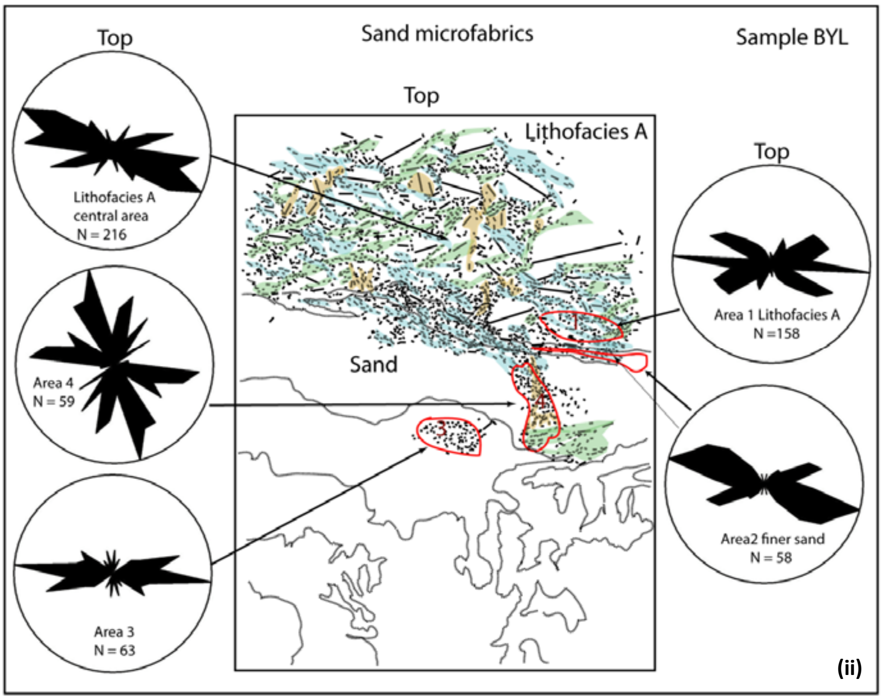

Figure 5.10a (i) Micro-structural map Thin Section BYL. (ii) 2-D Micro-fabrics Thin Section BYL, proximal flute zone, Area 3.

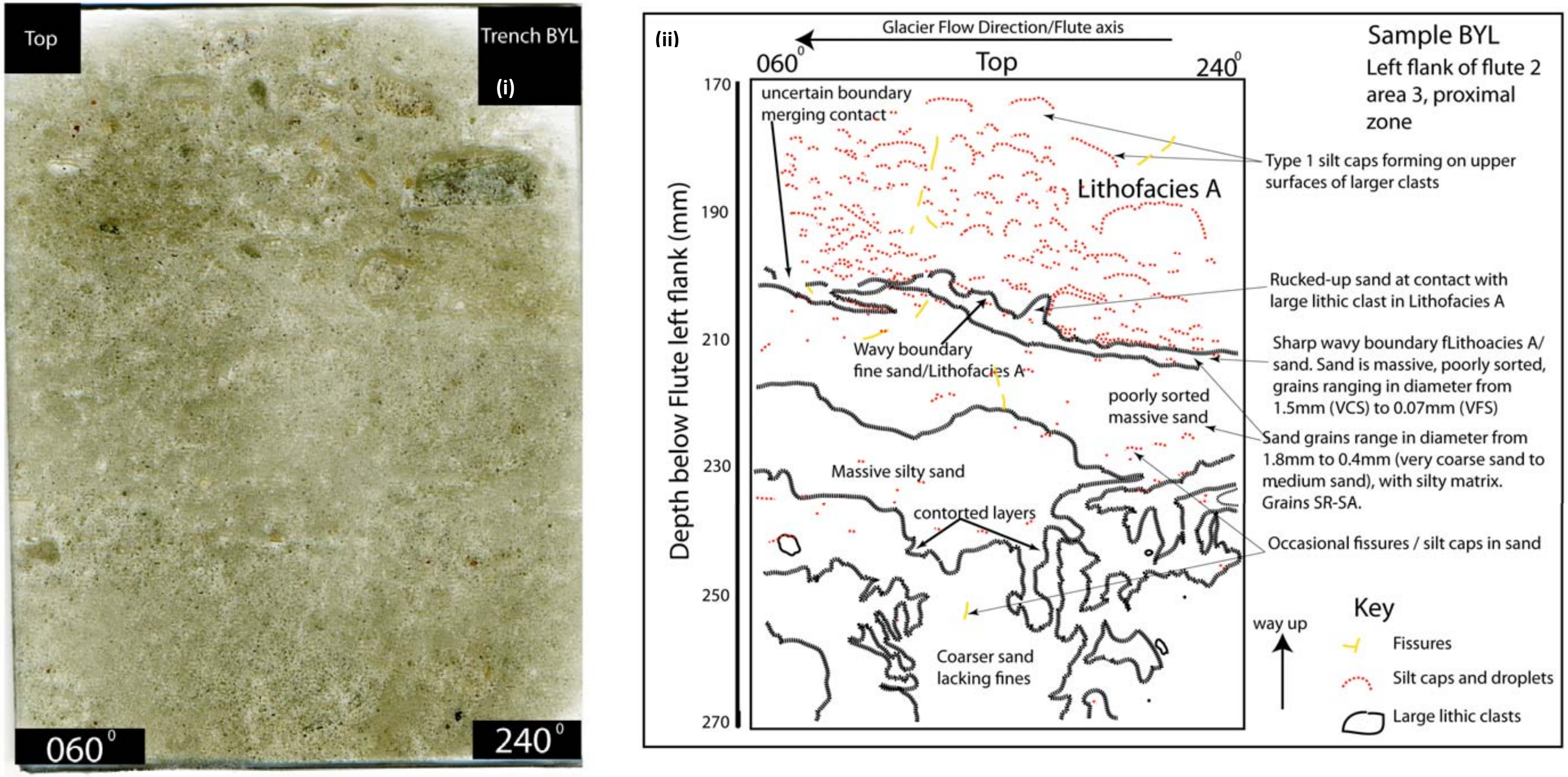

Figure 5.10b (i) Thin Section BYL. (ii) Lithofacies, fissures, and silt caps in Sample BYL, proximal flute zone, Area 3. Note the relatively large number of silt caps in Lithofacies A compared to the sand substrate.

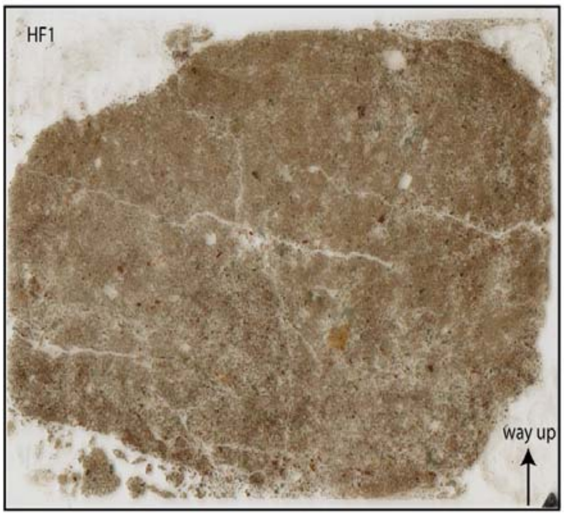

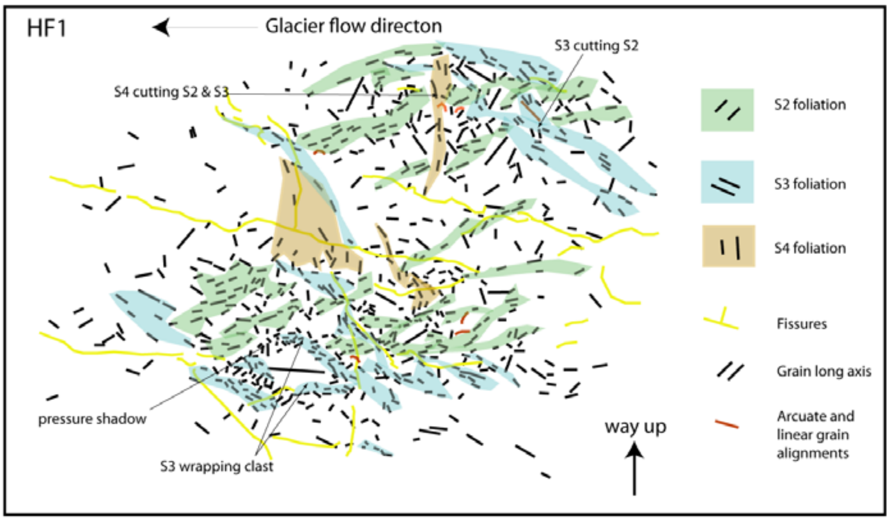

Figure 5.11 Thin Section HF1 and micro-structural map. HF1is from the proximal flute zone, Area 1, Flute 1, from 0.15m to 0.25m depth below the flute crest (the thin section covers a 10cm depth interval). This area was recently subaerially exposed (within the last ca. 30 years). Silt caps are fewer and thinner than in other Lithofacies A flute samples.

5.3 Micro-structural Maps of Flute Thin Sections

The micro-structural maps for the flute thin sections are shown in Figures 5.3 (MM9), 5.5 (MM8), 5.6 (D1), 5.9 (MMTT), 5.10 (BYL), and 5.11 (HF1). In each case, the 2-D long-axes orientations of clasts ranging in size from medium sand to fine gravel (grains with diameter of 0.1mm+) have been mapped to reveal clast micro-fabric foliations. A foliation is defined as a preferred clast or grain alignment that penetratively develops as a result of deformation (Phillips *et al*., 20011a).

The completed micro-structural maps for the flute thin sections are relatively complex and reveal four spaced and disjunctive clast micro-fabric domains. The earliest formed micro-fabric (designated S1, see Figure 5.1) is only observed in the samples from below 0.5m depth (Figure 5.11). The S1 clast micro-fabric consists of a sub-parallel foliation with grain inclinations <10°. In thin sections MMTT and D1 the S1 clast micro-fabric is defined by a series of well-developed, flat-lying domains (domain 1) that have short, rough to irregular lenticular shapes (the domains are between 2 and 22mm long in sample MMTT). Domain 1 is the dominant domain in sample MMTT where it is relatively intense and pervasive in the upper two thirds of the thin section. The domains have a wider spacing towards the base of the sample (spacing in the upper right section is 3, increasing to 6 in the lower section – see Figure 5.1 for an explanation of how spacing is measured). Domain 1 is less well-developed and intense in sample D1, especially towards the top of the thin section. The S1 clast micro-fabric is not observed to form distinct domains in any of the thin sections above 0.5m depth, although it is occasionally weakly developed in the intervening microlithons between domains 2 and 3, especially in sample BYL. In thin sections MMTT and D1 the intervening microlithons separating the S1 domains are massive.

The S1clast micro-fabric is cut by clast micro-fabrics S2 and S3. The S2 clast micro-fabric forms a spaced, anastomosing (disjunctive) foliation that is relatively steeply inclined down-flow (generally at 20° to 40°) and defines rough to irregular lenticular-shaped domains. S2 is relatively weakly developed in sample MM8 and in the lower sections of samples D1 and MMTT, but relatively well-developed in the upper sections of D1. S2 is much better developed and more intense in the thin sections from nearer the flute surface (HF1, BYL, and MM9) where it forms longer and more closely spaced domains (Figure 5.12). The S3 clast micro-fabric forms a similarly spaced, anastomosing (disjunctive) foliation to S2, but it is relatively steeply inclined up-flow (20° to 40°). It generally defines irregular to elongate lens-shaped domains. The S3 micro-fabric is well-developed in most samples and is the dominant clast micro-fabric in sample MM8, especially in the middle and lower sections of the sample, where it forms relatively thick lens-shaped domains. The spacing of the S3 domains generally becomes slightly wider with depth (Figure 5.12). In sample BYL from near the flute surface, domain 3 has a spacing of 5. In sample D1 from 0.5 to 0.6m depth the spacing of domain 3

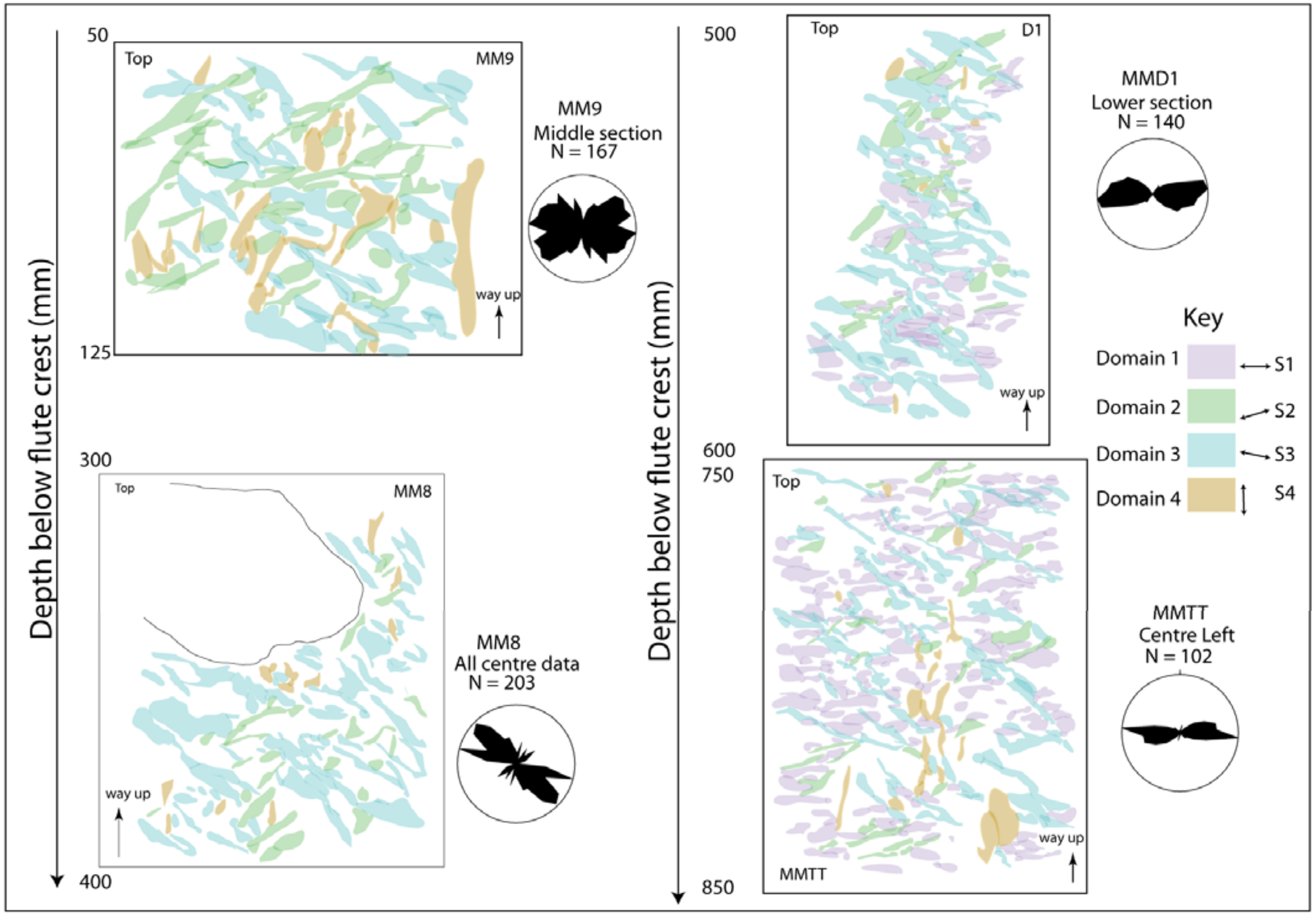

Figure 5.12 Variations in micro-fabrics with depth in flute thin sections.

is 6.6 in the upper section of the thin section. In the deepest sample MMTT, the spacing of domain 3 is relatively wide (10) and S3 forms thin long domains (up to 30mm long and 1 to 3mm thick).

The spacing of domains is affected by the concentration, distribution, and size of large lithic clasts. Larger clasts disrupt the S2 and S3 clast-micro-fabric domains; in general, the domains are better developed and more closely spaced in areas of the samples where there is a greater concentration of fine-grained matrix. This can be seen in sample MMTT. Here, the wider spacing of domains 1 and 3 towards the base of the thin section relate to the concentration of numerous larger clasts in this part of the sample (Figure 5.9). These domains exhibit closer spacing in the silt-rich parts of the matrix in the central and upper portions of the sample. Likewise, in sample MM8, there is a concentration of larger lithic clasts on the right-hand side of the thin section and domain 3 is relatively widely spaced compared to the left-hand side of the sample, which is finer-grained in the area below the large dolerite clast (Figure 5.5).

Clast micro-fabrics S2 and S3 form domains that have a complex relative age relationship as examples of domain 3 cross-cutting domain 2 and vice versa occur in close spatial proximity (for example, in sample MM9 in Figure 5.3 and sample MM8 in Figure 5.5). This suggests the timing of fabric development was reversed in different parts of the diamicton, with the S2 and S3 clast micro-fabrics developing penecontemporaneously and propagating at different rates through different parts of the diamicton (Phillips *et al*., 2011b). Moreover, the rose diagrams showing 2-D micro-fabrics in Figure 5.3 (MM9, especially the lower section), Figure 5.5 (MM8, especially the fabric for the area upper right), Figure 5.6 (sample D1), and Figure 5.10 (BYL Dm1, especially central area and area 1), have a 'bow-tie' appearance which shows the micro-fabric domains are forming a conjugate set (Phillips *et al*., 2011b). The two clast micro-fabrics, S2 and S3, are separated by an angle of approximately 60°. The S2-S3 conjugate set is well-developed in the samples from nearer to the flute surface, whereas it is moderately to weakly developed in samples from below 0.5m depth. In most thin sections, both the S2 and S3 clast-micro-fabrics are observed to wrap-around larger lithic clasts (examples can be seen in Figures 5.5 and 5.9). The larger clasts seem to have a moderately well-developed preferred alignment parallel to the enveloping fabric (Phillips *et al.*, 2011b). Pressure shadows (areas of low strain with no preferred fabric alignment, formed as the foliation wraps around rigid clasts) often occur adjacent to the largest clasts.

Asymmetric pressure shadows are occasionally observed, and these can be used to indicate the sense of shear (Figure 5.13). For example, in sample MMTT a large lithic clast, which has a long-axis steeply inclined up-flow, occurs in the top left of the thin section (Figure 5.9). The S3 foliation wraps around the large lithic clast. The clast geometry and developing asymmetric pressure shadows give a sinistral (top to left) sense of shear that is consistent with the glacier flow direction towards the east north-east.

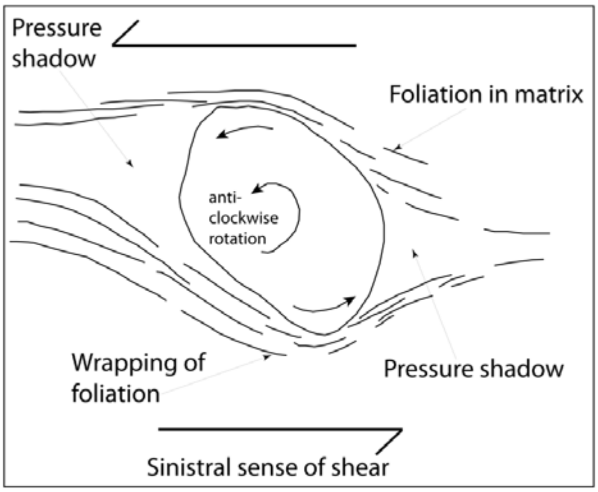

Figure 5.13 Sense of shear indicated by the development of asymmetric pressure shadows as foliation wraps-around a larger clast (after Phillips *et al*., 2011a).

The steeply inclined to near-vertical S4 clast micro-fabric shows a variable intensity of development with depth (Figure 5.12), being best-developed in the near-surface samples (BYL, HF1, and MM9). It forms a spaced (disjunctive) micro-fabric foliation consisting of short, rough to irregular shaped domains which are sometimes weakly anastomosing. Domain 4 is best developed in sample MM9 (Figure 5.3) where domains are up to 4mm long. It is poorly developed in samples MM8 and D1, suggesting its development is less intense with depth. However, in the deepest sample (MMT3, Figure 5.9) domain 4 occurs discontinuously throughout the central part of the thin section where it seems to be related to a zone of steeply inclined fissures and large open voids (Figure 5.9b). The age relationship between domain 4 and domains 2 and 3 is not always clear-cut; in many cases, where domain 4 is better developed, it appears to cross-cut other domains, for example, in the central areas of sample MMTT (Figure 5.12). However, in other areas, for example in sample MM9, it appears to be truncated by domains 2 and 3, which suggests the timing of the imposition of the micro-fabrics varied in Lithofacies A.

The orientation of sand-sized grains in Lithofacies A from sample MM8 are shown in rose diagrams in Figure 5.5. The long-axes of the sand-sized grains show multiple-orientations in the areas labelled centre right and centre (that is, just below and on the stoss-side of the large dolerite clast that dominates the upper section). The S_1 eigenvalues show that relatively weakly clustered micro-fabrics occur in these two areas (S_1 = 0.63 and 0.61 respectively, Table 5.2). However, the micro-fabric developed to the centre left of the sample is more strongly clustered (S_1 eigenvalue = 0.746) with the long-axes of sand-sized grains inclined up-flow. The up-flow inclination corresponds to the dominant S3 foliation in this part of the sample. The disruption to the micro-fabric in the centre right and centre areas is consistent with a pressure shadow developing adjacent to the large dolerite clast.

Below a depth of 0.5m, the 2-D micro-fabrics of sand-sized grains in Lithofacies A have relatively strong S_1 eigenvalues (generally >0.7 indicating strong linear clustering, see Table 2). Below 0.5m most S_1 eigenvalues are in excess of the steady-state S_1 eigenvalues obtained for sand-sized grains during simple shear in ring-shear experiments (Thomason and Iverson, 2006). Most sand-sized grains in sample MMTT correspond to the S1 foliation and are gently inclination up-flow, as is shown in the rose diagrams in Figure 5.9, except for those in area 4 where the grains are steeply inclined. In sample D1, a similar gentle up-flow inclination to sand-sized grains is apparent in the rose diagrams shown in Figure 5.6, especially in the lower section of the sample. However, the 2-D micro-fabric shows variation across the sample, with some rose diagrams being dominated by grains with steeper long-axes inclinations (20° to 40° or more, that is the S2 and S3 foliations), with either up-flow or down-flow directions dominating in different areas of the sample.

The 2-D micro-fabric S_1 eigenvalues for sand-sized grains in Lithofacies A generally become weaker towards the flute surface (generally <0.7 indicating relatively weak linear clustering, see Table 2). This reflects the increasing dominance and intensity of domains 2, 3 and 4 in the thin sections above 0.5m depth. Exceptions to this are the 2-D micro-fabrics from the Fronstjön sand layers in sample BYL, which have relatively strong S_1 eigenvalues dominated by grains with long-axes gently inclined up-flow (Figure 5.10), and the centre-left fabric previously described for Lithofacies A in sample MM8. Carr and Rose (2003) and Carr and

Goddard (2007) suggested that 2-D micro-fabrics are better developed in larger grain-size categories (>20mm diameter) compared to smaller sizes (0.25 to 1mm diameter). However, in sample MM8, 2-D micro-fabrics measured for different size-ranges show no increase in S_1 eigenvalue strength with increasing grain size (Figure 5.14). The rose diagrams in Figure 5.14 show that grains in all size-ranges (and especially those below 2mm diameter) show a preferred alignment that corresponds to the S3 micro-fabric, with secondary and tertiary modes corresponding to the S2 and S4 clast micro-fabrics. There are a greater number of steeply inclined clasts in the fine gravel size-ranges.

Table 5.2 S_1 eigenvalues for 2-D micro-fabrics from thin sections

Sample	**Location**	**N**	S_1
SL1	***SL1***		
Sydjåkk	zone 1	111	***0.776***
Dm plain	zone 2	112	0.687
	zone 3	115	***0.745***
	all Lithofacies Bii	338	**0.639**
	gravel	191	0.63
	sand	106	0.728
MMS2	***NL2***		
Nordjåkk	zone 1	64	0.680
Dm plain	zone 2	56	***0.798***
	zone 3	69	0.671
	zone 4	125	***0.730***
	zone 5 sand	98	***0.766***
	zone 6	134	0.620
Isfallsglaciären Flutes			
	Trench MMT3		
MM9	Upper area	159	0.601
Flute 3 Mid	Middle area	167	0.608
	Lower area	208	0.641
MM8	Upper Right	151	0.617
Flute 3 Mid	Centre left	69	***0.746***
	Mid section	203	0.684
	Centre-right	102	0.630
	Centre	53	0.610
	all lower area	535	0.613
	Base combined	221	0.608
	Bottom left	86	0.568
	Bottom right	314	0.625
D1	area 5	117	0.714
Flute 3 Mid	area 4	71	0.700
	area 3	76	***0.815***
	area 2 base	91	***0.828***
	area 1 lower left	140	***0.827***

MMTT	upper area 1	240	***0.759***
Flute 1 Distal	upper right	152	***0.888***
	upper combined	392	***0.808***
	vertical combined	174	0.599
	vertical lower	86	0.647
BYL	area 1	216	0.725
Flute 3 Proximal	area 2 lower right	158	0.698
	area 3 sand	58	***0.790***
	area 4 c sand	59	0.612
	area 5 massive sand	63	0.729

Note: S_1 eigenvalues in bold are equivalent to or greater than steady-state values obtained by pervasive shear in ring shear experiments (Thomason and Iverson, 2006). These do not indicate very high strain magnitude because steady-state sand micro-fabrics are achieved at relatively low strains (<10). The locations relate to areas where rose diagrams were constructed (see micro-structural maps). N refers to the number of clasts used in each rose diagram and S_1 calculation.

5.4 Interpretation and Discussion

5.4.1 The Extent of Periglacial Overprinting

An important question to address is the extent to which the micro-structures and features observed in the thin sections reveal subglacial or periglacial processes. Some of the observed structures are processing artefacts which are known to be associated with the manufacture of micromorphology thin sections (Carr, 2004; van der Meer *et al*., 2010a; 2010b). Large smooth-shaped voids, such as those observed centre-right in sample D1 and towards the base of sample MM9, are thought to result from sediment being removed during the grinding stage of thin section production from parts of the slide where resin failed to impregnate properly (van der Meer *et al*., 2010a; 2010b). The drying-out of sediment during thin section production is also known to result in sediment contraction and the opening of large voids, especially around larger clasts, and such contraction voids are observed in all the flute thin sections (see for example Figure 5.8). These processing artefacts result in an increased porosity and porosities measured in thin section samples are likely to be much higher than porosities observed in field settings (Kilfeather and van der Meer, 2008).

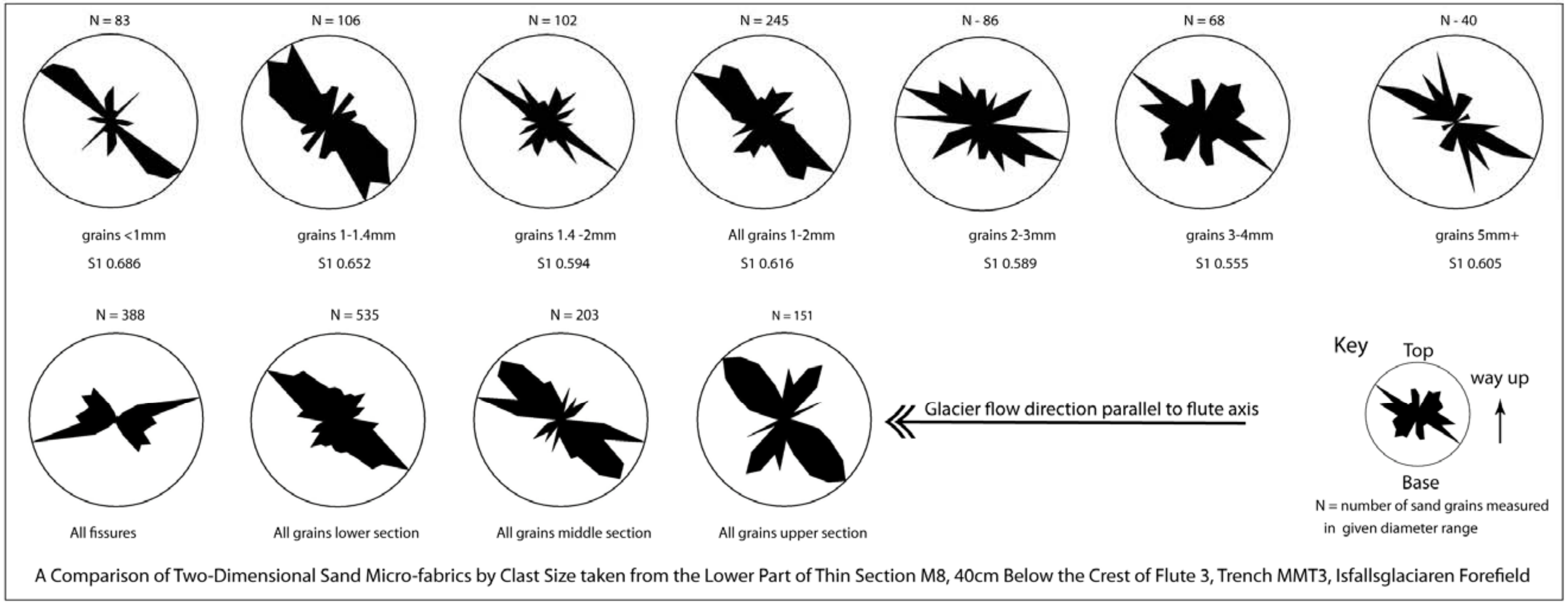

Figure 5.14 Variations in 2-D micro-fabric by grain size in Sample MM8. N is the number of grains measured in constructing each rose diagram and S_1 is the eigenvalue.
The top of the thin section is taken as ‘north’ in the rose diagrams. Note that similar dominant foliations are present at different grain sizes, with slightly more vertical to near-vertical grains in the larger clast sizes, and that there is small variation in the S1 eigenvalues.

The presence of large numbers of thick silt caps, and silt cutans, silt droplets, star-shaped vughs, and extensive sub-parallel linear voids suggests that periglacial overprinting has been quite extensive in the thin sections taken in the upper 0.35m of the flutes, and especially in sample MM9 from the upper 0.125m (Bockheim and Tarnocai, 1998; Harris, 1998; Van Vliet-Lanoe, 2010). Kilfeather and van der Meer (2008) found that fissile partings produced by shear strain in subglacial deformation tills were demarcated by strings of planar voids which had long, narrow, and elongated lens-shapes. The linear voids observed in the flute thin sections do not match this description; they are frequently sub-horizontal and consist of irregular to bubble-shaped-voids (strings of vughs). Similar irregular-shaped linear voids have been observed to form by frost action on arctic forefields in silty sediments which favour the formation of segregated ice (Bockheim and Tarnocai, 1998; Van Vliet-Lanoe, 2010). In Chapter 3.3.1 it was shown silt-sized material typically comprises up to a quarter of the matrix of Lithofacies A. This relatively high silt content renders Lithofacies A susceptible to the formation of segregated ice, which preferentially develops in silty sediments (Van Vliet-Lanoe, 2010). The growth of segregated ice lenses is known to produce star-shaped vughs (Van Vliet-Lanoe, 1985; 2010) such as those observed in sample MM9 and D1 (Figures 5.4 and 5.8).

The linear voids are quite extensive in sample MM8 and in the upper section of sample D1 and, in conjunction with contraction voids, they form distinct fissures (fissile partings) that separate the diamicton into platy structures. Platy structures and fissures are common features of sediments affected by cryogenesis in which the platy structure develops through a combination of compaction and cryo-desiccation between ice lenses (Harris, 1998; Bockheim and Tarnocai, 1998). However, such platy structures and fissures are usually sub-horizontal whereas the fissures in samples D1 and MM8 are relatively steeply inclined. As such, some of the more steeply inclined linear voids may represent original fissile partings produced by subglacial shear and subsequently affected by cryogenic processes. Two hypotheses are considered for the origin of the fissile partings:

Hypothesis 1 - they represent discrete subglacial shear planes which have subsequently been affected by segregated ice formation and water flow related to thaw consolidation and snow melt, which concentrated along pre-existing fissile partings which provided natural pathways for water movement through the diamicton (van der Meer *et al*., 2010b);

Hypothesis 2 - they are unrelated to subglacial shear but relate instead to sediment unloading and/or dewatering and subsequent cryogenic activity.

Some evidence to support hypothesis 1 comes the occasional development/preservation of linear grain alignments along the upper walls of some linear voids. Linear grain alignments are thought to represent the alignment of similar-sized grains along discrete shear planes (Menzies *et al*., 2006; Larsen *et al*., 2006). Short, steeply inclined grain alignments are associated with low strain magnitudes because linear grain alignments become longer and increasingly sub-horizontal at higher strain magnitudes (Thomason and Iverson, 2006; Larsen *et al*., 2006). However, linear grains alignments are very rare and the apparent alignment of the grains may be misleading as they are only being observed in 2-D. Moreover, micro-scale evidence for discrete brittle shear (such as faults or shear planes) is absent from the thin sections, and the alignment of the grains may relate to local water flow along the fissile partings following thaw of segregated ice.

Harris (1998), working on sediments affected by cryogenesis, argued that fissures related to shearing or water flow were likely to contain sediment deposited in the linear voids by these processes; clean linear voids were interpreted as recent structures that were opened-up by a late-stage of cryogenic activity. The linear voids in the flute thin sections are generally clean and devoid of deposits of sediment, except for occasional thin coatings of silt deposited along the void walls. These thin coatings of silt and occasional silt cutans observed in some vughs are consistent with silt translocation following thaw consolidation (Harris, 1998; van der Meer *et al*., 2010a). The clean nature of most linear voids suggests the fissile partings in Lithofacies A are relatively recent structures. This supports hypothesis 2 and suggests the fissile partings represent sediment de-watering or unloading structures (Muller, 1983). However, only a few extensive linear voids are observed in sample HF1, which has been subaerially exposed for the shortest time, compared to sample MM8 which has been exposed for longer. The more extensive linear voids (fissures) in the longer exposed sample suggest that fissure development relates to cryogenic processes. Linear voids are also less extensive in the deepest sample MMTT, which is consistent with a reduced cryogenic influence at depth (Van Vliet-Lanoe, 2010). The available thin section evidence suggests the fissile partings relate to a late-stage development of strings of linear voids which have certainly been affected, if not entirely produced, by cryogenesis. The clean nature of most linear voids and the general lack of micro-scale evidence of subglacial shear deformation along the voids suggest that the fissile partings are unlikely to be shear planes and, as such, hypothesis 2 is preferred in this study.

The presence of thick laminated silt caps and silt droplets in the upper flute samples provides further evidence of extensive periglacial overprinting of Lithofacies A (Harris, 1998; Carr, 2004; van der Meer *et al*., 2010a). Silt caps and silt droplets are classified as banded fabrics produced by cryogenesis (Bockheim and Tarnocai, 1998). Two explanations for silt cap formation occur in the literature. First, in subglacial sediments, they can be formed by simple washing processes (Harris and Ellis 1980; Harris, 1998; Van Vliet-Lanoe, 2010). This process occurs in areas where there is sufficient seasonal snow melt and seasonal thaw of segregated ice to initiate the downward illuviation of fines (Harris, 1998). The fines then collect on the upper surfaces of larger clasts (Type 1 silt caps) or, if there is sufficient water flow, coat the upper surfaces and sides of clasts (Type 2 silt caps). Silt illuviation can also result in thin silt bands being deposited in matrix voids, resulting in silt droplets (Harris, 1998). Type 3 silt caps, which encircle clasts, are thought to form in areas where clasts have been rotated; they are particularly associated with solifluction deposits and sediments affected by gelifluction processes (Harris and Ellis, 1980; Harris, 1998; Bockheim and Tarnocai, 1998). Alternatively, laminated silt caps exhibiting normal to inverse grading can be produced by the growth of segregated ice lenses in silty sediments (Van Vliet-Lanoe, 2010). As an ice lens grows it expels a thin film of water ahead of it. Coarser silt and sand grains are rapidly incorporated into the growing ice lens whereas fine silts are moved downwards by the thin water film and collect on the upper surfaces of larger clasts (Type 1 silt caps). Ice lenses form preferentially under larger clasts which experience vertical jacking, and this upward movement aids the accumulation of silt caps (Van Vliet-Lanoe, 2010). The greater number of steeply inclined grains in the gravel-size range in sample MM8 is consistent with preferential frost-jacking beneath larger clasts. The growth of segregated ice crystals can fragment earlier formed silt caps, as is seen in sample MM9 (Figure 5.4). Distinct laminations in a silt cap may relate to one frost cycle, and silt caps in laboratory studies have been observed to form after as few as 18-25 frost cycles (Coutard and Mücher, 1985). The presence of thin silt caps and silt droplets in sample HF1 demonstrates that even more recently exposed forefield sediments in the Tarfala Valley have been overprinted to an extent by cryogenic activity, and that silt caps and silt droplets are developed in diamictons exposed for *ca*. 30 years or less in the Tarfala Valley. Schytt (1963) observed frozen meltwater in flutes in a subglacial tunnel beneath the ice margin of Isfallsglaciären. If seasonal thaw of some of this frozen meltwater occurred, then it is possible that frost action began to affect Lithofacies A in an ice-marginal location prior to subaerial exposure.

The two processes of silt cap formation are not mutually exclusive and it is probable that both mechanisms have operated in the Isfallsglaciären flutes. Sample MM8 shows evidence of silt cap formation associated with water flow. For example, in Figure 5.7 the faint laminations that resemble micro-ripples in the triangular-shaped silt cap indicate deposition from water flow moving right to left (i.e. down-flute) along the upper surface of the dolerite clast. The faint laminations and graded laminations are truncated on the right hand side by silty laminations which indicate erosion and then deposition from water flow moving from top left to bottom right along a large linear void which intersects the right edge of the dolerite clast. In addition, the presence of Type 2 silt caps in the upper flute samples suggest formation by simple washing and silt illuviation has been an active process. Indeed, the open, porous appearance of sample MM9 and the presence of Type 3 silt caps in the upper few centimetres suggest considerable water movement has taken place through this sample. The restriction of Type 3 silt caps to the upper few centimetres of the flute indicate that only the top *ca*. 0.1m of Lithofacies A has experienced phases of gelifluction and grain rotation that post-date subglacial emplacement. The post-depositional rotation of some grains during saturated soil flow help to explain the fact that the weakest magnetic fabric was measured in sample MM9 (S_1 = 0.53). Below 0.1m depth there is less evidence of post-depositional grain rotation as Type 2 and Type 3 silt caps become very rare (especially below 0.35m depth). In samples MM8 and D1 silt caps occur on the upper surfaces of many steeply inclined clasts (Figures 5.5 and 5.6) suggesting the formation of the silt caps post-dates the development of the clast fabric. The reduction in silt cap size and frequency with depth suggests silt illuviation is unlikely to have had a major impact on magnetic fabrics measured below 0.35m depth, and these fabrics are generally stronger than near-surface samples and consistent with flow-parallel simple shear.

Comment [DJG34]: Includes interp

Comment [DJG35]: Interpretation

The lack of micro-scale evidence that the fissile partings are shear planes (that is, the lack of elongated voids, the absence of faults and the clean nature of the voids) and the evidence of extensive periglacial overprinting in the upper flute samples has a number of implications for the interpretation of Lithofacies A and for the wider interpretation of recently exposed subglacial diamictons, namely:

a) Care should be taken in using the presence of fissile partings as evidence to support the classification of diamictons as subglacial deformation tills at the macro-scale (Boulton 1996; Benn 1994; 1995; Etienne *et al*., 2003; Evans *et al*, 2010); micro-scale evidence is required to confirm the fissile partings are shear planes rather than cryogenic and/or de-watering/unloading structures.

b) The alignment of facets in Type 1 and Type 2 clasts along fissile partings (Chapter 3.3.1) does not necessarily support Benn's (1994) interpretation that the facets are caused by differential rates of shear along shear planes. Linear voids preferentially form beneath larger clasts in frost affected sediments (Van Vliet-Lanoe, 2010) and sediment shrinkage, related to de-watering or cryo-desiccation (Harris, 1998), would tend to result in finer matrix material contracting away from the faceted edges of larger clasts. Sediment contraction and the development of linear voids beneath the 'facted' faces of larger clasts, seen for example in Figure 5.8, would give the macroscopic appearance of facets being aligned with 'shear planes' (fissile partings).

c) Even subglacial diamictons that have been exposed relatively recently (*ca*. 30 years) reveal evidence of periglacial overprinting. Cryogenesis increases the porosity of sediments, illuviates fines, and disrupts fabrics (Bockheim and Tarnocai, 1998). Ice lensing jacks-up clasts and induces stresses that can re-orientate clasts into vertical alignment, producing a succitic fabric (Van Vliet-Lanoe, 2010). Some parts of domain 4 probably represent areas of Lithofacies A where cryogenesis has produced a near-vertical orientation of clasts. The increase in intensity of domain 4 in samples from shallower depths where cryogenesis is likely to have been more intense, is consistent with this interpretation. The relatively coarse nature of sample MM9 from nearest to the flute surface may reflect an element of vertical sorting and inverse grading induced by cryogenesis (Van Vliet-Lanoe, 2010). Sample MM9 has features that resemble Type A-horizons, such as an open, porous texture and fabrics with relatively weak linear clustering (Boulton and Hindmarsh 1987; Benn, 1994). However, the analysis of the thin section reveals extensive periglacial overprinting; the high porosity and weak fabrics relate, at least in part, to cryogenesis rather than subglacial deformation in a ductile A-horizon. The implication of this is that researchers working on recently exposed forefields that are subjected to seasonal frost action need to take care in the identification of near-surface sediments as A-horizons based on macroscopic observations alone (Boulton and Hindmarsh, 1987; Benn, 1994; 1995; Evans *et al*., 2010). Micro-scale evidence needs to be used to demonstrate that the features identified as indicative of A-horizons are not the consequence of periglacial overprinting but have been formed by ductile deformation, which is characterized by fold structures, rotational structures, strain caps and shadows, and necking structures (Carr, 2004).

d) The reduction in silt cap thickness and frequency with depth suggests the influence of cryogenic processes and the extent of periglacial overprinting of subglacially deformed sediments diminishes with depth. Harris and Ellis (1980) found that cryogenic processes were active in solifluction deposits in Norway to a depth of 1m. The flute thin sections suggest that the extent of periglacial overprinting is extensive in the upper 0.1m and extends to 0.35m depth, but become increasingly less intense at lower depths, although a mild degree of overprinting can be observed even at 0.8m. Strong flow-parallel clast a-axis macro-fabrics were recorded in the flutes. These were measured using clasts with a-axes 0.6cm to 6cm long and below 0.1m depth (Chapter 2.4.1). These strong macro-fabrics suggest cryogenesis has had a limited effect on the orientation of gravel-sized clasts below 0.1m depth (Chapter 4.1.15), even though the thin section analysis demonstrates that the matrix shows considerable evidence of silt illuviation and void development related to frost action.

Comment [DJG36]: error here

5.4.2 Soft-bed Deformation and Flute Formation

As in several other micromorphological studies of subglacial diamictons, plasma structures are not seen in the Isfallsglaciären thin sections because the matrix lacks sufficient clay for their development (Carr and Goddard, 2007; van der Meer *et al*., 2010a & 2010b; Phillips *et al*., 2011b). Furthermore, no evidence of structures related to glacio-tectonic deformation (such as faults, folds and turbate structures) have been observed at the micro-scale in any of the flute thin sections, an observation which is in keeping with some other studies of homogeneous subglacial diamictons from flutes on contemporary glacial forefields and from Quaternary till sequences (Phillips *et al*., 2007; van der Meer *et al*., 2010b; Phillips *et al*., 2011b). Despite this and despite the extent of periglacial overprinting, the micro-structural maps demonstrate that Lithofacies A has a complex polyphase subglacial deformation history and the variable intensity and spacing of the micro-fabric domains within and between thin section samples suggests deformation partitioning occurred within the matrix of Lithofacies A (Phillips *et al*., 2011b). The development of the cross-cutting clast micro-fabrics (S1 to S3) show that different phases of subglacial deformation affected Lithofacies A at different times, whilst the variable intensity of development and spacing of the clast micro-fabrics shows that, during each phase of deformation, the deformation was not homogeneous and continuous throughout the flute, but partitioned into discrete zones (Evans *et al*., 2006; Phillips *et al*., 2011b). Such heterogeneous deformation is at odds with Benn's (1995) model of flute formation by homogeneous cumulative shear.

The S1 micro-fabric is cross-cut by all subsequent micro-fabrics and so pre-dates them.As such, the earliest phase of deformation imposed the flat-lying S1 micro-fabric on Lithofacies A. The S1 clast micro-fabric does not form distinct domains in near-surface thin sections. This is either because it has been overprinted by the more intense development of domains 2-4, or because it represents an earlier phase of deformation unrelated to flute formation. Clast fabric data presented in Chapter 4.1.10 suggested that a weak layer occurred in the flutes at *ca.*0.5m depth and that this represents the depth at which shearing by overriding ice was unable to re-orientate clasts into flow-parallel alignment. If this is true, then the S1 micro-fabric, which is found below 0.5m depth, may represent a fabric that pre-dates the main events that formed the flutes. However, the S1 foliation is sometimes weakly developed in the microlithons that separate domains 2 and 3 in samples MM8 and BYL from above 0.5m depth, which indicates that the S1 has been overprinted by later phases of deformation in these samples.

The S1 micro-fabric is best developed in the sample taken from the greatest depth (MMTT) and it becomes more pervasive in that part of the thin section where there are fewer large clasts and a more silty matrix. The rose diagrams in thin section MMTT (Figure 5.9) suggest that the long-axes of most sand-sized grains in Lithofacies A are inclined at low angles up-flow. Similar sand grain alignments occur in ring shear experiments when tills are sheared pervasively to steady-state conditions (Thomason and Iverson, 2006). In these ring shear experiments, the up-flow inclination of the sand grain long-axes was thought to reflect the interaction of two sets of Riedel shears (Figure 5.15). The S_1 eigenvalues for 2-D sand micro-fabrics in Lithofacies A from samples MMTT and D1 are equivalent to steady-state values achieved in ring shear experiments. However, steady-state 2-D sand micro-fabrics are not necessarily indicative of high strain magnitudes as they can be achieved at low strains, with most of the evolution of the grain towards its steady-state position occurring at low strains (<7) (Thomason and Iverson, 2006). As such, weak S_1 eigenvalues recorded for 2-D sand micro-fabrics in Lithofacies A samples above 0.5m depth suggest only moderate to weak strain magnitudes. There is no micro-scale evidence of Riedel shears in the flute thin sections (possibly because there is a lack of clay in which plasma fabrics can develop; Riedel shears in ring shear experiments were identified in plasma fabrics). It is also possible that the inclination of the sand grains reflects the imposition of pure shear during sediment compaction, which acts to flatten the dip of clasts and sand grains (Evans *et al*., 2006). However, in thin sections D1 and MMTT, the reasonably strong S_1 eigenvalues, the low up-flow inclination of the sand grain long-axes, and the relatively well developed nature of the S1 micro-fabric are consistent with a phase of relatively pervasive deformation related to simple shear. Some clasts in domain 1 in sample MMTT have thin matrix coatings. Matrix coatings are thought to develop around freely rotating clasts in dilatant deformation tills (van der Meer *et al*., 2010a). The presence of clast coatings indicates relatively dilatant conditions during the imposition of the S1 micro-fabric.

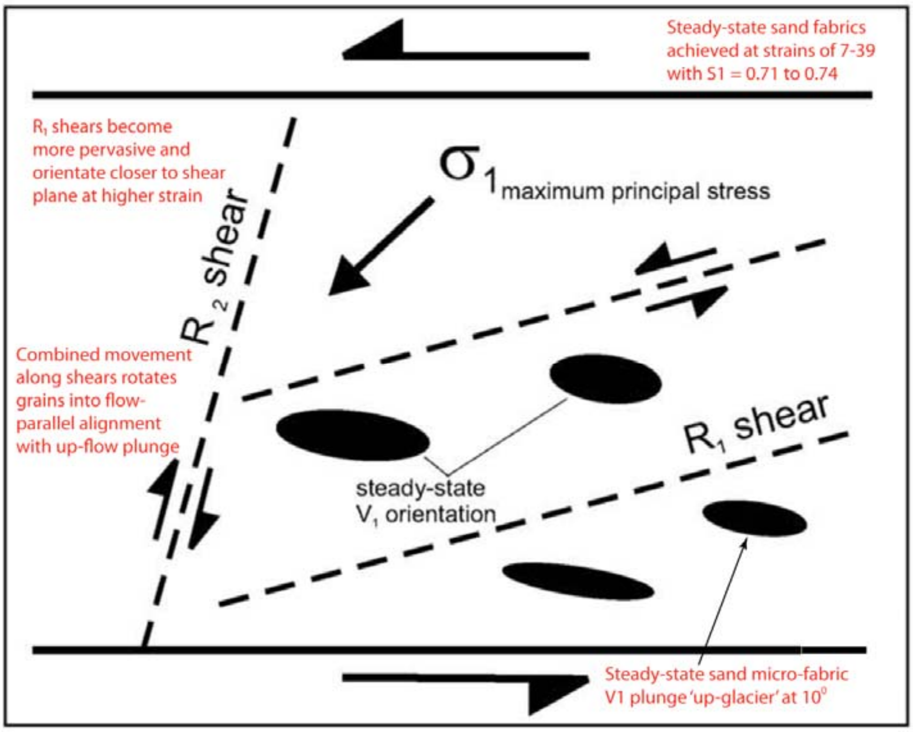

Figure 5.15 The Development of steady-state sand micro-fabric during pervasive shear in ring-shear experiments (after Thomason and Iverson, 2006). The low-angle up-flow dip of sand grains was explained by combined movement along two opposed sets of Riedel Shears (R_1 and R_2). Steady-state fabrics were achieved at generally low strain magnitudes with much of the rotation towards steady-state occurring at strains as low as 2.

Conjugate sets of spaced clast micro-fabrics, like those formed by the S2 and S3 micro-fabrics, were identified in micro-structural maps of subglacial deformation tills from Quaternary till sequences (Ferguson *et al*., 2011; Phillips *et al*., 2011b; Vaughan-Hirsch, *pers.comm*.) and from a flute sample taken at contemporary glacier margin (Phillips *et al*., 2011b). Despite the evidence of considerable periglacial overprinting in the flute thin sections, the occurrence of conjugate fabric sets (akin to the S2 and S3 micro-fabrics) in other subglacial tills suggests the development of these micro-fabrics relates to subglacial processes. S2 and S3 micro-fabrics are reasonably well developed in sample HF1 despite its more recent subaerial exposure, which also suggests these micro-fabrics relate to glacial rather than periglacial processes. The S2 and S3 conjugate sets are apparent in the near-surface thin section samples, although the increased presence of the S4 micro-fabric suggests periglacial overprinting is more intense at shallow depths and has disrupted some of the subglacial micro-fabrics.

The imposition of variably developed conjugate sets of micro-fabric domains on subglacial deformation tills was interpreted by Phillips *et al.* (2011a; 20011b) as a late-stage event related to a phase of partitioned deformation that occurred as the diamictons dewatered; dewatering reduced dilatancy and increased inter-grain contacts, causing the sediment to stiffen or 'lock-up'. Two features of the flute thin sections suggest the imposition of S2 and S3 micro-fabrics relate to a similar phase of sediment dewatering. First, the wrapping of the S2 and S3 foliations around larger clasts shows that the clasts acted as stiff, rigid bodies, suggesting parts of Lithofacies A were locking-up during micro-fabric development. Second, the closer spacing and more intense development of domains 2 and 3 in finer-grained and more matrix-rich parts of Lithofacies A indicates that deformation was preferentially partitioned into the softer and more easily deformed matrix-rich areas. Those parts of Lithofacies A which are relatively enriched in silty-matrix would have been associated with relatively retarded drainage and higher pore-water pressures compared to zones rich in larger clasts which would have been relatively better-drained. Dewatering would have encouraged a reduction in sediment dilation and more inter-grain contacts, leading to a cessation of grain rotation and effectively 'locking-up' the sediment (Phillips *et al*., 2011b). The silty-matrix zones would have dewatered more slowly and continued to deform and intensify fabric development after the more rigid larger clasts had become immobile.

The size and distribution of the larger clasts in Lithofacies A affect both the development of the enveloping micro-fabric domains and their spacing. In the flute thin sections, the S2 and S3 micro-fabric domains become more widely spaced in areas where there are more and/or larger clasts (for example, in Sample MM8, Figure 5.5). Phillips *et al*. (2011b) argued that where large clasts are packed closely together, a relatively rigid zone forms because clasts are not free to rotate as they interfere with each other. The lack of rotation hinders micro-fabric development. In matrix-rich zones exhibiting more open packing, the greater separation between detrital grains allows them to rotate more freely and this rotation promotes fabric development. Grain rotation is most likely to occur if the sediment is dilatant as this allows greater separation between grains (van der Meer, 1993; Evans *et al*., 2006). In sample BYL, the S3 micro-fabric is continuous across the Lithofacies A/fine sand boundary (Figure 5.10), suggesting that the deformation that produced domain 3 affected both lithofacies. The S3 micro-fabric is very well developed in the fine-sand layer, as would be expected in fine-grained sediment with relatively open packing that promotes micro-fabric development through a freer rotation of grains (Evans *et al*., 2006; Phillips *et al*., 2011b).

In Chapter 3.3.5 it was argued that differences in particle grain-size distribution between flutes and interflutes suggested fines were being moved from interflutes into flutes, possibly after the gravel-sized clasts had become immobile. The preferential partitioning of deformation into fine-grained matrix zones, with larger clasts acting as rigid bodies is consistent with this interpretation. Phillips *et al*. (2011b) found that a conjugate set of clast micro-fabrics were symmetrically disposed around a flute long-axis and concluded that the orientation of the micro-fabric was consistent with the strain pattern formed in the lee of an initiating boulder. The conjugate set of micro-fabrics was interpreted as representing a phase of ductile shearing directed towards the flute axis which produced cross-cutting ‘veinlets’ as the sediment dewatered. Given that the S2 and S3 micro-fabrics form a similar conjugate set in the Isfallsglaciären flute sections, it is argued here that the S2 and S3 micro-fabrics were imposed penecontemporaneously during a similar phase of ductile shearing and dewatering. The wrapping of foliations around clasts and the development of pressure shadows is consistent with ductile deformation (Phillips *et al*., 2011b). The increase in the dominance of the S2 and S3 micro-fabrics towards the flute surface indicate that this phase of deformation particularly affected the upper 0.5m of the flutes. The sense of shear in domain 3 accords with the glacier flow direction, which suggests that the S3 micro-fabric relates to stresses imposed by overriding ice. The sense of shear in the S3 micro-fabric is consistent with fine matrix material being advected down-flute, and so this domain probably post-dates any initial injection of sediment from interflutes into flutes. Benn (1995) argued that flutes propagate longitudinally by re-working earlier formed flute sediments and the sense of shear in the S3 micro-fabric is consistent with the down-flow advection of sediment. However, the generally weak 2-D micro-fabric S_1 eigenvalues, like the magnetic fabrics (Chapter 4.2), suggest strain magnitudes were limited.

The S4 micro-fabric is best developed in sample MM9 from the shallowest depth and in the near-surface samples it generally cross-cuts all other micro-fabrics and so post-dates them. The S4 foliation is generally associated with lithic clasts that have steeply inclined long-axes. The vertical orientation of clasts can be produced by cryogenic processes (Bockheim and Tarnocai, 1998) or the development of water escape structures (Phillips and Merrit, 2008). The growth of segregated ice can produce cryogenic pressures within sediments that result in some clasts becoming vertically orientated. For example, the formation of segregated ice results in preferential and localized frost-jacking beneath larger lithic clasts (Van Vliet-Lanoe, 2010). Some vertically orientated clasts in domain 4 in samples MM9, BYL and MMTT have Type 1 silt caps on one side of the clast, indicating that the clasts have attained their vertical orientation after silt cap formation, which suggests the vertical orientation of these clasts relates to cryogenic processes.

In the deepest sample, MMTT, the S4 micro-fabric is associated with a number of large voids and steeply inclined fissures, especially in the area to the lower left of the sample (Figure 5.9b). Some of the fissures and voids in this area have thin coatings of silt on their outside walls and patches of fine sand occur within the larger voids, suggesting this structure could represent a water escape structure (WES). WES are thought to form during or shortly after the consolidation of water-saturated, 'liquified' sediments (Lowe, 1975; Evans *et al*., 2006), and they have been observed in subglacial diamictons (van der Meer *et al*., 1999; 2010a). In thin sections, they appear as laminated sediment inclusions or voids coated by fine-grained deposits of sediment (Phillips 2006; Phillips and Merrit, 2008). As such, it is possible that some of the S4 micro-fabric relates to the development of WES formed as Lithofacies A compacted. This may explain why the relative age-relationship between the S2, S3 and S4 micro-fabrics is often uncertain, as each fabric was developing as the sediment dewatered.

Soft-sediment deformation related to the consolidation of water-saturated sediments may also explain the convoluted folds apparent in the lower sand layers in sample BYL. Convoluted bedding is known to be associated with WES during sediment compaction (Lowe, 1975). In sample BYL, the boundary between Lithofacies A and the Frontsjön sand unit is mostly sharp and wavy. However, towards the centre of the thin section the contact between Lithofacies A and the fine sand shows a rucked-up finger of sand pinching-up into the diamicton. This occurs on the lee-side of a relatively large lithic clast which is embedded in the base of the diamicton. The rucked-up sand could be a prow formed ahead of a lodged clast, or a loading structure. The boundary becomes increasingly uncertain and diffuse on the left-hand side of the sample, which is more characteristic of a deformable contact (Piotrowski *et al*., 2001). The rose diagrams for sample BYL show that the clast micro-fabric for the massive sand layer in area 3 (Figure 5.10) resembles the S1 foliation in that the long-axes of the sand grains are inclined at a low angle (<10°) up-flow. The 2-D sand micro-fabric shows relatively strong linear clustering with an S_1 eigenvalue of 0.79. Although no distinct S1 domains occur in Lithofacies A in this sample, the S1 foliation is apparent in the S2 and S3 microlithons and this can be seen in the rose diagram for area 1 (Figure 5.10). Here, a distinct mode of grains inclined at low angles is observed. The basal sections of subglacial deformation tills in Scotland have been shown to inherit preferred clast alignments from underlying substrate (Phillips and Auton, 2008). As such, in sample BYL, the S1 foliation preserved in the microlithons and apparent in the rose diagram for the base of Lithofacies A may have been inherited from the cannibalisation of the underlying sands.

5.4.3 Summary

The macroscopic appearance of homogeneous subglacial diamictons belies a more complex deformation history, and the application of the micro-structural mapping technique provides insights into the polyphase history of sediment deformation and flute formation that are not apparent at the macro-scale. The micro-structural maps suggest a three-stage deformation history for Lithofacies A:

Phase 1. A dilatant and relatively pervasive phase of ductile deformation in which the S1 micro-fabric develops.

Phase 2. The imposition of the S2 and S3 clast micro-fabrics during a phase of deformation in which the diamicton dewaters and locks-up. The S2 and S3 micro-fabrics formed a penecontemporaneous conjugate cross-cutting micro-fabric set which overprinted the S1 micro-fabrics in thin sections, especially in the upper 0.5m.

Phase 3. The development of the S4 micro-fabric, either related to the development of water escape structures and/or cryogenesis.

During each phase of deformation Lithofacies A was not necessarily deforming continuously, but only when elevated pore-water pressures reduce shear strength below the applied shear stress (Chapter 3.3.6). There may have been multiple phases of earlier deformation not recorded by micro-structural mapping as the evidence has subsequently been overprinted by later micro-fabric developments (Phillips *et al*., 2011b). Ductile deformation was relatively pervasive throughout the deforming layer during phase 1, but was more heterogeneous and partitioned into more matrix-rich areas during phase 2.

Matrix coating around grains suggest dilatant conditions occurred during the imposition of the S1 micro-fabric and this is consistent with the forced mechanism model of flute formation in which dilatant diamicton is injected into a subglacial cavity and subsequently advected down-flow (Boulton, 1976; Benn, 1995; Evans *et al*., 2006; Phillips *et al*., 2011b). The up-flow low-angle inclination of grains in the S1 micro-fabric and the relatively strong clast 2-D micro-fabric eigenvalues in the samples taken from depth are consistent with the S1 micro-fabric developing during a phase of relatively pervasive simple shear by overriding ice. Both the forced mechanism model of flute formation and instability model requires temperate ice and high pore-water pressures, and the dilatant nature of Lithofacies A in phase 1 is consistent with these requirements. The S1 micro-fabric does not form distinct domains above ca. 0.5m depth. It is well-developed in samples taken from below 0.5m in locations where Lithofacies A is relatively thick. This change in micro-fabric with depth corresponds to the changes in clast fabrics and magnetic fabrics with depth (Chapter 4). The clast fabric data suggested flutes formed during a phase of pervasive simple shear that occurred in a deforming bed that averaged 0.5m thick. The S1 micro-fabric relates to an early phase of deformation that is preserved in thicker samples below 0.5m depth possibly because, as the bed thickened, there was an upward movement in the loci of deformation (Alley, 2000). That is, Lithofacies A incremented and advected at the same time. The S1 micro-fabric – subsequently developed in the upper half a metre or so of the flute – was then overprinted by the imposition of the S2 and S3 micro-fabrics during phase 2. The S2 and S3 micro-fabrics become increasingly intense and well-developed above 0.5m depth, which suggests that the partitioned deformation in phase 2 was focused into the upper part of the flute. The available clast fabric and micro-fabric evidence is consistent with the following scenario:

a) An earlier phase of shearing by overriding ice imposes the S1 micro-fabric on Lithofacies A, which is in a dilatant state. Lithofacies A increments and advects at the same time and there is an upward movement in the loci of deformation. In the upper 0.5m of the developing flute soft-sediment is laterally transferred from interflutes to flutes and advected down-flow for relatively modest distances, which are sufficient to generate the S1 micro-fabric. Sediment being advected within the propagating flute is in a confined space, which limits clast rotations (Benn, 1994; 1995). Larger clasts act as passive markers once they have become flow-parallel and strong flow-parallel a-axis clast fabrics develop. As the sediment begins to dewater, increased inter-gain contact produces a more rigid framework which inhibits further grain rotations. The softer parts of the matrix remain relatively dilatant.

b) Further dewatering leads to the stiffening of the matrix. Deformation during this 'locking-up' phase generates micro-fabrics S2 and S3 which overprint the earlier micro-fabric (S1). Deformation during this phase is particularly focused into the upper parts of the flute and partitioned into the softer parts of the matrix. Larger matrix grains act as rigid bodies and the S2 and S3 micro-fabrics wrap around these. The locking-up of Lithofacies A acts as a break on glacier flow and localised sticky-spots form (Phillips *et al*., 2011b).

The available evidence is consistent with the forced mechanism model and the flow instability model of flute formation. The application of the latter model to Isfallsglaciären requires flutes 0.3 to 0.4m high to be formed in response to a flow instability that remoulds the soft-bed into quasi-regular dimensions. Schoof and Clarke (2008) demonstrated that flow instabilities can result in the transfer of sediment from interflutes to flutes, and ductile deformation in a *ca*. 0.5m thick bed could generate the required remoulding of the soft-bed.

5.5 Description of Thin Section Samples from the Storglaciären Diamicton Plain

The diamicton plain thin sections show a number of similarities to the Isfallsglaciären flute samples in terms of clast lithology, the degree of sediment sorting, and the presence of micro-structures related to periglacial overprinting. Sample MMS2 was taken from Log NL2 at 0.7 to 0.8m depth on the Nordjåkk side of the diamicton plain (Figure 5.16a). Sample SL1 was taken at log SL1 from 0.7 to 0.8m depth on the Sydjåkk side of the diamicton plain (Figure 5.16b). Both samples consist of poorly sorted diamicton (Lithofacies Bii). Dolerite and amphibolite are the dominant lithic clasts, with some of the largest clasts consisting of meta-sediments (Figures 5.17 and 5.18). Specimens of banded gneiss and garnet-mica schist also occur. Feldspar crystals in lithic fragments are very fresh and show little sign of chemical weathering or alteration. A few clasts exhibit matrix-filled fractures. Sample MMS2 resembles the flute samples D1 and MM8 in that the matrix is separated into platy aggregates by extensive sub-horizontal to steeply inclined fissures (fissile partings). As in the Isfallsglaciären flute samples, the fissures consist of contraction voids and strings of irregular-shaped linear voids, rather than elongated voids (Figure 5.17b). As in the flute samples, the voids are clean, except for occasional linings of thin silt observed at higher magnifications. Vughs occur frequently in the matrix of both diamicton plain samples, as do a few isolated spherical voids. As in thin section MMTT from Isfallsglaciären, which was taken at a similar depth to the Storglaciären diamicton plain thin sections, silt caps are thin (<0.1mm) and less common than in the shallow flute samples. Type 1 silt caps dominate, although Type 2 silt caps occur in both diamicton plain samples, especially on larger grains adjacent to the intersection of steeply inclined and sub-horizontal linear voids.

Comment [DJG37]: interpretation

Sample MMS2 was taken in an area where a gravel layer (SG) occurred in the Nordjåkk section. The sample was taken about 2m up-flow from Log 2 in an area where the gravel layer pinched out and a series of thin sand fingers appeared to squeeze-up into Lithofacies B (Chapter 3.7.1. and 3.8.4). The sample was taken across the contact between the sand fingers and Lithofacies B. The thin section can be divided into three areas (Figure 5.17a):

(1) The upper part, Area A, where Lithofacies B contains a darker looking matrix with a more dense concentration of silt and fine sand and a number of relatively large lithic clasts. Three sand inclusions form thin sub-horizontal bands extending up to 63mm across the thin section.

The sand layers have sharp upper and lowers contacts with the diamicton, are between 0.7 and 6mm thick, and massive. They are quite poorly sorted and contain occasional grains 1 to 2mm in diameter. Most grains are of fine sand-size and sub-angular to sub-rounded. At higher magnifications (x40) the sand is seen to contain included fragments of Lithofacies B (Figure 5.17d).

(2) The middle centre, Area B, where Lithofacies B has a lighter, 'washed' appearance and fewer relatively large lithic clasts occur (Figure 5.17a).

(3) The lower section, Area C, which is dominated by a large clast of metamorphosed dolerite (Figure 5.17a).

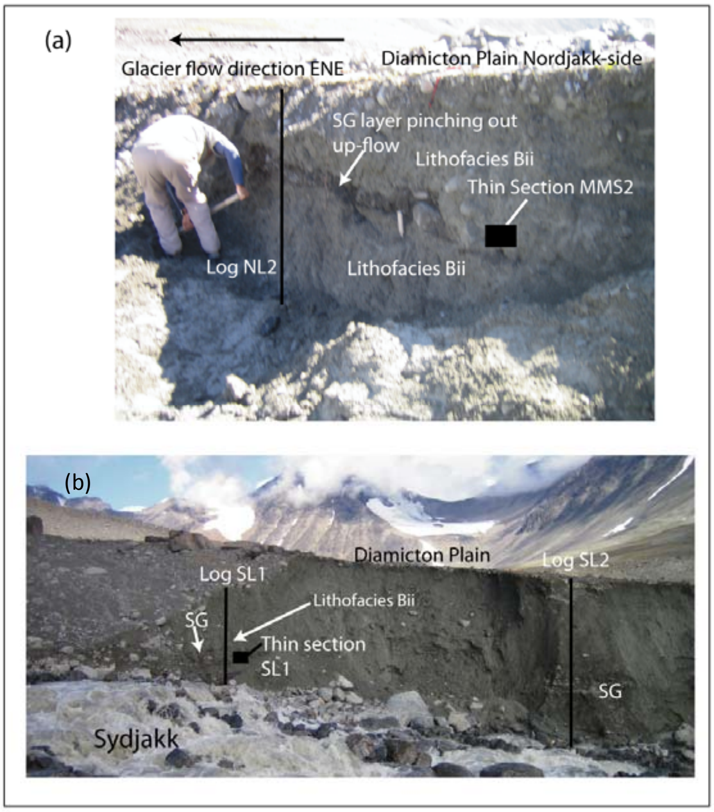

Figure 5.16(a) Location of thin section Sample MMS2, Nordjäkk; (b) Location of thin Section Sample SL1, Sydjåkk, Storglaciären diamicton plain.

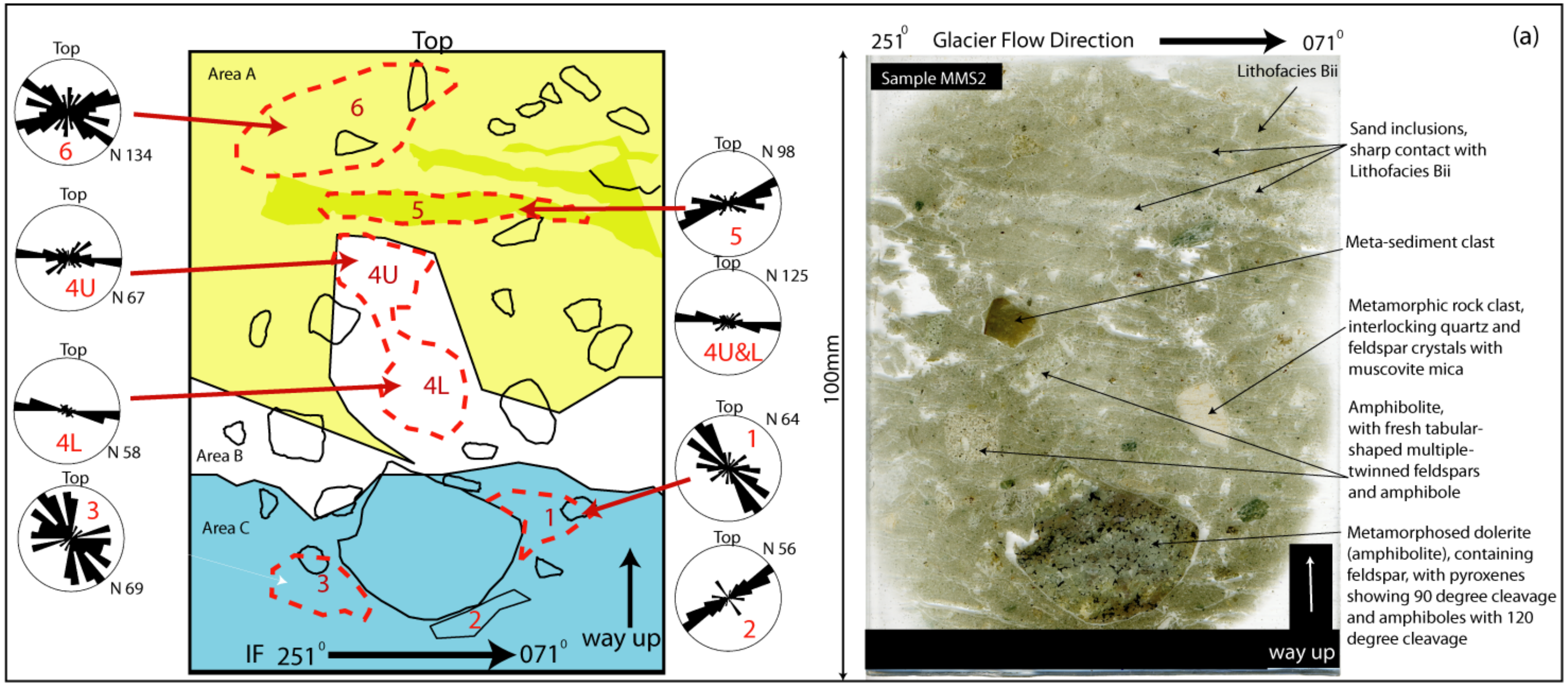

Figure 5.17(a) Sample MMS2, Nordjåkk, Storglaciären diamicton plain - 2-D micro-fabrics and thin section. Note the 'bow-tie' appearance of the conjugate micro-fabric set in zone 6, Area A, and the multimodal orientations in the rose diagram for zone 3, Area C, consistent with the development of an asymmetric pressure shadow.

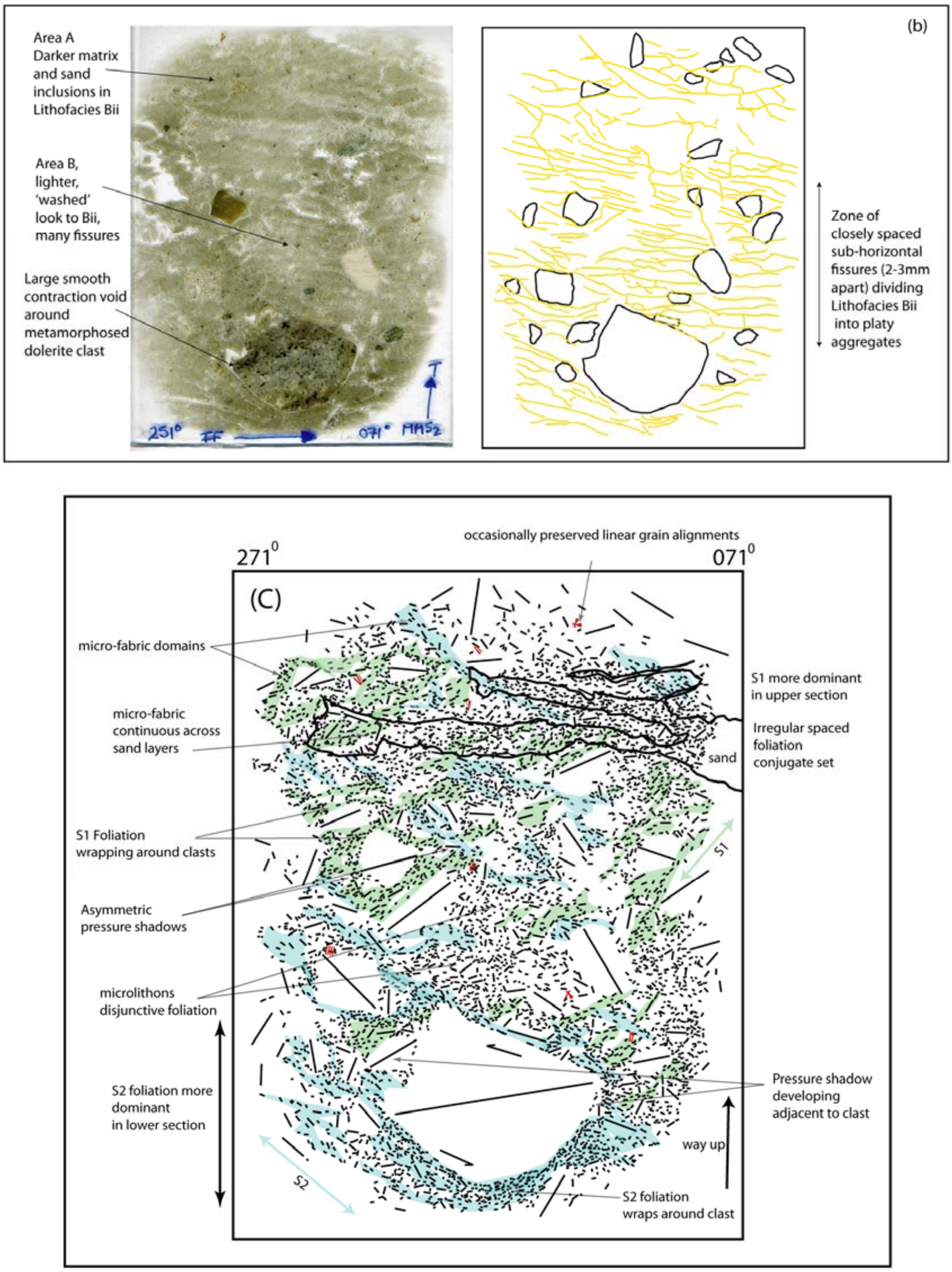

Figure 5.17 Sample MMS2, Nordjåkk (b) Fissures (c) Micro-structural Map (domain 1 in green, domain 2 in blue, grain alignments in red).

In the upper right-hand side of Area A lithic clasts display a crude preferred inclination down-flow, whereas on the left-hand side they are more inclined up-flow. On the left-hand side of Area C, lithic clasts tend to have a steep to near-vertical inclination. Fissures are well-developed in Areas B and C, where they are mostly sub-horizontal or inclined down-flow at 12° to 17°. Some fissures have steeper inclinations and are continuous across the sand/Lithofacies B boundary, suggesting their development post-dates the deposition of the sand. There is no evidence that the contact is offset either side of the steeply inclined fissures.

Sample SL1 from the Sydjåkk side of the diamicton plain was taken across the boundary of Lithofacies B and a layer of sandy gravel (Chapter 3.8.4). The thin section can be divided into two areas (Figure 5.18):

(1) Area A above the large clast of graded sandstone where Lithofacies B occurs;

(2) Area B to the left and below the large sandstone clast where sandy gravel (SG) occurs.

The long-axes of large lithic clasts in both lithofacies show a crude preferential inclination down-flow, with the Lithofacies B clasts inclined at 25° to 50°, and the gravel clasts at 15° to 20°. Lithic clasts in the SG, many of which have long-axes >5mm, range from rounded to angular. The large graded sandstone clast that dominates the thin section has a 68mm long-axis that is inclined down-flow at 8°. The contact between SG and Lithofacies B occurs above and to the left of the sandstone clast. In the lower part of the thin section, the SG layer exhibits crude sedimentary grading as it coarsens upwards and then fines-upwards towards the contact with Lithofacies B. To the left of the large sandstone clast, SG grades upwards to a thin sequence of sand and silty laminations that form a sharp wavy-contact with Lithofacies B. The sand is compositionally and texturally immature, consisting of angular grains of amphibole and feldspar, with subordinate quartz crystals. A thin layer of fine-sand/coarse silt occurs discontinuously across the top right-hand side of the large sandstone clast where it forms a merging contact with Lithofacies B. The silty laminations in the sand are cut by steeply inclined fissures, but show no evidence of being off-set by these. Nor is there any evidence of faulting or shear planes at the boundary between the sand and Lithofacies B. The matrix in Lithofacies B contains vughs, some of which contain silt cutans, and small, irregular-shaped packing voids (Kilfeather and van der Meer, 2008). Linear voids are fewer and not as laterally extensive as in sample MMS2. Some linear voids contain occasional thin linings of silt.

Comment [DJG38]: Is this relevant?

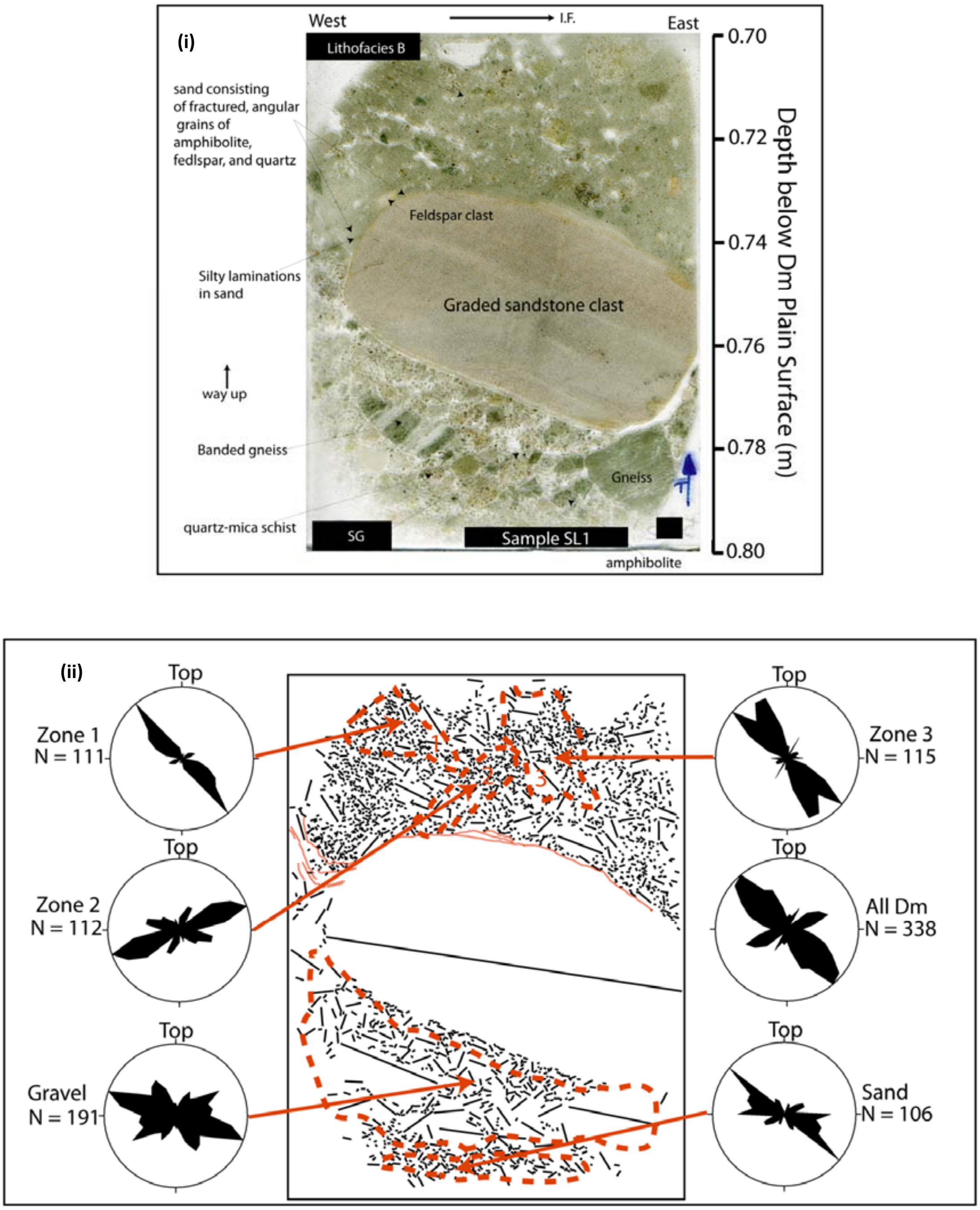

Figure 5.18(i) Thin Section SL1, Sydjåkk, Storglaciären diamicton plain; (ii) 2-D micro-fabrics. Note how the dominant orientations in Lithofacies A (e.g. zone 3 and for all Dm readings) resemble the modal orientations in the sand. The large graded sandstone clast is weakly metamorphosed and probably a meta-sediment from the Kebne Dyke Complex.

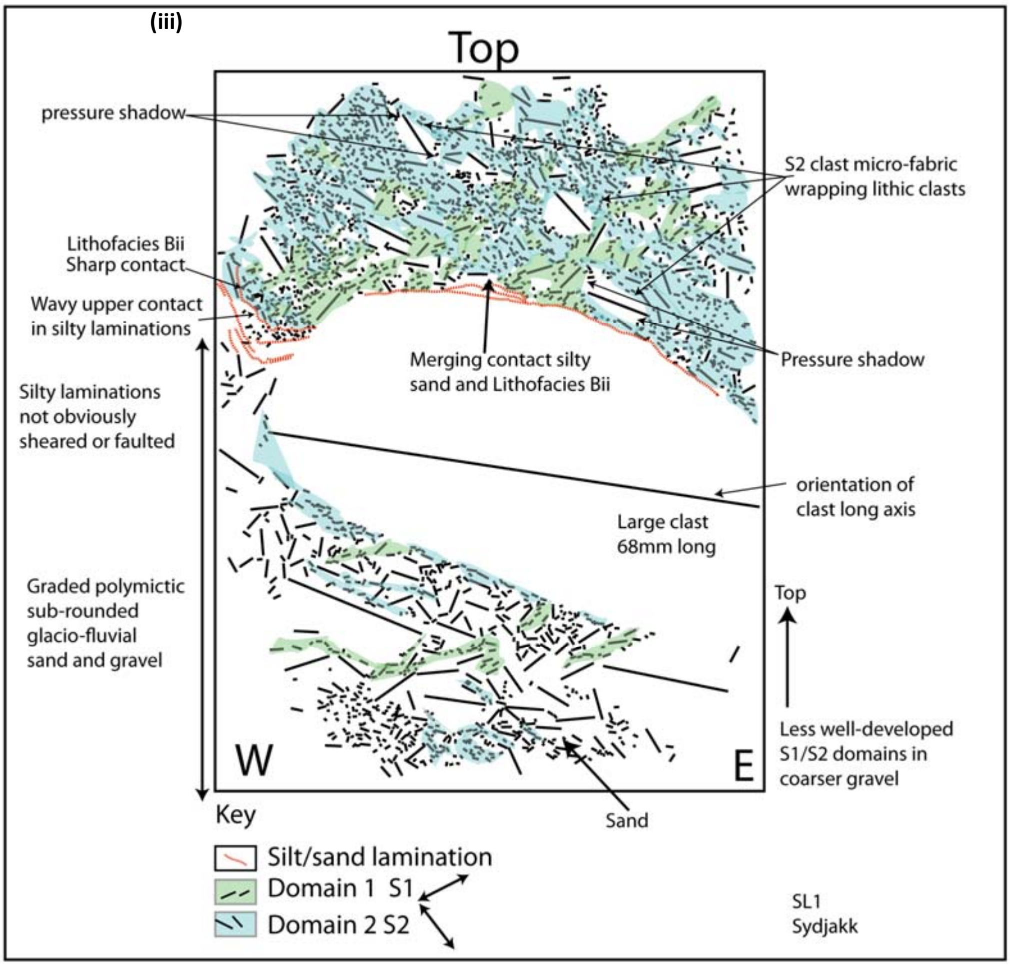

Figure 5.18(iii) Micro-structural map of thin section SL1, Sydjåkk. Note the relatively pervasive nature of the S2 foliation and domains in Lithofacies A.

5.6 Micro-structural Maps for Diamicton Plain Samples

5.6.1 Thin Section MMS2, Nordjäkk

The micro-structural map reveals two distinct clast micro-fabrics, S1 and S2 (Figure 5.17c). S1 forms a variably developed spaced (disjunctive) clast micro-fabric which defines short to irregular lens-shaped domains. The S1 micro-fabric forms more closely space domains in Area A where the sand layers occur and where there are relatively few larger lithic clasts (domain 1 has a spacing of 6.6 in Area A but this increases to between 10 and 30 in Area C).

Domain 1 is continuous across the sand/Lithofacies B contacts in area A. The S1 clast micro-fabric forms domains that are relatively steeply inclined up-flow (15° to 20°). The S1 micro-fabric is seen to wrap-around and envelop larger lithic clasts which tend to have similar up-flow inclinations, particularly in Area A. Asymmetric pressure shadows and clast geometry suggest a dextral sense of shear which is consistent with the glacier flow direction to the ENE. The intervening microlithons are massive, although they exhibit a crude flat-lying clast inclination reminiscent of the S1 micro-fabric from the lower flute samples at Isfallsglaciären, especially in Area B (see rose diagram for area 4 U&L, Figure 5.17a). As in the flute samples, occasional linear grain alignments seem to be associated with inclined linear voids and are short and inclined down-flow at 25° to 35° (Figure 5.17c).

Comment [DJG39]: interp

The S2 clast micro-fabric is much better developed in Area C where it wraps-around and envelopes the large clast of metamorphosed dolerite (Figure 5.17c). The S2 micro-fabric forms a weakly anastomosing spaced (disjunctive) micro-fabric which defines irregular-shaped domains which are inclined down-flow at 15° to 30°. The S2 micro-fabric is weakly developed in the upper left of Area A, and in the middle section of Area B. Like the S1 micro-fabric, the S2 micro-fabric is continuous across the sand/Lithofacies B contact in the upper right of Area A. The asymmetric pressure shadows developing adjacent to the large metamorphosed dolerite clast in Area C suggest a sinistral (top to left) sense of shear. The rose diagrams in Figure 5.17a show that the orientations of sand-sized grains in Lithofacies B become multi-modal in zone 3 and, to an extent, in zone 1, which are in the pressure shadow of the large dolerite clast. These 2-D micro-fabrics consequently have weak S_1 eigenvalues of 0.67 (Table 2). However, the rose diagram for zone 2, which lies just below the dolerite clast, shows a strong enveloping micro-fabric with an S_1 eigenvalue of 0.798. Where the S2 micro-fabric envelopes larger lithic clasts, the larger clasts tend to exhibit a crude preferred long-axes alignment down-flow. The variable micro-fabric development around the large dolerite clast, and the variable development, spacing and intensity of domains 1 and 2 across the thin section, suggest that, as in the flute samples from Isfallsglaciären, strain was partitioned and heterogeneous rather than homogeneous (Phillips *et al*., 2011b).

Like the S2 and S3 clast micro-fabrics in the Isfallsglaciären flute samples, the S1 and S2 micro-fabrics in the Storglaciären diamicton plain samples show a complex relative age relationship. The S2 micro-fabric mostly seems to cross-cut the S1 micro-fabric, especially in Area C, but examples of micro-fabric S1 cross-cutting S2 also occur, especially in Area A.

The rose diagram showing 2-D clast micro-fabrics in zone 6 (Figure 5.17a), a zone of Area A where both the S1 and S2 micro-fabrics are well-developed, shows a ‘bow-tie’ appearance, with the micro-fabrics forming a well-developed conjugate set (Phillips *et al*., 2011b). The S1 and S2 foliations are about 60° apart in this zone. The conjugate set is less well-developed in Areas B and C, suggesting Area A in the upper part of the thin section, experienced a more complex strain history.

5.6.2 Thin Section SL1, Sydjåkk

The S1 and S2 clast micro-fabrics also occur in the micro-structural map for sample SL1. The S1 clast micro-fabric is weakly developed throughout the thin section and forms short and discontinuous domains. It is best developed in zone 2 of Area A in Lithofacies B (Figure 5.18b). Here, the long-axes orientations of sand-sized grains shown in the rose diagram for a relatively weak fabric (S_1 eigenvalue = 0.678). The S1 micro-fabric is weakly developed in Area B. The S2 micro-fabric dominates the thin section and, in Lithofacies B, it forms a near-continuous domain that pervades the whole of Area A. It is more weakly developed in Area B, where it forms an irregular spaced (disjunctive) micro-fabric that develops in the sand-sized fraction of SG, especially in the area immediately beneath the large graded sandstone clast. The area of SG to the left of the large sandstone clast is massive, as might be expected in a pressure shadow developing adjacent to a large clast. The S1 and S2 clast micro-fabrics are variably developed within Lithofacies B. The S2 clast micro-fabric is much better developed in zones 1 and 3 of the thin section. In these zones, the 2-D micro-fabrics measured using the long-axes orientations of sand-sized grains (Figure 5.18b) exhibit relatively strong S_1 eigenvalues (0.776 and 0.745). By contrast, the 2-D micro-fabric for all sand-sized grain long-axes measured in Lithofacies B (N = 338) has a relatively weak S_1 eigenvalue of 0.639 (Table 2), although grain orientations reveal the dominance of the S2 foliation, which is relatively steeply inclined down-flow. The S2 clast micro-fabric wraps-around some larger clasts in Lithofacies B. The 2-D micro-fabric for the underlying gravel substrate reveals a weak S_1 eigenvalue (0.64), with grain long-axes having multiple orientations. Linear and turbate grain alignments were not observed in sample SL1.

5.7 Interpretation and Discussion

As in the flute samples from Isfallsglaciären, micro-scale evidence of subglacial deformation in the form of plasma fabrics, micro-scale folds and faults is not observed in the Storglaciären thin sections. However, the conjugate set of S1 and S2 micro-fabrics revealed by the micro-structural maps are consistent with a subglacial deformation origin for Lithofacies B as similar micro-fabric sets have been observed in other subglacial deformation tills (Phillips *et al*., 2011a; 2011b). The wrapping of the S1 and S2 foliations around large lithic clasts and the development of pressure shadows adjacent to large clasts is consistent with a phase of ductile deformation (Phillips *et al*., 2011b).

Lithofacies B contains clasts of unweathered meta-sediments (Figure 5.17a) that have originated from the Kebne Dyke Complex that crops out in the accumulation zone of Storglaciären (Anderson and Gee, 1989, see Chapter 2.1.4). The large sandstone clast in sample SL1 is probably also a meta-sediment - the contact between SG and Lithofacies B occurs above and to the left of the sandstone clast, suggesting the sandstone clast belongs to the SG. If meta-sediment clasts in Lithofacies B were derived from the cannibalisation of proglacial sediments which had experienced prolonged subaerial exposure, then they would appear more weathered. The presence of fresh meta-sediment clasts in Lithofacies B is consistent with it containing a relatively far-travelled component, which is a defining feature of subglacial deformation tills (Piotrowski *et al*., 2001). The short, relatively high-angle linear grain alignments observed in sample MMS2 are thought to be indicative of low to moderate strain magnitudes (Larsen *et al*., 2006; Thomason and Iverson, 2006). The S_1 eigenvalues for 2-D sand micro-fabrics in Lithofacies B are variable, with some equivalent to steady-state values (strain ≥7) obtained in the ring shear experiments of Thomason and Iverson (2006), whilst others show weaker values indicative of low strain magnitudes.

Comment [DJG40]: interp

Sample MMS2 shows many features indicative of cryogenesis and the growth of segregated ice in polar sediments, such as Type 1 and Type 2 silt caps, linear voids consisting of bubble-shaped to irregular-shaped vughs, and platy aggregates separated by distinct fissures consisting of contraction voids and linear voids (Harris, 1998; van Vliet Lanoe, 2010). In Chapter 3.4 it was shown that Lithofacies Bii from below ca. 30cm depthwas relatively enriched in silt-sized material compared to Lithofacies Bi from the top *ca*. 30cm of the diamicton plain. The presence of silt caps in Lithofacies Bii suggest that the difference in particle grain-size distribution is accounted for by the post-depositional illuviation of silt related to seasonal snowmelt and thaw consolidation. The development of Type 2 silt caps on larger clasts adjacent to the intersection of linear voids indicates sufficient illuviation following thaw consolidation and snow melt to coat the top and sides of some grains with silt (Harris, 1998).

There is little evidence in sample MMS2 that the fissures and linear voids (which demarcate the fissile partings) are the product of subglacial shearing. As in the flute samples, it is possible that the fissures have been opened-up along pre-existing shear planes by subsequent unloading/dewatering/cryogenesis, but the clean nature of most fissures, and the presence of bubble-shaped and irregular shaped vughs along the linear voids, suggests they are late-stage structures that have been developed/affected by cryogenesis (Harris, 1998). The occasional thin linings of silt along some voids are consistent with thaw consolidation (Bockheim and Tarnocai, 1998; Harris 1998). As in the flute samples, the linear grain alignments associated with liner voids may indicate a phase of discrete and brittle shear along the fissures. However, some fissures in sample MMS2 are seen to be continuous across the sand/Lithofacies B contact, which indicates that the fissures post-date the emplacement of the sand. There appears to be no offset of the contact either side of the fissures, as might be expected in the fissures represented shear planes. In sample SL1, fissures and linear voids are less evident and extensive, and silt caps are infrequent and thin. The reduced influence of periglacial overprinting probably reflects the shorter time this area has been subaerially exposed compared to sample MMS2 (Figure 3.2c). Historical aerial photographs show that the area where sample MMS2 was taken was subaerially exposed after 1917 but (well) before 1959, whereas the area where sample SL1 was taken was subaerially exposed between 1959 and 1969.

It is not possible to quantify the effect of silt illuviation on magnetic fabrics (Chapter 4.2.10) because fabric strength prior to subaerial exposure is unknown. The post-depositional translocation of silt possibly explains some of the deviations from simple shear seen in the diamicton plain aggregate strain ellipsoid, especially for the longer exposed Nordjåkk samples (Chapter 4.2.6). However, magnetic fabrics sample bulk volumes and silt caps are very thin and infrequent, so the quantity of undisturbed silt-sized material in the bulk sample at this depth is probably considerable, which suggests that the magnetic fabrics reflect a subglacial signature. Furthermore, there is no evidence of a pronounced succitic fabric (van Vliet-Lanoe, 2010) developing in samples MMS2 and SL1, which suggests at this depth, the influence of frost action on gravel a-axis macro-fabrics is minimal.

The Nordjåkk sample, MMS2, shows similarities with the flute samples from Isfallsglaciären in that a penecontemporaneous conjuctive set of spaced micro-fabrics is variably developed within the thin section. The micro-structural map for sample MMS2 shows that a cross-cutting conjugate set of micro-fabrics developed, probably as the sediment dewatered, lost dilatancy, experienced increased inter-grain contact, and 'locked-up' (Phillips *et al*., 2011b). A few clasts exhibit matrix-filled fractures which were probably formed by clast crushing (Phillips *et al*., 2011a). As the sediment dewatered, effective pressure would have increased as pore-water pressured reduced, which would have promoted grain-crushing.

Comment [DJG41]: interpretation

The variable development, spacing and intensity of the S1 and S2 micro-fabrics shows that deformation was partitioned within the matrix of Lithofacies B, whilst the complex relative age relations between the S1 and S2 clast micro-fabrics suggest a reversal in the timing of the imposition of the S1 and S2 micro-fabrics in different parts of the diamicton (Phillips *et al*., 2011a; 2011b). The wrapping of the S1 and S2 foliations around larger clasts suggests these acted as rigid bodies during the imposition of the fabric, consistent with the commencement of sediment stiffening and the preferentially partitioning of deformation into the finer fraction of the matrix. As with the flute samples, the granulometry seems to have exerted a control of strain partitioning, probably through controlling the pore-water pressure and the ease with which clasts could rotate (Evans *et al*., 2006; Phillips *et al*., 2011b).

Asymmetric pressure shadows indicate the sense of shear; the S1 macro-fabric gives a dextral (down-flow) sense of shear, whilst the S2 macro-fabric gives a sinistral sense of shear. The relatively steeply-inclined S2 micro-fabric resembles the steeply inclined Riedel shears that develop in ring shear experiments when subglacial tills are pervasively sheared (Figure 5.15, Thomason and Iverson, 2006). Sets of Riedel shears can develop during ductile or brittle deformation and can be inclined both up-flow and down-flow (Phillips *et al*., 2011a). Care must be taken in interpreting the sense of shear in the thin sections from the Tarfala Valley because grains are only being observed in 2-D. However, the 'apparent' S1 and S2 sense of shear are consistent with shearing induced by overriding ice (Thomason and Iverson, 2006; Phillips *et al*., 2011a) and, given the lack of evidence for brittle shear at the micro-scale, probably represent a relatively ductile phase of shearing along Riedel shears (Phillips, *pers.comm.*).

Ductile deformation is usually associated with high pore-water pressures and temperate ice conditions (Evans *et al*., 2006). Evidence that such conditions occurred in sample MMS2 is provided by the sand inclusions in Area A. The sharp contacts between the sand and Lithofacies B and the presence of included fragments of Lithofacies B in the sand, show that sand deposition post-dates Lithofacies B emplacement and that the contact is erosional. An explanation for this is that the sand layers represent a water escape structure (WES). WES consisting of massive sand with sharp contacts have been observed in other thin sections of unconsolidated sediments (Phillips, 2006). In Chapter 3.7.1 it was shown that the SG sheet in the Nordjåkk sections grades upwards in places to thin sandy layers at the contact with Lithofacies A. The sand fingers in sample MMS2 probably originated from consolidation of thin sandy layers. The presence of WES suggests that pore-water pressures were high. It was also argued in Chapter 3.7.1 that the SG sheet could have formed by subglacial meltwater incision (Boyce and Eyles, 2000), or by ice-marginal deposition during a Little Ice Age glacier oscillation (Karlén, 1973). In either case, the increase in overburden pressure brought about by the subsequent deposition of the overlying Lithofacies B would have encouraged sediment consolidation and the formation of WES where pore-water pressure were high. The S1 and S2 micro-fabrics are continuous across the sand-Lithofacies B contact which indicates the imposition of the micro-fabrics post-dated the emplacement of the sand.

The diamicton plain samples lack the flat-lying S1 micro-fabric and steeply inclined S4 micro-fabric observed in the flute samples, suggesting they had a less complex deformation history. However, 2-D sand micro-fabrics for zones 4U&L in Area B in sample MMS2 (see rose diagrams in Figure 5.17b), show a dominance of grain long-axes inclined at a low-angle down-flow in the S1 microlithons. This 'washed' zone lacks a dense silty matrix and is massive, or contains weakly developed S1 or S2 domains. The 2-D sand micro-fabrics are possibly picking-up a remnant of an earlier micro-fabric in the S1 microlithon, which, like the similar micro-fabric in the flute samples (S1), indicates an earlier phase of deformation.

Sample SL1 from Sydjåkk is distinct from all other thin section samplesin that:

a) no linear or turbate grain alignments have so far been observed in Lithofacies B;

b) the S2 micro-fabric, which is relatively steeply inclined, is pervasively developed and defines a near-continuous domain rather than a spaced micro-fabric across the whole of area A, which indicates a phase of pervasive deformation;

c) the S1/S2 conjugate set is very weakly developed.

Two hypotheses were presented in Chapter 3.8.4 to account for the origin of the heterogeneous sedimentary sequence observed in logs SL1 and SL2 on the Sydjåkk side of the diamicton plain, where Lithofacies B was interbedded with layers of SG and Sm. The micro-structural evidence is equivocal in that it appears to show evidence in support of both;

Hypothesis 1: a glaci-tectonised proglacial sequence formed during the Little Ice Age advance in which Lithofacies B originates as a subglacial traction till. Strain partitioning results in the incomplete homogenization of the coarser SG layers which are able to resist subglacial deformation more effectively than finer-grained layers. Evidence to support this hypothesis is that the S1 and S2 clast micro-fabrics occur in Lithofacies B and SG in thin section SL1, but they are weakly developed in the coarser gravel layer, as would be expected with strain partitioning in a glaci-tectonised sequence (Evans *et al*., 2006; Ó Cofaigh *et al*., 2011). Furthermore, the incomplete homogenisation of the SG would result in the retention of primary sedimentary structures (such as crude sediment grading and silty laminations seen in thin section SL1);

Hypothesis 2: ice-marginal sequence produced during Little Ice Age glacier oscillations. Evidence in support of this hypothesis comes from primary sedimentary origin of the SG layer in thin section SL1. In addition, there is a lack of evidence for glaci-tectonic deformation at the contact between the SG layer and Lithofacies B (no faults, shears, intraclasts). The S1 and S2 micro-fabrics may have been imposed during a stiffening/deformation phase as both lithofacies were frozen-on to the base of the glacier in the terminus region where cold-based ice occurs. Similar frozen-on sequences of SG and diamicton are observed at the present margin of Storglaciären (Moore *et al*., 2012). Alternatively, ice-marginal deposition and deformation occurred during Little Ice Age glacier oscillations, resulting in the interdigitation of SG with localised deformation tills (Menzies and Shilts, 2002). Diamicton and SG deposits are observed in close association beneath the terminus of contemporary Kaskasatjåkkaglaciären (Figure 5.19). The unweathered appearance of feldspar crystals in lithic clasts in SG and Lithofacies B suggests these lithofacies contain grains of recent origin that have not experienced prolonged exposure to weathering whilst being subaerially exposed in a proglacial zone. This is consistent with the SG layer being a relatively recent ice-marginal deposit rather than an older glaci-tectonised proglacial deposit. As such, hypothesis 2 is considered here to be the more likely explanation for the Sydjåkk sequence.

Figure 5.19 Sandy gravels and diamicton beneath the terminus of Kaskasatjåkkaglaciären. Note: the glacier is almost entirely temperate. SG is the dominant lithofacies of the forefield. In this view, looking up-flow beneath the snout of the glacier, the bed is seen to consist of a thin cover of grey-brown homogeneous diamicton and SG substrate, being eroded and re-worked by meltwater. The lithofacies resemble the gravel and diamicton sequences observed in the diamicton plain and diamicton sheet logs, but their preservation potential seems poor.

The magnetic fabrics from the Sydjåkk sections (Chapter 4.2.8; Table 4.8) and the relatively weak 2-D micro-fabric S_1 eigenvalues (Table 5.2) suggest Lithofacies B experienced moderate to weak strain magnitudes (<10) in this area (Larsen *et al*., 2006; Thomason and Iverson, 2006; Iverson *et al*., 2008). Moreover, clast fabrics from vertical sequences in the diamicton plain suggest Lithofacies B formed incrementally from thin deforming layers (Chapter 3.8.4). The available clast fabric and magnetic fabric data suggest that Lithofacies B in the diamicton plain formed by limited sediment advection in thin deforming layers of 0.3-0.6m thick. The micro-structural evidence suggests that a phase of ductile deformation occurred within each deforming layer, and that at times this was pervasive across parts of the thin section (for example, Llithofacies B in thin section SL1). However, within each deforming layer, strain was heterogeneous and partitioned into the softer and more easily deformed matrix-rich parts of Lithofacies B. In this regard, subglacial deformation was similar in Lithofacies A from the Isfallsglaciären flutes and Lithofacies B from the Storglaciären diamicton plain.

5.8 Conclusions

The micro-structural mapping approach provides insights into the polyphase history of sediment deformation that are not apparent at the macro-scale. Homogeneous diamictons from flutes are seen to have a complex 3-phase deformation history, with strain partitioned into softer and more easily deformed parts of the matrix. The earliest phase of deformation appears to have been relatively dilatant and pervasive and related to shearing imposed by overriding ice. The imposition of a conjugate set of cross-cutting micro-fabrics appears to have been related to dewatering, which resulted in a loss of dilatancy and increased inter-grain contacts. A similar conjugate set of micro-fabrics is variably developed in the diamicton plain samples and have been observed in other micro-structural maps of subglacial deformation tills. There is evidence to indicate that water escape structures developed in both the flute and diamicton plain samples, which suggests periods of relatively saturated sediment conditions prevailed subglacially. The micro-structural evidence is consistent with both the forced mechanism model of flute formation and the instability model of flute formation. Short and often steeply inclined linear grain alignments and weak S_1 eigenvalues in 2-D micro-fabrics suggest generally weak to moderate strain magnitudes, which are consistent with the magnetic fabric results.

The diamicton plain sample from the Nordjåkk section is similar to the flute samples and reveals a history of heterogeneous strain. The apparent sense of shear indicated by asymmetric pressure shadows, which developed as the S1 and S2 foliations wrapped around larger clasts, is consistent with shearing by overriding ice. The conjugate set of S1 and S2 micro-fabrics were produced during a relatively ductile phase of deformation as there is little evidence of brittle shear present in any of the thin sections.

The analysis of thin sections shows that recently exposed subglacial diamictons from flutes on the forefield of Isfallsglaciären have been subjected to quite extensive periglacial overprinting related to cryogenesis and the growth of segregated ice in the silty diamicton. This is particularly true of samples from the upper 0.35m. Evidence of cryogenesis is apparent even in diamicton subaerially exposed for as little as *ca*. 30 years or less. The influence of frost action reduces with depth. Nevertheless, evidence of silt illuviation, silt cap formation, and void development related to cryogenesis is apparent even at 0.8m depth in both Isfallsglaciären and Storglaciären. There is little micro-scale evidence to support the interpretation of fissile partings as shear planes, although post-depositional processes may have exploited existing fissile partings that originated as discrete shear planes. The clean nature of the irregular-shaped linear voids suggest they opened-up at a late-stage, possibly related to unloading or dewatering, and have been developed/affected by segregated ice growth and thaw consolidation. Type 3 silt caps in the upper 0.1m suggests that gelifluction has affected the upper few centimetres of the flutes, and the presence of succitic fabric, star-shaped vughs, and platy aggregates separated by fissures shows that cryogenesis has affected the porosity, void ratio, and fabric of the shallowest flute samples. As such, it is incumbent upon researchers working on diamictons on recently exposed forefields where seasonal frost action occurs to demonstrate that sediment characteristics observed only at the macro-scale, and attributed to subglacial processes, are not the product of periglacial overprinting. The integration of the micro-structural mapping approach with macro-observations would seem to provide the most comprehensive analysis of such sediments.

Chapter 6 Subglacial Deformation, Glacier Flow Dynamics and Landform Generation

Comment [DJG42]: I've changed the language of the whole doc to UK English

6.1 Introduction

In this chapter, observations from all scales are integrated into a synthesis which addresses the key questions identified in the research objectives, namely, what was the nature and extent of subglacial deformation, how thick was the deforming bed, what was the strain magnitude, to what extent did subglacial deformation control glacier dynamics, and what role did it play in the formation of the diamicton plain/sheet and flutes (Chapter 1.5.2). In addition, the wider implications of the research findings are discussed in relation to how the results relate to subglacial processes and dynamics are the larger scale beyond small polythermal valley glaciers.

Before proceeding with the interpretation, it is useful to briefly re-cap the key features of each of the subglacial traction tills (Lithofacies A-D) identified in Chapter 3 (Table 3.1). Lithofacies A is a homogeneous clast-rich sandy diamicton that comprises the flutes of each forefield and displays strong flow-parallel clast fabrics in flute crests. Lithofacies B is the dominant lithofacies in the diamicton plain (Storglaciären) and diamicton sheet (Kaskasatjåkka). It is a grey, generally homogeneous, sandy (to silty-sandy) clast-rich diamicton which displays strong fissile texture. Lithofacies C has restricted distribution at Isfallsglaciären where it forms the substrate to Lithofacies A in the proximal to mid-reaches of the flute field, but has a wider distribution at Kaskasatjåkka. It is a very clast-rich and coarse-grained diamicton containing many cobbles and boulders, but with a weak fissile texture. Lithofacies D forms the substrate to Lithofacies B in the upper reaches of the diamicton plain at Storglaciären, and forms the substrate to Lithofacies C at Isfallsglaciären and Kasakasatjåkka. It is a clast-rich and coarse-grained diamicton containing many cobbles and boulders. Many of the clasts are very badly weathered.

This chapter has three sections; it begins by considering the extent to which the integrated observations from the Tarfala Valley support different subglacial models and falsify the soft-bed deformation model. In section two a new model of flute formation is presented which combines aspects of the forced mechanism model of flute formation with the flow instability of flute formation. In the final section observations are integrated into a glacial-paraglacial landsystems model for the Tarfala Valley. The landsystems model links lithofacies-landforms associations to processes and has a specific emphasis on subglacial processes. The landsystems model represents a framework for understanding glacial processes and products in polythermal valley glaciers. The wider implications of the findings are discussed at the end of each section.

6.2 How Applicable are Different Subglacial Models to the Tarfala Valley?

The observational evidence that could be used to support different subglacial models was summarised in Table 1.4. This table is reproduced in Table 6.1 where it includes an assessment of the extent to which the integrated observations from the Tarfala valley support each model. The models are assessed below using the key questions identified in the research objectives.

Table 6.1 An Assessment of three subglacial models using evidence obtained in the Tarfala Valley (evidence is shown in rows entitled ***evidence*** and in *italics*). The number of crosses indicates the strength of the evidence – more crosses equate to greater strength).

Observational Evidence	**Soft-bed Deformation Model** ***After Boulton and Hindmarsh, (1987); Alley, (1991); Eklund and Hart, (1996); van der Meer et al., (2003)***	**Ice-bed Mosaic Model** ***After Piotrowski et al., (2004)***	**Fluid Flow Model** ***After Evans et al., (2006)***
Depth of Deforming Bed	Potentially deep and pervasive Up to 10m +	Limited, thin, maybe as little as a few centimetres in places	Deforming bed part of hybrid traction till; depth variable, but may be limited
Evidence	**X** ***Clast fabric vectors are consistently flow parallel in parts of diamicton plain/sheet 2m thick or more***	**XXXXX** ***Facies A in flutes averages 0.3m to 0.5m depth. Diamicton plain/sheet sequences interrupted by gravel deposits. Fabric strength variations with depth suggest Dm plain/sheet formed by accretion of thin traction tills over time***	**XXXX** ***Clast Fabrics at the macro-scale do not reflect strain partitioning as fabrics are strong/stronger in stiff, clast supported stony Lithofacies C than in softer Lithofacies A and B***
Extent of Deformation	Widespread. All subglacial tills are deformation tills. Deforming soft-beds can control glacier flow. Considerable till advection	Less widespread, lodged and melt-out sequences more common than previously realised. Deforming bed forms part of a patchy mosaic. Deforming bed may form an anastomosing network (Shumway and Iverson, 2009)	Variable in time and space
Evidence	**XX**	**XXXXX**	**XXXXX**

	Advection appears limited. Diamictons are hybrids, but deformation important process in their formation	***Lodgement an important process in formation of diamictons. Parts of Dm plain show little evidence of glaci-tectonic deformation. Part of deformation of Fronstjön sands may pre-date Dm emplacement or relate to non-tectonic soft-sediment deformation***	***Traction tills observed forming plains/sheets/flutes in central parts of each forefield, wider distribution likely but sediment re-worked by slush-flows/meltwater activity***
Strain Magnitude	Very high 10^2-10^5	Patchy, but generally low $< 10^2$. In laboratory experiments, steady state strain ellipsoids and fabrics are produced at moderate to high strains (7 to 30) by simple shear (Iverson *et al*., 2008)	Variable
Evidence	***Magnetic fabrics and sand micro-fabrics suggest strain magnitudes were not very high(<10)***	***XXXXX*** ***Lithofacies A aggregate strain ellipsoid consistent with shearing by overriding ice to moderate to high strains. S_1 eigenvalues variable, mostly indicative of low to moderate strains in Lithofacies A and B***	***XXXXX*** ***Magnentic fabric S_1 eigenvalues and vectors variable over small scales, consistent with strain partitioning. The plunge of AMS ellipsoids and sand grains affected by imposition of pure shear in ice-marginal & proglacial settings***
Vertical Strain profile	Non-linear simple gradational profile typical of pervasive deformation, with strain increasing towards ice-bed interface. However, vertical variations in sediment strength, pore water pressure, and effective pressure can result in décollement plane moving upwards over time as bed accretes, which produces more complex profile	Non-linear simple gradational profile may be typical of pervasive deformation, with strain increasing towards ice-bed interface. However, bed mosaic can produce complex profile with rapid changes in fabric vectors and strength over small depth intervals. Lodgement and bed accretion can produce uniform profile	Variable but complex. Strain may be distributed uniformly within bed, with variations in strain response reflecting variations in sediment strength and dilatancy, leading to strain partitioning
Evidence	***XXX*** ***Simple gradational profiles generally not observed. Sharp wavy contacts between Lithofacies A and Fronstjön sand unit consistent with décollement***	**XXXXX** ***Fabric strengths variable with depth. Uniform vector/strength profiles in top 0.4m of flutes also consistent with lodgement. Uniform vector profiles in Dm plain/sheet with variable strength consistent with lodgement and accretion***	**XXX** ***Strain portioning observed at the micro-scale, producing variations in sand micro-fabrics, but perhaps within a thin deforming bed. Coarser Dm has just as strong/ stronger fabrics than softer matrix-supported Dm at the macro-scale, suggesting strain partitioning does not account for clast variations at the macro-scale***
Typical Fabrics	Macro-fabric strength decreases with depth in non-linear pervasive profile, but with uniform vector orientations. In a thin deforming bed, may get uniformly strong flow-parallel a-axis fabrics. Macro-fabrics may weaken at	Fabric strength is a proxy for strain magnitude as fabric strength does not decrease at higher strain; meltout, lodgement and accretion of bed over time can produce a uniform profile with strong flow-	Variable, reflecting hybrid nature of traction till. Strong fabrics may be inherited from the melt-out of debris-rich

	higher strain (Carr and Goddard, 2007)) with clasts orientated transverse to flow, or may weaken in thicker deforming beds (Hart, 1994)	parallel a-axis macro-fabrics. In ring shear experiments, strong flow-parallel a-axis fabrics and magnetic lineations are produced at moderate to high strains under pervasive shear, with up-glacier plunge. Fabrics do not weaken with increased strain once steady-state is achieved. Deviations from the steady state fabric/strain ellipsoid suggest low strains and variable strains over time (Iverson *et al*., 2008)	basal ice. Dilatant 'fluidised' A-horizons produce variable macro-fabrics, with some weaker fabrics, akin to debris flows, and are characterised by ductile deformation. Fabrics will be stronger in B horizons where discrete brittle shear dominates
Evidence	**XXX** ***Consistent vectors in flute crests in top 0.4m and uniformly strong fabrics. Vectors also consistent in Nordjåkk profiles and Dm sheet. Weaker interflute clast fabrics consistent with Benn's (1994) model of non-constrained/constrained deformation in ice-walled furrow. Herringbone fabrics also consistent with bed-deformation model***	**XXXXX** ***Dm plain/sheet profiles reveal uniform vectors with variable fabric strengths, indicative of accretion from thin layers. No evidence flute clast fabrics weaken with increasing strain – strongest magnetic fabrics associated with sample sites where strong clast fabrics recorded. Magnetic fabrics and 2-D sand micro-fabrics are not indicative of very high strain magnitudes***	**XXXX** ***Diamictons macroscopically resemble B-Type horizons, but little micro-scale evidence of brittle shear. Fabrics may be inherited from cannibalisation of underlying sediments***
Nature of Diamicton and Deformation at macro-scale	Homogenised subglacial till produced at high strain. In non-linear pervasive profile, this may gradate into tectonised layers and then non-deformed sediments beneath a décollement plane at depth. Till may contain intraclasts and rafts/wedges of substrate. At the macro-scale, evidence of brittle deformation occurs lower in the profile e.g. faulting, with evidence of increasingly ductile flow at higher strains towards the ice-bed contact e.g. sheath folds, overturned folds etc. Homogenised till consists of admixture of local and far-travelled material, with strong planar fabric common; the planar fabric represents shear planes which may be visible at the micro-scale. Clasts in deformation tills are typically sub-round to sub-angular, with blocky shapes indicative of subglacial transport. Calcite precipitate may also occur in the lee of fractures on boulder surfaces, and stoss and lee forms are common. Subglacial tills typically have pseudo-fractal patterns with slopes of C.-2.9 (Hooke and Iverson, 1995)	There are no diagnostic criteria for deformation tills. Lodgement tills can also be homogeneous and have strong planar fabrics. Non-linear deformation profiles may be seen at the macro-scale, but these will be spatially variable and limited in extent. Deformation is typically partitioned into thin layers. Subglacial deformation profiles are characterised by a homogeneous appearance. Heterogeneous sequences are more typically of till accretion over time through meltout, lodgement, and deformation processes. Sand stringers within homogeneous till represent phases of ice-bed separation. Sand drapes over boulders, striae concentrated on upper boulder surfaces, the preservation of delicate material, and the presence of non-deformed weathering haloes within homogeneous till suggest a lodgement/meltout origin rather than deformation origin. Striae and wear marks all over clasts are more indicative of deforming beds. Stoss and lee boulders are indicative of lodgement; double stoss of lee boulders of ploughing followed by lodgement	Subglacial tills originate through a variety of processes which operate in close space and time at the glacier bed, e.g. meltout, lodgement, ploughing, deformation, and erosion, and so subglacial tills are hybrids, whose character reflects over-printing by multiple processes. At the ice-bed contact, tills are likely to be in a dilatant state and deforming in a ductile 'fluidized' layer. Stiffer B horizons may deform in a more brittle manner. The escape of over-pressurized water will produce numerous water escape structures
Evidence	**XXXX** ***Strong fissile texture observed at macro-scale. Type 1 and 2 clasts have facets aligned with major fissile partings. Fissile partings are***	**XXXX** ***Little macroscopic evidence of deformation (folds, faults, shears, intraclasts). Heterogeneous sequence at***	**XXXX** ***Strong evidence diamictons are subglacial in origin. Most diamictons***

	disrupted around embedded boulders. Some sand layers appear non-deformed beneath décollement plane in Frontsjön area. Some evidence of recumbent folding/open folding in Fronstjön sand beds. Dm contains clasts of fresh dolerites and meta-sediments from Kebne dyke complex, suggesting Dm contains a relatively far-travelled component. Some embedded boulders have striae on all surfaces in Dm plain consistent with rotation in a deforming bed	***Sydjåkk. Homogeneous Lithofacies B separated by SG in Dm plain/sheet profiles. Striae on upper boulder surfaces indicate lodgement is a key process in Dm genesis. Double stoss- and- lee forms suggest ploughing occurs in flutes. Variable nature of contact between Lithofacies A and Frontsjön sand unit over small spatial scales. Faults and folds in sands may pre-date Lithofacies A emplacement or relate to non-tectonic soft-sediment deformation. Fractal slope gradients are not diagnostic of deformation and variable in Lithofacies A. Few diffuse boundaries or intraclasts seen; contacts sharp and wavy***	***observed are best classified as hybrid traction tills because evidence of lodgement, erosion, and deformation occurring in close spatial proximity. Meta-sediments and dolerite could be inherited from cannibalisation of proglacial sediments***
Nature of Diamicton and Deformation at the Micro-scale	A range of S-matrix and Plasma fabrics and structures may be present such as rotational structures, till pebbles, water-escape structures, crushed grains, necking structures, kinking fabrics, unistrial and skelsepic plasma fabrics and crenulations foliations etc, depending on the exact nature of deformation e.g. brittle, ductile, compressional, extensional etc.	There are no diagnostic micro-structures and micro-fabrics for deformation tills. Discrete shear planes, represented by grain lineations and stacks become longer and lower in angle at higher strains, and the IL-index suggests strain magnitudes in deformation tills are low (Larsen *et al*., 2006a). Lodged clasts may have a sediment prow ahead of them with sand micro-fabrics draped over the top of the clast (Thomason and Iverson, 2006)	Micro-fabrics may be seen to wrap around larger rigid clasts in a pervasively deforming bed where strain is preferentially partitioned into softer and more easily deformed matrix (Phillips *et al*., 2011b)
Evidence	**XX** ***Rarely preserved, short, relatively steeply inclined linear grain alignments, observed along the upper walls of some linear voids, may indicate a phase of discrete, possibly brittle shear and indicate the steeper fissile partings are shear planes. Occasionally preserved turbate structures in S1 microlithons indicate a phase of dilatant deformation. Crushed clasts observed in thin sections. Feldspars are fresh, suggesting they have not been inherited from cannibalised proglacial sediments that have experienced prolonged subaerial exposure. The available thin section evidence indicates considerable periglacial over-printing related to segregated ice growth in silty Dm and cryogenesis. This has resulted in increased porosity, silt illuviation and micro-fabric disruption, especially in the upper 0.35m of flutes***	**XXX** ***Little evidence of glaci-tectonic deformation (folds, faults, shears, plasma fabric). Linear grain alignments are rare and may be 'apparent' alignments as only viewed in 2-D, or they may relate to water flow along voids. Turbate structures and crushed clasts are formed in various sediments and are not diagnostic of deformation. There is little evidence to suggest the fissile partings are shear planes – they seem to have opened-up at a late-stage and have been affected by cryogenesis. The contact between sand/Dm is not off-set either side of fissile partings. The apparent alignment of the facets of Type 1 and Type 2 clasts along fissile partings may represent the preferentially development of voids beneath larger clasts and contraction of sediment away from faceted faces. There is little evidence of deformation at the sand/Dm boundaries in the Dm plain samples***	**XXXX** ***Micro-structural maps suggest a polyphase history of deformation with strain partitioned into softer parts of matrix. Foliations wrap-around larger clasts, suggesting these acted as rigid bodies during fabric imposition. This suggests fabric was imposed as the sediment dewatered and locked-up. There is little evidence of a brittle phase of deformation. Deformation was heterogeneous. There is some evidence that WES developed at the SG/Lithofacies B boundary in the Nordjåkk sample consistent with deformation beneath temperate ice & high pore-water pressures***

6.2.1 How widespread was subglacial deformation?

The central zone in each forefield (below 1200m at Isfallsglaciären and Storglaciären and 1400m at Kaskasatjåkka) consists of fluted moraine and/or a diamicton plain/sheet comprising subglacial traction tills (Figure 3.22). Lithofacies A in each forefield, and Lithofacies B at Storglaciären and Kaskasatjåkka display similar physical properties and superposition which allows them to be correlated together; at the macro-scale, they appear homogeneous, matrix-supported and fissile (Chapter 3.1-3.4). They resemble subglacial diamictons whose formation has either been attributed to soft-bed deformation (Benn, 1994; 1995; Eklund and Hart, 1996; Kjaer *et al*., 2003;; Evans, 2003; Evans *et al*., 2011), subglacial lodgement (Benn *et al*., 2003, Larsen and Piotrowski, 2003; Piotrowski *et al*., 2006), *or* subglacial deposition (Gordon *et al*, 1992).

The evidence that Lithofacies A and B are hybrid traction tills is as follows:

1) Stoss-and-lee boulder forms with heavily striated upper surfaces, bullet-shaped clasts, clast clusters and flow-parallel clast fabrics with strong S_1 eigenvalues all indicate lodgement played an important role in the formation of these diamictons (Chapter 3.1-3.4).

2) Double stoss-and-lee boulder forms (Chapter 3.3.1) and sediment prows in deformed sand substrate (Chapter 3.3.2) indicate ploughing occurred.

3) Boulder pavements (Chapter 3.3.1) and stone lines (Chapter 3.4.1) indicate phases of localised erosion occurred at the ice-bed interface, whilst the occurrence of sheets of sandy gravel within the diamicton plain/sheet sequences (Chapter 3.7.1) point to phases of subglacial meltwater incision.

4) The disruption of fissile partings around embedded boulders and the alignment of Type 1 and Type 2 clasts along major fissile partings (Chapter 3.3.1&3.4.1) are consistent with the fissile partings being shear planes (although it was not possible to confirm this at the micro-scale; Chapter 5.2-5.4). However, a role for subglacial deformation in the genesis of Lithofacies A and B is suggested by deformable contacts with the Fronstjön sand unit (Chapter 3.2&3.3), flow-parallel clast fabrics with strong S_1 eigenvalues in flute crests and herringbone fabrics in flute flanks (Chapter 4.1), an aggregate strain ellipsoid for magnetic fabrics consistent with flow-parallel simple shear (Chapter 4.2), the presence of linear clast alignments observed at the micro-scale (Chapter 5.2-5.4), and the existence of conjugate micro-fabric sets (Chapter 5.4&5.7) which have been observed in other subglacial

deformation tills and related to ductile deformation and sediment dewatering (Phillips *et al*., 2011b).

The available evidence demonstrates that Lithofacies A and B are polygenetic, with soft-bed deformation, lodgement, ploughing and erosion occurring in close spatial proximity. As such, soft-bed deformation has not been the only process involved in the formation of the fluted moraine and diamicton plain/sheet. Consequently, it is more accurate to say that subglacial traction tills, rather than subglacial deformation tills, are a major component of each forefield. They form a near-continuous cover in the central areas where they are dissected by active and palaeo-meltwater channels. The subglacial diamicton probably had a wider distribution prior to the Little Ice Age recession, which initiated a phase of lateral meltwater incision and diamicton re-working by paraglacial processes (Chapter 3.8*)*. As such, outcrops of subglacial diamicton are rare at the lateral margins where sandy gravel, deposited in meltwater streams, is the dominant lithofacies (Figure 3.22). The relatively wide distribution of the most recent subglacial diamictons (Lithofacies A and B and Lithofacies C_{brown} at Kaskasatjåkka) corresponds to the central zones where the polythermal glaciers would have been thicker and temperate ice was most likely to occur as ice was near-to or at its pressure-melting point. The following observations indicateLithofacies A and B were produced under temperate ice conditions during the Little Ice Age *or* since recession from the Little Ice Age maxima:

1) Lithofacies A forms the upper surface of the main flute fields in each forefield whilst Lithofacies B forms the upper surface of the diamicton plain/flute. Lithofacies A is exposed in flutes that override the inner terminal moraine at Isfallsglaciären (Figure 3.22a), whilst Lithofacies C_{brown} is exposed in the inner terminal moraine at Kaskasatjåkka (Figure 3.16). These glaciers were observed to terminate at these locations during the Little Ice Age Maxima (Holmlund and Jansson, 2002). The superposition of Lithofacies A and B and the spatial distribution of Lithofacies A and C_{brown} indicate that they relate to the most recent glacial cycle and formed during the Little Ice Age advance or during glacier recession from the Little Ice Age maxima. By contrast, Lithofacies D contains heavily weathered clasts (Chapter 3.6) indicating it was exposed to a prolonged period of subaerial weathering and pre-dates the Little Ice Age advance (Baker and Hooyer, 1996).

2) Shear strength tests suggest elevated pore-water pressures were required for the subglacial deformation of Lithofacies A and B, which requires warm-based ice conditions (Chapter 3.3.6&7).

3) The widespread development of a conjugate set of cross-cutting micro-fabrics in Lithofacies A and B*,* interpreted here as micro-fabrics that developed as the diamicton dewatered, which likely formed under temperate ice conditions where pore-water pressures were high (Chapter 5.2-5.4).

4) The presence of sandy gravel layers interbedded with Lithofacies B in the diamicton plain/sheet sequences indicate considerable subglacial meltwater availability. The presence of water escape structures in thin section MMS2 from Storglaciären (Chapter 5.6&7) and the presence of loading structures and non-tectonic soft-sediment deformation structures in the Fronstjön sand unit (Chapter 3.3.2&3) indicate high pore-water pressures existed. These reduced sediment strength and encouraged soft-bed deformation, and at times of very high basal water pressures, would have encouraged basal sliding and ice-bed separation (Iverson *et al.,* 1995).

5) Flow-parallel wear marks concentrated on the upper surfaces of lodged boulders (Chapter 3.3.1&3.4.1) are consistent with subglacial abrasion associated with active basal sliding beneath temperate ice (Piotrowski *et al*., 2006).

6) Soft-bed deformation beneath temperate ice is producing a subglacial till beneath contemporary Storglaciären (Iverson *et al*., 1995). Lithofacies B from the diamicton plain closely resembles the subglacial till recovered from boreholes in terms of its matrix particle grain-size distribution, fractal slope gradient, and homogeneous grey appearance (Chapter 3.4.1&2). This suggests similar temperate ice conditions prevailed during the genesis of the diamicton plain. Towards the glacier margins, where ice was thinner, cold-based ice would have occurred and the glacier would have been frozen to its bed, restricting the formation of subglacial diamicton by deformation/lodgement processes to the central zones where temperate ice occurred.

Multiple processes are involved in the formation of hybrid tills. Subglacial deformation and lodgement have been an important process in the genesis of Lithofacies A and B and occurred widely beneath temperate ice across the lower central forefield zones of the polythermal glaciers during the Little Ice Age Advance and/or recession from the Little Ice Age maxima.

6.2.2 How thick was the deforming bed?

Macro-scale observations reveal the average thickness of Lithofacies A in flutes is between 0.3 and 0.5m thick and this shows little variation between forefields *(Chapter 3.3.8).* Where Lithofacies A appears to be greater than 1m thick in Area 3 of Isfallsglaciären, marked changes in clast fabric vectors and S_1 eigenvalues below 0.8m depth, and the separation of upper and lower diamictons by a 2cm thick massive sand layer, suggest the lower diamicton belongs to an earlier phase of deformation/lodgement when glacier flow or strain was directed towards the north rather than flow parallel towards the ENE (Chapter 4.1.7; Figure 4.8). At Isfallsglaciären, the boundary between Lithofacies A and Lithofacies C is often demarcated by a distinct boulder pavement which is interpreted here as representing a phase of erosion at the ice-bed interface (Chapter 3.5.1). The boundary is at 0.5-0.6m depth, which again suggests the deforming bed was approximately 0.5m thick during the flute construction phase.

Strong S_1 eigenvalues in flow-parallel clast a-axis fabrics are observed in the top 0.4m of flutes crests in Lithofacies A at Isfallsglaciären (Chapter 4.1), consistent with pervasive shear by overriding ice in a thin layer (Rose, 1991; Iverson *et al*., 2008). The aggregate strain ellipsoid derived from magnetic fabrics is also consistent with flow-parallel simple shear (Chapter 4.2.5). At approximately 0.5m depth a zone of clast macro-fabrics with weaker clast alignments and lower S_1 eigenvlaues occurs (Chapter 4.1.9). This weak layer probably represents the depth at which shearing by overriding ice was no longer able to re-orientate clasts into flow parallel alignment and so represents the base of the deforming bed (Boulton, 1976). This interpretation is consistent with the distinct change in micro-fabrics below 0.5m depth in the Isfallsglaciären thin sections (Chapter 5.3&5.4; Figure 5.12). The samples from the upper 0.5m of flutes are dominated by a variably developed cross-cutting conjugate set of micro-fabrics which seem to overprint an earlier and more pervasive micro-fabric which is dominant below 0.5m depth. This suggests that micro-fabric imposition related to sediment dewatering and 'lock-up' particularly affected the upper 0.5-0.6m of Lithofacies A at Isfallsglaciären and is consistent with a phase of partitioned deformation affecting a layer approximately 0.5m thick.

Lithofacies A mostly forms sharp wavy contacts with the underlying substrate, suggesting the boundary represents a décollement or depositional contact (Boulton *et al*., 2001; Piotrowski *et al*., 2001). In the Fronstjön area, the nature of the contact is variable over small spatial scales. Contrary to the pervasive deformation model of Eklund and Hart (1996), clast fabric S_1 eigenvalues show no simple decrease in strength with depth (Chapter 4.1.7-4.1.11). There is also little evidence of glaci-tectonic deformation at the micro-scale (such as folds, faults, shear planes) across the sand/Lithofacies A boundary in thin section BYL (Figure 5.10). However, the continuation of micro-fabric foliations across the sand/Lithofacies A boundary suggests the stress that induced the imposition of the fabric affected both lithofacies. Similarities in the orientation of sand-sized grains in the sand substrate and the S1 microlithons of Lithofacies A in sample BYL suggest some fabric was inherited from the cannibalisation of the sand beds. This is consistent with the sharp boundary representing a décollement surface where the base of Lithofacies A effectively planed across the Fronstjön sand layers and eroded sand into Lithofacies A.

Evidence that Lithofacies A is produced by the mixing of a relatively far-travelled sediment component with locally cannibalised materials is seen in the Fronstjön area where Lithofacies A has a very sandy matrix, contains unweathered clasts of meta-sediments derived from the Kebne Dyke Complex (which crops out up-valley), and where occasional lenses of coarse black sand – which are probably intraclasts derived from the sand substrate – are preserved behind pebbles (Chapter 3.3). In Figure 6.1, the particle grain-size distribution of silty sand (Zs) from the Fronstjön area has been merged with the particle grain-size distribution of sandy gravel (SG) derived from a nearby kame. The resulting particle grain-size distribution is very similar to the mean particle grain-size distribution for Lithofacies A obtained from 4 distal flute samples. Similarly, the merging of the particle grain-size distribution of Zs and SG taken from a flute produce a particle grain-size distribution that resembles some of the particle grain-size distributions of Lithofacies A obtained from flute samples (Table 6.2). This is not surprising given that Zs and SG probably originate, at least in part, from the glacio-fluvial re-working of subglacial diamictons (Etienne *et al*., 2003). However, the similarities in particle grain size-distribution between the merged samples and Lithofacies A (which have similar average and modal grain sizes, very poor sorting, and coarse silt/fine sand spikes) are consistent with Lithofacies A in eachforefield being the product of subglacial deformation in which local proglacial sediments were mixed with subglacially transported debris in a layer that averaged 0.3 to 0.5m thick. As SG is the dominant lithofacies in the proglacial area of each forefield (Figure 3.22a-c), it likely sourced some of the material that was incorporated into traction tills during glacier advances. The thickness of the deforming bed in each forefield was controlled by the rate of sediment input and output, the reduction in pore-water pressure with depth (especially where the substrate was more porous sand, leading to the effective evacuation of subglacial meltwater and the production of a relatively thin deforming bed), and increased sediment strength with depth as a consequence of increased effective pressure (Chapter 3.38&9).

The diamicton plain (Storglaciären) and diamicton sheet (Kaskasatjåkka) consist of multiple diamictons and are polygenetic, palimpsest landforms (Chapter 3.8.4). Lithofacies D predates the Little Ice Age advance. As such, the thickness of the diamicton plain/sheet does not equate to the thickness of the deforming-bed during the Little Ice Age Advance. Moreover, clast fabric profiles in Lithofacies B and C (Chapter 3.4&3.84) are not consistent with sequences that have deformed throughout their entire thickness at one time (Larsen and Piotrowski, 2003; Piotrowski *et al.,* 2006). S_1 eigenvalues do not decline with depth as would be expected in a simple pervasively deformed sequence (Piotrowski *et al.,* 2006), but vary in strength with depth, typically decreasing in strength over 0.2-0.6m depth intervals before increasing again. These variations are unlikely to be the consequence of strain partitioning throughout a thick deforming pile (Chapter 3.8.4). This is because sediments with greater gravel content would be expected to resist deformation more effectively and produce weaker clast alignments, but gravel-rich Lithofacies C at Kaskasatjåkka has S_1eigenvalues just as strong as or stronger than the less-gravel rich Lithofacies B (Table 3.9). The vertical changes in S_1 eigenvalues in the clast fabric profiles are consistent with Lithofacies B forming time-transgressively through the incremental accretion of traction layers that were 0.3-0.6m thick (Chapter 3.8.4). As such, the partitioning of strain observed at the micro-scale, evidenced by the increased intensity of micro-fabric development in the softer and more easily deformed parts of the matrix (Chapter 5.4&5.7), must have occurred within deforming layers of 0.3-0.6m thick that accreted over time as the loci of deformation moved upwards. This interpretation is supported by the rapid changes in shear strength with depth in Lithofacies B in the diamicton plain (Chapter 3.4.1). The measurements shown in Figure 3.17b&c show that shear strengths varied greatly with depth over small vertical intervals – shear strengths ranged from 100 to 35Kpa throughout the profiles, with shear strength varying by as much as 30KPa over 0.1m depth intervals. The presence of weak and strong layers indicates deformation was unlikely to have been pervasive or uniform throughout the sequence (Ó Cofaigh *et al*., 2007). Instead, deformation was particularly partitioned into weaker layers demarcated by closely-spaced fissile partings and characterised by a greater concentration of softer matrix and higher pore-water pressures in deforming beds of 0.2-0.6m thick (Chapter

Table 6.2 Particle grain size distribution (PGSD) of Lithofacies A from flutes compared to the particle grain size distribution of sediments produced by merging sandy gravel (SG) with silty sand (ZS)

PGSD Parameters **Matrix fraction <2mm size**	**SG + Zs (no.1)** **SG from flute Trench MMT3** **Z2 from Fronstsjön sand unit**	**Lithofacies A, Trench MMTT 0.8m depth, distal zone**	**Lithofacies A, Flute 3, Trench NT, Area 3, proximal zone**	**SG_F + Zs (no.2)** **SG from kame, Zs as for no.1**	**Lithofacies A, Mean 4 flute samples, distal zones of area 3**
% Sand	59.8	56.9	74.8	63.1	58.9
% Silt	35.4	36.7	20.4	32.9	34.8
% clay	4.8	6.4	4.8	4	6.6
PGSD	Bimodal	Bimodal	Polymodal	Polymodal	Polymodal
Sorting	Very poor	Very poor	Very poor	Very poor	Very poor
Mean (µm)	94.13	73.8	178.6	109	91.8
Mean	Very fine sand	Very fine sand	Fine sand	Very fine sand	Very fine sand
D_{10} (µm)	10.8	7.9	13	11.6	7.64
D_{50} (µm)	95.2	79.3	250.8	106	88.2
Mode 1 (µm)	152.5	107.5	855	107	75.4
Mode 2 (µm)	1700	427.5	107	37.5	151
Mode 3 (µm)	NA	NA	37.8	1200	427

Note: merger no.1 consists of a sandy gravel taken from a flute combined with a silty sand taken from the Fronstjön sand unit at 1m depth in flute 1, area 3, Isfallsglaciären. The resulting merger produces a sediment with a pgsd similar to some pgsds measured in Lithofacies A from flutes, e.g. sample from Trench MMTT at 0.8m depth. Both samples are bimodal, very poorly sorted, and have similar means and primary modes of very fine sand, and similar proportions of sand, silt and clay. Merger no.2 combines a SG_F from a kame deposit at Isfallsglaciären with the same Zs sample used in merger no.1. The resulting sediment pgsd is similar to the mean obtained from 4 Lithofacies A samples taken from the distal zones of flutes in area 3 where Lithofacies Acontains a higher proportion of silt in the matrix. Both samples are polymodal and very poorly sorted, with similar means and primary modes, and percentages of sand and silt. These similarities are not surprising given that much SG and Zs are probably produced by the glacio-fluvial re-working of diamictons. However, the mergers suggest that it is also possible to produce a diamicton with a similar matrix pgsd by cannibalising proglacial sediments. If subglacially transported boulders were added by lodgement, then cannibalisation combined with lodgement could produce a pgsd similar to Lithofacies A.

5.4&5.7). The thickness of the deforming bed suggested by the clast fabrics is consistent with estimates of relatively thin deforming bed thicknesses observed beneath contemporary glaciers, including Storglaciären (Iverson *et al*., 1995; Table 1.1).

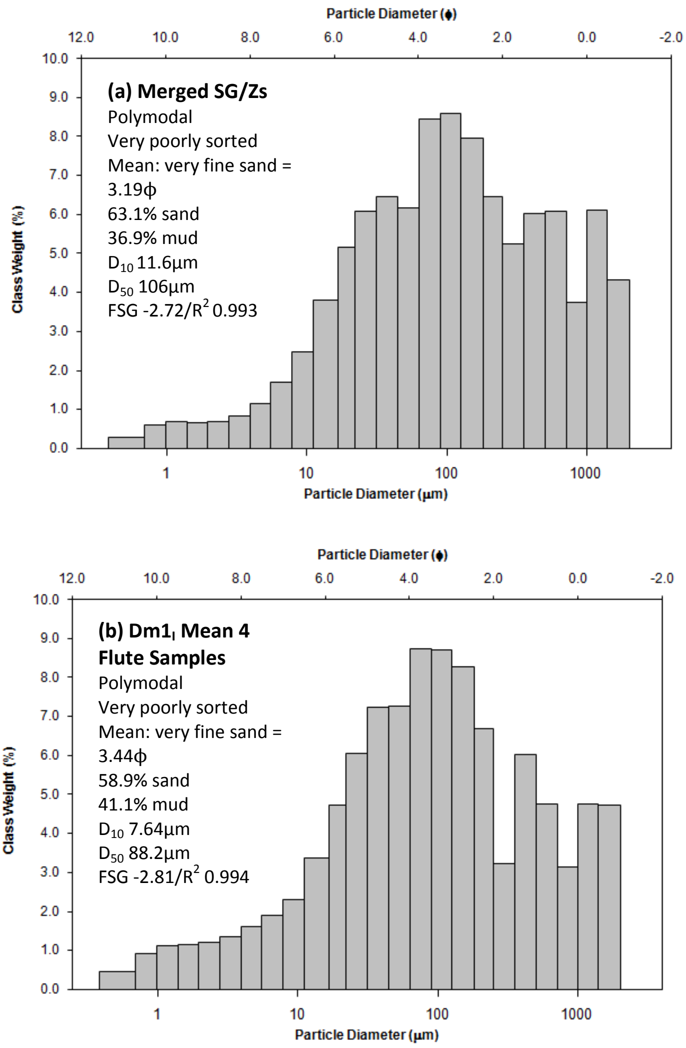

Figure 6.1 Particle Grain-size Distribution (PGSD) of a sediment produced by merging the PGSDs of SG and Zs compared to the PGSD of Lithofacies A from distal reaches of flutes; (a) PGSD produced by combining SG taken from a bar in a contemporary braided river channel with Zs taken from below the discontinuity in Trench T:1, Flute 1, Area 1 of Isfallsglaciären; (b) Mean PGSD of four Lithofacies A samples taken from the distal reaches of flutes. PGSD shows the matrix fraction <2mm in size in both graphs. FSG is the fractal slope gradient.

c) What was the strain magnitude?

Magnetic fabrics offer the best estimate of strain magnitude currently available for homogeneous subglacial tills (Shumway and Iverson, 2009). However, care must be taken in interpreting the magnetic fabrics from Lithofacies A and B as micro-scale observations show that cryogenic processes (in particular silt illuviation) have particularly affected near-surface samples in the upper 0.1 to 0.35m of flutes at Isfallsglaciären and at the Storglaciären diamicton plain (Chapter 5.4.1 &5.7). It is probable that the magnetic fabrics taken from shallow samples underestimate subglacial strain magnitude because post-depositional disturbances such as frost-jacking and silt illuviation (Chapter 5.4.1) have re-aligned silt-sized grains of magnetite (Chapter 4.2.10.d), which are the magnetic carrier in Lithofacies A and B (Chapter 4.2.2). However, even at depths where periglacial overprinting has been much less extensive, as evidenced by fewer and thinner silt caps in Lithofacies A and B thin sections (Figures 5.6; 5.9; 5.17; 5.18), magnetic fabrics do not indicate very high strain magnitudes ($\geqslant 10^2$-10^4). Moreover, occasionally developed or preserved short and relatively steeply inclined linear grain alignments observed in thin sections (Chapter 5.3&5.6) also indicate low to moderate strain magnitudes in both Lithofacies A and B (Thomason and Iverson, 2006; Larsen *et al*., 2006). Not all variations in magnetic fabrics necessarily reflect variations in deforming-bed conditions or post-depositional disruption, because some variations likely reflect the imposition of pure shear in ice-marginal and proglacial settings (Chapter 4.2.10), which acts to flatten strain ellipsoids and reduce the inclination of grains (Evans *et al*., 2006).

Clast a-axis fabrics, magnetic fabrics, and 2-D micro-fabrics for Lithofacies A from flutes at Isfallsglaciären reveal a consistent picture of strain that is consistent with simple shear by overriding ice and have similarities to steady-state fabrics produced in ring shear experiments (Thomason and Iverson, 2006; Iverson *et al*., 2008). These similarities include V_1 eigenvectors that are flow-parallel and plunge up-flow at shallow angles for clast fabrics (Chapter 4.1.5)and 2-D sand micro-fabrics (Chapter 5.3), and an aggregate strain ellipsoid defined by the principal magnetic susceptibility axes that is consistent with the aggregate strain ellipsoid produced by flow-parallel simple shear to moderate or high strains (~10-30) in laboratory experiments (Chapter 4.2.5). However, none of the S_1 eigenvalues derived from the different fabric measurements suggest strain magnitudes approached the **very** high strains ($\geq 10^2$-10^4) required by the deforming-bed model (Larsen *et al*., 2006; Iverson *et al*., 2008).

Indeed, many of the 2-D micro-fabrics and magnetic fabrics indicate low strain magnitudes (<10). This does not mean that bed-deformation did not occur, rather – and contrary to the bed-deformation model – that it was probably of insufficient magnitude to exert a major control on glacier dynamics(Iverson *et al*., 2008). In flutes at Isfallglaciären, clast fabrics in Lithofacies A were observed to rapidly increase in strength and vectors become increasingly flow-parallel over short distances away from large embedded boulders (S_1 eigenvalues increasing from 0.44 at 0.8m distance from the boulder, to 0.64 at 1.2m distance, to 0.84 at 4m distance; Table 4.1), consistent with strongly clustered clast fabrics being produced at moderate strains (Iverson *et al*., 2008). At Isfallsglaciären ,clast fabric S_1 eigenvalues and elongation indices show no increase in strength distally along flutes (Chapter 4.1.5), as might be expected if increasing cumulative strain produced stronger clast alignments (Benn, 1994; 1995; Eklund and Hart, 1996). Moreover, *in each* forefield, Lithofacies A does not increase in thickness down-flow outside of Area 3 at Isfallsglaciären (Chapter 3.3.8). The clast fabric data and deforming bed thicknesses indicate that sediment advection down-flute was probably limited, which is consistent with the low-to moderate strain magnitudes indicated by the magnetic and 2-D micro-fabrics.

A similar picture emerges from the diamicton plain at Storglaciären where some strongly clustered flow-parallel clast fabrics occur in Lithofacies B in the Nordjåkk logs (Table 3.8), but the magnetic fabrics indicate weak to moderate strain magnitudes (generally <10; Chapter 4.2), rather than the very high strain magnitudes required by the deforming-bed model ($\geq 10^2$-10^4). In the diamicton plain (Storglaciären) and diamicton sheet (Kaskasatjåkka), the strength of clast fabric a-axis alignments in Lithofacies B are spatially variable, and show no tendency to increase in value down-flow (Table 3.8&3.9).Strongly clustered clast fabrics can be produced at moderate strains (Iverson *et al.,* 2008). The magnetic fabrics for Lithofacies B indicate moderate to low strain magnitudes. As such, the available fabric data for Lithofacies B indicate that, although bed-deformation occurred, it was of insufficient magnitude to exert a major control on glacier dynamics. As Iverson *et al*. (2008) observed, the important question to understand in testing the bed-deformation model is not whether subglacial deformation occurred, but whether **enough** deformation occurred to exert a dominant control on glacier flow dynamics. If a valley glacier has a deforming bed 2m thick and advances 1km in 100years, then for bed-deformation to account for even half of the glacier movement a very high strain magnitude of $10^{2.4}$ would be required (strain magnitude = horizontal displacement divided by deforming bed thickness; Iverson *et al*., 2008).In the case of

Lithofacies A and B, the magnetic fabrics and 2-D micro-fabrics indicate strain magnitudes were well below the values required to support the deforming-bed model.

6.2.4 What was the nature of subglacial deformation?

Micro-structural maps show that micro-fabric domains are more closely-spaced and better developed in the softer and more easily deformed areas of the matrix of Lithofacies A and B and less well-developed in more clast-rich zones (Chapter 5.3&5.6). This shows that strain was not homogeneous at the micro-scale, but partitioned. The existence of cross-cutting micro-fabrics (S1-S4) in Lithofacies A from the Isfallsglaciären flutes demonstrates that bed-deformation was multi-phase (Chapter 5.3). In thin section MMS2 from the diamicton plain (Storglaciären), evidence of an earlier micro-fabric is preserved in the S1 and S2 microlithons in Lithofacies B (Figure 5.17a; Chapter 5.6.1), which again indicates multiple phases of bed deformation. As such, the appearance of the diamictons at the macro-scale is the consequence of a polyphase deformation history and represents cumulative strain, rather than homogeneous and uniform deforming bed conditions (Evans, 2003; Piotrowski *et al*., 2004; Evans *et al*., 2006). The following observations suggest subglacial deformation mostly occurred in the bed rather than in basal-rich debris ice:

i) Herringbone clast fabrics in flutes (Chapter 4.1) indicate strain in the deforming bed was directed towards the flute crest, whereas striae on nearby embedded boulders indicate glacier flow was directed down-flute (Benn, 1994).

ii) Linear grain alignments (Chapter 5.3) indicate brittle shear and such alignments do not occur in debris-rich basal ice where plastic deformation occurs (Thomason and Iverson, 2006).

iii) Striae and wear marks concentrated on upper surfaces of boulders embedded in Lithofacies A and B (Chapter 3.3.1&4.4.1) are consistent with abrasion by overriding ice.

iv) Double stoss-and-lee forms observed in Lithofacies A (Chapter 3.3.1) are thought to be formed by ploughing and lodgement in a deforming bed (Benn 1994; 2004).

v) Conjugate sets of cross-cutting micro-fabrics observed in Lithofacies A and B *(*Chapter 5.3&5.6) have been observed in micro-structural maps of known subglacial deformation tills (Phillips *et al*., 2011b).

vi) Flutes are not observed to deviate around boulders or to form across bedrock areas (Chapter 4.1.15), which were key pieces of evidence used by Gordon *et al*. (1992) to support the depositional model of flute formation from debris-rich basal ice.

Macroscopic observations alone provide only a partial picture of subglacial deformation. The occurrence of fissile partings and Type 1 and Type 2 clasts in Lithofacies A and B, and their porosities, void ratios, and particle grain-size distributions are consistent with B-horizons (Chapter 3.3.1& 3.4.1), which are characterised by brittle or brittle-to-ductile shear (Boulton and Hindmarsh, 1987; Evans *et al*., 2006). However, the integration of micro-scale observations, especially the results of the micro-structural maps, provides further insights (Chapter 5.3&5.6). In Lithofacies A and B, an early phase of relatively pervasive, dilatant and ductile deformation probably preceded a dewatering phase in which a penecontemporaneous set of conjugate micro-fabrics was imposed on the stiffening diamicton (Chapter 5.4.2 and 5.7). As shown in section 6.2.2, this relatively pervasive phase of deformation would have been in deforming beds averaging 0.5m thick in Lithofacies A at Isfallsglaciären, and 0.2-0.6m thick in Lithofacies B at Storglaciären. As the sediment began to dewater and lose dilatancy, inter-grain contacts and effective pressures increased as the sediment consolidated (Phillips *et al*., 2011b). Shear by overriding ice was sufficient to align clasts and produce strongly clustered fabrics (Table 3.8&9 and Table 4.2), although magnetic fabrics indicate these were achieved with limited sediment advection and modest (<10) strain magnitudes (section 6.2.3).Further dewatering and consolidation resulted in larger clasts becoming immobile. The finer matrix continued to deform in ductile manner and produced the conjugate micro-fabric sets which wrapped around the immobile clasts (Chapter 5.4&5.7). During this phase, strain was partitioned into the softer and more easily deformed parts of the matrix which retained higher pore-water pressures. Grain-crushing was initiated along grain bridges as inter-grain contacts and effective pressures increased. The fine sand/coarse silt spikes observed in Lithofacies A and B (Figure 3.3) suggest grain-crushing was significant during the non-dilatant phase (Haldorsen, 1981). The consolidation and accretion of the deforming layer reduced porosity and void ratios and produced diamictons that resemble B-type horizons at the macro-scale.

6.3 Discussion – Subglacial Models and Glacier Dynamics

6.3.1 Subglacial models and glacier dynamics in the Tarfala Valley

Glaciers in the Tarfala Valley receded from the Little Ice Age maxima ca. 1910 when average annual temperatures rose by 1°C (Holmlund and Jansson, 2002). Under the present climatic regime, bed-deformation and basal sliding contribute to the total basal slip of Storglaciären. Basal sliding across a soft-bed is the dominant control, accounting for *ca*.70% of the glacier's surface velocity (Iverson *et al*., 1995). In the ablation zone, pervasive subglacial deformation occurs intermittently within a thin layer (~0.3m thick) at times of rising basal water pressures and ice-bed separation occurs at times of very high basal water pressure (Iverson *et al*., 1995). Basal sliding also occurs beneath contemporary Isfallsglaciären, as evidenced by the existence of regelation ice at the glacier margin (Cook, *pers. comm*. 2013). The available evidence from the present study indicates that thick, pervasively deforming beds characterized by very high strain magnitudes ($\geqslant 10^2$-10^4) did not occur in the Tarfala Valley during the Little Ice Age advance or recent recession (Table 6.1). As such, bed-deformation probably did not exert a major control on former glacier dynamics. This conclusion is at odds with the view of Etienne *et al*. (2003) who argued that bed-deformation was an important control on Storglaciären's dynamics during drier climatic phases over centennial timescales during the Little Ice Age. However, shear strength tests (Chapter 3.3.6) demonstrate that elevated pore-water pressures were required to deform Lithofacies A and B, and this indicates that deformation required a well-lubricated bed – a situation that would also promote basal sliding. The evidence for temperate ice conditions and high pore-water pressures in Lithofacies A and B (Section 6.2.1) indicate that the glacier bed was indeed, at times, well-lubricated. The strain magnitudes and deforming-bed thicknesses indicate that Lithofacies A and B were generated under subglacial conditions akin to those prevailing beneath contemporary Storglaciären, with bed-deformation occurring intermittently in a thin layer at times of elevated pore-water pressures, with basal sliding the dominant control on glacier velocity. As such, the available evidence from small polythermal valley glaciers in the Tarfala valley does not support the deforming-bed model (Table 6.1).

Comment [DJG43]: Nice :-)

Because elevated pore-water pressures were required to initiate deforming-bed conditions, sediment granulometry, which influenced the efficiency with which subglacial water could be evacuated from the bed, played a key role in controlling the timing and location of sediment deformation. Subglacial deformation was polyphase and the appearance of Lithofacies A and

B at the macro-scale reflects cumulative strain (Piotrowski *et al*., 2001). As such, the subglacial environment is best characterised by the ice-bed mosaic model (Piotrowski *et al*., 2004; Chapter 1.4.6; Table 6.1). Consequently, the results of this study add to the growing body of evidence that challenges the deforming-bed paradigm (Piotrowski *et al*., 2001; 2004; Larsen *et al*., 2006; Thomason and Iverson, 2006; Iverson *et al*., 2008; Shumway and Iverson, 2009). Bed deformation did occur, but not continuously, not to great depth, and not to very high strains, and so it had a limited capacity to control glacier dynamics. These findings are consistent with other research findings for a variety of glaciers where the thickness of the deforming bed was seen to average 0.3-0.5m and basal sliding was seen to be the dominant control on glacier dynamics (Chapter 1.4.3; Table 1.1). The observation that Lithofacies A and B formed by multiple processes (such as deformation, ploughing, erosion and lodgement) that occurred in close spatial proximity, is also consistent with the ice-bed mosaic model (Table 6.1) which characterises the subglacial bed at any one time as a mosaic of stable, sticky, and deforming spots (Piotrowski *et al*., 2004).

The identification of multiple phases of deformation in Lithofacies A and the identification of a conjugate set of micro-fabrics probably related to sediment dewatering and stiffening also provides support for the ice-bed mosaic model (Piotrowski *et al*., 2004). In this model, subglacial tills are thought to undergo multiple phases of deformation related to variations in pore-water pressures. Sediment dewatering and stiffening could relate to the seasonal development of a more efficient subglacial drainage system, which would evacuate water more efficiently from the bed, as is thought to develop beneath contemporary Storglaciären in late-summer (Fischer *et al*., 1996). A reduction in pore-water pressures related to improved subglacial drainage is likely to stiffen parts of the bed as they dewater, leading to the localised development of sticky-spots (Kjaer *et al*., 2003; Evans *et al*., 2006; Phillips *et al*., 2011b). This would create a subglacial environment akin to that depicted in the ice-bed mosaic model (Piotrowski *et al*., 2004).

It is possible that micro-fabrics formed by earlier phases of subglacial deformation are not detected in micro-structural maps because they are destroyed by later events which re-work sediment into new foliations (Phillips *et al*., 2011b). As such, the processes of deformation, dewatering and sediment stiffening may have occurred multiple times, with cumulative strain representing multiple episodes of shearing. Such a scenario is again consistent with the ice-bed mosaic model (Piotrowski *et al*., 2004*)*. Alternatively, some of the stiffening and consolidation of Lithofacies A and B may relate to freezing-on in the cold-ice margin, where the locking-up of sediment might occur if the basal thermal gradient resulted in water being withdrawn from the till (Christoffersen and Tulaczyk, 2003). This process has been suggested for the production of stiff, over-consolidated tills beneath palaeo-ice streams on the Antarctic Peninsula (Ó Cofaigh *et al*., 2007). However, cross-cutting conjugate micro-fabric sets have been observed in subglacial tills in a flute formed beneath an entirely temperate glacier (Phillips *et al*., 2011b). Moreover, strain partitioning is thought to be indicative of deformation beneath warm-based ice where granulometry controls variations in pore-water pressures and hence the strain response (Evans *et al.*, 2006). As such, it is argued here that the conjugate micro-fabric set indicates formed as tills dewatered and stiffened beneath temperate ice.

A number of implications stem from the results of this study:

1) Homogeneous subglacial tills and strong flow-parallel clast a-axis fabrics can be produced at moderate strains and are not diagnostic of very high strain magnitudes and considerable till advection. This finding is contrary to the assumptions/findings of some previous research (Boulton, 1976; Boulton and Hindmarsh 1987; Rose, 1991; Benn 1994; 1995; van der Wateren *et al*., 2000), but is consistent with the fluid-flow model of massive till formation (Evans *et al*., 2006; Table 6.1) and the results of ring-shear experiments (Iverson *et al*., 2008).Nor do they indicate homogeneous strain as Benn (1995) argued. Likewise, fold types that are associated with very high strains in hard rocks, such as recumbent folds (observed at Isfallsglaciären in the Frontsjön sand unit) and sheath folds (van der Wateren *et al*., 2000), do not necessarily indicate very high strains in subglacial diamictons. Hard rock deformation and soft-sediment deformation are not comparable processes in terms of the strain magnitudes involved, because soft-sediments can deform subglacially under low strains if pore-water pressures are high (Phillips *et al*., 2011a). Macro-scale observations alone are insufficient to confirm high strain magnitudes and to falsify the deforming-bed model. The homogenisation of till at relatively low strains and the partitioning of strain observed at the micro-scale lends support to aspects of the fluid-flow model of massive till formation (Evans *et al*., 2006; Chapter 1.4.7. and Table 6.1). This model of deformation is compatible with the ice-bed mosaic model and micro-scale observations of deformation in Lithofacies A and B in that it predicts deformation will be time-transgressive, spatially variable, and controlled by variations in pore-water pressure.

2) Strong planar fabrics (fissile partings), which have been used to infer a subglacial deformation origin for homogeneous, matrix-supported tills (Boulton, 1976; Benn 1994; 1995; Etienne *et al*., 2003; Kjaer *et al*., 2003; Evans *et al*., 2010), may be formed by multiple processes such as unloading, sediment dewatering and cryogenic activity (Lundqvist, 1983; Muller, 1983; Chapter 3.4.2) and micro-scale evidence (faults, folds, shear planes, elongated voids) is required to confirm a deformation origin. This study shows that fissile partings do not necessarily denote discrete shear planes and brittle failure (cf. Benn, 1994; 1995) as, at the micro-scale, they are demarcated by irregular-shaped voids and contraction voids rather than elongate voids typically associated with shear planes(Kilfeather and van der Meer, 2008). Moreover, the clean nature of the voids suggests they are of recent origin and probably relate to sediment dewatering or unloading or cryogenesis (Chapter 5.4.1).

3) It is incumbent upon researchers working on recently exposed subglacial diamictons in areas of seasonal frost activity to demonstrate that sediment characteristics interpreted as subglacial signatures are not the consequence of periglacial overprinting. For example, A-horizons have been identified in tills in Iceland and Norway where they are characterised by weakly clustered clast a-axis fabrics, bubbly, open textures, and high porosities and void ratios (Boulton and Hindmarsh, 1987; Benn 1994; 1995; Evans *et al*., 2010). The thin sections in this study taken from shallow depths (for example, sample MM9) resemble A-horizons at the micro-scale in texture, porosity and appearance, and yet their characteristics are the consequence of periglacial overprinting (Chapter 5.4.1), which acts to increase porosity and disrupt fabrics (Bockheim and Tarnocai, 1999; van VlietLanoe, 2010). As such, micro-scale evidence (such as folds, faults, rotational structures, shear planes) is required to confirm the subglacial origin of diamictons that resemble A-type horizons, not least because dilatant horizons are thought to collapse and consolidate once shearing ceases (Craig, 1997). Moreover, as shown in this study, periglacial overprinting has an observable effect on diamictons subaerially exposed for as little as *ca*. 30 years (Chapter 5.2.2), and can even be active in ice-marginal locations (van Vliet-Lanoe, 2010), and so just because subglacial diamictons have been recently exposed, it does not follow that their properties are entirely glacigenic in origin. This is not to say that A-type horizons are not produced by subglacial deformation, but to argue that it cannot be **assumed** that this is the case based on macro-scale evidence alone.

The deforming-bed model (Chapter 1.4.1) has been the dominant paradigm in glaciology since the 1980's (Boulton, 1986) and numerous studies have used macro-scale observations of subglacial tills (such as homogenization and planar textures)to infer high strain magnitudes or thick deforming beds in support of this model (Boulton, 1983; Boulton *et al*., 1985; Boulton and Hindmarsh, 1987; Alley, 1991; Benn, 1994; 1995; Hart, 1994; Eklund and Hart, 1996). The deforming-bed model has been leading observations, with assumptions being made (for example, fissile partings are equivalent to shear planes) to match (often inadequate) macro-scale observations to deforming-bed processes. This approach only gives a partial view of till genesis and subglacial deformation processes. The results of the present study show that, whilst bed-deformation occurs, the thickness of the deforming-bed and the magnitude of strain are not as great as assumed by the deforming-bed model. The multi-dimensional approach adopted here allows for different scales of analysis, each of which provides additional insights that allow for a more complete interpretation of subglacial processes and a more rigorous test of subglacial models. The micro-structural mapping approach is particularly useful in revealing the polyphase and heterogeneous nature of sediment deformation (Chapter 5.4&5.7), whilst micromorphology reveals the extent of periglacial overprinting (Chapter 5.4.1), neither of which were previously known in the Tarfala Valley. The results of the multi-dimensional approach refute the model of pervasive deformation presented by Eklund and Hart (1996) for the formation of subglacial tills in the Isfallsglaciären flutes (Chapter 1.4.10 & Chapter 4.1.15a). Lithofacies A formed by multiple processes (Section 6.2.1) with subglacial deformation and lodgement being important, deformation was polyphase and partitioned in a bed averaging 0.5m thick, and sediment advection and strain magnitudes were limited. Detailed excavations in the Fronstjön area (Chapter 3.3.2) reveal variable contacts between Lithofacies A and the sand substrate, with evidence of folding and faulting that pre-dates Lithofacies A emplacement or relates to non-tectonic soft-sediment deformation (Chapter 3.3.3). The presence of erosional, deformed, and non-deformed contacts in close spatial proximity provides further support for the ice-bed mosaic model.

6.3.2 Subglacial Models and Subglacial Dynamics at Larger Scales

An important question to address is how applicable the results of this study are to large-scale glaciers, ice streams and ice sheets. What are the implications of rejecting the bed-deformation model in this study of small polythermal valley glaciers for our understanding of glacier and ice sheet dynamics and landform generation in general? This is important because ice streams in Antarctica and Greenland are responsible for most of the drainage of ice sheets and regulate ice sheet mass balance and contribution to sea level rise (Alley and

Bindschadler, 2001; Rignot and Kanagaratnam, 2006; Ó Cofaigh *et al*., 2007). Elongated landforms such as mega-scale glacial lineations (MSGL) and flutings have been associated with deforming-bed conditions and fast-ice flow in icestreams and outlet glaciers (Stokes and Clark 2002; Clark *et al*., 2003; Evans *et al*., 2005; Ó Cofaigh *et al*., 2007). The deforming-bed model has been used to account for fast-ice flow in ice streams, and the presence of acoustically transparent sediment layers used to infer thick pervasively deforming beds, for example, beneath the Whillans ice stream (Blankenship *et al.,* 1986; Alley *et al.,* 1986; Chapter 1.4.1). However, not all studies show evidence that the deforming bed is an important control on ice stream dynamics. For example, Englehardt and Kamb's (1997) borehole experiments in the Whillans ice stream demonstrated that the deforming bed was only a few centimeters thick, and that enhanced basal sliding associated with low effective pressures was an important control on ice stream dynamics. More recently, seismic and radar profiles of the fast-flowing Rutford ice stream provided evidence that supported aspects of the ice-bed mosaic model in that parts of the soft-bed were deforming pervasively, whereas other parts were stable (sticky spots) with low porosity tills that promoted a transition from deformation to basal sliding (Smith and Murray, 2009). As such, the findings of the present study are consistent with some research from large-scale glaciers and ice sheets that demonstrate that bed-deformation is not the major control of ice stream dynamics in all cases and that the subglacial environment is, at any one time, a mosaic of stable, sliding and sticky spots. The results from the Tarfala Valley support the ice-bed mosaic model in that they suggest it is changes in pore-water pressures that control whether any given patch of sediment is stable or deforming, and basal sliding is the dominant control on glacier velocity. Changes in ice stream dynamics have been related to a cessation or initiation of bed-deformation (Christoffersen and Tulaczyk, 2003), but if basal sliding is the dominant control on ice-stream dynamics, then it is the cessation or initiation of sliding that operates the primary control on ice stream dynamics and hence ice sheet stability.

Detailed investigations of sediment cores and marine geophysical data from some palaeo-ice streams of the West Antarctic Peninsula and Antarctic continental shelf, for example Marguerite Bay, have recently demonstrated that subglacial tills in MSGLs are hybrid traction tills and that subglacial deformation was focused and partitioned into weak beds of soft till 0.1-0.9m thick which accreted incrementally over time (Ó Cofaigh *et al*., 2007). Micro-scale investigations revealed evidence of deformation (shear planes and rotational structures) in the weak till and an underlying stronger lodgement till and, as such, the tills were interpreted as hybrids. These results mirror the findings of the present study in that subglacial tills formed by incremental accretion from thin layers and were generated by multiple processes, with both lodgement and deformation occurring close together in space and time. Furthermore, the shear strength of the soft till varied over small vertical intervals (0.1-0.5m) in the Marguerite Bay, which Ó Cofaigh *et al*. (2007) interpreted as evidence of variable pore-water pressure during till accretion. These results are very similar to the variations in shear strength observed in Lithofacies B at Storglaciären in the diamicton plain (Figure 3.1.7a&b), which indicates that similar time-transgressive processes of incremental till accretion from thin layers (in which deformation and lodgement took place) occurred at both glacier scales. The detailed multi-dimensional investigation of Ó Cofaigh *et al*. (2007) show that at least some sequences of homogeneous subglacial tills beneath palaeo-ice streams do not equate to pervasive deformation throughout a thick layer, and that subglacial deformation tills are, in reality, hybrid tills. This is consistent with the findings of the present study and one of the implications of both sets of findings is that pervasive subglacial deformation is not the major control on glacier dynamics, landform generation or till formation in glaciers at a range of scales. In the case of the Marguerite Bay, other mechanisms must control ice-stream dynamics and stability. For example, considerable till advection was thought to have occurred within thin deforming layers (this was indicated by a thickening of tills down-flow), which suggested bed-deformation in thin layers of soft-till combined with basal sliding probably initiated and sustained fast ice stream flow (Ó Cofaigh *et al*., 2007). If this is true, then magnetic fabrics from the soft-till should indicate very high strain magnitudes ($>10^2$). However, very few studies have so far measured strain magnitudes in order to verify the deforming-bed model, and this is an urgent requirement in glaciology (Piotrowski, *pers.comm*. 2012).

It should be noted that the results of the one study that has so far employed magnetic fabrics to estimate strain magnitude in a thick sequence of subglacial tills (the Douglas tills) deposited by the Superior Lobe of the Laurentide Ice Sheet in NW Wisconsin, did not find the very high strain magnitudes required by the deforming-bed model (Shumway and Iverson, 2009). As in the present study, K_1 vectors were variable with depth and S_1 eigenvalues varied over small vertical intervals (Chapter 4.2). Shumway and Iverson (2009) concluded that the magnetic fabrics showed that deformation occurred in thin, anastomosing beds (<1m thick) which accreted over time – the till was not shearing through its entire thickness at the same time. The model of till accretion from thin, anastomosing layers of deformation till is very similar to the characterization of the subglacial environment presented in the ice-bed mosaic model (Piotorowski *et al*., 2004). Till sequences formed beneath the continental-based Scandinavian ice sheet were also likely to have formed in a subglacial environment characterised by a mosaic of stable, sliding and sticky spots, with subglacial tills being formed by lodgement, deformation, and meltout processes, with basal sliding the dominant control on ice sheet dynamics (Piotrowski *et al*., 2001; Chapter 1.4.5). As such, the characterization of the subglacial environment in the present study is consistent with recent research findings from larger-scale ice sheets. Namely, at each scale, the subglacial environment is probably best characterized by the ice-bed mosaic model, with basal sliding the key control on glacier dynamics; bed deformation occurs, but in thin layers, time-transgressively, and to strain magnitudes that are not high enough to exert a major control on glacier velocity

This is not to invalidate the bed-deformation model entirely because it may be that some larger scale glaciers and ice sheets are characterised by subglacial environments in which bed-deformation has a more important control on glacier dynamics. For example, although the subglacial environment of the 2.2km thick Rutford Ice Stream is consistent with aspects of the ice bed-mosaic model, where bed-deformation does occur, it is thought to be relatively extensive and pervades up to several metres into the bed (Smith and Murray, 2009). Moreover, subglacial landforms become increasingly streamlined down-flow (King *et al*., 2007). These observations are consistent with considerable till advection and very high cumulative strains (although no estimates of strain magnitude have been reported in these studies), and provide evidence in support of the deforming bed-model. The deforming-bed model may be more applicable in these cases because different subglacial processes come into operation at the larger scale, such as groove-ploughing by ice keels, one process that has been proposed for the formation of large landforms such as MSGL (Clark *et al*., 2003; Chapter 1.4.8). It may also be that bed-deformation is particularly effective in areas where the substrate is clay-rich marine sediments, which occur beneath parts of the marine-based West Antarctic Ice Sheet, for example the Whillans Ice Stream (Alley *et al*., 1986). Soft, clay-rich marine sediments lacking coarser gravels are likely to be more effectively deformed than stiffer clast-rich diamictons such as those that dominate in the mountainous upland glaciers of the Tarfala Valley. In relatively stony diamictons, clasts exhibiting a greater degree of angularity are able to lock-together in a framework that produces greater frictional strength to resist bed-deformation (Head, 1982). As such, the deforming-bed model may be most applicable to regions of ice sheets and palaeo-ice sheets where soft and easily deformable marine sediments are overridden (Piotrowski *et al*., 2001).

There is another important potential difference between small valley glaciers and large-glaciers and ice sheets which renders comparisons of subglacial processes at different scales problematic, and that is the extent to which topography exerts a control on glacier dynamics. Topography exerts a major control on glacier dynamics in northern Sweden (Kleman *et al*., 2008; Goodfellow *et al*., 2008) and in small mountain glaciers in general (Benn *et al*., 2003). In the Tarfala Valley, longitudinal variations in valley cross-sectional areas and the existence of overdeepenings and riegels produce longitudinal variations in the glacier driving stresses and zones of extending and compressive flow (Hedfors *et al*., 2003). Topography also has an influence on basal thermal conditions in polythermal glaciers. Converging flow from accumulating basins generates sufficiently thick ice to generate temperate conditions in valley glaciers, whereas cold-based ice occurs at the thin lateral margins where the glacier may be frozen to its bed (Kleman *et al*., 2008). The frozen margins exert considerable lateral drag which takes-up a proportion of the driving stress (Hedfors *et al*., 2003). As such, topography plays an important role in controlling glacier dynamics in small polythermal glaciers, and glacier dynamics are not simply controlled by the relative contributions of basal sliding and bed-deformation to total basal slip. By contrast, ice sheets are generally thought to flow independently of topography (except in Greenland), although topography and ice margin thermal conditions may exert a significant control on the dynamics of outlet glaciers and ice streams (Benn and Evans, 2010). For example, in the Whillans Ice Stream, force-balance calculations suggest that up to 50% of the driving stress is resisted by lateral drag, which is far more significant than basal drag (Tulaczyk *et al*., 2001). As such, variations in the cross-sectional area of a valley, changes in bed-topography, and ice margin thermal conditions all exert major controls on glacier dynamics, particularly in polythermal valley glaciers, and glacier flow accelerations may be initiated by internal dynamics unrelated to soft-bed deformation (Benn and Evans, 2010).

Further evidence is required from Quaternary till sheets and from beneath active and palaeo-ice sheets and ice streams to test subglacial models at larger scales. Specifically, whether soft-beds are deformed pervasively through thick layers and to the very high strains required by the bed-deformation model, or whether the subglacial environment is a mosaic with basal sliding the key control on dynamics, with landforms and tills generated by multiple subglacial processes such as lodgement and deformation acting in close space and time. This requires the use of a multi-dimensional approach and the use of magnetic fabrics to estimate strain magnitudes. This research is important because it has implications for our understanding of ice sheet dynamics and stability, and the processes that generate subglacial landforms and tills.

6.4 Flute Formation

6.4.1 A Model of Flute Formation

A model of flute formation which accounts for the integrated observations from the Tarfala Valley is presented in Figure 6.2. The model specifically accounts for the long and parallel-sided flutes observed at Isfallsglaciären and Kaskasatjåkka where topography has an important control on the location of the most prominently fluted areas. These occur just down-flow of major bedrock riegels (Chapter 3.8.2). This new model is novel in that it combines – for the first time – aspects of the forced-mechanism model of flute formation beneath warm-based ice (Chapter 4.1.15b) with the flow instability model of flute formation (Chapter 4.1.15d).

Force-balance calculations demonstrate that flow convergence and valley narrowing at Storglaciären results in accelerated and extending flow across riegels (Hedfors *et al*., 2003). Consequently, during the Little Ice Age advance, basal shear stresses across riegels were high and active basal sliding and subglacial erosion occurred. Evidence for this comes from the multitude of striae and grooves observed on subaerially exposed riegels at Isfallsglaciären and Kaskasatjåkka which were formed by subglacial abrasion, and the presence of roche moutonnée at Kaskasatjåkka which demonstrate that plucking also occurred (Figure 3.2). In addition, estimates of basal shear stresses at Isfallsglaciären, based on the extent of the glacier in 1910 when it was near to its Little Ice Age Maxima (Karlén, 1973), show high basal shear stresses across the lower riegel (Figure 6.3). Below the riegel, the glacier surface slope reduced as the glacier escaped the confines of the valley and radiated out across the lower forefield, which reduced glacier velocity. At Isfallsglaciären, flutes begin to form in the area below the riegel where there was a reduction in velocity and basal shear stress, a transition from a hard- to a soft-bed, and a switch from subglacial erosion to subglacial deformation and lodgement (Figure 3.2a; Chapter 4.1.15).

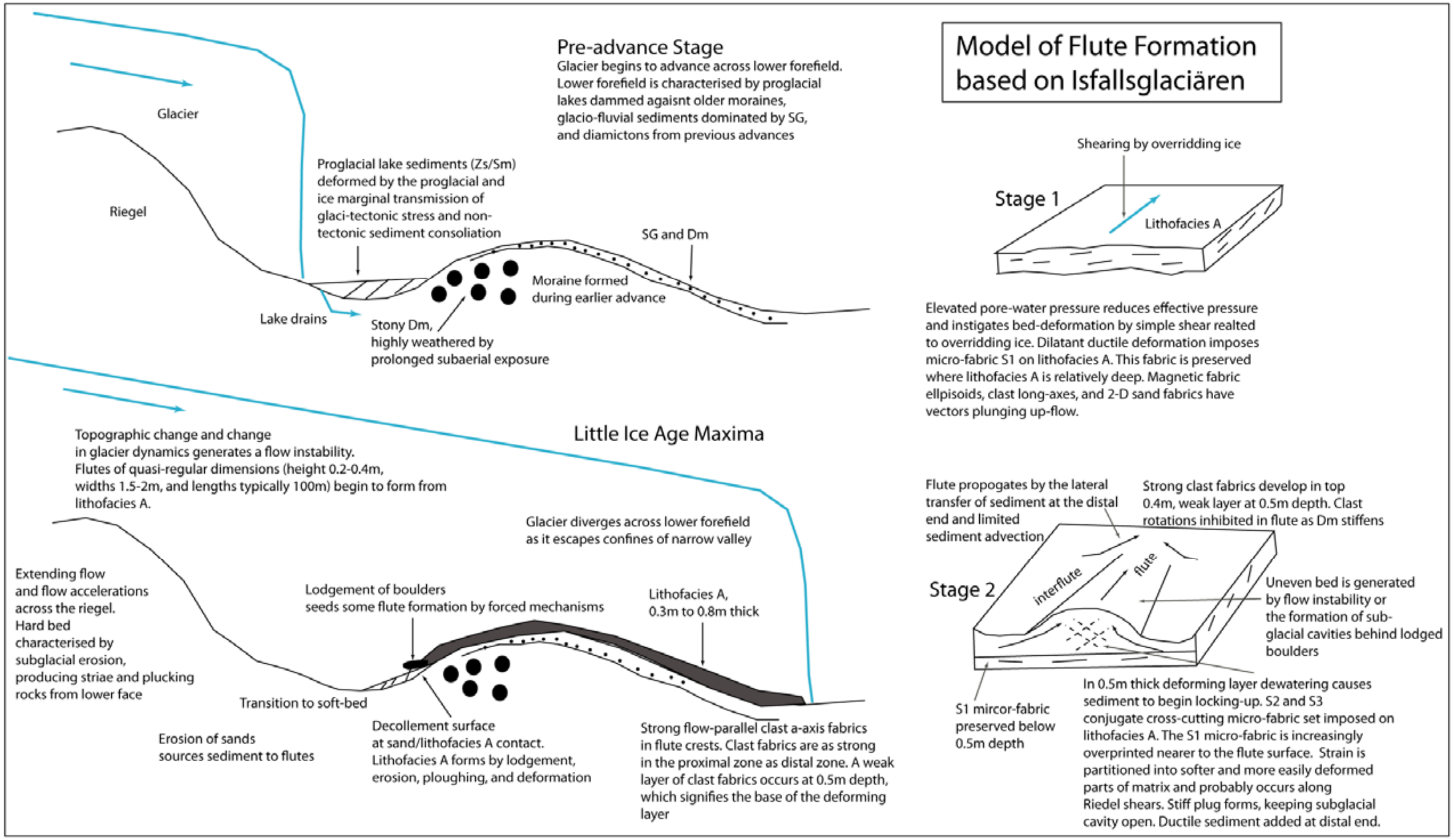

Figure 6.2 A model of flute formation.

Likewise at Kaskasatjåkka, the main fluted area occurs just down-flow from a prominent riegel, where areas of glacially eroded bedrock outcrop, and there was likely to have been a shift in the subglacial conditions down-flow from erosion to deformation and lodgement (Figure 3.2b). At Storglaciären, flutes are less well developed or preserved, but a relatively small area of fluted moraine consisting of Lithofacies A occurs just down-flow from a topographic break of slope (Figure 3.2c). It is suggested here that the change in topography instigated a flow-instability that generated flutes (Fowler, 2000; Schoof and Clarke, 2008; Chapter 1.4.10).

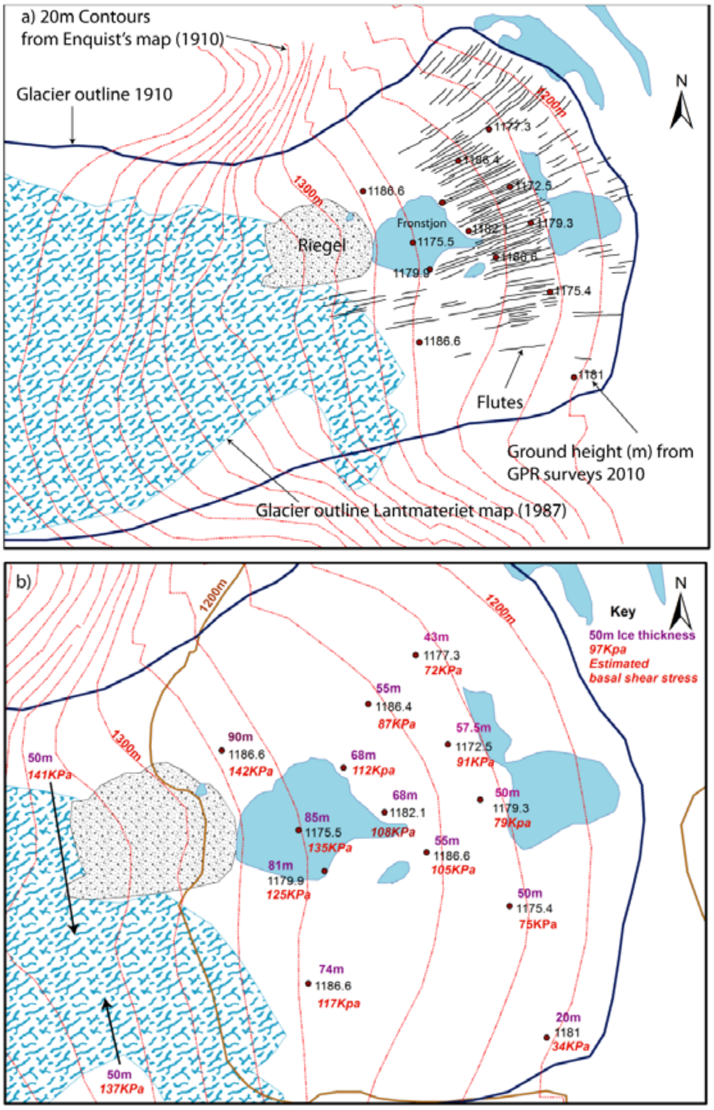

Figure 6.3 Estimates of basal shear stress and glacier thickness beneath Isfallsglaciären, 1910 (see Chapter 2 method).

Flow instabilities can be generated by natural variations in till thickness (Hindmarsh, 1998; Schoff and Clarke, 2008). Where the bed thickens, increased effective pressure results in a stalling of bed-deformation. The till then accretes as the loci of deformation moves upwards (Fowler, 2000). Positive feedback acts to enhance the initial topographic differences and favours the formation of bedforms (flutes) of certain wavelengths (Fowler, 2000). An initial phase of ductile deformation imposed the S1 micro-fabric on Lithofacies A (Chapter 5.4) as the glacier advanced across the forefield. It is argued here that as the bed thickened and stiffened just down-flow from the transition zone from a hard-bed to a soft-bed, a flow instability was generated which resulted in the bed being moulded into flutes of quasi-regular dimensions (Chapter 3.8.2). The dewatering and stiffening of Lithofacies A may have contributed to the flow instability as it would have produced localised sticky spots where bed-deformation was stalled and the bed was likely to thicken by accretion and an upward movement in the loci of deformation.

Boulders plucked from the bedrock riegels were lodged in thin deforming beds and seeded flute formation by forced mechanisms (Chapter 4.1.15b), which was superimposed on flute formation related to flow instabilities. The observed flute dimensions and properties are explained by the synchronous operation of two flute-forming mechanisms: flow instabilities generate flutes without the need for initiating boulders and over half the flutes observed in this study had no initiating boulder (Chapter 4.1.15d). They also account for the quasi-regular geometry of flute heights and widths and interflute widths in each forefield (Figure 3.23ae). However, the irregular spacing of flutes along transects at Isfallsglaciären (Figure 3.23f) can be explained by the random superimposition of flutes formed by forced-mechanisms on flutes formed by flow instabilities. The close association between boulders and about half of flutes observed is also explained by the forced-mechanism model. In these flutes, sediment was injected into lee-side cavities by ductile flow and advected short-distances down-flow as part of a deforming bed. Subsequent dewatering promoted the stiffening of the diamicton and the formation of the conjugate set of micro-fabrics, which overprinted the S1 micro-fabric (Figure 6.2).

6.4.2 Discussion of Flute Model

A topographic control on flute formation was identified by Hubbard and Reid (2006) in the Saskatchewan Glacier Valley where flutes formed on a 'moraine high' just down-flow from a proglacial lake basin. That is, flutes formed in a situation similar to that at Isfallsglaciären. In both cases, high pore-water pressures in the lake sediments probably encouraged bed-deformation and sourced material to subglacial traction tills. Estimates of basal shear stress beneath Isfallsglaciären suggest elevated pore-water pressures were required to deform Lithofacies A (Table 6.3). The estimates of strain magnitude derived from magnetic fabrics suggest that Lithofacies A in flutes must have stiffened and locked-up after relatively modest sediment advection; the strongest S_1 eigenvalues suggest a strain magnitude of ~10, which in a deforming bed ~0.5m thick approximates to sediment advection over a maximum distance of 5m. In the distal reaches of Area 3 at Isfallsglaciären, the deforming bed thickness achieves a maximum at ~0.8m thick and sediment advection approximates to a maximum value of ~8m. The siltier matrix in Lithofacies A in this zone probably induced higher pore-water pressures which allowed the bed to deform at lower shear stresses, and this probably explains the slight thickening of the bed in this area (Chapter 3.3.8&9).

In flutes formed by forced mechanisms sediment is laterally transferred from interflutes to flutes (Boulton, 1976). Evidence for the lateral transfer of sediment from interflutes to flutes in the Tarfala Valley is provided by herringbone fabrics and the differences in particle grain size distributions and fractal slope gradients in Lithofacies A samples taken from flutes and adjacent interflutes (Chapter 3.3.5). The dewatering and subsequent stiffening of Lithofacies A in lee-side subglacial cavities after relatively limited sediment advection would have created a solid plug of diamicton. According to Schoof and Clarke (2008), density contrasts between the sediment plug and glacier ice should result in the closure of the subglacial cavity, which imposes a limit on flute lengths. However, it is argued here that the injection of fine-grained ductile material from interflutes to flutes helped to keep the subglacial cavities open. If the lateral injection of fine-grained sediment was added to the distal end of the developing sediment plug, then viscosity contrasts between the cavity filled with ductile sediment and glacier ice would keep the cavity open (Benn and Evans, 2010). Keeping the subglacial cavity open would enable the flute to propagate by a combination of the lateral addition of locally sourced deforming sediments at the distal end and the shearing and advection of some sediment down-flow by overriding ice. Keeping the subglacial cavity open and propagating the flute by the addition of till at the distal end provides a mechanism for producing long, parallel-sided flutes such as those observed at Isfallsglaciären (Benn and Evans, 2010).

Table 6.3 Elevated pore-water pressures required to deform Lithofacies A, Isfallsglaciären

Estimated glacier dimensions	**Glacier Thickness (m)**	**Glacier Surface Slope (°)**	**Normal Pressure (KPa)** $\rho g h$	**Basal Shear Stress (KPa)** $\tau_b = \rho g h \sin\alpha$
	80	10	706	122
Estimated peak shear strength of Lithofacies A measured in shear box experiments*			Normal Load (KPa)	Peak shear strength (KPa)
			175	121

Note: the peak shear strength was measured using normal loads up to 100 KPa. The shear strength at 175 KPa has been estimated using the linear regression line (R^2 = 0.99) for the relationship between peak shear strength and normal load established during shear box tests (y = 0.662x + 4.863). Basal shear stress is calculated using equation 1.2 where p is the density of ice ($0.9 gcm^{-3}$), g is gravitational acceleration ($9.81 ms^{-2}$), h is ice thickness (m), and α is the glacier surface slope. Shear strength was calculated using equation 1.3. A lower basal shear stress would be required for deformation once the sediment has been sheared to its residual shear strength. The estimates of basal shear stress given here are in the range quoted for other glaciers, where it has been estimated that elevated pore-water pressures are required to take-up to 90% of the confining pressure in order to facilitate bed deformation (Paterson, 1994).

Shearing by overriding ice and sediment advection was sufficient to induce strong flow-parallel clast a-axis fabrics in flute crests where deformation was confined (Benn, 1994). The removal of sediment from interflutes explains why weaker clast fabrics are generally measured in interflutes (Chapter 3.3.5). In a deforming bed, where shearing by overriding ice is orientating clasts into flow-parallel alignment, the initiation of flute formation would have resulted in clasts being laterally transferred towards low-pressure subglacial cavities (Boulton, 1976). The lateral transfer of sediment would have been particularly effective in the softer and more easily deformed finer-grained matrix fraction of Lithofacies A, which continued to deform even after the stiffer framework of skeletal grains began to lock-up (Chapter 5.3). In interflutes, lateral sediment transfer disrupted fabric development and resulted in the development of a coarser and stiffer diamicton, which resisted deformation and clast alignment more effectively.

Flutes without initiating boulders have been interpreted here as flutes that formed due to a topographically controlled flow instability. Flutes without boulders were more common than flutes with boulders, suggesting that the flow instability mechanism was more dominant than the forced mechanism of flute formation. The same flute/interflute contrasts in Lithofacies A were observed in flutes without initiating boulders, so the flow instability must have resulted in the lateral transfer of sediment from interflutes to flutes (Schoof and Clarke, 2008). It is suggested here that the topographically controlled flow instability produced a wavy ice-bed interface characterised by ice-walled furrows of quasi-regular dimensions into which sediment was injected. As in flutes formed by forced mechanisms, flutes were propagated through a combination of lateral sediment transfer and sediment advection (Figure 6.2).

Flute formation by forced mechanisms requires the operation of two subglacial processes: the lodgement of an initiating boulder, and subsequent bed deformation. Lithofacies A must, at times, have been sufficiently stiff to generate enough drag to cause boulders to lodge in the bed. The occurrence of double stoss-and-lee boulders, thought to be formed by ploughing (Benn, 1994; 2004), suggest that, at other times, Lithofacies A was sufficiently soft to allow boulders to plough through the bed. These variations in the shear strength of Lithofacies A are consistent with variable pore-water pressures controlling the nature of subglacial processes (Piotrowski *et al*., 2004). The locking-up of Lithofacies A in flutes is evidenced by the formation of the S2 and S3 conjugate micro-fabrics and the wrapping of these foliations around coarser clasts, which is related here to sediment dewatering (Chapter 5.3&4). The limited sediment advection suggested by moderate strain magnitudes (Chapter 4.2.9) and the lack of correlation between clast fabric S_1 eigenvalues and distance downflute (Chapter 4.1.5), indicate that sediment dewatering occurred rapidly after sediment was injected into subglacial cavities/ice-walled furrows. This could have been achieved by effective drainage through the soft-bed, or by freezing-on to the base of the glacier (Section 6.3.1). The latter mechanism is consistent with the flute-forming mechanism suggested by Roberson *et al*. (2011) in which Robin's heat-pump effect creates a cold patch of ice in a subglacial cavity beneath temperate ice onto which injected sediment freezes-on.

Lithofacies A (and B) resemble over-consolidated B-horizons with relatively low porosities. Similar diamictons have been identified as lodgement tills in palaeo-ice stream deposits (Ó

Cofaigh *et al*., 2007), in till sheets (Larsen and Piotrowski, 2003), and in forefields of some valley glaciers (Benn *et al*., 2003). As Lithofacies A and B began to stiffen, they would have generated more drag and encouraged lodgement of coarser debris. Subglacial deformation, ploughing and lodgement processes are linked together by variations in pore-water pressure; a soft ductile till facilitates ploughing, whereas lodgement is encouraged as the till begins to dewater and stiffen. The stiffening of Lithofacies A and the increase in basal drag would have acted as a brake on glacier flow.

6.4.3 The Wider Application of the Flute Model

The model presented in Section 6.4.1 is different from previous models of flute formation in that it combines two models of flute formation in order to account for the observed features of flutes in the Tarfala Valley. Unlike the Eklund and Hart (1996) model (Chapter 4.1.15a), it is based on detailed observations and attempts to explain the quasi-regular dimensions of flutes. It is distinct from the Hoppe and Schytt (1953) model of flute formation in that it recognizes that flute formation occurred beneath temperate ice (Chapter 1.4.10).

Flutes occur in a wide-range of glacial environments and they may have multiple modes of formation, including erosion, deposition and deformation (Gordon *et al*., 1992; Benn, 1994). As such, no one model is likely to account for **all** flute fields (Benn, 1995). Nevertheless, the model presented here may explain flute formation in other forefields where flutes with and without initiating boulders have been observed, especially where flutes have quasi-regular dimensions (Boulton, 1976; Gordon *et al*., 1992; Benn 1994; 1995; Evans *et al*., 2010; Benn and Evans, 2010). The operation of the two-flute forming mechanisms would be particularly applicable to forefields where bedrock topography instigated flow instabilities and the erosion of riegels seeded flute formation through boulder lodgement. The importance of lodgement processes in seeding flute formation was recently recognised by Evans *et al*. (2010) in Icelandic forefields. The evidence from the present study accords with Benn and Evan's (2010) suggestion that most researchers favour a deforming bed origin for flutes. However, this is only part of the picture because detailed observations show that both lodgement and bed-deformation are important processes in flute formation in the Tarfala Valley.

The results of this study show that uniform deforming bed conditions and very high strain magnitudes cannot be assumed based on macroscopic observations of homogeneous diamictons in long, parallel-sided flutes with strong flow-parallel clast a-axis fabrics (cf. Rose

1989; 1991; Benn 1994; 1995; Eklund and Hart, 1996). Moreover, the locking-up of sediment after relatively limited advection, the moderate strain magnitudes, and the deceleration of Isfallsglaciären below the riegel suggest that long, parallel-sided flutes formed under conditions of continuous glacier flow rather than fast flow. Similarly, Benn (1994) argued long, parallel-sided flutes in polythermal valley glaciers in Norway formed under conditions of steady, continuous flow.

Large subglacial landforms such as MSGL and mega-flutings have been linked to fast flow beneath ice streams and to deforming-bed conditions produced by ice-keel ploughing (Tulaczyk *et al*., 2001; Clark *et al*., 2003; Chapter 1.4.8). The evidence for fast flow is inferred from the great length of MSGLs, and their close spacing and increased elongation in ice steam trunk zones (Stokes and Clark, 2002). The evidence for groove-ploughing is inferred from the distribution of MSGLs down-flow of rough bedrock elements in onset areas which could have generated ice keels (Tulaczyk *et al*., 2001), and the reduction in groove and ridge dimensions down-flow – which is consistent with less effective ploughing as ice keels attenuated (Clark and Stokes, 2003). However, not all MSGLs can be accounted for by the ice-groove ploughing hypothesis, which suggests that, like flutes in the present study, multiple processes may be involved in their formation (Benn and Evans, 2010). For example, MSGLs in Marguerite Bay do not always form down-flow of rough eroded bedrock areas where ice keels would form, and the spacing between grooves changes down-flow (suggesting it does not relate to the spacing of ice keels), whilst ridges often divide (Ó Cofaigh *et al*., 2005). As in the Tarfala Valley flutes, the subglacial till forming the MSGL was interpreted as a hybrid till formed by lodgement and deformation (Ó Cofaigh *et al*., 2007). MSGLs were interpreted as forming by two processes – both groove-ploughing and, where till was sufficiently thick and stiff to produce sticky spots, localized bed deformation from point sources (Ó Cofaigh *et al*., 2005). The model of flute formation presented in the present study is consistent with these findings in that at both glacier scales subglacial bedforms are observed to be generated by multiple processes and the synchronous operation of two mechanisms.

It maybe that larger subglacial bedforms, like the smaller Tarfala flutes, can also be produced by continuous steady – rather than fast – flow. The quasi-regular dimensions of bedforms like MSGLs may also relate to flow instabilities rather than the spacing of ice keels (Schoof and Clarke, 2008). As such, the model of flute formation presented here may be applicable to the formation of subglacial bedforms at larger scales. To confirm that such landforms are formed by high cumulative strains and bed-deformation, estimates of strain magnitude are required, but relatively little research has currently been completed on the composition of MSGLs (Ó Cofaigh *et al*., 2007) or on estimating strain magnitudes in associated landforms such as drumlins. Interestingly, a recent study of a drumlin formed at the bed of the Rutford ice stream suggested the drumlin formed by either subglacial sediment deformation into an ice-groove formed in the base of the glacier as it flowed over a bedrock obstruction further up-flow (that is, a mechanism akin to the forced-mechanism model of flute formation), or in response to flow instabilities in the bed (Smith *et al*., 2007). It is speculated here that both mechanisms may have operated at the same time. If this is true, then the flute model presented in this study may be applicable to the formation of other landforms at larger glacier scales, and these landforms are polygenetic features.

6.5 Landsystem Model

6.5.1 A Glacial-Paraglacial Landsystems Model for the Tarfala Valley

The characteristics of the contemporary forefields are the result of glacial-paraglacial interactions and the observations from different scales of analysis have been integrated into a glacial-paraglacial landsystems model for the Tarfala Valley which is shown in Figure 6.4. Many of the features of the model have already been discussed in the previous sections of this Chapter, for example, the topographic control of glacier dynamics and the nature of subglacial processes and flute formation. As such, the main features of the model are briefly summarised below.

A near-continuous cover of subglacial traction tills forms in the central lower forefield beneath temperate ice where elevated pore-water pressures facilitate subglacial deformation and the cannibalisation of overridden proglacial sediments sources material for till genesis. Subglacial deformation related to shearing by overriding ice is not a continuous process but controlled by variations in pore-water pressure. Strain is partitioned, polyphase and cumulative. The diamicton plain/sheet is built-up by the accretion of thin layers of traction till over time. Lodgement, ploughing, erosion and deformation processes occur in close spatial proximity, with lodgement and deformation being the dominant processes. Larger particles preferentially lodge in the bed as they experience greater drag (Benn, 2004), whilst deformation is partitioned into softer and more easily deformed parts of the matrix. An initial phase of ductile and dilatant deformation is followed by sediment dewatering and stiffening and the imposition of a conjugate set of micro-fabrics. The over-consolidation of the diamicton produces traction tills that resemble B- horizons and the stiffening of the diamicton generates sticky-spots. Glacier thermal structure, bedrock topography, basal sliding, and soft-bed deformation all exerted a control on glacier dynamics. Basal sliding is the major contributor to total basal slip. At times of very high basal water pressures, glaciers de-couple from their beds and flow accelerations occur (Iverson *et al*., 1995), whilst subglacial meltwater incision deposits sandy gravels across parts of the diamicton plain/sheet. Overridden fluted moraine and diamicton plains/sheets are palimpsest landforms consisting of multiple lithofacies. When glaciers advance moraines are overridden but with little modification, although flutes form at a relatively late-stage on their proximal and distal slopes. Sediment freezes-on to the base of at the glacier margin. Older moraines act as barriers to glacier advance and compressive flow causes the thickening, stacking and elevation of debris-rich basal ice at the ice margin (Ó Cofaigh and Evans, 2003; Moore *et al*., 2011; Chapter 3.8.2).

Individual glaciers vary in the quantity of supraglacial sediment they carry, which includes medial moraine, material sourced from rockfalls and frost shattering of valley sides, and debris mounds of subglacial/englacial debris elevated to the surface by compressive flow at the glacier margin. Nevertheless, the amount of supraglacial sediment carried is relatively limited as subglacial traction tills are well-exposed on the forefield and not masked by extensive cover of supraglacial moraine or dump moraines. Large lateral-frontal moraines occur and diamictons in these moraines contain sediment sourced from subglacial and supraglacial transport pathways (Chapter 3.6.1&2). The largest lateral-frontal moraines are ice-cored and so sufficient sediment was deposited to insulate glacier ice. The distal slopes of the lateral-frontal moraines are characterised by deposits of sandy gravels, massive sands, block gravels, and occasional patches of diamicton (Chapter 3.8.6). Sediments frozen-on to the base of the glacier during winter advances melt-out in summer and are deposited on the distal slopes of the moraines (Evans, 2003). Ice-marginal streams developed where meltwater could not penetrate cold-based ice.

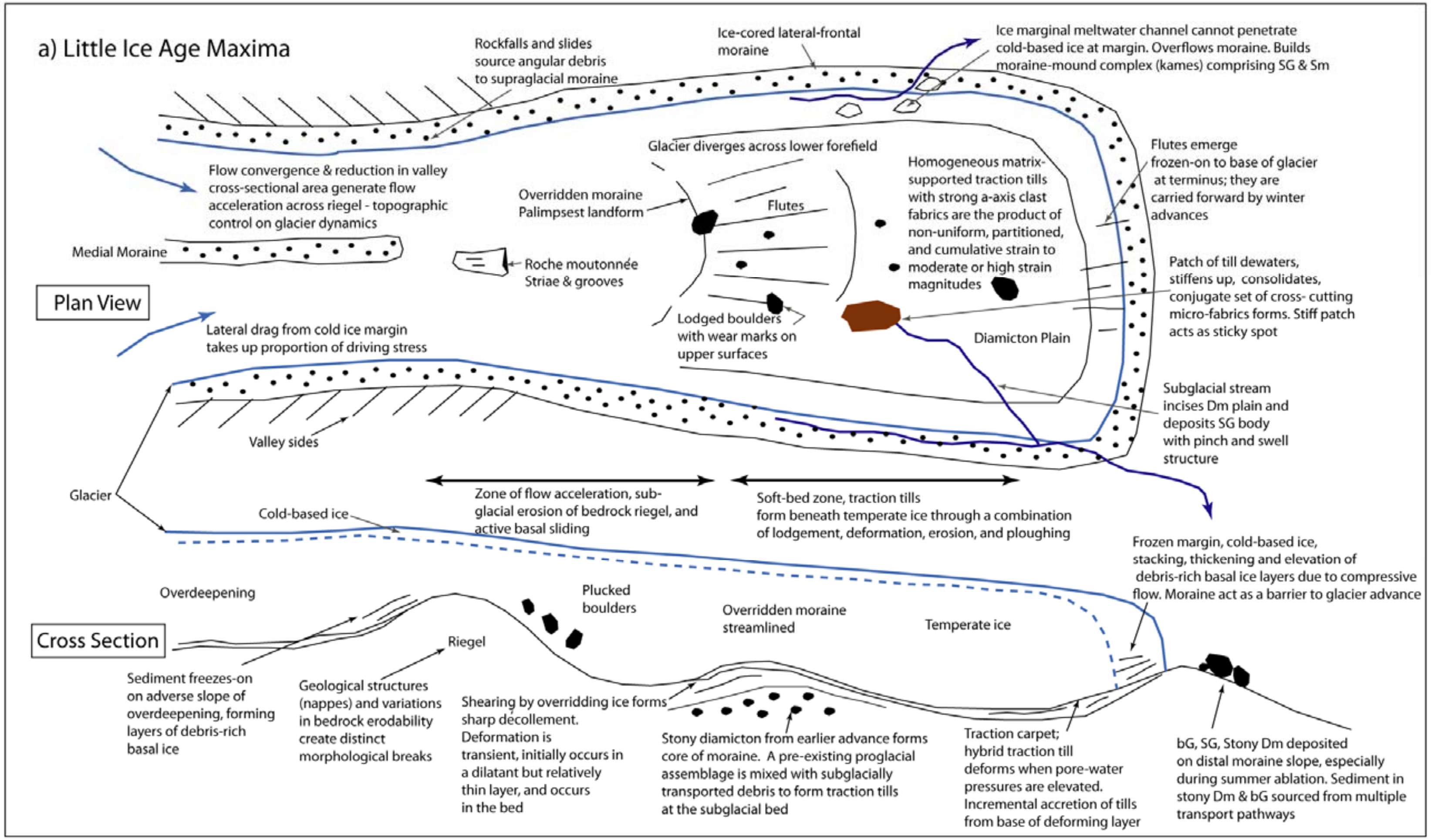

Figure 6.4(a&b) A glacial-paraglacial landsystems model for the Tarfala Valley; (a) the situation during the LIA Maxima.

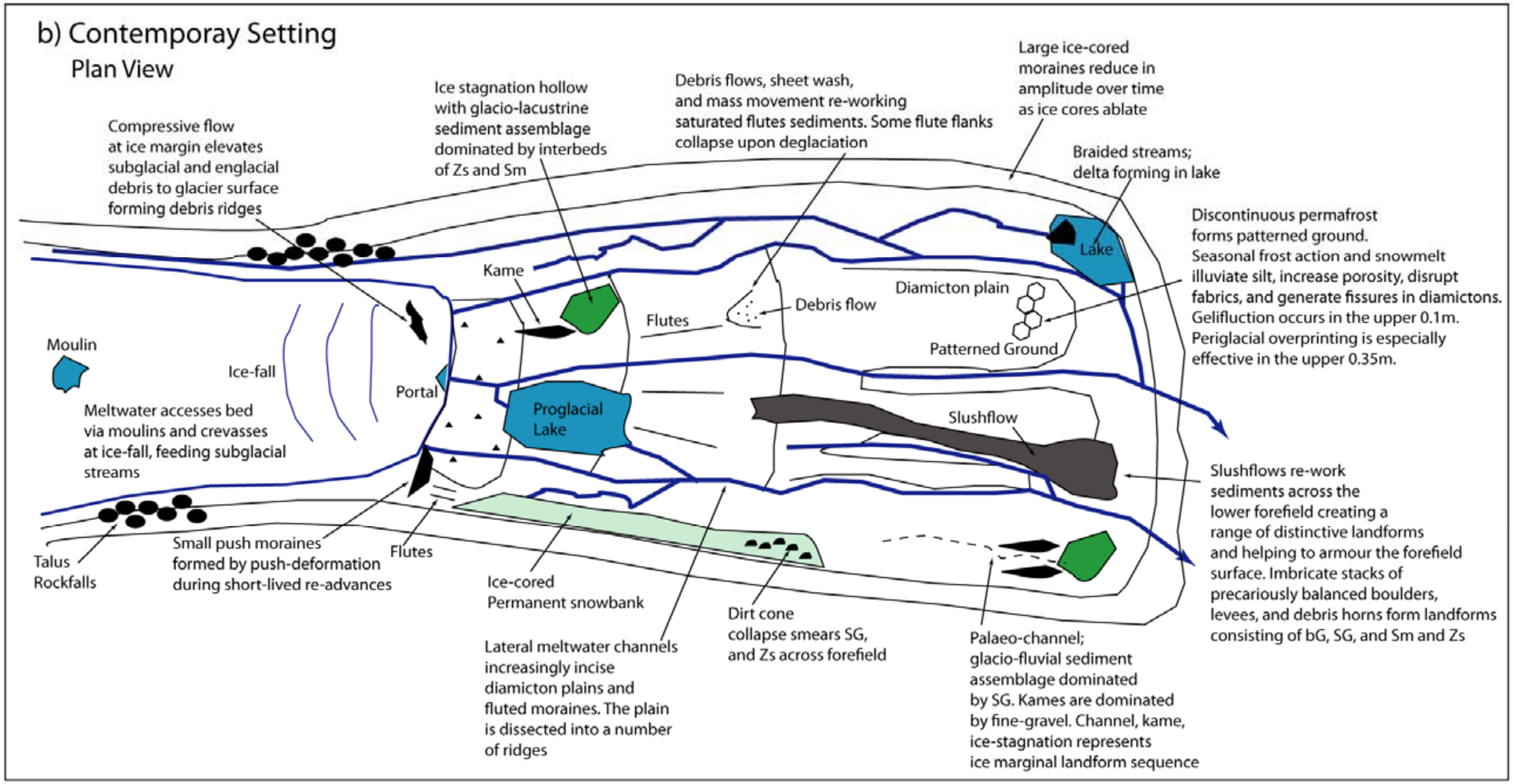

Figure 6.4 continued (b) The contemporary setting.

During glacier recession, extensive active and modified glaciofluvial terrain occurs in the proglacial areas where sandy gravel is the dominant lithofacies. Ice stagnation topography occurs particularly towards the lateral margins of the forefields where kames and ice stagnation hollows develop. These landforms consist of glaciofluvial and glacio-lacustrine sediment assemblages characterised by sandy gravels, massive sands, and silty sands (Chapter 3.7). Lateral meltwater streams incise into the diamicton plains and fluted moraines and re-work subglacial diamictons. Small glacier advances produce small push moraines characterised by block gravels which contain boulders sourced from subglacial and supra-glacial transport pathways (Chapter 3.8.1). Glacier oscillations are capable of generating an ice-marginal sediment assemblage in some parts of the diamicton plain which are characterised by the interdigitation of subglacial diamictons, sandy gravels and massive and silty sands (Chapter 3.8.4).

Once glaciers recede, paraglacial processes actively and rapidly begin to modify the subaerially exposed subglacial sediments and landforms. The combination of summer snowmelt and heavy summer storms, which saturate poorly drained diamictons, and some steep slopes renders diamictons unstable and mass movement events are common. These include slumps, slides, falls, gelifluction and debris flows (Chapter 3.8.3). Mass movements disrupt and mask flutes and disrupt some flute clast fabrics, particularly in the upper 0.1m. High magnitude-low frequency slushflows are initiated during rapid spring warming events and subglacial sediments are eroded and re-worked across the lower forefield. Slushflows generate a unique assemblage of landforms including precariously stacked boulders, levees and debris horns. Slushflow deposits mask areas of fluted moraine and erode sections of diamicton plains/sheets. Wind-blown sediment and sediment derived from slides, falls, and meltwater flow deliver debris to the surface of permanent snowbanks. Ablation of permanent snowbanks results in the production of dirt cones and smears sandy gravels and silty sands across the forefield. Paraglacial processes help to armour the forefield surface. Braided meltwater streams incise into forefield sediments at times of higher discharge and, where they flow into moraine dammed lakes, form small deltas. Extensive scree slopes develop through active frost shattering of the valley sides. The eventual ablation of ice-cores leads to the reduction in height of ice-cored lateral-frontal moraine-mound complexes (Holmlund and Jansson, 2002). Seasonal frost action leads to the vertical jacking of clasts, the formation of patterned ground, silt illuviation, and the growth of segregated ice in silty diamictons. Periglacial overprinting is extensive in the upper sections of traction till, where it results in increased porosity and void ratios and disruption to clast fabrics. The extent of periglacial overprinting decreases with depth, but is still evident at 1m depth (Chapter 5.4.1).

6.5.2. Discussion of the Landsystems Model

The model presented in Figure 6.4 is a framework for understanding the landsystems of polythermal valley glaciers in northern Sweden. Individual glaciers will show deviations from the model depending on their exact thermal structure, topography, elevation, and aspect. These factors control the extent of temperate ice and the amount of basal sliding and subglacial deformation that occurs, and the rate at which paraglacial activities modify the forefield. For example, the initiation of slushflows by rapid warming events is much more likely to occur at Kaskasatjåkka due to its south facing aspect. In addition, the glacier is almost entirely composed of temperate ice at present (Holmlund and Jansson, 2002) and in summer, considerable meltwater is produced which results in the more active incision and re-working of subglacial diamictons. Despite individual deviations from the model, the results of this study suggest that similar processes operated in each forefield and produced a common suite of lithofacies-landforms associations typical of polythermal glaciers.

The model has similarities with elements of other glacial landsystem models, but is also distinct from them. For example, the subglacial sediment assemblage associated with ice-marginal terrestrial landsystems with active temperate margins (Evans, 2003) has similarities with the Tarfala Valley model. Similarities include overridden fluted moraines, the incremental accretion of traction tills, ductile deformation, the importance of pore-water pressure in controlling the timing and location of deformation, and the cumulative and distributed nature of strain. In addition, the elevation of subglacial material at the ice margin through compressive flow, and the formation of large frontal-lateral moraines are also features of the ice-marginal terrestrial landsystem. By contrast, evidence of extensive glaci-tectonic deformation of pre-existing proglacial sediments and extensive large-scale water escape structures, which are features of the landsystem of active temperate margins in Iceland (van der Meer *et al*., 1999; Evans, 2003), are not in evidence in the Tarfala Valley model. Here, subglacial deformation is focused into relatively thin beds typified by sharp contacts with underlying sediments which are indicative of erosion/décollement. Moreover, extensive low-amplitude dump, push and squeeze- moraines do not occur in the Tarfala Valley model, although small push moraines form in response to short-lived glacier advances.

In the Tarfala Valley model, topography plays an important role in controlling glacier dynamics and the distribution of landforms as it is also known to do in the glaciated valley landsystem (Benn *et al*., 2003). However, the supply of supraglacial moraine to the forefield is much more restricted than in some dirty Alpine valley glaciers, which allows good forefield exposure of subglacial sediments. In the landsystem of sub-polar glacier margins of the High Arctic (Ó Cofaigh and Evans, 2003), thick layers of debris-rich basal ice exist because temperate ice erodes and transports material which then freezes-on at the cold margin, leading to the accretion of thick debris layers. Compressive flow then thickens and elevates the layer, and a similar process is thought to operate beneath Storglaciären where it produces debris ridges at the glacier surface (Moore *et al*., 2012). However, unlike many High Arctic glaciers (and many Svalbard glaciers; Glasser and Hambrey, 2003), the Tarfala Glaciers do not surge, and there is an absence of extensive continuous permafrost cover. Surging has been implicated in the formation of very thick basal-rich debris ice layers and landforms such as thrust-block moraines (Ó Cofaigh and Evans, 2003; Glasser and Hambrey, 2003). The presence of extensive permafrost is thought to play a vital role in the formation of thrust-block moraines and the extensive glaci-tectonic deformation of proglacial sediments in High Arctic glaciers where the base of the aggrading permafrost acts as a décollement surface (Ó Cofaigh and Evans, 2003).

As the model presented here contains elements of other glacial landsystems it should be considered a hybrid that falls part-way between the temperate ice-marginal terrestrial landsystem, the glaciated valley landsystem, and the landsystem of the High Arctic. It varies from each of these models in turn by the extent of permafrost cover, the influence of topography on glacier dynamics, the absence of surging behaviour, and the availability of subglacial meltwater to facilitate basal sliding and soft-bed deformation. As such, the model is distinct and significantly different from other landsystem models that only partly account for the lithofacies-landform associations of the Tarfala Valley. The model is probably most applicable to other small polythermal glaciers in areas having similar bedrock geology, topography and climate to northern Sweden.

Chapter 7 Conclusions

7.1 Conclusions Related to Observations in the Tarfala valley

7.1.1 The subglacial environment of the Tarfala Valley is best characterised by the ice-bed mosaic model. Ploughing, lodgement, deformation and erosion occurred in close spatial proximity, and subglacial deformation was multi-phase and time-transgressive; variations in pore-water pressure controlled the timing and location of deformation events. The available evidence from macroscopic observations and fabric studies indicate that thick deforming beds and very high strain magnitudes ($>10^2$) did not occur. Observations on deforming-bed thickness and strain magnitude (derived from magnetic fabrics) indicate that in flutes, sediment advection was probably limited to a maximum of ~5-8m, whilst strain magnitudes in recently exposed subglacial traction tills were modest (<10). As such, the results of this study add to the growing body of detailed observational evidence that is at odds with the very high strain requirements of the soft-bed deformation model. Subglacial deformation did occur, but not continuously, not to great depth, and not to very high strain magnitudes, and so it had a limited capacity to control glacier dynamics. Basal sliding beneath temperate ice and topography exert strong controls on glacier dynamics in small, polythermal valley glaciers.

7.1.2 Subglacial deformation in Lithofacies A and B was polyphase. An initial ductile phase of deformation occurred under relatively dilatant conditions in deforming layers that averaged 0.2-0.6m thick. Till in these layers accreted incrementally. Deformation was partitioned into the softer and more easily deformed parts of the matrix, especially during the later imposition of a cross-cutting penecontemporaneous conjugate set of micro-fabrics. These micro-fabrics developed as the sediment dewatered and locked-up, a process driven either by effective evacuation of pore-water through the deforming bed, or the freeze-on of sediment to the base of the glacier. The resulting homogeneous diamictons are the product of heterogeneous and cumulative strain. The stiffening of the diamicton would have acted as a brake on glacier dynamics as local sticky-spots developed.

7.1.3 Similar lithofacies-landform associations are associated with each of the glaciers in the Tarfala Valley. This suggests similar processes occurred in each valley glacier, and this allows for the development of a glacial-paraglaciallandsystemsmodel. Topography, aspect, elevation and glacier thermal structure are key controls on glacial-paraglacial processes in the Tarfala Valley. Diamicton plains/sheets and fluted moraines are palimpsest and polygenetic landforms which contain clast-supported diamictons that pre-date the Little Ice Age Advance. Detailed observations reveal that the diamicton plain of Storglaciären and the fluted moraine of Isfallsglaciären are more complex landforms than previously reported. The diamicton plain consists of heterogeneous sequences of ice-marginal sediments, sandy gravel layers possibly formed by subglacial meltwater incision, and traction tills formed by incremental accretion from the base of relatively thin deforming layers and that appear homogeneous at the macro-scale. Lodgement was also an important process in the formation of Lithofacies A and B in fluted moraines and the diamicton plain.

7.1.4 Long parallel-sided flutes with quasi-regular dimensions are common subglacial landforms associated with all of the glaciers in the Tarfala Valley. The most prominent fluted areas occur beneath distinct topographic breaks of slope. Flutes formed in response to a topographically controlled flow instability and forced mechanisms related to the lateral movement of ductile sediment into lee-side subglacial cavities which formed behind initiating boulders. Ductile till stiffened-up as it dewatered and consolidated after relatively limited advection. Shearing by overriding ice was sufficient to induce strong flow-parallel clast a-axis fabrics in flute crests, and to produce an aggregate strain ellipsoid in magnetic fabrics similar to the steady-state strain ellipsoid produced at moderate to high strains by simple shear in ring shear experiments. Flutes were propagated through a combination of sediment advection and the lateral transfer of ductile till from interflutes to flutes, which added sediment to the distal end of the developing flute. The lateral sediment transfer helps to explain the differences in particle-grain size distribution, fractal slope gradients, and clast fabric strengths between interflutes and flutes.

7.1.5 Thin section analysis reveals evidence of periglacial overprinting of subglacial diamictons which have been subaerially exposed for less than *ca.* 30 years to at least 1m depth. Periglacial overprinting relates by the growth and thaw consolidation of segregated ice in siltydiamictons. It is quite extensive in the upper 0.15m of flutes where the presence of Type 3 silt caps demonstrates gelifluction occurred. Silt caps are formed by silt illuviation related to thaw consolidation and seasonal snowmelt. Type 1 silt caps dominate and silt caps become fewer and thinner with depth. Fissile partings are demarcated by clean linear voids and contraction voids and probably opened-up at a late-stage due to dewatering or unloading and subsequent cryogenic action. There is little micro-scale evidence to suggest they are shear planes, although occasionally developed/preserved linear grain alignments formed along the outside walls of linear voids that demarcate steeply inclined fissile partings may indicate a phase of earlier discrete shear. A late-phase of brittle shear would be expected in a stiffening diamicton that was losing dilatancy. Seasonal frost action increased porosity and disrupted fabrics in the upper 0.15m.

7.1.6 Paraglacial processes are rapidly re-working subglacial sediments exposed in the Tarfala Valley. They are particularly active at south-facing Kaskasatjåkka where high magnitude-low frequency slush flows produce a number of distinctive landforms not previously reported in the Tarfala Valley. The extent to which paraglacial processes are re-working subglacial sediments and landforms explains some of the contrasts in appearance between each forefield.

7.2 Conclusions Related to the Wider Implications of the Research and Future Research Directions

7.2.1 An important implication of this study is that mascroscopic observations revealing a homogeneous, matrix-supported subglacial diamicton with strong flow-parallel clast a-axis fabrics are not diagnostic of high strain magnitudes. Likewise, brittle discrete shearing cannot be assumed just because a diamicton contains fissile partings and faceted clasts. Researchers should be careful not to make assumptions about deforming-bed processes which lead to an over-interpretation of subglacial diamictons based on limited macro-scale observations alone; micro-scale observations may provide a different picture of deforming-bed processes. The results of this research demonstrate the value of a multi-dimensional landsystems approach. The micro-structural mapping technique provides useful insights into the polyphase history of sediment deformation that are not apparent at other scales of analysis. Magnetic fabrics allow strain magnitudes to be estimated, which allows one of the main tenets of the bed-deformation model to be tested. In this study, the magnetic fabrics, clast fabrics, and 2-D sand fabrics in tills from flutes provide a consistent picture of strain, which suggests magnetic fabrics taken in tills where periglacial overprinting was less extensive probably gave a reliable estimate of shear strain magnitude.

7.2.2 There is a need to apply a multi-dimensional approach more widely to the study of Quaternary till sheets and till sequences beneath active and palaeo-ice sheets and ice streams, and to landforms such as MSGLs, so as to verify subglacial models. Previous research has inferred that MSGLs relate to fast-flow and bed-deformation, and pervasive deformation has been inferred from the presence of acoustically transparent sediment layers from beneath ice streams. However, further observational evidence is required to corroborate these inferences. Magnetic fabrics should indicate very high strain magnitudes in tills in MSGLs if they have been formed by bed-deformation and extensive sediment advection. Likewise, if thick pervasively deforming beds are controlling ice stream dynamics, then sediments recovered from the bed should have magnetic fabrics consistent with very high strain magnitudes.

7.2.3 Some recent research suggests tills in MSGLs are hybrid traction tills formed by lodgement and deformation processes in relatively thin, accreting beds – a situation similar to till formation in the Tarfala Valley. Moreover, recent research provides evidence that the ice-bed mosaic model – the model favoured as the best characterisation of the former subglacial bed in the Tarfala Valley – also best characterises the subglacial environment beneath the Rutford Ice Stream. The deforming-bed model and ice-bed mosaic model probably represent end members in a range of possible subglacial environments. Bed-deformation might exert a particularly effective control on glacier dynamics where ice sheets override soft, fine-grained marine and lacustrine sediments that deform more readily than granular tills. Further research is required to characterise the subglacial environments beneath a range of glaciers at different scales to see how the nature of the sediments that comprise the soft-bed exert a control on the partitioning between bed-deformation and basal sliding. This research is urgently required in order to better understand the way in which subglacial conditions exert a control on ice sheet stability and dynamics, and on landform generation. The application of a multi-dimensional approach would allow for the wider testing and falsification of subglacial models beneath different types of glaciers at a variety of scales, a better understanding of the relation between strain magnitudes, sediment advection and glacier velocity, and a better understanding of the polyphase nature of sediment deformation.

7.2.4 The synchronous operation of two flute-forming mechanisms incorporated into the model of flute formation in the Tarfala Valley may account for flutes observed on other forefields where flutes with and without initiating boulders occur, and where flutes have quasi-regular heights and widths, but variable spacing. This model may also explain landforms formed beneath some large-glaciers, where flow instabilities in the bed and forced-mechanisms related to sediment deformation may occur concurrently. Further research is required to relate theoretical models of flow instabilities to direct observations. For example, whether flow instabilities at Isfallsglaciären are capable of producing flutes of the quasi-regular dimensions observed, and whether flow instabilities beneath ice streams scale-up to produce landforms such as MSGLs and drumlin fields. The exact mechanisms that induce flow instabilities in subglacial beds also need to be identified, both in theory and practice.

7.2.5 Ring shear experiments demonstrate that strongly aligned clast fabrics occur at moderate strains even in dilatant layers. Weakly aligned fabrics are thought to equate to low strains, and yet in a pervasively deforming bed, the highest strain is supposed to occur nearest to the glacier sole. However, in this zone, A-Type horizons are supposed to form and these are characterized by some weakly clustered clast fabrics. The origin of such weak fabrics remains unexplained. The results of the present study suggest that weakly clustered clast fabrics can be produced in a deforming bed where high compressive stress occurs near to lodged boulders (a situation not found in ring-shear experiments). Furthermore, the results show that some of the weakly clustered fabrics may be the product of periglacial overprinting in the top 0.1m of recently exposed tills. As such, micro-scale evidence is required to confirm sediment characteristics interpreted as subglacial signatures (such as A-Type horizons) are not the consequence of periglacial overprinting. Further research is required to understand the processes that generate some weakly clustered clast fabrics in A-type horizons and to understand how the high porosity, void ratio, and dilatant state of such layers is maintained after the cessation of shear (at which point dilatant layers are supposed to collapse and consolidate). There is also a need for further research to understand the origin of fissile textures in subglacial tills, especially at the micro-scale. Such thin sections need to be recovered from subglacial tills which are actively shearing and which have not been exposed to paraglacial and periglacial processes.

7.2.6 There is a need for further research to see how applicable the periglacial-paraglacial landsystems model presented here is to other sub-polar and arctic glaciers, and to formerly glaciated areas. This model is distinct in that it contains elements of the temperate valley glacier landsystem, the ice-marginal glacier landsystem, and high arctic glacier landsystem, and in that it emphasis the interactions between glacial and paraglacial processes in accounting for Lithofacies-Landform Associations. The model is probably most applicable to valley glaciers where bedrock topography and glacier thermal structure exerted a major control on glacier dynamics.

Acknowledgements

I would like to thank the British Geomorphological Society, the Gilchrist Education Expedition Trust and the Quaternary Research Association for funding support towards fieldwork and laboratory costs. I would like to thank the staff at the Tarfala Research Centre for fieldwork assistance and advice, especially Professor P. Jansson, Mr A. Mercer, and Professor P. Holmlund of Stockholm University, who also supplied aerial photographs and historical photographs of glaciers in the Tarfala Valley. I am indebted to Dr A. Palmer at the Centre for Micromorphology, Royal Holloway University for thin section preparation, and Mr E. Fleming, Department of Geology, University of Birmingham for carrying out AMS measurements and thermo-magnetic experiments. I am grateful to Dr S. Carr and Professor J. van der Meer at the Centre for Micromorphology, Queen Mary College, University of London for training in micromorphology, and Dr E. Phillips of the British Geological Survey for training in micro-structural mapping techniques and for many stimulating discussions concerning subglacial deformation processes. I am grateful to Dr D. Benn and Dr T. Ringrose for supplying me with a copy of their Matlab bootstrapping programme and granting permission to use it. I would like to thank Dr S. Cook for advice on the basal ice facies of Storglaciären and Isfallsglaciären. I am also grateful to Dr. M. Frost, Department of Civil Engineering, Loughborough University for technical advice concerning shear box tests. I am grateful to my supervisors, Dr J. Evans and Dr D. Graham for fieldwork assistance and ongoing support. Finally, I would like to thank Dr T. Matthews for his help in digging pits and trenches and his unfailing good humour and company during two summer fieldwork campaigns in Sweden.

I would like to dedicate this work to all those family and friends who have either seen too little of me over the last few years or have seen too much of my back! Special thanks for the forebearance and support of Lara, Dale and Joanna.

References

Allen, J.R.L., 1982. *Sedimentary structures, their character and physical basis.Vol.2.* Elservier, Amsterdam, pp 645.

Alexanderson, H., Johnsen, T. & Murray, A. S. 2010. Re-dating the Pilgrimstad Interstadial with OSL: a warmer climate and a smaller ice sheet during the Swedish Middle Weichselian (MIS 3)? *Boreas*, Vol. 39: 367–376.

Alley, R., Blankenship, D., Bentley, C., Rooney, S. 1986. Deformation of till beneath Ice Stream B, West Antarctica. *Nature* 322: 57-59.

Alley, R. 1991. Deforming bed origin for southern Laurentide till sheets? *Journal of Glaciology*, 37, 125: 67-76.

Alley, R., Agustdottir, M., Fawcett, P. 1999 Ice-core evidence of late-Holocene reduction in North Atlantic Ocean heat transport. In P.U. Clark, R.S. Webb, and L.D. Keigwin, (eds). *Mechanisms of Global Climate Change at Millennial Time Scales*. Geophysical Monograph v. 112, American Geophysical Union, Washington, DC: 301-312.

Alley, R. B. 2000. Continuity comes first; recent progress in understanding subglacial deformation. In Maltman, A, Hubbard, B., Hambrey, M.J, (eds) (2000) Deformation of glacial materials, *Geological Society Special Publication* no. 176, (London), pp. 344.

Alley, R. B., and R. A. Bindschadler (Eds.) (2001), *The West Antarctic Ice Sheet: Behaviour and Environment, Antarctic Research. Ser.*, Vol. 77, AGU, Washington, D. C.

Åmark, M. 1980. Glacial flutes at Isfallsglaciären, Tarfala, Swedish Lapland. *Geologiska Foreningens I Stockholm Forhandlingar*, Vol, 102. Pt.3: 251-259.

Andersson, P. and Gee, D. 1989. Bedrock Geology and Morphology of the Tarfala Area, Kebnekaise Mountains, Swedish Caledonides. *Geografiska Annaler* 71. A (3-4): 235-239.

Annan, A. 1999. *Practical processing of GPR data*. Sensors and Software, Ontario.

Ashley, G. M. 2002. Glaciolacustine Environments, (chapter 11) in: *Modern and Postglacial Environments*, Menzies, J. (ed.), Buterworth Heinemann, Oxford, pp. 529.

Baker, R. and Hooyer, T. 1996. Multiple till layers beneath Storglaciären.In Jansson, P. (ed) (1996) *Tarfala Research Station Annual Report 1994-5*, Stockholm University, pp. 66.

Bakker, M.A.J. 2002. A comparison of ground-penetrating radar facies and sediment characteristics in a Pleistocene push moraine in the Netherlands. In: Koppenjan, S.K., and Lee, H. (eds.). 2002. Ninth International Conference on Ground-Penetrating Radar. *Proceedings of SPIE,* Vol 4758.

Banerjee, I. and McDonald, B.C. 1975. Nature of esker sedimentation. In: Evans, D.J.A., (ed.), 2004. Geomorphology, Vol. IV, *Glacial Geomorphology*, Routledge, London: 372 – 410.

Bell, R., Studinger, M., Shuman, C., Fahnestock, M., and Joughin, I. 2007. Large subglacial lakes in East Antarctica at the onset of fast-flowing ice streams. *Nature*, 445 (7130): 904-907.

Benn, D, I. and Ballantyne, C. 1994. Reconstructing the transport history of glacigenic sediments: a new approach based on co-variance of clast form indices. *Sedimentary Geology*, 91: 215-27.

Benn. D.I. 1994. Fluted moraine formation and till genesis below a temperate valley glacier: Slettmarkbreen, Jotunheimen, southern Norway. *Sedimentology* 41: 279-292.

Benn. D. I. 1995. Fabric signature of subglacial sediment deformation, Breiðamerkurjökull, Iceland. *Sedimentology*, 42: 735-747.

Benn, D.I. and Ringrose, T. 2001. Random variation of fabric eigenvalues: implications for the use of a-axis fabric data to differentiate till facies. *Earth Surface Processes and Landforms*, 26: 295-306.

Benn, D, I. and Gemmell, A.M.D. 2003. Fractal dimensions of diamictic particle-size distributions: simulations and evaluation. *Geological Society of America*, Bulletin, v.141. no.5: 523-528.

Benn, D. I. 2004. Clast Morphology (chapter 4) and Macrofabric (chapter 5) in: Evans, J.A. and Benn, D.I. (eds). 2004. *A practical Guide to the study of glacial sediments*, Hodder Education, London, pp. 266.

Benn, D. I. and Evans, D. J. 2010. *Glaciers and Glaciation* (2nd edition), Hodder Education, London, pp. 789.

Bennett, M.R., and Glasser, N.F.1996. *Glacial Geology: Ice Sheets and Landforms*. John Wiley, London, pp 364.

Bennett, M.R., Hambrey, M.J., Huddart, D. 1997. Modification of clast shape in the High-Arctic environment. *Journal of Sedimentary Research*, 67 (3): 550-559.

Bennett, M.R., Waller, R., Glasser, N., Hambrey, M., and Huddart, D. 1999. Glacigenic clast fabrics; genetic fingerprint or wishful thinking? *Journal of Quaternary Science*, 14: 125-35.

Bennett, M.R. 2001. The morphology, structural evolution and significance of push moraine. *Earth Science Reviews* 53: 197-236.

Bennett, M.R., Huddart, D., Waller, R., Cassidy, N., Tomio, A., Pzukowsky, J., Midgley, N., Cook, S., Gonzalez, S., and Glasser, N. 2004. Sedimentary and tectonic architecture of a large push moraine: a case study from Hagafellsjökull-Eystri, Iceland. *Sedimentary Geology* 172: 269-292.

Berglund, B., Barnekow, L., Hammarlund, D., Sandgren, P., Snowball, I. 1996. Holocene forest dynamics and climate changes in the Abisko area, northern Sweden – the Sonesson model of vegetation history re-considered and confirmed. *Ecological Bulletins* 45: 5-30.

Betterton. M. D., 2001. Formation of structure in snowfields: penitentes, suncups, and dirt cones. *Physical Review E,* Vol 63, 056129. DOI: 10.1103/PhysE.63.056129

Beylich, A., and Gintz, D. 2004. Effects of high magnitude/low frequency fluvial events generated by intense snowmelt or heavy precipitation in arctic periglacial environments in northern Swedish Lapland and northern Siberia. *Geografiska Annaler*, 86 A (1): 11-29.

Bindschadler, R., Harrison, W., Raymond, C, and Crosson, R. 1977. Geometry and dynamics of a surge type glacier. *Journal of Glaciology* 18: 181-194.

Blake, E. W. 1992. *The deforming bed beneath a surge-type glacier: measurement of mechanical and electrical properties*. (Ph.D. thesis, University of British Columbia.), cited in: Fischer, U., and Clarke, G. 1997. Stick-slip sliding behaviour at the base of a glacier, *Annals of Glaciology*, 24: 390-396.

Blankenship, D., Bentley, C., Rooney, S., Alley, R. 1986. Seismic measurements reveal a saturated porous layer beneath an active Antarctic ice stream. *Nature,* Vol. 322: 54-57.

Blikra, L., and Nemec, W. 1998. Postglacial colluvium in w. Norway: depositional processes, facies and palaeoclimatic record. *Sedimentology* 1998, 45: 909-959.

Blott, S. and Pye, K. 2001. Gradistat: A grain-size distribution and statistics package for the analysis of unconsolidated sediments. *Earth Surface Processes and Landforms*, 26: 1237-1248.

Bockheim, J.G., and Tarnocai, C. 1998. Recognition of cryoturbation for classifying permafrost affected soils. *Geodema* 81: 281-293.

Boulton, G.S. 1976. The origin of glacially fluted surfaces – observations and theory. *Journal of Glaciology*, Vol 17, No. 76: 287 -309.

Boulton, G.S. 1983. A theory of drumlin formation by subglacial sediment deformation. In: Menzies, J. and Rise, J. (eds.). 1987. *Drumlin Symposium*. Balkema, Rotterdam, pp.360.

Boulton, G., Smith, G., Jones, A., Newsome, J. 1985. Glacial geology and glaciology of the last mid-latitude ice sheet. *Journal of the Geological Society of London*. 142: 447-474.

Boulton, G. 1986. A paradigm shift in glaciology, *Nature*, 322: 18.

Boulton, G. 1987 A theory of drumlin formation by subglacial sediment deformation. In Menzies, J., and Rose, J. (eds) *Drumlin Symposium*. Balkema, Rotterdam: 25-80.

Boulton, G. and Hindmarsh, R. 1987. Sediment deformation beneath glaciers; rheology and sedimentological consequences. *Journal of Geophysical Research*, 92, B9: 9059-82.

Boulton, G., Dobbie, K., Zatsepin, S. 2001. Sediment deformation beneath glaciers and its coupling to the subglacial hydraulic system. *Quaternary International* 86: 3-28.

Boulton, G. and Hagdorn, M. 2006. Glaciology of the British Isles Ice Sheet during the last glacial cycle; form, flow, streams and lobes. *Quaternary Science Reviews*, 25 (23-24): 3359-3390.

Boyce, J.J., and Eyles, N. 2000. Architectural element analysis applied to glacial deposits; internal geometry of a late Pleistocene till sheet, Ontario, Canada. *Geological Society of America Bulletin*, 112: 98-118.

British Standard BS 1377-7. 1990. Incorporating Amendment No.1., Methods of test for Soils for Civil Engineering Purposes – Part 7: *Shear strength tests (total stress),* The British Standards Institution.

Bronge, C. 1996. The excavation of Storglaciären Trough during the Quaternary. *Geografiska Annaler* 78. A (2-3): 163-170.

Busby, J.P. Merritt, J.W. 1999. Quaternary deformation mapping with Ground-Penetrating Radar. *Journal of Applied Geophysics* 41: 75-91.

Carr, S.J. 2001. Micromorphological criteria for distinguishing subglacial and glacimarine sediments: evidence from a contemporary tidewater glacier, Spitsbergen. *Quaternary International*, 86: 71-79.

Carr, S, J. and Rose, J. 2003. Till fabric patterns and significance; particle response to subglacial stress. *Quaternary Science Reviews*, 22: 1415-26.

Carr, S., J. 2004. Microscale features and structures. In Evans, J.A. and Benn, D.I. (eds). 2004. *A practical guide to the study of glacial sediments*, Hodder Education, London, pp. 266.

Carr, S.J. and Goddard, M.A. 2007. Role of particle size in till fabric characteristics: systematic variation in till fabric from Vestri-Hegafellsjokull, Iceland. *Boreas.* Vol.36: 371-385.

Christoffersen, P. and Tulaczyk, S. 2003. Signature of Palaeoicestream stagnation: till consolidation induced by basal freeze-on. *Boreas,* Vol. 32: 114-129.

Clark, C. D., Tulaczyk, S., Stokes, C., Canals, M. 2003. A groove-ploughing theory for the production of MSGL and implications for ice-stream mechanics. *Journal of Glaciology,* Vol. 49, no.165: 240-256.

Clark, C. D. Stokes, C. 2003a. Palaeo-ice stream landsystems. In: Evans, D. J. (ed). 2003. *Glacial Landsystems*, Arnold, London, pp. 532.

Clark, C.D. and Stokes, C. 2003b. The Dubawnt Lake palaeo-ice stream; evidence for dynamic ice sheet behaviour on the Canadian Shield and insights regarding the controls on ice-stream location and vigour. *Boreas,* 32 (1): 263-279.

Clarke, G. 2005. Subglacial Processes. *Annual Review of Earth and Planetary Sciences* 33: 247-76.

Clark, P.U. 1994. Unstable behaviour of the Laurentide Ice Sheet over deforming sediment and its implications for the climate change. *Quaternary Research* 41: 19-25.

Clark, P.U., Licciardi, J., MacAyeal, D., and Jenson, J. 1996. Numerical reconstruction of a soft-bedded Laurentide Ice Sheet during the Last Glacial Maximum. *Geology,* v. 24. No. 8: 679-82.

Clark, P.U. and Pollard, D. 1998. The origin of the middle Pliestocene transition by ice sheet erosion of regolith. *Paleoceanography,* 13 (1): 1-9.

Clark, P., Licciardi, J., MacAyeal, D., Jenson, J. 1996. Numerical Reconstruction of a Soft-bedded Laurentide Ice Sheet. *Geology,* Vol 24. no.8: 679-682.

Coutard, J.P., and Müncher, H., 1985. Deformation of laminated silt loam due to repeated freezing and thawing. *Earth Surface Processes and Landforms* 10: 309-319.

Craig, R.F. 1997. *Soil mechanics*, sixth edition, E&F Spon, London, pp. 481.

Cuffey, K.M. and Paterson, W.S.B. 2010. *The Physics of Glaciers*, 4th edition, Elsevier, Amsterdam, pp. 683.

Donner, J. 1995. *The Quaternary history of Scandinavia*. Cambridge University Press, pp. 200.

Dowdeswell, J.A. and Sharp, M.J. 1986. Characterization of pebble fabrics in modern terrestrial glacigenic sediments. *Sedimentology*, 33: 699-710.

Dreimanis, A. 1984. Discussion: Lithofacies types and vertical profile models; an alternative approach to the description and environmental interpretation of glacial diamict and diamictite sequences. *Sedimentology* 31: 885-886.

Dreimanis, A. 1988. Temporal and spatial relationships of till types. In: Goldthwaite, R.P. and Matsch, C.L. (eds.).1988. *Genetic classification of glacigenic deposits*. A.A. Balkema, Rotterdam, pp.294.

Echelmeyer, K. and Wang, Z. 1987. Direct observation of basal sliding and deformation of basal drift at sub-freezing temperatures. *Journal of Glaciology*, Vol. 33, no. 113: 83-98.

Eklund, A. and Hart, J. 1996. Glaciotectonic deformation within a flute from Isfallsglaciären, Sweden. *Journal of Quaternary Science,* 11 (4): 299-310.

Englehardt, H.F. and Kamb, B. 1997. Basal hydraulic system of a West Antarctic Ice Stream; constraints from borehole observations. *Journal of Glaciology*, 43: 207-231.

Etienne, J., Glasser, N., Hambrey, M.J. 2003. Proglacial sediment-landform associations of a polythermal glacier; Storglaciären, Northern Sweden. *Geografiska Annaler* Vol. 85, Issue 2: 149-164.

Evans, D.J., 2000. A gravel outwash/deformation till continuum, Skalafellsjojull, Iceland. *Geografiska Annaler* Vol. 82A (4): 449-512.

Evans, D.J. (Ed.) 2003. *Glacial Landsystems*. Arnold, London, pp. 523.

Evans, D.J. 2003. Ice-marginal terrestrial landsystems of active temperate glacier margins. In: Evans, D.J. (Ed.). 2003. *Glacial Landsystems*. Arnold, London, pp. 532.

Evans, J, A. and Benn, D.I. (eds). 2004. *A practical Guide to the study of glacial sediments*, Hodder Education, London, pp. 266.

Evans, D.J.A., Phillips, E.R., Hiemstra, J.F., Auton, C.A. 2006. Subglacial till: formation, sedimentary characteristics and classification. *Earth-Science Reviews* 78: 115-176.

Evans, D.J.A., Nelson, C.D., Webb, C. 2010. An assessment of fluting and 'till esker' formation on the foreland of Sandfellsjokull, Iceland. *Geomorphology,* 114: 453-465.

Evans, J., Dowdeswell, J.A., Ó Cofaigh, C. 2004. Late Quaternary submarine bedforms and ice-sheet flow in Gerlache Strait and on the adjacent continental shelf, Antarctic Peninsula. *Journal of Quaternary Science* 19: 397-407.

Evans, J, Pudsey, CJ, Ó Cofaigh, C, Morris, P, Domack, E (2005) Late Quaternary glacial history, flow dynamics and sedimentation along the eastern margin of the Antarctic Peninsula Ice Sheet, *Quaternary Science Reviews*, 24 (5-6): 741-774, ISSN: 0277-3791. DOI: 10.1016/j.quascirev.2004.10.007.

Eyles, N., Eyles, C. H., and Miall, A. D. 1983. Lithofacies types and vertical profile models; an alternative approach to the description and environmental interpretation of glacial diamict and diamictite sequences. *Sedimentology* 30: 395-410.

Eyles, N. and Boyce, J.I. 1998. Kinematic indicators in fault gouge; tectonic analog for soft-bedded ice sheets. *Sedimentary Geology* 116: 1-12.

Ferguson, A., van der Meer, J., Phillips, E. 2011. Micromorphological analysis of deformation structures. In Phillips, E., Lee., J.R., Evans, H.M. (eds.). 2011a. *Glacitectonics*, Quaternary Research Association, pp.263, Chapter 2: 32-53.

Fischer, U., Grace, E., Hanson, B., LeB, Hooke, R., Jansson, P. 1996. Basal till rheology studies on Storglaciären. In Jansson, P. (ed). 1996. *Tarfala Research Station Annual Report 1994-5*, Stockholm University, pp. 66.

Fischer, U. and Clarke, G. 2001. Review of subglacial hydro-mechanical coupling: Trapridge Glacier, Yukon Territory, Canada. *Quaternary International* 86: 29-43.

Fitzsimons, S.J., Lorrain, R.D., Vandergoes, M.J. 2000. Behaviour of subglacial sediment and basal ice in a cold glacier. In: Maltman, A.J., Hubbard, B., Hambrey, M.J. (eds.). 2000. *Deformation of glacial materials.* Geological Society (London) Special Publication 176: 259-278.

Fjeldskaar, W. 2000. Isostatic test of the hypothesis of ice-free mountain areas during the last glaciation. *Norsk Geologisk Tidsskrift* 80: 51-60.

Fleming, E.J., Stevenson, C.T.E., Petronis, M.S. 2013. New insights in the deformation of a Middle Pleistocene glaciotectonised sequence in Norfolk, England through magnetic and structural analysis. *Proceedings of the Geologists' Association, Special Issue, Glaciotectonics,* Vol.124, Issue 5: 172-179.

Flint, R. F., Sanders, J. E., and Rodgers, J. 1960. Diamictite, a substitute term for symmictite. *Geological Society of America Bulletin*, 71 (12): 1809 – 1810.

Folk, R.L. and Ward, W.C. 1957. Brazos River bar: a study in the significance of grain size parameters. *Journal of Sedimentary Petrology*, 27: 3-26.

Fountain, A., Jacobel, R., Schlichting, R., Jansson, P. 2005. Fractures as the main pathways of water flow in temperate glaciers. *Nature*, Vol. 433: 618-621.

Fowler, A.C. 2000. An instability mechanism for drumlin formation. In: Maltman, A.J., Hubbard, B., Hambrey, M.J. (eds.). 2000. *Deformation of glacial materials.* Geological Society (London) Special Publication 176: 259-278.

Fredin, O. and Hatterstrand, C. 2002. Relict lateral moraines in northern Sweden – evidence for an early mountain-centred ice sheet. *Sedimentary Geology* 149: 145-156.

Fuller, S. and Murray. T. 2000. Evidence against pervasive bed deformation during thr surge of an Icelandic glacier. In:Maltman, A., Hubbard, B., Hambrey, M.J. (eds). 2000. *Deformation of Glacial Materials*. Geological Society (London) Special Publication 176: 259-278.

Gibbard, P.L., Pasanen, A.H., West, R.G., Lunkka, J.P., Boreham, S., Cohen, K.M., Rolge, C. 2009. Late Middle Pleistocene glaciations in East Anglia, England. *Boreas,* Vol. 38: 504-528.

Glen, J.W., Donner, J.J., West, R.G. 1957. On the mechanism by which stones in till become orientated. *American Journal of Science*. 255: 194-265.

Goodfellow, B., Stroeven, A., Hattestrand, C., Kleman. J., Jansson, K. 2008. Deciphering a non-glacial/glacial landscape mosaic in the northern Swedish mountains. *Geomorphology.* 92: 213-232.

Gordon, J.E., Whalley, W.B., Gellatly, A.F., Vere, D.M. 1992. The formation of glacial flutes: assessment of models with evidence from Lyngsdalen, North Norway. *Quaternary Science Reviews*. Vol. 11: 709-731.

Graham, D.J. and Midgley, N.G. 2000a. Graphical representation of particle shape using triangular diagrams: An Excel spreadsheet method. Technical Communication, *Earth Surface Processes and Landforms*, 25: 1473-1477.

Graham, D.J. and Midgley, N.G. 2000b. Moraine-mound formation by englacial thrusting: the Younger Dryas moraines of Cwm Idwal, North Wales. In: Maltman, A., Hubbard, B., Hambrey, M.J. (eds). 2000. *Deformation of Glacial Materials*. Geological Society (London) Special Publication 176: 259-278.

Grudd. H., Briffa, K., Karlén, W., Bartholin, T., Jones, P., Kromer, B. 2002. A 7400-year tree-ring chronology in northern Swedish Lapland; natural climatic variability expressed on annual to millennial timescales. *The Holocene.* 12: 657.

Grudd, H. and Schneider, T. 1996. Air temperature at Tarfala research station 1946-1995. *Geografiska Annaler*78. A (2-3): 115-120.

Gusmeroli, A., Murray, T., Jansson, P., Pettersson, R., Aschwanden, A., and Booth, A. 2010. Vertical distribution of water within the polythermal Storglaciären, Sweden. *Journal of Geophy. Res*., 115 (F4), F04002. (doi: 10.1029/2009/F00153a).

Gusmeroli, A., Jansson, P., Pettersson, R., and Murray, T. 2012. Twenty years of cold surface layer thinning at Storglaciären, sub-Arctic Sweden, 1989-2009. *Journal of Glaciology*, Vol. 58, No. 207: 3-10.

Haldorsen, S. 1981. Grain-size distribution of a subglacial till and its relation to glacial crushing and abrasion. *Boreas*, Vol. 10: 91-105.

Hambrey, M. J. 1994. *Glacial Environments*. UCL Press, London: pp. 304.

Hambrey, M.J. and Lawson, W.J. 2000. Structural styles and deformation fields in glaciers; a review. In: Maltman, A., Hubbard, B., Hambrey, M.J. (eds). 2000. *Deformation of Glacial Materials*, Geological Society (London) Special Publication 176: 59-84.

Ham, N.R. and Mickelson, D.M. 1994. Basal till fabric and deposition at Burroughs Glacier, Alaska. *Geological Society of America* Bulletin. 106: 1552-1559.

Harris, C. and Ellis, S. 1980. Micromorphology of soils in solifluction materials, Okstindan, N.Norway. *Geoderma* 23: 11-29.

Harris, C. 1998. The micromorphology of paraglacial and periglacial slope deposits: a case study from Morfa Bychan, W.Wales, UK. *Journal of Quaternary Science 13* (1): 73-84.

Hart, J.K. and Boulton, G.S. 1991.a. The interpretation of glaciotectonism and glaciodepositional processes within the glacial environment. *Quaternary Science Reviews*, 10: 335-350.

Hart, J.K. and Boulton, G.S. 1991.b. The Glacial Geology of North East Norfolk, in Rose. J., Gibbard, P., and Elhers, J (eds.), *The Glacial deposits of Britain*. Balkema, Rotterdam, pp. 233-244.

Hart, T. 1994. Till fabric associated with deformable beds. *Earth Surface Processes and Landforms*. 19: 15-32.

Hart, J. and Rose, J. 2001. Approaches to the study of glacier bed deformation. *Quaternary International* 86: 45-58.

Head, K.H. 1982. *Manual of soil laboratory testing. Volume 2: permeability, shear strength and compressibility tests*. Pentech Press Ltd, Plymouth, UK, pp. 743.

Hedfors, J., Peyaud, V., Pohjola, V., Jansson, P., Pettersson, R. 2003. Investigating the ratio of basal drag and driving stress in relation to bedrock topography during a melt season on Storglaciären, Sweden, using force-bedget analysis. *Annals of Glaciology*, 37: 263-268.

Hicock, S.R., Goff, J.R., Lian, O.B., Little. E.C. 1996. On the interpretation of subglacial till fabric. *Journal of Sedimentary Research*. A66: 928-934.

Hiemstra, J. F. and van der Meer, J. 1997. Pore water controlled grain fracturing as an indicator for subglacial shearing in tills. *Journal of Glaciology*, 43: 446-54.

Hiemstra, J. F. and Rijsdijk, K.F. 2003. Observing artificially induced strain: implications for subglacial deformation. *Journal of Quaternary Science*, 18: 373 – 383.

Hiemstra, J.F., Rijsdijk, K.F., Evans, D.J.A., van Der Meer, J. 2005. Integrated micro and macro-scale analysis of Last Glacial Maxima Irish Sea diamicts from Abermawr and Treaeth Y Mwnt, Wales, Uk. *Boreas*, 34, 1: 61-74.

Hindmarsh, R. 1997. Deforming beds; viscous and plastic scales of deformation. *Quaternary Science Reviews*, 16: 1039-56.

Hindmarsh, R. 1998. Drumlinisation and drumlin-forming instabilities; viscous till mechanism. *Journal of Glaciology*, 44: 293-314.

Hock. R. and Holmgren. B. 1996. Some aspects of energy balance and ablation of Storglaciären, northern Sweden. *Geografiska Annaler*78. A (2-3): 121-132.

Hoey, T. 2004. The size of sedimentary particles. In: Evans, D.J. and Benn, D.I.(eds). 2004. *A practical guide to the study of glacial sediments*, Hodder Education, London pp. 266.

Holmlund, P. and Eriksson, M. 1989. The cold surface layer, Storglaciären. *Geografiska Annaler*, Series A, 71 (3-4): 241-244.

Holmlund, P., Wigjorn, K., Grudd, H. 1996a. Fifty years of mass balance and glacier front observations at Tarfala Research Station. *Geografiska Annaler* 78. A (2-3): 105-114.

Holmlund, P., Naslund, J., Richardson, C. 1996b. Radar surveys on Scandinavian glaciers; in search of useful climate archives. *Geografiska Annaler* 78. A (2-3): 147-154.

Holmlund, P. and Jansson, P. 1999. Tarfala mass balance programme. *Geografiska. Annaler*. 81A (4): 621-631.

Holmlund, P. and Jansson, P. 2002. *Glaciological Research at Tarfala Research Station*. Tryckindustri Information AB, Universitet Stockholm, pp. 48.

Hooke. R. and Pohjola, V. 1994. Hydrology of a segment of a glacier situated in an overdeepening, Storglaciären, Sweden. *Journal of Glaciology*. Vol. 40. No. 34: 140-148.

Hooke, LeB, R. and Iverson, N. 1995. Grain-size distribution in deforming subglacial tills: Role of grain fracture. *Geology*, v.23, No.1: 57-60.

Hooke, LeB, R., Hanson, B., Iverson, N., Jansson, P., Fischer, U. 1997. Rheology of till beneath Storglaciären, Sweden. *Journal of Glaciology*, Vol. 43, No. 143: 172-179.

Hooyer, T.S., Iverson, N.R., Lagroix, F., Thomason, J.F. 2008. Magnetic fabric of sheared till: a strain indicator for evaluating the bed deforming model of glacier flow. *Journal of Geophysical Research*, Vol. 113. F02002, doi:10. 1029/2007 JF 000757, 15p.

Hoppe, G., and Schytt, V. 1953. Some observations on fluted moraine surfaces. *Geografiska Annaler*, Vol. 35, No. 2: 105-15.

Houmark-Nielsen, M. 2010. Extent, age and dynamics of Marine Isotope Stage 3 glaciations in the SW Baltic Basin. *Boreas*, Vol. 39, issue 2: 343-359.

Houmark-Nielsen, M. and Kjær, K. 2003. SW Scandinavia, 40-15 kyr BP: Palaeogeography and environmental change. *Journal of Quaternary Science*, 18 (8): 769-786.

Hubbard, B. and Maltman, A.J. 2000. Laboratory investigations of the strength, static hydraulic conductivity and dynamic hydraulic conductivity of glacial sediments. In: Maltman, A., Hubbard, B., Hambrey, M.J. (eds). 2000. *Deformation of Glacial Materials*, Geological Society (London) Special Publication 176: 231-244.

Hubbard, B. and Glasser, N. 2005. *Field Techniques in glaciology and glacial geomorphology*, Wiley and sons, Chichester, pp .400.

Hubbard, T. D. and Reid, J. R. 2006. Analysis of flute forming conditions using ice sheet reconstructions and field techniques. *Geomorphology* 74: 137-151.

Humphrey, N., Kamb, B., Fahnestock, M., Engelhardt, H. 1993. Characteristics of the bed of the lower Columbia Glacier, Alaska. *Journal of Geophysical Research* 98(B1): 837–846.

Iverson, N.R., Jansson, P., Hooke, R. 1994. In-situ measurement of the strength of deforming subglacial till. *Journal of Glaciology*, Vol.40, No. 136: 497-503.

Iverson, N.R., Hanson, B., LeB. Hooke, R., Jansson, P. 1995. Flow mechanisms of glaciers on soft beds. *Science*. Vol 267: 80-81.

Iverson, N.R., Baker, R., Hooke, LeB, R., Hanson, B., Jansson, P. 1999. Coupling between effective pressure and local shear stress determined for till elasticity. *Journal of Glaciology*, Vol. 45, No. 149: 31-40.

Iverson, N.R. and Iverson, R. 2001. Distributed shear of subglacial till due to Coulomb slip. *Journal of Glaciology*, Vol. 47. no. 158: 481-488.

Iverson, N.R., Hooyer, T.S., Fischer, U.H., Cohen, D., Moore, P.L., Jackson, M., Lappegard, G., Kohler, J. 2007. Soft-bed experiments beneath Engabreen, Norway: regelation infiltration, basal slip and bed deformation. *Journal of Glaciology*, Vol. 53, No. 182: 323-341.

Iverson, N.R., Hooyer, T., Thomason, J., Graesch, M., Shumway, J. 2008. The experimental basis for interpreting particle and magnetic fabrics of sheared till. *Earth Surface Processes and landforms* 33: 627-45.

Iverson, N.R. and Shumway, J.R. 2009. Magnetic fabrics of the Douglas Till of the Superior lobe: exploring bed-deformation kinematics. *Quaternary Science Reviews* 28: 107-119.

Jakobsen, P.R. and Overgaard, T. 2002. Georadar facies and glaciotectonic structures in an ice-marginal deposits, Northwest Zealand, Denmark. *Quaternary Science Reviews*, Vol.21, No.8-9: 917-927.

Jansson, P. and Hooke, R. 1989. Short-term variations in strain and surface tilt on Storglaciären, Kebnekaise, northern Sweden, *Journal of Glaciology*. Vol. 35. No. 120: 201-208.

Jansson, P. 1995. Water pressure and basal sliding on Storglaciären. Northern Sweden. *Journal of Glaciology*, Vol. 41, No. 138: 232-240.

Jelinek, V. 1981. Characterization of the magnetic fabric of rocks. *Tectonophysics* 79, T.63-T67.

Johansson, H. 1951. Petrology and tectonics of the Kebnekaise region and their morphological importance: A preliminary account. *Geografiska Annaler* 39: 95-120.

Johnson, W.H. and Menzies, J. 2002. Supraglacial and Ice-Marginal deposits and landforms, (chapter 10) in: *Modern and Postglacial Environments*, Menzies, J. (ed.). 2002. Buterworth Heinemann, Oxford, pp. 529.

Jol, H. and Bristow, C. (eds). 2003. Ground-penetrating radar in sediments. *Geology Society Special Publications* 211. London.

Kamb, B. 1991. Rheological nonlinearity and flow instability in the deforming-bed mechanism of ice-stream motion. *Journal of Geophysical Research*, 96B: 16585-95.

Karlén, W. 1973. Glacier and climatic variations, Kebnekaise Mountains, Swedish Lapland. *Geografiska Annalar.* Vol.55. Series A: 29-63.

Kezdi, A. 1974. *Handbook of soil mechanics*, *Volume 1, soil physics*. Elsevier, Amsterdam, pp.294.

Khan, M.A. 1962. The AMS of some igneous and metamorphic rocks. Journal of Geophys. Res. 67: 2873-2885.

Kilfeather, A.A. and van der Meer, J. 2008. Pore size, shape, and connectivity in tills and their relationship to deformation processes. *Quaternary Science Reviews*, 27: 250-266.

King, E., Woodward, J., Smith, A. 2007. Seismic and radar observations of subglacial bed froms beneath the onset zone of Rutland Ice stream, Antarctica. *Journal of Glaciology*, Vol. 53 no. 183: 665-672.

Kjaer, K.H. and Krüger, J. 1998. Does clast size influence fabric strength? *Journal of Sedimentary Research*, 68: 746-749.

Kjær, K.H., Krüger, J., and van der Meer, J.M. 2003. What causes till thickness to change over distance? Answers from Myrdalsjökull, Iceland. *Quaternary Science Reviews*, 22: 1687-1700.

Kjær, K., Sultan, L., Krüger, J., Schomacher, A. 2004. Architecture and sedimentation of outwash fans in front of the Myrdalsjökull ice cap, Iceland. *Sedimentary Geology* 172: 139-163.

Kjellstrom, E., Brandefelt, J., Naslund, J.-O., Smith, B., Strandberg, G.and co-authors. 2010. Simulated climate conditions in Europe during the Marine Isotope Stage 3 stadial. *Boreas* 39: 436–456.

Kleman, J., Stroeven, A., Lundqvist, J. 2008. Patterns of Quaternary ice sheet erosion and deposition in Fenno-Scandinavia; a theoretical framework for explanation. *Geomorphology* 97: 93-90.

Kleman, J. 1992. The palimpsest landscape of NW Sweden. *Geografiska Annalar*, 74A: 305-325.

Kostic, B. and Aigner, T. 2007. Sedimentary architecture and 3D ground-penetrating radar analysis of gravelly meandering river deposits (Necker Valley, SW Germany), *Sedimentology* 54: 789-808.

Krüger, J. 1984. Clasts with stoss-lee forms in lodgement tills: a discussion. *Journal of Glaciology*, 30: 241-3.

Krüger, J. and Kjær K. 1999. A data chart for field description and genetic interpretation of glacial diamicts and associated sediments – with examples from Greenland, Iceland, and Denmark. *Boreas*, 28. 8: 84-90.

Lambeck, K., Purchell, A., Zhao, J., Svensson, N, O. 2010. The Scandinavian ice sheet: from MIS 4 to the end of the LGM. *Boreas*. Vol 39: 410-435.

Largerback, R. 2007. Ventifacts – means to reconstruct glacial developments and palaeo-environments in northern and central Sweden. *GFF* Vol. 129, Issue 4: 315-324.

Larsen, N. and Piotrowski, J.A. 2003. Fabric pattern in a basal till succession and its significance for reconstructing subglacial processes. *Journal of Sedimentary Research*, 73: 725-34.

Larsen, N., Piotrowski, J., Christiansen, F. 2006a. Microstructures and microshears as proxy for strain in subglacial diamicts; implications for basal till formation. *Geology,* Vol.34, No. 10: 889-892.

Larsen, N., Piotrowski, J.A., Christoffersen, P., Menzies, J. 2006b. Formation and deformation of basal till during a glacier surge; Elisebreen, Svalbard. *Geomorphology*, 81: 217-234.

Larsen, N., Piotrowski, J., Menzies, J. 2007. Microstructural evidence of low-strain, time-transgressive subglacial deformation. *Journal of Quaternary Science* 22 (6): 593 – 608.

Lawson, D.E. 1979. A comparison of the pebble orientation in ice and deposits in the Matanuska Glacier, Alaska. *Journal of Glaciology*, 87: 629-645.

Lemke, P., Ren, J., Alley, R.B., Allison, I., Carrasco,J., Flato, G., Fuiji, Y., Kaser, G., Mote, P., Thomas, R.H., and Zang, T. 2007. *Observations: changes in snow, ice and frozen ground. In: Climate Change 2007, The Physical Science Basis, Contribution of working group I to the 4th Assessement Report of the Intergovernmental Panel on Climate Change, 2007*, (eds.) Solomon, S., Qin, D., Manning, M., Chen, Z., Marquis, M., Averyt, K.B., Tignor, M., Miller, H.L. Cambridge University Press, IK.

Lowe, D.R., 1975. Water escape structures in coarse-grained sediments. *Sedimentology* Vol.22, issue 2: 157-204.

Lukas, S., Coray, S., Graf, A., Schluchter, C. 2010. The influence of clast lithology and fluvial reworking on the reliability of clast shape measurements in glacial environments – a case study from a temperate Alpine glacier. In: Bridgland, D.R. (ed.) *Clast Lithological analysis. Technical Guide.* London, QRA (in press).

Lundqvist, J. 1983. Tills and moraines in Sweden. In: Ehlers, J. (ed.). 1983. *Glacial deposits in North-West Europe*. A.A.Balkema, Rotterdam, pp. 83-91.

Lundqvist, J. 2004. Glacial history of Sweden. In: Ehlers, J. and Gibbard, P. 2004. *Quaternary Glaciations- Extent and Chronology*. Elsevier, Developments in Quaternary Science, editor Rose, J. Part 1. Europe, pp. 401.

MacAyeal, D. 1993. Binge/purge oscillations of the Laurentide ice sheet as a cause of the North Atlantic's Heinrich Events. *Paleocenography,* Vol.8, No. 6: 755-784.

Maizels, J. 2002. Sediments and landforms of modern proglacial terrestrial environments. In: Menzies, J. (ed.). 2002. *Modern and Postglacial Environments*, Chapter 9. Buterworth Heinemann, Oxford, pp. 529.

Mangerud, J. 2004. Ice sheet limits in Norway and on the Norwegian continental shelf. In: Ehlers, J. and Gibbard, P. (eds.) 2004. *Quaternary Glaciations- Extent and Chronology*. Elsevier, Developments in Quaternary Science, editor Rose, J. Part 1. Europe, p. 271.

Mangerud, J., Svendsen, J., Astakhov, I. 1999. Age and extent of the Barents and Kara Ice Sheets in Northern Russia. *Boreas* 28: 46-80.

Mark, D.M. 1973. Analysis of axial orientation data, including till fabrics. *Geological Society of America Bulletin*, 84: 1369-74.

Mark, D.M. 1974. On the interpretation of till fabrics. *Geology,* 2: 101-4.

Markgren, M. 1964. *Geomorphological studies in Fennoscandinavia*. *Vol. II: Chute slopes northern Fennoscandinavia.* A-B Medd. Lunds University, Geografiska Institute, Avhandl. XLV. 136 p.

Mason, C. 2011. *Particle size analysis for supporting Biological Analysis*. National Marine Biological AQC Coordinating Committee, Best Practice Guide, pp.72.

McCarroll, D., and Rijsdijk, K,F. 2003. Deformation styles as a key for interpreting glacial depositional environments. *Journal of Quaternary Science.*, Vol. 18: 473-489.

Menzies, J. 1987. Towards a general hypothesis on the formation of drumlins. In: Menzies, J. and Rose, J. (eds.). 1987. *Drumlin Symposium*. Balkema, Rotterdam: 9-24.

Menzies, J. and Shilts, W.W. 2002. Subglacial environments. In: Menzies.J. (ed.). 2002. *Modern and postglacial environments*. Butterworth Heinemann, Oxford, pp. 529.

Menzies, J., van der Meer., J., Rose, J. 2006. Till as a glacial tectomict, its internal architecture, and the development of a typing method for till differentiation. Binghampton Symposium, 2003. Geomorphology, Vol.75: 172-200.

Menzies, J., and Brand, U. 2007. The internal sediment architecture of a drumlin, Port Byron, New York State, USA. *Quaternary Science Reviews* 26: 322-55.

Miller, G., Brigham-Grette, J., Alley, R., Anderson, L., Bauch, H., Douglas, M., Edwards, M., Elias, S., Finney, B., Fitzpatrick, J., Funder, S., Herbert, T., Hinzman, L., Kaufman, D., MacDonald, G., Polak, L., Robock, A., Serreze, M., Smol, J., Spielhagen, R., White, J., Wolfe, A., Wolff, E. 2010. Temperature and precipitation history of the Arctic. *Quaternary Science Reviews* 29: 1679 – 1715.

Moncrieff, A. C. M. 1989. Classification of poorly-sorted sedimentary rocks. *Sedimentary Geology*. Vol. 65, Issue 1-2: 191-194.

Møller, I. and Jakobsen, P. 2002. Sandy till characterized by ground-penetrating radar. In: Koppenjan, S.K., and Lee, H. (eds.). 2002. Ninth International Conference on Ground-Penetrating Radar. *Proceedings of SPIE* Vol.4758.

Moore, P. L., Iverson, N. R., Uno, K. T., Dettinger, M. P., Brugger, K. A. & Jansson, P. 2012: Entrainment and emplacement of englacial debris bands near the margin of Storglaciären, Sweden. *Boreas*, Vol. 42, Issue 1: 71-83.

Moorman, B. and Michel, F. 2000. Glacial hydrological system characterisation using ground-penetrating radar. *Hydrological Processes*, 14 (15): 2645-2667.

Muller, E. H. 1983. Dewatering during lodgement of till. In: Evenson, E., Schluchter, Ch., Rabassa, J. (eds.) 1983. *Tills and related deposits*. Proceesings of the INQUA Symposia on the genesis and lithology of Quaternary deposits, USA 1981, Argentina 1982. Balkema, Rotterdam, 1983, pp. 453.

Murray, T. 1997. Assessing the paradigm shift: deformable glacier beds. *Quaternary Science Reviews,* Vol. 16: 995-1016.

Nasje, A. 2009. Late Pleistocene and Holocene alpine glacier fluctuations in Scandinavia. *Quaternary Science Reviews* 28: 2119-2136.

Nasje, A. and Dahl, S. 1992. Geometry, thickness and isostatic loading of the late Weichselian Scandinavian Ice Sheet. *Norsk Geologisk Tidsskift* 72: 271-273.

National Snow and Ice Data Center. 1999, updated 2009. *World glacier inventory*. World Glacier Monitoring Service and National Snow and Ice Data Center/World Data Center for Glaciology. Boulder, CO. Digital media.

Neal. A. 2004. Ground-penetrating radar and its use in sedimentology: principles, problems and progress. *Earth-Science Reviews*, no.66: 261-330.

Ó Cofaigh, C., Pudsey, C.J., Dowdeswell, J.A., Morris, P. 2002. Evolution of subglacial bedforms along a paleo-ice stream, Antarctic Peninsula continental shelf. *Geophysical Research Letters 29*, doi: 10.1029/2001GL014488.

Ó Cofaigh, C., Evans, D.J., England, J. 2003. Subpolar glacier margins of the Canadian and Greenland High Arctic. In: Evans, D.J. (Ed.) 2003. *Glacial Landsystems*. Arnold, London, pp 532.

Ó Cofaigh, C., Dowdeswell, J.A., Allen, C.S., Hiemstra, J.F., Pudsey, C.J., Evans, J., and Evans, D.J. 2005. Flow dynamics and till genesis associated with a marine-based Antarctic palaeo-ice stream. *Quaternary Science Reviews* 24: 709-40

Ó Cofaigh, C., Evans, J., Dowdeswell, J.A., and Larter, R.D. 2007. Till characteristics, genesis and transport beneath Antarctic paleo-ice streams, *Journal of Geophysical Research*., 112, F03006, doi:10.1029/2006JF000606.

ÓCofaigh, C., Evans, D. J. A. & Hiemstra, J. F. 2011. Formation of a stratified subglacial 'till' assemblage by ice-marginal thrusting and glacier overriding. *Boreas*, Vol. 40: 1–14.

Olsen, L. 1983. A method for determining total clast roundness in sediments. *Boreas*, Vol, 12: 17-21.

Overgaard, T. and Jakobsen, P.R. 2001. Mapping of glaciotectonic deformation in an ice-marginal environment with ground-penetrating radar, *Journal of Applied Geophysics*, Vol. 47: 191-197.

Palmer, A., Lee, J., Kemp, R., and Carr, S. 2008. *Revised laboratory procedures for the preparation of thin sections from unconsolidated sediments*. Centre for Micromorphology, Royal Holloway and QMUL.

Park, R.G. (1989) *Foundations of Structural Geology* (2nd edition), Blackie, Glasgow and London, pp.145.

Passchier, S., Laban, C., Mesdag, C., Rijsdijk, K. 2010. Subglacial bed conditions during Late Pleistocene glaciations and their impact on ice dynamics in the southern North Sea. *Boreas*, 39: 633-647.

Paterson, W. 1994. *The Physics of Glaciers* (3rd edition), Butterworth Heinemann, Oxford. pp. 473.

Patterson, C.J., and Hooke, R. LeB. 1996. Physical environment of drumlin formation. *Journal of Glaciology* 4: 30-8.

Paul, M.A. and Eyles, N. 1990. Constraints on the preservation of diamict facies (melt-out tills) at the margins of stagnant glaciers. *Quaternary Science Reviews* 9: 51-69.

Pettersson, R., Jansson, P., and Holmlund, P. 2003. Cold surface layer thinning on Storglaciären, Sweden, observed by repeated ground penetrating radar surveys. *J. Geophys. Res*., 108 (F1), 6004, doi: 10.1029/2003/F000024.

Phillips, E. and Auton, C. 1998. Micromorphology and deformation of a Quaternary glaciolacustrine deposit, Speyside, Scotland. *British Geological Survey Technical Report* WG/98/15.

Phillips, E, R. and Auton, C.A. 2000. Micromorphological evidence for polyphase deformation of glaciolacustrine sediments from Strathspey, Scotland. In: Maltman, A.J., Hubbard, B., Hambrey, M.J. (eds.). 2000. *Deformation of Glacial Materials*. 176. The Geological Society of London, Special Publication: 279-291.

Phillips, E.R. Micromorphology of a debris flow deposit: evidence of basal shearing, hydrofracturing, liquefaction and rotational deformation during emplacement. *Quaternary Science Reviews* 25: 720-738.

Phillips, E. R., Merritt, J.W., Auton, C.A., Golledge, N.R. 2007. Microstructures developed in subglacially and proglacially deformed sediments; faults, folds and fabrics, and the influence of water on the style of deformation. *Quaternary Science Reviews*, 26: 1499-1528.

Phillips, E.R., and Auton, C., 2008. Microtextural analysis of a glacially 'deformed' bedrock: implications for inheritance of preferred clast orientations in diamictons. *Journal of Quaternary Science*, 23 (3): 229-240.

Phillips, E.R., and Merrit, J., 2008. Evidence of multiphase water-escape during rafting of shelly marine sediments at Clava, Invernesshire, NE Scotland. *Quaternary Science Reviews* 27: 988-1011.

Phillips, E., Lee., J.R., Evans, H.M. (eds.). 2011a. *Glacitectonics*, Quaternary Research Association, pp.263.

Phillips, E.R., van der Meer, J.M., Ferguson, A. 2011b. A new 'microstructural mapping' methodology for the identification, analysis and interpretation of polyhase deformation within subglacial sediments. *Quaternary Science Reviews*, 30: 2570-2596.

Piotrowski, J.A., Micklesen, D., Tulaczyk, S., Kryzszkowski, D., Junge, F. 2001. Were deforming subglacial beds beneath polar ice sheets really widespread? *Quaternary International,* 86: 139-150.

Piotrowski, J.A., Mickelson, D,M., Tulaczyk, S., Krzyszkowski, D., Junge, F,W. 2002. Reply to comments by G.S. Boulton, K.E. Dobbie, S. Zatsepin on: Deforming soft beds under ice sheets: how extensive were they? *Quaternary International,* 97-98: 173-177.

Piotrowski, J.A., Larsen, J., Junge, F. 2004. Reflections on soft bed subglacial deformation as a mosaic of deforming and stable spots. *Quaternary ScienceReviews* 23: 993-1000.

Piotrowski, J. A., Larsen, N.K., Menzies, J., Wysotta, W. 2006. Formation of subglacial till under transient bed conditions: deposition, deformation and basal decoupling under a Weichselian ice sheet lobe, central Poland. *Sedimentology,* 53: 83-106.

Porter, P. and Murray, T. 2001. Mechanical and hydraulic properties of till beneath Bakaninbreen, Svalbard. *Journal of Glaciology*, 47: 167-75.

Powers, M.C. 1953. A new roundness scale for sedimentary particles. *Journal of Sedimentary Petrology*, 23: 117-19.

Rapp, A. 1960. Recent development of mountain slopes in Kärkevagge and surroundings, Northern Scandinavia. *Geografiska Annaler*, 42: 71-2100.

Rees, A.I. and Woodall, W.A. 1975. The magnetic fabric of some laboratory-deposited sediments. *Earth and Planetary Science Letters* 25: 121-130.

Reynolds, J. 1997. *An introduction to applied and environmental geophysics*. Wiley, Chichester, pp.796.

Rhodes. J.J., Armstrong. R.L., and Warren. S.G.1987. Mode of formation of "ablation hollows" controlled by dirt content of snow. *Journal of Glaciology*, 33: 135–139.

Rignot, E., and P. Kanagaratnam (2006), Changes in the velocity structure of the Greenland Ice Sheet, *Science*, 17: 986–990.

Röller, K. and Trepmann, C. 2012. Stereo32 software, Institut für Geologie, Ruhr University, Bochum. http://www.ruhr-uni-bochum.de/hardrock/downloads.html

Roberson, S., Hubbard, B., Coulson, H. and Boomer, I. 2011. Physical properties and formation of flutes at a polythermal valley glacier: Midre Lovénbreen, Svalbard. *Geografika Annaler: Series A, Physical Geography*, 93: 71–88.

Rose, J. 1987. Drumlins as part of a glacier bedform continuum. In: Menzies, J. and Rose, J. (eds.). 1987. *Drumlin Symposium*. Balkema, Rotterdam: 103-117.

Rose, J. 1989. Glacier stress patterns and sediment transfer associated with the formation of superimposed flutes. *Sedimentary Geology*, 62: 151-176.

Rose, J. 1991. Subaerial modification of glacier bedforms immediately following ice wastage. *Norsk geogr. Tidsskr*, Vol 45: 143-153.

Rosqvist, G., Jonsson, C., Yam, R., Karlén, W., Shemesh, A. 2004. Diatom oxygen isotopes in pro-glacial lake sediments from northern Sweden: a 5000 year record of atmospheric circulation. *Quaternary Science Reviews*, 23: 851-859.

Rousselot, P. and Fischer, U. 2007. A laboratory study of ploughing. *Journal of Glaciology*, Vol. 53. No. 181: 255-231.

Sadura, S., Martini, I.P., Endres, A.L., Wolk, K. 2006. Morphology and GPR stratigraphy of a frontal part of an end moraine of the Laurentide Ice Sheet; Paris Moriane near Guelph, ON, Canada. *Geomorphology* 75: 212-225.

Sammis, C., King, G., and Biegel, R. 1987. The kinematics of gouge formation. *Pure and Applied Geophysics*, 125: 777-812.

Sappa, H. and Hammarlund, D. 2000. Pollen-stratigraphical evidence of Holocene hydrological change in northern Feno-scandia supported by independent isotopic data. *Journal of Paleolimnology* 24: 69-79.

Scherer, D., Gude, M., Gempeler, M., Parlow, E. 1998. Atmospheric and hydrological boundary conditions for slushflow initiation due to snowmelt *Annals of Glaciology* 26: 377-380.

Schneider.T. and Bronge, C. 1996. Suspended sediment transport in the Storglaciären drainage basin. *Geografiska Annaler*78. A (2-3): 155-162.

Schoof, C. and G.K.C. Clarke. 2008. A model for spiral flows in basal ice and the formation of subglacial flutes based on a Reiner-Rivlin rheology for glacial ice. *J. Geophys. Research. Solid Earth,* 113, B05024.

Schwamborn, G., Heinzel, J., and Schirrmeister, L. 2008. Internal characteristics of ice-marginal sediments deduced from georadar and sediment properties (Brøgger Peninsula, Svalbard). *Geomorphology* 95; 74-83.

Schwehr, K. and Tauxe, L. 2003. Characterization of soft-sediment deformation: Detection of cryptoslumps using magnetic methods. *Geology* 31: 203-206.

Schytt, V. 1963. Fluted moraine surfaces, *Journal of Glaciology,* Vol, 4. Pt 36: 825-837.

Shakesby, R.A., Matthews, J.A., Winkler, S. 2004. Glacier variations in Breheiman, southern Norway: relative-age dating of Holocene moraine complexes at six high-altitude glaciers. *The Holocene* 14, 6: 899-910.

Shaw, J. and Freschauf, R.C. 1973. A kinematic discussion of the formation of glacial flutings. *Canadian Geogr*., 18: 19-35.

Shaw, J. (1983). Forms associated with boulders in melt-out till. In, Evenson, E.B., Schlüchter, Ch., Rabassa, J. (1983) (Ed.) *Tills and Related Deposits*. Balkema, Rotterdam: pp. 453.

Shumway, J.R., and N.R. Iverson, 2009. Magnetic fabrics of the Douglas Till of the Superior lobe: exploring bed-deformation kinematics. *Quaternary Science Reviews*, 28, 107-119.

Siegert, M. 2000. Radar Evidence for Water-saturated Sediments beneath the E. Antarctic Ice Sheet.In: Maltman, A., Hubbard, B., Hambrey, M.J. (eds). 2000. *Deformation of Glacial Materials*, Geological Society (London) Special Publication 176: 259-278.

Sladen, J.A. and Wrigley, W. 1983. Geotechnical properties of lodgement till – a review. In: Eyles, N. (ed.). 1983. *Glacial Geology, an introduction for engineers and earth scientists*. Chapter 8: 184 – 212. Pergamon Press, Oxford: pp. 409.

Smalley, I.J. and Piotrowski, J.A. 1987. Critical strength/stress ratios at the ice-bed interface in the drumlin forming process: from dilatancy to cross-over. In: Menzies, J. and Rose, J. (eds.), 1987. *Drumlin Symposium*. Balkema, Rotterdam: p.360.

Smith, A. 2006. Microearthquakes and subglacial conditions. *Geophysical Research Letters* Vol. 33. L24501, doi. 10.29/2006GL027.

Smith, A.M., Murray, T., Nicholls, K.W., Makinson, K., Athalgeirsdottir, G.,Behar, A. and Vaughan, D.G. 2007. Rapid erosion and drumlin formation observed beneath a fast-flowing Antarctic ice-stream. *Geology* 35: 127-30.

Smith, A. and Murray, T. 2009. Bedform topography and basal conditions beneath a fast-flowing West Antarctic ice stream. *Quaternary Science Reviews*. 28: 584-596.

Snead, E.D and Folk, R.L. 1958. Pebbles in Lower Colorado River, Texas, a study of particle morphogenesis. *Journal of Geology*, 66 (2): 114-150.

Stokes, C. and Clark, C.D. 2002. Are long subglacial bedforms indicative of fast flow? *Boreas* 31: 239-49.

Swift, D.A. 2002. The *provenance of suspended sediment in subglacial drainage systems.* Ph.D thesis, Department of Geography and Topographic Science, University of Glasgow.

Tarling, D.H. and Hrouda, F. 1993. *The Magnetic Anisotropy of Rocks*. Chapman and Hall, London: pp. 213.

Thomason, J. and Iverson, N. 2006. Microfabric and microshear evolution in deformed till. *Quaternary Science Reviews*, v.25: 1027-1028.

Thomason, J. and Iverson, N. 2008. A laboratory study of particle ploughing and pore-pressure feedback: a velocity-weakening mechanism for soft glacier beds. *Journal of Glaciology*, Vol. 54, No. 184: 169-181.

Thomason, J. and Iverson, N. 2009. Deformation of the Batestown till of the Lake Michigan Lobe, Laurentide Ice Sheet. *Journal of Glaciology*, Vol. 55. No. 189: 131-146.

Tulaczyk, S., Scherer, R., Clark, C. 2001. A ploughing model for the origin of weak tills beneath ice streams; a qualitative treatment. *Quaternary International* 86: 59-70.

Tulaczyk, S. 2006. Scale independence of till rheology. *Journal of Glaciology*, Vol. 52, No. 178.

Truffer, M., Harrison, W. D., Echelmeyer, K. A. 2000. Glacier motion dominated by processes deep in underlying till. *Journal of Glaciology* 46(153): 213–221.

Udden, J.A. 1914. Mechanical composition of clastic sediments. *Bulletin of the Geological Society of America*. 25: 655-744.

Van der Meer, J. 1993. Microscopic evidence of subglacial deformation. *Quaternary Science reviews*, 12: 553-87.

Van der Meer, J.A., Kjaer, K.H., Krüger, J., 1999. Subglacial water escape structures and till structures, Sléttjökull, Iceland. *Journal of Quaternary Science*, Vol.14, issue 3: 191-205.

Van der Meer, J., Menzies, J., Rose, J. 2003. Subglacial till: the deforming glacier bed. *Quaternary Science Reviews* 22: 1659 – 1685.

Van der Meer, J., Menzies, J., and Rose, J. 2010a. Handbook for the 7th International workshop: *Micromorphology of glacial sediments*, QMUL and Royal Holloway, Centre for Micromorphology.

Van der Meer, J.M., Carr. S.J., Kjær, K.H. 2010b. Myrdalsjökull forefield under the microscope. The micromorphology of meltout and subglacial tills. *Developments in Quaternary Sciences*, Vol. 13: 159-180.

Van der Veen, C.J. 1999. *Fundamentals of glacier dynamics*. A.A. Balkema, Rotterdam: pp. 460.

Van der Wateren, F., Kluiving, S., and Bartek, L. 2000. Kinematic indicators of subglacial shearing. In: Maltman, A., Hubbard, B., Hambrey, M.J. (eds). 2000. *Deformation of Glacial Materials*. Geological Society (London) Special Publication 176: 259-278.

Van Vliet-Lanoe B. 1985. Frost effects in soils. In *Soil and Quaternary Landscape Evolution*, J. Boardman (ed), J. WILEY Publ: 115-156

Van Vliet-Lanoe, B. 2010. Frost Action. In: Stoops, G., Marcelino, V., and Mees, F. (eds.). 2010. *Interpretation of micromorphological features of sands and regoliths*. Chapter 6: 81-108. Elsevier, Amsterdam: pp. 725.

Walker, S. and Mattheas, J. 2010. Observations on terminal moraine-ridge formation during recent advances of Southern Norwegian glaciers. *Geomorphology,* 116: 87-106.

Waller, R., Murton, J., Whiteman, C. 2009. Geological evidence for subglacial deformation of Pleistocene permafrost. *Proceedings of the Geologists' Association*, 120: 155-162.

Wentworth, C.K. 1922. A scale of grade and class terms for clastic sediments. *Journal of Geology*, 30: 377-392.

Whiteman, C.A. 2002. Processes of terrestrial glacial deposition. In: Menzies, J. (ed). 2002. *Modern and Post-glacial Environments*. Chapter 7. Butterworth Heinemann, Oxford: pp.529.

Wohlfarth, B. 2010. Ice-free conditions in Sweden during Marine Oxygen Isotope Stage 3. *Boreas*, Vol. 39: 377-398.

World Glacier Monitoring Service and the National Snow and Ice Data Center. 1989, updated 2012. *World Glacier Inventory*. Compiled and made available by the WGMS, Zurich, Switzerland, and the NS&IDC, Boulder, Co. USA. Digital Media.
http://nsidc.org/data/docs/noaa/g01130_glacier_inventory/

World Glacier Monitoring Service, Preliminary Glacier Mass Balance Data 2007/8 and 2009/9:
http://www.geo.uzh.ch/wgms/mbb/sum08.html

Appendix 1 Glossary of Key Terms

Acoustic Impedance: Seismic waves travel at different velocities through different materials – the degree of impedance can be used to infer something about the physical properties of the ground materials – impedance is the product of seismic velocity and material density. In water saturated materials or water layers, acoustic impedance is low, but it is higher for rock layers.

Aliasing Data: Sampling radar and seismic wave reflections at intervals rather than measuring continuously can introduce false frequencies (aliasing) into the data in a range equivalent to half the sampling frequency down to zero (Doyle, 1995). Filters can be used to cut-off frequencies above half the sampling frequency (i.e. the Nyquist frequency) or sampling intervals increased to avoid aliasing.

Basal Shear Stress: Stress is a force per unit area; the component of stress imposed on a bed by a glacier which acts in a direction parallel to the surface is the basal shear stress. It is opposed by a parallel traction stress acting in the opposite direction. Basal shear stress is usually equated with the glacier driving stress, but this ignores lateral and longitudinal stress components.

Constructional Deformation: Viscous pervasive deformation produces a non-linear deformation profile because sediment strength increases with depth and because maximum strain occurs at the glacier-bed interface. As such, some vertical till sequences show a transition from non-deformed sediments, to glacio-tectonised sediments, to fully homogenised sediments, reflecting the vertical increases in stress and strain towards the former glacier bed. This vertical sequence is referred to as constructional deformation.

Coulomb Plastic Rheology: The way tills behave in laboratory experiments approaches the ideal behaviour of a Coulomb plastic material in which stress is accommodated by elastic strain up to a failure point (where stress > sediment strength). Once the critical point (also known as the yield stress) has been exceeded, the sediment fails plastically. The point of failure is linearly dependent on the effective pressure. Failure can be along discrete planes with strain being accommodated by slippage between grains (Benn and Evans, 2010).

Deformation Till: A diamicton that has been homogenised by subglacial deformation and which incorporates an admixture of advected material and local material. This is distinct from a ***glacio-tectonite*** which is a subglacial diamict that has not been homogenised and does not include far-travelled material, but which has been deformed by glacier-imposed stresses which typically caused folding, faulting, and shearing. ***Lodgement till*** is also produced subglacially by deposition and subsequent vertical accretion of debris directly from the basal ice layer of the glacier. ***Melt out tills*** are produced by ablation and static ice volume reduction, or by deposition in subglacial cavities.

Deviatoric Stress: The differential between any given average stress condition in a glacier's stress field and an observed stress. Normal and shear stresses interact and vary across and down glacier to produce deviations in the average stress field conditions and principal stress directions, which can be thought of as deviations in compressive and tensional stress.

Diamicton: A non-genetic term used to describe immature sediment deposits that are poorly sorted and contain a wide-range of clast sizes and finer matrix. Deposits can be clast-supported or matrix-supported. Most tills are classed as diamictons (the term diamict is also sometimes used), but the term can also be used for other deposits such as debris flows.

Dilation: A form of strain in which the sediment responds to stress by increasing volume so as to allow grains to rotate and slide over one another. Dilation is usually associated with pervasive shear. Opinion differs as to whether dilation results in an increase (strain hardening) of decrease (strain weakening) in sediment strength.

Disharmonic Folds: A fold structure in which different styles of folding occur in beds or horizons with different levels of competence. Competent beds resist ductile failure and may fracture in a brittle manner, whereas relatively incompetent beds may flow. Such disharmonic folding produces bedding plane slip in which weaker layers are buckled into drag folds by more competent layers slipping over them.

Distributed Shear and Discrete Shear: Homogenised subglacial tills appear to show distributed shear throughout the whole volume of the deforming body when viewed macroscopically. However, careful examination of till sequences often reveals multiple phases of deformation, with shear being accommodated along discrete, partitioned failure planes.

Eigenvector and Eigenvalue: In clast fabric analysis, the principal orientation of the a-axis is statistically given by the first eigenvector, V_1. The degree of clustering of data around V_1 is given by the first eigenvalue, S_1. S_1 values > 0.7 are considered to represent strongly clustered clast fabrics.

Facies, Lithofacies, and Radar-facies: A facies is a bed or unit of sediment which is distinct in appearance and is recognisably different from neighbouring facies. A lithofacies is a descriptive, non-genetic term used to log and describe facies. A radar-facies is a distinct layer separated by bounding surfaces which can be recognised on radar profiles.

Fast Glacier Flow: Usually seen in an ice stream or outlet glacier which draws down vast volumes of ice from ice sheets, but also seen in surging glaciers. The term is also used loosely to describe any region of a glacier experiencing relatively enhanced velocities.

Fault Gouge: A pulverised rock layer produced by shearing along a tectonic fault.

Forefield/Proglacial Area: The area in front of a glacier snout which includes recently deposited subglacial sediments and landforms.

Force Balance Equations: Glacier driving stresses are resisted by drag and ice viscosity and these are usually close to being in balance for most glaciers such that accelerations can be ignored. This is the starting point for force-balance calculations which provide a framework for studying glacial dynamics (Benn and Evans, 2010). As lateral and longitudinal drag are considered in force balance calculations such calculations give a more accurate estimation of basal drag and the basal shear stress.

Ground-Truthing: the correlation of observed sediment sequences with GPR profiles, such that distinct radar-facies can be linked to known sediment facies, and these associations used to aid analysis of other GPR profiles.

Jeffery and March-type Clast Rotation: In Jeffery-type clast rotation clasts are free to rotate and roll continuously in a medium that is deforming viscously. Clast rotation occurs because of velocity variations within the deforming layer and will only cease when deformation stops. Jeffery-type rotation results in weakened fabrics as clasts align with a-axis in planes oblique or transverse to the flow direction. By contrast, March-type rotation involves clasts acting as passive strain markers in a deforming medium and which simply rotate so that the a-axis is parallel to the main direction of strain. Clasts cease to rotate once this efficient stress-minimising position is reached and so March-type rotation produces strong fabrics. March-type rotation is observed in laboratory experiments and is consistent with a Coulomb-plastic rheology (Benn and Evans, 2010), but some field experiments report Jeffery-type rotation.

Kubiena Tins: Specialist sampling tins used to collect samples for micromorphology. The sample is carefully cut and the tin enclosed around it to limit deformation. Resin is poured into the tin to harden the sample in situ prior to thin section production.

Micro-fabric Domains: In micro-structural mapping, the S1-Sn micro-fabrics (see S1 below) may dominate certain areas of the thin section where they produce distinct domains – the S1 domains will be areas where the S1 micro-fabric is dominant. These domains may have certain shapes and orientations that can be described e.g. they may be anastomosing, continuous, discontinuous and so on.

Normal Stress: Stress imposed on the bed by the weight of the overlying glacier and which acts perpendicular to the surface.

Overdeepened Basin: A bowl-shaped hollow carved out by glacial erosion and often terminating in a riegel. The basins often contain lakes and alluvial fans, especially after deglaciation.

Riegel: A rocky bar which forms an irregularity in the long profile of a glacier (similar to a rock step). Riegels usually separate overdeepened basins or near-level treads. They are formed by resistant outcrops of (usually crystalline) rock crossing the valley floor which may be eroded into roches moutonnées.

S1 Micro-fabrics: In micro-structural mapping, micro-fabrics are recognised by distinct foliations (alignments of clast axes). The earliest formed micro-fabric is designated S1. The next formed micro-fabric, which cuts S1, is called S2 and so on.

S-Matrix and Plasma Structures and Fabrics: These structures are seen in thin section and have many origins. The S-matrix refers to the skeleton matrix of the sample and includes sand grains and clasts. S-matrix structures include clast rotational structures and grain alignments. Plasma fabrics refers to alignments made by the very fine grained clays in the sediment whose individual grains cannot be discerned under normal thin section magnification.

Step Size: In GPR surveys, the distance between radar traces. The step size depends on antenna frequency but should be sufficiently small to prevent aliasing data.

Silt Caps, Silt Droplets, and Silt Cutans: Silt caps are banded structures formed by cryogenic action (see text for mode of formation). These consist of fine layers of silt, often graded, formed on larger clasts. The growth of interstitial ice produces lens-shaped pores which can have fine deposits of translocated silt deposited them – these are silt cutans. Where translocated silt forms enriched areas/bands/layers within the matrix these are referred to as silt droplets.

Sticky Spot: A point or area on the glacier bed which accommodates a disproportionately high amount of basal shear stress. It may represent an outcrop of hard rock, lodged boulders, or a patch of particularly well-drained and stiff till.

Stacking Density: In GPR surveys, the number of wave pulses used to derive an average for any given trace. The average trace eliminates or reduces much of the random noise.

Strain, Strain Rate, Cumulative Strain, and Strain Magnitude: Strain is a dimensionless term expressing the ratio of displacement length to displacement depth, whereas the strain rate is strain/time. Strain magnitude is a measure of the amount of strain the sediment has been previously exposed to. Cumulative strain embodies the idea that strain is times-transgressive and that total strain is the sum of all previous strain events. Elastic strain is recoverable; permanent strain is not. Permanent strain includes brittle and ductile (plastic) failures, and dilation/compression. Strain is usually defined by either pure shear or simple shear: in pure shear, material is flattened and stretched, whereas in simple shear, material is rotated like a sheared pack of cards. Simple shear is assumed to dominate in subglacial deformation tills (Benn and Evans, 2010).

***Succitic Fabric**:* A cryogenic fabric - clast a-axes become increasingly vertically aligned under the influence of frost-jacking in periglacial environments. This preferentially affects larger clasts which favour the formation of segregated ice.

Texturally and Compositionally Immature Sediments: During sediment transport sediment can be sorted by grain-size. Sediments that undergo limited transport, or experience limited sorting, are referred to as texturally immature and have a range of grain-sizes present. If they also polymictic, that is, they contain a range of mineral and lithic fragments, then they are also compositionally immature.

Thermal Characteristics: Warm-based glaciers consist of ice at the pressure melting point. As such, the ice-bed interface is characterised by the presence of a lubricating film of melt water and basal slip occurs. Cold-based ice is below the pressure melting point and the glacier is frozen to the bed. Most glaciers are polythermal and consist of cold-based ice at the frozen margins and on the surface, and warm-based ice in the central zones where ice is thicker and pressure melting at the glacier sole produces melt water. The thermal regime is sensitive to climatic oscillations and the warm-cold transition zone can retreat up glacier during retreat phases. SBD is associated with warm-based, active ice. Continental glaciers contain more cold-based ice and maritime glaciers more warm-based ice.

Till: Sediment that has been deposited from a glacial with little or no sorting of sediment by water (Benn and Evans, 2010). Tills are usually poorly sorted diamictons.

Till Rheology: The material behaviour of till deposits defined by the relationship between stress and strain.

Velocity Weakening: The idea that an increase in the strain rate brought about by accelerated glacier flow can progressively weaken sediment strength by increases pwp in the prow of a ploughing clast. Reduced strength results in increased strain and faster velocity; this feedback mechanism may result in catastrophic glacier acceleration.

Viscous Till Rheology: The strain rate increases linearly with stress in a classic Newtonian viscous fluid and the material deforms pervasively (particle by particle) throughout its entire dilating volume (distributed shear). In a Bingham material, the same relationship holds once stress > sediment strength. In a non-viscous till rheology the relationship between stress and strain takes the form of a power function.

Appendix 2 The Quaternary History of northern Sweden

Epoch/Stage	Main Events relevant to northern Sweden/Tarfala area	Source of Evidence
Holocene	Post 1916 – 2010: Alpine glaciers in the Tarfala Area in retreat; small maritime glaciers respond to temperature rise rapidly and are now more in equilibrium and 'stable'. Larger, continental glaciers have longer response times (50-100 years) and are still responding to LIA changes.	Holmlund and Jansson (2002) and Jansson (2010, personal communication).
	1900-1916 Photographs and maps show alpine glaciers in the Kebnekaise Mountains advancing, but after 1916 they begin to retreat, leaving a distinctive frontal moraine line on Storglaciären. Ice retreats in response to a 1° C summer temperature rise at the beginning of the century and an increasingly maritime climate in the Tarfala area.	Holmlund and Jansson (2002); Karlen (1973)
	AD 1100 LIA, culminates in the 17th Century in northern Sweden AD 1000 Mediaeval Warm Period AD 500 -900 Cold 'Dark Ages' 1st Century AD Roman Warm Period. 600 – 1BC Very cold conditions and glaciers expand to Holocene maximum, possibly linked to volcanic eruptions in 330 BC.	Grudd *et al*. (2002) dendrochronoly and Tornetrask Lake Chronology of northern Sweden.
	A series of well-preserved and fresh moraines consisting of fluted and non-fluted 'undifferentiated drift sheets', stratified lacustrine sediments, small deltas, eskers, outwash trains and moraine ridges up to 1.5 km wide and approximately 0.7 km from present glacier fronts reveal a series of Holocene glacier advances, dated at 8500-7900, 7200, 6300-6100, 5900-5800, 5600, 5300, 5100-4800, 4600-4200, 3400-3200, 3000-2800, 2700, 2000, 1900-1600, and culminating in the Little Ice Age advance in the 17th and 18th Centuries. The maximum LIA expansion was at 1500-1640.	Karlen (1973) mulit-proxy approach based on extrapolation of lichen growth curves and a very limited number of absolute ^{14}C dates.
	Alternatively, northern Sweden was ice-free during early-Holocene climatic optimum corresponding to a 9% increase in summer insolation driven by orbital forcing. Rosqvist *et al.* (2004) found no clear evidence of early Holocene ice advances from lake sediment records in northern Sweden. No systematic timing in the reformation of glaciers during the Neoglaciation (6100 – 2100 ka yr) or LIA. Rosqvist *et al.* (2004) recognise ice advances at 4300, 3100, 2200, 1800 years BP and during the last 1300 years; abrupt changes in lake sediments in Lake Vuolep Allakasjaure occur at 5000 years ago, and interpreted as a climatic switch to conditions dominated by more frequent Arctic rather than Atlantic air flows. Oxygen isotope depletion records suggest an average temperature decline of 2.3 to 4° C during the mid-late Holocene, which agrees with a 2° C fall recorded in the Greenland Ice Sheet ice cores.	Nasje (2009) climate model; Grudd *et al*. (2002) dendrochronology and Tornetrask Lake Chronology. Rosqvist *et al*.(2004) oxygen isotope records in freshwater lake diatoms in northern Sweden. Alley *et al*. (1999) GIS ice cores.
LGM	Ice retreated west into valleys of the Kebnekaise Mountains. The last remnants are near present ice fronts and may date from 9640 years ago, but these moraines now subdued compared to fresher and more prominent Holocene moraines.	Karlen (1973) Lichenometry and cross-cutting moraines
	Alternatively, asynchronous deglaciation across Scandinavia. SIS thin and rapidly declines at 10 thousand years ago (ka yr). Lakes in northern Sweden drain west before eastern routes open, indicating mountains ice-free first.	Grudd *et al*. (2002) Dendrochronology and Tornetrask Lake Chronology
	12 – 11.7 ka yr Younger Dryas asynchronous re-advance, eustatic re-bound 10-20 m, Goteburg moraine glacio-tectonised by extra-marginal folding and extensive marginal moraines deposited in Scandinavia. Deglaciation progresses to the west,	Mangerud (2004) ^{14}C dating marine molluscs on

north, and inland from continental shelf.	continental shelf; Lundqvist (2004) geomorphology and till analysis.
MIS 2 LGM greatest extent at 21 ka with mean Arctic temperature 20° below present temperatures.	Miller *et al*. (2010) Review of multiple temperature and precipitation proxies
LGM SIS equilibrium line falls 350-600 m and ice-divide migrates eastwards to centre on Gulf of Bothnia. Maximum ice thickness estimated at 3km with ice velocity at 300-400 m/yr. Ice flows W-E from ice- divide and produces zones of flutings and drumlins, veiki and rogen moraines, and De Geer moraines which reflect changes in thermal conditions and ice dynamics. However, little erosion in central and northern Sweden as cold-based ice.	Ice sheet models driven by temperature records from cores from the Greenland Ice Sheet ice and North Atlantic marine records. Boulton *et al*. (1985) and Nasje (2009).
Alternatively, the ice-divide was centred over central Sweden with thinner ice (max. 2800 m) and sea level fall less severe.	Glacier rebound inversion model (Lambeck *et al*.2010)
23-16 ka yr SIS reaches edge of Norwegian continental shelf, although geometry and thickness of ice sheet unknown. Mountain summits in western Norway and northern Sweden may have been ice-free nunataks, or covered by a cold-based ice sheet.	Mangerud (2004) continental shelf cores. Nesji and Dahl (1992) cosmogenic dating. Fjeldskaar (2000) ice sheet inversion model.
Various positive feedback cycles operate in the Arctic to produce Late Weichselian ice sheet expansion which coincides with maximum orbital forcing. Expansion of sea ice prevents Atlantic waters penetrating Arctic waters; ice sheet albedo reduces insolation inputs whilst thick ice increases average elevations, reducing temperatures; a colder ocean produces less evaporation and reduces greenhouse gas emissions (water vapour); drier and sparsely covered continental interiors produce more atmospheric dust which filters out sunlight. Strong feedbacks, but variable in space and time, hence asynchronous SIS advances and retreats.	Miller *et al*. (2010) review of multiple temperature and precipitation proxies across the Arctic.
SIS covers Scandinavian mountains throughout MIS 4-2 with no major deglaciation. Probably a warmer North Atlantic, but cold-based ice in northern and central Sweden advances to 60° north. Ice streams reach the Baltic by MIS 4, but southern Sweden only in MIS 2.	Lundqvist (2004) limited ^{14}C dates and geomorphology/till analysis
Western Norway ice-free at 41-38 and 34-28 cal. kyr BP.	Mangerud *et al*. (2010) Cave stratigraphy using AMS ^{14}C of bones
Cold conditions prevail 12-44 cal. kyr BP with average surface temperatures 5° colder than present, but warmer than the LGM; drier conditions with permafrost extending to 62° North.	Kjellstrom *et al*. (2010) fully-coupled continent-ocean global/regional climate model
Northern and central Sweden ice-free 60-35 cal. kyr BP. according to Wohlfarth, and 52-36 cal. kyr BP according to Alexanderson *et al*. LGM advance as late as 35 cal. kyr BP. MIS 3 characterised by Dansgaard – Oescher cycles with Interglacials lasting 500 – 5000 years and 8-16° temperature shifts.	Wohlfarth (2010) ^{14}C dating O seds beneath LGM tills. Alexanderson *et al*. (2010) OSL O lake Seds C. Sweden.

Mid-Late Weichselain	Relict moraines in east-west trending mountains in the eastern foothills of the Kebnekaise Mountains in Sweden pre-date the LGM, but their exact age is poorly constrained. However, they suggest the existence of an Early-Mid Weichselian MIeS.	Lundqvist (2004). Fredin and Hatterstrand, (2002).
	Two distinct phases of ice stream advance across the Baltic basin at 34 – 19 cal. kyr BP (the Klintholm ice stream advance) and at 55 – 46 cal. kyr BP (the Ristinge ice stream), at a time when western Norway and central and northern Sweden ice-free. The ice stream advance may have been controlled by changing ice-bed dynamics.	Houmark-Nielsen and Kjaer (2003) and Houmark-Nielsen (2010) Multi-proxy litho-stratigraphy, OSL, ^{14}C.
	MIS 4 Cold pahase deposition of a distinct blue-clayey till in Sweden which contains re-worked ventifacts and aeolian silt produced during the intense periglacial conditions of the Tarendo interstadial.	Lagerback (2007) till analysis and ^{14}C O seds.
	MIS 5a. The Tarendo Interstadial. Severe periglacial conditions in Sweden facilitate an intense phase of ventifaction and production of aeolian sand and silt deposits so distinct they act as a stratigraphic marker. Prevailing NW wind. Ventifaction produced by sand and ice crystal blasting.	Lagerback (2007) till analysis central and northern Sweden.
	MIS 5b. Cold phase. Erratics in tills in Swedish Lapland suggest a western provenance, indicating existence of a MIeS (of unknown extent). Little erosion as veiki moraines preserved.	Lundqvist (2004) geomorphology and till analysis.
	MIS 5c. Perapohjola Interstadial (not seen in Finland)	Lundqvist (2004)
Early Weichselian	MIS 5d. 117 – 105 cal. kyr BP. Cold conditions and first major Weichselian SIS advance in Sweden. Warm-based ice as very erosive. Contemporary landscape initiated at this time. Ice extended from Swedish mountains to the Baltic. Drumlins have NW orientation and till provenance in Sweden is from the north. A distinct arc of 3 hummocky recessional moraines (Veiki moraines) deposited in Swedish Lapland as deglaciation proceeds towards the mountain centre.	Lundqvist (2004)
Pre-Weichselian	130 – 120 kyr BP Interglacial conditions across the Arctic with average summer temperatures 5° warmer and sea level 5m higher than today. All glaciers melted except the Greenland Ice Sheet.	Miller *et al*. (2010) review paper of multiple data sources
	Little detail known in Sweden due to lack of deposits, but assume complete ice sheet cover in Saalian and Elsterian based on European deposits. Recession towards the Sarek Mountains.	Lundqvist (2004) moraine/till distribution
	MIS 8-10 Finnmarksvidda terrestrial till deposited, Norway	Mangerud (2004)
	1.1 ma. Fedje till deposited by ice streams on the Norwegian continental shelf 800-1000 m below present S.L.	Mangerud (2004) IRD/Shelf sediment cores
	European deposits suggest extensive ice sheet by 2.8 ma. with a 41 kyr glacial cycle linked to the tilt of the earth's axis, changing to a 100 kyr cycle at 700 kyr BP.	Miller *et al*. (2010) review paper